Clear Lake Watershed and Lake Remediation: Final Report

Prepared for: State of California Natural Resources Agency

Grant Agreement: GF2141-0

Prepared by: University of California, Davis

January 2026

Clear Lake Watershed and Lake Remediation: Final Report

Prepared for: State of California Natural Resources Agency

Grant Agreement: GF2141-0

Prepared by:
Alicia Cortés, University of California, Davis
Alexander L. Forrest, University of California, Davis
Steven Sadro, University of California, Davis
Sergio A. Valbuena, University of California, Davis
S. Geoffrey Schladow, University of California, Davis

With Contributions by:
Charles N. Alpers, United States Geological Survey
Jennifer A. Curtis, United States Geological Survey
Joseph L. Domagalski, United States Geological Survey
Dina K. Saleh, United States Geological Survey
Michelle A. Stern, United States Geological Survey
Daniel R. Wise, United States Geological Survey

Editor:
Alicia Cortés, University of California, Davis

Suggested citation: *Cortés, A. (2026) "Clear Lake Watershed and Lake Remediation: Final Report. University of California, Davis, prepared for State of California Natural Resources Agency, Grant GF2141-0". Zenodo. https://zenodo.org/records/18376136*

January 2026

0 Executive Summary

Motivation and Goals

Clear Lake is essential for the communities living in its watershed due to **key water uses**: drinking water supply, cultural activities, recreational activities (boating, fishing, swimming, scenic beauty), economic growth (tourism), and an ecological niche for a wide variety of aquatic and terrestrial species. However, the lake is affected by multiple **environmental challenges** that are compromising these beneficial water uses. These include mercury contamination, fish kills, cultural eutrophication (increase in nutrient concentrations), frequent cyanobacterial harmful algal blooms (CHABs), taste and odor formation from CHABs that increase water treatment costs for human consumption, extreme wildfires, pesticide and herbicide runoff, and the introduction of non-native species, among others. These environmental challenges are the result of a combination of processes occurring both within the lake and in its watershed, with the two largely connected by the multiple creeks entering the lake. The greatest barrier to effective water-quality restoration at Clear Lake is the absence of quantitative data on the anticipated response to: (a) environmental changes in the lake and creeks; (b) restoration projects; and (c) long-term changes such as climate change and altered land use. Overcoming this barrier requires a combination of **measurements (via monitoring)** across the watershed and lake, which will allow for the development of **quantitative predictions (via modeling)** of lake responses.

Thus, the **main goal** of this joint effort between the University of California Davis, Tahoe Environmental Research Center (UCD-TERC), and the United States Geological Survey (USGS) is to develop the **watershed and in-lake monitoring and modeling** (Figure 0-1) needed to:

- Better **understand** the processes contributing to poor water quality;
- **Predict** watershed and lake responses to changing environmental conditions; and,
- **Evaluate** the impacts and unintended consequences of potential management and restoration activities.

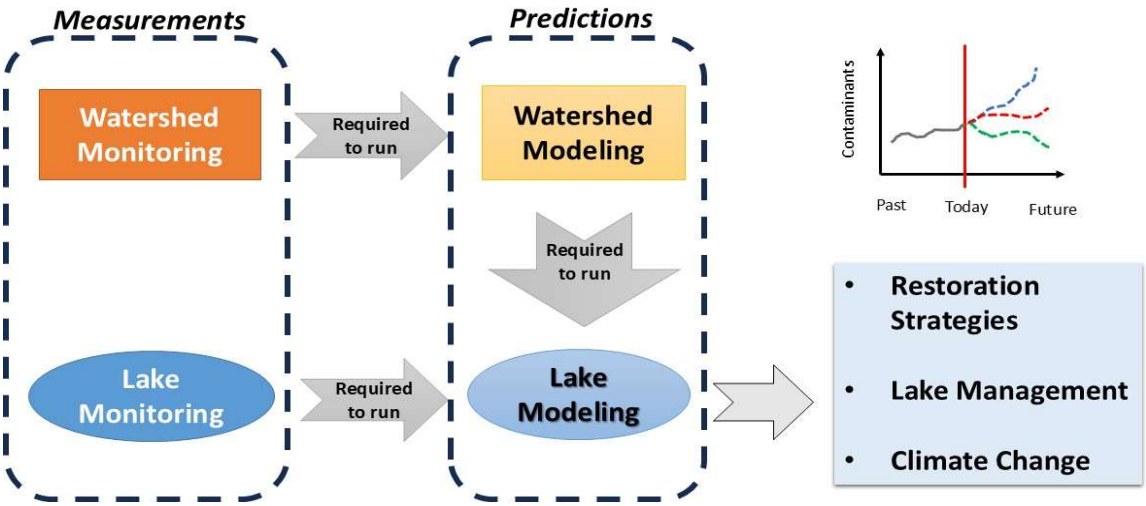

Figure 0.1. Diagram showing the main tasks and goals of this project

Background and Novelty

Over time there have been numerous monitoring efforts by a range of entities including the Department of Water Resources (DWR), Lake County, and Native American Tribes living around the lake. However, these sampling programs have focused on specific sites with infrequent and variable sampling schedules. Such programs cannot characterize the highly dynamic nature of Clear Lake and its watershed, with storm-driven flashy creeks experiencing high interannual hydrological variability and a lake that can mix and re-stratify within a week, with anoxic (no oxygen) conditions establishing within days, and with strong, highly variable currents that rapidly transport water (and contaminants) between the three basins. In other words, a system-wide understanding of Clear Lake and its watershed could not be built on such past efforts. The novelty of this joint project between UCD-TERC and USGS is the creation of a systemwide understanding, upon which future restoration efforts can be based. Components include:

- Collection of watershed and in-lake **continuous, high-resolution, high-frequency in-situ data** for hydrological (flow, water temperature, turbidity), lake physical (temperature, currents, light climate), lake water-quality (dissolved oxygen, nutrients, algae) variables and meteorological conditions (***monitoring***).
- **Prediction** of **the creeks, lake, and their combined response** to environmental forcings to inform lake managers and stakeholders due to the current water-quality challenges (***modeling***).
- **Evaluation** of the impacts, and unintended consequences of implementing particular **restoration projects or strategies** (***model scenario testing***).

Main accomplishments of USGS Watershed Monitoring

- Monitoring of discharge (streamflow) and water quality in several tributaries to Clear Lake was accomplished during 2022–24 by a team of scientists with the U.S. Geological Survey (USGS), Lake County Watershed Protection District (LCWPD), and the University of California, Davis (UCD). **Four new gaging stations** were constructed by USGS after necessary permits were obtained in 2022, and real-time, continuous discharge was reported online during the wet seasons of water years 2023 (October 2022 to May 2023) and 2024 (October 2023 through May 2024). These new gaging stations were: Clover Creek Bypass at Elk Mountain Road (USGS station (11449235), Cole Creek at Kelseyville (11449820), Molesworth Creek near Old Highway 53 (11449370), and Scotts Creek below Tule Lake near Highway 29 (11449255). In addition to discharge, these stations recorded and transmitted data for water temperature and turbidity at 15-minute intervals. The California Department of Water Resources (CA-DWR) began stream gaging during Jan. 2024 at Adobe Creek at Soda Bay Road near Finley (DWR station ACF). Where available, we obtained historical streamflow data from gages to match historical water-quality data for samples collected prior to water year 2022.
- **Water-quality samples** were collected at the four new USGS gaging stations and at several other stream locations in the Clear Lake drainage basin. The additional locations include three other active gaging stations maintained by USGS — two in the upper Scotts Creek watershed (11448750 and 11448800, funded by the Bureau of Land Management) and one on upper Kelsey Creek near Kelseyville (11449500, funded jointly by LCWPD and USGS) — and three stations maintained by CA-DWR — Scotts

Creek at Eickhoff Road (DWR station SCS), Middle Creek at Rancheria Road (MCU), and Kelsey Creek at Soda Bay Road (KCK). Continuous measurements of turbidity and water temperature were made by UCD at the three CA-DWR gaging stations during 2019–24. Some water-quality samples were also collected by USGS at ungaged locations on Adobe Creek and upper Middle Creek.

- Sampling events targeted high flows during and after rain events as well as some lower flow baseline conditions during the wet season (typically December through April) during water years 2022, 2023, and 2024. Three different sets of analyses (schedules A, B, and C) were assigned to selected sampling locations. **Schedule A (116 samples at 6 locations)**, the most complete, included mercury (Hg) species (total Hg (THg) and methylmercury (MeHg), both filtered and particulate), dissolved organic carbon (DOC) and optical properties of dissolved organic matter, filtered and unfiltered nutrients (various forms of nitrogen (N) and phosphorus (P)), and total suspended sediment (TSS). **Schedule B (148 samples at 10 locations)** consisted of the same analyses as Schedule A but without mercury species, DOC, or optical properties. **Schedule C** analyses consisted of unfiltered nutrients at selected storm drains. Two storm drains (North Lakeport, Nice, and (or) Lucerne as the alternate) were analyzed for Schedule B constituents during selected storm events. At the time of sample collection, field data were collected to document the following parameters at most locations: water temperature, specific conductance, pH, dissolved oxygen, and turbidity. Sampling locations and data for gaging stations and water-quality monitoring for both the USGS and Lake County can be seen at: https://ca.water.usgs.gov/apps/clear-lake-water-monitoring.html.
- Some **key findings**: Concentrations of bioavailable phosphorus (soluble reactive phosphorus, or SRP), and the ratio of SRP to total phosphorus (TP), varied at each of the sampling locations. The highest ratio of SRP to TP was measured at the Molesworth Creek site at 48%. The second highest was measured at the Cole Creek site (37%). The site with the lowest measured ratio was Middle Creek (8%). The range of ratios of SRP to TP at the other sites was from 13 to 22%. Another operationally defined form of phosphorus, dissolved phosphorus (DP), was only slightly higher than the concentrations of SRP. **Nitrate (NO_3-) in filtered samples accounted for about 30% of total N (TN**) in unfiltered samples and the remainder of N was mainly organic or in a particulate form. Concentrations of ammonia (NH_3) and ammonium (NH_4^+) were typically low, and given the pH conditions of the creeks, most of this was in the form of ammonium. Molesworth Creek and the storm drains, representing urbanized areas in the Clear Lake basin, had the highest concentrations of N and P species, turbidity, and suspended sediment among monitored tributaries, but relatively low discharge. Measured concentrations of nutrients and streamflow were used to estimate mass loading to the lake on daily, monthly, and annual time steps. **The highest annual loading of total nitrogen in both 2023 and 2024 water years was from Middle Creek. The highest loading of total phosphorus was from Scotts Creek.** Loadings of total nitrogen and total phosphorus from Kelsey Creek were about half of that recorded for either Middle or Scotts Creek. The annual loads of total nitrogen from Clover Creek were about 10% of that from Middle Creek and for total phosphorus between 11 and 14% of that from Scotts Creek for these two water years. Loadings of total nitrogen and total phosphorus from Cole Creek were about 3% of the loadings from either

Middle or Scotts Creek. Loadings of total nitrogen or total phosphorus from Molesworth Creek were between 1 to 3% of that from either Scotts or Middle Creek.

Main accomplishments of UCD-TERC In-lake Monitoring

- UC Davis Tahoe Environmental Research Center (UCD-TERC) developed a **high-resolution, continuous network of in-situ measurements in Clear Lake between 2019 and 2023.** This monitoring program focused on gathering essential information to understand the rapidly changing processes characterizing Clear Lake's poor water quality, and to develop predictive tools for evaluating lake responses to natural conditions and management actions such as restoration projects. **Data collection and analysis** include stream properties at three locations (Middle, Scott, and Kelsey Creeks); meteorological variables at seven locations around the perimeter of the lake; continuous lake temperature and dissolved oxygen at multiple depths and six locations across the lake (fixed water quality stations); and measured nutrient concentrations, phytoplankton speciation, and multi-variable profiles throughout the water column and across all three lake basins. Data are publicly available via the TERC-Clear Lake website.
- Historical monitoring data and more recent monitoring have shown that **periods of low dissolved oxygen (hypoxia) occurring in the summer/fall,** when the lake develops temperature gradients in depth (i.e. stratification), are a **major explanatory factor in the poor water quality** and ecological health of Clear Lake because it controls the nutrient availability for phytoplankton growth. We developed a **method to predict when and for how long low dissolved oxygen levels occur** in the lake using basic meteorological information and lake surface temperature. Results show this method to be highly accurate when predicting the timing of hypoxia without computing actual lake oxygen values. Our results endorse the newly developed method as a **cost-effective tool** for predicting the timing of hypoxic events. We believe this method can be incorporated into an important **decision-making tool** for management actions when aquatic ecological challenges due to hypoxia get accentuated. This method was published in a peer-reviewed journal and can be found here.
- Clear Lake has had **recurring cyanobacteria harmful algal blooms (CHABs)** for over a century despite reductions in external phosphorus (P) loadings. Internal P loadings from lake sediments can also alter nutrient availability. **We quantified both external watershed P loads and internal P loads from 2019-2023**. We combined high-frequency measurements of water temperature and dissolved oxygen, discrete grab sampling for nutrient chemistry, and remote sensing to understand the potential drivers of the observed variability and the spatiotemporal dynamics of CHABs. Comparative estimates of external and internal phosphorus loading indicate that **internal sources accounted for 70 – 95% of the total P input** to the water column during the study period. Contrary to other lakes, the intensity of the summer bloom season correlated to the **timing and duration of anoxia** rather than the magnitude of spring runoff. Internally released P shifted the system from phosphorus to **nitrogen limitation during the summer**, potentially favoring the proliferation of nitrogen-fixing cyanobacteria. Details of this study can be found here. We also produced "The phosphorus (P) budget for the Clear Lake watershed from 2019 - 2022", published on our website. Clear Lake's P budget demonstrates that the annual cycling of P in the system is largely controlled by internal fluxes between lake sediments and the water column. The overwhelming influence of the internal process on P cycling in Clear Lake suggests that focusing on

controlling in-lake internal P loading will be critical to mitigating cyanobacteria blooms in the future.

- **Cyanobacteria measurements** are intrinsically complicated due to the **high spatial and temporal variability of the blooms.** Understanding the spatial and temporal variability of these blooms helps design adequate sampling plans that inform lake managers and local communities about their ability to rely on the lake for key water uses. We studied the spatial heterogeneity of cyanobacteria blooms in Clear Lake by collecting coincident **measurements at varying scales and resolutions**. We collected discrete boat-based measurements (in situ spectroscopy and water samples), Autonomous Underwater Vehicle (AUV) optical measurements, multispectral imagery from small Unmanned Aerial System (sUAS) flights; and multispectral imagery from the Ocean and Land Color Instrument (OLCI) sensor on the Sentinel-3a satellite. A semi-variogram analysis of the high-resolution AUV and sUAS data found the **Critical Scale of Variability for cyanobacterial blooms to range from 70 to 175 m**, which is finer than what is resolvable by the satellite data. We thus observed high spatial variability within each 300 m satellite pixel. The peer-reviewed publication of this study can be found here. We also used the data collected for this study and from our 5-year water quality monitoring program dataset to **evaluate the Cyanobacteria Index (CI) remote sensing algorithm**, which estimates cyanobacteria abundance from the top portion of the water column from OLCI data, and it is publicly available from https://fhab.sfei.org/. The CI tool is valuable because it provides near-daily measurements of cyanobacteria abundance across the entire lake. Our validation found the **current modified version of the CI algorithm to not be effective for Clear Lake and found better performance with the initially developed CI algorithm**.

Main accomplishments by USGS and UCD-TERC combined watershed and in-lake monitoring.

The combined watershed and in-lake monitoring efforts have provided an improved understanding of the nutrient dynamics in the Clear Lake system. Figure 0.2 and Figure 0-3 show the linkage between watershed and lake nutrients at short-term and long-term time scales. We defined **short-term changes** as those occurring on a seasonal basis (e.g. winter vs summer), and **long-term changes** when variability is observed between years (e.g. wet vs. dry years). Different patterns were observed for different nutrients.

- The main source of **total phosphorus (TP)** in the lake in the **short-term** is the sediments during the warm, dry season, as **summer** hypoxia and stratification trigger internal loading. As a result, TP increases in the lake when the creeks are not running. On a **long-term** basis, TP in the lake is higher during summer in **dry years**, when the watershed inputs are minimal (Figure 0.2).
- On the other hand, the main source of **nitrate** (NO_3^-) in the lake is the creeks during the **wet season**, showing that the availability of NO_3^- in lake water is directly correlated with the creeks' loads on a seasonal or short-term basis. As a consequence, NO_3^- availability in the lake is higher during **wet years in the long term**. Summer concentrations of NO_3^- are one order of magnitude lower than in winter, with minimum values observed in the summer of dry years (Figure 0.3).

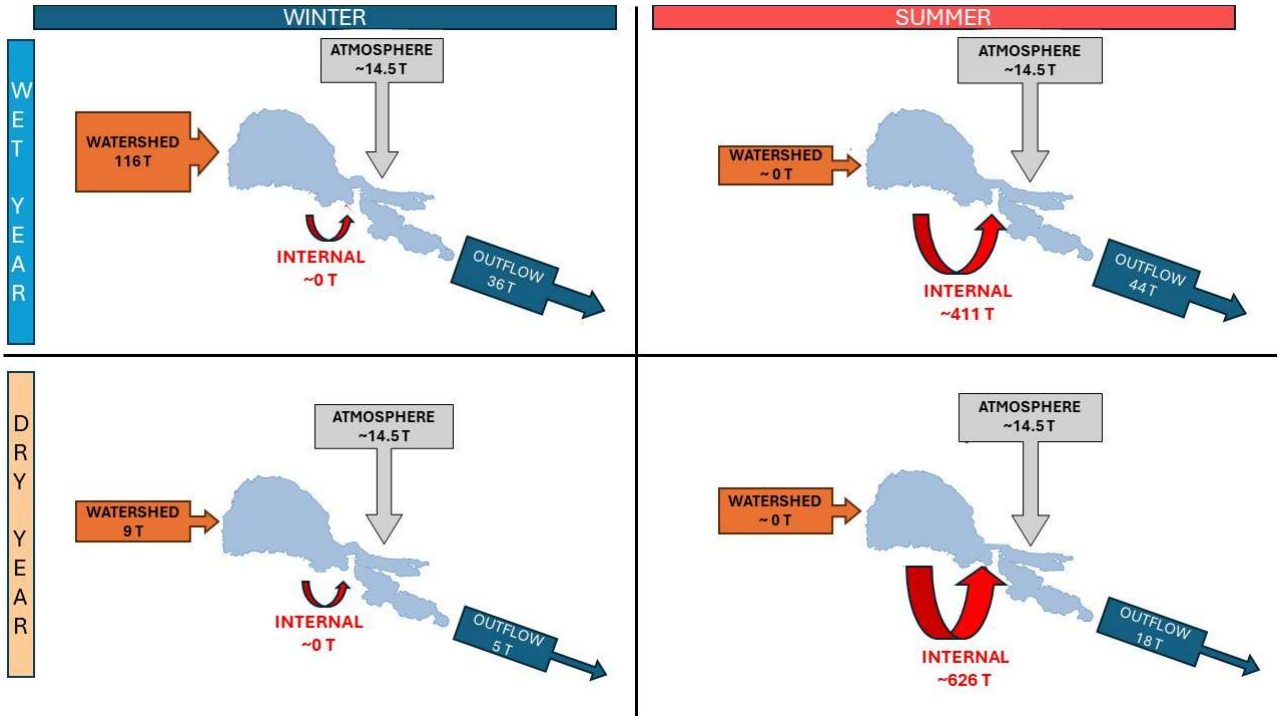

*Figure 0.2. Clear Lake **Total Phosphorus (TP)** flow chart showing the mass sources and sinks (mass balance) which vary seasonally (winter/summer) and interannually (wet/dry years). The figure shows mean values of metric tons (T) obtained during the monitoring period (2019-2023).*

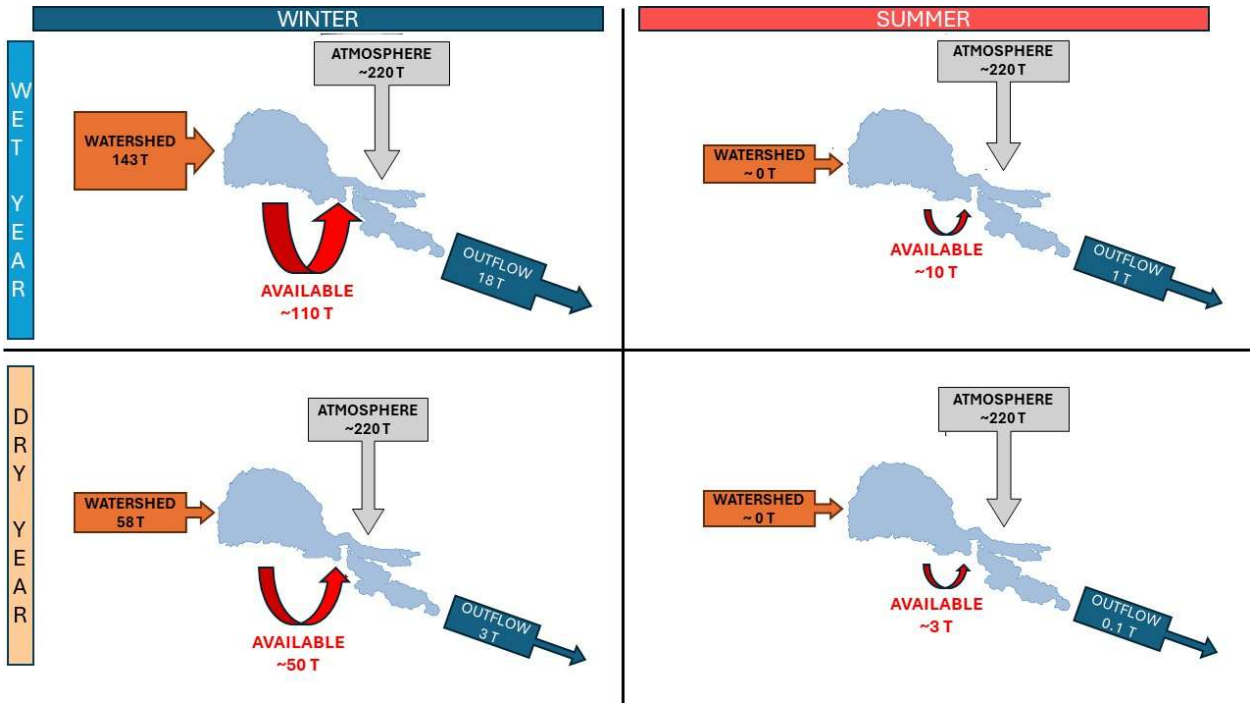

*Figure 0.3. Clear Lake **Nitrate (NO_3^-)** flow chart showing the mass sources and sinks (mass balance) which vary seasonally (winter/summer) and interannually (wet/dry years). The figure shows mean values of metric tons (T) obtained during the monitoring period (2019-2023).*

The joint monitoring efforts in the watershed and lake water argue, for the first time, the **root cause of the water quality problem** in Clear Lake: The **low oxygen** or hypoxia near the sediments during the warm dry season, triggers internal loading or release of **nutrients** from the sediments. The addition of nutrients (especially P) is linked to the increase in CHABs capable of producing toxins and causing fish kills. Low oxygen also favors the production of methylmercury, the form that bioaccumulates, causing risks to human health and fish-consuming biota. Thus, low dissolved oxygen in Clear Lake is impacting human and wildlife health (Figure 0.4).

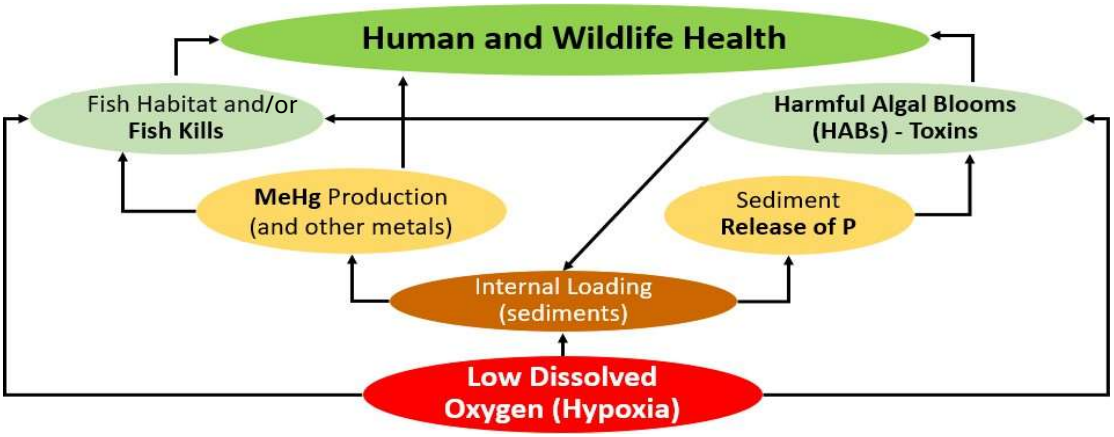

Figure 0.4. Diagram showing the cause and consequences of poor water quality in Clear Lake

Main accomplishments by USGS Watershed Modeling

- The USGS used a **multi-model approach** to watershed modeling. Three modeling strategies were used, each with different strengths and complementary outcomes. **Hydrological Simulation Program – FORTRAN (HSPF)** is a comprehensive model of watershed hydrology and water quality, facilitating the integrated simulation of land and soil constituent runoff processes. We used the HSPF watershed model to simulate continuous streamflow and sediment transport. A **SPARROW (SPAtially Referenced Regressions On Watershed attributes) model** was developed to evaluate the spatial distribution of total nitrogen (TN) and total phosphorus (TP) sources, loads, watershed yields, and factors affecting the transport and delivery of these nutrients in tributary streams that drain into Clear Lake, focusing on a decadal time frame originally centered on 2012 and updated by recent changes in land use and land cover projected to 2020 conditions and fertilizer use during 2017, to understand average loading of TN and TP. **Sediment fingerprinting** for Clear Lake and its tributaries was implemented by collecting and analyzing 590 samples of soil and sediment for more than 60 major and trace elements, plus forms of carbon, stable isotopes of carbon and nitrogen, and particle size distribution. Statistical techniques were used to compute mixing relationships for target sediments at downstream locations, including 25 locations in Clear Lake (representing all three arms) and three locations in Rodman Slough delta, which receives sediment from Scotts Creek, Middle Creek, and Clover Creek.

- Results of **SPARROW** modeling indicate that the largest contributors to **TN** and **TP** loading to Clear Lake originate from the combined outflows from Adobe, Kelsey, Middle, and Scotts Creeks (77% for TN and 71% for TP). Sources of TN to the watershed, and subsequent transport to the lake, include atmospheric deposition, fertilizer and manure, developed land, shrubland, and forested land. Principal sources of TP include natural geological background, fertilizer and manure, and developed land. SPARROW modeling showed that, **although fertilizer is a source of TP to the lake, about 90% of phosphorus applied in fertilizer is not transported to the lake**. Natural geological background includes phosphorus in soils and other geological materials. **Identification of areas undergoing erosion from various natural or anthropogenic activities is one area of potential nutrient source reduction to the lake.** The SPARROW modeling also showed that the upper portion of the headwaters of Scotts Creek releases TP from geological materials, more so than other portions of the Scotts Creek watershed, clearly indicating erosion as a source of phosphorus. In contrast, **the lower Middle Creek watershed, representing the combined flow of Middle and Clover Creeks, releases TP from agricultural activities with higher amounts than other watersheds, indicating a potential area of interest for watershed best management practices to reduce the loading.**
- Results from **HSPF** modeling include calibrated watershed models for **flow, temperature, and sediment transport**. The outputs of the HSPF watershed models were linked to the UCD three-dimensional (3-D) numerical in-lake model. Streamflow results indicated the largest tributary contribution of flow to Clear Lake is Scotts Creek, followed by Middle Creek and Kelsey Creek; interannual variability can affect the relative contributions significantly. Sediment load contributions were also highest for these three tributaries; however, **Tule Lake effectively traps an average of 36% of the sediment loads from the Scotts Creek watershed**, depending on flow conditions. **Scotts Creek contributes roughly 52% of the streamflow, but only 34% of the sediment discharge to the lake. Middle Creek restoration scenarios indicate that a trapping efficiency of a similar magnitude may be attainable**. Future climate scenarios indicate a potential increase in temperature of 5 to 8 degrees Fahrenheit by the end of the 21st century, with mixed projected changes in precipitation of -8% to +25%. These changes lead to potential decreases or increases in streamflow and sediment load, depending on the scenario. The drier scenarios resulted in decreased streamflow and sediment, whereas the wetter scenarios resulted in large increases in streamflow and sediment transport. The hottest and wettest scenario, TaiESM1, resulted in average annual increases of streamflow and sediment discharge of 29% and 89%, respectively, by the end of the 21st century.
- Results from **sediment fingerprinting** were computed using available data, which include complete analyses for more than 60 major and trace elements, forms of carbon, stable isotopes of carbon and nitrogen, and particle-size distribution in 590 samples of soils and sediments from Clear Lake and ten tributaries. Results of Linear Discriminant Analysis (LDA) indicate **distinct geochemical signatures for four tributary source groups**: 1) Adobe Creek, Manning Creek, and Scotts Creek, 2) Cole Creek and Kelsey Creek, 3) Burns Valley, Molesworth Creek, and Schindler Creek, and 4) Clover Creek and Middle Creek. Source group 1 is the dominant source of sediment to Clear Lake, representing about 60% based on 26 target samples distributed in all three arms

of the lake. Source group 3 accounts for about 25% of Clear Lake sediment, predominantly in the Lower Arm and Oaks Arm. Source group 4 is the source of about 15% of Clear Lake sediment, predominantly in the Upper Arm. A separate set of calculations showed **a distinct geochemical signature for upper Scotts Creek (South Cow Mountain area)** compared with middle and lower Scotts Creek and the Clover Creek and Middle Creek source group.

- Comparing **phosphorus concentrations in soil and sediments** among tributary watersheds, the **highest** overall median values (830 mg/kg, N=131) were **in lower and middle Scotts Creek, Middle Creek, and Clover Creek**. Considering only soils, the highest median phosphorus concentrations were in lower and middle Scotts Creek (980 mg/kg, N=24). Median phosphorus concentration in Clear Lake sediments was 1,300 mg/kg (N=28); concentrations were higher in the Lower Arm and Oaks Arm compared with the Upper Arm. Fe-Al-associated phosphorus and loosely bound phosphorus are the forms most likely to contribute (during anoxic conditions) to soluble reactive phosphate (SRP), a bioavailable form that can stimulate algal blooms. **The proportion of Fe-Al-associated phosphorus relative to total phosphorus in sediment ranged from 21% to 25% in the three arms of the lake**. In tributaries, the proportion of Fe-Al-associated phosphorus relative to total phosphorus ranged from 4% in Kelsey Creek to 17% in Cole Creek. Other tributaries with greater than about 10% Fe-Al-associated phosphorus were Burns Valley and Molesworth Creek, Manning Creek, Schindler Creek, and Scotts Creek. Loosely-bound phosphorus represented less than 5% of total phosphorus both in tributaries and lake sediments.

Main accomplishments by UCD-TERC In-lake Modeling and Bathymetrical Survey

- The field measurements collected by TERC researchers between 2019 and 2023 have been essential to building, calibrating, and validating an **in-lake three-dimensional (3D) processed-based model for Clear Lake** capable of making predictions. The processes the model simulates are organized into two groups: those that characterize how the water moves (i.e., **hydrodynamics**) and those that quantify nutrients, oxygen, and algae in the lake (i.e., **water quality**). The water quality model simulates the evolution of dissolved oxygen (DO), nitrogen (N) species, phosphorus (P) species, and the four major phytoplankton divisions (diatoms, green algae, cryptomonads, and cyanobacteria). For this project, we will refer to the newly developed coupled 3-D hydrodynamic Aquatic Ecological Model as **Si3D-AEM.** The coupled model operates on any sub-daily time step to resolve algal processes. We have also **coupled** this **in-lake model with the watershed model** developed by USGS using HSPF and obtained an appropriate representation of the contribution from the creeks to the nutrient pool available in the lake during the wet season.
- The poor quality of existing bathymetric data (i.e. lake bottom topography) from 2002 with a relatively coarse horizontal resolution of 100 m represented a severe constraint on the in-lake predictions. The TERC team conducted a **bathymetric survey in 2024** using an interferometric sonar mapping system to obtain a bathymetric map with a **horizontal resolution of 1 m.** The benefits of this **improved and refined representation of the lake bottom topography** include more robust lake model predictions and the capability to resolve fine-scale processes such as the fate of inflows (i.e., where does the inflow water go?), their impacts, and changes with restoration strategies. This survey has also provided sonar data to better characterize the lakebed substrate. The

hydrographic products from the mapping of Clear Lake provide information to a broad range of stakeholders working on the lake and help reduce the cost of the implementation of restoration strategies.

- Lake **restoration strategies to mitigate CHABs** can be grouped into physical (dredging of the sediment, weed removal, water drawdown, harvesting of algae/nutrients, aeration, oxygenation, ozonation, water mixing, water shading, sediment capping, flocculants/nutrient sequestration, ultrasonic exposure, UV exposure), chemical (copper/peroxide based algaecides, organic algaecides), and biological (microbial/food web manipulations, barley/rice straws, wetland restoration, shoreline stabilization) strategies. Between 2022 and 2023, pilot projects to test four lake restoration strategies at Clear Lake have been recommended and approved by the Blue Ribbon Committee. Those restoration strategies include **dissolved oxygen enhancement (e.g., hypolimnetic oxygenation), algae and nutrient harvesting, ultrasonic algae control, and sediment phosphorus (P) sequestration**. All these techniques have proved to improve the water quality of the sites where they have been previously tested. However, Clear Lake is a unique system with a large surface area, very strong currents, high nutrient and algae concentrations, and a highly dynamic mixing regime. Thus, we have used the newly developed in-lake model to evaluate the effects of the recommended pilot projects on Clear Lake's water quality. Scenario testing has allowed us to identify key variables in the design of the different pilot restoration projects that should be further explored and carefully quantified before the projects move into the implementation phase. This modeling exercise points out the technologies that only provide localized benefits for the water quality and those whose implementation can be challenged due to the dynamic nature of Clear Lake (strong currents). A detailed cost-benefit analysis should be performed to evaluate if the capital investment and maintenance costs of the strategies are worth the water-quality improvement obtained. However, **because the lack of dissolved oxygen is the root cause of the problem, hypolimnetic oxygenation has proved to be the most appropriate solution to Clear Lake's water quality.** Hypolimnetic oxygenation is also the most economical and viable solution in the short and long term due to its ability to treat the full lake with a feasible number of facilities as it takes advantage of the highly dynamic environment. Model results of the four pilot restoration projects are summarized here:
    - *Hypolimnetic oxygenation*: UCD-TERC researchers recommend a pilot project that consists of the direct addition of pure oxygen to the bottom of the Oaks Arm using two diffusers of 1 km long each in the deepest hole of this basin, allowing **DO concentrations to remain above 3.5 mg/L across the Oaks Arm (3,500 acres, 14.2 km^2)** after 2 weeks of treatment. Model results including oxygen injection show a **~50 % reduction in P concentrations and a ~20% reduction in algae compared to the model scenario without oxygen injection**. We obtained these results using a DO injection flow rate of 500 cubic feet per minute (cfm) at the diffuser. To achieve that, we will require ~20 tons/day of liquid oxygen (LOX) or ~3,500 gallons/day. This flow rate also matches the amount of LOX required to overcome the sediment oxygen demand across the Oaks Arm (~0.9 $g/m^2/day$). As a result, we will **treat 10% of the lake** surface using approximately $4M funding based on estimates from 2022.

- *Algae and nutrient harvesting*: AECOM is leading a proposal that recommends a pilot project to operate an algae harvester to remove algal biomass, nutrients (phosphorus and nitrogen), and cyanotoxins from the lake between the inflow water (coming from Clear Lake) and effluent water (clean and oxygenated). Following recommendations from the pilot project leads, we used a flow rate at the intake and effluent of 1 million gallons per day or 0.04 m^3/s, treating the top 50 cm of a **control area of 0.5 acres (0.002 km^2) near Redbud Park (Lower Arm) for 3 weeks** for the model scenario testing**.** The cost of this pilot project is ~$1.3M and uses only one harvester. Model results of the scenario with the harvester did yield **improvements in key water quality variables in the control area compared to model results without the harvester**: the water column remained oxygenated; P concentration remained similar to values at the beginning of the study period; and the algae concentrations were reduced ~10% by the end of the 3-week test period. However, model results using a larger control area (50 acres, 0.2 km^2, 0.1% of the lake surface) were not favorable due to the continuous transport of nutrient and algae-rich water from outside the control area.
- *Ultrasonic algae control*: LG Sonic is proposing a pilot project to deploy 16 LG MPC Buoys, which use ultrasonic waves to form continuous pressure around algal cells, preventing their growth. Each buoy is capable of **treating 50 acres (0.2 km^2).** A pilot project near Redbud Park in the Lower Arm is estimated to cost ~$1.5M. Model results showed **limited improvement** in key water quality variables (DO, P concentrations, and algae biomass), due to the transport of untreated lake water into the control region. We observed a reduction in algae growth by 10% underneath the buoy, and less than 1% algae biomass reduction when evaluating spatially averaged results in the control area (50 acres).
- *Sediment phosphorus sequestration*: We have used the in-lake model to test aspects of the sediment phosphorus sequestration remediation pilot project recommended by EutroPHIX. The numerical model considers the **dispersion, settling, and resuspension** of suspended particles with physical characteristics of the lanthanum-modified bentonite (LMB). Our model results indicate:
  - Clear Lake currents can transport the applied LMB to untargeted locations (**dispersion**) and **delay the settling**, potentially reducing the application efficiency to targeted areas. These processes increase the **uncertainty of the amount of product** required to reduce internal P loading from the sediments. Methods to account for this should be taken into account in dosing calculations.
  - Clear Lake currents and waves can **resuspend sediments from the lakebed** during windy days, which may lead to the horizontal redistribution of the **deposited LMB**. Although this may benefit sequestering phosphorus at different locations on the lakebed until the material's capacity is reached, the resuspension of the deposited LMB and subsequent transport may lead to lower efficiency of treatment at targeted locations. Thus, the transport and resuspension of sediments at Clear Lake must be considered when defining the areas to be treated and designing the dosing required to treat the targeted area.

- Model results aim to provide the quantitative basis for the **up-scaling** of the different

recommended **CHAB mitigation pilot projects** presented to the Blue Ribbon Committee and assist their mission to revitalize Clear Lake. However, we have been only able to do that for Hypolimnetic Oxygenation due to the limited information provided by the proponents of the other proposals.

  - Preliminary model results show that the lake-wide implementation of hypolimnetic oxygenation should use at least six HOS facilities (three in the Upper Arm, two in the Lower Arm, and one in the Oaks Arm). This will add $20-30 M in cost to the pilot project in the Oaks Arm. Annual operation, management, and monitoring (O&M&M) for 10 years of the full lake HOS facilities may cost ~$25 M. As a result, the total capital investment plus O&M&M for 10 years of the full lake HOS may be of the order of ~$50 M.

- We have also produced a report to address concerns raised about possible toxicity threats from metals in Clear Lake if the proposed Hypolimnetic Oxygenation (HO) pilot project in the Oaks Arm is executed, which can be found on our website.

Recommendations for future work

- **Management implications**: Our study shows that the key remediation goal should focus on **increasing dissolved oxygen at the lake bottom** to r**educe the release of nutrients from the sediments during** the warm, dry season **(summer)**. That nutrient reduction (particularly P) will prompt the reduction of CHABs. Preliminary estimates of the magnitude of nutrient reduction required to improve water quality indicate that a ~50% reduction of P concentrations in the lake translates into a ~20% reduction of algae. Since the P loads in the lake are not directly linked to the creeks in the short term, any reduction in the P loads in the creeks will only reduce the available P concentration in the sediments to move into the water column during the warm, dry season. Despite the need to focus on the reduction of nutrients in the summer to mitigate CHABs, monitoring and modeling efforts conducted in this project showed the importance of a multidisciplinary approach to improving the lake's water quality that combines **in-lake restoration strategies in the short-term (seasonal scale) and watershed restoration strategies in the long-term (annual to multi-year scale).**

- Potential remediation strategies:

  a. ***Stream*** *Strategies*: SPARROW modeling indicated the release of phosphorus from geological materials indicating that erosion produces up to 1,500 kg/yr of phosphorus in the upper portion of the Scotts Creek watershed (South Cow Mountain area). The release may be from unpaved roads or other sources, and candidate areas should be assessed for remediation. **Identification and mitigation of the most problematic areas subject to erosion** would represent a good short-term solution for reduction of watershed phosphorus loads. Phosphorus in streams was also sourced from **agricultural sources** with the combined flow of Middle and Clover Creeks transporting up to 2,500 kg of total phosphorus in an average year. The planned **Middle Creek restoration** project may reduce that load, although full implementation is still several years out. Another remediation strategy for that location and other sub-watersheds is a **better understanding of actual fertilizer use and optimization of fertilizer use** where practical. USGS based its fertilizer assessment on sales in Lake County in 2017, with estimated applied amounts based on agricultural locations. An assessment of actual use from individual farms

would provide better information. SPARROW analysis also showed the locations of soils with high clay content which are more easily erodible and a potential source of phosphorus. These soils with the highest clay contents tend to be near the lake shoreline. Those areas should be assessed for best management practices (BMPs) to reduce erosion because of the proximity to the lake. **Erosion control measures in support of existing Lake County BMPs may help reduce sediment and nutrient loadings to Clear Lake in the short and long term**. Reducing sediment and nutrient transport in areas with relatively high sediment and phosphorus loads such as **Scotts Creek, Kelsey Creek**, and the agricultural areas in **Middle and Clover Creeks** should be prioritized. The **Tule Lake** restoration has resulted in **reducing sediment loads by ~36% from Scotts Creek;** a **similar restoration below the confluence of Scotts Creek, Middle Creek, and Clover Creek** would likely reduce the sediment and nutrient loadings to Clear Lake significantly. The proposed and ongoing efforts to restore the Rodman Slough / Middle Creek area through wetland restoration, and reducing channelized flow in between levees, are likely to significantly reduce sediment and nutrient loads into Clear Lake.

b. ***In-lake*** *strategies*: Because the **lack of dissolved oxygen is the root cause of the water-quality problem in Clear Lake, hypolimnetic oxygenation has proved to be the most appropriate solution.** Hypolimnetic oxygenation is also the most economical and viable solution in the short and long term due to its ability to treat the full lake with a feasible number of facilities as it takes advantage of the highly dynamic environment. The overall conclusions from our in-lake model results are that, by maintaining the oxygenated conditions near the lake bottom, P concentrations may be capped to typical winter values (~100 mg/m^3) preventing the excessive P releases that cause a shift in nutrient limitation (P >> N), and thus a relative deficit in nitrogen for all algae. This favors CHABs which are capable of fixing atmospheric nitrogen and thrive in a harsh environment.

- We recommend a **sustained, long-term, community-led, science-based monitoring program** at Clear Lake defined as a cooperative effort with a well-defined science-based framework that provides an opportunity for the community to lead the efforts, ensure technology transfer, capacity building for the local communities, and the development of an engaged science community at Clear Lake with guidance from regional expertise. Continuous monitoring at Clear Lake is necessary for multiple reasons: to ensure standards for drinking water supply, as well as cultural and recreational activities; to evaluate the effectiveness of restoration strategies; to ensure the ecosystem continues as a niche for several endangered wildlife species; and to provide a continued understanding of the long-term changes in the watershed and within the lake under natural and anthropogenic stressors (e.g. climate change, land uses). In addition, it is recommended that further understanding of the interactions of groundwater and surface water is needed to better determine the timing and locations of when and where streams are gaining and losing and how this might affect fish reproduction and populations, especially necessary for the sustainability of the Hitch population.
- The novelty of this project focuses on the **newly developed models** to (1) accurately anticipate or **predict conditions** in the creeks and lake, and their combined response to the environmental changes, which will inform lake managers and stakeholders of

recurrent or new water-quality challenges; and (2) quantitatively **evaluate** the effectiveness, impacts, and potential unintended consequences of implementing particular restoration strategies. This project represents the initial effort in the development and use of those predictive tools. However, we recommend to **continue using the newly developed watershed and in-lake models** in Clear Lake as we move forward in the task of rehabilitating the lake, which will be facing new challenges due to changes in climate and land use, but also to **update their predictive capabilities by recalibrating the models with new monitoring data as it becomes available**. As an example, the California Natural Resources Agency has recently funded a modeling effort to couple a mercury model to the water quality model. This expansion to the Clear Lake's predictive tools will enable state and federal agencies to explore lake remediation strategies that ameliorate mercury concentrations accumulated in the lake water and the sediments, that ultimately move to the biota.

- **Improve the biogeochemical water quality in-lake model** to include more complex processes which may be key to correctly predicting cyanobacteria blooms: Incorporate dynamic intracellular storage of nutrients for algae dynamics; Include nitrogen fixation as part of the nitrogen cycle to overcome the N limitation during the summer; incorporate dynamic modeling of nutrient fluxes in the sediments; and include the effect of microbial community dynamics at the sediment-water interface on cyanobacteria algal blooms.

1 Table of Contents

2 List of Figures

3 List of Tables

4 Introduction

4.1 Background and Motivation

Clear Lake, CA is the largest lake in surface area in California (151 km^2), the oldest lake in North America (~2.5 million years old), and vital for the local culture and economy of Lake County, yet the lake is highly impaired in key water uses. Clear Lake is essential for the cultural activities and economies of seven Native American Tribes living around the lake, a vital source of drinking water supply for many communities, a niche for several endangered fish species, and crucial for tourism and recreational activities such as fishing and boating. However, the lake is affected by multiple environmental challenges that are compromising these beneficial water uses, such as mercury contamination (Suchanek 2008), fish kills, cultural eutrophication (i.e., increase in nutrient loads), frequent cyanobacteria harmful algal blooms (CHABs) (Richerson et al. 1994), which may produce toxins that increase water treatment costs for human consumption, extreme wildfires, pesticide overuse, or introduction of invasive species.

Cyanobacteria Harmful Algal blooms (CHABs) have been observed in Clear Lake throughout the 20th century with blooms becoming more frequent and well-documented starting in the early 1970s (Horne 1975). Since 1986, Clear Lake has been on the Clean Water Act Section 303(d) List of Impaired Water Bodies because of these CHABs. Clear Lake suffers major economic losses stemming from HABs, and a 1994 study estimated that Lake County loses between $7-10 million in tourist revenue annually due to HABs (Goldstein & Tolsdorf 1994). This value likely underestimates current tourism losses and maintaining the economic viability of Clear Lake is paramount since it is located in the poorest county in the state. Past study results and data analyses conducted by Richerson et al. (1994) and Tetra Tech (2004) suggest that controlling phosphorus inputs into the lake is the best approach to addressing the CHABs. As such, the Clear Lake watershed is currently subject to a Total Maximum Daily Load (TMDL) requirement for phosphorus loading which was adopted in June 2006 following the Central Valley Regional Water Quality Control Board's (CVRWQCB) and EPA approval the following year (2007).

Winder et al. (2010) reviewed the lake data collected at Clear Lake from the late 1960s to 2008 to update the current thinking on the cause(s) of high primary productivity and troublesome algal blooms in Clear Lake. The specific objectives were to investigate the status and trends of available water quality parameters such as nutrient concentrations (both N and P), phytoplankton, zooplankton, fish, and Secchi depth from the early 1990s to 2008. They concluded that the increase in lake clarity observed in the 1990s in Richerson et al. (1994) analysis was not a result of a reduction in nutrient concentration but rather due to a trophic cascade that ended in reduced zooplankton predation and a subsequent increase in cladoceran and rotifer densities. More recently, Thirkill et al. (2021) compare present nutrient trends to trends observed by Winder et al. (2010), assess how the status and trends of nutrient concentrations have changed since the 1970s, and quantify whether the internal phosphorus concentrations have decreased since the placement of the Central Valley Regional Water Quality Control Board's (CVRWQCB) phosphorus TMDL in 2006. The historical analysis of nitrogen and phosphorus data from Clear Lake indicated that the lake continues to suffer from excessive phosphorus loading

even though the TMDL has forced a reduction in external inputs. This work confirms that the continuation of regular water quality monitoring is strongly recommended.
Still today, the greatest barrier to effective water quality restoration at Clear Lake is the absence of quantitative data on the anticipated response to restoration projects. Watershed and in-lake monitoring and modeling are needed to better understand the processes contributing to poor water quality, predict watershed and lake response to changing environmental conditions, and evaluate the impacts, costs, and unintended consequences of potential management activities.

4.2 Objectives of the Report

This project will conduct upper watershed and in-lake monitoring and modeling and measure in-lake bathymetry to develop and evaluate remediation strategies and projects for the watershed and lake.

4.3 Clear Lake Site Description

Clear Lake has a surface area of 151 km^2 and volume (V) of 1.11 km^3 located in the Coast Ranges of California, approximately 120 km northwest of Sacramento. It is a shallow (average depth ~8 m, maximum depth ~18 m), warm (5-28°C), hypereutrophic (rich in nutrients) lake, with 4.5 years of residence time, and its circulation is strongly influenced by wind-driven currents. Because of the temperate Mediterranean climate and Clear Lake's low elevation the lake never freezes. Finally, because of its relatively shallow depth, and the influence of strong west/northwest winds, Clear Lakes experiences frequent mixing events (i.e. polymictic). It is a multi-basin lake, with the largest basin named Upper Arm (63% of V) on the western side connected via a channel (Narrows) to two smaller basins on the east (Oaks Arm and Lower Arm, 12% and 25% of V, respectively) (Figure 4-1).

Clear Lake has several tributaries. These tributaries include Adobe Creek, Burns Valley Creek, lover Creek, Forbes Creek, Kelsey Creek, Manning Creek, Middle Creek, Molesworth Creek, Morrison Creek, Schindler Creek, and Scotts Creek. Of these tributaries Scotts Creek and Middle Creek provide the most input into the system, draining about 30% of the watershed (Richerson et al. (1994). The lake's only outlet is through Cache Creek, which flows out of the Lower Arm.

Land use in the watershed is primarily forested, shrubland, and grassland. Both the Mendocino National Forest and the Bureau of Land Management (BLM) own lands within the Middle Creek and Scotts Creek watersheds respectively and use it for livestock grazing and timber harvesting. Agricultural and urban land uses are primarily located in the lowland areas along the lake shoreline. Vineyards have increasingly become the major crop in Lake County over the last few decades. The Clear Lake watershed is sparsely populated, with only 2.5% of the lake's surrounding area being urbanized in 2004 (Tetra Tech, 2004). Wetlands and other habitat areas along the shoreline of the lake support a variety of waterfowl and songbirds, both resident and migratory, and the county depends heavily on tourism for its economic growth. Fishing and swimming in Clear Lake are the two primary recreational activities that bring tourists to the area.

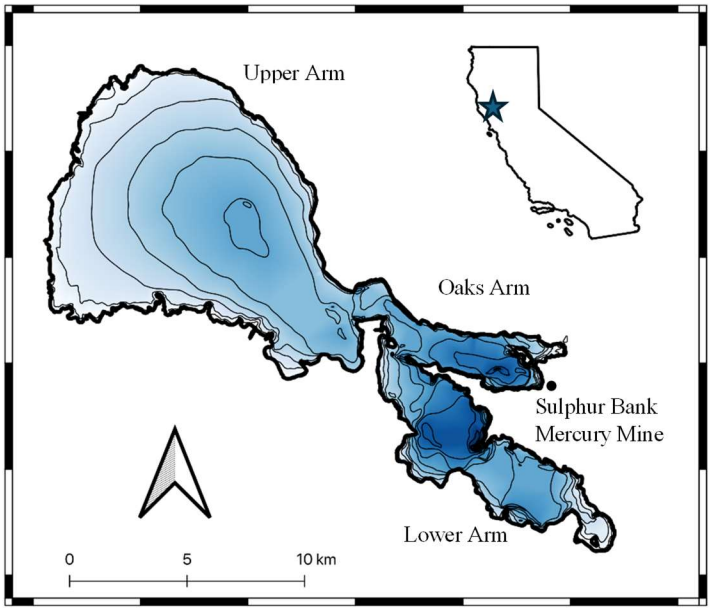

Figure 4.3.1. Clear Lake Map. Isodepths are every 2 m (~6 ft)

Water quality data suggest that the lake experiences nitrogen-limiting conditions during the summer periods when algal productivity is highest. Watershed loading of phosphorus and subsequent accumulation in lakebed sediment provides a large source of internal phosphorus further contributing to this nitrogen limitation. This nutrient enrichment/limitation problem has occurred in Clear Lake for several decades, and historical records show evidence that this problem may have begun as early as 50 years ago (Tetra Tech 2004). As a result of this nutrient enrichment, Clear Lake suffers from frequent blooms of noxious scum forming cyanobacteria. These cyanobacteria scums are typically formed by *Microcystis, Anabaena,* and *Aphinozomenon*. *Aphanizomenon* and *Anabaena* have a competitive advantage in the phosphorus-rich waters of Clear Lake because of their ability to fix atmospheric nitrogen (Winder et al., 2010).

4.4 Structure of the Report

This report is structured as follows:

- Upper Watershed Monitoring: Stream discharge and water quality monitoring
- Upper Watershed Modeling: SPARROW, HSPF, Sediment Fingerprinting
- In-Lake Monitoring
- In-Lake Modeling
- In-Lake Bathymetric Survey
- Coupling of Upper Watershed and In-Lake Modeling
- Conclusions
- Recommendations

5 Upper Watershed Monitoring (USGS)

5.1 Stream flow at Gaging Stations

Authors: Dina Saleh and Charles N. Alpers

5.1.1 Methods

Streamflow monitoring was used in this study to document tributary inflows to Clear Lake, for the planning of water quality sample collection, and to support modeling of nutrient and sediment sources and delivery to the lake along with the UC Davis Lake hydrodynamic model (Si3D, Smith, 2006). There were 11 river discharge monitoring stations available for this study. Of these, seven were maintained by the U.S. Geological Survey (USGS) and four by the California Department of Water Resources (DWR). One of the DWR sites, Adobe Creek near Finley at Soda Bay Road, had the shortest record (less than one full water year) and was not used for calculating nutrient or sediment loads. The names of the stations, location coordinates, site identifiers, site locations, periods of record, and website links are available in Table 5.1.1. A map showing the locations of the gaging stations is provided in Figure 5.1.1.

Table 5.1.1. Station names, US. Geological Survey station numbers, California Department of Water Resources station abbreviations, latitude (NAD83), longitude (NAD83), and streamflow record periods. Links to websites for each station are provided. Note the Molesworth Creek near Clear Lake, California, gage is no longer active.

Station Name	U.S. Geological Survey Station Number	Station ID	Latitude (Decimal Degrees, NAD 83)	Longitude (Decimal Degrees, NAD 83)	Stream-Flow Record
South Fork Scotts Creek near Lakeport CA	11448750	SFS	39.04028	-122.983306	2020-11-05 to present
Scotts Creek below South Fork Scotts Creek near Lakeport, CA	11448800	SBS	39.04194	-122.980833	2020-11-05 to present
Scotts Creek above State Route 29 at Upper Lake, CA	11449255	TLS	39.15764	-122.920733	2022-10-01 to present
Scotts Creek above Eickhoff Road Bridge near Lakeport CA	390544122574201	SCS[2]	39.09545	-122.961044	2008-04-16 to present
Clover Creek Bypass at Elk Mountain Road near Upper Lake, CA	11449235	ACS	39.17578	-122.902889	2022-10-01 to present
Molesworth Creek near Clear Lake, CA	11449370	MCH	38.93894	-122.628889	2022-10-01 to 2024-04-30
Kelsey Creek near Kelseyville, CA (Upper Kelsey)	11449500	KCU	38.92740	-122.843605	1946-10-01 to present
Kelsey Creek below Kelseyville, CA (Lower Kelsey)	390030122502101	KCK/KCS[*1,2]	39.00840	-122.839219	2010-02-16 to present
Cole Creek at Kelseyville, CA	11449820	CCK	38.97933	-122.830578	2022-10-01 to present
Middle Creek near Upper Lake at Rancheria, CA	391057122544301	MCU/MCS[*1,2]	39.18252	-122.911842	2008-05-20 to present
Adobe Creek near Finley at Soda Bay Road, CA	390054122521501	ACF[2]	39.01486	-122.870676	2024-01-19 to present

[*1] This site has two name abbreviations, the first is the DWR Station ID, and the second is the abbreviation used by USGS and Lake County, [*2] DWR sites

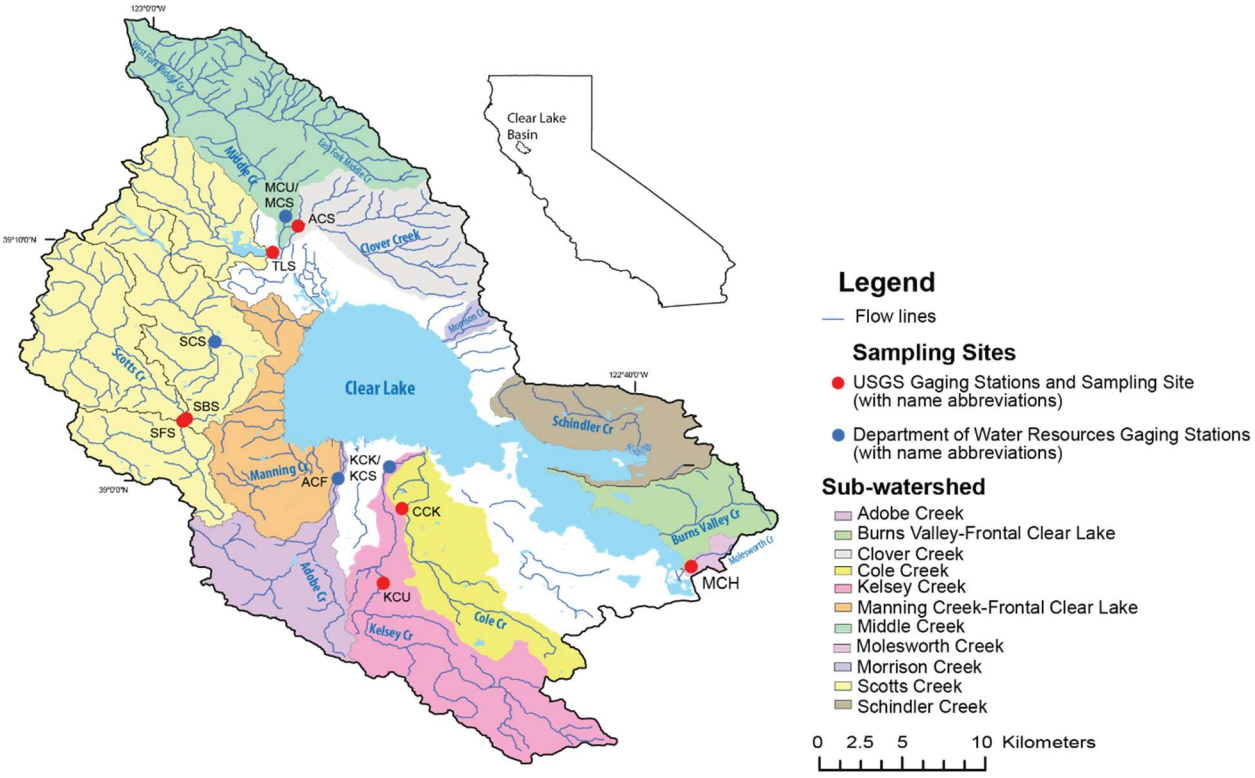

Figure 5.1.1. Locations of water-quality sampling sites.

Streamflow monitoring provided a record of the amount of water delivered to Clear Lake and was also used to schedule water-quality sampling based on the amount of flow following rainfall events, and in between events, so that samples could be collected across the range of flows. In general, predicted streamflow above 14.2 cubic meters per second (m^3/s) (500 cubic feet per second, cfs) at the larger streams was used as a threshold for collecting water quality samples to capture conditions associated with higher flows that could transport more sediment, nutrients, or other constituents. Streamflow, along with water-quality measurements, was used to calculate mass loading of nutrients and sediment. Mass loading of nutrients or sediment were used to either calibrate, validate, or compare watershed models (SPARROW, HSPF, Sediment Fingerprinting, discussed in other chapters).

The Adobe Creek site had the shortest record, and that flow record did not sufficiently overlap with the water-quality monitoring to calculate mass loads of nutrients or sediment for this project. Four stations, SCS, KCK/KSC, MCU/MCS, and ACF are maintained by the DWR, and the hyperlinked websites lead to web pages maintained by DWR. USGS station numbers for those four sites can be used to access water-quality data measured by USGS.

Streamflow at all locations is collected at 15-minute intervals and then aggregated into mean daily values. Methods for measuring river stage and streamflow are summarized by Wahl et al. (1995) and are also available from Turnipseed and Sauer (2010). Data for streamflow can be obtained from either the USGS National Water Information System (2024; https://nwis.waterdata.usgs.gov/nwis) for stations managed by USGS or from the

California Data Exchange Center (https://cdec.water.ca.gov) for sites managed by DWR.

5.1.2 Results

Streamflow data were used to schedule water sampling visits, to calculate mass loads of nutrient and sediment, and to calibrate or validate other watershed models. Some additional information on the streamflow records at these locations related to this study is as follows.

Four gaging sites, Scotts Creek above State Route 29 at Upper Lake, Clover Creek Bypass at Elk Mountain Road Near Upper Lake, Molesworth Creek near Clearlake, and Cole Creek at Kelseyville, were installed and maintained specifically for this study; the record for these sites began on October 1, 2022 (the first day of water year 2023). Therefore, those sites had the shortest periods of record. The site with the longest historical record in the Clear Lake basin is Kelsey Creek near Kelseyville, maintained by USGS, with a streamflow record starting in October 1946. This long-term record provides valuable information on the variation in streamflow in this watershed and how climatic conditions (rainfall) have affected streamflow over this period. The mean daily streamflow for the entire period of record at Kelsey Creek near the Kelseyville site is shown in Figure 5.1.2. The streamflow record provides insights into climatic conditions over this 78-year record. Streamflow is "flashy" with rapid increases in response to rainfall, which also drop rapidly in the days after a storm. Streamflow may drop to zero at some or most sites in the summer through fall, prior to the start of the next rainy season (Figure 5.1.1 and Figure 5.1.2A).

There is considerable year-to-year variability in streamflow. Annual instantaneous peak flows for the KCU site are shown in Figure 5.1.2B. Peak flows provide a useful metric of dry versus wet years because streamflow is usually zero in the summer months. Peak flows for each year were obtained from the National Water Information System (2024; https://nwis.waterdata.usgs.gov/nwis). The regression line and equation, and associated statistics, shown in Figure 5.1.2B were produced using the R Project for Statistical Computing (https://www.r-project.org) package, ggplot2 (version 3.5.1, https://ggplot2.tidyverse.org). The grey shading surrounding the regression line indicate 95% confidence intervals, also produced using ggplot2. Instantaneous peak flows (Figure 5.1.2B) vary considerably at this location with no statistically significant temporal trend as indicated by the p-value of the regression line (0.75). The regression line fitted through the data shows a Pearson's Correlation Coefficient, R, of 0.038. Although there is a slight negative trend as indicated by the linear regression (peak flow = 120 - 0.00027 x) equation, there is no statistical significance, given the p-value of 0.75 and the low value of the correlation coefficient. The lowest annual peak flow was recorded in January 1977 at 2.86 cubic meters per second (101 cfs), and the highest in March 1995, at 243.5 cubic meters per second (8,600 cfs). The median annual peak flow is 120.6 cubic meters per second (4,259 cfs) with a standard deviation of 59.5 cubic meters per second (2,101 cfs). This analysis shows that there are no significant trends in peak stream flows over the period of record shown in Figure 5.1.2B (1946-2023).

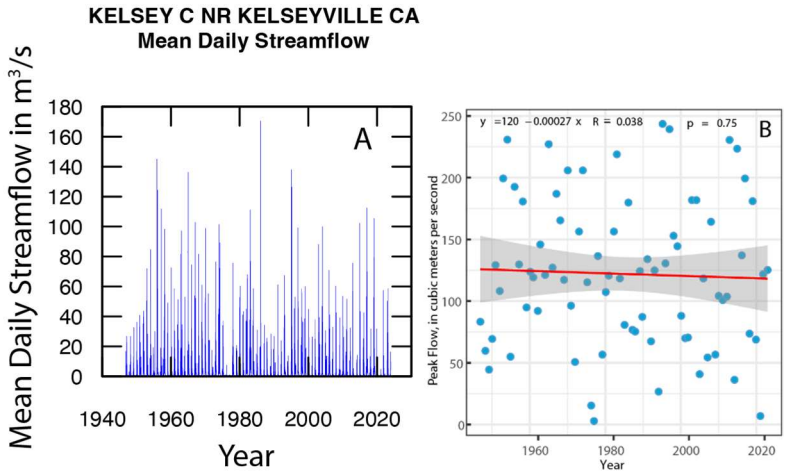

Figure 5.1.2. A (left). Long-term record of stream flows at the Kelsey Creek near Kelseyville location (station KCU). Data from Kelsey Creek Near Kelseyville, CA; B (right). Yearly record of peak flows at the Kelsey Creek near Kelseyville location. Gray shaded areas are the 95% percent confidence interval.

Streamflow was also used in this study to calculate or simulate daily mass loads of nutrients and to support watershed and lake hydrodynamic models. Water-quality sampling began in October 2021 for most sites. Some sites had historical water-quality data, such as the Kelsey Creek site below Kelseyville, which dates to 2010. A partial record of daily mean discharge from 2016 to the spring of 2024 for the site Kelsey Creek above Soda Bay Road near Kelseyville, CA is shown in Figure 5.1.3 to illustrate the variability in streamflow over the past 8 years.

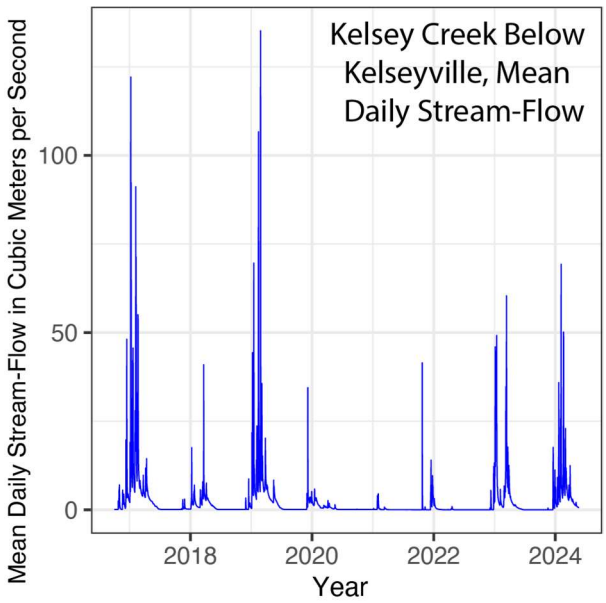

Figure 5.1.3. Mean daily streamflow at the lower Kelsey Creek site (KCK/KCS), 2016-2024

The flow record at the lower Kelsey Creek location (Kelsey Creek above Soda Bay Road near Kelseyville, CA, site KCK/KCS) starting from 2016 to 2024 (Fig 5.1.3) shows the year-

to-year variability in streamflow, and near-zero tozero flow between rainy seasons. Streamflow during 2020 to 2022 was very low and then increased in 2023. The variability in stream flows cause variability in mass loading of nutrients and sediment to the lake.

Streamflow is highly skewed at each of the gaging stations, with most of the discharge occurring during the rainy season (October through March). The peak flows occur before most of the primary productivity in Clear Lake begins. The highest amount of nutrient delivery is therefore disconnected from when peak primary productivity in Clear Lake happens. Streamflow drops to near zero or zero flow during the summer, accounting for the highly skewed results. Box plots of all discharges used in the modeling for the 10 modeled locations are shown in Figure 5.1.4. Monthly box plots for the Scotts Creek below South Fork Scotts Creek (SBS) site are shown in Figure 5.1.5.

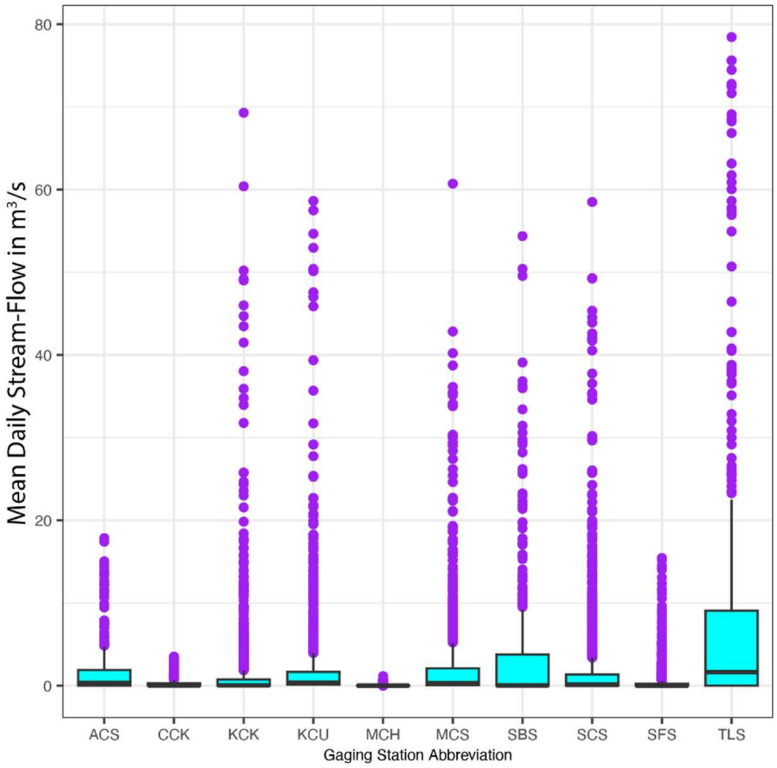

Figure 5.1.4. Box plots of mean daily streamflow at sampling locations (water years 2023 and 2024. Abbreviations: ACS: Clover Creek Bypass; CCK: Cole Creek; KCK/KCS; Lower Kelsey Creek; KCU: Upper Kelsey Creek; MCH: Molesworth Creek; MCU/MCS: Middle Creek; SBS; Scotts Creek below South Fork Scotts Creek; SCS: Scotts Creek near Lakeport (at Eickhoff Road); SFS: South Fork Scotts Creek; TLS: Scotts Creek above State Route 29 at Upper Lake. Locations are shown in Table 5.1.1. Each box shows the range of concentrations measured. Lower boundary of box is the 25th percentile, upper boundary of box is the 75th percentile, line through the central portion of the box is the median or 50th percentile, whiskers are calculated using 1.5 times the interquartile range, dots are outliers.

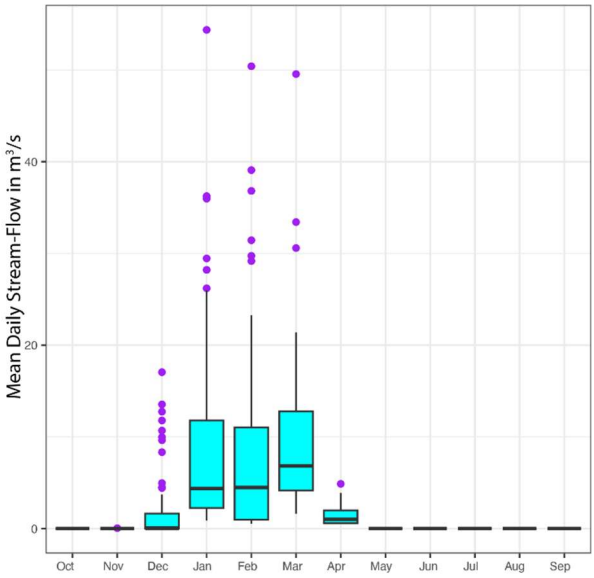

Figure 5.1.5. Box plots of monthly streamflow at the Scotts Creek below South Fork Scotts Creek location. Months are in water year order. Water year begins on October 1 and ends on September 30. Data are for water years 2023 and 2024.

The box plots by month at the Scotts Creek below South Fork Scotts Creek location show that streamflow typically starts in the late fall or early winter with maximum streamflow in January through March, decreased streamflow during April and May, and low to zero streamflow in the summer months. A similar pattern is observed at all the gaging stations.

Mean daily streamflow at the two Kelsey Creek (KCU and KCK/KCS, respectively) sites is shown for water years 2022–24 in Figure 5.1.6. Streamflow at the two Kelsey Creek locations is very close because of the proximity of the two gages (Figure 5.1.6). At the end of the wet season of water year 2022, streamflow is slightly higher at the upper (KCU) site relative to the lower (KCK/KCS) site, suggesting a loss of water through the streambed.

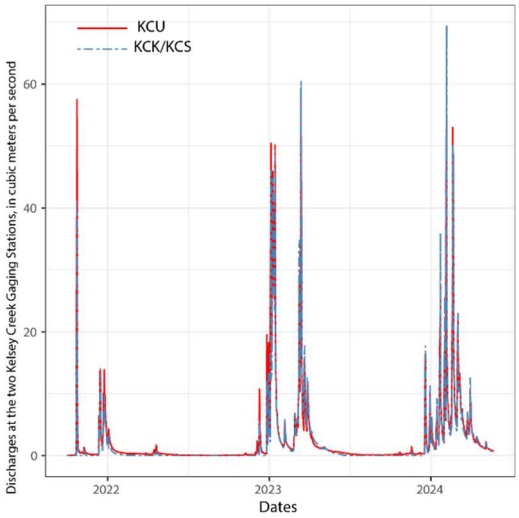

Figure 5.1.6. Mean daily discharge at the two Kelsey Creek Locations.

The total annual streamflow for six gaging stations is shown in Table 5.1.2. The six locations are the Scotts Creek above State Route 29 at Upper Lake (TLS), Middle Creek near Upper Lake at Rancheria (MCU/MCS), Kelsey Creek below Kelseyville (KCK/KCS), Clover Creek Bypass at Elk Mountain Road near Upper Lake (ACS), Cole Creek at Kelseyville (CCK), and Molesworth Creek near Clear Lake (MCH). These six locations were chosen for comparison because they have similar locations in the watershed (near the outflows of each creek to the lake) and relative contributions to annual streamflow to the lake.

Table 5.1.2. Water balance (total streamflow) for water years 2023 and 2024 in cubic meters for six locations. [Abbreviations: TLS, Scotts Creek Above State Route 29 at Upper Lake; MCU/ MCS, Middle Creek near Upper Lake; KCK/KCS Lower Kelsey Creek; ACS, Clover Creek Bypass; CCK, Cole Creek; MCH, Molesworth Creek].

Stream	2023 Water Year Total Streamflow, cubic meters	2024 Water Year Total Streamflow, cubic meters
TLS	169,802,339	166,399,794
MCU/MCS	101,559,948	90,157,334
KCK/KCS	88,642,393	83,355,205
ACS	32,665,130	27,222,683
CCK	4,425,113	9,381,525
MCH	721,983	586,834
Totals	**397,816,906**	**377,103,285**

The combined streamflow of Scotts Creek, Middle Creek, and Kelsey Creek make up about 90 percent of the discharge for these six locations for these two water years. In addition to these sites, other streams that are not gaged such as Adobe Creek, Manning Creek, and Burns Valley, among others, contribute to the water balance of the Clear Lake watershed. Previous estimates have shown that Scotts Creek, Middle Creek, and Kelsey Creek account for 73 percent of the total amount of water entering the lake from all streams surrounding the lake (Richerson et al., 1994). The HSPF model (section 6.3) estimates that the average contribution of flow to Clear Lake from Scotts Creek, Middle Creek (not including Clover Creek), and Kelsey Creek from water years 1980 to 2023 is 84 percent.

5.2 Water Quality Monitoring at Tributary Locations

Authors: Dina Saleh and Charles N. Alpers

5.2.1 Methods

Water-quality monitoring was completed for this project during water years 2022–24 at the streamflow gaging stations discussed in section 5.1 of this report and at additional ungaged tributaries to Clear Lake. Methods for collecting water-quality samples, for either field measurements or laboratory analysis, depend on site conditions and safety considerations (https://www.usgs.gov/special-topics/water-science-school/science/water-quality-sampling-techniques). In all cases, sampling crews attempted to collect the most representative sample for the environmental conditions. Methods for water-quality sampling are given in the U.S. Geological Survey National Field

Manual (https://www.usgs.gov/mission-areas/water-resources/science/national-field-manual-collection-water-quality-data-nfm). The link to the National Field Manual provides detailed information on methods for measuring field parameters such as dissolved oxygen concentration, specific conductance, turbidity, pH, and other instantaneous measurements. The National Field Manual also provides guidance on the collection of discrete samples for laboratory analysis. This guidance provides information on the proper equipment, bottle types, any necessary preservatives, holding times prior to analysis, and refrigeration requirements of the sample prior to analysis. Locations of sampling sites are shown in Figure 5.2.1.

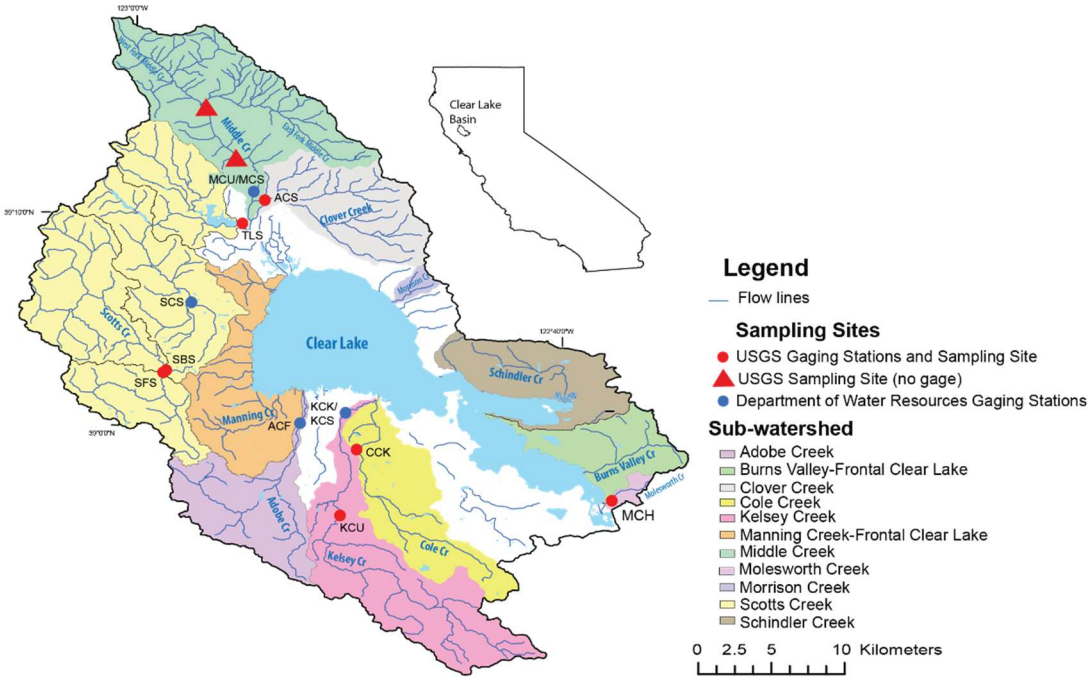

Figure 5.2.1. Locations of water-quality sampling sites.

The types of water-quality samples collected varied at individual sites. A comprehensive list of all sampling sites, including location, dates of sampling, and results of either discrete laboratory analyses or field measurements, is available from Sushch et al. (2025). Three different analytical schedules designated as Schedules A, B, or C were used throughout this project for discrete samples. Schedule A (116 samples at 6 locations), the most complete, included mercury species (total mercury and methylmercury, both filtered and particulate), dissolved organic carbon (DOC), optical properties, filtered and unfiltered nutrients (various forms of nitrogen (N) and phosphorus (P)), and suspended sediment (SS). Schedule B (148 samples at 10 locations) consisted of the same analyses as Schedule A but without mercury species, DOC, or optical properties. Schedule C analyses consisted of unfiltered nutrients (total nitrogen and total phosphorus) at selected storm drains. Data for the storm drains are available from the CEDEN Query Tool (https://ceden.waterboards.ca.gov). [Note: An exception to the information given above is that some sites in the Scotts Creek drainage (funded by the Bureau of Land

Management, BLM) had measurements of DOC and optical properties, but not mercury species. Those could be considered as a hybrid of schedules A and B, or "Schedule B+."]

In addition to the discrete samples, continuous measurements of turbidity and temperature were completed at a subset of sites, by both the U.S. Geological Survey (USGS) and University of California at Davis (UCD), but those measurements will not be discussed in this report. The continuous turbidity and temperature data collected at USGS gaging stations (USGS National Water Information System (2024; https://nwis.waterdata.usgs.gov/nwis) are available at the links in Table 5.1.1. Continuous data collected by UCD at three gaging stations maintained by the California Department of Water Resources (DWR) are available at https://tercdev.github.io/Clear_Lake_Website_Data_Visualization/.

The focus of this report is on discrete water-quality samples collected for analysis of various types of nutrients (ammonium, nitrate, Kjeldahl nitrogen, total nitrogen, soluble reactive phosphorus, dissolved phosphorus, and total phosphorus) at sites with continuous streamflow monitoring. Water-quality samples collected at continuous flow monitoring stations were used to estimate daily concentration and mass loads to support simulations of watershed nutrient transport (as described in sections 6.1 and 6.2) and to support the UCD Water Quality Lake Model (as described in section 8.3). Timing of sample collection relative to streamflow for this study and previous studies prior to October 2021 is shown graphically for the monitoring sites in Figure 5.2.2.

Forms of nutrients were analyzed in both filtered and unfiltered water samples. Total Kjeldahl nitrogen is measured from unfiltered water samples and is the sum of organic nitrogen plus ammonia (NH_3) and ammonium (NH_4^+). For the pH range of the streams in the Clear Lake watershed, the dominant form is likely ammonium, with only minimal ammonia. Total nitrogen is defined as the sum of Kjeldahl nitrogen plus nitrate (NO_3^-) and nitrite (NO_2^-). The amount of nitrite is typically quite low. Ammonium plus ammonia, nitrate plus nitrite, soluble reactive phosphorus (SRP, commonly referred to as orthophosphate), and dissolved phosphorus are measured from filtered water samples (using a 0.45 micrometer filter). Total phosphorus was measured in unfiltered water.

Nutrient analyses for this study were mostly completed by the UCD Tahoe Environmental Research Center (TERC) Laboratory in Incline Village, Nevada. However, samples from Scotts Creek were analyzed by the USGS National Water Quality Laboratory (NWQL) in Denver, Colorado, because those sites were also part of a separately funded study, by the U.S. Bureau of Land Management (BLM), which began in water year 2019. Scotts Creek samples from water years 2019, 2021, and 2022 were sent to the USGS NWQL for nutrient analyses, and additional samples from water years 2023 and 2024 were sent to the UCD TERC Laboratory. Analytical methods for USGS NWQL are given by Fishman and Friedman (1985) and Fishman (1993). Analytical methods for the TERC Laboratory are given by Murphy and Riley (1962), Kamphake et al. (1967), Solorzano (1969), Strickland and Parsons (1972), Liddicoat et al. (1975), and Kempers and Luft (1988). The detection limit for ammonium plus ammonia at USGS NWQL was higher relative to the TERC Laboratory. As a result, some samples collected from Scotts Creek sites had undetectable ammonium plus ammonia.

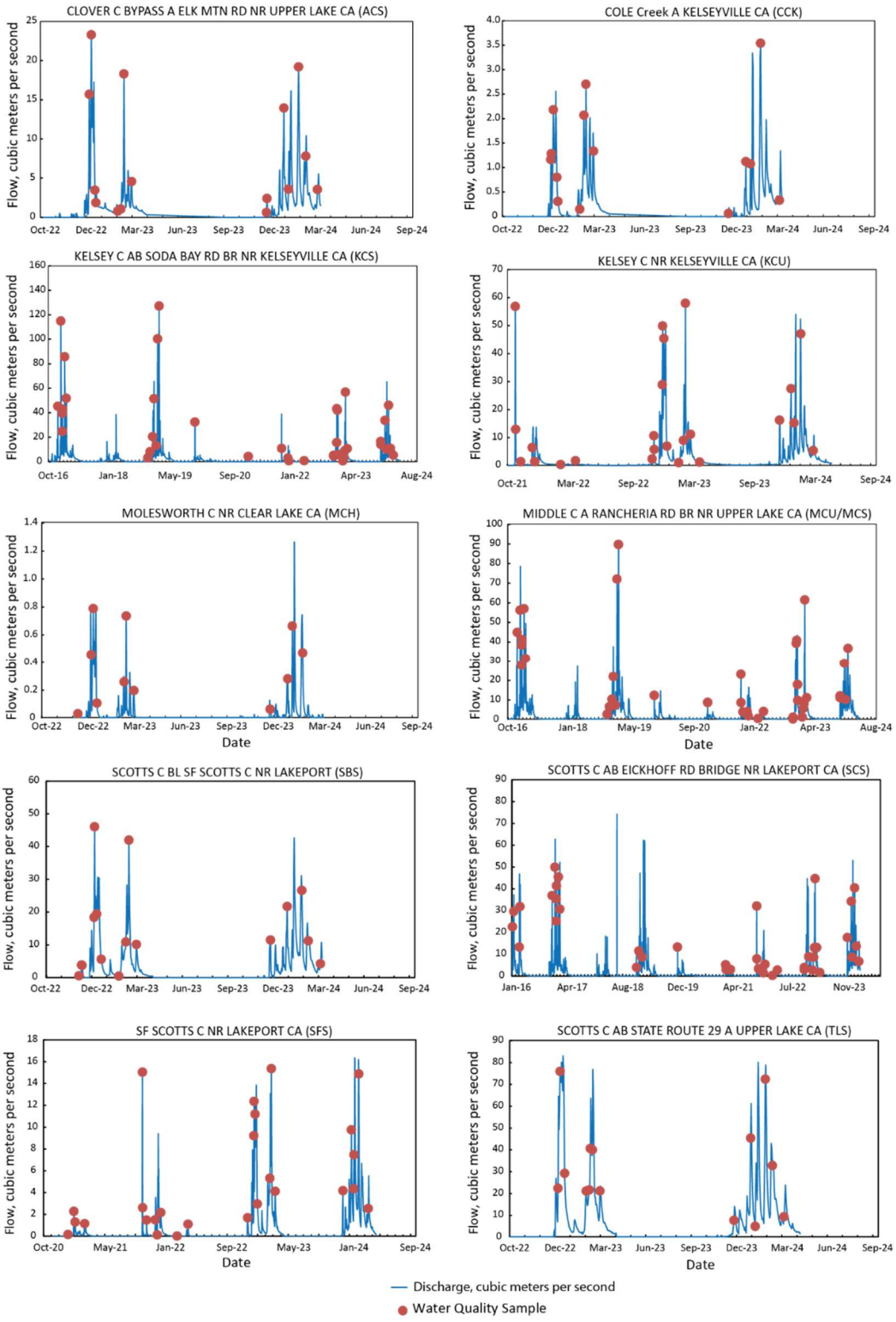

Figure 5.2.2. Streamflow at sampling sites and timing of discrete water sample collection relative to streamflow. For this study, samples were collected during water years 2022-24 (October 2021 to September 2024). Samples prior to October 2021 were collected by Lake County and others. Samples collected at some sites during water year 2022 (no stream gaging) are not shown.

5.2.2 Results

The ranges of nutrient concentrations measured at the tributary sites during water years 2022–2024 are shown as boxplots in Figure 5.2.3. The samples used to construct these box plots are shown graphically in Figure 5.2.6 and the Appendix. The range of suspended sediment concentrations are shown in Figure 5.2.4. Note that the scale for suspended sediments is a logarithmic axis. Each box shows the range of the data collected for each parameter at each site. The structure of the box is explained in the figure caption. At most sites, total nitrogen is mostly composed of total Kjeldahl nitrogen. One exemption is Molesworth Creek, an urban location, where nitrate accounts for most of the total nitrogen, and has the highest concentrations of total nitrogen and nitrate. At all the tributary sites sampled for this study, ammonium concentrations are much less than nitrate or Kjeldahl nitrogen. Dissolved phosphorus and soluble reactive phosphorus are uniformly low at all locations. As would be expected, total phosphorus measured in unfiltered samples, is higher than either dissolved phosphorus or soluble reactive phosphorus because phosphorus on particles is also measured as part of the method.

Two sites were sampled on Kelsey Creek (Figure 5.2.3). Pairwise test of the mean concentrations of total nitrogen using the Tukey Honestly Significant Difference (HSD) indicates that total nitrogen of the lower site is significantly different from that of the upper (KCU) site, with a *p*-value of 0.05. Pairwise test of the medians was slightly less significant with a *p*-value of 0.09. Mean nitrate concentrations are not significantly different. The upper Kelsey Creek site (KCU) drains some agricultural land and urban land is more abundant as the creek flows to the lower site (KCK/KCS).

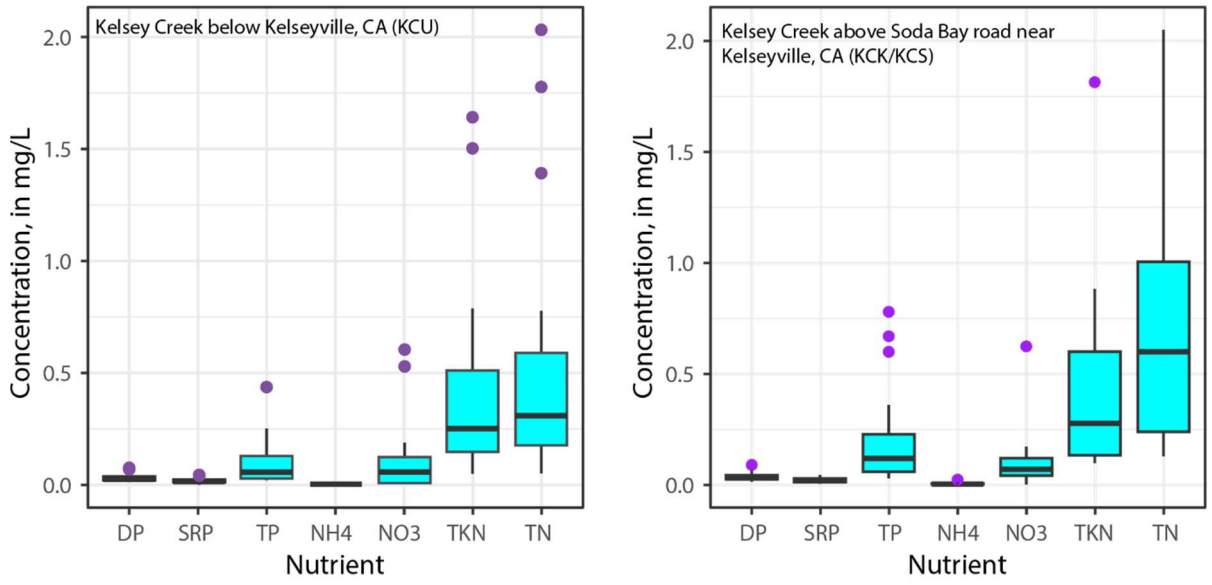

(continue)

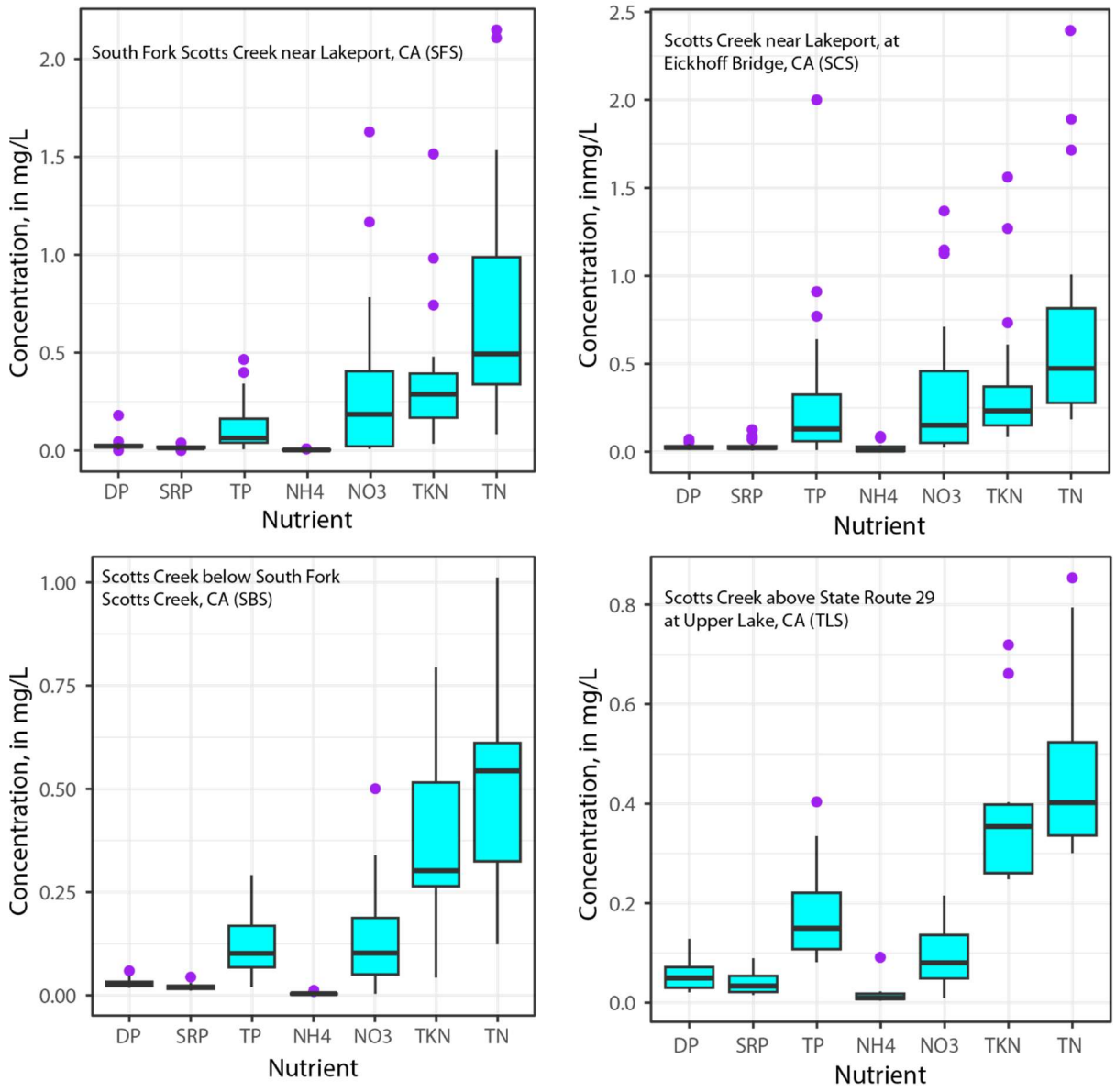
South Fork Scotts Creek near Lakeport, CA (SFS)
Concentration, in mg/L
2.0
1.5
1.0
0.5
0.0
DP
SRP
TP
NH4
NO3
TKN
TN
Nutrient
Scotts Creek near Lakeport, at Eickhoff Bridge, CA (SCS)
Concentration, inmg/L
2.5
2.0
1.5
1.0
0.5
0.0
DP
SRP
TP
NH4
NO3
TKN
TN
Nutrient
Scotts Creek below South Fork Scotts Creek, CA (SBS)
Concentration, in mg/L
1.00
0.75
0.50
0.25
0.00
DP
SRP
TP
NH4
NO3
TKN
TN
Nutrient
Scotts Creek above State Route 29 at Upper Lake, CA (TLS)
Concentration, in mg/L
0.8
0.6
0.4
0.2
0.0
DP
SRP
TP
NH4
NO3
TKN
TN
Nutrient

(continue)

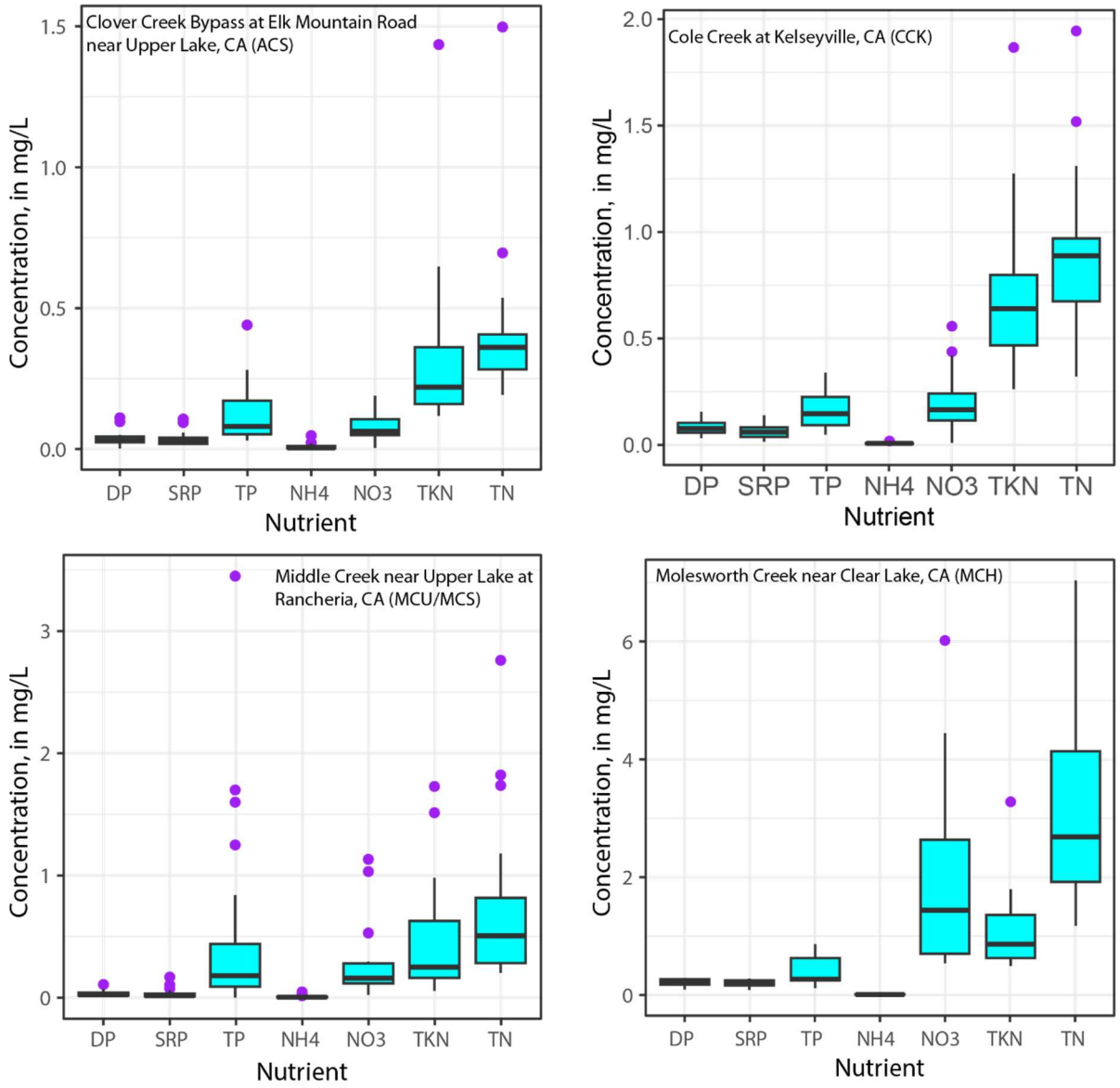
Clover Creek Bypass at Elk Mountain Road near Upper Lake, CA (ACS)
Cole Creek at Kelseyville, CA (CCK)
Middle Creek near Upper Lake at Rancheria, CA (MCU/MCS)
Molesworth Creek near Clear Lake, CA (MCH)
Concentration, in mg/L
Nutrient
DP
SRP
TP
NH4
NO3
TKN
TN

(continue)

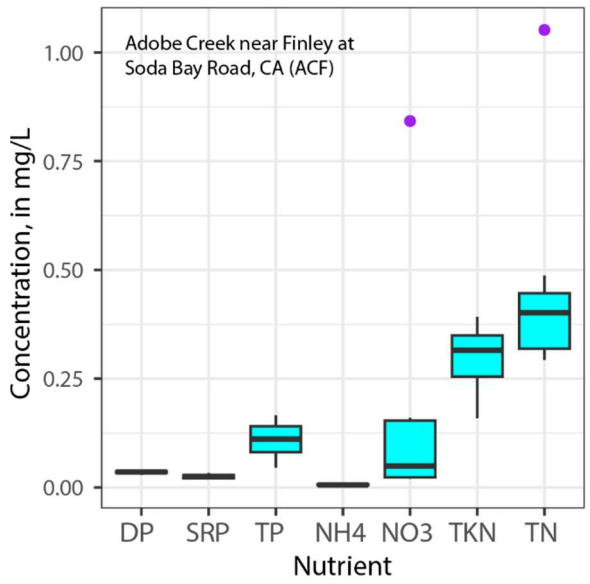

Figure 5.2.3. Box plots of nutrient concentrations at Clear Lake tributary monitoring locations for samples collected during water years 2022–24. [DP: dissolved phosphorus; NH4: ammonium plus ammonia; NO3: nitrate plus nitrite; SRP: soluble reactive phosphorus; TKN: total Kjeldahl nitrogen; TN: total nitrogen; TP: total phosphorus. Each box shows the range of concentrations measured. Lower boundary of box is the 25th percentile, upper boundary of box is the 75th percentile, line through the central portion of the box is the median or 50th percentile, whiskers are calculated using 1.5 times the interquartile range, dots are outliers.]

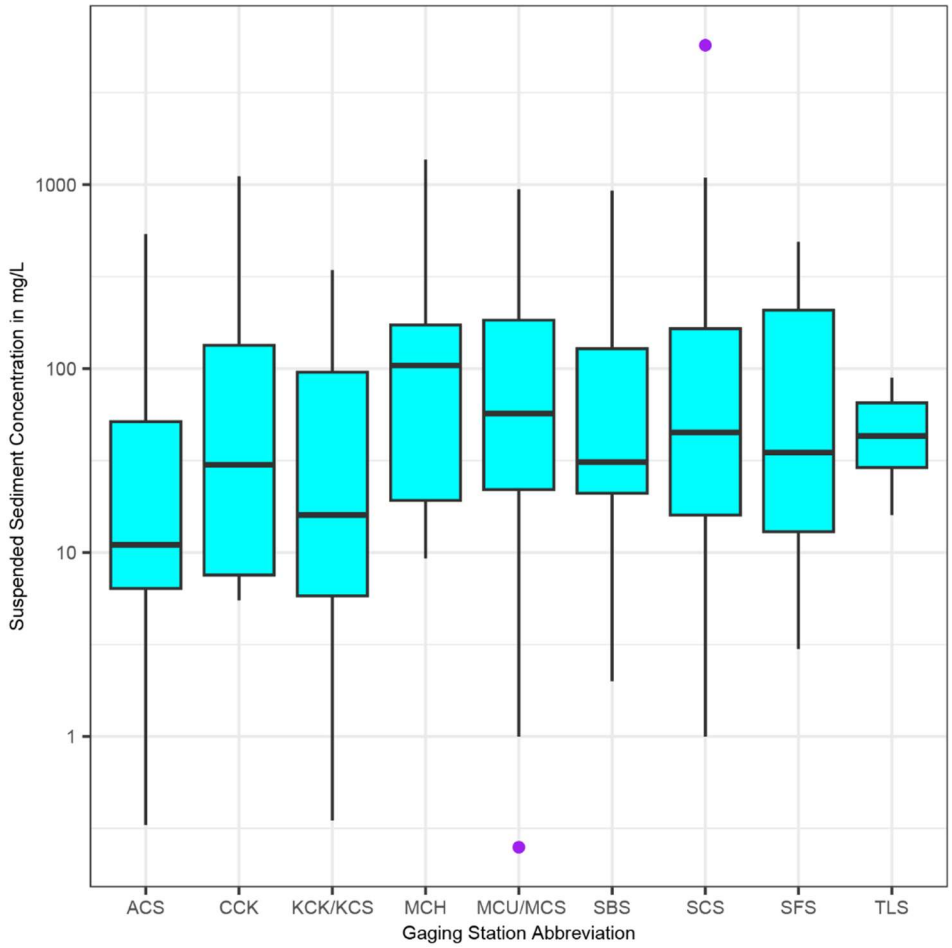

Figure 5.2.4. Boxplots of suspended concentrations at Clear Lake tributary monitoring locations. Suspended sediment concentrations are displayed on a logarithmic scale. [Station IDs: ACS: Clover Creek Bypass; CCK: Cole Creek; KCK/KCS: lower Kelsey Creek; MCH: Molesworth Creek; MCU/MCS: Middle Creek; SBS: Scotts Creek below South Fork Scotts Creek; SCS: Scotts Creek at Eickhoff Road near Lakeport; SFS: South Fork Scotts Creek; TLS: Scotts Creek above Route 29 at Upper Lake. Each box shows the range of concentrations measured. Lower boundary of box is the 25th percentile, upper boundary of box is the 75th percentile, line through the central portion of the box is the median or 50th percentile, whiskers are calculated using 1.5 times the interquartile range, dots are outliers.]

The box plots show that nutrient species measured on whole-water samples (Kjeldahl nitrogen, total nitrogen, and total phosphorus) as a group are higher in concentration than the nutrient species measured in filtered water samples (dissolved phosphorus, soluble reactive phosphorus, ammonium plus ammonia, and nitrate plus nitrite).

Nutrients that are considered bioavailable and may stimulate primary productivity as the streams flow into Clear Lake are ammonium, nitrate, and soluble reactive phosphorus. Ammonium concentrations, as indicated by the box plots, are uniformly low relative to nitrate in the tributaries to Clear Lake. (This is in contrast to typically higher ammonium concentrations compared with nitrate in the lake; see section 7.) On average, concentrations of filtered (dissolved) phosphorus (DP) were about half of unfiltered (total) P concentrations (TP). Soluble reactive phosphorus (SRP) made up about 70 percent of DP and about 35 percent of TP. Nitrate plus nitrite in filtered samples accounted for about 30 percent of total N (TN) in unfiltered samples. The remainder of N was mainly organic and concentrations of ammonia (NH_3) plus ammonium (NH_4^+) were typically low.

Suspended sediment concentrations were tested for differences among sites by the pairwise test of the mean concentrations using the Tukey Honestly Significant Difference (HSD). There are no significant differences by site for the suspended sediment concentrations.

Ratios of bioavailable nutrients on a molar scale are sometimes used as an indicator of which nutrient may be limiting for primary productivity. The Redfield ratio (Redfield, 1958) has long been used to determine whether nitrogen or phosphorus might limit primary productivity. The Redfield ratio of 16N to 1P, on a molar scale, has been used to compare bioavailable nitrogen and phosphorus concentrations. The Redfield ratios calculated from the monitoring data for the Clear Lake tributaries are shown in Figure 5.2.5. Water with a molar ratio of nitrogen to phosphorus greater than 16:1 is considered phosphorus limited whereas waters with ratios less than 16:1 are considered nitrogen limited. Molar ratios of nitrogen to phosphorus in the tributary streams measured during this study are highly variable. For example, for site SCS (Scotts Creek near Lakeport), the ratio ranges from 374:1 to 1:1, with a median of 20:1, indicating phosphorus limitation overall. In contrast, site TLS (Scotts Creek at Hwy 29 near Upper Lake) has a range of molar ratios of 11:1 to 1.3:1 with a median of 6:1, indicating nitrogen limitation. Site SBS (Scotts Creek below South Fork Scotts Creek) has a range of molar ratios of nitrogen to phosphorus of 94:1 to 0.6:1 with a median of 11:1, generally indicating nitrogen limitation. Site SFS (South Fork Scotts Creek) has a range of molar ratios of nitrogen to phosphorus of 143:1 to 1.6:1 with a median of 30:1, generally indicating phosphorus limitation. Site MCU/MCS (Middle Creek near Upper Lake) also shows a high degree of variability in nitrogen-to-phosphorus molar ratios with a range of 155:1 to 3:1, and a median of 17:1, suggesting phosphorus limitation overall. Site KCU (upper Kelsey Creek) had measured molar ratios of nitrogen to phosphorus of 42:1 to 0.25:1, with a median of 7:1, whereas site KCK/KCS (lower Kelsey Creek) had a range of ratios of 35:1 to 0.2:1 with a median of 8:1, again indicating nitrogen limitation. Other sites from this study generally showed ratios indicating nitrogen limitation overall as well. These ratios are shown graphically in Figure 5.2.4. The red dashed line on the graph indicates the Redfield ratio. The lowermost site on Scotts Creek, TLS, has a range of N:P ratios very much below those of the other locations on Scotts Creek. The TLS site drains into a portion of the lake with periodic reverse flows and probable changes in stream velocity, which may account for this difference in the ratios due to nutrient cycling or other processes.

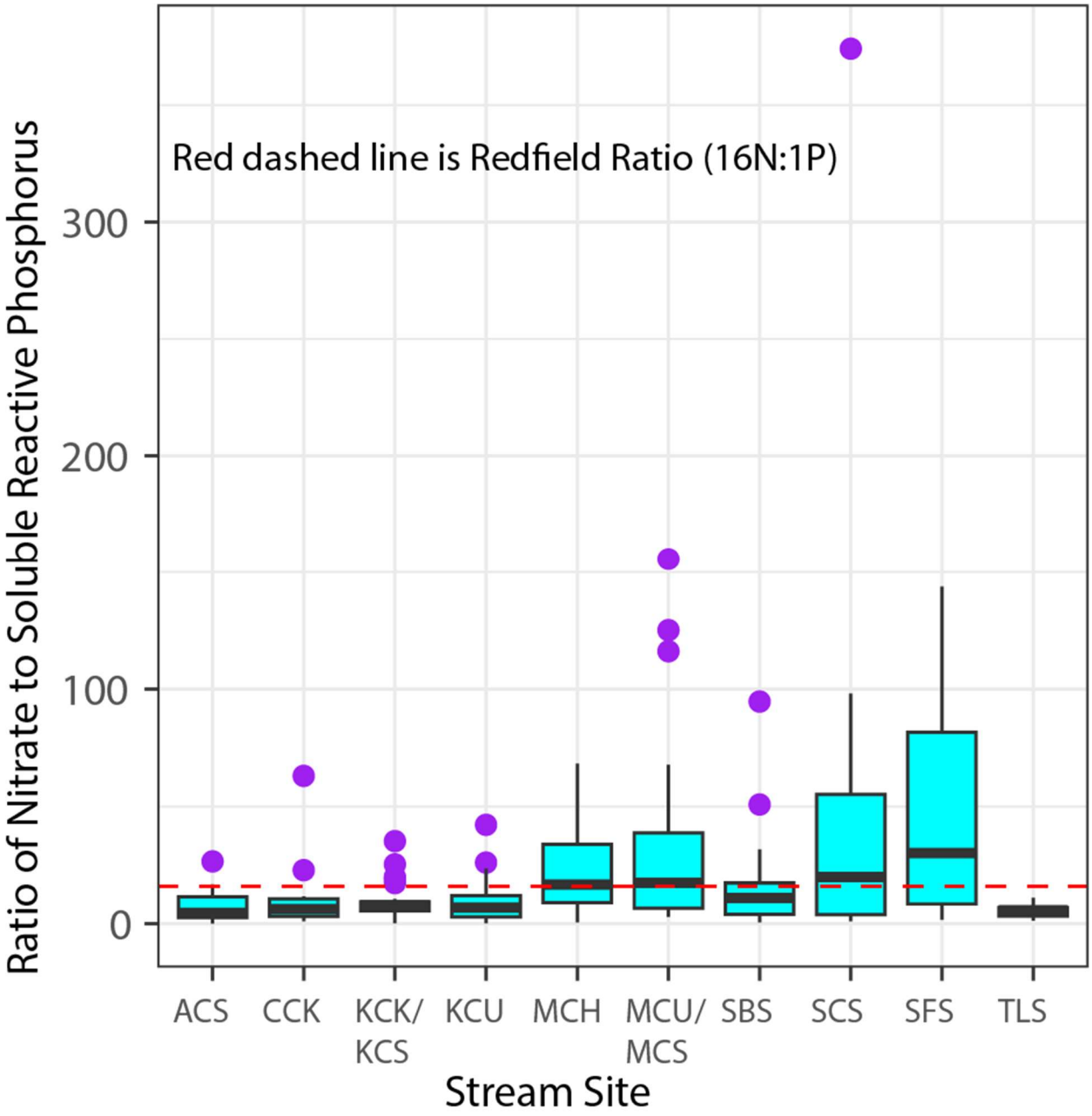

Figure 5.2.5. Box plots of bioavailable nutrient molar ratio (nitrate to soluble reactive phosphorus) at Clear Lake tributary monitoring locations. [ACS: Clover Creek; CCK: Cole Creek; KCK/KCS: lower Kelsey Creek; KCU: Upper Kelsey Creek; MCH: Molesworth Creek; MCU/MCS: Middle Creek; SBS: Scotts Creek below South Fork Scotts Creek; SCS: Scotts Creek at Eickhoff Road near Lakeport; SFS: South Fork Scotts Creek; TLS: Scotts Creek above Route 29 at Upper Lake. Lower boundary of box is the 25th percentile, upper boundary of box is the 75th percentile, line through the central portion of the box is the median or 50th percentile, whiskers are calculated using 1.5 times the interquartile range, dots are outliers.]

Other ways to visualize the discrete water quality data are plots of either concentration versus flow or concentrations versus time. These plots are shown to demonstrate either the changes in concentration over the sampling period or the response of concentration to streamflow. Representative plots are shown in Figure 5.2.6 and the remainder are in the Appendix (Section 15).

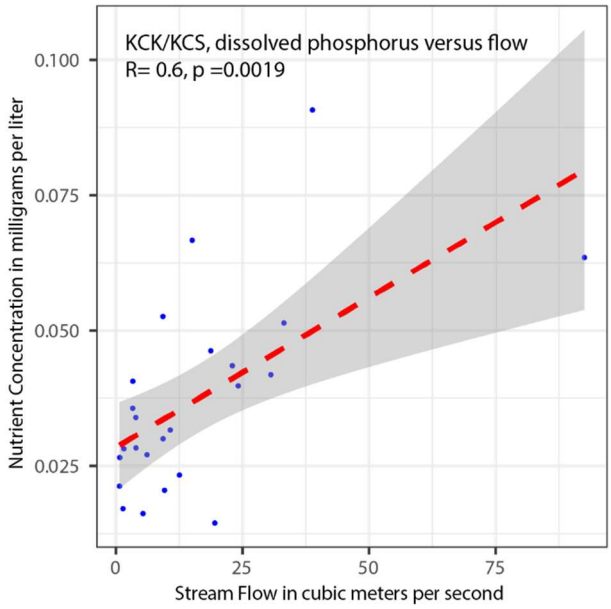
KCK/KCS, dissolved phosphorus versus flow
R= 0.6, p =0.0019
Nutrient Concentration in milligrams per liter
0.100
0.075
0.050
0.025
0
25
50
75
Stream Flow in cubic meters per second

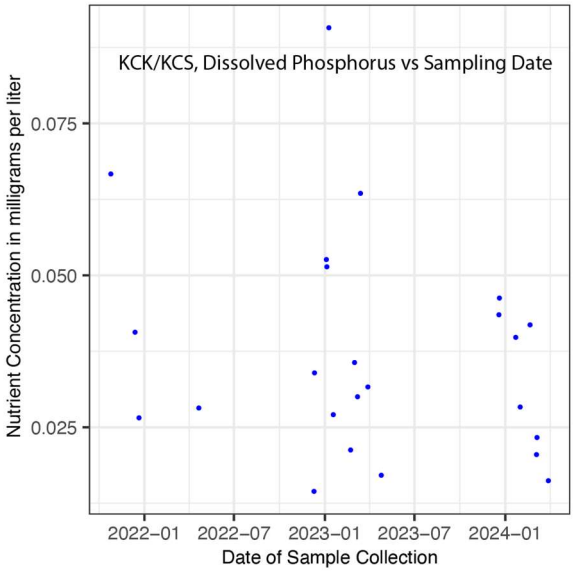
KCK/KCS, Dissolved Phosphorus vs Sampling Date
Nutrient Concentration in milligrams per liter
0.075
0.050
0.025
2022–01
2022–07
2023–01
2023–07
2024–01
Date of Sample Collection

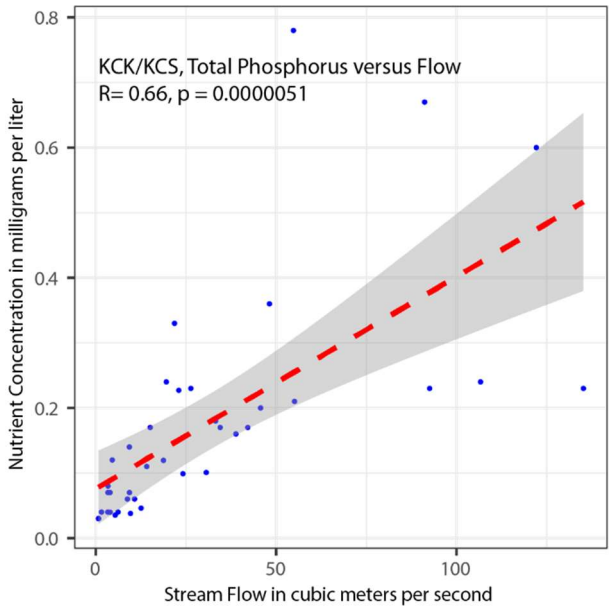
KCK/KCS, Total Phosphorus versus Flow
R= 0.66, p = 0.0000051
Nutrient Concentration in milligrams per liter
0.8
0.6
0.4
0.2
0.0
0
50
100
Stream Flow in cubic meters per second

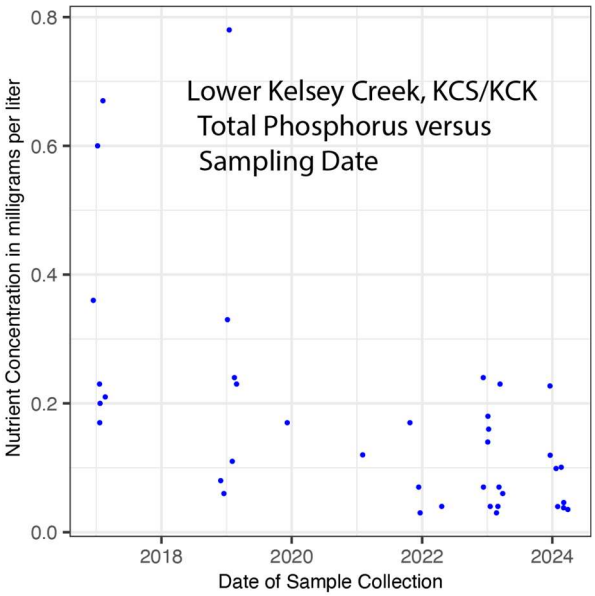
Lower Kelsey Creek, KCS/KCK
Total Phosphorus versus
Sampling Date
Nutrient Concentration in milligrams per liter
0.8
0.6
0.4
0.2
0.0
2018
2020
2022
2024
Date of Sample Collection

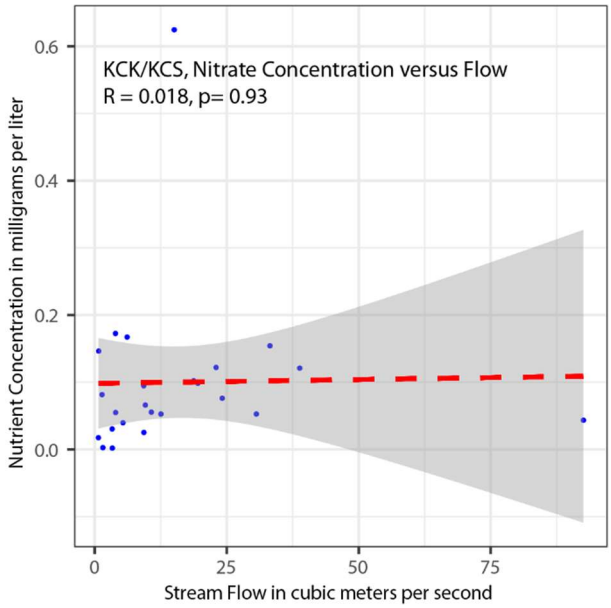
KCK/KCS, Nitrate Concentration versus Flow
R = 0.018, p= 0.93
Nutrient Concentration in milligrams per liter
0.6
0.4
0.2
0.0
0
25
50
75
Stream Flow in cubic meters per second

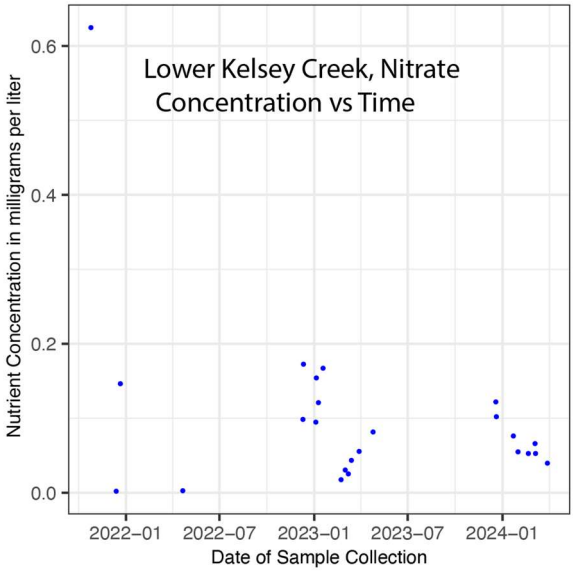
Lower Kelsey Creek, Nitrate
Concentration vs Time
Nutrient Concentration in milligrams per liter
0.6
0.4
0.2
0.0
2022–01
2022–07
2023–01
2023–07
2024–01
Date of Sample Collection

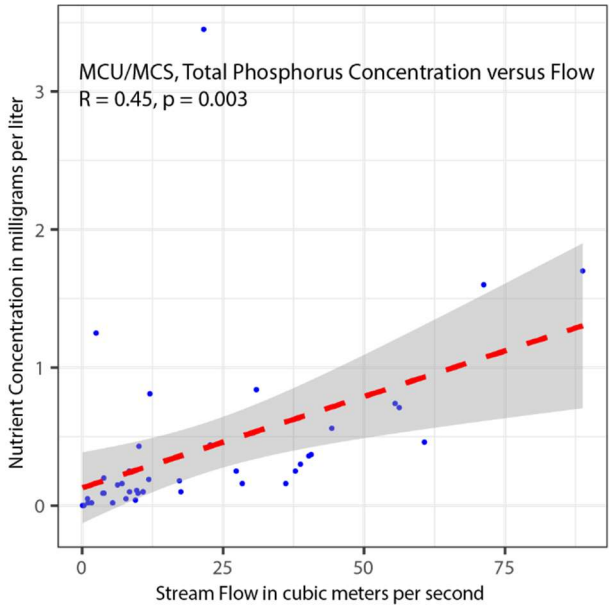
MCU/MCS, Total Phosphorus Concentration versus Flow
R = 0.45, p = 0.003
Nutrient Concentration in milligrams per liter
3
2
1
0
0
25
50
75
Stream Flow in cubic meters per second

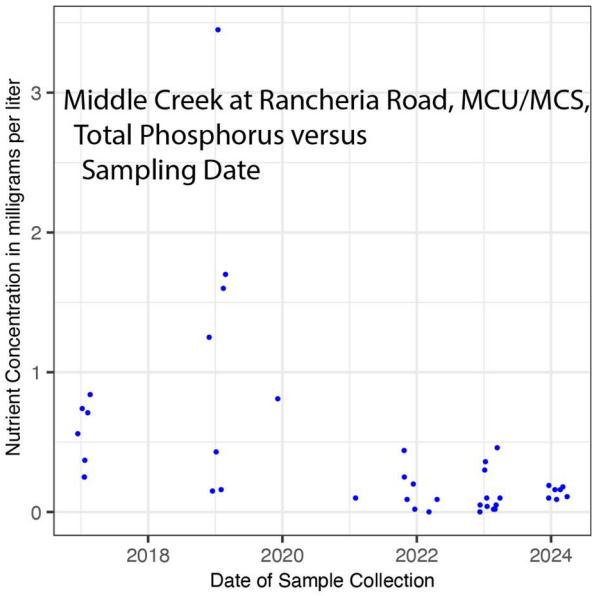
Middle Creek at Rancheria Road, MCU/MCS,
Total Phosphorus versus
Sampling Date
Nutrient Concentration in milligrams per liter
3
2
1
0
2018
2020
2022
2024
Date of Sample Collection

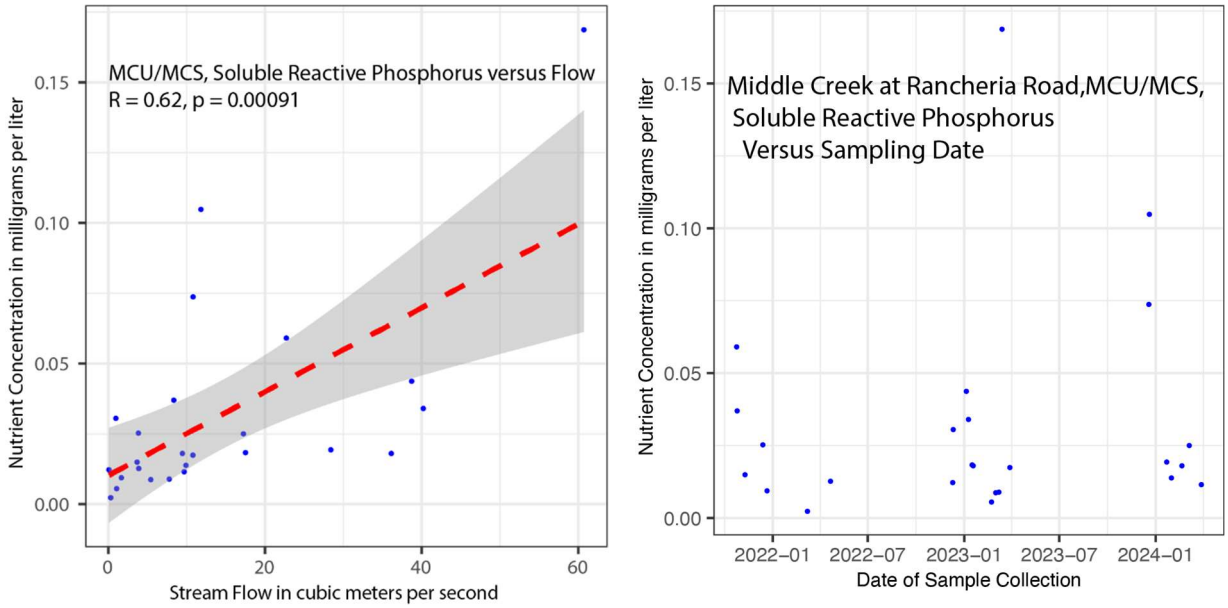

Figure 5.2.6. Streamflow versus concentration and time versus concentration for selected nutrients in Clear Lake tributaries. Value of R is Pearson's Correlation Coefficient. Gray shaded areas are the 95% percent confidence interval.

In general, more samples were taken at relatively low flows rather than at higher flows. It was not always possible for sampling crews to be at the sites during the highest flows, and the higher flows tended to happen at shorter time scales. For safety reasons, no sampling is done at night, and no autosamplers were used for water-quality sampling. (The only exception is that an autosampler was used for suspended sediment sampling at site SBS [Scotts Creek below South Fork Scotts Creek]). Weak correlations between concentration and flow can be seen at some locations and no correlation at other locations. For example, correlation coefficients (*R*) near 0.6 were obtained at some sites. The weakest correlation shown is 0.018 for nitrate concentrations measured at the lower Kelsey Creek site (KCK/KCS). The *p*-value shown on each plot indicates the significance of the regression line. A *p*-value less than 0.05 is typically interpreted as indicating a statistically significant relation of the linear regression line. Sites with a statistically significant regression line on these plots of concentration versus flow are more likely to have a statistically significant predictive model of concentration as a function of flow, whereas sites with no relation between concentration and flow, such as nitrate at the lower Kelsey Creek site (KCK/KCS), will not be able to have a predictive model relating concentration to flow. More samples taken across the full range of flow conditions would likely have resulted in better correlations and better predictive models of concentration based on flow. Predictive models for nutrient concentrations are discussed in section 6.1.

6 Upper Watershed Modeling (USGS)

6.1 RLOADEST Modeling of nutrient and sediment concentrations and loads

Authors: Dina K. Saleh and Charles N. Alpers

6.1.1 Model Description

Models of daily mass loads of nutrient species and suspended sediment at tributary locations using water quality and streamflow data from river gaging stations were developed to estimate mass loads of nutrients and sediment in tributaries to Clear Lake. Site locations are discussed in sections 5.1 and 5.2. Streamflow is measured continuously at 15-minute intervals, but water samples are only collected periodically at a much lower frequency. Therefore, it is necessary to estimate daily concentrations with a suitable model to calculate daily mass loads. Mass loads are calculated by multiplying stream discharge, measured as volume per time, by constituent concentration, measured in mass per volume.

The chosen model to accomplish load calculations for this study is LOADEST (Runkel et al., 2004). The original LOADEST model was written in the FORTRAN language but has subsequently been written for the R computing framework (https://www.r-project.org). The code for LOADEST in R is available at https://github.com/USGS-R/rloadest. LOADEST models complete a regression of the natural logarithm of concentration as a function of either flow, the square of flow, decimal time, seasonality, or some combination of these terms.

Water-quality data at some locations in the Scotts Creek drainage were available starting in the fall of 2018 as part of a companion study funded by the Bureau of Land Management (BLM), or from historical data sources compiled by Lake County. Most locations had water-quality samples from the fall or winter of 2021 to the spring of 2024 (water years 2022–24). Ideally, the LOADEST model requires at least 20 water-quality measurements for an acceptable model, but some sites had fewer measurements than the ideal. The forms of nitrogen measured and modeled included ammonium (NH_4^+), nitrate (NO_3^-), total Kjeldahl nitrogen (TKN, which is a sum of organic nitrogen plus ammonium), and total nitrogen (TN), which includes the sum of nitrate and Kjeldahl nitrogen. It was assumed that ammonia (NH_3) and nitrite (NO_2^-) were negligible (see section 5.2). Ammonium and nitrate were measured in filtered water samples whereas total Kjeldahl nitrogen was measured in unfiltered samples. The forms of phosphorus measured and modeled included soluble reactive phosphorus (SRP), dissolved phosphorus (DP), and total phosphorus (TP). Soluble reactive and dissolved phosphorus were measured in filtered water samples and total phosphorus in unfiltered samples.

As described in Section 5.2, most of the water-quality analyses for nutrients in samples collected during water years 2022–24 were completed by the Tahoe Environmental Research Center (TERC, https://tahoe.ucdavis.edu). However, some water-quality data (for sites on Scotts Creek during water years 2019, 2021 and 2022) were measured at the National Water Quality Laboratory of the U.S. Geological Survey (https://www.usgs.gov/labs/national-water-quality-laboratory). This happened because

of a companion study on the Scotts Creek location that began 1 year prior to this study. At the start of this study, all nutrient samples were sent to the TERC laboratory. Although data from the two laboratories are mostly comparable, the detection limits for ammonium were higher at the U.S. Geological Survey lab, and as a result, non-detections of ammonium were recorded early in the project for some of the samples collected from sites on Scotts Creek. This limited the number of sites where ammonium loads could be calculated.

All water-quality data used for load calculations in this study are available from Sushch et al. (2025). Streamflow is available from the U.S. Geological Survey, 2024, USGS water data for the Nation: U.S. Geological Survey National Water Information System database, accessed [December 01, 2024], at https://doi.org/10.5066/F7P55KJN or from the State of California Department of Water Resources California Data Exchange Center (CDEC, https://cdec.water.ca.gov). Internet links for access to streamflow data are available in section 5.1 of this report (Table 5.1.1).

The LOADEST model is structured to require two input files. The first file has water-quality data with the date of sample collection, river discharge at the time of water sample collection, and constituent concentration. The second file contains the date and daily mean discharge for the location for the time frame to be modeled. LOADEST has nine default models that regress the natural logarithm of concentration as a function of either stream discharge, the square of stream discharge, or a combination of decimal time, stream discharge, and seasonality terms (sine and cosine of decimal time). See Runkel et al. (2004) for the model equations. The best possible model for a given constituent at a given site is chosen by the user based on summary statistics, including the Akaike Information Criterion (AIC) and the corrected Akaike Information Criterion (AIC_c) (Runkel et al., 2004). Although both are provided with the model output, the corrected version is considered the better metric (Hurvich and Tsai, 1989). Other metrics are evaluated to select the best model, including the statistical significance of model terms (*p*-values), model bias, and the Nash-Sutcliffe index (Jain and Sudheer, 2008). The best model is then selected after consideration of all the model statistics and diagnostic plots. Model output consists of daily concentrations and loads and standard error of prediction. LOADEST input and output files and R scripts for this study are available from Saleh and Alpers (2025) for the sites and constituents shown below for which successful models were derived.

6.1.2 Results

LOADEST models of daily concentration and daily loads were attempted for nutrient constituents and suspended sediment, mentioned in the section 6.1.1. Most, but not all, attempts were successful. The models were considered successful when they are statistically significant, with a low model bias and Nash-Sutcliffe index greater than 0.5 (Jain and Sudheer, 2008). A list of successful load models by site is given in Table 6.1.1. For a map with locations of sampling sites, see Section 5.1 (Figure 5.1.1).

LOADEST model output includes the daily predicted concentration, in milligrams per liter, and the daily predicted mass load, in kilograms of constituent per day. Loads are aggregated by the model so that monthly and yearly loads are also calculated. The model output also includes the standard error, standard error of prediction, and the upper and lower bounds of prediction. The standard error of prediction is the most useful metric for evaluating the suitability of a particular model (Runkel et al., 2004).

Table 6.1.1. Successful load models by site [NH4, ammonium, NO3, nitrate, TKN, total Kjeldahl nitrogen, TN, total nitrogen, DP, dissolved phosphorus, SRP, soluble reactive phosphorus, TP, total phosphorus, SS, suspended sediment].

Site ID and Short Name	Successful Load Models
ACS, Clover Creek Bypass at Elk Mountain Road near Upper Lake, CA	TKN, TN, DP, SRP, TP
CCK, Cole Creek at Kelseyville, CA	NH4, NO3, TKN, TN, DP, SRP, TP
KCK/KCS, Kelsey Creek below Kelseyville, CA (Lower Kelsey)	NH4, TKN, TN, DP, SRP, TP, SS
KCU, Kelsey Creek near Kelseyville, CA (Upper Kelsey)	NH4, TKN, TN, DP, SRP, TP
MCU/MCS, Middle Creek near Upper Lake at Rancheria, CA	NO3, TKN, TN, DP, SRP, TP, SS
MCH, Molesworth Creek near Clear Lake, CA	NH4, TKN, TN, DP, TP
SBS, Scotts Creek below South Fork Scotts Creek near Lakeport, CA	NH4, TKN, TN, DP, SRP, TP
SCS, Scotts Creek above Eickhoff Road Bridge near Lakeport CA	TKN, TN, DP, SRP, TP
SFS, South Fork Scotts Creek near Lakeport CA	NH4, NO3, TKN, TN, DP, SRP
TLS, Scotts Creek above State Route 29 at Upper Lake, CA	TKN, TN, DP, SRP, TP

A graphical example of daily simulated concentrations of total phosphorus, daily simulated mass load, and standard error of prediction is shown in Figure 6.1.1 for the lower Kelsey Creek site. Annual loads of all nitrogen and phosphorus forms analyzed for all stream locations are shown in Tables 6.1.2 and 6.1.3.

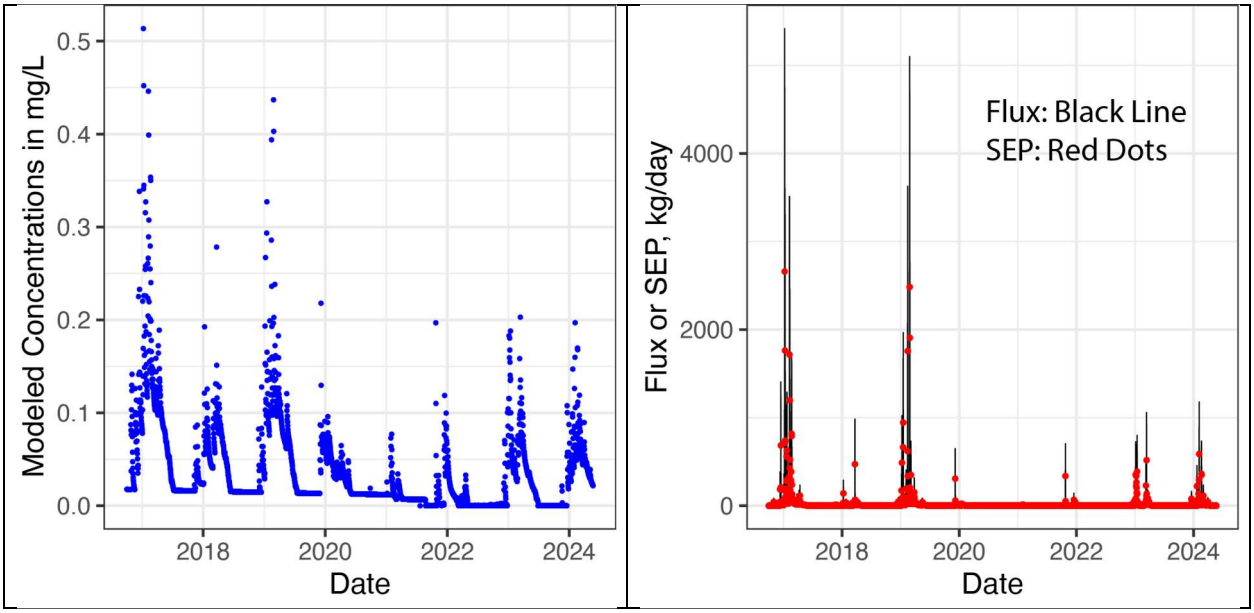

Figure 6.1.1. Daily simulated concentration of total phosphorus, daily load (flux) of total phosphorus, and standard error of prediction (SEP): lower Kelsey Creek site.

Most of the accepted models for constituents shown in Tables 6.1.2 and 6.1.3 regressed the natural log of concentration as a function of stream discharge (model 1 of Runkel et al., 2004), but some models included stream discharge, the square of stream discharge, and/or decimal time. For all models, the input files, the script for executing LOADEST in R, and the output files (simulated daily concentration and daily loads) are available from Saleh and Alpers (2025).

Table 6.1.2. Annual loads, in kilograms by water year, of various forms of nitrogen in Clear Lake tributaries. [Abbreviations: SFS, South Fork Scotts Creek; SBS, Scotts Creek below South Fork Scotts Creek; SCS, Scotts Creek at Eickhoff Road near Lakeport; TLS, Scotts Creek above State Route 29 at Upper Lake; MCS/MCU, Middle Creek near Upper Lake; KCU, Upper Kelsey Creek; KCK/KCS Lower Kelsey Creek, ACS, Clover Creek Bypass; CCK, Cole Creek; MCH, Molesworth Creek; NH4, ammonium; NO_3, nitrate; TKN, total Kjeldahl nitrogen; TN, total nitrogen; blank entries indicate no successful load model], (--, no data).

Site ID	2023 NH4	2023 NO3	2023 TKN	2023 TN	2024 NH4	2024 NO3	2024 TKN	2024 TN
SFS	91	4032	10279	16355	93	1229	10537	8801
SBS	394	--	31681	49928	379	--	30545	18445
SCS	--	--	43487	71059	--	37562	--	63816
TLS	--	--	61964	77846	--	--	62898	78237
MCU/MCS	--	24011	50849	146982	--	7825	40045	115907
KCU	365	8856	40488	50487	331	4854	22057	25589
KCK/KCS	590	12328	44954	67054	540	11077	40009	59550
ACS	282	3043	10234	13830	244	2545	7679	11530
CCK	32	893	3188	4709	35	413	3547	3207
MCH	7	--	867	2316	6	--	702	1870

Table 6.1.3. Annual loads, in kilograms by water year, of various forms of phosphorus in Clear Lake tributaries. [Abbreviations: SFS, South Fork Scotts Creek; SBS, Scotts Creek below South Fork Scotts Creek; SCS, Scotts Creek at Eickhoff Road near Lakeport; TLS, Scotts Creek above State Route 29 at Upper Lake; MCS, Middle Creek near Upper Lake; KCU, Upper Kelsey Creek; KCK Lower Kelsey Creek, ACS, Clover Creek Bypass; CCK, Cole Creek; MCH, Molesworth Creek; DP, dissolved phosphorus; SRP, soluble reactive phosphorus; TP, total phosphorus, blank entries indicate no successful load model], (--, no data).

Stream	2023 DP	2023 SRP	2023 TP	2024 DP	2024 SRP	2024 TP
SFS	828	618	4075	552	623	3835
SBS	2452	1761	11035	2343	1682	10388
SCS	3628	4861	34099	3134	3972	25912
TLS	9404	6956	29998	8832	6550	29713
MCU/MCS	3911	3734	24891	3165	2852	14218
KCU	2997	2227	9834	2006	1952	6148
KCK/KCS	3863	2540	10300	2589	1631	8264
ACS	1495	1183	4281	1236	1002	3504
CCK	367	290	779	410	323	867
MCH	157	--	327	127	--	269

The highest annual loads of total nitrogen are higher than those for total phosphorus at all locations. The highest annual load for total nitrogen was 147 metric tons (147,000 kilograms) during water year 2023 for the Middle Creek site (MCU/MCS). The highest measured annual load of total phosphorus was at the Scotts Creek at Eickhoff Road site (SCS, 35 metric tons per year) during water year 2024, followed by Scotts Creek at Upper Lake (TLS, 30 metric tons per year) in both water years 2023 and 2024. Cole Creek (CCK) and Molesworth Creek (MCH) had the smallest loads of both total phosphorus and total nitrogen, consistent with the lower flow in these streams (Table 5.1.1).

At most sites, total Kjeldahl nitrogen (TKN) made up more than half of the total nitrogen load in both water years 2023 and 2024. Two exceptions to this, in both water

years, are Middle Creek (MCU/MCS) and Molesworth Creek (MCH); at these two sites, median concentrations of nitrate (NO_3) plus nitrite were close to or exceeded median concentrations of TKN (see section 5.2, Figure 5.2.3). At two sites (SBS and SFS), TN loads were less than TKN loads for water year 2024. These results are within the uncertainty of the annual load estimates, expressed as the standard error of prediction (Saleh and Alpers, 2025).

The bioavailable form of phosphorus, soluble reactive phosphorus (SRP), on average makes up about 15 to 20 percent of the total phosphorus load at these sites. SRP made up 14 percent of the total phosphorus load at the Scotts Creek at Eickhoff Road site in 2023 and 15 percent in 2024. Soluble reactive phosphorus made up 23 percent of the total phosphorus load at the Scotts Creek at Upper Lake site in 2023 and 22 percent in 2024. For both total nitrogen and total phosphorus, the combined loads of lower Scotts Creek, Middle Creek, and lower Kelsey Creek are the highest, relative to other streams.

Soluble reactive phosphorus is immediately available for biological utilization (Wetzel, 2001). With respect to nitrogen forms, ammonium and nitrate are immediately available for biological utilization (Wetzel, 2001). The molar ratio of nitrate (NO_3) to soluble reactive phosphorus (SRP) in annual loads was computed using available data for water years 2023 and 2024 (Table 6.1.4). The results are similar to those for individual water samples (Figure 5.2.5)—most sites have an NO3/SRP ratio lower than the Redfield ratio of 16N to 1P for both water years investigated, which indicates that nitrogen is the limiting nutrient. Four sites (SFS, SCS, MCU/MCS, and KCK/KCS) had NO3/SRP molar ratios greater than 14 to 1 for one of the water years investigated. Of these four sites, three (SFS, SCS, MCU/MCS) had median values of the NO3/SRP ratio greater than the Redfield ratio for individual water samples (Figure 5.2.5), indicating that phosphorus may be the limiting nutrient some of the time in some Clear Lake tributary locations.

Table 6.1.4. Molar ratios of nitrate loads to soluble reactive phosphorus loads, for water years 2023–24 for Clear Lake tributaries. [Abbreviations: SFS, South Fork Scotts Creek; SBS, Scotts Creek below South Fork Scotts Creek; SCS, Scotts Creek at Eickhoff Road near Lakeport; TLS, Scotts Creek above State Route 29 at Upper Lake; MCS, Middle Creek near Upper Lake; KCU, Upper Kelsey Creek; KCK Lower Kelsey Creek, ACS, Clover Creek Bypass; CCK, Cole Creek; MCH, Molesworth Creek; DP, dissolved phosphorus; SRP, soluble reactive phosphorus; TP, total phosphorus, blank entries indicate no successful load model], (--, no data).

Site ID	2023 NO_3/SRP	2024 NO_3/SRP
SFS	14.4	4.4
SBS	-	-
SCS	-	20.9
TLS	-	-
MCU/MCS	14.2	6.1
KCU	8.8	5.5
KCK/KCS	10.7	15.0
ACS	5.7	5.6
CCK	6.8	2.8
MCH	-	-

6.2 SPARROW

Authors: Dina K. Saleh and Daniel R. Wise

6.2.1 Model Description

The SPARROW (Spatially Referenced Regression on Watershed Attributes) model is a spatially explicit, hybrid statistical and process-based tool that estimates constituent loads in streams by integrating monitoring data with watershed characteristics and constituent sources. By utilizing a hydrologic network to route loads through the stream system, SPARROW enhances prediction accuracy and offers valuable insights into nutrient transport processes (Alexander et al., 2019). SPARROW utilizes a hybrid methodology that combines statistical and process-based approaches, using non-linear least squares regression with mass balance constraints. This framework captures spatial relationships between estimated constituent loads and transport dynamics, enabling accurate predictions of loads at unmonitored stream reaches across the network (White et al., 1992; Smith et al., 1997; Schwarz et al., 2006). In this study, the Extended National Hydrography Data Set Plus, version 2.1 (ENHDPlusV2_us)(Schwarz and Wieczorek, 2018) was used in developing the SPARROW model, which encompasses various hydrologic features such as rivers, streams, lakes, and streamgages within the study area. The Extended National Hydrography Data Set Plus shows the location of catchments (sub-watersheds), with each catchment having the reach of a single stream segment. The direction of water flow is given in this dataset and other information can be added, including soil characteristics, land use, etc. SPARROW's streamflow conceptual model and hypothetical catchments are shown in Figure 6.2.1 (Miller et al., 2021a). This structured approach facilitates detailed analysis and modeling of nutrient loads.

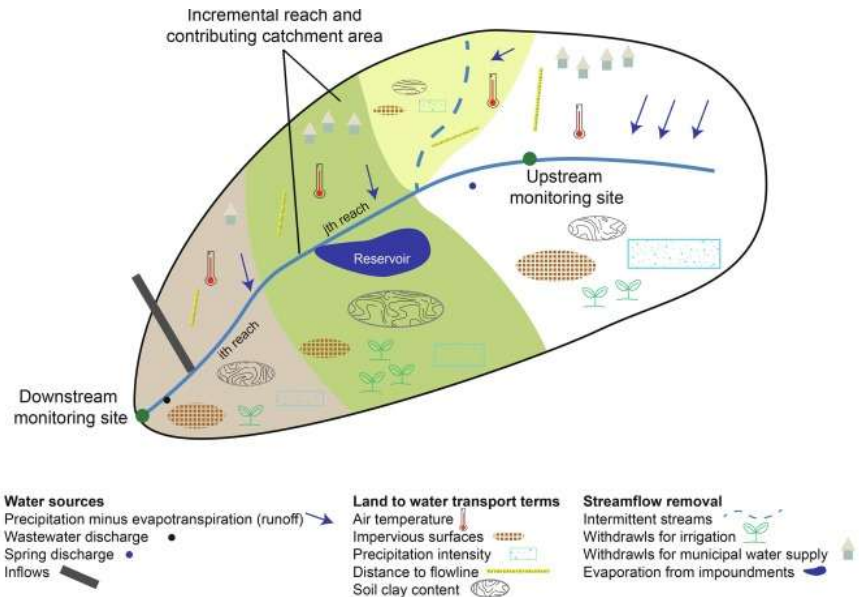

Figure 6.2.1. Hypothetical catchment modeled by SPARROW showing stream, reservoir, and sources of water and catchment area. Figure from Miller et al., 2021a.

The basic equations derived for the SPARROW model were originally discussed by Smith et al. (1997). The governing equation for the SPARROW model can be shown as:

$$L_i = A_i L_{i-1} + A_i^{'} \sum_{n=1}^{N} \alpha_n S_{ni} \exp(\sum_{m=1}^{M} \delta_{mn} \theta_m Z_{mi})$$

The load leaving an individual catchment, L_i, is a function of the incoming load (L_{i-1}), aquatic decay ($A_i^{`}$), constituent sources within that catchment ($\alpha_n S_{ni}$) composed of an array of source variables, S_{ni}, where n range from 1 to the number of source variables N, and associated source-specific coefficient, α_n. The land to water delivery variable ($\exp(\sum_{m=1}^{M} \delta_{mn} \theta_m Z_{mi})$) is similarly composed of an array of catchment attributes, Z_{mi}, where m indexes the M land-to-water variables; δ_{mn} represents a set of indicator variables that take the value of 1 if land-to-water variable m is to interact with source variable n, and 0 otherwise; and θ_m is a coefficient controlling the effect of the $m-th$ land-to-water variable. Finally the processing term A_i, is specified for instream or reservoir processing. The aquatic decay term accounts for a variety of physical or biogeochemical processes resulting in loss of constituents during in-stream transport.

As shown by the equation, the SPARROW model predicts in-stream load based on sources (e.g., fertilizers, urban land, livestock), delivery variables (e.g., soil permeability, land slope), and aquatic decay processes (Smith et al., 1997; Schwarz et al., 2006; Alexander et al., 2008). These variables account for the influences of natural and anthropogenic factors on constituent transport. Sources of constituents, such as nutrients, to the stream might include applied fertilizers, urban land, livestock, population density, atmospheric deposition, natural background geologic sources, wastewater discharges, and others (Smith et al., 1997). Sources, land cover and land use, and delivery variables for the Nation have been compiled for the extended hydrologic network and are available at (Wieczorek et al., 2018 and Wieczorek et al., 2024). The amounts of total nitrogen (TN) from atmospheric deposition to the catchments are available from Schmadel and Peterman-Phipps (2023).

In this study, we adapted existing long-term total nitrogen (TN) and total phosphorus (TP) steady-state SPARROW models, originally developed on a regional scale for the Pacific region of the United States with a 2012 base year (Wise, 2019) for application to the Clear Lake watershed. Model statistics for the explanatory variables included in the original SPARROW TN and TP models are detailed by Wise (2019). The original model, developed using the Statistical Analysis System (SAS) program, was converted to run in the R code for this analysis.

The calibrated SPARROW model identified four primary sources of TN and five sources of TP. TN sources include agricultural fertilizer, which includes both commercial fertilizers and livestock manure applied to cultivated crops and pastureland, atmospheric deposition for nitrogen, runoff from developed land, and runoff from grasslands and scrublands. TP sources include natural geological sources, including erosion from stream channels and bedrock phosphorus in the geologic landscape, runoff from developed land, agricultural fertilizer applied to cultivated crops and pastureland, and manure from grazing cattle deposited on grazing land. The TN SPARROW model identified three significant land-to-water delivery variables: soil clay content, soil organic matter content, and incremental

water runoff. The TP sparrow model identified four significant land-to-water delivery variables: soil clay content, natural phosphorus from geological sources, incremental water runoff, and the area affected by wildfire. These variables influence the transport of nutrients from the land to the stream system, either promoting or limiting nutrient delivery. For example, highly erodible clay soils on hillslopes can enhance nutrient transport through erosion. Results calibrated using TN and TP SPARROW models developed by Wise (2019) with the 2012 base year, including model variables and their estimated coefficients, are summarized in Table 6.2.1.

Table 6.2.1. Model statistics for the explanatory variables included in the SPARROW (SPAtially Referenced Regression On Watershed attributes) total nitrogen (TN) and total phosphorus (TP) models modified from the Pacific region of the United States 2012 models (Wise, 2019)

[ft_3/s: cubic foot per second; kg/yr, kilogram per year; km, kilometer; km^2, square kilometer; m/yr, meter per year; *p*-value, probability value; RMSE, root mean square error; R^2, coefficient of determination; yr/m, year per meter]. Table revised from Wise, 2019.

Variable	Variable unit	Coefficient unit	Model coefficient value	90-percent confidence interval for the model coefficient		Standard error of the model coefficient	(p-value)	t-statistic	Variance inflation factor
				Low	*High*				
TN Model Sources									
Atmospheric deposition	kg/yr	Fraction, dimensionless	0.100	0.039	0.161	0.037	0.0077	2.71	11.3
Scrub and grass land	km^2	$(kg/km^2)/yr$	42.3	12.8	71.8	17.8	0.0192	2.37	2.92
Developed land	kg/yr	Fraction, dimensionless	246	37.4	455	126	0.0530	1.95	1.76
Spring discharge	ft3/s	mg/l	1.81	0.59	3.02	0.73	0.0152	2.46	1.01
Agricultural fertilizer	kg/yr	Fraction, dimensionless	0.109	0.072	0.147	0.023	<0.0001	4.80	2.35
TN Model Land-to-water delivery									
Ln(incremental water yield)	Unitless	Unitless	0.618	0.453	0.782	0.099	<0.0001	6.22	9.02
Ln(soil organic matter)	Unitless	Unitless	0.270	0.035	0.504	0.141	0.0588	1.91	2.49
Ln(soil clay content)	Unitless	Unitless	0.333	0.094	0.573	0.144	0.0227	2.31	1.59
TP Model Sources									
Stream channels	km	kg/km-yr	4.01	1.16	6.86	1.72	0.0209	2.33	6.68
Upland geologic sources	km^2	kg/km^2-yr	0.0014	0.0003	0.0024	0.001	0.0303	2.18	10.7
Developed land	km^2	kg/km^2-yr	11.06	0.00	23.39	7.46	0.1400	1.48	2.37
Agricultural fertilizer	kg/yr	Fraction, dimensionless	0.0290	0.0121	0.0458	0.0102	0.0050	2.84	1.46
Grazing cattle	kg/yr	Fraction, dimensionless	0.0471	0.021	0.073	0.016	0.0033	2.97	2.64
TP Model Land-to-water delivery									
Ln(incremental water yield)	Unitless	Unitless	1.332	1.106	1.559	0.137	<0.0001	9.7	11.4
Ln(wildfire disturbance)	Unitless	Unitless	0.486	0.272	0.702	0.130	0.0002	3.74	1.77
Ln(geologic phosphorus)	Unitless	Unitless	3.047	1.294	4.801	1.061	0.0045	2.87	4.59
Ln(soil clay content)	Unitless	Unitless	0.731	0.261	1.201	0.284	0.0109	2.57	2.17

The hydrologic framework of the Clear Lake watershed consists of 568 individual catchments (Figure 6.2.2). The adapted model was modified for catchments within the Clear Lake watershed by incorporating updated source data. These updates included utilizing the 2019 National Land Cover Database (NLCD, Dewitz, 2021) for land use and cover data, updating agricultural chemical application data to reflect 2017 county-level fertilizer and manure inputs specific to Lake County, and refining the spatial distribution of wildfire-affected areas to include the impacts of the 2017 and 2018 wildfires in the

Clear Lake watershed. The updated SPARROW models were then run in prediction mode to estimate TN and TP loads and yields to project the year 2020 conditions. These projections utilized SPARROW models calibrated to the 2012 base year. Table 6.2.2 summarizes the updated source and delivery variables included in the modified TN and TP SPARROW models.

Previous studies have been run in prediction mode using projected climate data (Miller et al. 2021a,b). An advantage of this approach, as compared to developing a model specific to the Clear Lake watershed, is that SPARROW models produce better results using a larger spatial or temporal framework allowing for better model calibration (Smith et al., 1997, Schwarz et al., 2006; Alexander et al., 2008).

Table 6.2.2. Updated source and delivery variables used in the Clear Lake TN and TP SPARROW models, projected to the year 2020 conditions. [kg/yr, kilogram per year; km, kilometer; km^2, square kilometer; mm/yr, millimeter per year]

Variables updated for the Clear Lake watershed			
Total Nitrogen (TN)	**Variable unit**	**Total Phosphorus (TP)**	**Variable unit**
Sources			
Atmospheric deposition, 2020	kg/yr	Developed land, 2019	km^2
Scrub and grass land, 2019	km^2	Agricultural fertilizer, 2017	kg/yr
Developed land, 2019	km^2	Grazing cattle, 2019	kg/yr
Agricultural fertilizer, 2017	kg/yr		
Land-to-water delivery[1]			
Incremental water yield, 2016-2024	mm/yr	Incremental water yield, 2016–2024	mm/yr
		wildfire disturbance area, 2017, 2018	km^2
Incremental flow data also used from the Extended National Hydrography Data Set, version 2.1			

[1]*Natural log transformation is applied to all land-to-water delivery variables in the SPARROW model.*

Maps showing the spatial distribution of TN and TP sources and delivery variables for each catchment in the Clear Lake watershed are provided in Appendix 15.6.2.

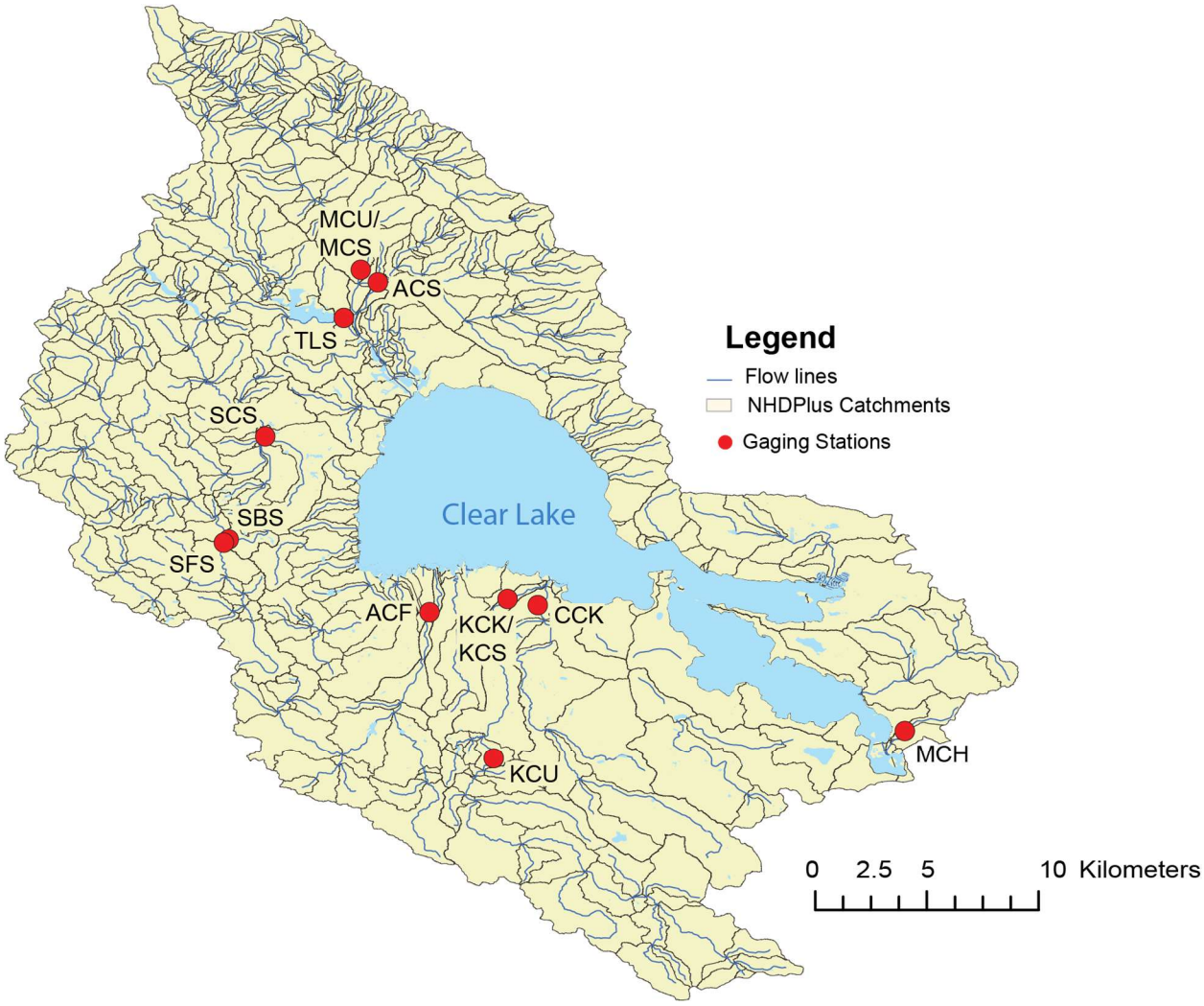

Figure 6.2.2. Map showing the Clear Lake watershed with locations of stream gaging and water-quality sampling; catchments delineated by the Extended National Hydrography dataset. Gaging station name abbreviations correspond with table 5.1.1.

The output of the SPARROW model includes information on the loading (mass per time) and yield (mass per area) of TN and TP sourced from each catchment and delivered to downstream catchments (Figure 6.2.1). Generally, the delivered loads are lower than the sourced amounts due to losses occurring during transport through the stream network. Understanding the loading, delivery, and sources of TN and TP within a watershed can be used to help guide watershed nutrient management decisions. SPARROW input and output files and R scripts for this study are available (Saleh, 2025).

6.2.2 Results

The total nitrogen (TN) and total phosphorus (TP) SPARROW models developed for the Pacific region of the United States and calibrated to the 2012 base year (Wise, 2019) were applied in prediction mode to estimate TN and TP loads and yields in Clear Lake watershed projected for the year 2020 conditions. Results of the two models are described below.

6.2.2.1 Total Nitrogen (TN)

The total nitrogen (TN) SPARROW model projected that during the 2020 conditions, approximately 299 metric tons per year of TN are delivered to Clear Lake from upstream watersheds. Of this, about 77 percent (or 229 metric tons) comes from four primary upstream watersheds: Middle and Clover Creeks, Scotts Creek, Adobe Creek, and Kelsey Creek. The remaining 23 percent comes from other sub-watersheds, including Cole Creek, and other areas within the Clear Lake watershed. Commercial fertilizers and livestock manure applied to cultivated crops and pastureland account for 33 percent, atmospheric deposition for nitrogen account for 29 percent, runoff from grasslands and scrublands account for 26 percent, and runoff from developed land accounts for 11 percent of the TN loads to Clear Lake from these sub-watersheds.

Figure 6.2.3 (A) and (B) show delivered total nitrogen (TN) loads and TN yields, respectively, as estimated by the SPARROW model. The delivered loads are calculated as the sum of the incremental catchment loads (the loads generated by the local catchment) plus the loads from upstream catchments draining into that stream reach and accounting for aquatic decay, which refers to the natural reduction in nitrogen loads as the loads travel through subsequent catchments. Figure 6.2.3 (B) shows the TN yields, which are calculated by dividing the TN total delivered load by the catchment area. Yield is useful for comparing the nutrient contributions from catchments of varying sizes, as it normalizes the loads relative to the area of the catchment. This helps identify regions that are more nutrient rich or have higher nutrient contributions per unit area, allowing for more effective comparisons across different catchments in the watershed.

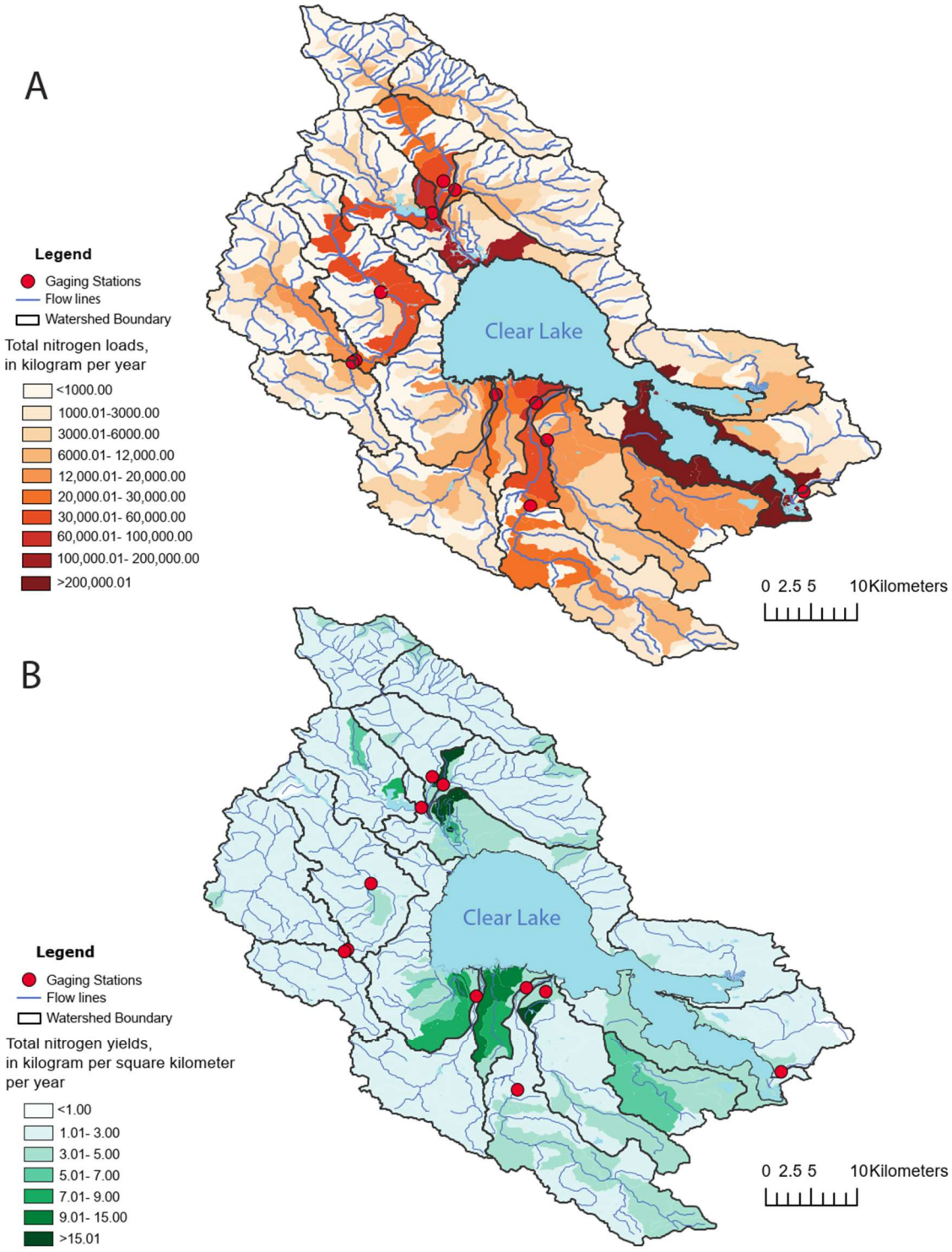

Figure 6.2.3. (A) Delivered total nitrogen loads, (B) delivered total nitrogen yields.

Figure 6.2.4 illustrates the distribution of total nitrogen (TN) loads and their primary sources across sub-watersheds within the four main creeks discharging to Clear Lake (Adobe Creek, Kelsey Creek, Middle and Clover Creeks, and Scotts Creek (fig 5.1.1)). The TN loads vary significantly among sub-watersheds, largely influenced by land use patterns and agricultural activities. For example, in sub-watersheds with high agricultural activity like Adobe Creek, TN from fertilizer and manure applications makes up about 48 percent of the TN load. In contrast, in sub-watersheds like Kelsey Creek, where atmospheric deposition plays a more dominant role, about 43 percent of TN loads are attributed to this source (Figure 6.2.4 A). Overall, fertilizer and manure application along with atmospheric deposition are the two main sources, 33 and 30 percent respectively, of TN in these four Clear Lake main sub-watersheds. Grasslands and scrubland account for 25 percent and runoff from developed (urban) lands accounts for the remaining 11 percent.

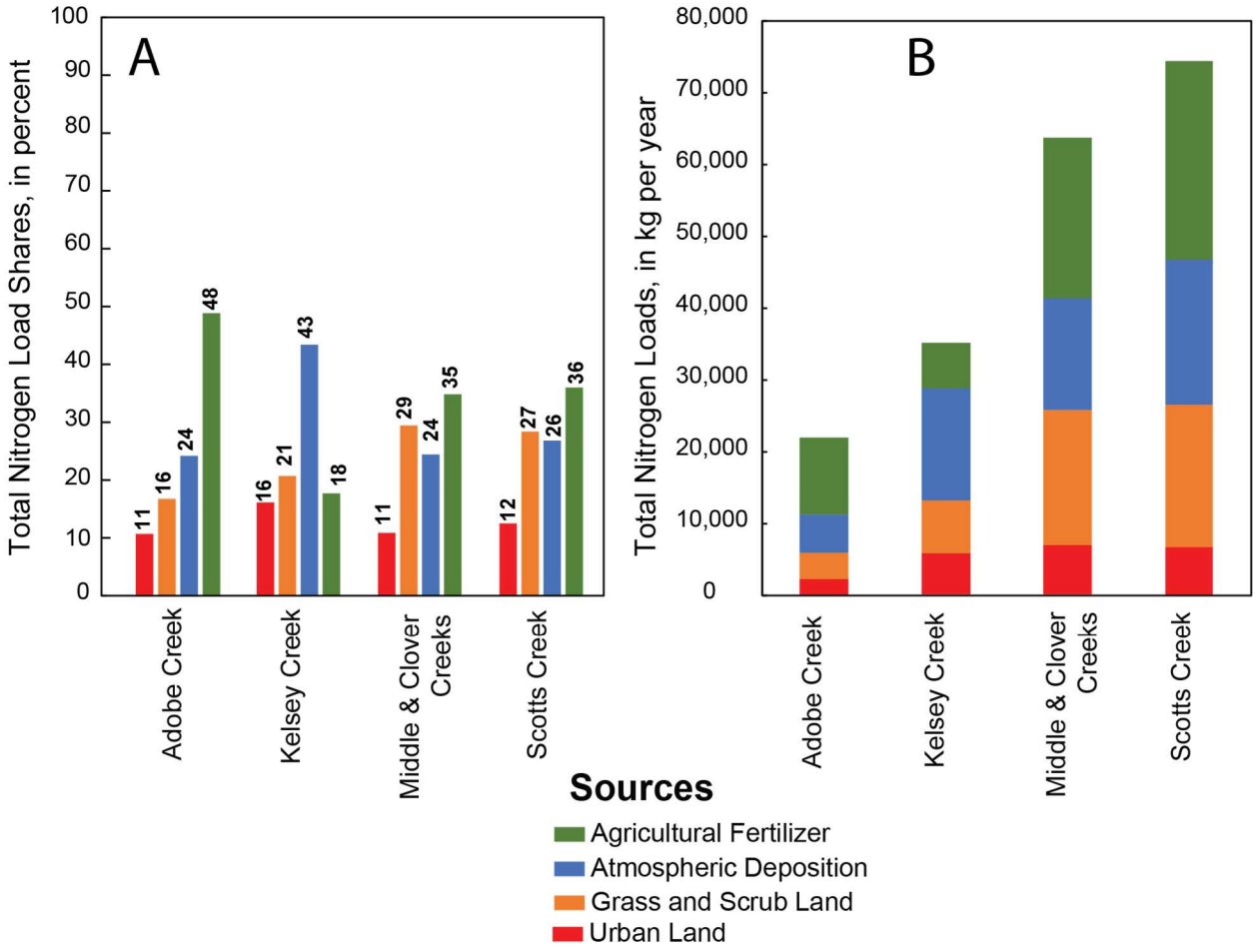

Figure 6.2.4. Predicted mean annul total nitrogen loads, by source, for selected sub-watersheds in the Clear Lake watershed projecting the year 2020 conditions. A) Percent load share from each source, B) total nitrogen load in kilograms per year.

Figure 6.2.5 shows sources of TN loads in the four main creeks in the Clear Lake watershed along an elevational gradient starting from their headwaters to their outlets. Adobe Creek (Figure 6.2.5 A) runs approximately 21 kilometers (km) from its headwaters to its

outlet at Clear Lake. Initially, atmospheric deposition is the dominant TN source in the sub-watershed. However, around the 12 km mark, Highland Creek joins Adobe Creek, introducing TN loading from agricultural fertilizer on cultivated crops and pasture lands, as shown in Figure 6.2.6. Kelsey Creek (Figure 6.2.5 B) runs approximately 37 km from its headwaters to Clear Lake. TN sources in the first 25 km are mainly from atmospheric deposition, grass and scrub lands, and urban runoff. Beyond this point, as Kelsey Creek flows through areas with cultivated crop and pasture lands, agricultural fertilizer applications increase (Figure 6.2.6).

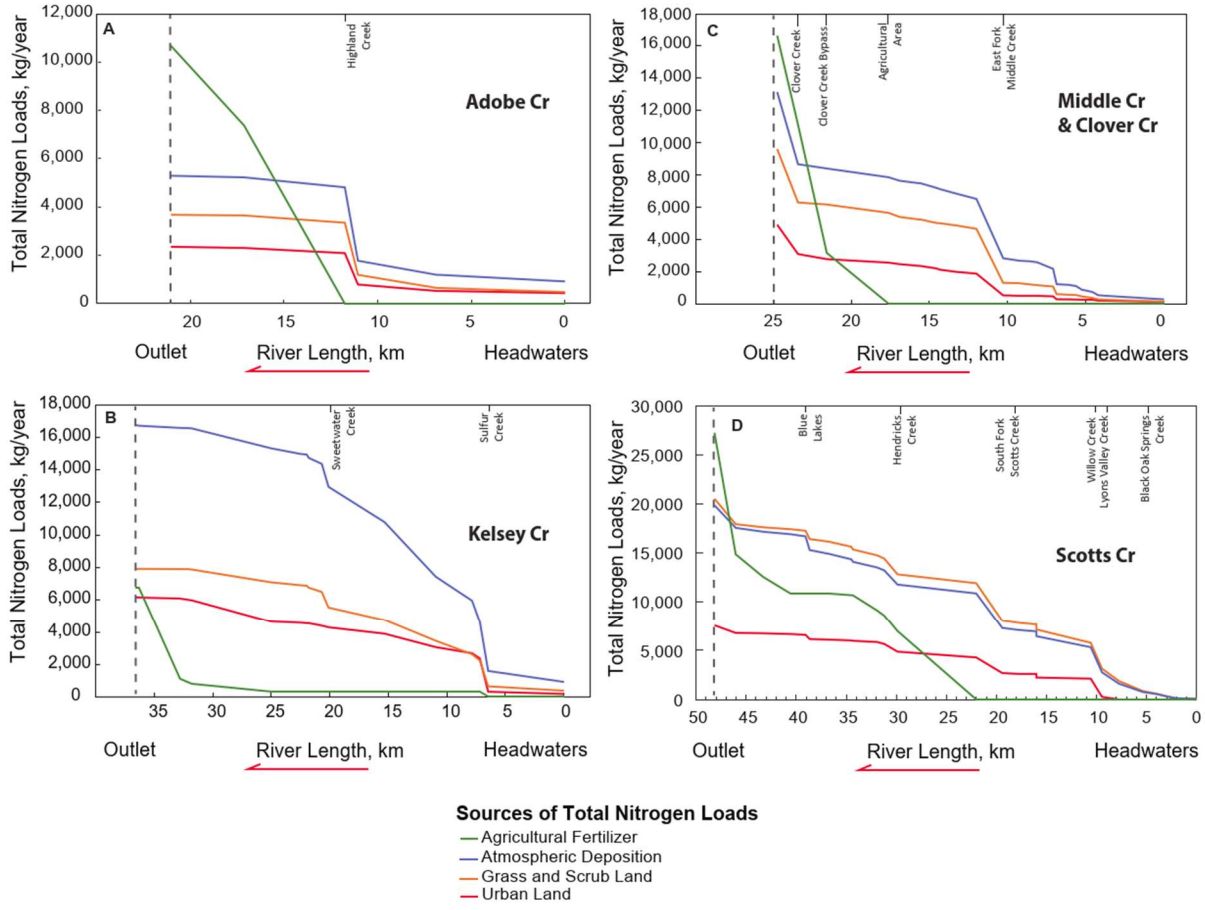

Figure 6.2.5. Sources of total nitrogen loads for (A) Adobe Creek, (B) Kelsey Creek, (C) Middle Creek, and (D) Scotts Creek, estimated by the SPARROW model reflecting projected 2020 conditions. Dashed vertical line represents creek discharge at outlet.

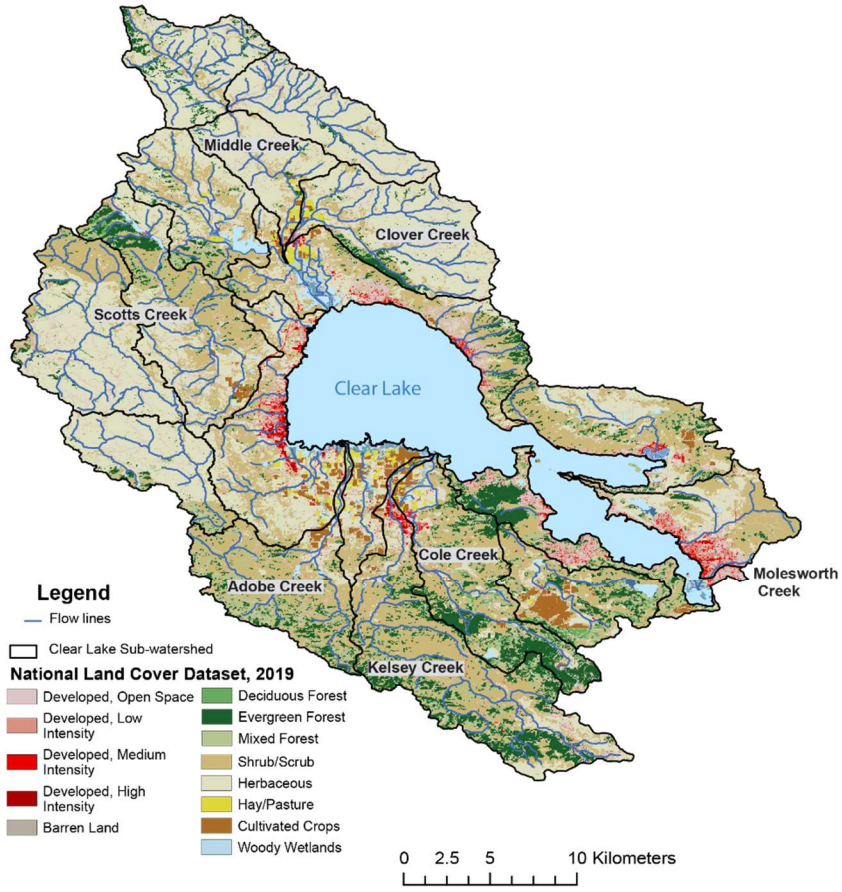

Figure 6.2.6. Land cover for each sub-watershed in Clear Lake. Data from the National Land Cover Dataset (Dewitz, 2021)

Middle Creek (Figure 6.2.5 C) flows approximately 25 km from its headwaters to where it meets Scotts Creek, about 1.5 km below Tule Lake. Near the headwaters, TN loads come predominantly from atmospheric deposition and grass and scrub lands. Around the 10 km mark, the east fork of Middle Creek introduces an increase in TN, primarily from grass and scrub lands and urban areas. As the creek progresses to the 18 km mark, TN loads increase due to agricultural fertilizer applications as the creek enters agricultural areas. Other notable increases in TN occur near the 22 and 24 km marks, where Clover Creek Bypass and Clover Creek joins Middle Creek, contributing TN loading from cultivated crop and pasture lands (Figure 6.2.6). Scotts Creek (Figure 6.2.5 D) extends for approximately 43 km. The primary sources of TN in this sub-watershed are atmospheric deposition, grass and scrub lands, urban runoff, and agricultural applications. The TN loads along Scotts Creek increase as inflows from both Lyons Valley, Willow Creek, and from South Fork Scotts Creek contribute to the main stem around the 10 km and 19 km marks, respectively. At the 23 km mark, another increase in TN is observed where the creek flows into areas of cultivated crop and pasture lands, further raising the TN load (Figure 6.2.6).

6.2.2.2 Total Phosphorus (TP)

The total phosphorus (TP) SPARROW model projected that during 2020 conditions, approximately 31 metric tons per year of TP are delivered to Clear Lake from upstream watersheds. Of this, 71 percent (about 22 metric tons) originates from four primary upstream watersheds: Adobe Creek, Kelsey Creek, Middle and Clover Creek, and Scotts Creek. The remaining 29 percent comes from other sub-watersheds, including Cole Creek, and other locations within the Clear Lake watershed. Natural geological sources, including erosion from stream channels and bedrock phosphorus in the geologic landscape, account for 37 percent of the TP loads. Agricultural fertilizer applied to farmlands contributes 34 percent of the TP load, and manure from grazing cattle makes up 18 percent of the TP loads. Runoff from urban land accounts for the remaining 12 percent of the TP load.

Figure 6.2.7 (A) and (B) show total delivered phosphorus (TP) loads and TP yields, respectively, estimated by the SPARROW model. Figure 6.2.7 (A) shows the delivered TP loads for each stream reach, calculated similarly to TN. It includes the sum of incremental catchment loads and upstream catchment contributions, also accounting for aquatic decay. Figure 6.2.7 (B) illustrates TP yields, calculated by normalizing the total phosphorus delivered load to the catchment area, enabling effective comparison across catchments of varying sizes. This highlights areas with greater phosphorus contributions per unit area, useful for identifying phosphorus-rich regions or areas with heightened TP transport.

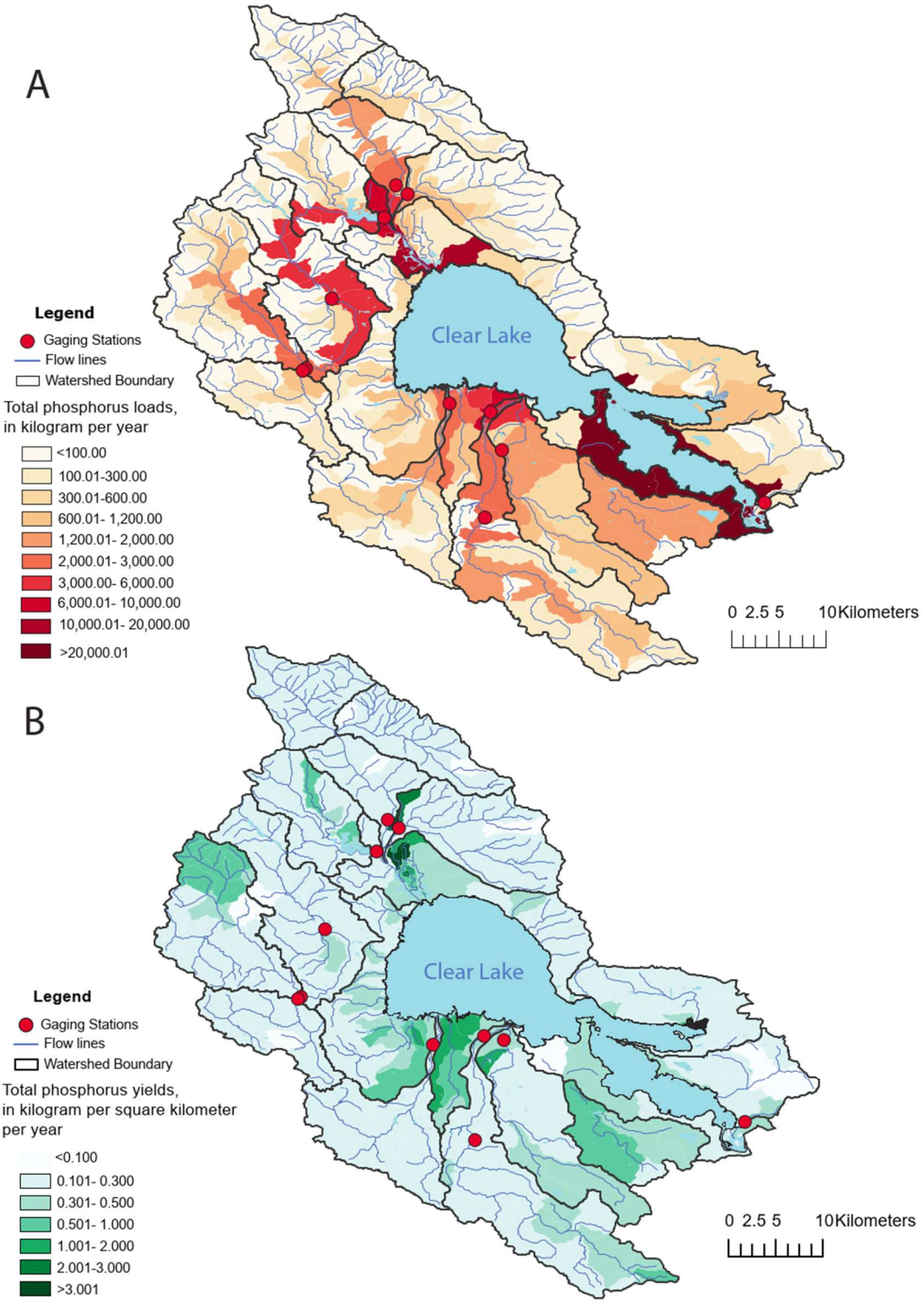

Figure 6.2.7. (A) Delivered total phosphorus loads, (B) delivered total phosphorus yields.

Figure 6.2.8 shows the distribution of TP loads and their primary sources across sub-watersheds within the Clear Lake watershed. The TP loads vary considerably across sub-watersheds and are heavily influenced by the spatial distribution of natural geological sources and agricultural activities. In the Scotts Creek sub-watershed, about 49 percent of the TP loads originate from natural background geological sources and stream channels, primarily due to streambed erosion and contributions from the surrounding geologic formations. In sub-watersheds with more significant agricultural activities, such as Adobe Creek and Middle and Clover Creeks, the main source of TP is fertilizer applied on farmlands. In Adobe Creek, 45 percent of the TP load is attributed to agricultural fertilizer, whereas in Middle and Clover Creeks, fertilizer accounts for 38 percent of the TP load. These variations emphasize the impact of land use and geological factors on phosphorus transport within the Clear Lake watershed, with some sub-watersheds dominated by natural erosion processes, whereas others are more influenced by agricultural practices.

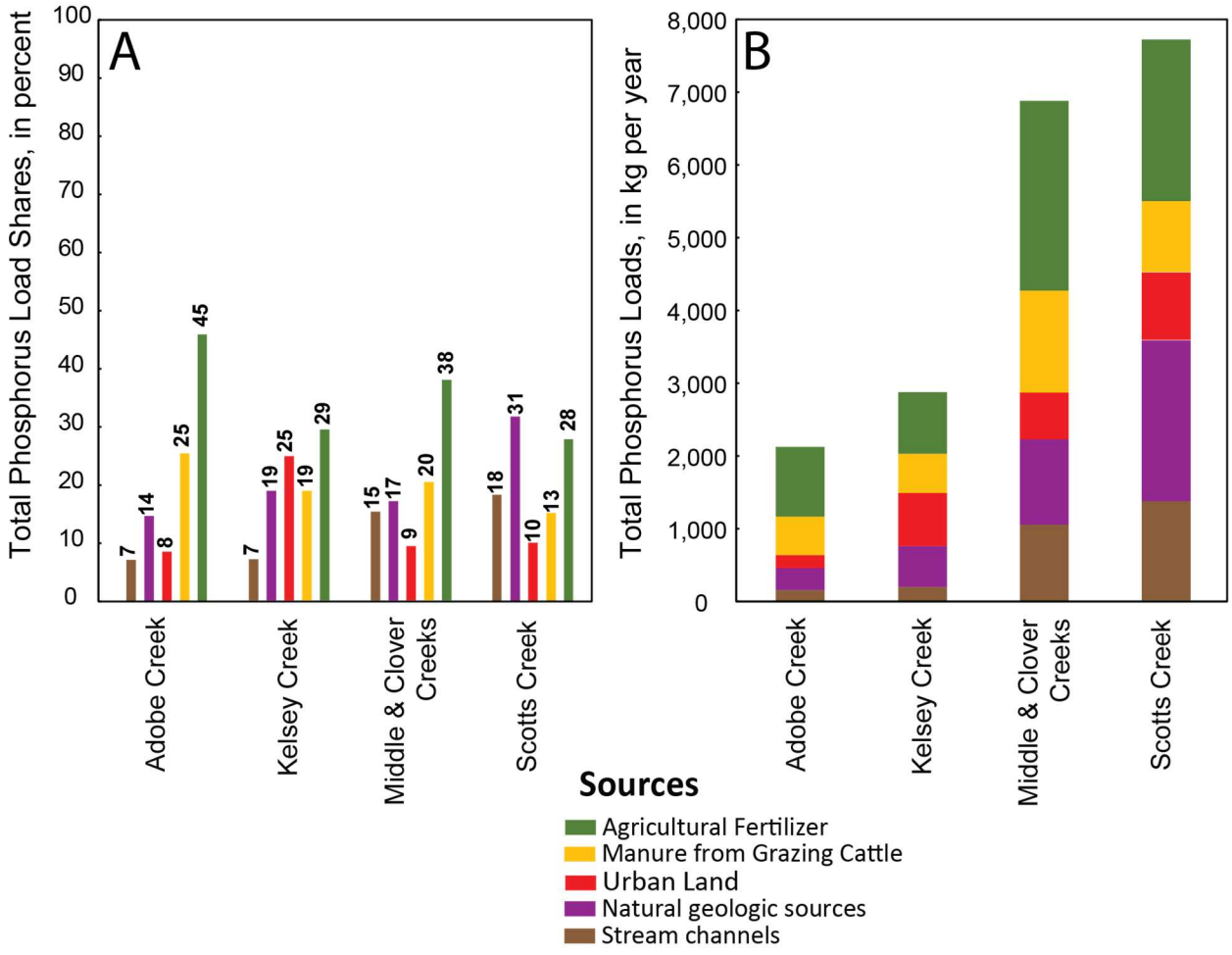

Figure 6.2.8. Predicted mean annual total phosphorus loads, by source, for selected sub-watersheds in the Clear Lake watershed projecting the year 2020 conditions. A) Percent load share from each source, B) total phosphorus load in kilograms per year

Figure 6.2.9 shows sources of TP loads in the four main creeks in the Clear Lake watershed along an elevational gradient starting from their headwaters to their outlets. Adobe

Creek (Figure 6.2.9 A) runs approximately 21 km from its headwaters to its outlet at Clear Lake. Initially, erosion from stream channels and natural geologic sources are the dominant TP source in the Adobe Creek sub-watershed. Downstream of the 12 km mark, where Highland Creek joins Adobe Creek, TP increases from agricultural fertilizer applications on cultivated lands and manure from livestock grazing areas. Kelsey Creek (Figure 6.2.9B) runs approximately 37 km from its headwaters to Clear Lake. TP sources in the first 33 km are mainly from natural geologic sources and urban runoff. Beyond this point, as Kelsey Creek flows through areas with cultivated crop and pasture lands, TP loads from agricultural fertilizer applications and manure from livestock grazing areas increase. Middle Creek (Figure 6.2.9 C) flows approximately 25 km from its headwaters to where it meets Scotts Creek, about 1.5 km downstream from Tule Lake. Initially, TP loads come predominantly from erosion of stream channels and natural geologic sources. Around the 10 km mark, the east fork of Middle Creek introduces an increase in TP, from urban areas as well as stream channels and natural geologic sources. As the creek progresses past the 18 km mark, TP loads increase due to agricultural fertilizer applications and manure from grazing cattle as the creek enters an area with agriculture and ranching. Scotts Creek (Figure 6.2.9 D) extends for approximately 43 km. The primary sources of TP throughout the entire reach of Scotts Creek are from erosion of stream channels and natural geologic sources. Around the 22 km mark, there is an increase in TP loads where the creek flows into areas of cultivated crop and pasture lands, further raising the TP load from agricultural fertilizer applications and manure from livestock grazing areas (Figure 6.2.6).

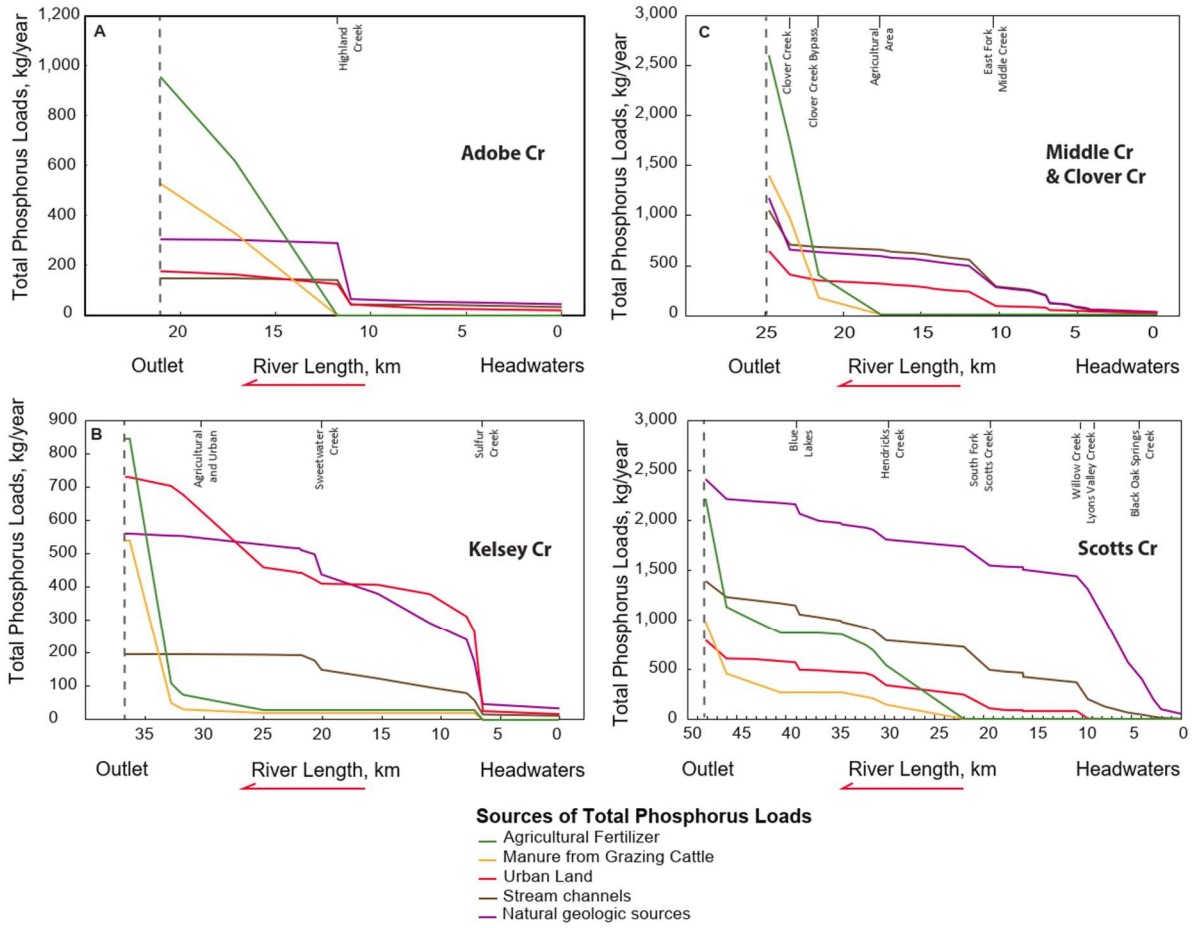

Figure 6.2.9. Sources of total phosphorus loads for (A) Adobe Creek, (B) Middle Creek, (C) Kelsey Creek, and (D) Scotts Creek. Estimated by the SPARROW model reflecting projected 2020 conditions. Dashed vertical line represents creek discharge at outlet.

6.2.3 Discussion

To better assess the sources and transport of total nitrogen (TN) and total phosphorus (TP) from upstream sub-watersheds into Clear Lake, we utilized the SPARROW model developed for the Pacific region of the United States (Wise, 2019) with the 2012 base year. This model provided essential spatial variation and helped address data limitations specific to the Clear Lake watershed. This model was updated with several new datasets to reflect more recent changes in agricultural practices and land use classifications (Table 6.2.2). Furthermore, streamflow and incremental water yield data were revised to align with hydrologic conditions representative of 2020 conditions for these updated SPARROW models. Additionally, spatial data from the wildfires of 2017–2018 were incorporated into the TN and TP models to capture the impact of these disturbances. Specifically, the Sulfur Fire of 2017 and the Mendocino Complex Fire of 2018 had a considerable influence on land use in the Clear Lake watershed, with approximately 44 percent of the watershed being burned (De Palma-Dow et al., 2022). This comprehensive update enables a better analysis of nutrient loads and transport mechanisms by accounting for both anthropogenic activities (e.g., agricultural changes) and natural

disturbances (e.g., wildfires), enhancing the model's utility for future water-quality management in the Clear Lake watershed.

Figure 6.2.10 shows the percent change in land use areas in the sub-watersheds affected by wildfire calculated by comparing the area classifications of the 2019 National Land Cover Database (NLCD, Dewitz, 2021) to areas of the 2011 NLCD used in developing the Pacific region of the United States (Wise, 2019). Figure 6.2.10 shows the effect of the fire on land use in Clear Lake as shown by the decrease in forest land area and increase in barren land. This effect on land use composition is also reflected on the estimated TN and TP sources.

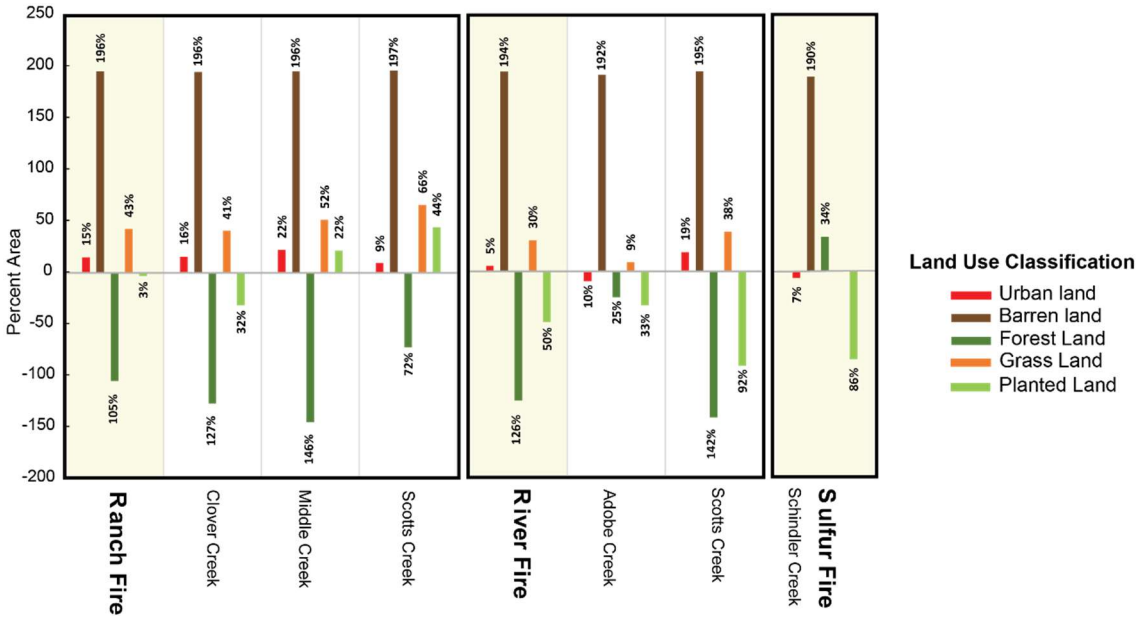

Figure 6.2.10. The effect of wildfires on areas of land use in the main sub-watersheds of Clear Lake, expressed as percent change between 2011 NCLD and 2019 NLCD.

The results of the updated Clear Lake SPARROW model, projecting 2020 annual conditions, were compared to the output of the Pacific region model (Wise, 2019), which used a 2012 base year. Overall, the models indicated a 41 percent increase in total nitrogen (TN) loads and a 30 percent increase in total phosphorus (TP) loads in 2020 compared to 2012. The primary source of this increase in nutrient loads was identified as agricultural fertilizer, which includes both commercial fertilizers and livestock manure applied to cultivated crops and pastureland. This rise in nutrient loads is closely related to the amount of fertilizer and livestock manure applied in the Clear Lake sub-watersheds. Table 6.2.2 shows the county-level data on commercial nitrogen and phosphorus fertilizer sales in kilograms. These data reveal a 52 percent increase in TN fertilizer and a 69 percent increase in TP fertilizer applied to incremental catchments in 2017 (Gronberg and Spahr, 2012; Gronberg and Arnold, 2017; Falcone, 2021).

Table 6.2.3. Lake County commercial nitrogen and phosphorus fertilizer sales applied to cultivated crops and pastureland. [kg/yr, kilogram per year]

Year	Nitrogen Farm Fertilizer, kg/yr	Phosphorus Farm Fertilizer, kg/yr
1987	817,438	104,945
1992	718,141	90,029
1997	709,766	111,292
2002	1,311,100	226,405
2007	1,156,172	189,867
2012	415,910	42,138
2017	868,506	134,704

Management of the Clear Lake watershed requires both understanding of nutrient loads and sources and how any source reduction strategy may or may not improve lake water quality. For example, any reduction in nitrogen loading may have only a minimal, if any, effect on improving lake water-quality conditions because of the high amount of nitrogen added to the lake by nitrogen-fixing bacteria. It has been known since 1972 (Horne and Goldman, 1972) that up to 500 metric tons of nitrogen can be added to the lake in a single year by nitrogen-fixing bacteria. That amount is higher than the 2020 watershed SPARROW model prediction of watershed contribution to the lake. Watershed contributions tend to vary greatly from year to year depending on wet or dry conditions. For example, load calculations from monitored tributaries to the lake showed that 313 metric tons were delivered by the combined outflows of Middle Creek, Scotts Creek, Kelsey Creek, Clover Creek, Cole Creek, and Molesworth Creek in water year 2023, and 270 metric tons in water year 2024 (see section 6.5.1). These watershed nitrogen loadings are less than that estimated by Horne and Goldman (1972) from biological fixation in the lake, suggesting that watershed reductions of nitrogen loads may not be effective for improving lake water quality.

Although the Clear Lake SPARROW model showed that about 52 percent of the total phosphorus loading to the lake is from agricultural practices, that amount needs to be considered relative to how much agricultural phosphorus was applied to the land surface from either phosphorus fertilizer or livestock manure. Those two amounts from all the agricultural catchments are 151.7 metric tons. The loading to the lake relative to the amount applied shows that only 10.5 percent of the applied agricultural phosphorus, from fertilizer and livestock manure, contributes to lake loading. Therefore, most applied phosphorus remains on the landscape, potentially being released to streams or the lake at a later time, depending on groundwater residence times, or is taken up by plants and does not contribute to immediate runoff into the lake. Geological sources and stream channels were shown to contribute 37 percent of the total phosphorus load to the lake. Reduction of some amount of phosphorus loads may be possible by identifying areas subject to erosion.

In summary, in the Clear Lake watershed, total nitrogen (TN) and total phosphorus (TP) loadings closely align with hydrologic conditions and peak stream flows from key

tributaries like Adobe, Kelsey, Middle, and Scotts Creeks. Although SPARROW model results identify anthropogenic sources of TN and TP, further comparison with in-lake nutrient cycling could help fully understand their relative impact. The SPARROW models, calibrated using measured TN and TP loads that include both dissolved and particulate forms, offer an accurate depiction of nutrient transport dynamics; however, not all transported nutrients are immediately bioavailable for algal growth, an important factor for lake eutrophication and algal bloom potential, as detailed in the water quality monitoring chapter. The SPARROW model's alignment with load estimates from monitoring and LOADEST methods provides confidence in its ability to guide targeted management strategies and assess nutrient sources across the watershed.

6.3 Hydrological Simulation Program – FORTRAN (HSPF)

Authors: Michelle A. Stern and Charles N. Alpers, U.S. Geological Survey

6.3.1 Model Description

A watershed model was developed for the tributaries that flow into Clear Lake to simulate continuous hourly streamflow, water temperature, and sediment transport. The purpose of this model is to evaluate long-term trends of hydrology and water quality flowing into Clear Lake. Hydrological Simulation Program – FORTRAN (HSPF; Bicknell et al., 2001) was chosen for this study because it is a comprehensive process-based watershed model that can be used to simulate hourly streamflow and water quality constituents over decadal time scales. HSPF has been used to model natural and developed watersheds globally and has complex surface and subsurface hydrology and water quality processes. Importantly, HSPF allows the simulation of alternative scenarios to evaluate a possible reduction of sediment loads in conjunction with changes in air temperature and (or) precipitation. HSPF is a spatially distributed and temporally continuous simulation model that uses lumped parameter segments. Each subbasin is considered homogeneous with the same set of parameters. HSPF is modular and is typically calibrated in steps beginning with hydrology, then sediment, then nutrient modules. The hydrological processes are divided into a PERLND module representing pervious land, an IMPLND module representing impervious ground, and the RCHRES module that simulates processes in streams or reservoirs. Sediment sources are simulated in HSPF as wash-off of detached sediment in surface storage and scour of the soil matrix, and as bedload scour in the stream. Sediment transport is simulated as an advective, non-reactive constituent of streamflow, with deposition and scour dependent on the simulated flow velocity and particle size of the sediment. Longitudinal bedload transport and bidirectional flow are not simulated in HSPF. Model inputs and outputs for historical and future model runs, along with simulated time series of streamflow and sediment loads, are available online (Stern, 2025).

6.3.2 Model inputs and calibration data

To simulate water quality, HSPF requires a continuous time series of climate data including air temperature, precipitation, solar radiation, potential evapotranspiration, cloudiness, dewpoint, and wind speed. Two methods for developing the climate data were considered: local climate station data and gridded data from the North American Land Data Assimilation System (NLDAS). Station data in the area were downloaded from multiple networks and assessed for use as input but were found to contain many erroneous values and large gaps in records that would have led to errors in the hydrology and water quality simulations. One common argument against using gridded data is that it does not accurately reflect local conditions; however, localized rainfall events can often be missed by stations due to missing data, station errors, or a lack of spatial density of stations. Errors or uncertainties may also exist in gridded climate data, but for easier reproducibility and updates, a lack of missing data, consistent processing, and consistent quality assurance and quality control, gridded climate data inputs were chosen instead of individual station data for this study. The variables required for HSPF were downloaded through the BASINS 4.5 (U.S. Environmental Protection Agency [EPA], 2024) interface that directly accesses data from NLDAS (Xia et al., 2012), which provides the hourly climate

data required to produce the full water quality simulations. NLDAS is published by the National Aeronautical and Space Administration (NASA) at a 1/8-degree grid over central North America, with the available historical observed period of 1979 to the present.

Future climate data were downloaded from the Weather Research and Forecasting (WRF) dataset (Rahimi et al., 2023), extracted for the nearest centroid to the NLDAS grid center near Lakeport, California (Figure 6.3.1). Four Global Circulation Models (GCMs) were chosen based on data availability for bias corrected models from the California 5th Climate Assessment for their skill in representing the historical climate in California (Krantz et al., 2021). The four models are listed in Table 6.3.1, and are all SSP 370, or the "business as usual" "medium warming" global emissions and socioeconomic policies. The GCMs are run multiple times using different initial conditions, physics calculations, and forcings; therefore, the run information is provided to identify the specific iteration used in this study.

Table 6.3.1. Global Circulation Model (GCM) name and scenario iteration for the four scenarios used in this study.

Name	**Iteration**
EC-Earth 3	r1i1p1f1
MIROC6	r1i1p1f1
MPI-ESM1-2-HR	r3i1p1f1
TaiESM1	r1i1p1f1

The 3-kilometer resolution WRF variables are outputs from a Regional Climate Model that dynamically downscaled the GCM outputs for a smaller area (Rahimi-Esfarjani et al., 2023). These outputs provide variables close to what are needed to drive the HSPF model, but some conversions were required to ensure consistency to the historical climate inputs. The variables downloaded from WRF that were used to calculate input climate data for HSPF can be found in Table 6.3.2. Potential evapotranspiration was calculated using the method of Singer et al. (2021). Each scenario is bias corrected (Rahimi-Esfarjani et al., 2023) to the 1981–2013 historical period and run through 2100 using emissions forcings beginning in 2014. Thirty-year periods were chosen to represent the early (2010–2039), middle (2040–2069), and late (2070–2099) century climatology. The historical run of each scenario (1981–2013) was used as a baseline condition to calculate change in streamflow and sediment for each respective future scenario period. The historical climate runs (1981–2023) were used as a qualitative check against the GCM historical period data.

Table 6.3. 2. Hydrological Simulation Program – FORTRAN (HSPF) input climate parameters and Weather Researching and Forecasting (WRF) model parameters used.

HSPF input	**WRF variable(s)**
Precipitation	rainnc, rainc (non-convective and convective cumulative precipitation)
Air temperature	t2 (2-meter temperature)

Wind	u10, v10 (10-meter u-component and v-component of the wind
Solar radiation	swdnb, swupb, lwdnb, lwupb (short wave and longwave downwelled and upwelled solar radiation, clear sky and all sky)
Potential evapotranspiration	Wind, dewpoint, temperature, solar radiation, psfc (surface pressure)
Dewpoint	t2, q2 (2-meter temperature and 2-meter specific humidity)
Cloudiness	swdnb, swdnbc (shortwave downwelled clear sky and all sky solar radiation)

6.3.3 Model parameterization

Watershed segmentation was done to discretize the Clear Lake watershed into smaller, discrete sub-watersheds for modeling and analysis, with each sub-watershed and land use type containing homogeneous properties. The Clear Lake tributaries (Figure 6.3.1) were partitioned into 11 sub-models (Table 6.3.3) based on each major tributary and further subdivided using the National Hydrography Dataset Plus Version 2 (NHDPlusV2. U.S. Geological Survey (2024b); Available at https://www.epa.gov/waterdata/get-nhdplus-national-hydrography-dataset-plus-data) High Resolution subbasins.

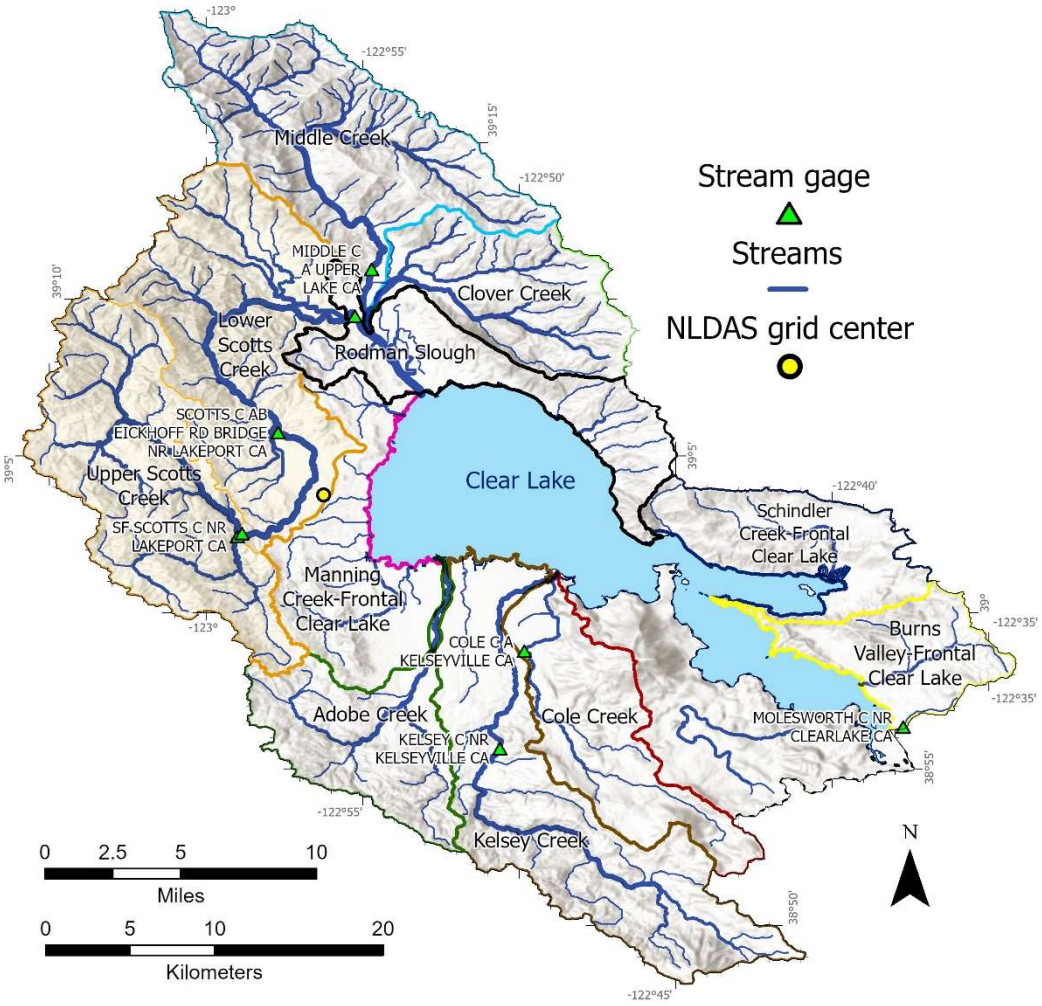

Figure 6.3.1. Location of Clear Lake tributary sub-models and streamflow calibration gages. Stream thickness indicates the stream order, with thicker lines indicating higher order streams that contain higher flows on average. Base map from Esri and its licensors, copyright 2025.

The largest tributary, Scotts Creek, was divided into two sub-models, containing 66 subbasins in the upper watershed and 61 in the lower watershed. There was a total of 440 subbasins across 11 sub-models (Figure 6.3.2, Table 6.3.3), with Middle Creek divided into 99 subbasins, Clover Creek into 45, the frontal streams into 36, Kelsey Creek into 37, Adobe Creek into 20, Manning Creek into 39, Cole Creek into 8, Burns Valley into 11, and Schindler Creek into 18.

Table 6.3. 3. Watershed model names and number of subbasins for each model.

Model	Number of subbasins
Upper Scotts Creek	66
Lower Scotts Creek	61
Middle Creek	99
Clover Creek	45

Rodman Slough	36
Schindler Creek	18
Burns Valley / Molesworth Creek	11
Cole Creek	8
Kelsey Creek	37
Adobe Creek	20
Manning Creek	39
	440

Each subbasin is further discretized by land use. Therefore, each subbasin contains separate parameters for each land use type defined by the National Land Cover Database (NLCD, Jin et al., 2019, available at https://www.mrlc.gov/data) (Table 6.3.4, Figure 6.3.2). For comparison, the Loading Simulation Program C++ (LSPC) model developed for the total maximum daily load study (Tetra Tech, 2004) consisted of 54 subbasins to represent the entire Clear Lake watershed. The smaller subbasins in this study were developed to better represent the spatial variability of soil, geology, terrain, and land use properties, and based on the recommendation that the average flow time through the stream length represented by one subbasin should be close to the model simulation time step, which in this case is one hour.

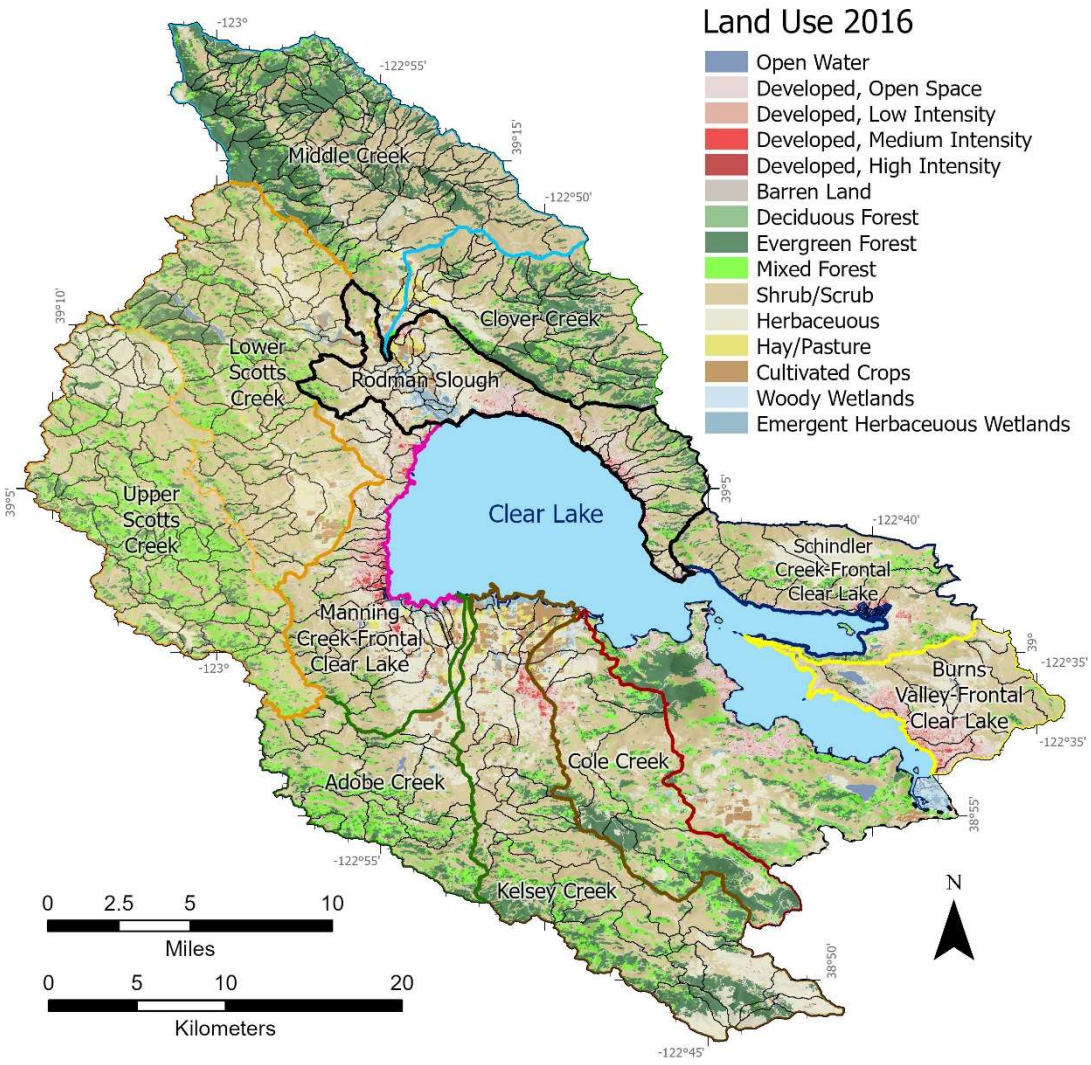

Figure 6.3.2. Subbasins for each sub model in the watershed model, with 2016 National Land Cover Dataset (NLCD; Jin et al., 2019) land use shown.

Initial parameterization of the 11 sub-models was completed using gridded environmental properties that enabled a consistent quantification of hydrology and water quality response variables across all models. Gridded environmental data, including elevation, geology, land use, and soil properties were used to characterize hydrologic response characteristics of the model segments (Table 6.3.4). Each subbasin represents a contributing area to a downstream model reach, or a stream or lake. These reaches (RCHRES) were characterized by stream elevation difference from the top to the bottom segment, stream width, and rating tables that consist of a depth-surface area-volume-outflow relationship. These relationship tables (FTABLEs) were developed from channel characteristics available from USGS gaged streams. For ungaged streams, FTABLE parameters from similar gaged streams were used or were scaled according to the ratio of watershed areas of the gaged and ungaged watersheds. FTABLES for large reservoirs including Tule Lake and the Blue Lakes in the Scotts Creek watershed were developed based on historical published information relating surface area and depth (Ewing, 2014).

6.3.3.1 Sediment parameterization

Sediment parameter values were initially determined using the BASINS Technical Note 8 (EPA, 2006), which gives guidance on setting ranges of sediment parameters based on soil type, land use, slope, and geology. These parameter values were further adjusted during the calibration process. To further characterize the upper Scotts Creek sediment parameters due to high trail densities, trail density and vegetated to non-vegetated ratios were developed from high resolution satellite imagery (Bond and Curtis, 2024). Sediment transport parameters were increased for subbasins that had the highest trail densities and non-vegetated area.

6.3.3.2 Middle Creek restoration

To simulate an ongoing major restoration effort in the Middle Creek/Rodman Slough area near the northern side of Clear Lake (https://www.lakecountyca.gov/1273/Middle-Creek-Restoration-Project), FTABLEs were adjusted in a similar way to Tule Lake in the Scotts Creek watershed. Stream widths, volume, and outflows were adjusted to simulate behavior of a wider channel that is not constrained by levees. The simulation was run before restoration for the historical period (1981–2023), then run again with the adjusted FTABLEs and parameters to simulate restoration conditions.

Table 6.3.4. Environmental data and sources used to build and parameterize the model.

Category	Name	Grid size or scale	Source/Reference
Land use	National Land Cover Database (NLCD) 2016	30 meters	Jin et al., 2019; available online at https://doi.org/10.3390/rs11242971 https://www.mrlc.gov/
Geology	Geologic Map of California	1:750,000	Jennings et al. (2010)
Soil Properties	SSURGO	1:12,000 to 1:63,360	Soil Survey Staff (2024)
Elevation	NED	30 meters	U.S. Geological Survey (2024a)
Hydrography	NHDPlus v2	1:24,000 or higher	U.S. Geological Survey (2024b)

6.3.4 HSPF model calibration

The calibration approach for this study maintained spatial relationships of physical properties used to estimate preliminary hydrologic and sediment parameters across the domain to compensate for sparse calibration data. BASINS Technical Note 6 (EPA, 2000) was used to guide initial parameter values and the appropriate ranges of values during calibration. The parameter values corresponded to distributed physical properties that varied by land use type and were scaled up or down during the calibration process. After the streamflow calibration, water temperature and sediment modules were added, and the initial parameters were developed using the guidance documents and the gridded environmental data (Table 6.3.4), when appropriate. HSPEXP+, a tool built by HSPF developers to standardize the calibration process, was used to calibrate streamflow in locations with data. Calibration was accomplished by adjusting the model parameters

until the simulated and observed water budgets matched within a predefined margin of error. After a satisfactory fit between simulated and observed water budgets was obtained, the hydrologic response to storm events was calibrated. Ungaged watersheds received calibrated parameters from similar basins. A lack of daily time step sediment transport data did not allow for the use of HSPEXP+ for calibrating sediment and necessitated an unguided trial and error calibration approach for sediment transport.

Nine streamgages were used for streamflow calibration (Figure 6.3.1, Table 6.3.5) to ensure an accurate representation of the hydrology across the diverse Clear Lake tributaries. Due to the climate data availability starting in 1979, only streamflow and water quality data after 1979 were collected for calibration. Visual comparisons of hydrographs in addition to a range of statistical metrics were performed to assess a goodness of fit of simulated to measured data. A range of goodness of fit metrics were used to quantify the simulated to observed fit, including Pearsons correlation (R), coefficient of determination (R^2), mean error, percent bias (PBIAS), mean absolute error (MAE), root mean squared error (RMSE), and Nash-Sutcliffe efficiency (NSE). The goodness of fit metrics R, R^2, and NSE describe the measured to simulated fit with low values close to 0 representing a poor fit, and the high values close to 1 representing a good fit. These metrics tend to be biased toward the higher values and one outlier value can bring down the metric significantly. The mean error, PBIAS, MAE, and RMSE are used to describe the goodness of fit characterizing differences between observed and simulated volumes and can be related directly to the units of the model parameter, like streamflow.

Table 6.3.5. Streamflow gages used for hydrology calibration and approximate dates of available data. DWR = station data provided by California Department of Water Resources (www.ca.cdec.gov)

Station name	Station ID	Hourly data available
SF Scotts C Nr Lakeport	11448750	2020–2024
Scotts C BL SF Scotts C Nr Lakeport	11448800	2020–2024
Scotts Creek at Eickhoff Road Bridge	SCS (DWR)	2008–2024
Scotts C AB State Route 29 A Upper Lake	11449255	2022–2024
Middle Creek Nr Upper Lake	MCU (DWR)	2008–2024
Molesworth C Nr Clearlake	11449370	2022–2024
Cole C A Kelseyville	11449820	2022–2024
Kelsey C Nr Kelseyville	11449500	2007–2024
Kelsey Ck Below Kelseyville	KCK (DWR)	2010–2024

6.3.5 Historical climate variability

The average annual air temperature between 1980 and 2023 was 53.5 degrees Fahrenheit (°F), ranging between 50.9 and 56.6 °F. There is a statistically significant ($p<0.05$) increasing trend in average air temperature (Figure 6.3.3), even with a relatively cooler water year in 2023 with an average of 52.1 °F. The 30-year long term average between 1981 and 2010 was 53.1 °F, whereas the more recent long-term average between 1991 and 2020 was 53.7 °F, an increase of 0.6 °F. The average annual water

year precipitation between 1980 and 2023 was 38.9 inches, ranging from 15.7 inches in 2021 to 76 inches in 1983. There is a statistically significant ($p<0.01$) decreasing trend of precipitation over the 1980–2023 period (Figure 6.3.4). The long-term average precipitation between 1980 and 2010 was 42 inches, and the more recent 1991–2020 period was 3 inches less at 39 inches. In summary, within the post-1980 period, air temperature has increased and precipitation has decreased in this area.

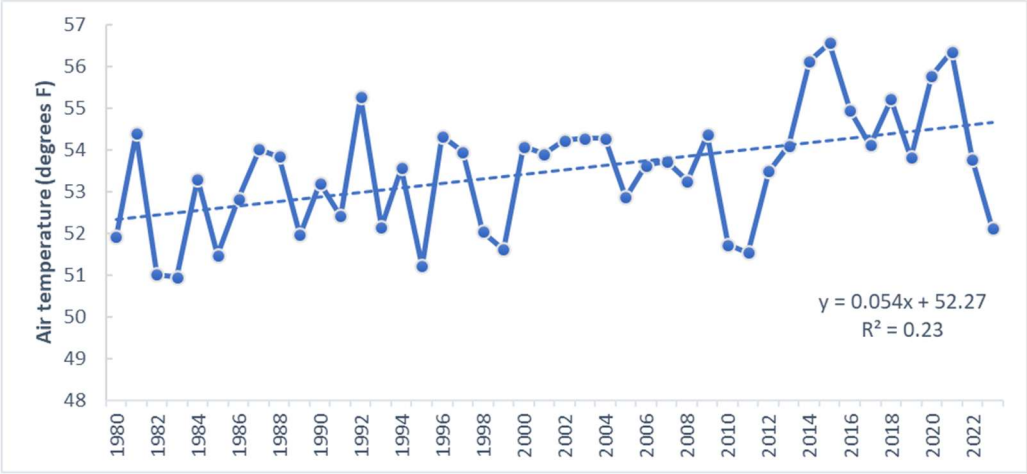

Figure 6.3.3. Annual average air temperature from water years 1980-2023.

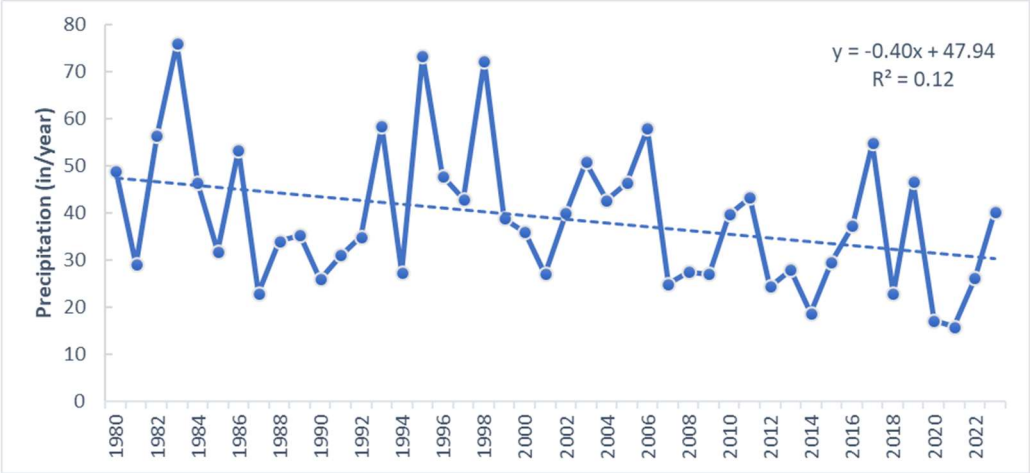

Figure 6.3.4. Annual water year precipitation from 1980 to 2023.

The climate data used for average trends in Figures 6.3.3 and 6.3.4 was extracted from the NLDAS grid point nearest to Lakeport (Figure 6.3.1) and was used because there is a nearby climate station for comparison. It is important to note the high variability in precipitation and air temperature across the Clear Lake watershed (Figure 6.3.5). The amount of precipitation varies through time and across the watershed. The southeast portion of the watershed receives much less precipitation than the northernmost edge (Figure 6.3.5A) and the highest elevation areas along the west and southern edges of the watershed. Precipitation directly over Upper Lake, Lakeport, and Big Valley is significantly less than the upper watershed. Average annual maximum air temperatures are highest over Clear Lake and the surrounding urban areas (Figure 6.3.5B), with lower temperatures at the northern and southern ends and in the highest elevations around the watershed.

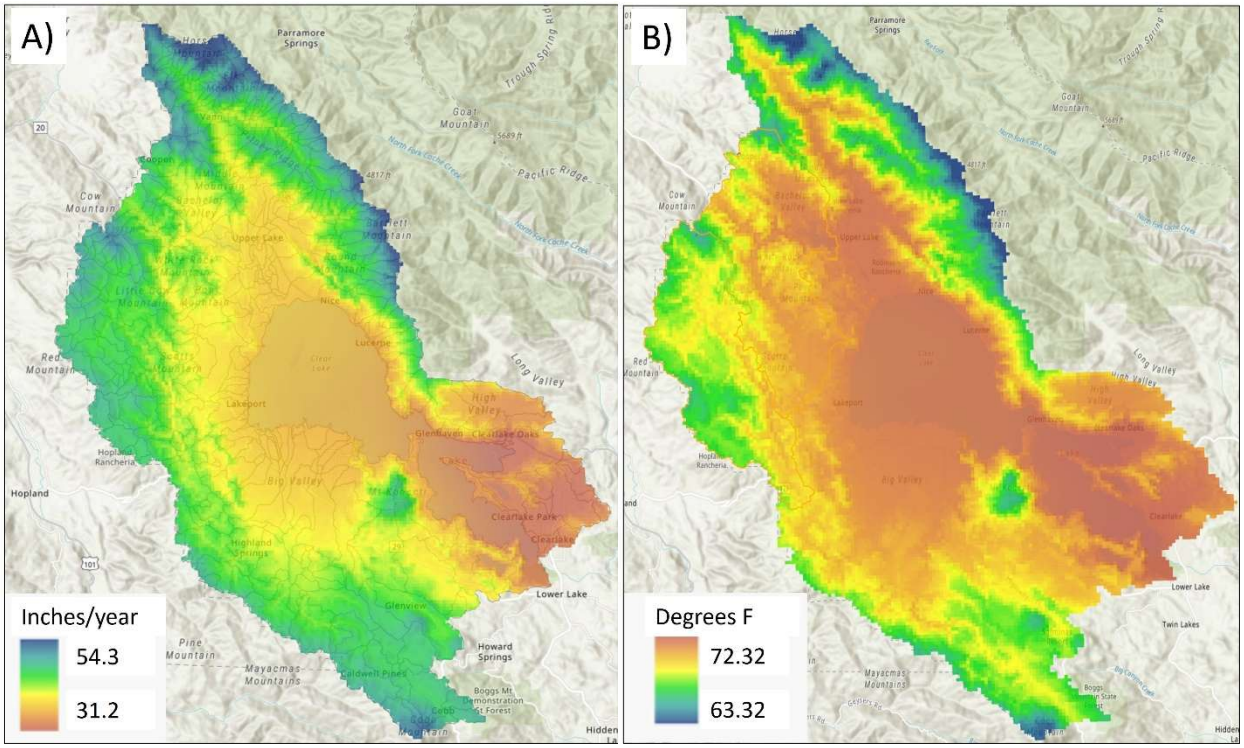

Figure 6.3.5. Average annual A) precipitation (inches per year) and B) maximum air temperature (degrees Fahrenheit) in the Clear Lake watershed (PRISM Climate Group, [2024], PRISM gridded climate data: Oregon State University, accessed [September 12, 2024], at https://prism.oregonstate.edu). Base map from Esri and its licensors, copyright 2025.

6.3.6 Streamflow calibration results

Results from the hydrologic calibration are presented visually through time series comparisons of hourly or daily streamflow, and statistically using the seven goodness of fit metrics described above. In general, the hydrologic calibration was successful with an average daily R^2 of 0.79 (Table 6.3.6), indicating a very good calibration (Stern et al., 2016). The monthly statistics showed an average R^2 of 0.90 (Table 6.3.6), indicating an excellent calibration result. The calibration results varied by location, with all gages resulting in a fair to excellent calibration designation. The daily NSE average was 0.74, or good, and the monthly NSE average was 0.84, or very good. Mean error estimates averaged 5.8 cubic feet per second (cfs) across the sites at a daily time step and were on average 7.4 cfs at a monthly time step.

Table 6.3.6. Calibration statistics for streamflow gages in the Clear Lake watershed. R = Pearson's coefficient, R^2 = coefficient of determination, PBIAS = percent bias, MAE = mean absolute error, RMSE = root mean squared error, NSE = Nash-Sutcliffe efficiency, cfs = cubic feet per second.

Streamgage location		Mean flow (cfs)	R	R^2	Mean Error (cfs)	PBIAS (%)*	MAE (cfs)	RMSE (cfs)	NSE
Daily	SF Scotts C Nr Lakeport	33.4	0.82	0.67	-0.09	-0.6	7.7	35.6	0.63
	Scotts C BL SF Scotts C Nr Lakeport	103.0	0.90	0.81	0.36	1.0	16.5	72.1	0.77
	Scotts C at Eickhoff Road Bridge	116.0	0.92	0.84	-1.8	-2.7	26.8	92.0	0.81
	Scotts Creek AB State Route 29 A Upper Lake	326.0	0.92	0.84	45.1	11.0	136.7	142.3	0.81
	Middle C Nr Upper Lake CA	105.7	0.89	0.79	1.1	1.8	29.5	103.8	0.73
	Molesworth C Nr Clearlake	1.33	0.80	0.64	1.4	110	1.18	2.16	0.42
	Kelsey C Nr Kelseyville	54.5	0.92	0.85	1.0	1.8	21.6	78.5	0.85
	Kelsey Ck Bl Kelseyville	64.7	0.93	0.86	4.8	7.2	28.8	103.0	0.86
	Cole C A Kelseyville	3.07	0.91	0.83	-0.1	-1.3	5.3	10.8	0.80
Monthly	SF Scotts C Nr Lakeport	33.4	0.97	0.94	0.1	0.6	3.89	8.55	0.94
	Scotts C BL SF Scotts C Nr Lakeport	103.0	0.97	0.95	0.7	2.0	10.4	22.4	0.94
	Scotts C at Eickhoff Road Bridge	116.0	0.97	0.95	-1.8	-2.7	16.4	31.5	0.95
	Scotts Creek AB State Route 29 A Upper Lake	326.0	0.97	0.94	43.5	11.7	86.7	86.8	0.92
	Middle C Nr Upper Lake CA	105.7	0.96	0.92	1.3	2.0	21.6	40.4	0.91
	Molesworth C Nr Clearlake	1.33	0.89	0.80	16.4	110	39.42	42.24	0.32
	Kelsey C Nr Kelseyville	54.5	0.97	0.93	1.0	1.9	14.5	30.1	0.93
	Kelsey Ck Bl Kelseyville	64.7	0.96	0.93	4.9	7.2	19.5	40.3	0.93
	Cole C A Kelseyville	3.07	0.86	0.74	0.4	3.9	5.0	7.4	0.73
		* Positive bias indicates over simulation of streamflow							

Examples of calibration hydrographs are shown in hourly and daily time steps (Figures 6.3.6–6.3.9). Figure 6.3.6 shows the calibration results for the uppermost gage in the Scotts Creek watershed, South Fork Scotts Creek near Lakeport, at a daily time step. Precipitation is shown on the top of the hydrograph to visually compare the hydrologic response to precipitation events. Some peaks are over-simulated, and some are under-simulated, but the overall hydrologic response is well simulated by the model. Further downstream, the Scotts Creek at Eickhoff Road Bridge gage (Figure 6.3.1) had a much longer period of record of hourly streamflow, allowing a more robust comparison and confidence in the calibration through year-to-year precipitation variability. Figure 6.3.7 shows a very good calibration result, representing the hydrologic response to precipitation, with some over- and some under-simulated peaks.

Downstream of Tule Lake, the Scotts Creek above State Route 29 at Upper Lake gage (Figure 6.3.1) calibration result (Figure 6.3.8) showed a good fit between simulated and observed streamflow, except when the observed discharge values are negative. Negative observed streamflow indicates a reversal of flow direction. HSPF is not capable of simulating bidirectional flow, which caused discharge to be over-simulated (Table 6.3.6). The model calibration still resulted in a very good calibration, except for the mean errors that were higher than other stations. Observed peak discharges at the Scotts Creek at Eickhoff Road Bridge gage were reduced by roughly half or more after flowing through the rest of the Scotts Creek watershed and finally discharging to Tule Lake. More data is needed at this location to better represent the hydrology of this complex area.

Figure 6.3.9 shows the daily calibration results for the Kelsey Creek near Kelseyville gage, with an excellent calibration. The long-term data available at this gage (Table 6.3.5) allows for higher confidence in the model calibration result, which is especially important for the tributaries that contribute the highest amount of streamflow and thus sediment and nutrients to Clear Lake.

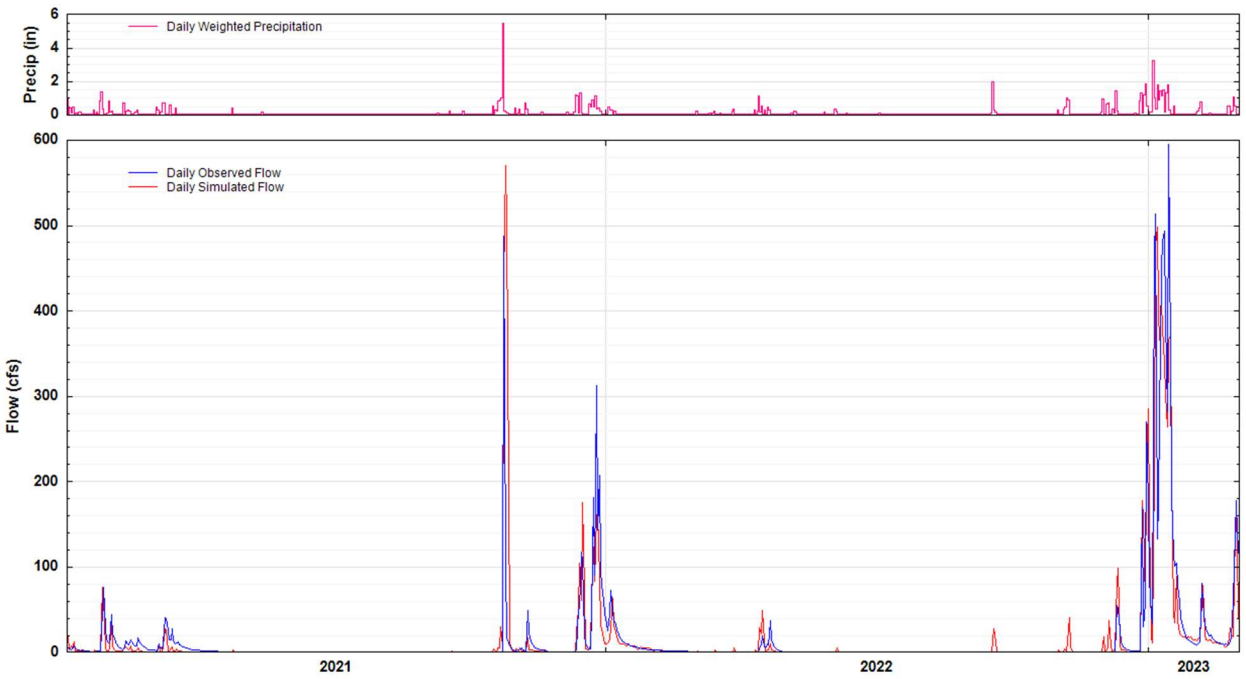

Figure 6.3.6. Daily observed (blue) and simulated (red) streamflow, with precipitation in the auxiliary plot for the South Fork Scotts Creek near Lakeport gage (station 11448750). cfs, cubic feet per second; in, inches.

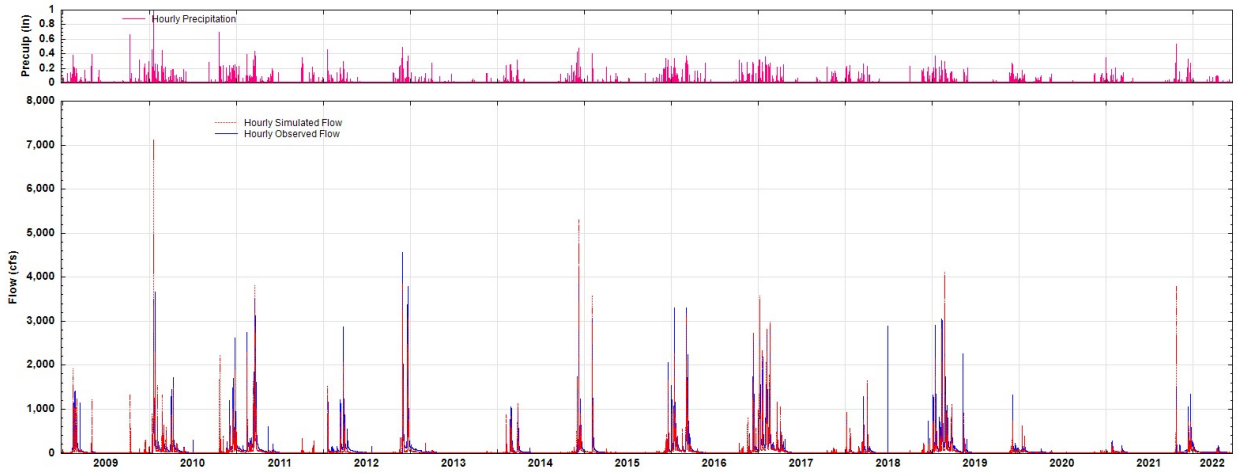

Figure 6.3.7. Hourly observed (blue) and simulated (red) streamflow, with precipitation in the auxiliary plot for the Scotts Creek at Eickhoff Road Bridge gage. cfs, cubic feet per second; in, inches.

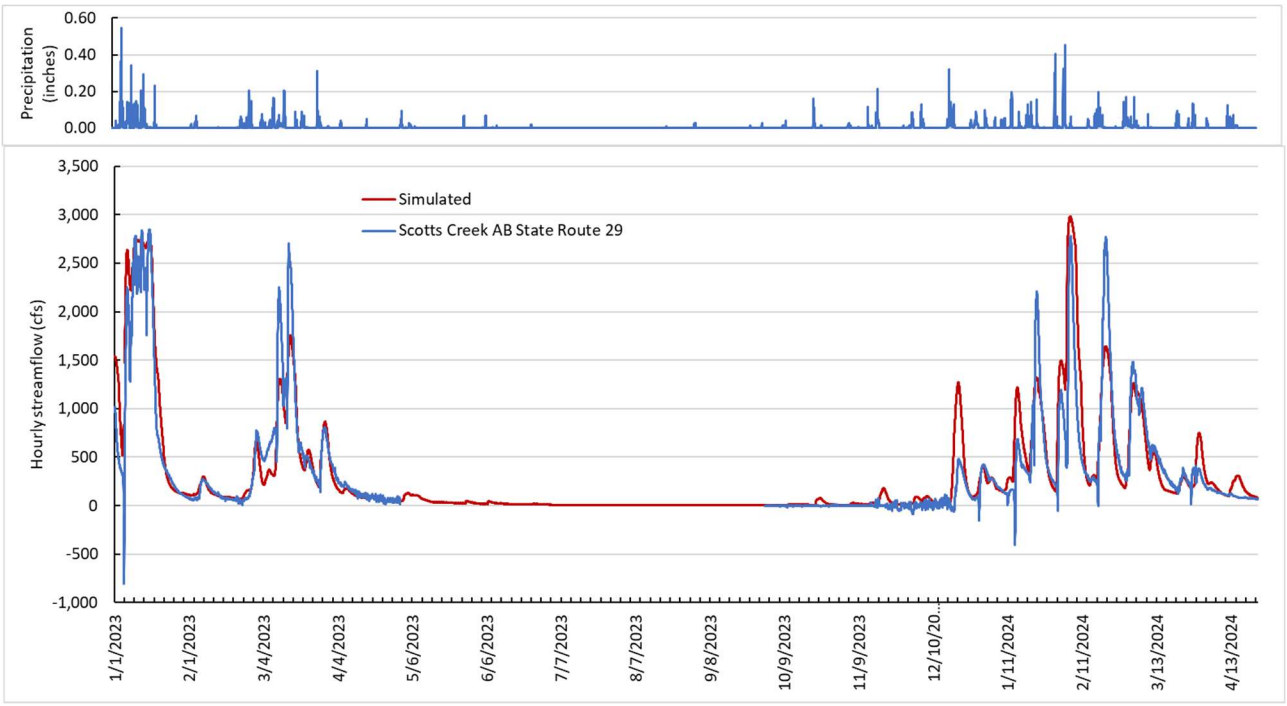

Figure 6.3.8. Hourly observed (blue) and simulated (red) streamflow, with precipitation in the auxiliary plot for the Scotts Creek above State Route 29 at Upper Lake gage (station 11449255). cfs, cubic feet per second; in, inches.

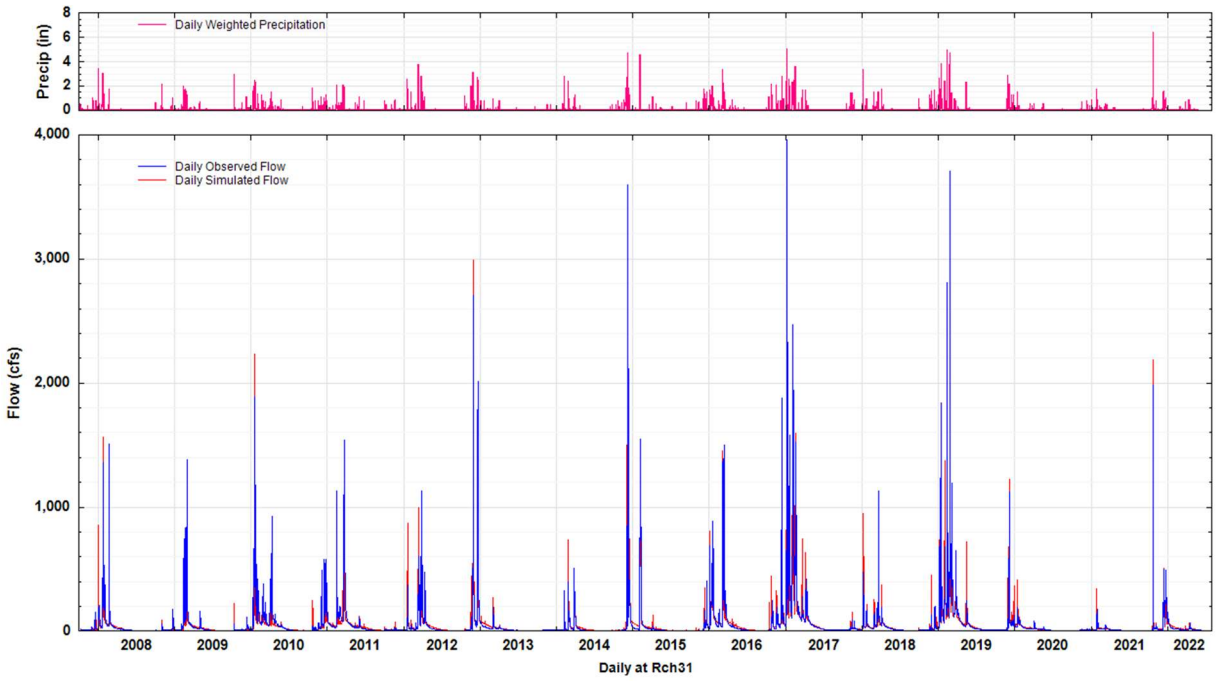

Figure6.3.9. Daily observed (blue) and simulated (red) streamflow, with precipitation in the auxiliary plot for the Kelsey Creek near Kelseyville gage (station 11449500). cfs, cubic feet per second; in, inches.

6.3.7 Water temperature calibration results

Water temperature time series data were collected from all the gages in Table 6.3.5 except for the Kelsey Creek near Kelseyville gage, which did not have stream temperature data. Simulated water temperature generally followed the patterns that were seen in the observed data, with some variations. For example, the Scotts Creek at State Route 29 gage showed a good relationship between observed and simulated stream temperature (Figure 6.3.10), especially during the spring and fall months when temperatures were increasing and decreasing rapidly. Winter water temperatures did not show as good of a simulation result. This resulted in an R^2 of 0.83 over the one year of data available (Figure 6.3.11). There is no water temperature data during the summer months when flow reaches zero.

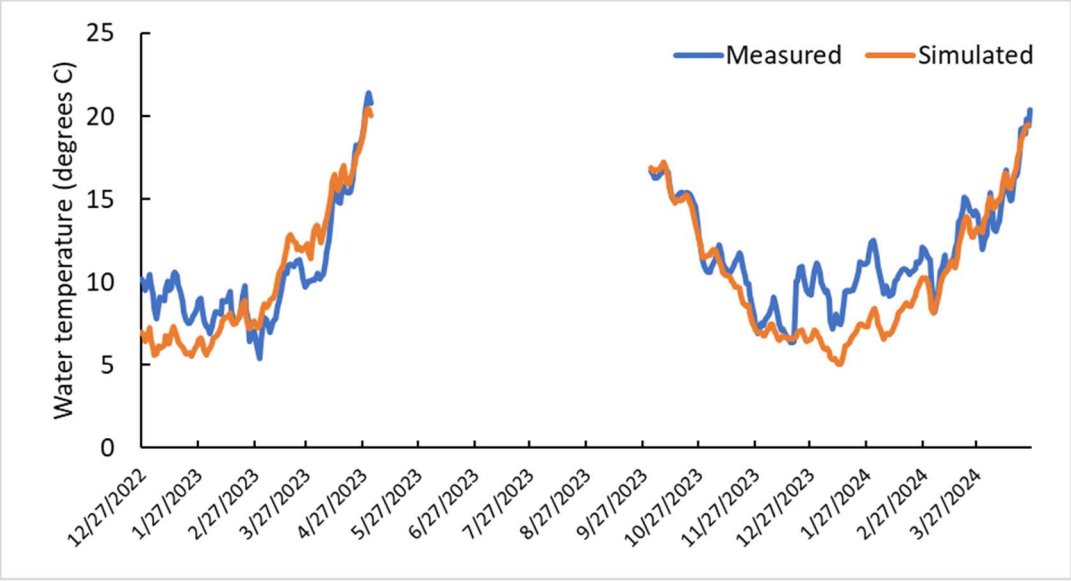

Figure 6.3.10. Comparison between daily observed (blue) and simulated (orange) water temperature for the Scotts Creek at State Route 29 gage.

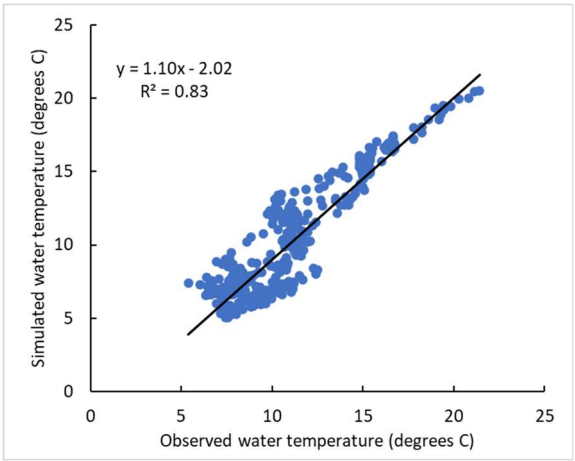

Figure 6.3.11. Scatter plot comparing daily observed (x-axis) and simulated (y-axis) water temperature for the Scotts Creek at State Route 29 gage.

6.3.8 Sediment calibration results

Sediment transport calibration was guided by the BASINS Technical Note 8 (EPA, 2006) where values of sediment-process parameters from the PERLND and HYDR modules were changed iteratively using a trial-and-error approach to produce the best match between simulated and measured data. Daily suspended sediment concentrations and sediment loads were available at the Scotts Creek below South Fork Scotts Creek near Lakeport gage (1144880), the only daily sediment record available in the Clear Lake watershed. Instantaneous suspended sediment concentrations (SSC) were also used for calibration in nine locations across the watershed (Table 6.3.7, Sushch et al., 2025), increasing the amount of calibration data. Most of the sample data were collected between 2021 and 2024 (Table 6.3.7) with or without coincident flow measurements. Table 6.3.7 shows the calibration statistics for the daily sediment record at Scotts Creek below South Fork Scotts Creek and the instantaneous SSC calibration results at the nine other locations. The R^2 and RMSE for the daily SSC and sediment discharge data were 0.50 and 72.6 milligrams per liter (mg/L), and 0.55 and 426 tons/day, respectively (Table 6.3.7). HSPF generally underpredicted SSC and sediment discharge in the lower half of the distribution, but represented the highest values well, especially for sediment discharge (Figure 6.3.12).

Table 6.3.7. Daily sediment and instantaneous suspended sediment concentration (SSC) calibration results. R^2, coefficient of determination; RMSE, root mean squared error.

Daily sediment					
Station Name	**Station ID**	**Constituent**	**Dates**	**R^2**	**RMSE**
Scotts Creek Below South Fork Scotts Creek	8800	SSC	1/13/2021 to 3/29/2023	0.50	72.6 mg/L
		Sediment discharge	1/13/2021 to 3/29/2023	0.55	425.8 tons/day

Suspended Sediment Concentration (SSC) instantaneous data					
Location	**Station ID**	**Samples**	**Dates**	**R^2**	**RMSE (mg/L)**
South Fork Scotts Creek Nr Lakeport	11448750	19	1/5/2021 to 3/29/2023	0.14	243
Scotts C BL SF Scotts C Nr Lakeport	8800	237	1/13/2021 to 3/29/2023	0.21	246
Scotts Creek A Eickhoff Bridge Road	SCS	42	2/9/2007 to 4/24/2023	0.12	974

Scotts Creek above State Route 29 A Upper Lake	9255	13	1/5/2023 to 3/29/2023	0.51	27
Middle Creek Near Upper Lake	MCU	21	10/24/2021 to 3/28/2024	0.57	173
Clover Creek Bypass	ACS	19	10/25/2021 to 3/28/2024	0.12	7
Kelsey Creek Below Kelseyville	KCK	22	10/25/2021 to 3/28/2024	0.38	125
Cole Creek A Kelseyville	9820	15	1/4/2023 to 3/28/2024	0.73	158
Molesworth C Nr Clearlake	9370	11	12/10/2022 to 2/20/2024	0.84	174
Average				0.41	236

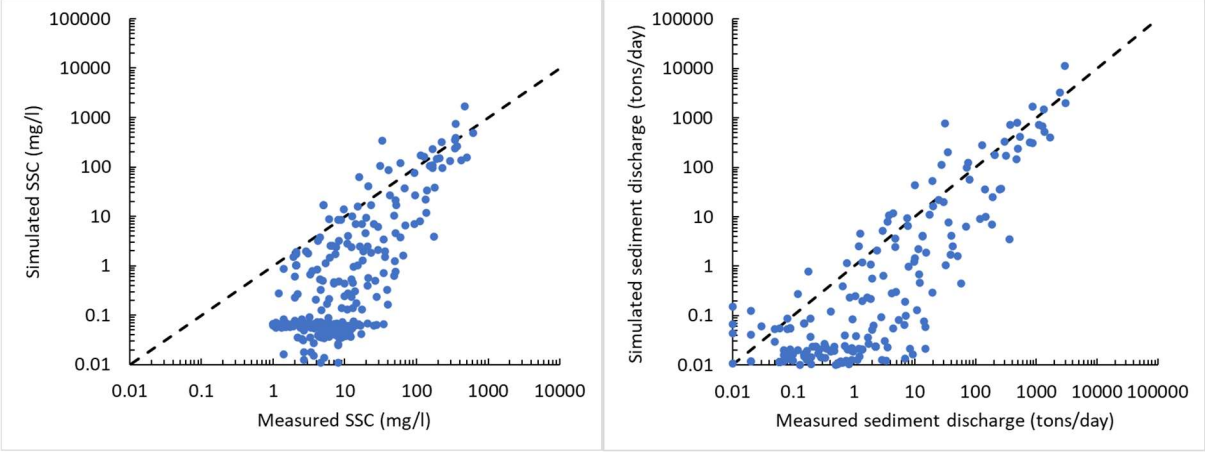

Figure 6.3.12. Scatter plots of observed versus simulated suspended sediment concentrations (SSC, left) and sediment discharge (tons/day, right) at the Scotts Creek below South Fork Scotts Creek (station 8800) gage. The black dashed line indicates a one-to-one relationship.

The instantaneous data calibrations generally showed poorer statistics because any minor shift in the timing or magnitude of streamflow between measured and simulated data will greatly affect the goodness-of-fit statistics for SSC. The average R^2 for instantaneous SSC samples was 0.41 and ranged between 0.12 to 0.84. The average RMSE across all nine sites was 236 mg/L, and ranged from 7 to 974 mg/L. All except one of the RMSE values were lower than 300 mg/L. The number of SSC samples ranged from 11 to 237, and samples during high flows were generally not taken due to logistical and safety considerations. Figure 6.3.13A–H show that HSPF provided a satisfactory match to measured SSC for these locations; however, some timing issues resulted in HSPF over- or under-simulating SSC at a given time step relative to the grab samples. SSC in this watershed is very flashy, with rapid increases and decreases, making it difficult to

calibrate to instantaneous data. The locations with the most amount of SSC data generally showed that HSPF underpredicted at the low to middle SSC values but represented the higher values well (Figures 6.3.13A, C, F).

There are inherent limitations to using the instantaneous data directly for calibration, including a difference in time step between an hourly model and a discrete grab sample, and a lack of samples taken during high flow events. Daily sediment data also have large uncertainties as the daily values are simulated using the same discrete samples and a flow-concentration statistical relationship. Without samples taken at both high and low flows, the highest values are often extrapolated using relationships built with lower sediment concentrations. A "weight of evidence" approach (EPA, 2006) was used during calibration to ensure reasonable values (values considered to be within bounds observed in other studies; e.g., Stern et al., 2016) were achieved considering the data available for calibration. More long-term sediment data are needed to increase confidence in the calibrations, especially in ungaged tributaries.

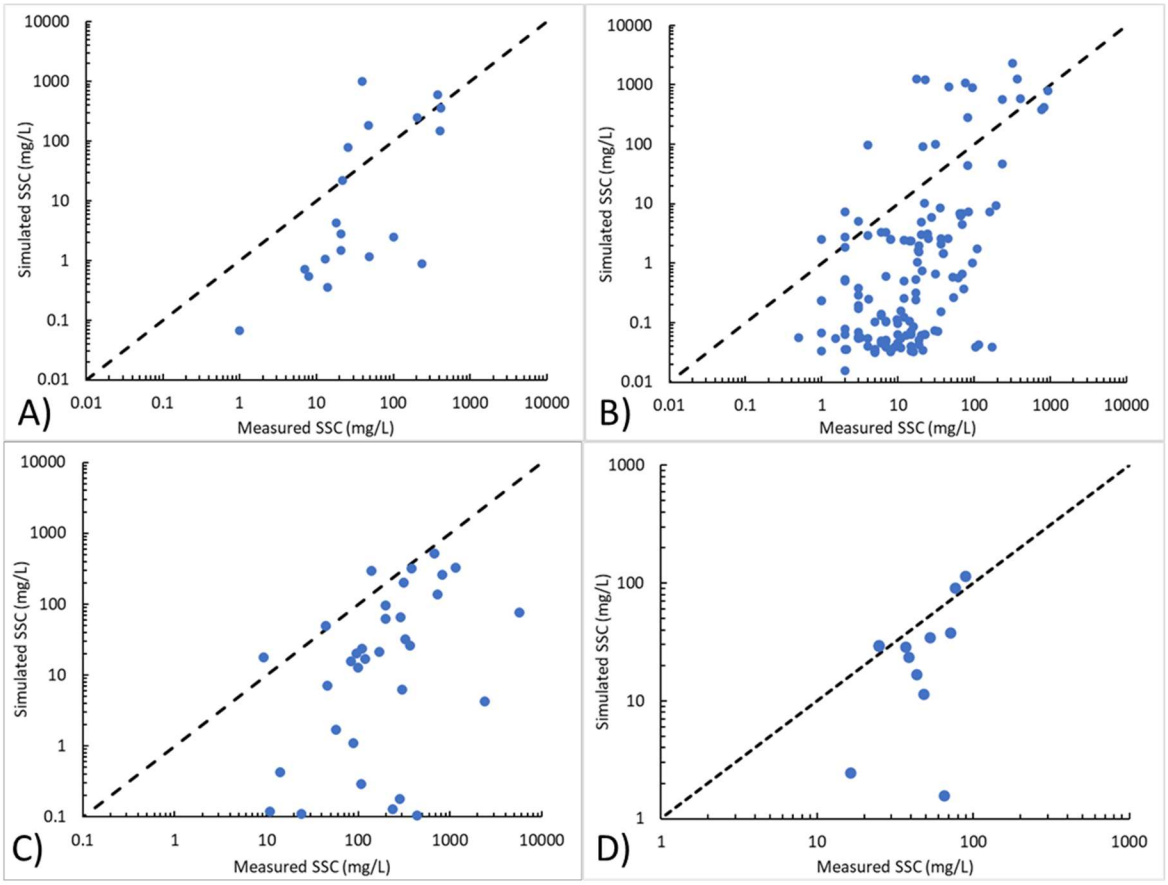

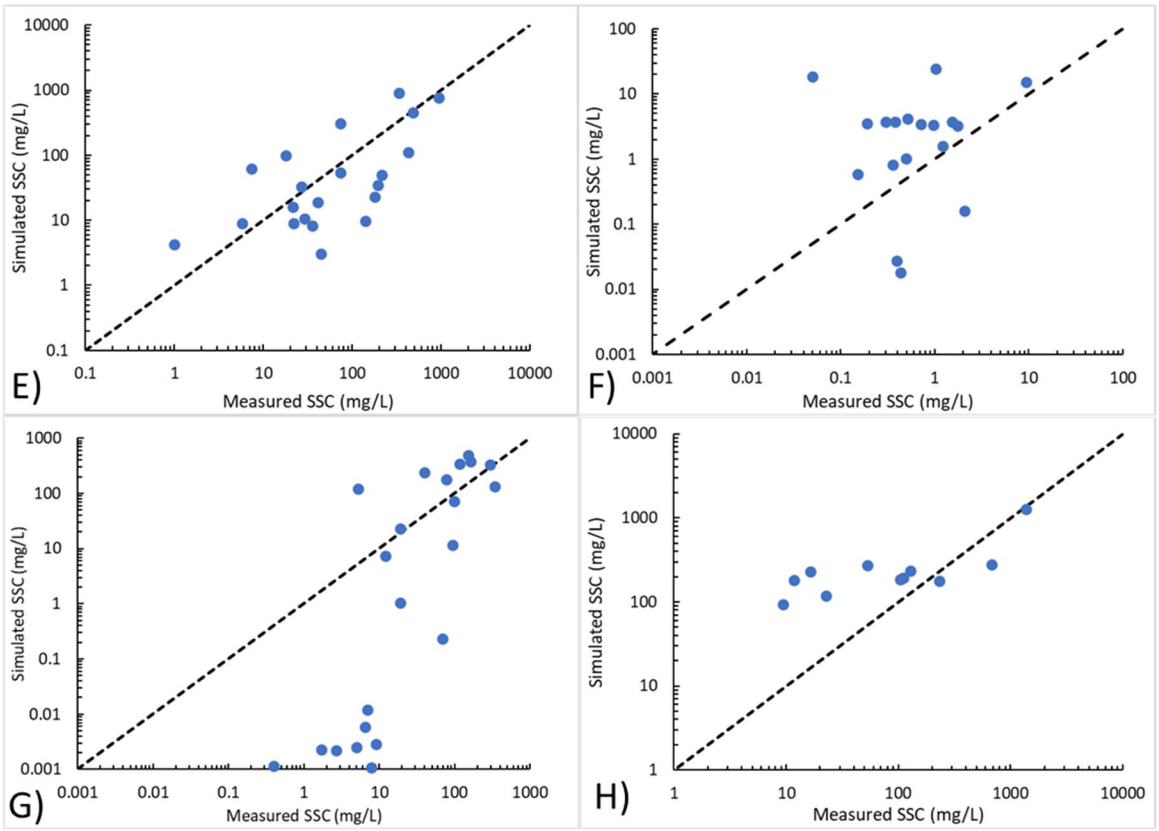

Figure 6.3.13. Scatter plots of observed versus simulated suspended sediment concentrations (SSC) in milligrams per liter (mg/L) at A) South Fork Scotts Creek near Lakeport, B) Scotts Creek below South Fork Scotts Creek near Lakeport, C) Scotts Creek at Eickhoff Bridge Road, D) Scotts Creek above State Route 29 at Upper Lake, E) Middle Creek near Upper Lake, F) Clover Creek Bypass, G) Kelsey Creek below Kelseyville, and H) Molesworth Creek near Clearlake. The black dashed line indicates a one-to-one relationship.

6.3.9 Historical streamflow and sediment discharge results

Simulated streamflow and suspended sediment discharge for all major Clear Lake watershed tributaries were combined to quantify total inflows to Clear Lake and were aggregated to water-year totals to assess long-term trends. Figure 6.3.14 shows the annual streamflow and sediment data by water year from 1981 to 2023. These time series show the high degree of annual variability in the simulated streamflow and sediment discharge inflows to Clear Lake. The high degree of annual variability in streamflow and sediment discharge causes multi-year average streamflow and sediment discharge to Clear Lake to be significantly dependent on the years that are being averaged. The 1981–2023 average of streamflow and sediment discharge is 776 cfs/year and 56,212 tons/year; however, the first 15 years were much wetter than the last 15 years. The streamflow and sediment discharge from 2010 to 2023 was just 509 cfs/year and 25,939 tons/year, respectively. The highest inflows of sediment and streamflow occurred in water year 1983, with 296,000 tons/year and 1,460 cfs/year, respectively. The last 15 years coincided with four extremely dry drought years (2012, 2014, 2020, and 2021). The wetter years in the last 15 years were also not as high or frequent as the wetter years from before 2000.

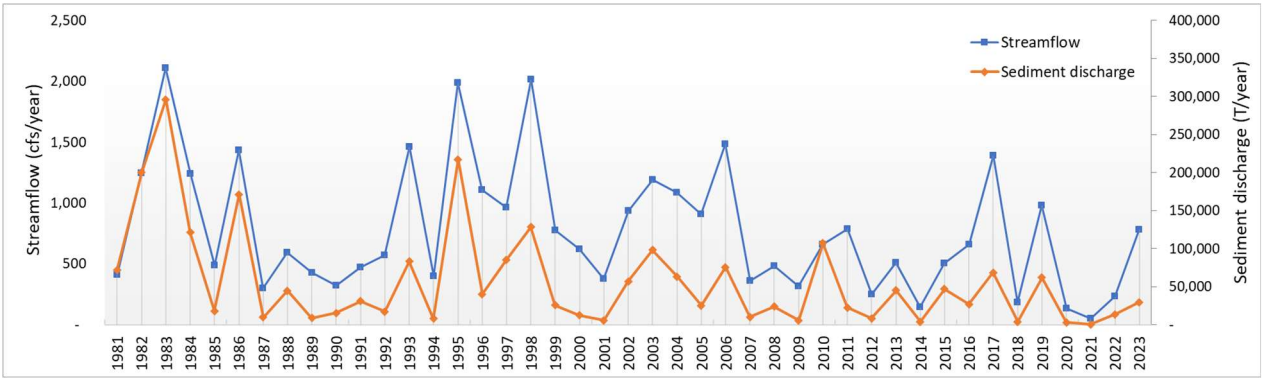

Figure 6.3.14. Water year streamflow (cubic feet per second per year; cfs/year) and sediment discharge (tons per year; T/year) for Clear Lake tributaries.

The calibrated watershed model allows the direct comparison between tributaries, and it is possible to quantify the contribution of each to Clear Lake, including ungaged tributaries. Figure 6.3.15 shows the minimum, maximum, and average annual flow contributions to Clear Lake from 1981 to 2023. The largest contributors on average are Scotts Creek (52%), Middle Creek (20%), and Kelsey Creek (12%), but the contributions vary significantly from year to year. The northernmost inlet to Clear Lake (Figure 6.3.1) includes Scotts Creek, Middle Creek, and Clover Creek, which contributed 48–96% of the streamflow each year, or 73% on average.

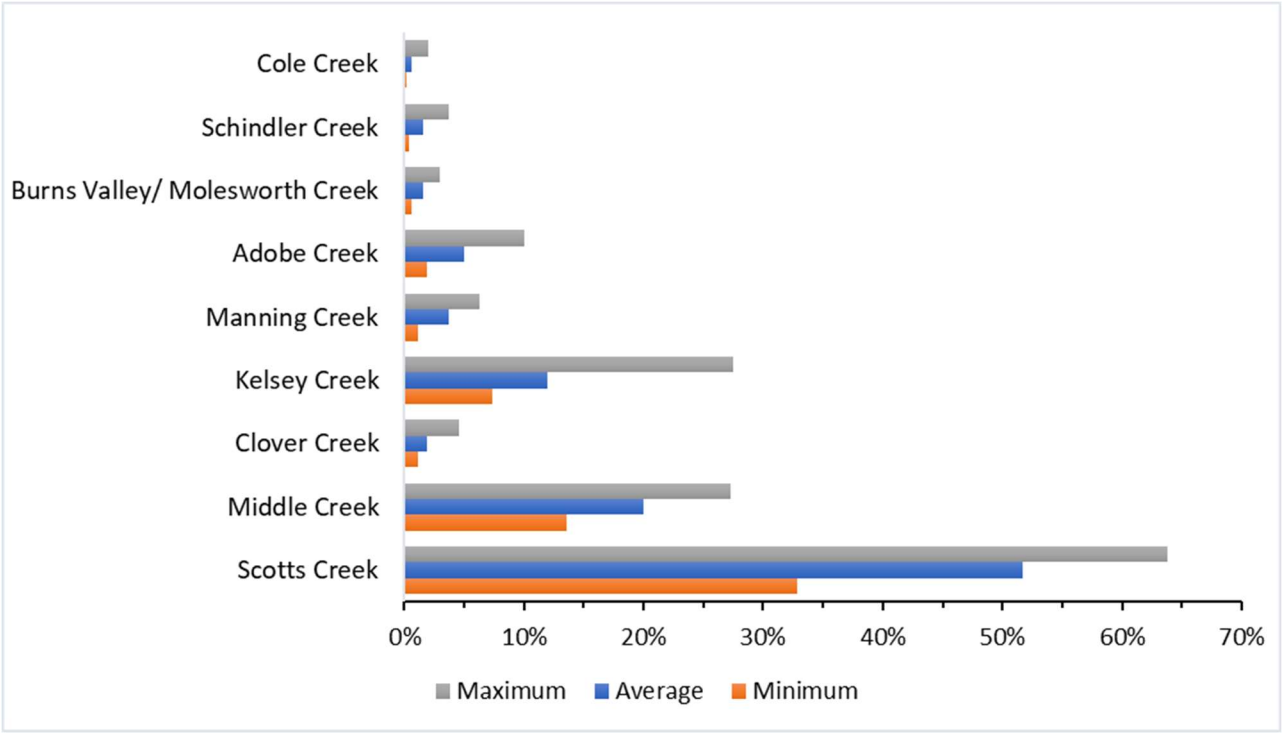

Figure 6.3.15. Relative streamflow contributions to Clear Lake, showing the minimum (orange), maximum (grey), and average annual contribution between 1980 and 2023.

Figures 6.3.16 and 6.3.17 show the average streamflow and sediment watershed inputs to Clear Lake by tributary, respectively. Although there is higher uncertainty in the ungaged watersheds, most of the major tributaries had streamflow calibration data. As

Figure 6.3.15 shows, contributions significantly vary year to year compared to the average value due to annual precipitation. The top four contributors of streamflow were also the highest contributors of sediment discharge to Clear Lake. Although the biggest contributor by far, Scotts Creek below Tule Lake contributes relatively lower sediment discharge due to the trapping efficiency of sediment in Tule Lake. Scotts Creek below Tule Lake contributes roughly 52% of the streamflow on average, but only 34% of the sediment discharge (Figure 6.3.18A and B). There is a roughly 36% reduction in sediment loads from the Scotts Creek at Eickhoff Bridge Road gage to Scotts Creek below Tule Lake. Middle Creek and Kelsey Creek contribute 17% and 10% of the streamflow, but relatively higher sediment discharge at 27% and 15% (Figure 6.3.18A and B).

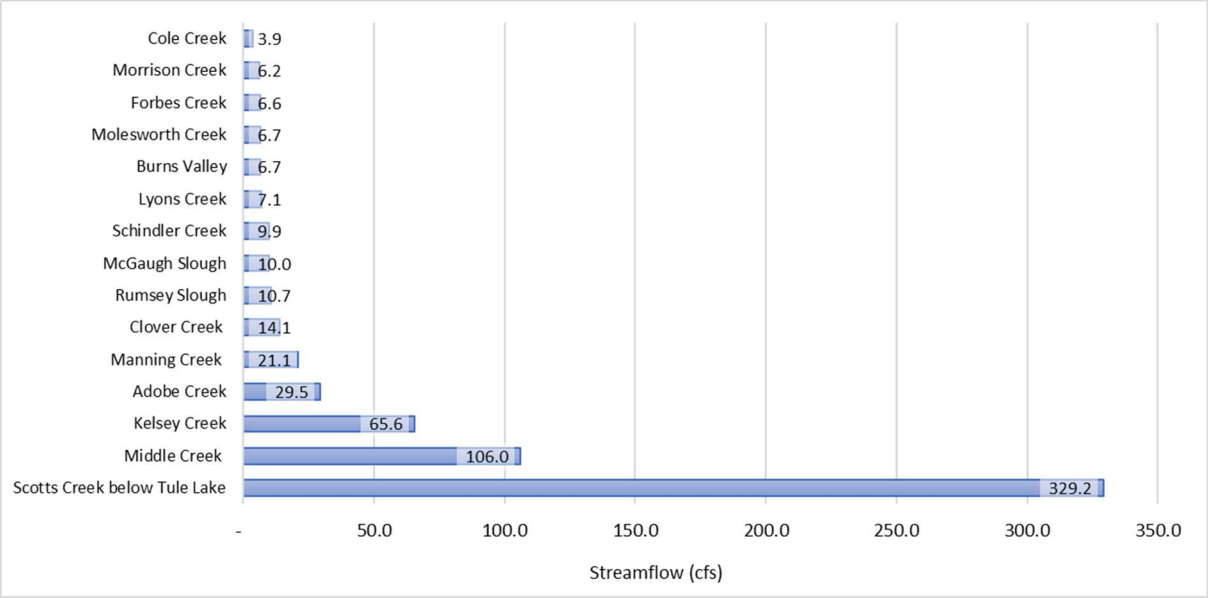

Figure 6.3.16. Average water year contribution of streamflow (in cubic feet per second [cfs]) to Clear Lake, summarized by major tributary inputs.

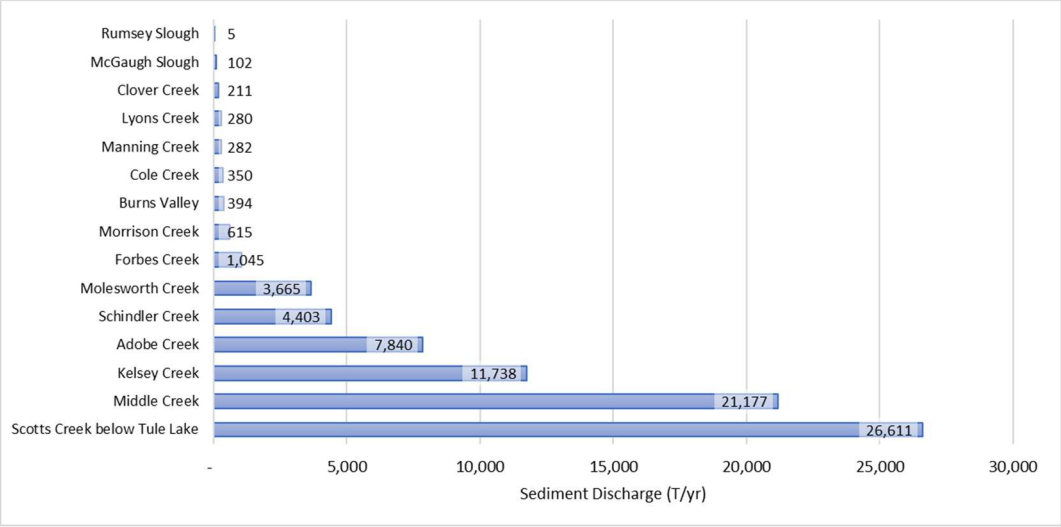

Figure 6.3.17. Average water year contribution of sediment discharge (in tons per year [T/year]) to Clear Lake, summarized by major tributary inputs.

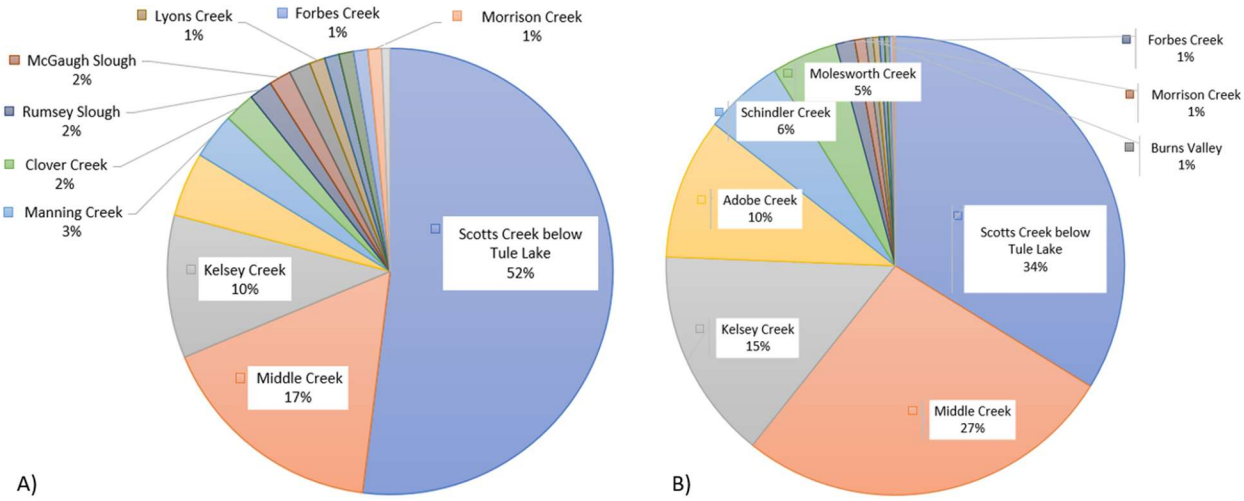

Figure 6.3.18. Average contribution of A) streamflow and B) sediment discharge to Clear Lake from 1981 to 2023.

6.3.10 Scotts Creek

As the largest contributor of streamflow and sediment to Clear Lake, it is necessary to quantify Scotts Creek streamflow and sediment sources and potential ways to reduce the effects to Clear Lake through sediment and nutrient transport. More than 75% of the total samples were collected in the Scotts Creek watershed, and the only daily sediment record was available below the confluence of South Fork Scotts Creek. This enabled a higher resolution calibration of streamflow and sediment processes in this watershed. The upper Scotts Creek watershed can be divided into three main components: the South Fork Scotts Creek and Benmore Creek tributary to the south, the northernmost tributary Black Oak Springs and Lyons Valley Creek, and the westernmost tributaries, Willow Creek and Eightmile Valley (Figure 6.3.19). Within Willow Creek and Eightmile Valley lies the South Cow Mountain off-highway vehicle (OHV) Park, and a high density of unpaved roads.

Figure 6.3.19. Upper Scotts Creek tributary subbasins, major streams, and South Cow Mountain off-highway vehicle (OHV) routes. Base map from Esri and its licensors, copyright 2025.

Of the three tributaries, Benmore Creek and South Fork Scotts Creek contributed the highest amount of streamflow, around 41% of the total flow during 1981–2023 (Figure 6.3.20). Black Oak Springs and Lyons Valley Creek contributed 30% of the streamflow, just higher than Willow Creek and Eightmile Valley at 29%. In contrast, the highest contributions of sediment discharge were from Willow Creel and Eightmile Valley at 40% on average. Black Oak Springs and Lyons Valley Creek contributed slightly less at 39% (Figure 6.3.21). Benmore and South Fork Scotts Creek contributed 20% of sediment discharge on average. The relative contributions of Black Oak Springs and Lyons Valley Creek and Willow Creek and Eightmile Valley are more difficult to quantify, as there is no calibration data for these locations. Benmore Creek and South Fork Scotts Creek have a calibration gage before the confluence with Scotts Creek, upstream of the Scotts Creek below South Fork Scotts Creek near Lakeport gage.

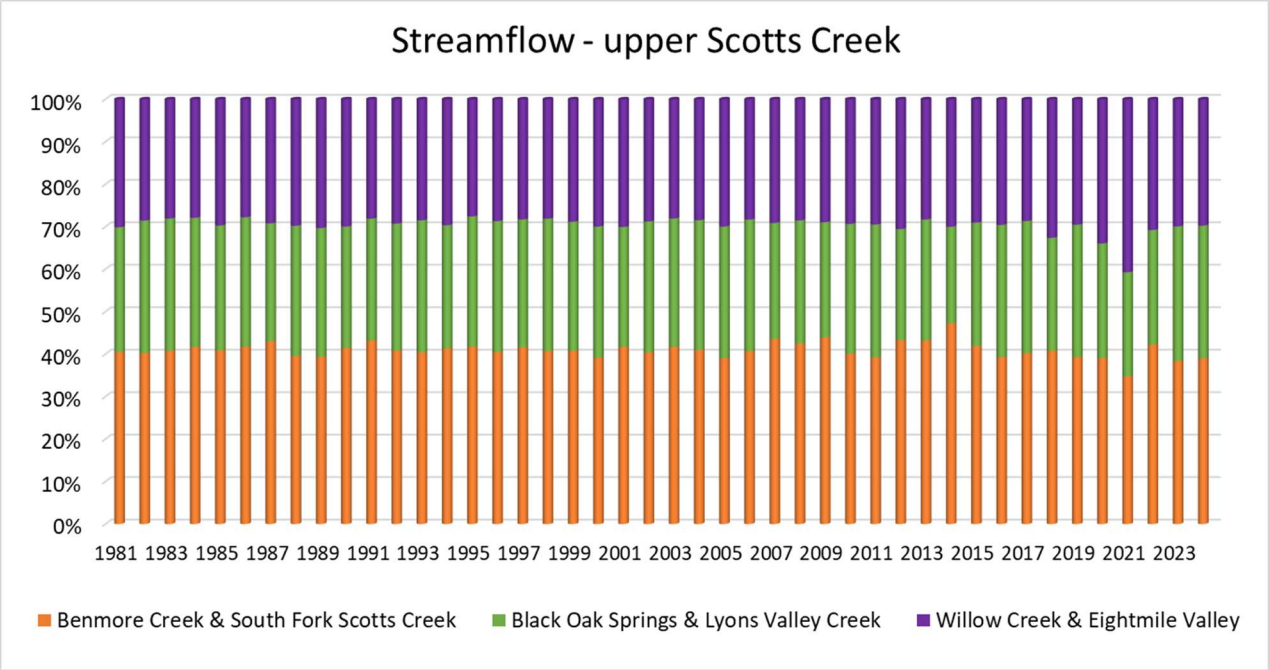

Figure 6.3.20. Stacked bar chart showing the relative contributions of streamflow for three major tributaries above the Scotts Creek below South Fork Scotts Creek near Lakeport gage.

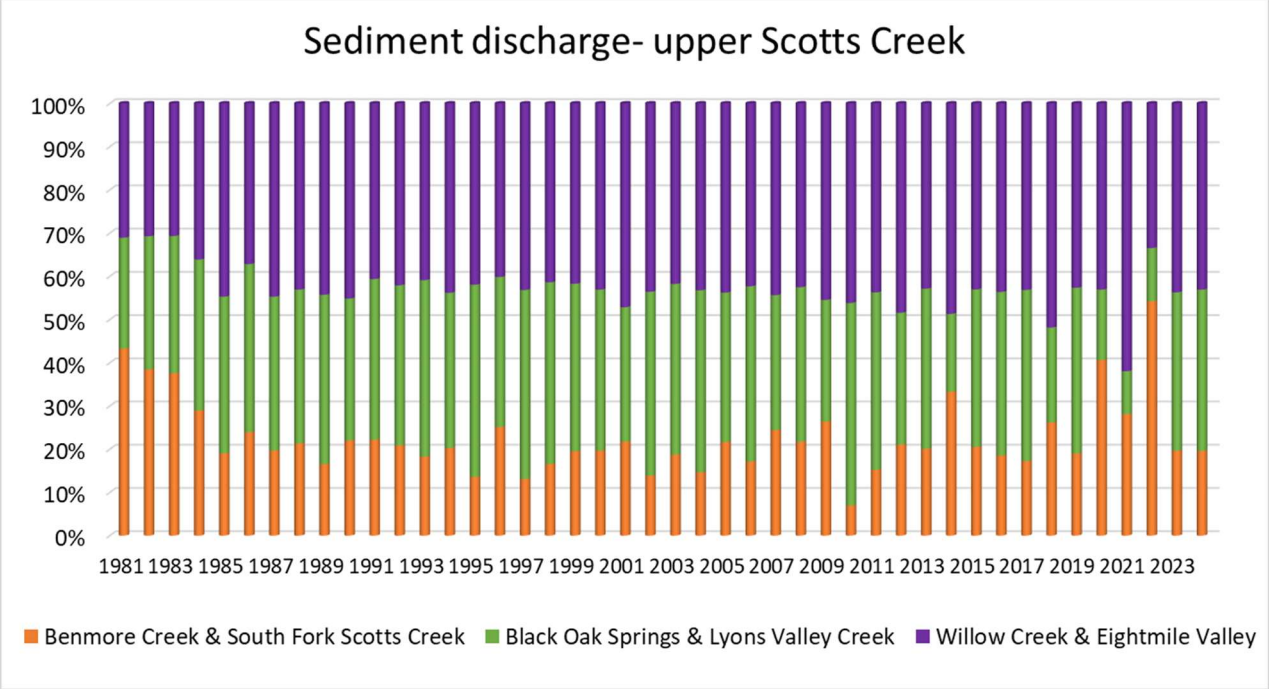

Figure 6.3.21. Stacked bar chart showing the relative contributions of sediment discharge for three major tributaries above the Scotts Creek below South Fork Scotts Creek near Lakeport gage.

Streamflow data below Tule Lake beginning in 2022 has led to a more complete understanding of the flow and sediment dynamics above and below Tule Lake. Streamflow peaks can be dampened and delayed by Tule Lake (Figure 6.3.22), and sediment dynamics are particularly sensitive to these changes in hydraulics. During storms

(periods of heavy precipitation), low flows occurring prior to the onset of the rising limb of the hydrograph, the flow will often switch directions for a few hours, flowing from Clear Lake to Tule Lake rather than from Tule Lake to Clear Lake. Although HSPF does not model bidirectional flows, the simulated streamflow shows a strong relationship to measured data and represents the flow dynamics well (Figure 6.3.8). More data during extreme high flows are needed to better understand the high flow dynamics of this system.

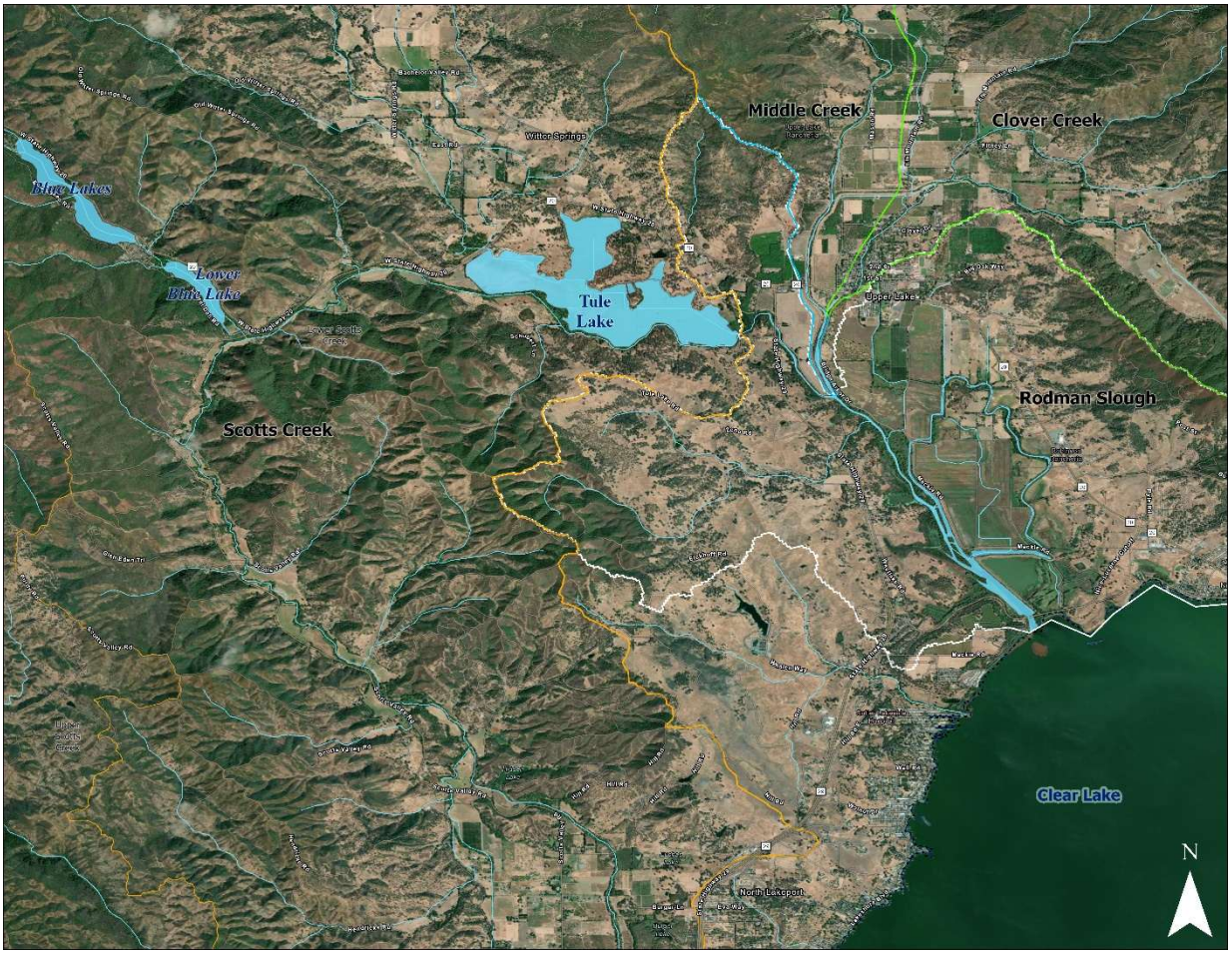

Figure 6.3.22. Lower Scotts Creek including Blue Lakes, Tule Lake, and the confluence of the Scotts Creek, Middle Creek, and Clover Creek watersheds. Base map from Esri and its licensors, copyright 2025.

Although many samples were taken in this watershed to characterize sediment transport dynamics, only 13 samples were taken below Tule Lake, and none were taken directly upstream of Tule Lake. However, the relationship between simulated and observed SSC at this location was good (Table 6.3.7) and resulted in a calibrated sediment transport model that determined Tule Lake has a roughly 36% trapping efficiency on average at an annual time step. The trapping efficiency of individual events or days will vary widely due to antecedent conditions, wind, temperature, and streamflow conditions. More data collection is needed to validate the relative contributions of Willow Creek and Eightmile Valley and the Black Oak Springs and Lyons Valley Creek locations to enable better understanding and management of sediment loads to Clear Lake.

6.3.11 Middle Creek restoration

An ongoing effort to restore the Middle Creek outflow to Clear Lake would reduce the channelization of the confluence of the three northern tributaries: Scotts Creek, Middle Creek, and Clover Creek by removing levees and adding more wetland area for the creeks to meander. The Clean Lakes Study (Richerson et al., 1994) recommended the restoration project to reduce the frequency and magnitude of harmful algal blooms, reduce erosion, and increase wetland and riparian restoration. The three streams flow into Rodman Slough and predominantly come from Scotts Creek, the largest tributary in the Clear Lake watershed. Scotts Creek contributed about 73% of the flow to Rodman Slough during 1981–2023. Middle Creek and Clover Creek contributed 24% and 3%, respectively (Figure 6.3.23). Scotts Creek contributed about 55% of the sediment discharge to Rodman Slough, whereas Middle Creek and Clover Creek contributed 44% and 0.4%, respectively (Figure 6.3.24).

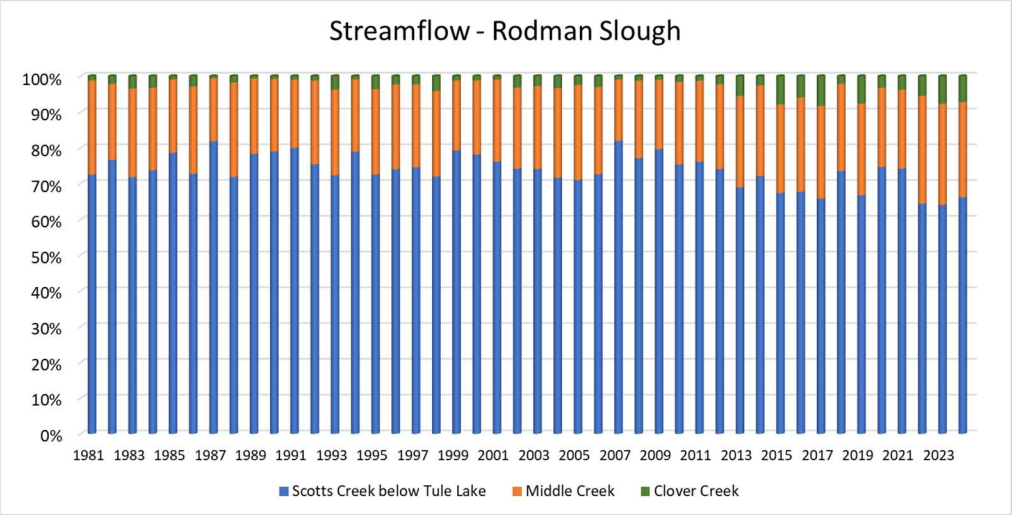

Figure 6.3.23. Stacked bar chart showing the relative contributions of streamflow for three major tributaries above Rodman Slough.

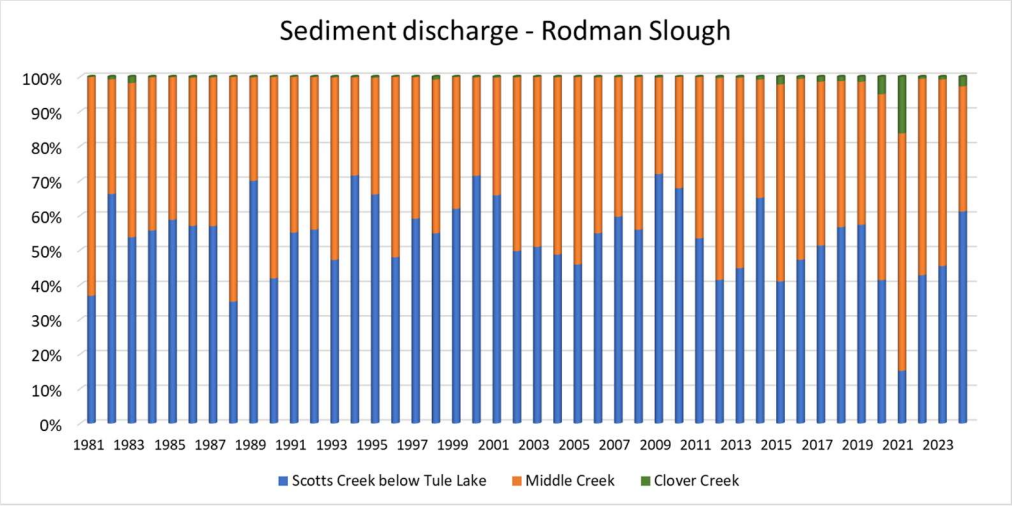

Figure 6.3.24. Stacked bar chart showing the relative contributions of sediment discharge for three major tributaries above Rodman Slough.

Building on the successful calibration of streamflow and sediment at Scotts Creek above and below Tule Lake, a hypothetical scenario was developed to simulate potential changes in streamflow and sediment to Clear Lake from the confluence of Scotts, Middle, and Clover Creeks (Rodman Slough). In HSPF, FTABLEs and sediment parameters were changed to achieve similar results to Scotts Creek above and below Tule Lake. These changes resulted in slightly lower flows; −1% on average but larger decreases in drought or dry years (Figure 6.3.25). Sediment discharge was more sensitive to these changes and resulted in a 33% reduction in sediment transport on average from 1981 to 2023 (Figure 6.3.26). However, the simulated reduction in sediment was widely variable depending on annual precipitation. In drought years like 2014, 2020, and 2021, sediment discharge decreased by 53%, 69%, and 83%, respectively. The average reduction in sediment discharge over the last 10 years was 43%.

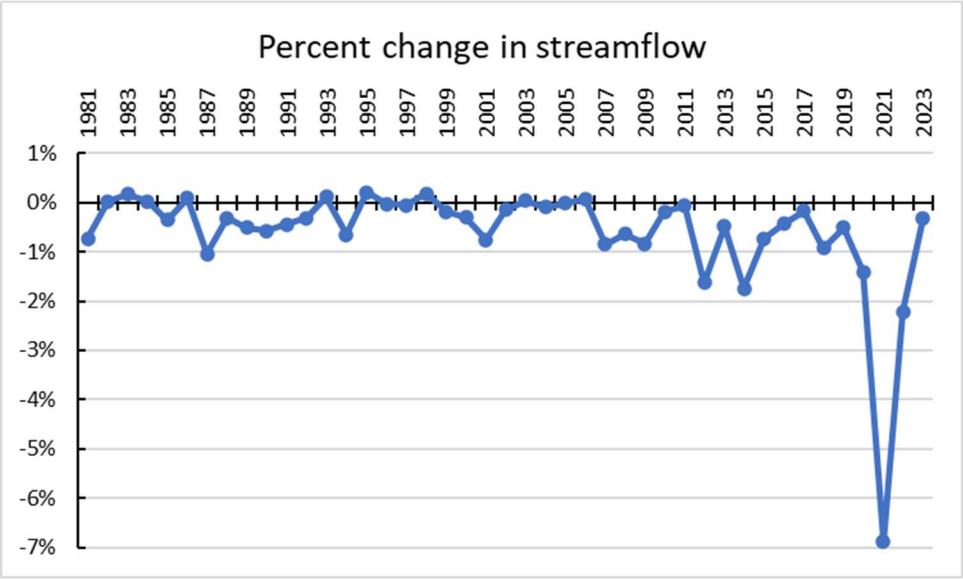

Figure 6.3.25. Percent change in annual streamflow at Rodman Slough post-restoration simulation.

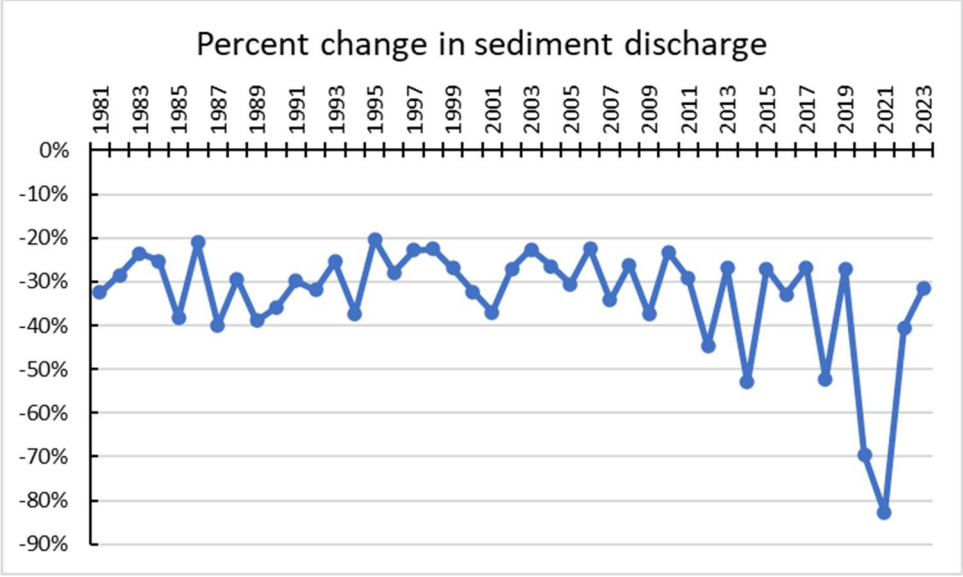

Figure 6.3.26. Percent change in annual sediment discharge at Rodman Slough post-restoration simulation.

6.3.12 Future climate scenario results

Four climate change scenarios were simulated using the calibrated HSPF tributary models. The hourly climate data were used as inputs, but the other model parameters remained the same to determine the potential impact on streamflow and sediment discharge to Clear Lake. Annual precipitation from the four climate scenarios is shown in Figure 6.3.27 along with the historical NLDAS precipitation data for reference. The historical precipitation data was generally less variable and lower in magnitude than any of the scenario baseline periods, especially pre-2000. Minimum temperature (Figure 6.3.28) showed a similar historical increasing trend as the NLDAS data; however, three out of four scenarios were shifted up by approximately 0.8 °F, and the MIROC6 scenario was shifted down by about the same amount. To reduce any potential bias from differences in these historical baselines, the historical period from each scenario was used to calculate future changes.

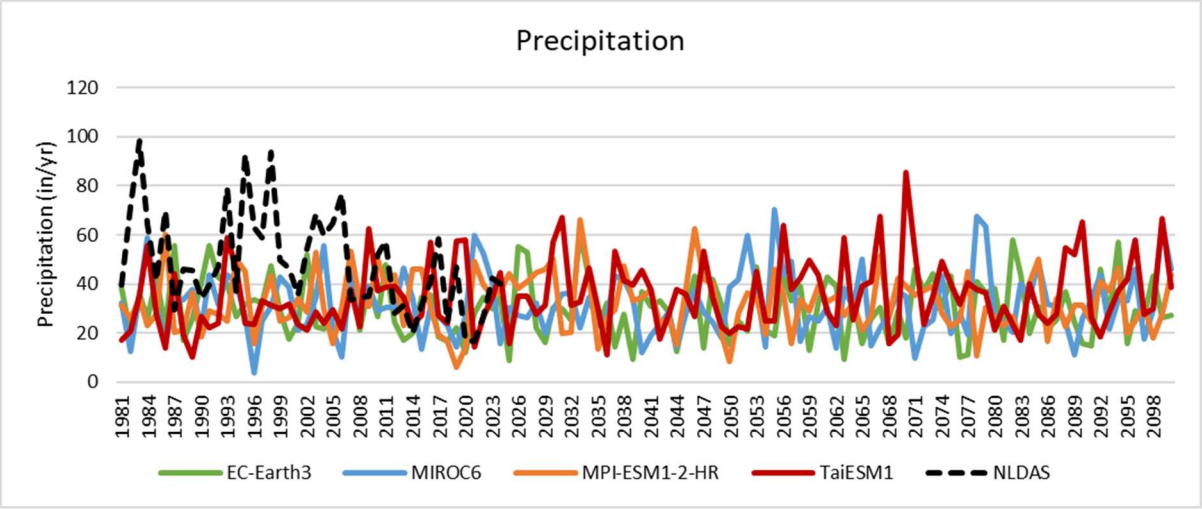

Figure 6.3.27. Water year total precipitation in inches per year for the four future scenarios and the historical NLDAS data used to calibrate the watershed model.

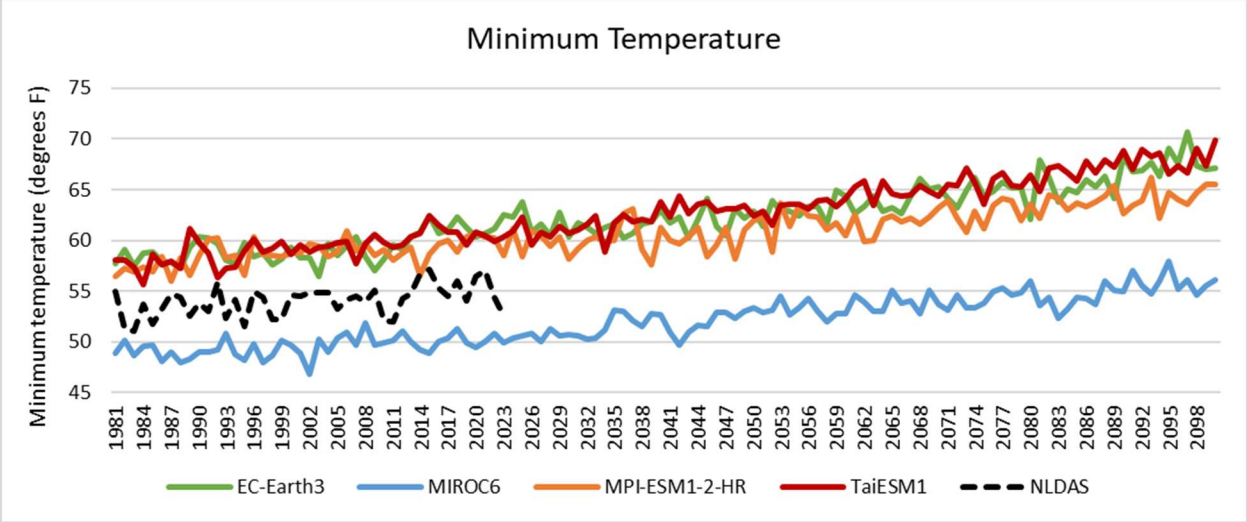

Figure 6.3.28. Water year average minimum temperature for the four future scenarios and the historical NLDAS data used to calibrate the watershed model.

By looking at the change between the scenario's historical period and three future 30-year periods, it is easier to see the average projected changes in air temperature and precipitation for this location (Figures 6.3.29A–C). The climate and hydrology results were summarized into the historical baseline (1981–2013), early century (2010–2039), mid-century (2040–2069), and end of century (2070–2099). Emissions forcings began in the year 2014, so the earliest 30-year period includes three years of historical baseline. The bias correction of each scenario was done using the 1980–2013 period. Minimum temperatures increased on average by 1.8 °F by early century, 3.9 °F by mid-century, and 6.4 °F by end of century. The TaiESM1 scenario was the warmest, increasing by 7.9 °F by end of century, and the coolest scenario was MPI-ESM1-2-HR, showing an end of century increase of 5.1 °F. Precipitation changes were not as clear, varying between −13% and +19% in early century, −13% to +14% in mid-century, and −8% to +25% by end of century. The TaiESM1 scenario is the hottest and wettest scenario overall, whereas the other scenarios tend to stay drier and relatively cooler than TaiESM1.

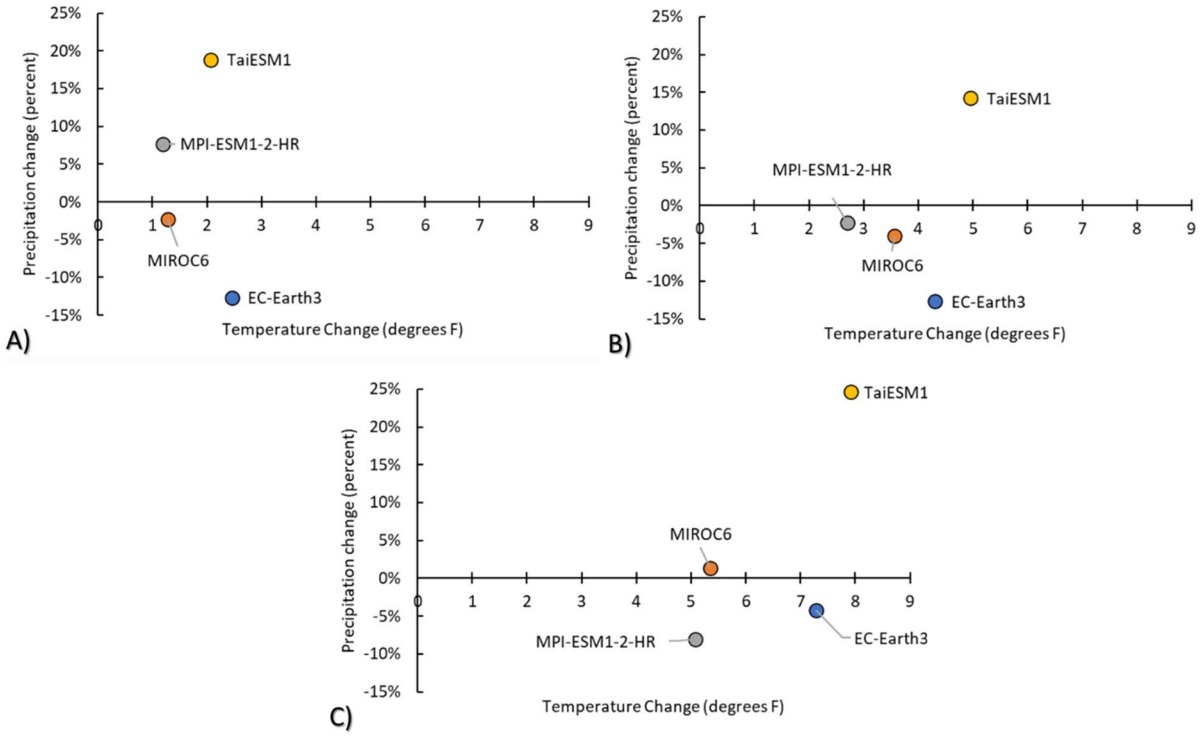

Figure 6.3.29. Change in temperature (x-axis) in degrees Fahrenheit, and changes in precipitation (y-axis) in percent for three 30-year averages: A) 2010–2039, B) 2040–2069, and C) 2070–2099.

Translating the changes in climate to changes in streamflow and sediment showed that streamflow is less sensitive to changes in temperature and precipitation than sediment discharge (Figure 6.3.30, Table 6.3.8). The EC-Earth3 scenario showed an increase of over 7 °F and a slight reduction in precipitation of 5%, which resulted in decreases of streamflow and sediment discharge of 13% and 14% by end of century, respectively (Figure 6.3.30, Table 6.3.8). The mid-century period for the EC-Earth3 scenario had the largest decrease in precipitation and led to decreases in streamflow and sediment discharge of 26% and 34%, respectively. The MIROC6 scenario showed smaller changes in precipitation and was cooler than the TaiESM1 and EC-Earth3 scenarios, resulting in a slight increase in streamflow of 2% and an increase in sediment discharge of 28% by the

end of the century. The MPI-ESM1-2-HR scenario had a wetter early century period and switched to drier by the middle and end of the century, resulting in decreases of 27% in streamflow and 32% in sediment discharge. TaiESM1 was the hottest and wettest scenario, resulting in the largest increases in streamflow and sediment discharge of 29% and 89%, respectively, by the end of the century.

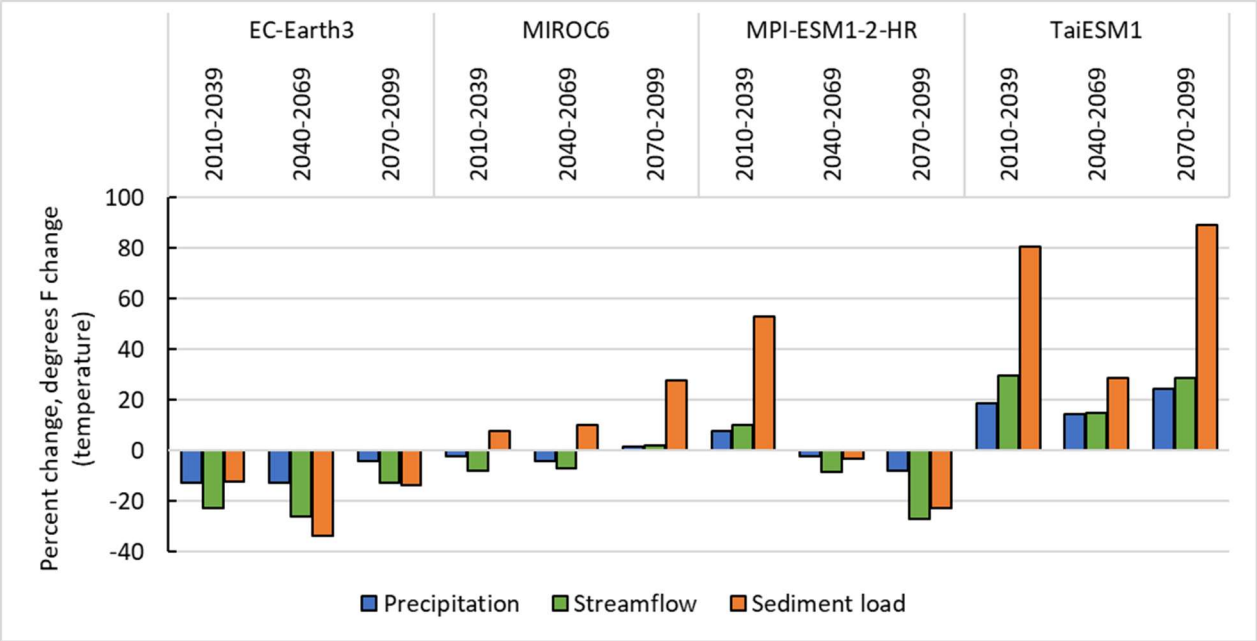

Figure 6.3.30. Percent change in precipitation, streamflow, and sediment loads for four climate scenarios and three 30-year periods.

Table 6.3.8. Streamflow and suspended sediment future climate scenario results summarized by 30-year period. T/yr, tons per year.

	EC-Earth3				MIROC6			
	Streamflow (cfs)	Sediment load (T/yr)	Streamflow change (%)	Sediment load change (%)	Streamflow (cfs)	Sediment load (T/yr)	Streamflow change (%)	Sediment load change (%)
1981–2012	490	108,000	-	-	392	92,200	-	-
2014–2039	377	95,000	−23	−12	360	99,400	−8	8
2040–2069	363	71,900	−26	−34	365	101,000	−7	10
2070–2099	426	93,400	−13	−14	400	118,000	2	28
	MPI-ESM1-2-HR				**TaiESM1**			
1981–2012	399	74,000	-	-	379	80,000	-	-
2014–2039	440	113,000	10	53	502	144,000	29	81
2040–2069	365	71,700	−9	−3	443	103,000	15	29
2070–2099	292	57,000	−27	−23	502	151,000	29	89

Any use of trade, firm, or product names is for descriptive purposes only and does not imply endorsement by the U.S. Government.

6.4 Sediment Fingerprinting

(by Charles N. Alpers, Jennifer A. Curtis, Connor J. McVey*, Michelle A. Stern, and Dina Saleh U.S. Geological Survey; *current affiliation, California State Water Resources Control Board)

6.4.1. Introduction

6.4.1.1 Background

Measures to improve water quality in Clear Lake (Figure 4.3.1) include efforts to reduce nutrient and sediment loads. Nutrient and sediment load estimates (see sections 6.1, 6.2, and 6.3) provide valuable water-quality datasets to assess the general location and the timing of nutrient and sediment delivery to Clear Lake. Water-quality data collected at gaged sites integrate nutrient and sediment delivery for large areas; however, the spatial resolution of these data may be insufficient for prioritizing restoration activities and determining the efficacy of implemented restoration projects.

Sediment fingerprinting approaches to determine sediment sources in watersheds have been developed and refined over the past two decades (Walling, 2005, 2013; Walling and Collins, 2005; Collins et al., 2010, 2012, 2017, 2020; Xu et al., 2022). The approach uses multivariate data to determine characteristics of sediment source types, and also may consider geologic rock types and land uses such as agriculture, forests, and urban sources (Carter et al., 2003; Gellis et al., 2015; Cashman et al., 2018; Williamson et al., 2023). In addition, sediment fingerprinting has been used to identify the contributions of tributaries (Zhang et al., 2012; Haddadchi et al., 2015; Habibi et al., 2019), an approach employed in this study.

This study tested the feasibility of discriminating the relative contribution of particulate nutrients and sediment to Clear Lake from watershed sources on the basis of the geochemical composition of source sediments using source attribution methods (Gellis and Walling, 2013) referred to as "sediment fingerprinting." Ad-hoc and opportunistic restoration projects have a lower likelihood for successfully reducing nutrient and sediment loads compared with strategic restoration accomplished by identifying land uses or stream reaches where implementation will have the highest likelihood of nutrient and sediment load reductions on the basis of a robust sediment source analysis.

Our approach to sediment fingerprinting for this project was to collect new geochemical and isotopic data for a representative suite of soil and sediment samples in the largest tributary watersheds to Clear Lake as well as samples of lakebed sediments in all three arms of the lake and delta sediments from Rodman Slough. We analyzed the fingerprinting data with a systematic statistical approach (Gellis et al., 2016, 2018; Gorman Sanisaca et al., 2017) to put constraints on tributary sediment sources.

6.4.1.2 Objective and Scope

The main objective of this sediment fingerprinting study was to determine the relative magnitude of sources of fine-grained sediment transported to Clear Lake with regard to geographic distribution, by tributary watershed. The first step in fingerprinting studies is to identify an **optimal set of tracers** for determining **diagnostic characteristics** for various **sediment sources.**

Once a suite of tracers is determined that identify source groups, multi-variate statistical techniques and mixing analyses are used to determine the relative contributions from various sediment sources for **target samples**. The target samples represent sediment mixtures composed of various proportions of sediment derived from the source groups.

In this report, source groups were discriminated by tributary watershed and two sets of target samples were evaluated: 1) 25 sample locations for shallow (top 4 centimeters, cm) sediment deposited in Clear Lake (total drainage area 1,099 square kilometers, km^2), and 2) three sediment sample locations in the Rodman Slough delta, which is the largest tributary (drainage area 467 km^2) to Clear Lake. The Rodman Slough delta samples were used to evaluate the relative contributions of sediment from the Scotts Creek, Middle, Creek, and Clover Creek watersheds, which are upstream of Rodman Slough (figures 6.4.1, 6,4,2, and 6.4.3).

The remainder of this section titled Sediment Fingerprinting (6.4) is divided into subsections on Methods (6.4.2), Results (6.4.3), Discussion (6.4.4), and Summary and Conclusions (6.4.5). The Results section includes subsections with details of two separate fingerprinting analyses (referred to as Trial 1 (6.4.3.1) and Trial 2 (6.4.3.2)), and additional subsections on Nutrient Speciation (6.4.3.3) and Mercury (6.4.3.4).

6.4.2. Methods

The strategy for choosing the number and types of soil and sediment sample locations for sediment fingerprinting calculations is explained below in the subsection on Study Design (6.4.2.1). Methods of sample collection, handling, and storage are explained in the subsection on Field Methods (6.4.2.2). Analytes and corresponding analytical methods are described in the subsection on Laboratory Methods (6.4.2.3). Statistical methods of data analysis used to determine **sediment source groups** are described in the subsection on Statistical Methods (6.4.2.4).

6.4.2.1 Study Design

In the Clear Lake watershed, sediment eroded from upland hillslopes and stream channels is transported and delivered to downstream receiving waters by various geomorphic processes (Lundquist and Smythe, 2010). The geochemical and isotopic fingerprint of sediment sources may reflect both current and past land-cover and land-use history, making it difficult to distinguish different source groupings on the basis of spatial criteria alone (Miller et al., 2015). We hypothesized that the sediment fingerprints for source samples collected from the tributary watersheds would be geochemically and isotopically distinct because of large variations in underlying geologic material.

The geologic map of the Clear Lake basin (Figure 6.4.4) shows a wide variety of rock types that are distributed in different proportions around the lake. A table indicating the percentages of area underlain by different geological formations in each tributary watershed to Clear Lake is provided in Appendix Table 15.6.4.1. An example of geological heterogeneity is that Quaternary volcanics are dominant in the Cole Creek watershed (84%) and are also present in the Kelsey Creek and Molesworth Creek watersheds (28% and 17%, respectively), but do not occur in the other tributary watersheds. Ultramafic rocks that are elevated in magnesium (Mg) and iron (Fe) may contain high concentrations of other metals including nickel (Ni), chromium (Cr), and

cobalt (Co), and are present in the Kelsey Creek watershed (12%) and the Adobe Creek watershed (5.5%) with a small proportion in the Scotts Creek watershed (0.34%).

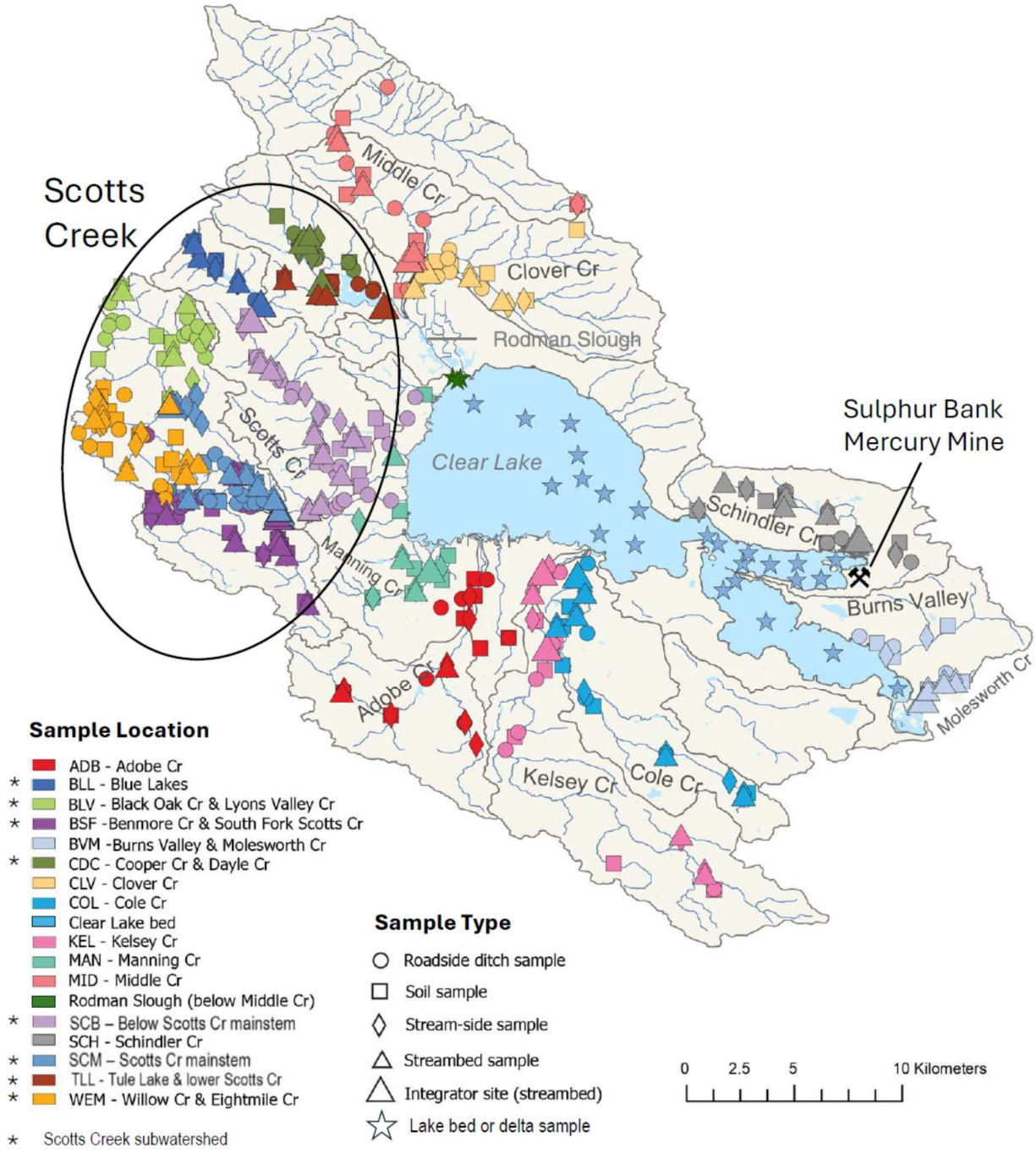

Figure 6.4.1. Map of the Clear Lake drainage basin showing locations of samples in the sediment fingerprinting study, indicating sixteen watershed and subwatersheds areas, Rodman Slough, and lakebed samples in Clear Lake, and location of Sulphur Bank Mercury MIne. Eight subwatersheds in the Scotts Creek watershed are indicated.

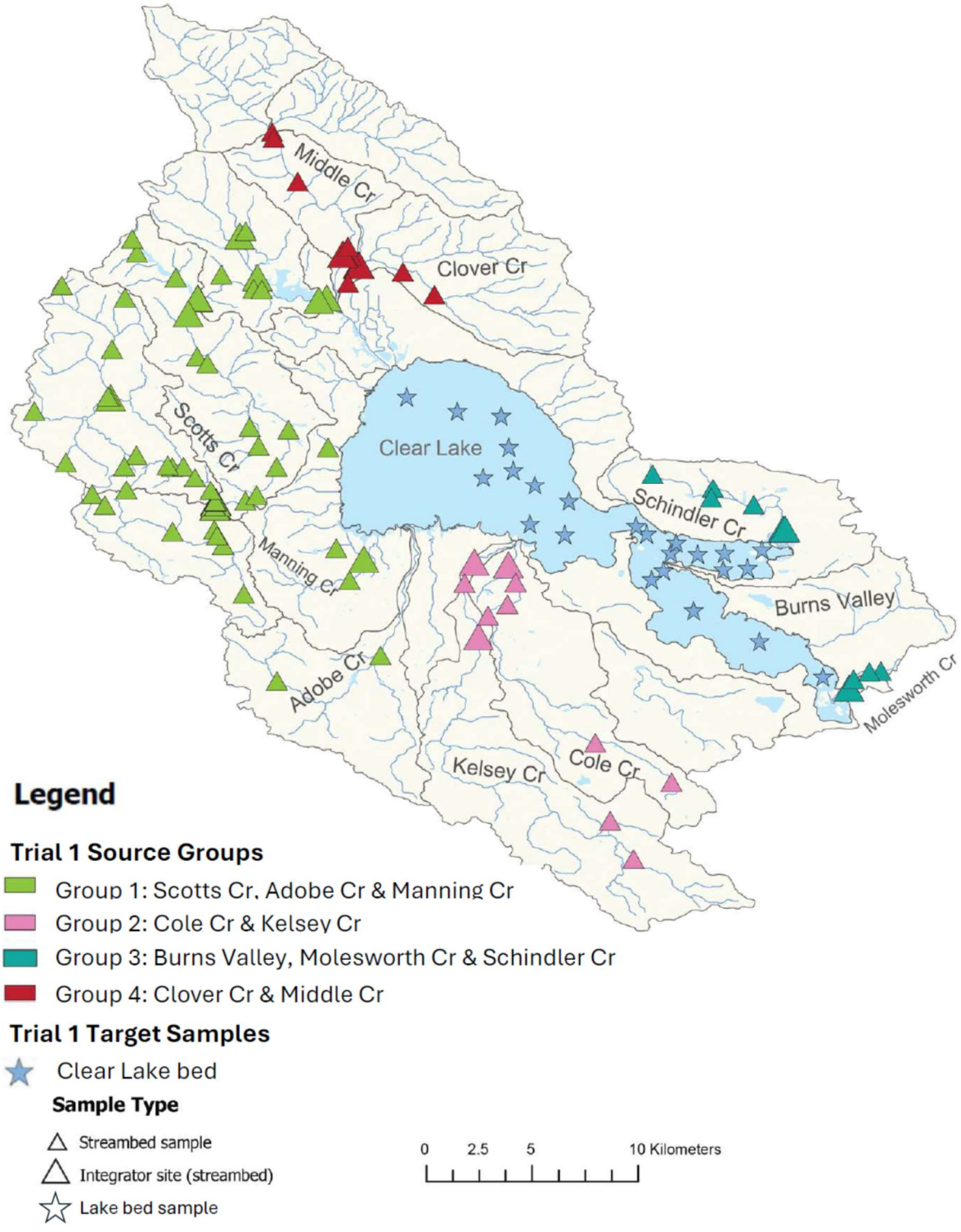

Figure 6.4.2. Map of the Clear Lake drainage basin showing locations of samples in the sediment fingerprinting study, indicating four source groups in tributary watersheds and lakebed target samples used in Trial 1 calculations.

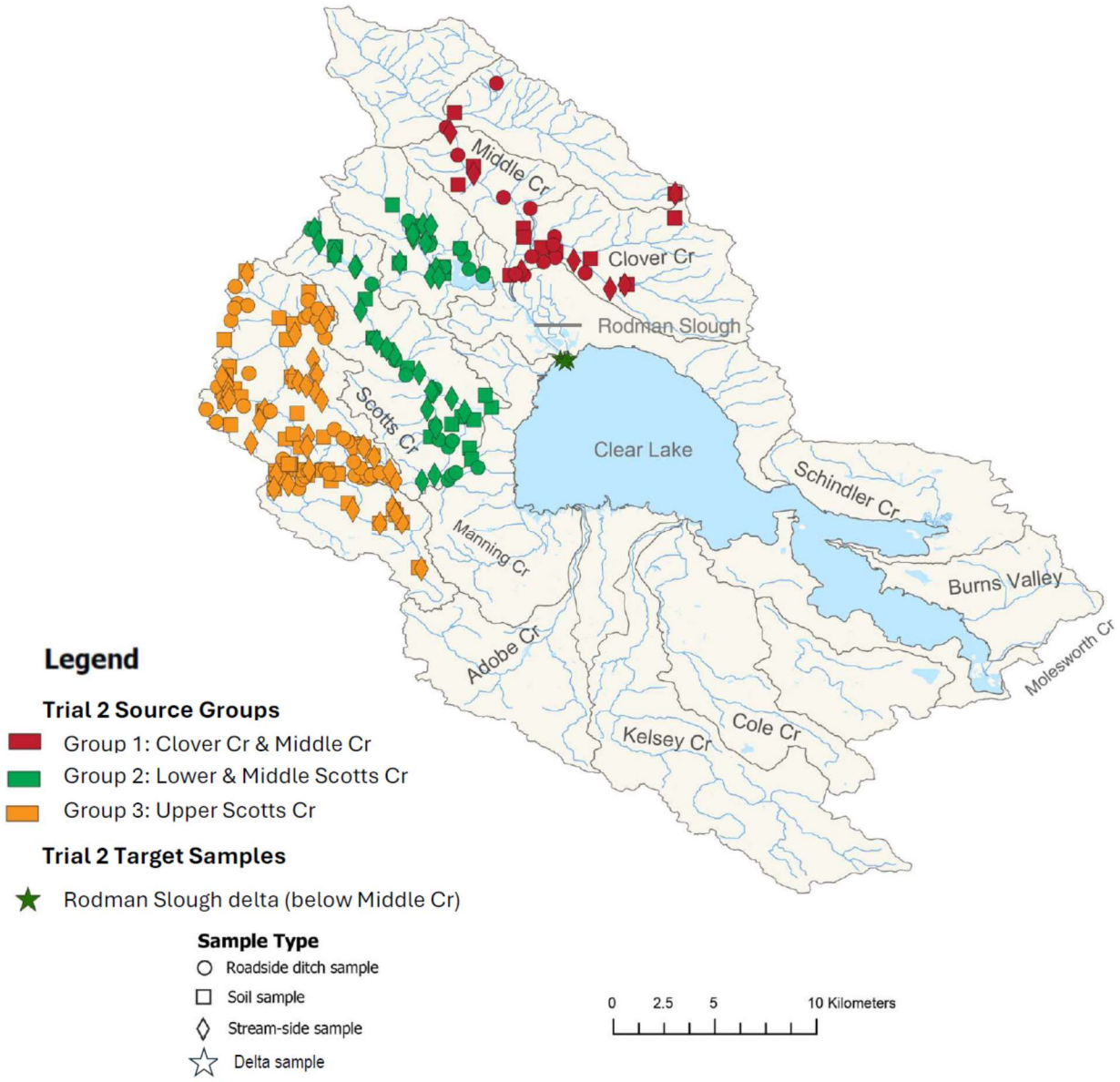

Figure 6.4.3. Map of the Clear Lake drainage basin showing locations of samples in the sediment fingerprinting study, indicating three source groups in tributary watersheds and target samples from Rodman Slough used in Trial 2 calculations.

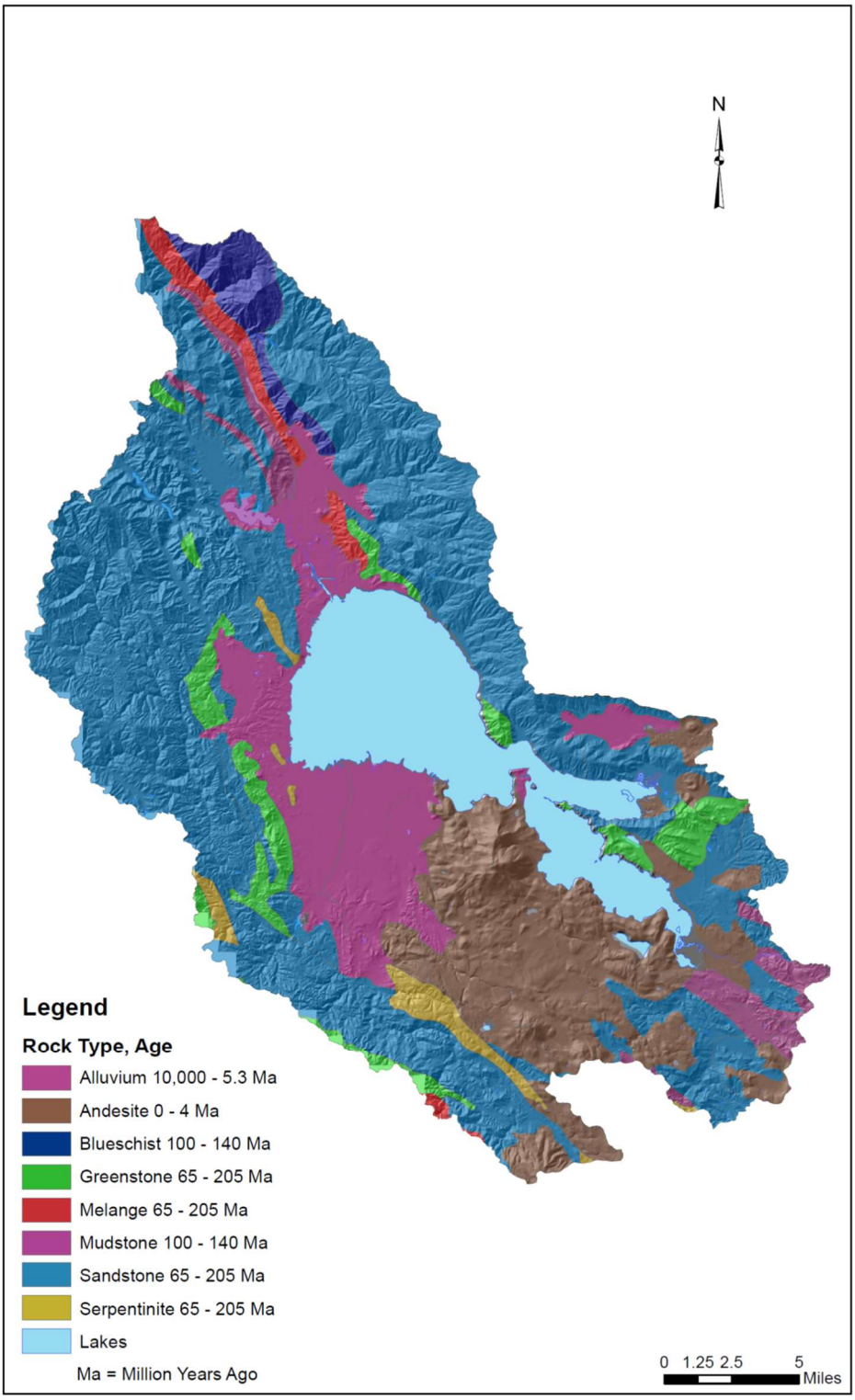

Figure 6.4.4. Geologic map of the Clear Lake drainage basin. From Lundquist and Smythe (2010). Map available at: https://www.lakecountyca.gov/DocumentCenter/View/4226/09-Plate-2-Clear-Lake-Watershed-Geology-PDF

During the summer and fall 2021, field observations indicated that sediment sources in the Clear Lake tributary watershed include: 1) **soils**, 2) **roadside ditches**, 3) **stream-side** sediment, and 4) **streambed** sediment. Stream-side sediment consists of true streambanks (floodplain deposits) and (or) colluvium or other sediment located adjacent to stream channels. The majority of stream-side samples collected for this study are interpreted as actual streambanks, i.e. alluvium or material deposited by the stream.

The sampling plan included nine of the largest tributary watersheds in the Clear Lake basin (Figure 6.4.1): Adobe Creek (ADB, 68 km^2), Burns Valley and Molesworth Creek (BVM, 33 km^2), Clover Creek (CLV, 70 km^2), Cole Creek (COL, 73 km^2), Kelsey Creek (KEL, 114 km^2), Manning Creek (MAN, 30 km^2), Middle Creek (MID, 129 km^2), Schindler Creek (SCH, 32 km^2), and Scotts Creek (268 km^2). The total drainage area of these nine watersheds is 817 km^2, which represents 74% of the entire Clear Lake drainage basin area (1,099 km^2).

The lowest streambed sampling location in each tributary watershed or subwatershed was designated as an **integrator** site. There were a total of 14 integrator sites, of which 9 sites represented entire tributary watersheds (designated as **lower integrator** sites) and 5 sites represented subwatersheds within Scotts Creek (Figure 6.4.1). The integrator sites are indicated by the larger triangles in Figures 6.4.1, 6.4.2, and 6.4.3. The integrator sites were located typically within 2 km of the downstream tributary confluence.

Streambed sediments are an effective surrogate for characterizing the geochemical character of watershed-derived sediment (Miller and Orbock Miller, 2007; Horowitz et al., 2012; Collins et al., 2013; Miller et al., 2015). The geochemical characteristics of select elements in the bed sediment may change over time (Collins et al., 2013). It is assumed that temporal variability represents variability in the proportion of various sources within the drainage rather than variability in the composition of the sources themselves. To incorporate temporal variability into the source sample datasets, streambed sediment was sampled monthly from July 2023 to December 2023 at the lower integrator sites.

The Scotts Creek drainage is the largest tributary to Clear Lake in surface area and in modeled flow of water and sediment transport (see section 6.3 on HSPF modeling). There is additional interest in quantifying sediment sources in upper Scotts Creek, particularly in the South Cow Mountain Off-Highway Vehicle (OHV) Management Area, which is maintained by the Bureau of Land Management (BLM). A total of **eight subwatersheds were sampled separately in the Scotts Creek watershed** (Figure 6.4.1). Four of the subwatersheds are in upper Scotts Creek: Benmore Creek / South Fork Scotts Creek (BSF), Black Oak Creek / Lyons Valley (BLV), Scotts Creek mainstem (SCM), and Willow Creek / Eightmile Creek (WEM); and four of the subwatersheds are in middle and lower Scotts Creek: Below Scotts Creek mainstem (SCB), Blue Lakes (BLL), Cooper and Dayle Creeks (CDC), and Tule Lake and lower Scotts Creek (TLL). The streambed site below Tule Lake is considered a lower integrator site, representing contributions from the entire Scotts Creek watershed.

The minimum number of samples needed for a robust statistical analysis for a complex study involving many variables can vary with physical scale. A sample size of 10 to 15 observations per explanatory variable (Babyak, 2004) is a widely used guideline. Other recommendations often cited in the literature are 10 to 20 observations per explanatory variable (Harrell, 2001) and 50 observations plus 8 additional observations for each

explanatory variable (Green, 1991). The Sediment Source Assessment Tool (**Sed_SAT**) used in this project recommends at least 10 samples per sediment source type (Gorman Sanisaca et al., 2017). Smaller samples sizes (5<N<20) can provide useful results but typically have non-normal distributions that require non-parametric statistics, which have less statistical power (Ingre, 2013).

Sediment and soil sampling locations were chosen to ensure **similar sample densities** across **land use and land cover** categories (Dewitz, 2023), **bedrock geology** (McLaughlin et al., 2018), and **wildfire history** (Monitoring Trends in Burn Severity, 2021). The chosen analytes (discussed below in the section on Laboratory Methods, 6.4.2.3) required a minimum of 15 grams of fine material (< 0.063 mm). Some samples that were collected did not have a sufficient amount of fine material after sieving, so they were not analyzed. Most of the samples with insufficient fine material were streambed sediments. These sites were not resampled because of time constraints. This resulted in some imbalance in the distribution among sample types (Table 6.4.1).

In all, 579 samples were collected during 2021–23 that had sufficient fine material for all analyses (Watanabe et al., 2025). Of these, 400 samples were selected for a mixing model analysis in two trials. In Trial 1, 140 stream sediment samples from all nine tributaries, were divided into four source groups (Table 6.4.1; Figure 6.4.2), and 26 shallow bed sediment samples collected from Clear Lake (Table 6.4.1, Figure 6.4.5) were used as target samples for unmixing calculations. In Trial 2, 231 samples of soil, roadside ditch, and streamside sediment from the Clover Creek, Middle Creek, and Scotts Creek watersheds were divided into three source groups (Table 6.4.2, Figure 6.4.3) and 3 samples from the Rodman Slough delta (Figure 6.4.3) were used as targets for unmixing calculations. There were at least 14 streambed samples from each of the four source groups in Trial 1, and at least 9 samples of each of the three site types in each of the three source groups in Trial 2. Samples that were analyzed but not used in modeling described in this report included field replicates designated for sampling and laboratory QA/QC, and soil, roadside ditch, and streamside samples from the watersheds not included in Trial 2. Those samples may be used in future modeling efforts focused on individual watersheds.

Table 6.4.1. Sample counts used in modeling watershed source groups and target samples in Trial 1. All source samples were from streambeds (including integrator sites). Field replicate samples were excluded, with one exception noted.

Trial 1 Source Groups		**Number of samples**
1	Scotts Cr, Adobe Cr & Manning Cr	92
2	Cole Cr & Kelsey Cr	14
3	Burns Valley, Molesworth Cr & Schindler Cr	18
4	Clover Cr & Middle Cr	16
	Total	140

Trial 1 Target Samples	Number of samples
Clear Lake - Upper Arm	11
Clear Lake - Oaks Arm*	9
Clear Lake - Lower Arm	6
Total	26
* includes one field replicate	

Table 6.4.2. Sample counts used in modeling for watershed source groups and target samples in Trial 2. Field replicate samples were excluded.

Trial 2 Source Groups		Site Type - Number of samples			
		Soil	Streamside	Roadside Ditch	Total
1	Clover Cr & Middle Cr	11	9	13	33
2	Lower & Middle Scotts Cr	24	25	25	74
3	Upper Scotts Cr	42	39	43	124
	Total	77	73	81	231

Trial 2 Target Samples	Number of samples
Rodman Slough delta	3

Figure 6.4.5. Map of Clear Lake showing target sample locations for Trial 1. Yellow symbols, Upper Arm; red symbols, Oaks Arm; green symbols, Lower Arm. Numbers 902-928 refer to sample numbers SFS-0902 through SFS-0928 in Watanabe et al. (2025).

At a subset of sampling locations (9 lower integrator sites, 1 upper integrator site, and 26 Clear Lake sites), a split of sediment was collected for nutrient speciation analysis by the University of California, Davis (UCD) Tahoe Environmental Research Center (TERC) laboratory. These splits were frozen in the field at the time of collection, as described in the next subsection (6.4.2.2). At the integrator sites, a six-month time series of samples was collected during July–December 2023 to assess seasonal variations. In all, 101 samples were analyzed for nutrient speciation, representing 29 bed sediment samples from Clear Lake and 72 samples from tributaries (including field replicates). Additional details are provided below in the sections on Field Methods (6.4.2.2), Laboratory Methods (6.4.2.3) and Results (6.4.3).

6.4.2.2 Field Methods

Soil, roadside ditches, streamside, and streambed source samples were collected using a modification of standard USGS methods (Shelton and Capel, 1994). Rather than sieving in the field, the samples were dry sieved after air-drying at the USGS laboratory in Denver, Colorado, as described in the next subsection on Laboratory Methods (6.4.2.3). Samples were collected using single-use plastic scoops and clean-hands methods; for example, a new pair of disposable powder-free nitrile gloves were used for each sample. Where necessary, a clean stainless-steel trowel or shovel was used to clear away vegetation or coarse material.

Samples of soil, roadside ditches, streamsides, and streambed sediment were collected from October 2021 to December 2023 in the tributary watersheds. Samples of lakebed sediment in Clear Lake were collected during September 12–14, 2023.

For each sample from the tributary watersheds, approximately 3 kilograms of solid material was collected in a gallon-sized zippered plastic bag (double-bagged). Pebbles and organic matter greater than 1 centimeter in size were excluded by hand-picking. For soil sampling, material was scooped from six locations within one meter from a central location (Figure 6.4.6). At each streambed and roadside ditch sampling site, sediment was collected from six locations with recently deposited or representative sediment.

Streambed sampling methods differed slightly in dry and wet channels. If the streambed was dry, six pits were made along a cross-section perpendicular to the streamflow direction and sediment was sampled to a depth of 5 cm. If the stream channel had water, fine-grained sediment was collected near the water's edge on or both sides of the stream at six representative locations over a 100-meter reach.

Roadside ditches were sampled opportunistically at six representative locations, typically along a reach of 10 to 100 meters along unpaved roads. Streamside sampling locations included streambanks, colluvium, or alluvium and were sampled along vertical channels excavated with hand tools with the goal of representing the entire vertical section of material potentially mobilized by bank erosion.

After collection, the samples were stored in a cooler on wet ice, then transferred to a refrigerator. The samples were shipped to the USGS laboratory in the Geology, Geophysics, and Geochemistry Science Center in Denver, Colorado for processing.

For splits of the samples collected at integrator streambed sites intended for nutrient speciation analysis, approximately 1 kg of material was placed in a zippered plastic bag (double-bagged) and placed on dry ice in the field. For frozen splits at lake sites,

approximately 20 grams of material was placed in two 20 mL plastic scintillation vials. Following collection, the samples were stored in a freezer, then shipped on dry ice to the Tahoe Environmental Research Center laboratory in Incline Village, Nevada.

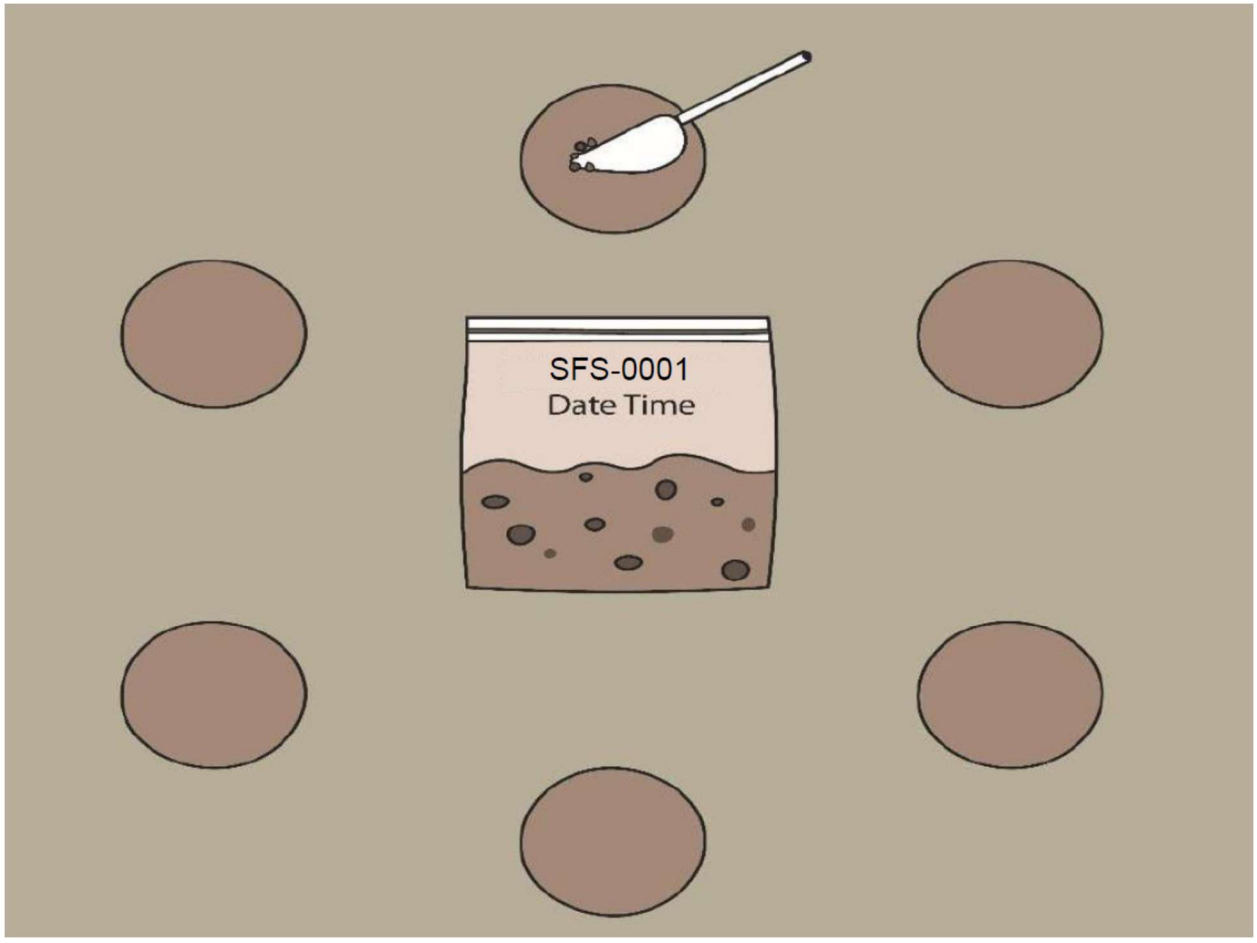

Figure 6.4.6. Layout for soil samples (modified from McVey, 2023). The six pits are located approximately one meter from a central location.

Lakebed samples were collected using a stainless steel Eckman dredge, a device that is set vertically on the lake bottom and spring-loaded jaws are activated by sending a messenger weight down the connecting cable. The collection area is square, 6 inches (15 cm) on each side. When successfully deployed, the Eckman dredge collects a representative sample from the sediment-water interface. In this study, the top 1.5 inches (4 cm) of sediment were recovered using a 3-inch (8 cm) diameter plastic core liner and a thin, rigid plastic sheet. Samples were transferred to pre-cleaned glass jars and stored on wet ice.

Field replicate samples were taken at a rate of about 12% across all sample types. For tributary sites, the replicates were collected from the same excavations as the primary samples and composited in a separate bag. For lake sites, an additional Eckman dredge sample was collected for each replicate.

In the field, sample locations and photographs were recorded using the ArcGIS Field Maps application (Esri, Redlands, California). A paper field data sheet was used for notes,

sketches, and a written backup of sample location coordinates. Paper field sheets were photographed or scanned for archival purposes.

6.4.2.3 Laboratory Methods

At a USGS laboratory in Denver, Colorado (Geology, Geophysics, and Geochemistry Science Center, GGGSC, Sample Control Laboratory), soil and sediment samples were air dried (typically over a period of one to three weeks), then sieved to less than 0.063 millimeters (mm) (63 micrometers, µm, or 0.0025 inches; No. 230 mesh). A minimum of **15 grams of fine material** was needed for the analyses listed in Table 6.4.3. Method references and detailed lists of analytes are available in a USGS data release (Watanabe et al., 2025).

Table 6.4.3. *Analytes, methods, and laboratories for analyses on < 0.063 mm size fraction of soils and sediments for sediment fingerprinting study. [USGS, U.S. Geological Survey; UCD, University of California, Davis; SIF, Stable Isotope Facility; TERC, Tahoe Environmental Research Center; WDXRF, wavelength dispersive x-ray fluorescence; ICP-OES-MS, inductively coupled plasma – optical emission spectrometry – mass spectrometry; C, carbon; Li, lithium; N, nitrogen; Na, sodium]*

Analytes	Laboratory	Method	Reference
Total Sulfur and Total Carbon	USGS Contract Lab	Combusion, infrared	USGS (2022) Methods 2 and 3
Carbonate Carbon (inorganic Carbon)	USGS Contract Lab	Coulometry	USGS (2022) Method 4
Total Mercury (Hg)	USGS Contract Lab	Cold vapor atomic absorption	USGS (2022) Method 5
Loss on Ignition	USGS Contract Lab	Heating, weighing	USGS (2022) Method 15
Major elements	USGS Contract Lab	WDXRF, Li-borate fusion	USGS (2022) Method 15
61 elements	USGS Contract Lab	ICP-OES-MS, Na-peroxide fusion	USGS (2022) Method 18
C-N isotopes and concentrations	UCD SIF	Mass spectrometry	UCD SIF (2024)
Particle Size Distribution	UCD TERC	Laser diffraction	Beckman Coulter Inc. (2019)

Concentrations of total organic carbon (TOC) were calculated by subtracting carbonate carbon (CarbC) from total carbon (TC). The TOC concentrations were used to determine the optimal amount of material to be loaded into foil capsules for analysis of carbon and nitrogen (C and N) stable isotopes by the UCD Stable Isotope Facility (SIF) laboratory. Loading of the foil capsules was done by the UCD College of Agriculture and Environmental Sciences Analytical Laboratory (Anlab). Samples which had detectable carbonate carbon were acid-treated to remove the carbonate, so the C-isotope analyses obtained for this study pertain only to the organic fraction of the soil or sediment. Measurements of carbon and nitrogen stable isotopes by the UCD SIF were made by mass spectrometry after combustion using Elementar Vario EL Cube or Micro Cube elemental analyzer (Elementar Analysensysteme GmbH, Hanau, Germany) interfaced to either an Isoprime VisION IRMS (Elementar UK Ltd, Cheadle, United Kingdom) or a PDZ Europa 20-20 isotope ratio mass spectrometer (Sercon Ltd., Cheshire, United Kingdom)(University of California, Davis, Stable Isotope Facility, 2024). Concentrations of total organic nitrogen (TON) and TC were determined by the UCD SIF using the elemental analyzer. There was excellent agreement between TC carbon concentrations reported by UCD SIF and the TOC values computed using data for TC minus CarbC from the USGS Contract Lab (SGS, Inc., Burnaby, British Columbia Canada). The carbon stable isotope ratio $^{13}C/^{12}C$ was reported as $\delta^{13}C$ relative to Vienna Pee Dee Belemnite (VPBD) and the nitrogen stable isotope ratio $^{15}N/^{14}N$ was reported as $\delta^{15}N$ relative to air; both were reported in parts per thousand (per mil).

Loss on ignition (LOI), measured by percentage mass lost by heating to 550 °C, is well known to correlate with TOC in soils (De Vos et al., 2005) and in lake sediments, and is sometimes used to estimate TOC. In some studies, plots of LOI versus TOC show linear (or slightly non-linear) trends with a slope of approximately 0.5 to 0.6. Regressions lines from some studies pass through the origin, or near to it, with small intercept values (e.g., Sutherland, 1998; Leipe et al., 2011); that is, TOC typically makes up about half of the total organic content, interpreted as the mass lost in LOI analyses. A plot of the data from this study (Figure 6.4.7) indicates that many samples have LOI values in the approximate range of 4% to 10% with very low concentrations of TOC (< 1%) which implies a non-organic source of volatiles lost during heating. The data in Figure 6.4.7 also show a quasi-linear trend at higher LOI and TOC values with a slope of approximately 0.5.

The line on Figure 6.4.7 labelled with equation (1) goes through the origin (0,0) with a y-intercept of 0. The line labelled with equation (2) has a y-intercept of –2.5, and the line labelled with equation (3) has a y-intercept of –5.

$$TOC = 0.5*LOI \quad (1)$$

$$TOC = 0.5*LOI - 2.5 \quad (2)$$

$$TOC = 0.5*LOI - 5 \quad (3)$$

Most of the data from this study plot between the lines defined by equations (2) and (3), below the line with no intercept (equation 1). This is likely caused by the presence of clay minerals such as kaolinite and illite/smectite, which contain structural water that is released at the temperature of the LOI measurement (550 °C; Sun et al., 2009). Because LOI is highly correlated with TOC, rather than use LOI in the sediment fingerprinting calculations we introduced the tracer LOI-2TOC which was computed as follows:

$$LOI\text{-}2TOC = LOI - 2*(TOC) \quad (4)$$

where LOI is the loss on ignition (in percent, %), and TOC is the concentration of organic carbon determined by the difference of total carbon and carbonate carbon, using analyses from the USGS Contract Lab. Values of LOI-2TOC in the source samples range from 0.7 to 12.8 % with a median of 5.3%. This tracer is considered to be proxy for the abundance of minerals with structural water such as kaolinite and smectite, and is similar to the mineral structure water loss (SWL) parameter of Sun et al. (2009).

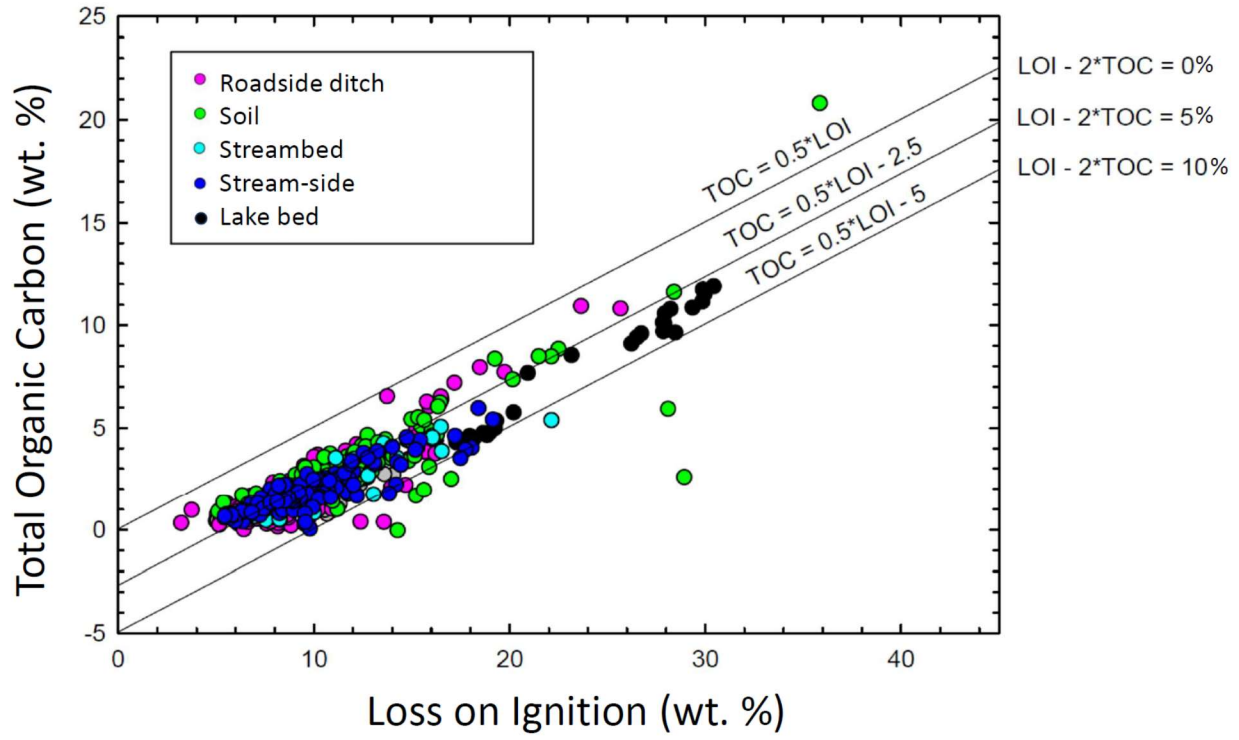

Figure 6.4.7. Plot of Loss on Ignition (LOI) versus total organic carbon (TOC) concentration. See text for explanation of diagonal lines. Data summarized from Watanabe et al. (2025).

For selected sediment samples collected at integrator sites, and all lake sites (Figures 6.4.2 and 6.4.5), a split sample was frozen in the field using dry ice as described in the Field Methods section (6.4.2.2), and stored frozen until delivered to the UCD TERC laboratory (Incline Village, Nevada). These samples were analyzed for nutrient speciation, as detailed in Table 6.4.4. These samples were not sieved in the field, but were sieved to < 2 mm at the TERC laboratory after thawing.

Table 6.4.4. *Analytes for selected frozen split samples, sieved to < 2 mm at the University of California, Davis Tahoe Environmental Research Center laboratory. [TKN, total Kjeldahl nitrogen]*

Forms of Phosphorus (P)	
	Loosely Bound P
	Iron-Aluminum associated P
	Calcium-associated P
	Residual P

Forms of Nitrogen (N)	
	Organic, ammonia, and ammonium (TKN)
	Nitrate and nitrite
Particle Size Distribution	

Particle size distributions (PSD) for both sample sets (chilled samples sieved to < 0.063 mm and frozen samples sieved to < 2 mm, Tables 6.4.3 and 6.4.4, respectively) were determined at the UCD TERC lab using an LS 13 320 laser diffraction analyzer (Beckman Coulter Life Sciences, Indianapolis, Indiana). Median particle size (D50) was determined directly by the instrument. Each sample was analyzed in duplicate. If the D50 values had a relative percent difference (RPD) greater than 10%, a third analysis was made. The two analyses with the closest D50 values were averaged. The raw PSD data were input to a MATLAB (Mathworks, Inc., Natick, Massachusetts) routine that combined the two runs and computed detailed statistics including 50 particle-size bins (at ¼-phi intervals) and cumulative distributions at 5 percentile intervals.

6.4.2.3.1 Quality Assurance and Quality Control

Rigorous quality-assurance and quality-control (QA/QC) procedures were followed for all analytes. Reference samples of known composition were submitted for chemical analyses along with samples at rate of about 10%.

Five reference materials (SAR-L.1, SAR-L.2, SAR-M.1, SAR-M.2, and SAR-H) were analyzed routinely along with the environmental samples. In all, 85 analyses by reference materials were done by wavelength dispersive x-ray fluorescence (WDXRF; major elements) and inductively coupled plasma – optical emission spectrometry – mass spectrometry (ICP-OES-MS; 61 elements). The analyses of reference materials indicated that analyses for nearly all elements were routinely within 15% of the expected amount present (Watanabe et al., 2025). Some elements (and methods) for which results for reference samples were more than 15% different than expected concentrations were: boron (by ICPMS), beryllium (ICPMS), and vanadium (WDXRF).

Results for field replicates (n = 57 for most analytes) had median relative percent difference (RPD) values less than 15% for all analytes and less than 10% for nearly all analytes. The analytes (and methods) with median RPD values between 10% and 15% were: antimony (ICPMS), mercury (by cold vapor atomic absorption spectroscopy, CVAAS), and barium (WDXRF).

QA/QC analyses for C-isotopes ($\delta^{13}C$) and N-isotopes ($\delta^{15}N$) by the UCD SIF were made on 15 reference materials. The average absolute difference in $\delta^{13}C$ for reference materials from the expected values was 0.08 per mil (‰) based on 448 analyses. For $\delta^{15}N$, the average absolute difference from the expected values of the reference materials was 0.06 ‰ based on 472 analyses (Watanabe et al., 2025).

Analyses of total C and total N concentrations by the UCD SIF were checked using a glutathion reference material. Total C (78 analyses) and total N (52 analyses) were both within about 1% of the expected amounts (recovery of 100.9% for C and 101.1% for N).

Variability of results for nutrient speciation (90 environmental samples) was assessed using 11 field replicates. Median values of RPD for field replicate pairs were less than 15% for iron (Fe)-aluminum (Al)-associated phosphorus, calcium (Ca)-associated phosphorus, and total phosphorus. Values of RPD were greater than 15% for loosely bound phosphorus (18%), residual phosphorus (18%), total nitrogen (17%), and nitrate plus nitrite (42%)(Watanabe et al., 2025). Additional details regarding laboratory methods and associated QA/QC are provided by Watanabe et al. (2025).

6.4.2.4 Statistical Methods

We used the Sediment Source Assessment Tool (**Sed_SAT**), jointly developed by the USGS and the U.S. Environmental Protection Agency (EPA; Gellis et al., 2016; Gorman Sanisaca et al., 2017; Gellis et al., 2018), to determine the relative contributions of fine-grained (< 0.063 mm) sediment to Clear Lake and to the Rodman Slough delta from various upstream sediment sources using standardized statistical methods. The Sed_SAT tool optimizes a minimal set of geochemical characteristics, or "sediment fingerprint" for user-defined source groups. The "sediment fingerprints" for each source group were used to determine the relative contributions from each sediment source for each target sample using an unmixing model (Collins et al., 2010).

Sed_SAT uses the mean concentration values of the geochemical and isotopic tracers and linear discriminant analysis to determine representative sediment fingerprints for each source group. The use of the mean concentration values is physically realistic because target samples represent sediment mixtures that are composed of material mobilized and delivered from various upstream sediment sources. The composite fingerprints for target samples defined using the mean concentrations of source samples collected from a range of locations and site types throughout the basin are assumed to represent natural mixing of sediment sources during transport and delivery (Collins et al., 2010).

6.4.2.4.1 Source Groups and Target Samples

In Trial 1, we used 140 samples of streambed sediment from 9 tributary watersheds to Clear Lake as the source materials for the fingerprinting calculations, and we used 26 lakebed sediments from Clear Lake as targets. In Trial 2, we used 231 samples of soil, roadside ditch sediment, and stream-side sediment from three tributary watersheds as source materials, and 3 samples of delta sediment from Rodman Slough as targets.

For Trial 1, the source materials were organized into 4 source groups (Table 6.4.1, Figure 6.4.2). The distribution of samples among the source groups was weighted heavily toward source group 1 (Scotts Cr., Adobe Cr., and Manning Cr.), which represented 66% of the samples. The other three source groups each represented 10% to 13% of the samples. Target samples for Trial 1 were distributed fairly evenly among the three arms of Clear Lake (Table 6.4.1) and in proportion to their relative area, with 42% in the Upper Arm (the largest of the three arms), 35% in the Oaks Arm, and 23% in the Lower Arm.

For Trial 2, the source samples were organized into 3 source groups (Table 6.4.2, Figure 6.4.3). The distribution of samples among the source groups was weighted toward source group 1 (Upper Scotts Cr.) which represented 54% of the samples. Source group 2 (Lower and Middle Scotts Cr.) was represented by 32% of the samples, and the remaining 14% of the samples were from source group 3 (Clover Cr. and Middle Cr.). The distribution of the three sample types (soil, roadside ditch sediment, and streamside sediment) was balanced among the three source groups (Table 6.4.1).

We used **Linear Discriminant Analysis (LDA)** initially within JMP Statistical Software (v.17; JMP Statistical Discovery LLC, Cary, North Carolina) to determine the *a priori* effectiveness of the source groups and to confirm that the source groups could be discriminated on the basis of geochemical and isotopic characteristics. LDA is a multi-variate statistical method used to determine a combination of tracers that explains differences between the source groups, assuming normality and equal within-group covariance matrices. This analysis confirmed that there are differences in geochemical and isotopic characteristics among the source groups. Additional LDA calculations were performed within the **Sed_SAT** tool, as described in the following subsection (6.4.2.4.2).

6.4.2.4.2 Effective Geochemical Fingerprints

We followed a standardized fingerprinting approach using the **Sed_SAT** tool developed by Gorman Sanisaca et al. (2017). Sed_SAT is a freely available, comprehensive tool with user prompts that follow a step-by-step workflow. The steps include: (1) imputation (replacing missing values) for censored (non-detect) data, (2) transformations to meet statistical assumptions of normality and homoscedasticity (homogeneity of variance), (3) outlier test (using 3 standard deviations, or 3σ, from the mean), (4) corrections to control for particle size and organic content when relationships show statistically significant (R^2 > 0.5) regressions, (5) "bracket test" to ensure each tracer concentration for the target samples is conservative relative to the concentrations in source samples (±10%), (6) stepwise discriminant function analysis to discriminate fingerprints for each sediment source, (7) source apportionment using an unmixing model to determine the relative contributions from each sediment source, and (8) error analysis using 1,000 Monte-Carlo simulations to examine sensitivity of the results. See Gorman Sanisaca et al. (2017) for more information on the statistical procedures.

Missing values in source samples can be imputed, but target samples cannot (Gorman Sanisaca et al., 2017). Each source type is assumed to be unique and unrelated to the other source types; therefore, the tracer relationships should be maintained and imputation can be run. Target samples cannot be imputed because each sample is considered unique and therefore independent. Tracers with non-detects for target samples that were excluded from the Sed_SAT analysis included: sulfur (S), silver (Ag), arsenic (As), beryllium (Be), cadmium (Cd), germanium (Ge), indium (In), molybdenum (Mo), rhenium (Re), selenium (Se), tin (Sn), tantalum (Ta), tellurium (Te), thallium (Tl), and tungsten (W). One tracer (silicon, Si), with values that exceeded the lab reporting limit, was excluded from the **Sed_Sat** analysis.

We implemented multivariate normal (MVN) imputation in JMP (v. 17) to estimate missing values for non-detects. MVN computes least-squares predictions from source samples for each source type.

- Trial 1: Clear Lake targets
    - Tracers with non-detects (values less than the lab detection limits) that were imputed in JMP using MVN imputation included: bismuth (Bi) (N=12)
- Trial 2: Rodman Slough targets
    - Tracers with non-detects (values less than the lab detection limits) that were imputed in JMP using MVN imputation included: Bi (N=18), lead (Pb) (N=1), and antimony (Sb) (N=1)

Outliers can cause bias in statistical tests (Zimmerman, 1974); however, outliers should not be removed automatically because they can contain valuable data (Helsel et al., 2020). In the **Sed_SAT** program, outlier removal is a manual procedure. We used the default value of 3 standard deviations, or 3σ, from the mean to identify and remove outliers from the source sample datasets.

The source and target samples were corrected for particle size because finer-grained materials have greater surface area, which provides additional sites where tracers can attach by adsorption, leading to higher concentrations (Collins et al., 2010; Horowitz and Elrick, 1987) that may bias the study results. Similarly, samples with higher organic content have additional sites for sorption of tracers (Collins et al., 2010; Horowitz and Elrick, 1987). The rationale for applying correction factors for particle size and organic content to source samples in relation to target samples for Sed_SAT calculations is explained in detail by Gellis et al. (2016).

The optimization of geochemical and isotopic characteristics and definition of sediment fingerprints for each sediment source heavily influences the reliability of the study results (Walling, 2013). **Tracers that do not meet the assumptions** inherent in unmixing modeling **are eliminated** and **tracers that are most effective for discriminating** sediment sources **are identified** resulting in a robust and parsimonious unmixing model.

Unmixing models require that tracers display conservative behavior with no enrichment or depletion of tracer values by physical (e.g. hydraulic sorting) or chemical processes (e.g. weathering) during transport and deposition (Mukundan et al., 2012). We used three methods to **eliminate potential biases** related to non-conservative behavior:

1. We constrained our sediment source analysis to fine sediment (< 0.063 mm) and therefore results of the fingerprinting analysis for the target samples only apply to fine-sediment fraction;

2. Using a "bracket test," we identified non-conservative tracers and removed them from the analysis; and

3. We corrected for the effects of particle size (using D50) and organic matter (using TOC).

In all, 52 tracers were used in the **Sed_SAT** analysis (Table 6.4.5).

Table 6.4.5. *Analytes used as potential tracers in the Sed_SAT tool. [δ13C, carbon stable isotope ratio 13C/12C relative to Vienna Pee Dee Belemnite (VPBD); δ15N, nitrogen stable isotope ratio 15N/14N relative to air; CarbC; carbonate (inorganic) carbon; TOC, total organic carbon; TON, total organic nitrogen; Al, aluminum; Ca, calcium; Fe, iron; K, potassium; Mg, magnesium; Na, sodium; Si, silicon; Ti, titanium; B, boron; Ba, barium; Ce, cerium; Co, cobalt; Cr, chromium; Cs, cesium; Cu, copper; Dy, dysprosium; Er, erbium; Eu, europium; Ga, gallium; Gd, gadolinium; Hf, hafnium; Ho, holmium; La, lanthanum, Li, lithium; Lu, lutetium; Mn, manganese; Nb, niobium; Nd, neodymium; Ni, nickel; Pb, lead; Pr, praseodymium; Rb, rubidium; Sb, antimony; Sc, scandium; Sm, samarium; Sr, strontium; Tb, terbium; Th, thorium; Tm, thulium; U, uranium; V, vanadium; Y, yttrium; Yb, ytterbium; Zn, zinc; Zr, zirconium; LOI, loss on ignition]*

Groups	**Parameters**
Forms of Carbon	Carbonate (CarbC), Organic (TOC)
Forms of Nitrogen	Organic (TON)
Stable Isotopes	$\delta^{13}C$, $\delta^{15}N$
8 major elements	Al, Ca, Fe, K, Mg, Na, Si, Ti
38 minor / trace elements	B, Ba, Bi, Ce, Co, Cr, Cs, Cu, Dy, Er, Eu, Ga, Gd, Hf, Ho, La, Li, Lu, Mn, Nb, Nd, Ni, Pb, Pr, Rb, Sb, Sc, Sm, Sr, Tb, Th, Tm, U, V, Y, Yb, Zn, Zr
LOI-2TOC	see text and equation (4)

We ran the Sed_SAT tool using the recommended default parameters. After identifying and removing non-conservative tracers and correcting for particle size and organic matter, we used a forward stepwise discriminant function analysis (DFA) to identify optimal sediment fingerprints. TOC was used to correct for the effects of organic matter and was also used as a model parameter.

6.4.2.4.3 Unmixing Model and Uncertainty Analysis

A significant source of uncertainty in the fingerprinting approach is the inherent variability of the geochemical characteristics for the source samples that can result in multiple statistically equivalent solutions that result in similar model performance for different source contributions (Collins et al., 2010; Rowan et al., 2012). This uncertainty is commonly referred to as the equifinality problem.

Additional sources of error that may contribute to uncertainty in the sediment fingerprinting approach include: poor sampling density for one or more sources, lab analytical errors associated with characterization of geochemical tracers, and non-conservative behavior during transport or due to weathering following deposition that changes the physical or chemical characteristics of source sediments.

Errors associated with sampling density were addressed by designing a robust field sampling campaign and determining source groups with near-equal numbers of samples. Lab errors were minimized by QA/QC procedures explained in the Laboratory Methods section (6.4.2.3) and the associated data release (Watanabe et al., 2025). Non-conservative tracers were identified using a bracket test that ensures the range of tracer values measured for the target samples falls within the range of values measured for the sources sampled. Note that the bracket test often eliminates soluble elements or ions (e.g. sodium (Na), chloride (Cl^-), and P) and elements associated with organic matter (Miller et al., 2015). Corrections for particle size and organic matter were applied using standardized methods explained by Gellis et al. (2016).

After identifying optimal fingerprints for each source group, we used the **unmixing model** (Gorman Sanisaca et al., 2017) to quantify the relative source contributions for each target sample. Model error (sensitivity and uncertainty) related to inherent variability in the source samples (Small et al., 2004; Collins et al., 2010, 2017) was quantified using 1,000 Monte Carlo simulations using a "leave-one-out" approach for each model run. All other model parameters used in Sed_SAT trials were default values (Gorman Sanisaca et al., 2017). Input files for Sed_SAT Trials 1 and 2 (data for source and target samples) are provided in Watanabe et al. (2025).

6.4.2.4.4 Analysis of Variance (ANOVA)

Differences in the sediment fingerprints between the source groups were evaluated for each of the tracers selected by the Sed_SAT model using the Kruskal-Wallis one-way variance on ranks, a form of analysis of variance (ANOVA), using SigmaPlot (v. 15, Inpixon, Palo Alto, California). Analysis on ranks is a **non-parametric test** that **does not require a normal distribution** of data. SigmaPlot (v.15, Inpixon (now Grafiti), Palo Alto, California) was used for the calculations. **Groups that differ from the others were isolated** using an all pairwise multiple comparison procedure (Dunn's Method), run as a post-hoc, non-parametric test. Letters were assigned to signify differences and displayed on box plots. For example, A and B are statistically different groups, whereas AB indicates overlap with both groups A and B.

6.4.2.4.5 Unmixing Model Trials

Trial 1. Basin Scale: Clear Lake targets with 4 watershed source groups

In Trial 1, the Sed_SAT source discrimination and unmixing model tools were run with 4 watershed source groups and 1,000 Monte Carlo simulations for 26 target lake samples (Figure 6.4.5). The 4 source groups included: 1) Scotts Creek, Adobe Creek, and Manning Creek, 2) Cole Creek and Kelsey Creek, 3) Burns Valley, Molesworth Creek, and Schindler Creek, and 4) Clover Creek and Middle Creek (Figure 6.4.2).

Trial 2. Partial Basin Scale: Rodman Slough delta targets with 3 watershed source groups

In Trial 2, the Sed_SAT source discrimination and unmixing model were run with 3 watershed source groups and 1,000 Monte Carlo simulations for 3 target samples collected from the Rodman Slough delta, where it drains into Clear Lake (Figure 6.4.3). The three source groups included: 1) Clover Creek and Middle Creek, 2) Lower and Middle Scotts Creek, and 3) Upper Scotts Creek (Figure 6.4.3).

6.4.3 Results

6.4.3.1 Trial 1 - Basin Scale: Clear Lake targets with 4 watershed source groups

6.4.3.1.1 Classification in Trial 1

In Trial 1, after starting with 140 streambed sediment samples from all nine tributary watersheds sampled, outlier analysis excluded 25 samples (18%) leaving 115 samples for further analysis. No corrections were needed for particle size or organic matter. Tracers excluded from the analysis because of non-conservative behavior included: Na, mercury (Hg), niobium (Nb), neodymium (Nd), P, lead (Pb), praseodymium (Pr), antimony (Sb), silicon (Si), samarium (Sm), terbium (Tb), titanium (Ti), thulium (Tm), TOC, TON, and zirconium (Zr).

The DFA correctly classified 94.79 % of the source samples in the 4 source groups. The biplot (Figure 6.4.8) shows that there was good discrimination among some of the source groups, but source groups 1 and 4 overlap when only the axes LD1 and LD2 are considered. For additional discussion of uncertainty and model error, see section 6.4.3.1.4, below.

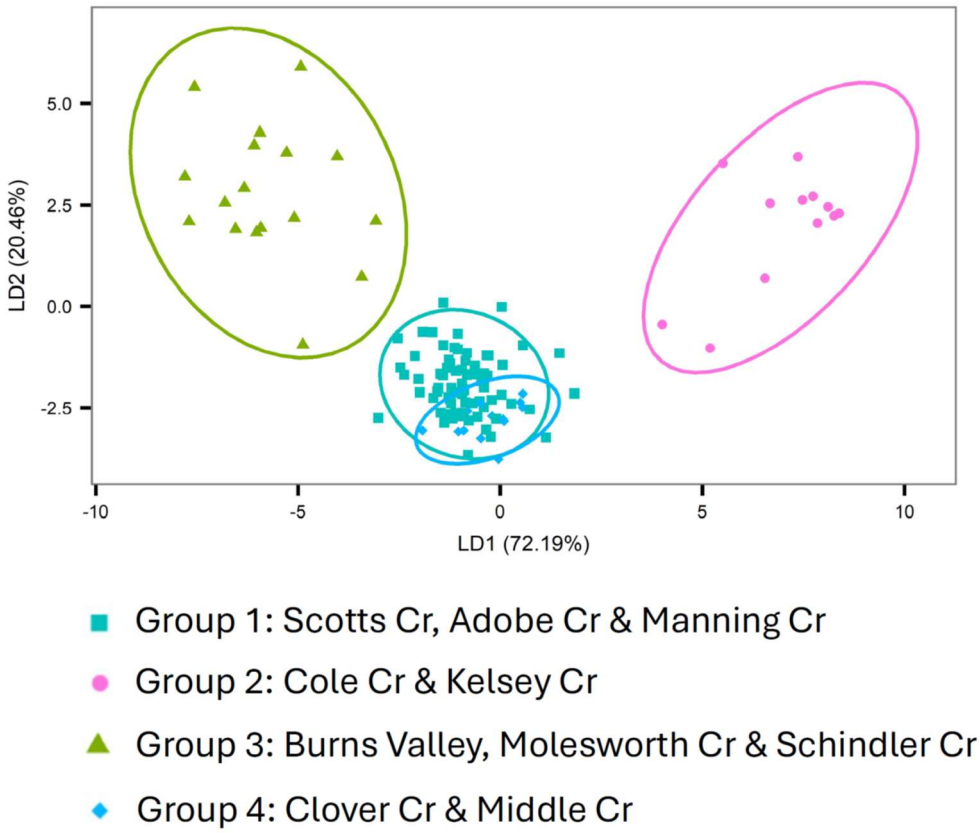

Figure 6.4.8. Linear Discriminant Analysis (LDA) results biplot for Trial 1 from the Sediment Source Assessment Tool (Sed_SAT), showing overlap among two of the four source groups. The LDA biplot shows predicted values from the first two linear discriminants. The first two linear discriminants do not show the full discriminatory power of the analyses when there are 3 or more source groups. The confusion matrix for Trial 1 (Appendix Table 15.6.4.4) shows the percentage of samples correctly classified by the complete linear discriminant function for each source group. Sed_SAT input data from Watanabe et al. (2025). [LD1, linear discriminant 1; LD2, linear discriminant 2]

6.4.3.1.2 Tracers in Trial 1

In Trial 1, 12 tracers were found by Sed_SAT to have utility in distinguishing among the four source groups. The diagnostic tracers were (in order of decreasing discriminatory power): potassium (K), rubidium (Rb), chromium (Cr), cesium (Cs), Mg, lithium (Li), LOI-2TOC (see equation (4)), barium (Ba), strontium (Sr), uranium (U), scandium (Sc), and yttrium (Y)(Appendix Table 15.6.4.2). Box plots showing concentration data for these tracers in the four source groups are provided in Figures 6.4.9 through 6.4.14. These figures also show the results of ANOVA testing of significant differences among source groups for each tracer.

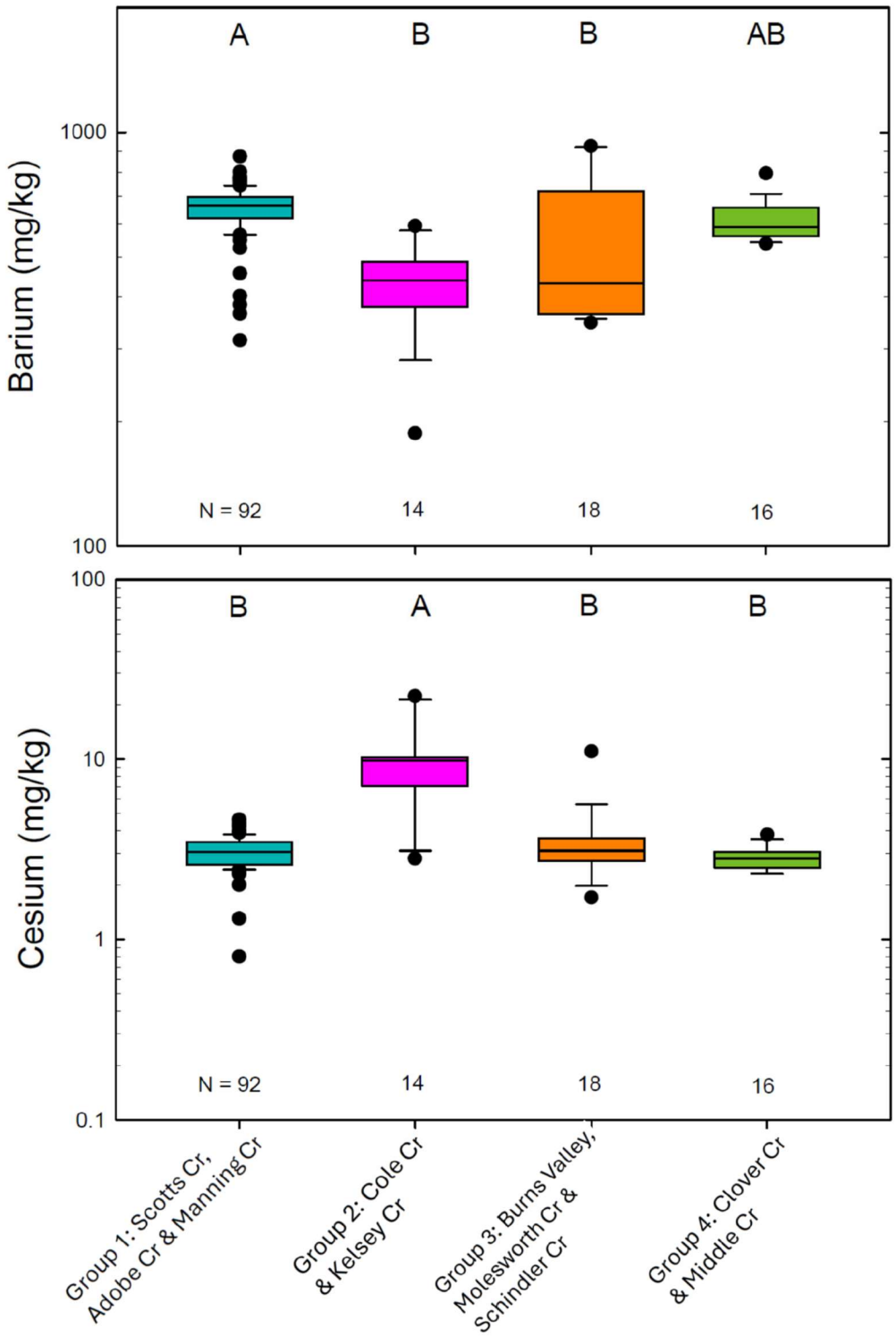

Figure 6.4.9. Box plots for barium and cesium (logarithmic scale). Letters at top indicate statistical differences among four source groups in Trial 1, using analysis of variance (ANOVA) on ranks. Boxes indicate interquartile range; horizontal lines indicate median; whiskers indicate 10th and 90th percentiles; circles indicate results below 10th percentile or above 90th percentile. Numbers at the bottom indicate the number of samples (N) in each source group. Colors match those used in Figures 6.4.15 and 6.4.16, which show the unmixing model results. Data summarized from Watanabe et al. (2025). [mg/kg, milligram per kilogram]

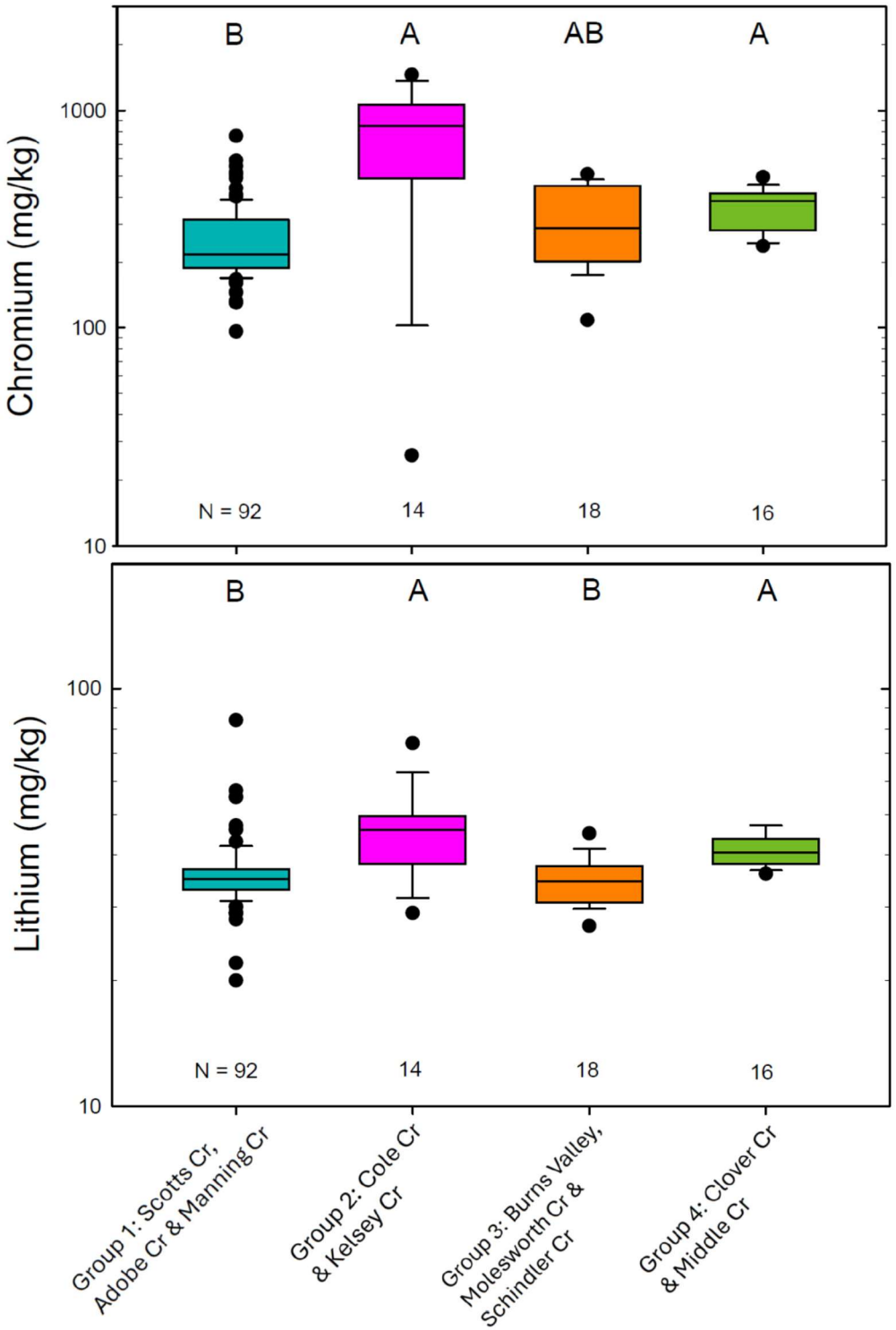

Figure 6.4.10. Box plots for chromium and lithium (logarithmic scale). Letters at top indicate statistical differences among four source groups in Trial 1, using analysis of variance (ANOVA) on ranks. Boxes indicate interquartile range; horizontal lines indicate median; whiskers indicate 10th and 90th percentiles; circles indicate results below 10th percentile or above 90th percentile. Numbers at the bottom indicate the number of samples (N) in each source group. Colors match those used in Figures 6.4.15 and 6.4.16, which show the unmixing model results. Data summarized from Watanabe et al. (2025). [mg/kg, milligram per kilogram]

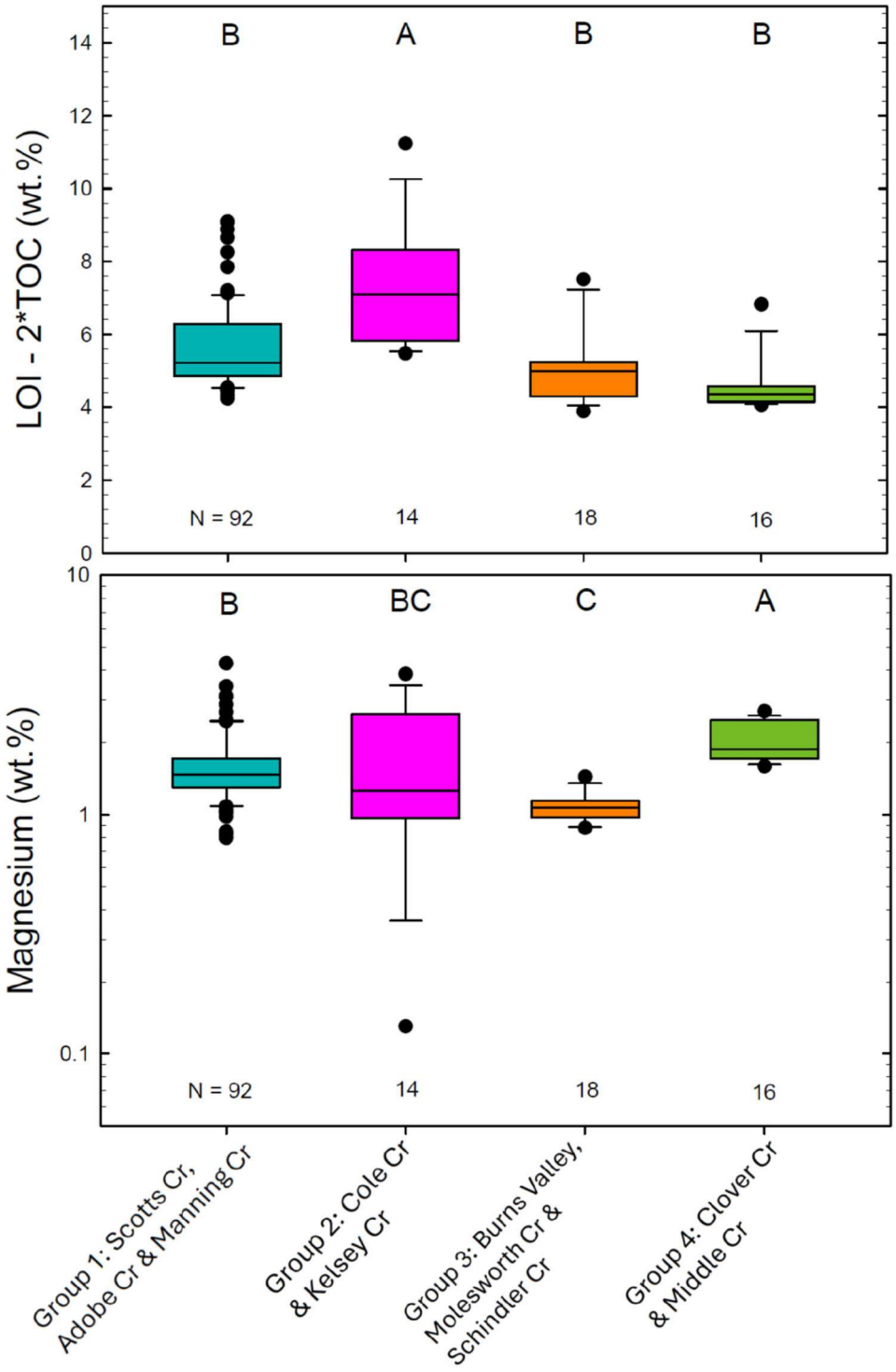

*Figure 6.4.11. Box plots for loss on ignition minus 2 times organic carbon (LOI-2*TOC; see text) (linear scale) and magnesium (logarithmic scale). Letters at top indicate statistical differences among four source groups in Trial 1, using analysis of variance (ANOVA) on ranks. Boxes indicate interquartile range; horizontal lines indicate median; whiskers indicate 10th and 90th percentiles; circles indicate results below 10th percentile or above 90th percentile. Numbers at the bottom indicate the number of samples (N) in each source group. Colors match those used in Figures 6.4.15 and 6.4.16, which show the unmixing model results. Data summarized from Watanabe et al. (2025). [wt.%, weight percent]*

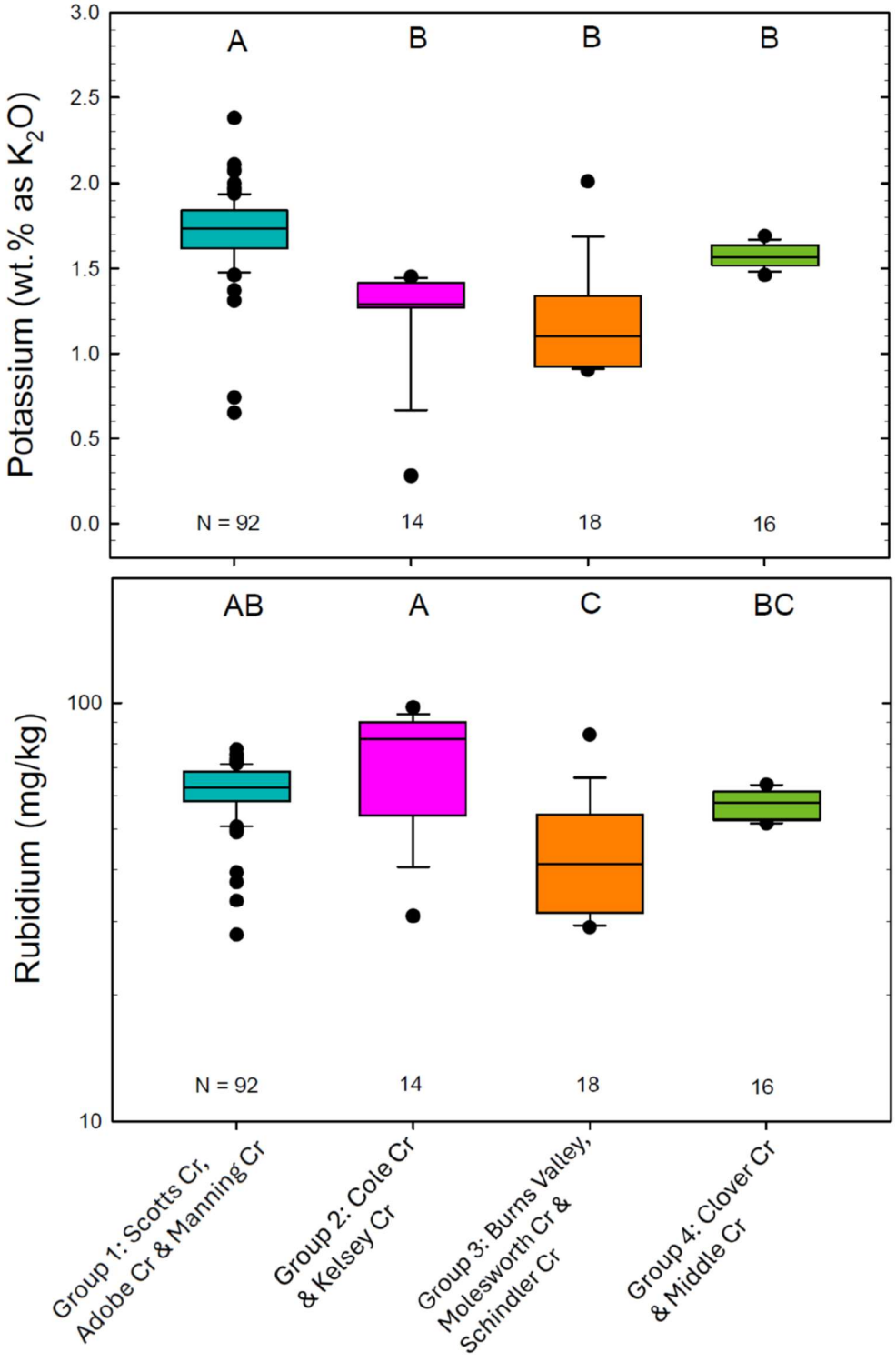

Figure 6.4.12. Box plots for potassium (linear scale) and rubidium (logarithmic scale). Letters at top indicate statistical differences among four source groups in Trial 1, using analysis of variance (ANOVA) on ranks. Boxes indicate interquartile range; horizontal lines indicate median; whiskers indicate 10th and 90th percentiles; circles indicate results below 10th percentile or above 90th percentile. Numbers at the bottom indicate the number of samples (N) in each source group. Colors match those used in Figures 6.4.15 and 6.4.16, which show the unmixing model results. Data summarized from Watanabe et al. (2025). [wt.%, weight percent; mg/kg, milligram per kilogram]

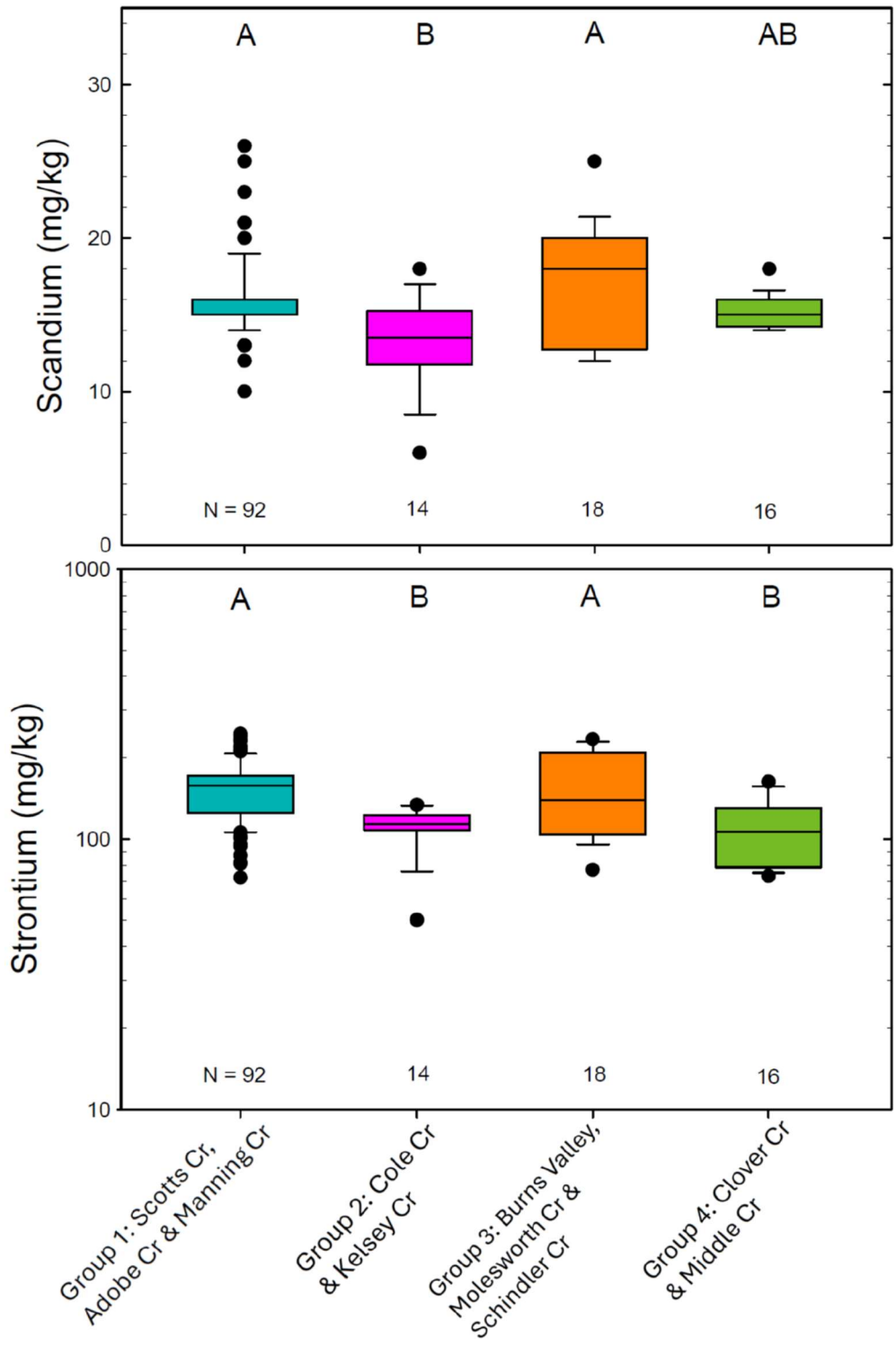

Figure 6.4.13. Box plots for scandium and strontium (logarithmic scale). Letters at top indicate statistical differences among four source groups in Trial 1, using analysis of variance (ANOVA) on ranks. Boxes indicate interquartile range; horizontal lines indicate median; whiskers indicate 10th and 90th percentiles; circles indicate results below 10th percentile or above 90th percentile. Numbers at the bottom indicate the number of samples (N) in each source group. Colors match those used in Figures 6.4.15 and 6.4.16, which show the unmixing model results. Data summarized from Watanabe et al. (2025). [mg/kg, milligram per kilogram]

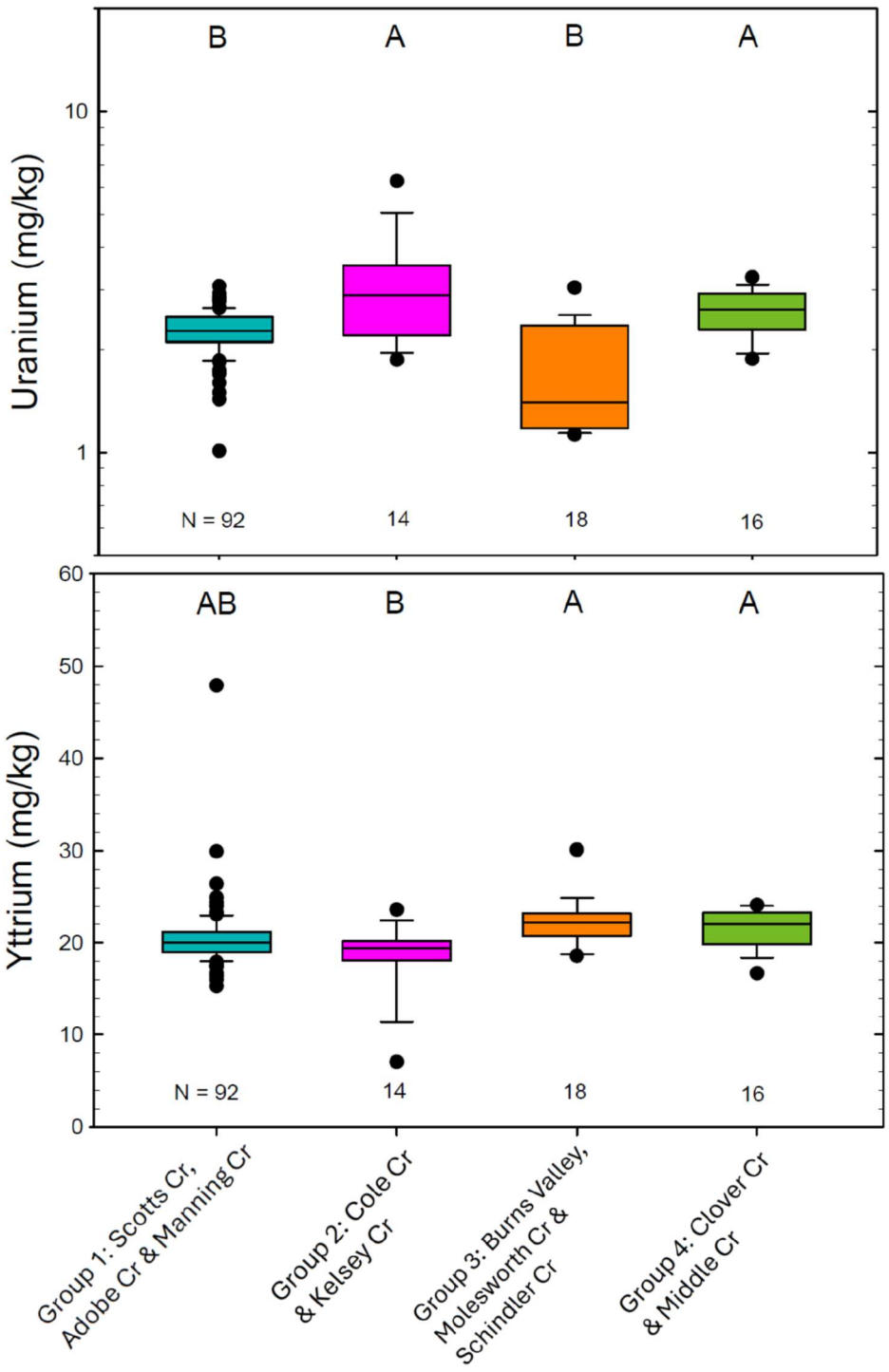

Figure 6.4.14. Box plots for loss on uranium (logarithmic scale) and yttrium (linear scale). Letters at top indicate statistical differences among four source groups in Trial 1, using analysis of variance (ANOVA) on ranks. Boxes indicate interquartile range; horizontal lines indicate median; whiskers indicate 10th and 90th percentiles; circles indicate results below 10th percentile or above 90th percentile. Numbers at the bottom indicate the number of samples (N) in each source group. Colors match those used in Figures 6.4.15 and 6.4.16, which show the unmixing model results. Data summarized from Watanabe et al. (2025). [mg/kg, milligram per kilogram]

A summary of the ANOVA results for the diagnostic tracers for Trial 1 is provided in Table 6.4.5. Diagnostic tracers are apparent for each of the source groups, and in some cases, these can be related to the underlying geology (see Appendix, Table 15.6.4.1).

*Table 6.4.6. Trial 1 optimal geochemical tracers showing results of analysis of variance (ANOVA) on ranks testing for streambed sediment samples from four source groups. The tracers are listed in order of decreasing influence. Letters (A, B, AB etc.), emphasized by color shading, indicate statistical differences (see section 6.4.2.4.4). Box plots for the 12 tracers are in Figures 6.4.9 through 6.4.14. Input data from Watanabe et al. (2025). [K, potassium; Rb, rubidium; Cr, chromium; Cs, cesium; Mg, magnesium; Li, lithium; LOI-2*TOC, loss on ignition minus two times total organic carbon; Ba, barium; Sr, strontium, U, uranium, Sc, scandium; Y, yttrium]*

	Group 1	Group 2	Group 3	Group 4
Tracer	**Scotts, Adobe & Manning Cr**	**Cole & Kelsey Cr**	**Burns Valley, Molesworth & Schindler Cr**	**Clover & Middle Cr**
K	A	B	B	B
Rb	AB	A	C	BC
Cr	B	A	AB	A
Cs	B	A	B	B
Mg	B	BC	C	A
Li	B	A	B	A
LOI-2*TOC	B	A	B	B
Ba	A	B	B	AB
Sr	A	B	A	B
U	B	A	B	A
Sc	A	B	A	B
Y	AB	B	A	A

Source group 1 (Scotts Cr., Adobe Cr., and Manning Cr.) is distinguished from the other source groups in Trial 1 by having higher concentrations of Ba (Figure 6.4.9) and K (Figure 6.4.12), and lower concentrations of Cr (Figure 6.4.10). These chemical characteristics are consistent with the presence of K-Ba-rich silicate minerals such as feldspars, which may occur in arkosic sandstone or other sedimentary rocks found in the Franciscan Complex. This source group has the largest proportion (more than 75%) of a geologic unit consisting of Cretaceous and Jurassic Franciscan Complex sandstone with smaller amounts of slate, chert, limestone, and conglomerate (Figure 6.4.4; Appendix Table 15.6.4.1, Kjf).

Source group 2 (Cole Cr. and Kelsey Cr.) is associated geologically with the Quaternary Clear Lake volcanic field (Figure 6.4.4) which has a wide range of compositions including

basaltic andesite, andesite, dacite, and rhyolite (Hearn et al., 1995). Streambed sediment from this area showed higher concentrations of Cs (figure 6.4.9) and Rb (Figure 6.4.12) and a lower concentration of Y (Figure 6.4.14) than the other three source groups. These elements occur in stream sediments from source group 2 at levels that are comparable to concentrations in the Clear Lake volcanics (Hammersley and DePaolo, 2006). Another tracer that is highest in source group 2 is LOI-2*TOC, which indicates elevated presence of minerals with structural water such as kaolinite and illite/smectite.

Source group 3 (Burns Valley, Molesworth Cr., and Schindler Cr.) had lower concentrations of Mg (Figure 6.4.11) and Rb (Figure 6.4.12) in streambed sediments than the other three source groups and relatively high Y (Figure 6.4.14).

Source group 4 (Clover Cr. and Middle Cr.) is distinguished by relatively elevated concentrations of Li (Figure 6.4.10) and Mg (Figure 6.4.11). A geologic map unit that occurs only in the Clover and Middle Creeks area is "blueschist and semi-schist of the Franciscan Complex" (Saucedo et al., 2000). Blueschist is a relatively rare metamorphic rock that forms at high pressure and relatively low temperature at depth in subduction zones; it is often associated with serpentinite, a Mg-rich rock (Essene et al., 1965). Two other geologic map units that are relatively abundant in the Clover and Middle Creeks area are Upper and Lower Cretaceous sandstone, shale, and conglomerate (Appendix Table 15.6.4.1). It is possible that these units are responsible for the relatively high observed Li concentrations, which are associated with lake sediments and shale in other settings (for example, Liu et al., 2024; Phan et al., 2016).

6.4.3.1.3 Targets in Trial 1

Results from the Sed_SAT analysis for the 26 Clear Lake target samples from Trial 1 unmixing calculations are shown in Figure 6.4.15. The six target samples from the Lower Arm are on the left; nine target samples from Oaks Arm are in the middle; and 11 target samples from the Upper Arm are on the right. The Oaks Arm samples include one field replicate (SFS-0915, a replicate of SFS-0914).

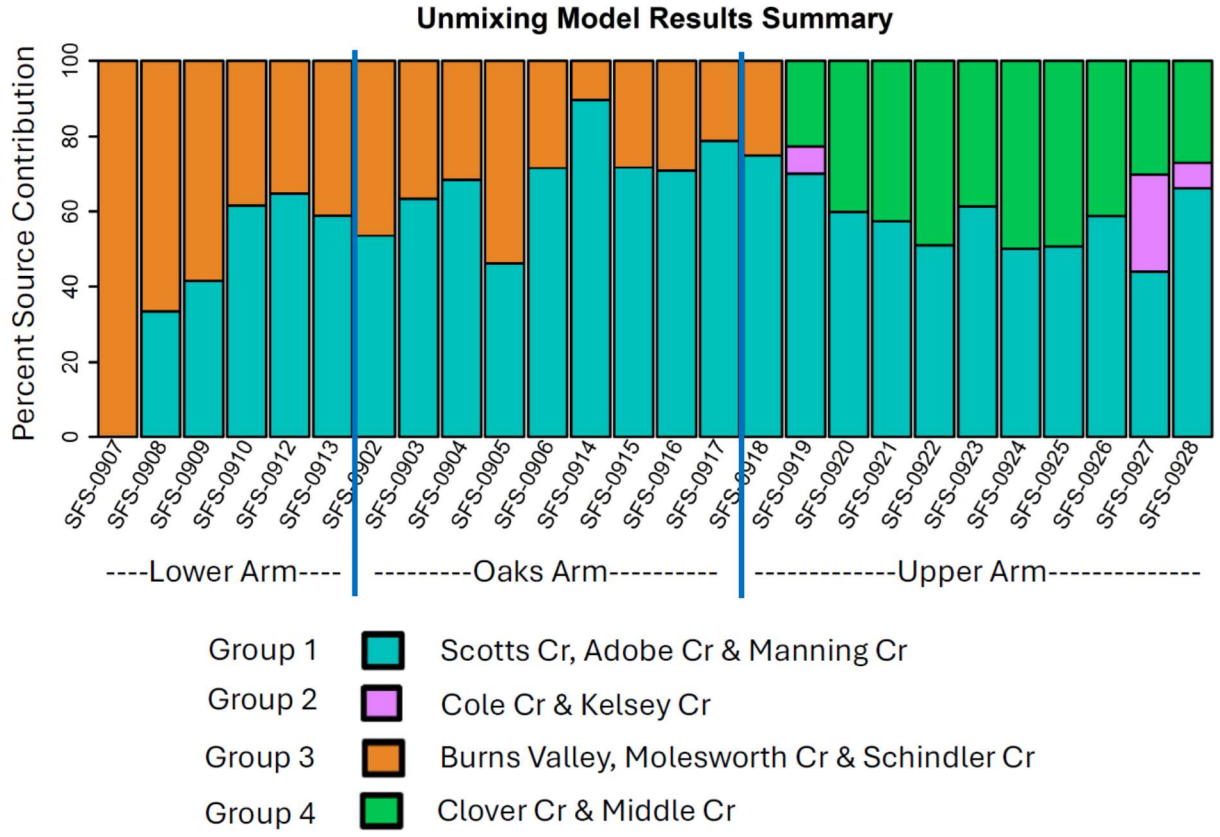

Figure 6.4.15. Vertical bar charts showing Trial 1 unmixing model results from the Sediment Source Assessment Tool (Sed_SAT), indicating estimated source contributions for each target sample. Colors for source groups are consistent with box plots in Figures 6.4.9 through 6.4.14. Locations of target samples shown in Figure 6.4.5. Input data to Sed_SAT from Watanabe et al. (2025).

Results from Trial 1 are consistent with the geographic distribution of the target samples. All of the samples from the Lower Arm and Oaks Arm show contributions of sediment from source group 3 (Burns Valley, Molesworth Creek, and Schindler Creek) which are tributaries to these two arms of the lake (Figure 6.4.2). Sample SFS-0907, which shows a 100% contribution from source group 3, is located at the farthest downstream end of the Lower Arm, near the input of Burns Valley and Molesworth Creek (Figure 6.4.5). Sample SFS-0918 also has a contribution of sediment from source group 3; although this sample is grouped with the Upper Arm samples, it is located in the Narrows area that connects the Upper Arm with the Oaks Arm.

Three of the target samples (SFS-0919, -0927, and -0928) indicate contributions from source group 2 (Cole Creek and Kelsey Creek). These samples are located in the southeastern part of the Upper Arm (Figure 6.4.5), near the outlets of those two creeks to Clear Lake. All of the samples from the Upper Arm show sediment contributions from source group 4 (Clover Creek and Middle Creek) which flow into Clear Lake through Rodman Slough at the northwestern end of the Upper Arm (Figures 6.4.2 and 6.4.5). Contributions from source group 1 (Scotts, Adobe, and Manning Creeks) the largest group of tributaries, are seen in all of the Clear Lake samples except SFS-0907,

Averaged results for Trial 1 are shown in Figure 6.4.16. At the basin scale, there are two source groups that contributed 83.4% of the sediment to Clear Lake. The relative

contributions from source group 1 (Scotts, Adobe, and Manning Creeks) and source group 3 (Burns Valley, Molesworth Creek, and Schindler Creek) were 58.4% and 25.0%, respectively. Clover and Middle Creeks (source group 4) contributed 15.1% and Cole and Kelsey Creeks (source group 2) contributed only 1.5%.

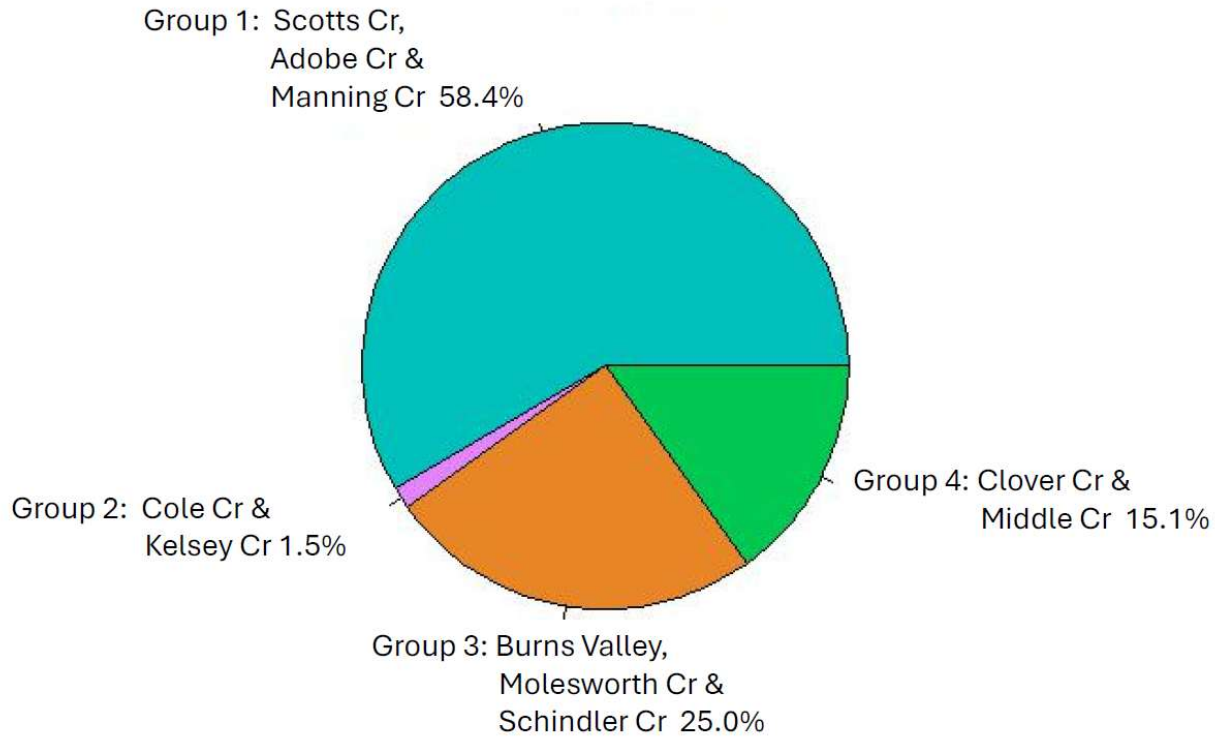

Figure 6.4.16. Pie chart showing averaged results for Trial 1 from the Sediment Source Assessment Tool (Sed_SAT) for all 26 Clear Lake target samples (lakebed sediments). Colors for source groups are consistent with Figures 6.4.9 through 6.5.15. Input data to Sed_SAT from Watanabe et al. (2025).

6.4.3.1.4 Uncertainty in Trial 1

Three distinct quantitative measures for evaluating uncertainty are built into the Sed_SAT tool: an error analysis, a "confusion matrix," and a source verification test. For Trial 1, the results of these evaluations are summarized in Appendix Tables 15.6.4.2, 15.6.4.3, and 15.6.4.4, respectively.

The error analysis is based on the results of 1,000 Monte Carlo simulations, which provided a percent error for each target sample, along with a standard deviation (Table 15.6.4.3). For Trial 1, the mean value of the errors was 3.94%. Standard deviation values for each target sample were typically less than 0.2%.

The "confusion matrix" for Trial 1 (Appendix Table 15.6.4.4) shows the percentage of samples that were correctly classified in each of the source groups. The vertical columns in the matrix indicate the actual sample source, and the rows indicate the source group classification selected using the Sed_SAT tool. The percentage classified correctly ranged from 88.2% for source group 3 to 100% for source group 2. After removal of outliers, 115 samples were used in Trial 1 and 111 (or 96.5%) were classified correctly.

The source verification test (SVT; Appendix Table 15.6.4.5) shows results when each source sample is run as a target sample. The SVT table shows the percentage of samples in each source group that were correctly classified by the Sed_SAT tool, and these values are highlighted in Table 15.6.4.5 with blue shading. A high predicted contribution from the correct source group (e.g., Upper Scotts Cr. predicted as Upper Scotts Cr.) indicates effective model prediction and discrimination between source groups. The percentages (and standard deviations) of correct source contributions in the SVT table ranged from 59% (± 36%) for source group 2 (Cole and Kelsey Creeks) to 85% (± 24%) for source group 4 (Clover and Middle Creeks).

Uncertainty was assumed to be equal to the sum of individual errors in quadrature, a standard technique for propagating random errors using the square root of the sum of the squares. Taken together, the sampling error (estimated using the average error from the 1,000 Monte Carlo runs), source grouping error (estimated as the average error reported in the confusion matrix), and classification error (estimated using the average SVT error) indicate that results from Trial 1 have an overall uncertainty of 27%.

6.4.3.2 Trial 2 - Rodman Slough delta targets with 3 watershed source groups

6.4.3.2.1 Classification in Trial 2

Trial 2 includes target samples collected from the Rodman Slough delta, an area that receives sediment from Scotts Creek, Middle Creek, and Clover Creek (Figure 6.4.3). Three source groups were used for the Sed_SAT analysis in Trial 2: 1) Clover Creek and Middle Creek; 2) Lower and Middle Scotts Creek; and 3) Upper Scotts Creek

In Trial 2, after starting with 231 samples, the outlier analysis excluded 46 samples (20%) leaving 185 samples for further analysis. Two tracers (hafnium (Hf) and zirconium (Zr)) were corrected for particle size for the Clover and Middle Creeks source group, and two tracers (Hf and TON) were corrected for organic material. No tracers were excluded from the analysis for non-conservative behavior. The DFA correctly classified 89.47% of the source samples, and the biplot (Figure 6.4.17) shows that the 3 source groups are fairly well discriminated. For additional discussion of uncertainty and model error, see section 6.4.3.2.4, below.

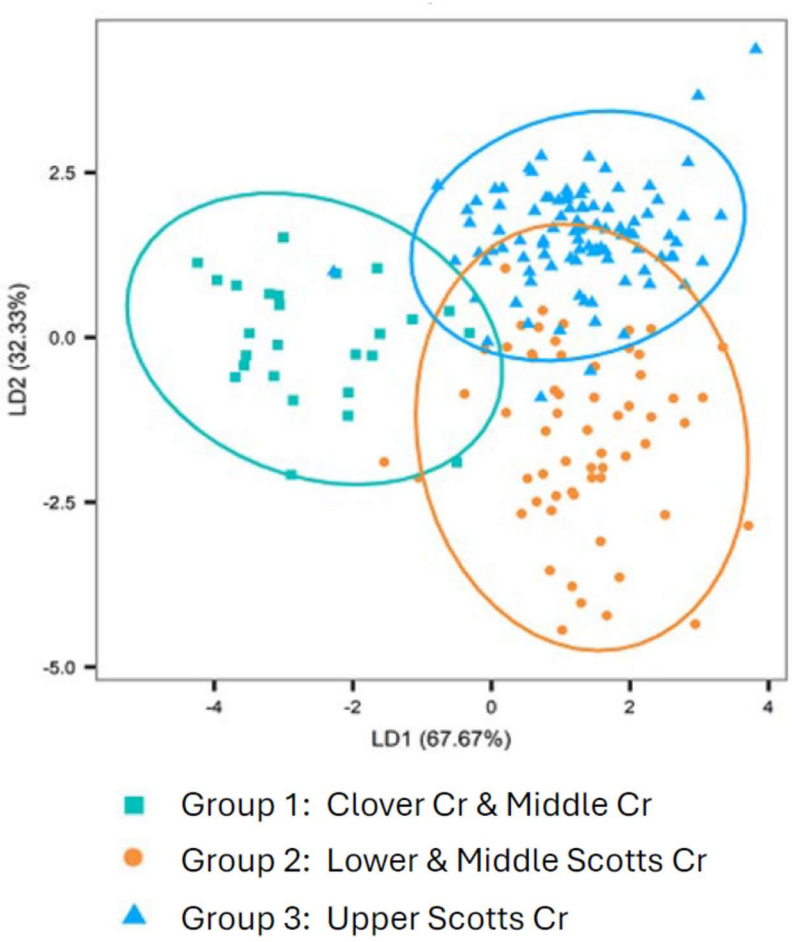

Figure 6.4.17. Linear Discriminant Analysis (LDA) results biplot for Trial 2 from the Sediment Source Assessment Tool (Sed_SAT), showing some overlap among the three source groups. The LDA biplot shows predicted values from the first two linear discriminants. The first two linear discriminants do not show the full discriminatory power of the analyses when there are 3 or more source groups. The confusion matrix for Trial 1 (Appendix Table 15.6.4.) shows the percentage of samples correctly classified by the complete linear discriminant function for each source group. Input data to Sed_SAT from Watanabe et al. (2025). [LD1, linear discriminant 1; LD2, linear discriminant 2]

6.4.3.2.2 Tracers in Trial 2

In Trial 2, twelve tracers were found by Sed_SAT to have utility in distinguishing among source groups. The diagnostic tracers, in order of discriminatory weighting factor, were: Hf, zinc (Zn), Mg, Li, Cs, niobium (Nb), LOI-2TOC, $\delta^{15}N$, manganese (Mn), gallium (Ga), Cr, and Sr (Appendix *Table 15.6.4.6*). Box plots showing concentration data for these 12 tracers in the three source groups are provided in Appendix Figures 15.6.4.1 through 15.6.4.6. These figures also show the results of ANOVA testing of significant differences among source groups for each tracer. A summary of the ANOVA results for the Trial 2 tracers is given in Table 6.4.6, which has letters indicating statistically significant differences for tracers among the 3 source groups, as in Table 6.4.5 for Trial 1 tracers.

*Table 6.4.7. Trial 2 optimal geochemical tracers showing results of analysis of variance (ANOVA) on ranks testing for 3 source groups. The tracers are listed in order of decreasing weighting factor. Letters (A, B, AB etc.) indicate statistical differences (see section 6.4.2.4.4). Input data from Watanabe et al. (2025). Box plots showing variations of tracers are in Appendix Figures 15.6.4.1 through 15.6.4.6. [Hf, hafnium; Zn, zinc; Mg, magnesium; Li, lithium; Cs, cesium; Nb, niobium; LOI-2*TOC, loss on ignition minus two times total organic carbon; δ15N, delta-15-nitrogen, the ratio of 15N to 14N relative to air; Mn, manganese; Ga, gallium; Cr, chromium; Sr, strontium]*

	Group 1	Group 2	Group 3
Tracer	**Clover & Middle Cr**	**Lower & Middle Scotts Cr**	**Upper Scotts Cr**
Hf	B	B	A
Zn	A	A	B
Mg	A	B	B
Li	A	B	B
Cs	A	B	A
Nb	A	A	B
LOI-2*TOC	B	B	A
$\delta^{15}N$	B	A	B
Mn	A	A	A
Ga	B	B	A
Cr	A	A	A
Sr	B	A	A

Six of the twelve tracers selected by Sed_SAT for Trial 2 *(*Table 6.4.6*) were* also selected for Trial 1 (Table 6.4.5). Comparison of Table 6.4.6 (for Trial 2) with Table 6.4.5 (for Trial 1) and related box plots (Figures 6.4.9 through 6.4.14 for Trial 1 and Appendix Figures 15.6.4.1 through 15.6.4.6 for Trial 2) reveals that the variability of tracers for Trial 2 is consistent with that determined for Trial 1 for the six tracers common to both trials. For the tracers unique to Trial 2, Hf and Ga were highest in Upper Scotts Creek, Zn and Nb were lowest in Upper Scotts Creek, and $\delta^{15}N$ values were highest in Lower and Middle Scotts Creek.

6.4.3.2.3 Targets in Trial 2

Results from Sed_SAT for the three Rodman Slough target samples from the Trial 2 unmixing calculations are shown in Figure 6.4.18. The three target samples from the Rodman Slough delta (Figure 6.4.3) show some differences in computed sediment source areas. The average results for the three target samples are show in Figure 6.4.19.

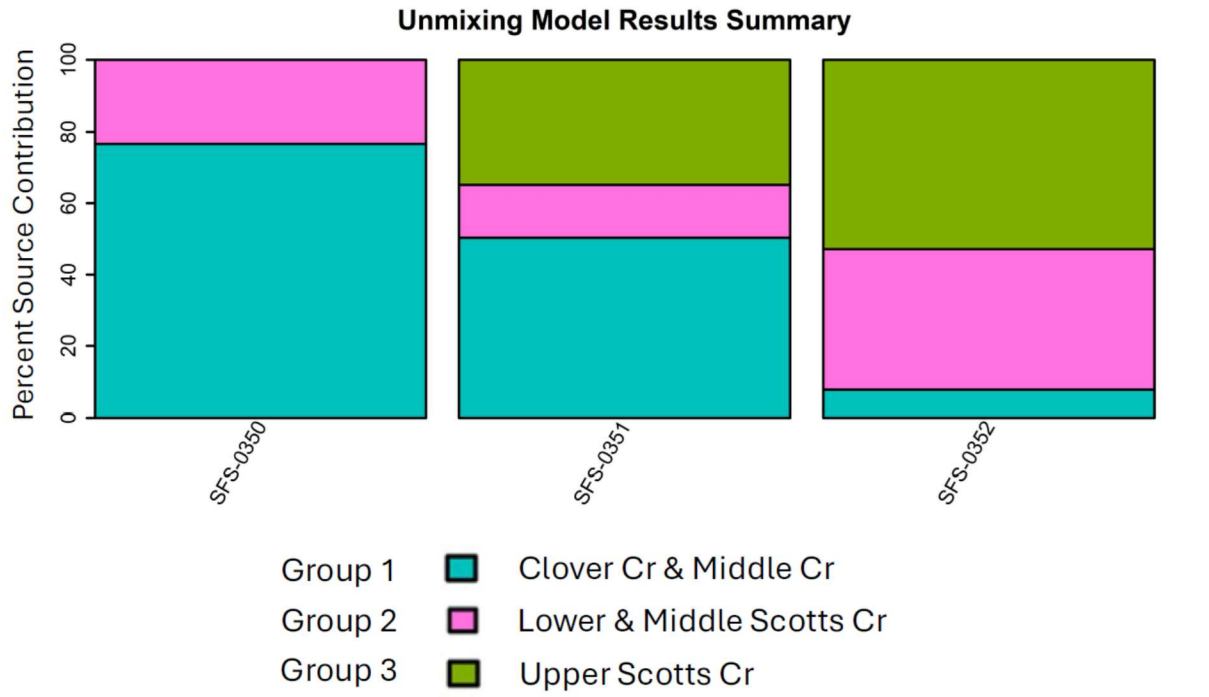

Figure 6.4.18. Vertical bar charts showing Trial 2 mixing model results from the Sediment Source Assessment Tool (Sed_SAT), indicating estimated source contributions for each target sample. Locations of target samples shown in Figure 6.4.3. Input data to Sed_SAT from Watanabe et al. (2025).

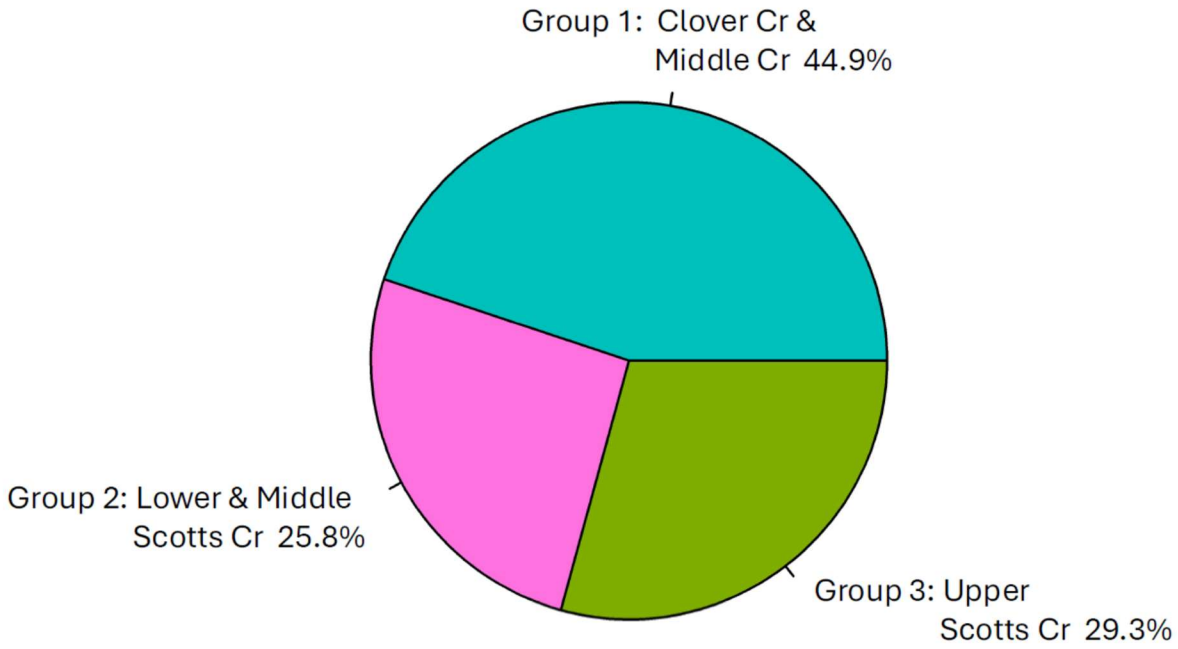

Figure 6.4.19. Pie chart showing averaged results for Trial 2 from the Sediment Source Assessment Tool (Sed_SAT) for three target samples from the Rodman Slough delta. Input data to Sed_SAT from Watanabe et al. (2025).

According to the Trial 2 results, the largest source of sediment to the Rodman Slough Delta is source group 1 (Clover and Middle Creeks), contributing 44.9%. The second largest contributor is source group 3 (Upper Scotts Creek), contributing 29.3%. Source group 2 (Lower and Middle Scotts Creek) is estimated to have contributed 25.8%. The areas of the source groups as a fraction of the area modeled in Trial 3 are source group 1 with 42.6%; source group 2 with 30.1%, and source group 3 with 27.3%. Therefore, source groups 1 and 3 show slightly higher contributions than their relative drainage area in the results from Trial 2, and source group 2 shows a slightly lower contribution than its relative drainage area (Table 6.4.8).

6.4.3.2.4 Uncertainty in Trial 2

The error analysis, confusion matrix, and source verification test (SVT) results for Trial 3 are summarized in Appendix Tables 15.6.4.7, 15.6.4.8, and 15.6.4.9, respectively. The error analysis indicates that the mean error for individual target samples was 0.68%. The confusion matrix indicates that classification of source area samples was relatively good (compared with results for Trial 1), ranging from 85% correct for source group 2 to 94.9% for source group 3 (Appendix Table 15.6.4.8). After removal of outliers, 185 source samples were used in the analysis, of which 168 were classified correctly, an average of 90.8% classified correctly. The SVT resulted in predicted contributions (with standard deviations) of 68% ± 40% for source group1, 72% ± 28% for source group 2, and 69% ± 38% for source group 3 (Appendix Table 15.6.4.9).

As with Trial 1, uncertainty in Trial 2 was assumed to be equal to the sum of indivdual errors in quadrature, a standard technique for propagating random errors. Taken together, the sampling error (estimated using the average error from the 1,000 Monte Carlo simulations), source grouping error (estimated as the average error reported in the confusion matrix), and classification error (estimated using the average SVT error) 0 indicate that results from Trial 2 have an overall uncertainty of 32%, slightly higher than that for Trial 1.

6.4.3.3 Concentrations and speciation of nutrients

Concentrations of total phosphorus (P) and total organic nitrogen (TON) were determined for 587 soil and sediment samples collected for this study and sieved to < 0.063 mm. The samples were analyzed for P by two methods: inductively-coupled plasma optical-emission spectroscopy (ICP-OES) and wavelength-dispersive x-ray fluorescence (WDXRF); results are available in the accompanying data release (Watanabe et al., 2025). The WDXRF analyses of P had better quality-assurance performance for standard reference materials than the results by ICP-OES, so the WDXRF results for P are discussed below. Data for TON for this sample set were reported by the UCD SIF along with analyses of $\delta^{15}N$.

For the 101 sediment samples preserved frozen in the field and subsequently analyzed for nutrient speciation, four forms of phosphorus were determined: 1) loosely bound, 2) Ca-associated, 3) Fe-Al-associated, and 4) residual. Two forms of nitrogen were measured: 1) nitrate plus nitrite, and 2) Kjeldahl nitrogen, which includes ammonia, ammonium, and organic forms. Complete results of the nutrient speciation analyses are available in Watanabe et al. (2025); a summary of results is presented here.

6.4.3.3.1 Concentrations of phosphorus

Box plots showing the distribution of total P in selected soil and sediment samples from tributaries to Clear Lake are included in Figure 6.4.20. The results are organized using six watershed groups; three of the groups are identical to source groups 2–4 used in Trial 1 (Table 6.4.1). Source group 1 from Trial 1 (Scotts, Adobe, and Manning Creeks) is broken out into three parts for the nutrient plots: A) Adobe Cr. and Manning Cr., B) Lower and Middle Scotts Creek, and C) Upper Scotts Creek.

In the upper part of Figure 6.4.20, data for 418 soil and sediment samples are included. This data set removes field replicates and integrator sites, but includes soils, roadside ditch sediments, streamside sediments, and streambed sediments (those from upstream locations not considered Integrator sites). The lower plot in Figure 6.4.20 includes data for only the soil samples (N=115). The two watershed groups with highest median P concentrations (both 830 mg/kg) were Clover and Middle Creeks and Lower and Middle Scotts Creek. The lowest median P concentrations (both 650 mg/kg) were found in Cole and Kelsey Creeks and Upper Scotts Creek. Considering only the soil samples, the highest median concentration (980 mg/kg) was in Lower and Middle Scotts Creek, whereas the lowest median concentration (610 mg/kg) was in Clover and Middle Creeks. Considering all sample types as well as only soils, the P concentrations in samples from Upper Scotts Creek were significantly lower than those from Lower and Middle Scotts Creek. This may reflect the influence of agriculture at lower elevations in the Scotts Creek watershed.

The data for P in Clear Lake sediment samples (Figure 6.4.21) show that median concentrations were typically higher than those from the tributaries. The overall median P concentration for Clear Lake samples was 1,300 mg/kg compared with an overall median of 700 mg/kg for samples from the tributaries. Significant variation was observed in P concentrations in sediment from the three arms of Clear Lake; median P concentrations ranged from 1,200 mg/kg in the Upper Arm to 1,800 mg/kg in the Lower Arm, with intermediate values in the Oaks Arm. The higher concentrations of total P in the Oaks and Lower arms relative to the Upper Arm are consistent with the higher prevalence and intensity of algal blooms in the Oaks and Lower arms (Kalra et al., 2025).

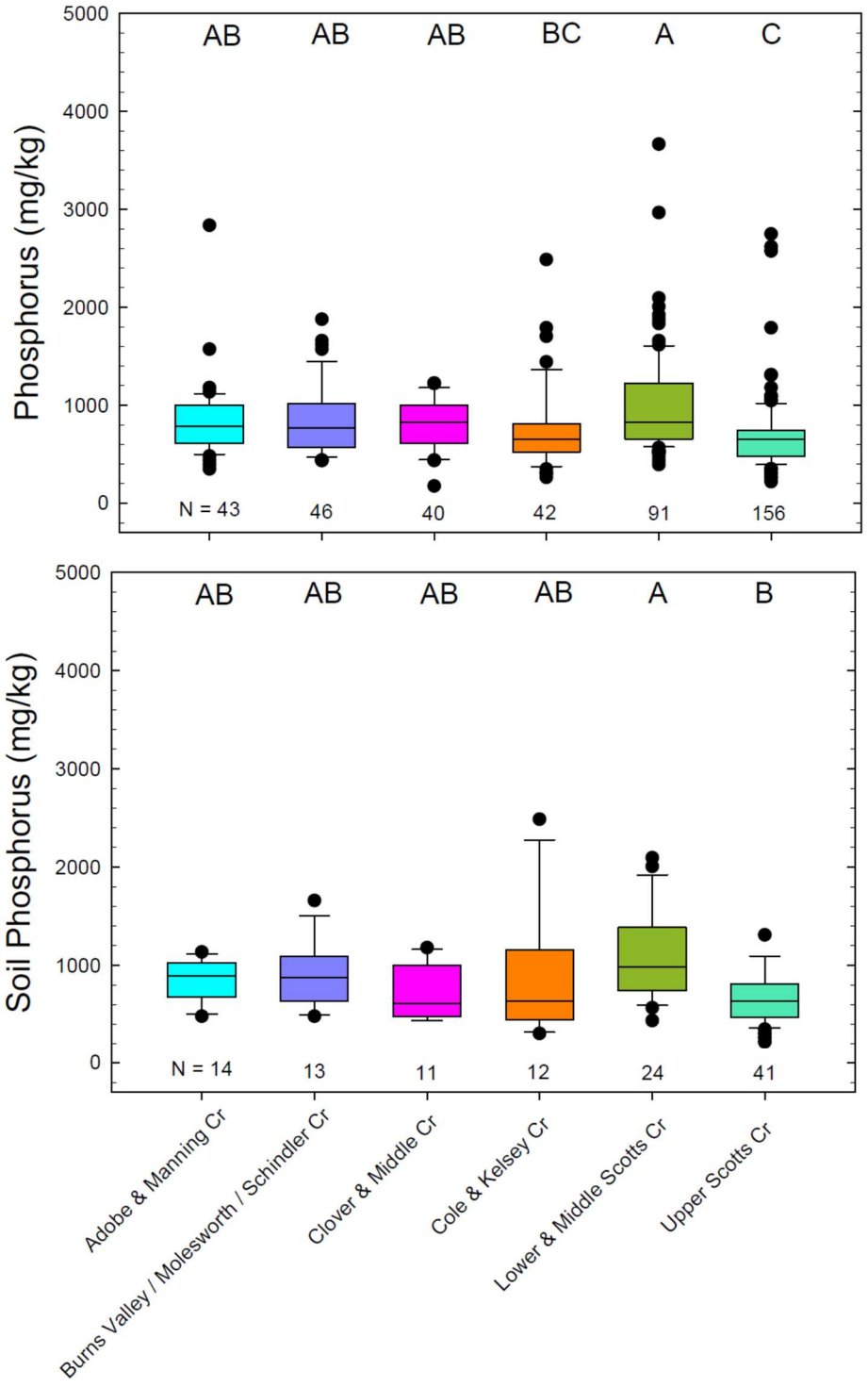

Figure 6.4.20. Box plots for phosphorus in soils and sediments from Clear Lake tributaries. Top plot is all soils and sediments (excluding field replicates and integrator sites). Bottom plot is only soils – same vertical scale. Letters at top indicate statistical differences among watersheds groups, using analysis of variance (ANOVA) on ranks. Numbers at bottom indicate number of samples (N) for each tributary watershed group. Boxes indicate interquartile range; horizontal lines indicate median; whiskers indicate 10th and 90th percentiles; circles indicate results below 10th percentile or above 90th percentile. Data summarized from Watanabe et al. (2025).

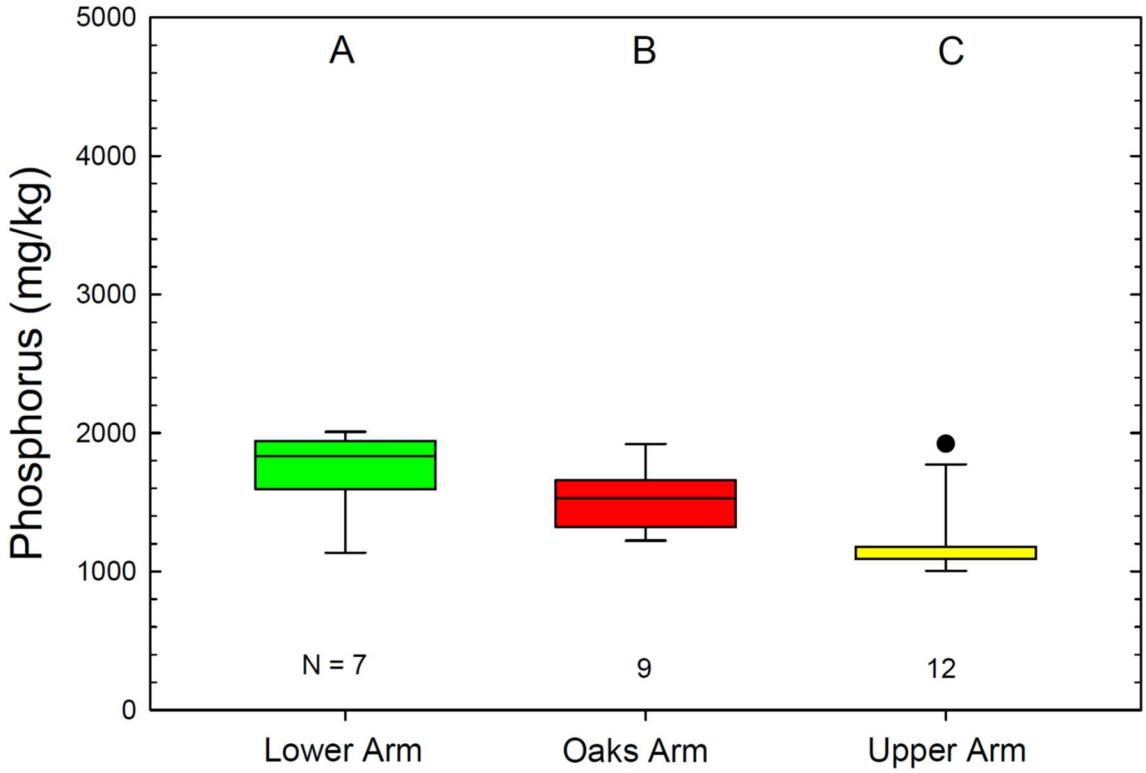

Figure 6.4.21. Box plots for phosphorus in sediment from the three arms of Clear Lake. Letters at top indicate statistical differences using analysis of variance (ANOVA) on ranks. Numbers at bottom indicate number of samples (N) from each arm of the lake. Boxes indicate interquartile range; horizontal lines indicate median; whiskers indicate 10th and 90th percentiles; circles indicate results below 10th percentile or above 90th percentile. Same vertical scale as Figure 6.4.20. Colors match locations in Figure 6.4.5. Data summarized from Watanabe et al. (2025).

6.4.3.3.2 Forms of phosphorus

Forms of P in Clear Lake sediment (top 4 cm) are summarized in Figure 6.4.22. The proportion of Fe-Al-associated P ranged from 21% to 25% of total P in the three arms of the lake. Average Ca-associated P ranged from 30% to 36% of total P in the three arms. Loosely bound P was less than 1% of total P in all samples. The remainder of P (average of 42% to 43% in the three arms) was residual P, which includes organic forms. The samples were collected during September 2023 when bottom water conditions were generally oxic; however, there had been several periods of anoxic conditions during May-August 2023 (see section 7, Figure 7.3.6) that likely affected redox conditions in shallow sediment. Anoxic conditions can lead to mobilization of Fe-associated P in situations where Fe in the ferric (oxidized) state, such as P adsorbed to hydrous ferric oxides (Swann et al., 2024).

Results for forms of P in tributary bed sediment are shown in Figure 6.4.23. The proportion of Fe-Al-associated P ranged from 4% in Kelsey Creek to 17% in Cole Creek. Other tributaries with greater than about 10% Fe-Al-associated P were Burns Valley and, Molesworth Creek, Manning Creek, Schindler Creek, and Scotts Creek. This form of P is most likely to contribute to soluble reactive phosphate (SRP), a bioavailable form that

can stimulate algal blooms, when low-dissolved-oxygen conditions occur in Clear Lake bottom water. It is worth noting that proportions of Fe-Al-associated P in samples from Clear Lake tributaries (Figure 6.4.23) are approximately half of those observed in Clear Lake sediments (Figure 6.4.22). It was well documented by Swann et al. (2024) that P cycling accounts for 70 to 95% of P loading in the Clear Lake water column. Ca-associated P ranged from 40 to 61% of total P in samples from the tributaries (Figure 6.4.23), a higher proportion than in the lake sediments (Figure 6.4.22). Because P and its forms are not conservative tracers, they were not used in the sediment fingerprinting analysis with Sed_SAT.

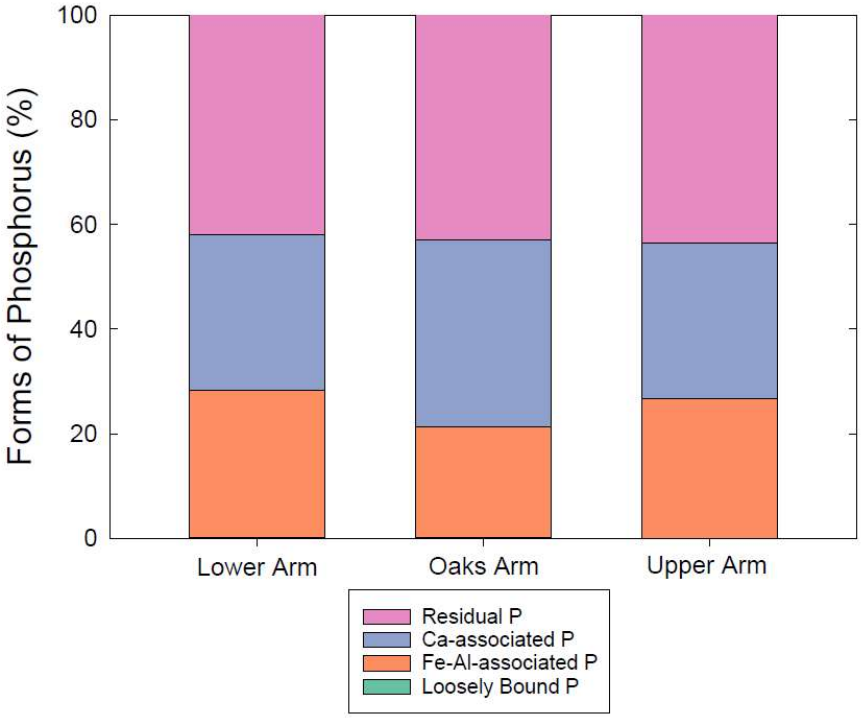

Figure 6.4.22. Stacked bar chart showing average percentages of phosphorus (P) species in shallow sediment (top 4 cm) from the three arms of Clear Lake. Loosely bound P was less than 1% in all samples, and therefore does not appear on the bar chart. Data summarized from Watanabe et al. (2025).

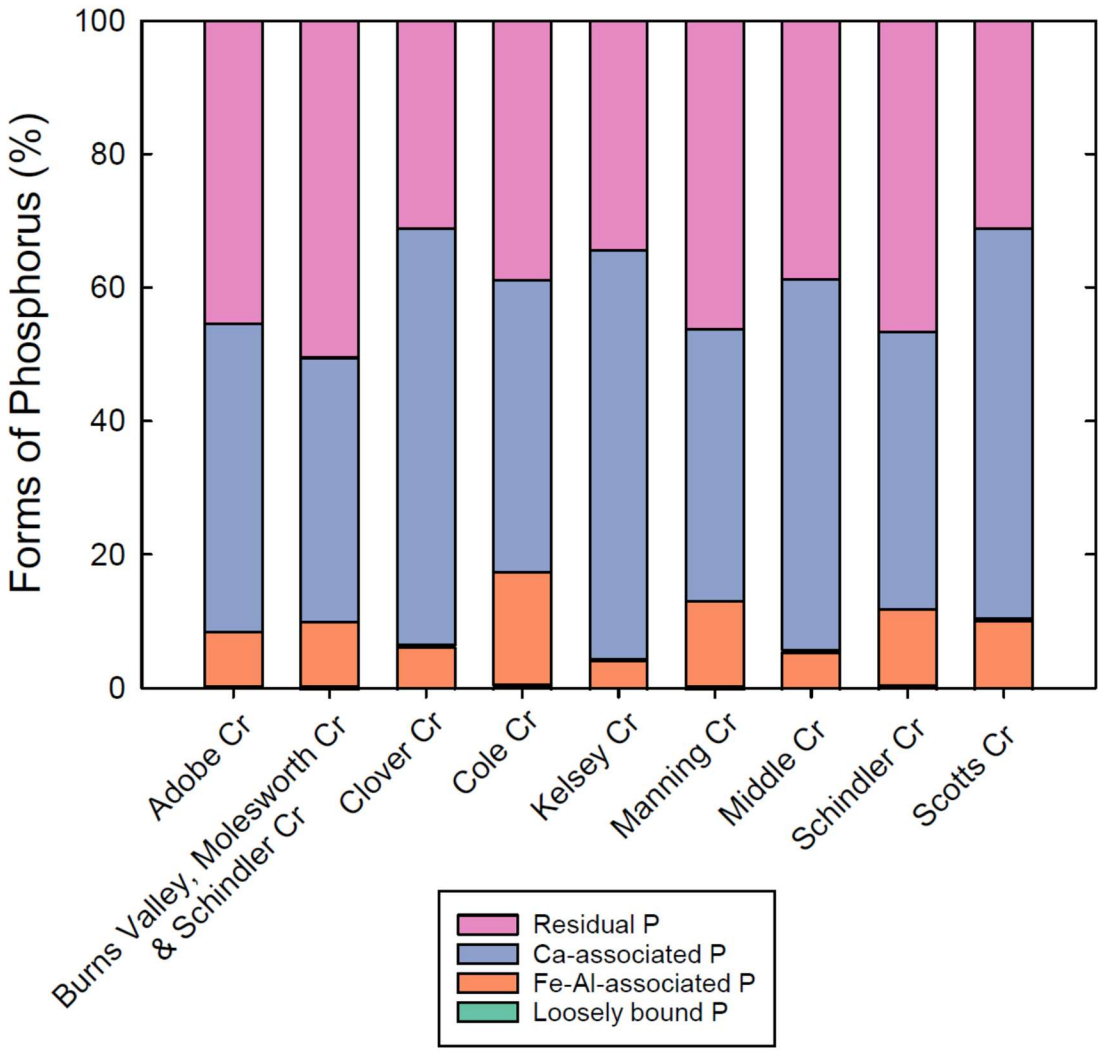

Figure 6.4.23. Stacked bar chart showing average percentages of phosphorus (P) species in streambed sediment (integrator sites) from tributaries to Clear Lake. Data summarized from Watanabe et al. (2025). [Ca, calcium; Fe, iron; Al, aluminum]

6.4.3.3.3 Concentrations of nitrogen

Total organic nitrogen (TON) had a median concentration of 0.15 weight percent (wt. %) in the 418 soil and sediment samples from the tributary source areas considered in the previous section for P concentration. The distribution of TON concentrations in the six tributary watershed groups considered above for P (Figure 6.4.24) indicates concentrations were lower in Upper Scotts Creek compared with most of the other source areas.

The median TON concentration from shallow sediment in Clear Lake was 1.2 wt. %, eight times larger than that for the tributaries. The much larger TON concentration in lake sediments compared with the tributaries is attributed to the activity of nitrogen-fixing bacteria within Clear Lake. Cyanobacteria have the ability to fix atmospheric nitrogen, which allows them to thrive in areas with limited nitrogen availability (Paerl et al., 2001).

TON concentrations in the Lower Arm and Oaks Arm were greater than those in the Upper Arm by approximately a factor of two (Figure 6.4.25). A similar relationship was found in data for LOI and organic carbon (Watanabe et al., 2025). This is consistent with the more frequent prevalence of cyanobacterial harmful algal blooms (CHABs) in the Lower Arm and Oaks Arm compared with the Upper Arm (see sections 7 and 8 of this report). Nitrogen exhibits strongly non-conservative behavior, so it was not used as a tracer in Sed_SAT sediment fingerprinting analysis for this study.

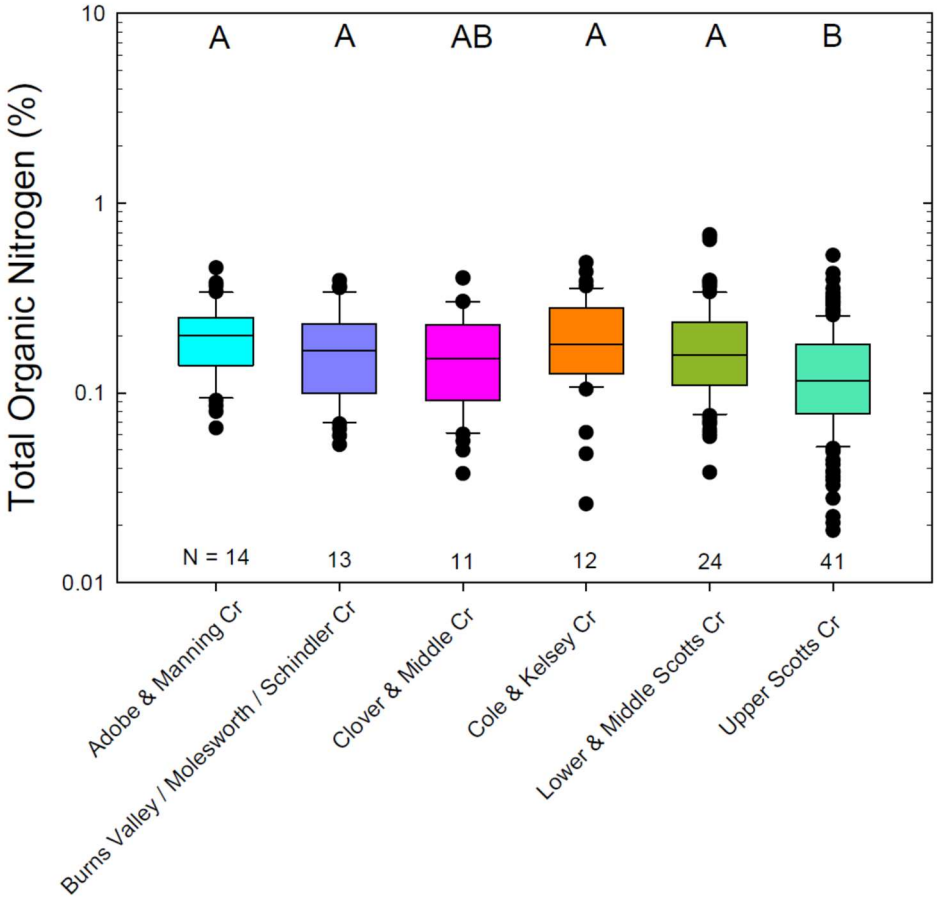

Figure 6.4.24. Box plots for total organic nitrogen in soils and sediments from Clear Lake tributaries. Letters at top indicate statistical differences using analysis of variance (ANOVA) on ranks. Numbers at bottom indicate numbers of samples (N) from each tributary watershed group. Boxes indicate interquartile range; horizontal lines indicate median; whiskers indicate 10th and 90th percentiles; circles indicate results below 10th percentile or above 90th percentile. Same vertical scale as Figure 6.4.25.

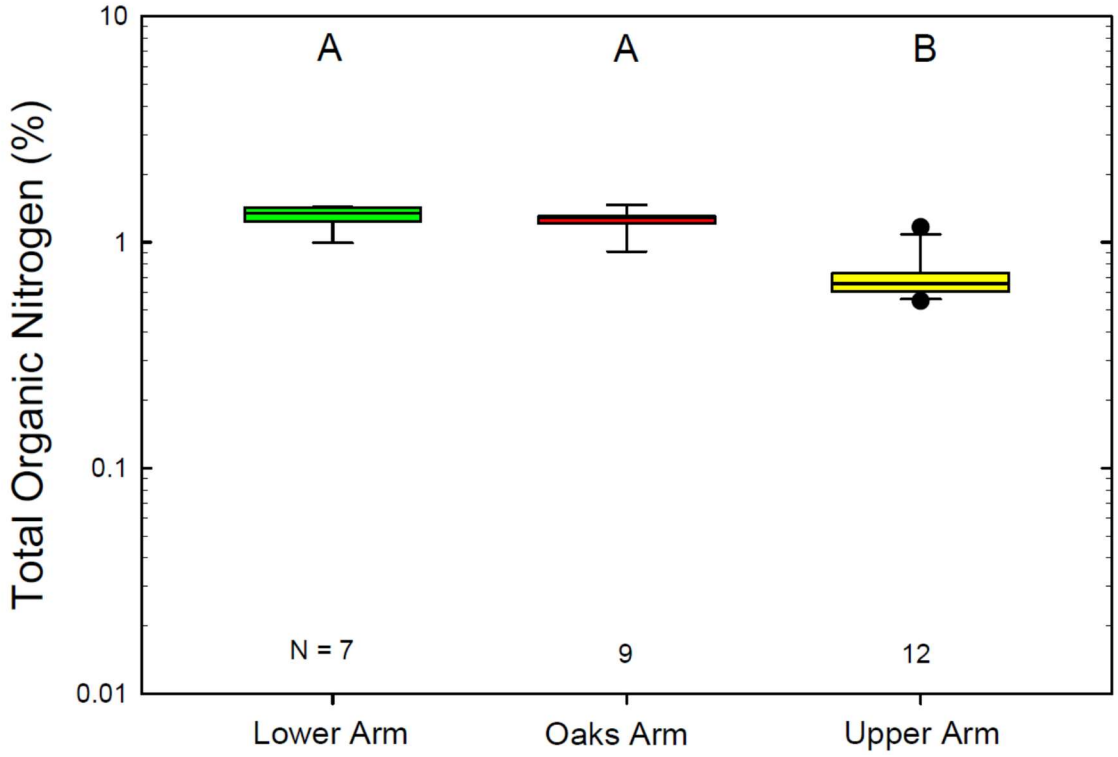

Figure 6.4.25. Box plots for total organic nitrogen in shallow sediment (top 4 cm) from the three arms of Clear Lake. Letters at top indicate statistical differences using ANOVA on ranks. Numbers at bottom indicate number of samples (N) from each arm of the lake. Boxes indicate interquartile range; horizontal lines indicate median; whiskers indicate 10th and 90th percentiles; circles indicate results below 10th percentile or above 90th percentile. Same vertical scale as Figure 6.4.24. Data summarized from Watanabe et al. (2025).

6.4.3.3.4 Forms of nitrogen

Two forms of nitrogen (N) were analyzed in frozen sediment samples: nitrate plus nitrite (NO_3^-+ NO_2^-) and Total Kjeldahl Nitrogen (TKN), which represent ammonia (NH_3), ammonium (NH_4^+), and organic N. In the tributary samples (Figure 6.4.26), the nitrate + nitrite component (the more oxidized N species) represented 24% to 36% of the N in all of the watersheds except for Scotts Creek, where it represented only 3.5% of N. The sampling location for the lower integrator site in the Scotts Creek stream channel below Tule Lake was inundated with water at the time of sampling, whereas all of the other sampling sites were dry; this may account for the presence of less of the oxidized N species at the Scotts Creek location.

Another difference in sampling between Scotts Creek and other watersheds is that the other watersheds were sampled monthly from July to December 2023 whereas Scotts Creek was sampled on only one occasion, in November 2023. Although there was some variability in the proportions of the two N species, there were no clear temporal trends in the N species data.

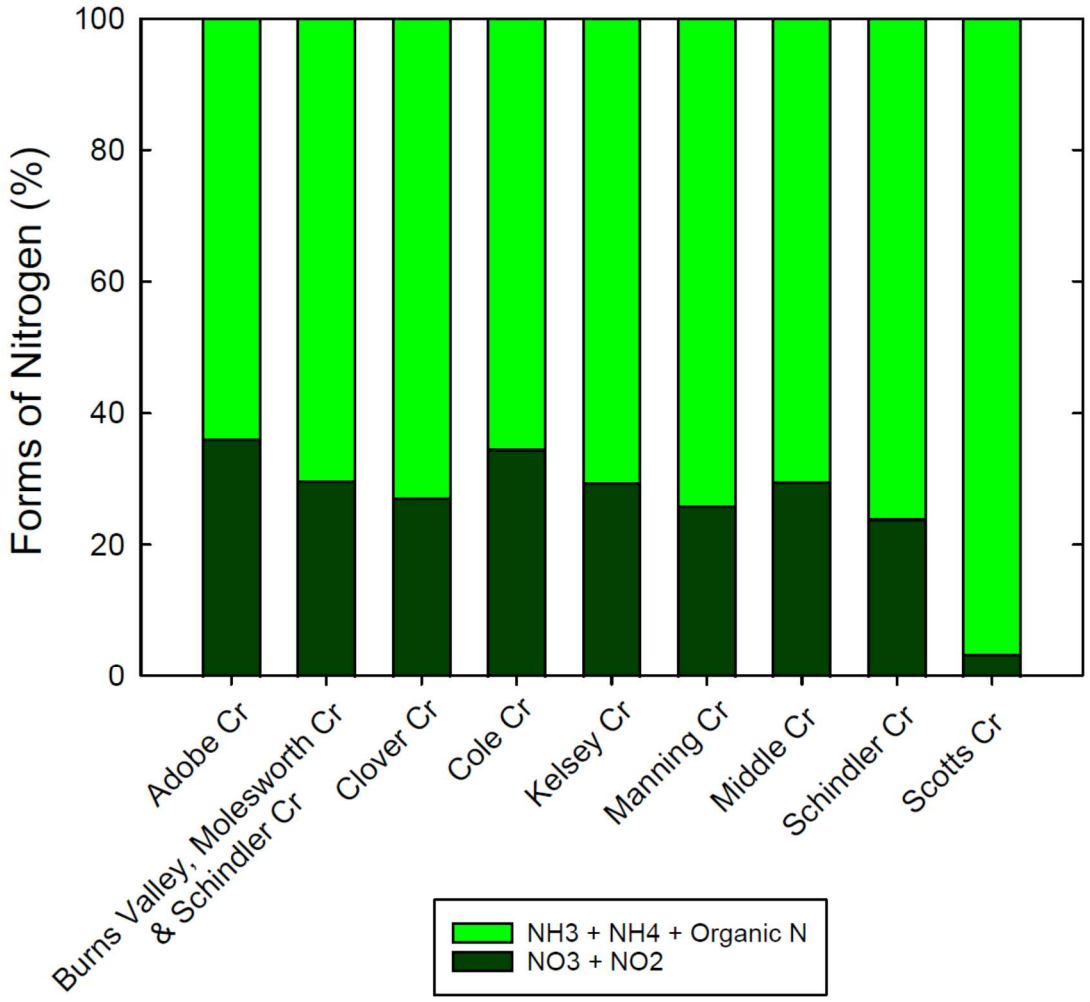

Figure 6.4.26. Stacked bar chart showing average percentages of nitrogen (N) species in stream bed sediment from tributaries to Clear Lake. Data summarized from Watanabe et al. (2025). [NH3, ammonia; NH4, ammonium; NO3, nitrate; NO2, nitrite]

The N speciation data for Clear Lake sediments (Figure 6.4.27) were dominated by TKN, the more reduced N species. The Clear Lake sediments were sampled during September 2023 after several months with anoxic events (section 7). Ammonium in water tends to be most abundant in Clear Lake during late summer and fall (section 7), consistent with the sediment chemistry.

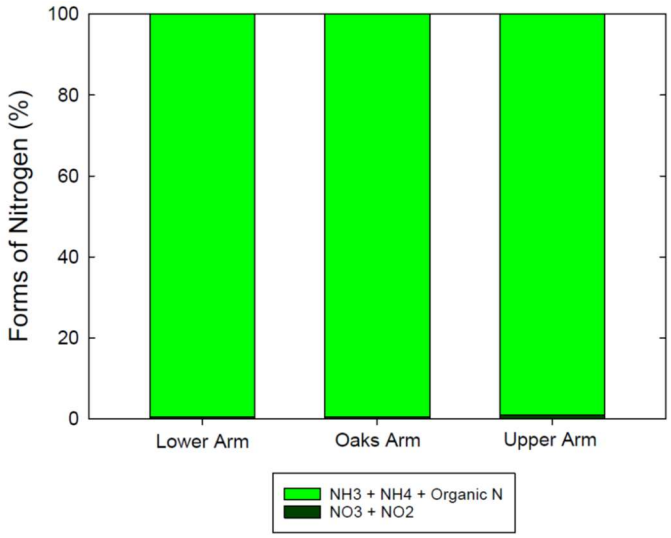

Figure 6.4.27. Stacked bar chart showing average percentages of nitrogen (N) species in shallow sediment (top 4 cm) from the three arms of Clear Lake. Data summarized from Watanabe et al. (2025). [NH3, ammonia; NH4, ammonium; NO3, nitrate; NO2, nitrite]

6.4.3.4 Mercury

It is well known that elevated mercury concentrations are found in the Oaks Arm of Clear Lake, associated with the Sulphur Bank Mercury Mine (e.g., Suchanek et al., 2008). The mine produced mercury from underground workings during 1873–1906, and from open-pit mining during 1927–1957. During open-pit mining, mine waste contaminated with elevated mercury concentrations was placed directly into Clear Lake, at the eastern end of the Oaks Arm. The EPA placed the mine site on the Superfund National Priorities List in 1990. In 1992, EPA regraded the shoreline of Clear Lake adjacent to the mine and placed a soil cover which greatly reduced erosion of mercury-laden mine waste into the lake (U.S. Environmental Protection Agency, 2023).

Results from this study for mercury concentrations in shallow (top 4 cm) sediments from Clear Lake (Figure 6.4.28) are consistent with prior work (Suchanek et al., 2008). Concentrations of mercury in the Oaks Arm were in the range of 13 to 53 mg/kg, with a median of 26 mg/kg. In the Upper Arm, mercury concentrations ranged from 1 to 8 mg/kg with a median of 2.1. The highest mercury concentration in the Upper Arm was in a sample from near the Narrows area that connects the Upper Arm with the Oaks Arm. In the Lower Arm, the range of concentrations was 0.8 to 4.8 mg/kg with a median of 2.9 mg/kg.

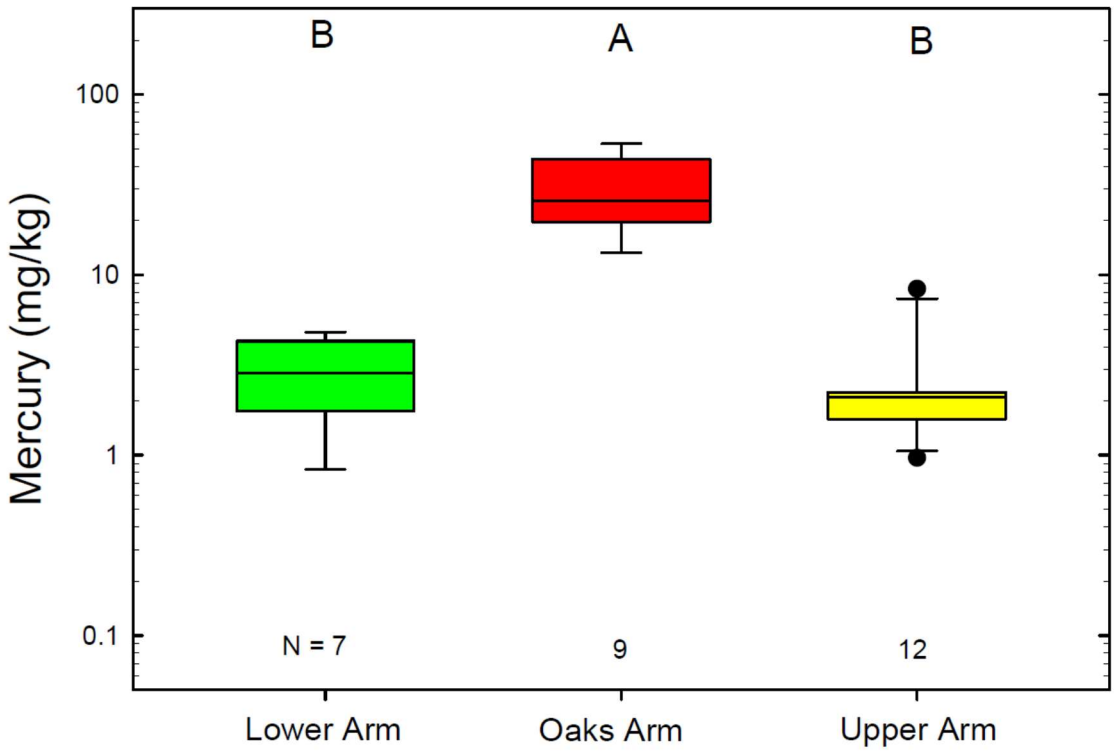

Figure 6.4.28. Box plots for mercury in shallow sediment (top 4 cm) from the three arms of Clear Lake. Letters at top indicate statistical differences using analysis of variance (ANOVA) on ranks. Numbers at bottom indicate number of samples from each arm of the lake. Boxes indicate interquartile range; horizontal lines indicate median; whiskers indicate 10th and 90th percentiles; circles indicate results below 10th percentile or above 90th percentile. Same vertical scale as Figure 6.4.29. Colors match locations in Figure 6.4.5. Data from Watanabe et al. (2025).

In tributaries to Clear Lake sampled for this study, nearly all of the samples had mercury concentrations less than 1 mg/kg (Figure 6.4.29). The overall median concentration was 0.06 mg/kg. The plot showing data for mercury concentrations in Clear Lake tributaries (Figure 6.4.29) displays data for six watershed groups, similar to the plots for P and TON (Figures 6.4.20 and 6.4.24). Mercury concentrations in samples from Burns Valley, Molesworth Creek, and Schindler Creek were significantly higher than those from the other five areas; median mercury concentration was 0.22 mg/kg. The median mercury concentration in the other five watershed areas ranged from 0.046 to 0.084 mg/kg (Figure 6.4.29). The Burns Valley, Molesworth Creek, and Schindler Creek watersheds are located closer to Sulphur Bank Mercury Mine than the other sediment source areas sampled for this study (Figure 6.4.1). It is possible that atmospheric transport of mercury vapor (e.g. Engle et al., 2005) or contaminated particulates from the mine site have affected these adjacent watersheds. Another possibility is that these watersheds are weakly mineralized as a manifestation of the Geysers - Clear Lake geothermal system that is responsible for the mercury mineralization at Sulphur Bank and for related hot springs; the geothermal system remains active. Although the Burns Valley, Molesworth Creek, and Schindler Creek watersheds have higher mercury concentrations in soil and sediment than the other source areas sampled for this study, these areas are not a significant source of mercury to Clear Lake, given that their concentrations are typically below 1 mg/kg (Figure 6.4.29) and nearly all lake sediments are above 1 mg/kg (Figure 6.4.28).

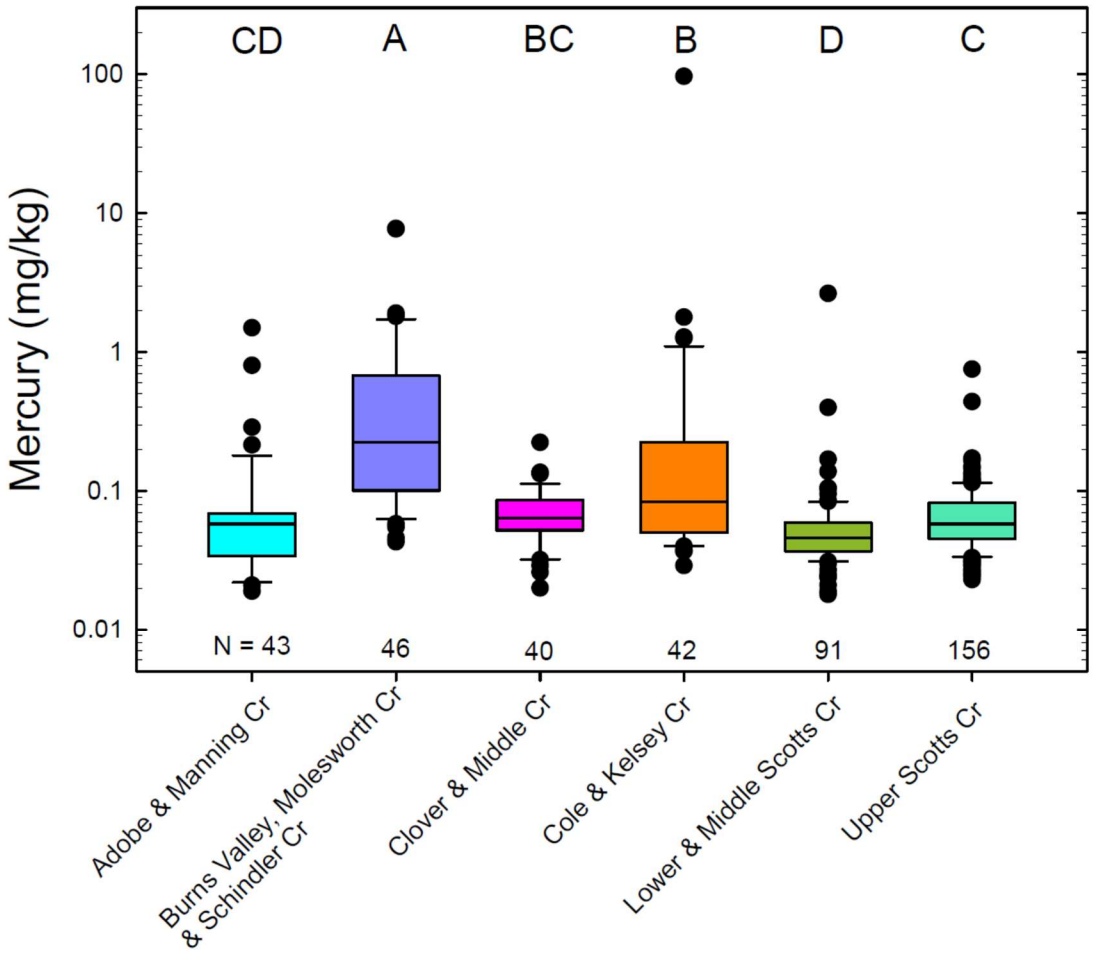

Figure 6.4.29. Box plots for mercury in soils and sediments from Clear Lake tributaries. Letters at top indicate statistical differences using analysis of variance (ANOVA) on ranks. Numbers at bottom indicate number of samples (N) from each tributary group. Boxes indicate interquartile range; horizontal lines indicate median; whiskers indicate 10th and 90th percentiles; circles indicate results below 10th percentile or above 90th percentile. Same vertical scale as Figure 6.4.28. Data summarized from Watanabe et al. (2025).

Mercury fails the "bracket test" for determining non-conservative behavior within Sed_SAT so it was not used a tracer for sediment fingerprinting calculations in this study.

Incorporation of geochemical data from mine waste and soils at Sulphur Bank Mercury Mine could potentially allow that source to be added for future refinements of the analysis presented in this report. A rough estimate of the contribution of sediment from the mine to the lake can be made by looking at mercury concentrations in terms of their order of magnitude. Concentrations of mercury in the mine waste are typically 500 to 5000 mg/kg (McVey et al., 2023). Given the observed concentrations in lake sediment sampled for this study (Figure 6.4.28), using only mercury as a tracer, the mine waste could represent 0.5 to 5% of the sediment in the Oaks Arm, and 0.1 to 1% of the sediment in the Upper and Lower Arms.

6.4.4 Discussion

6.4.4.1 Comparison of Sed_SAT model results with Hydrological Simulation Program–FORTRAN (HSPF) model results and drainage area

Results of Sed_SAT modeling are compared with results from Hydrological Simulation Program–FORTRAN (HSPF) sediment modeling and watershed areas in Table 6.4.8. Results of HSPF simulations (section 6.3) agree with Sed_SAT results regarding the two largest sources of sediment to Clear Lake — Scotts Creek and Middle Creek. The models diverge regarding the influence of Kelsey Creek. HSPF results indicate that Kelsey Creek is a strong third-place contributor of sediment, whereas Sed_SAT modeling (which combined Cole Creek with Kelsey Creek in Trial 1) indicates a much smaller contribution.

Table 6.4.8. Summary of Sediment Source Assessment Tool (Sed_SAT) results and comparison to watershed drainage areas and Hydrological Simulation Program–FORTRAN (HSPF) modeling (section 6.3). HSPF results represent averages of simulations from 1981– 2023. [T/yr, tons per year]

	Source group	Watersheds	Area (sq. mi.)	Area (sq. km)	% of modeled area	Sed_SAT % sediment source	HSPF % sediment discharge	HSPF sediment discharge (T/yr)	% area burned 2018
Trial 1	1	ScottsC+AdobeC+ManningC	141.4	366.2	44.8%	58.4%	45.3%	34,733	54.2%
	2	ColeC+KelseyC	72.3	187.3	22.9%	1.5%	15.8%	12,088	0.0%
	3	BurnsValley+MolesworthC+SchindlerC	24.8	64.2	7.9%	25.0%	11.0%	8,462	10.2%
	4	CloverC+MiddleC	76.8	198.9	24.4%	15.1%	27.9%	21,388	87.4%
		Totals	315.3	816.6	100%	100%	100%	76,671	46.5%
		Uncertainty				27%			
Trial 2	1	CloverC+MiddleC	76.8	198.9	42.6%	49.9%	44.6%	21,388	87.4%
	2	LowerScottsC+MiddleScottsC	54.3	140.6	30.1%	19.0%	55.4%	26,611	40.9%
	3	UpperScottsC	49.3	127.6	27.3%	31.1%			75.4%
		Totals	180.4	467.1	100%	100%	100%	47,999	70.1%
		Uncertainty				32%			

For Trial 1, the main source watersheds are source group 1 (Scotts, Adobe, and Manning Creeks) and source group 3 (Burns Valley, Molesworth Creek, and Schindler Creek). These two areas contributed 58.4% and 25.0% of sediment to Clear Lake, respectively, in the Sed_SAT Trial 1 results. Both of these source groups yielded sediment in a proportion greater than their watershed drainage areas: 44.8% and 7.9%, respectively (Table 6.4.8). The other two source groups considered in Trial 1 contributed a lower percentage of sediment compared with their drainage areas; Cole and Kelsey Creeks (source group 2) contributed only 1.5% of the sediment to Clear Lake in Trial 1 despite representing 22.9% of the modeled area; Clover and Middle Creeks (source group 4) contributed 15.1% of the sediment to Clear Lake in Trial 1 whereas these watersheds represent 24.4% of the modeled area (Table 6.4.8). Uncertainty in Trial 1 is estimated at 27% for Trial 1 and 32% for Trial 2 based on the sum of individual errors in quadrature.

In the HSPF model results, the sediment discharge contributions were closer to the relative watershed areas for all four source groups in Trial 1 of the Sed_SAT analysis. HSPF results for Cole and Kelsey creeks (15.8% contribution to sediment discharge) were somewhat lower than the drainage area (22.9%), but higher than the Sed_SAT Trial 1 model results

for this source group (1.5%; Table 6.4.8). The HSPF results for the other three source groups in Trial 1 were within 4% of their respective drainage areas (Table 6.4.8).

An important factor in comparing HSPF model results to the Sed_SAT analysis is that HSPF integrated results on sediment discharge to Clear Lake for the period 1981–2023, whereas Sed_SAT used target samples from Clear Lake taken from the top 4 cm, which may represent more recent deposition. Total sediment discharge computed by HSPF (section 6.3) corresponds to about 7.2×10^7 kg per year. Over the lake area of 180 km^2, this equals about 400 grams per m^2. Depending on assumptions regarding organic content, water content, and sediment density, the sedimentation rate appears to be similar to the long-term rate of about 0.4 to 1.0 mm/year computed by Sims and White (1982) over the past ~40,000 years. The top 4 cm of lakebed sediment sampled for this study would correspond to 40 years of deposition assuming an average deposition rate of 1 mm/yr, which is comparable to the 52-year interval modeled by HSPF. However, it is possible that the top 4 cm of lakebed sediment that was sampled for this study represents primarily more recent sediment that is heavily influenced by deposition since the 2018 Mendocino Complex Fire (Ryan, 2018), especially if the fire caused enhanced rates of sediment transport and deposition.

For Sed_SAT Trial 2, sediment source contributions were estimated as 49.9%,19.0%, and 31.1%, respectively from the three source group areas (Table 6.4.8). These percentages differ somewhat from the relative areas of the source groups. Group 1 (Clover and Middle creeks) and source group 3 (Upper Scotts Creek) have sediment source percentages in Sed_SAT Trial 2 somewhat higher than their relative areas by 7.3% and 3.8%, respectively. Source group 2 (Lower & Middle Scotts Creek) has a lower sediment source percentage compared to its relative area by about 11.1%(Table 6.4.8). Uncertainty of the Trial 2 Sed_SAT analysis is estimated at 32% based on several statistical metrics.

There are many possible factors that can influence sediment yield from watersheds, including slope, geology, soils, vegetation, unpaved roads, other land use types, and fire history (Curtis et al., 2005). A large portion of the Clear Lake drainage basin has been affected by wildfire over the past decade. Wildfire can cause large increase in erosion rates because removal of vegetation exposes bare soil, and other geomorphic processes (e.g., East et al., 2024, 2025). The most significant fire affecting the field area for this study during that period was the Mendocino Complex Fire (De Palma-Dow et al., 2022) which burned more than 1,850 km^2 during July 2018 through January 2019. In Table 6.4.8, the percentage area that burned during 2018 is indicated for the source groups in Trials 1 and 2 of the Sed_SAT analysis. The overall percentage burned in 2018 for the area modeled in Trial 1 was 46.5%. For Trial 2, the percentage are burned in 2018 was 70.1%.

In Trial 1, the only source group that did not burn in 2018 was source group 2 (Cole and Kelsey Creeks). Source group 2 yielded proportionally less sediment than its drainage area in both the Sed_SAT model and the HSPF model (Table 6.4.8). The lack of burning in that area could have contributed to the relatively low sediment yield.

In Trial 2, source group 1 (Clover and Middle Creeks) and source group 3 (Upper Scotts Creek) had the largest proportions of burned area (87.4% and 75.4%, respectively); these two source groups also contributed sediment to the target sites (Rodman Slough delta) at rates higher than their drainage areas. In contrast, source group 2 (Lower and Middle Scotts Creek) had the lowest proportion of burn area (40.9%) and it contributed sediment

to the target sites at a rate lower than its drainage area (30.1%). Wildfire history is but one of many factors that may have influenced sediment yield in the study area.

6.4.4.2 Qualifications and limitations of Sed_SAT modeling

The Sed_SAT tool (Gorman Sanisaca et al., 2017) was specifically designed to assist resource managers and regulatory agencies in applying the sediment fingerprinting approach to quantify sediment sources within the sediment framework for TMDLs (Total Maximum Daily Loads) – a provision of the Clean Water Act for impaired water bodies (U.S. Environmental Protection Agency, 2025). To interpret the unmixing model results for Trial 1, it is important to consider the extent of exchange of water and sediment between the arms of Clear Lake based on work by UCD (section 8 of this report). It appears that strong currents are capable of resuspending lakebed sediment and allowing for mixing of lake sediments between the Upper Arm, Oaks Arm, and Lower Arm.

Mercury was not used in the mixing calculations for this sediment fingerprinting analysis because it failed the "bracket test"—mercury concentrations in Clear Lake sediments are considerably higher (by a factor of 5x to 100x) compared with concentrations for nearly all samples collected in the monitored tributaries (see section 6.4.3.3). This is potentially related to the influence of the Sulphur Bank Mercury Mine, located on the eastern shoreline of the Oaks Arm (Figure 6.4.1). Evidence suggests that the principal source of mercury to Clear Lake sediments originated in the Oaks Arm, and that mercury is now dispersed in sediments throughout the lake (e.g., Suchanek et al., 2008; Marvin-DiPasquale et al., 2021) indicating that there is likely sediment exchange and mixing between the arms of the lake.

Inherent variability in the geochemical characteristics of the source groups increased uncertainty and diminished the discriminatory power of the LDA analysis. A higher density of sampling of watershed soils and sediment in some tributaries (for example, Burns Valley, Molesworth Creek, and Schindler Creek) may allow more narrowly defined source groups to be defined in support of more focused studies of sediment sources in the Oaks Arm and Lower Arm.

In this study, we used a standardized multivariate approach, but single tracers or ratios could also be effective tracers. For example, Takeda et al. (2004) found that phosphate fertilizers typically contain 10–200 times more U than soils but they also contain lower Th concentrations than the soils. The U/Th ratio can be an effective fingerprinting tool for watersheds with high phosphate loading (Evrard et al., 2013).

Size fractionation for this study was done using dry sieving after air-drying and gentle mechanical disaggregation. Wet sieving, an alternative approach that is more labor-intensive and therefore more costly, could have resulted in better separation between coarse and fine particles because of improved disaggregation, and could have increased the yield of fine particles (e.g. Gelhardt et al., 2021). However, wet sieving is prone to its own limitations—soluble minerals are lost and very fine particles may be lost with the wash water unless centrifugation methods are used.

Unmixing model results may also be improved by using a Bayesian mixing model (e.g., MixSIAR; Stewart et al., 2015; Stock et al., 2018). When there are source groups with a small number of samples, the use of Bayesian statistics enables prior knowledge about

river processes to increase the number of samples for discriminant analysis and mixing models (Walling and Collins, 2005; Collins et al., 2013; Cooper et al., 2014).

The statistical analyses and unmixing calculations described in this report are a small fraction of what could be done with the available dataset (Watanabe et al., 2025) to understand sediment sources and transport in the Clear Lake drainage basin. By choosing target samples at the lower integrator sites (9 tributaries) and upper integrator sites (7 subwatersheds in the Scotts Creek drainage), it may be possible to derive information about sediment sources with regard to processes (hillslope erosion versus in-channel processes), as well as land use and land cover (e.g. forests, unpaved roads, agriculture, urban, etc.).

Some additional potential tracers may provide more robust results for sediment source analysis in future studies. Strontium isotopes ($^{87}Sr/^{86}Sr$) are known to vary among tributaries to Clear Lake (Feyrer et al., 2019). This spatial variation is likely attributable to variations in rock type (Figure 6.4.4; Hammersley and DePaolo, 2006; Linn et al., 1992; Nelson, 1995). Pyrogenic (fire-related) carbon (e.g. Cotrufo et al., 2016) could be useful in tracking sediment from areas that have experienced recent wildfire. Microplastics are an emerging contaminant that may also provide some insight into sediment sources (e.g., Yang et al., 2021). If available, data for these tracers could be incorporated into future fingerprinting calculations to better constrain sediment source contributions to Clear Lake.

6.4.5 Summary and Conclusions

Sediment source analysis was done using data for several hundred soil and sediment samples collected during 2021–23 in the Clear Lake drainage basin. The sediment samples were collected from roadside ditches, stream sides (representing streambanks, alluvium, or colluvium), streambeds, and lakebed sediment. The samples were sieved to < 0.063 mm and analyzed for major elements, trace elements, organic and inorganic (carbonate) carbon, carbon and nitrogen stable isotopes, and particle size distribution.

Streambed sediment samples (n=140) from 9 tributary watersheds were used as source samples (divided into four source groups) in a basin-scale model (Trial 1) in which 26 lakebed sediments were used as target samples for unmixing calculations (Figure 6.4.2). A second model at a partial basin scale (Trial 2) used 231 samples of soils, roadside ditch sediment, and stream-side sediment as sources with three sediment samples from the Rodman Slough delta (Figure 6.4.3) as target samples.

Linear Discriminant Analysis (LDA) within the Sed_SAT program was used to determine which elements are the most effective natural tracers for different combinations of watershed source groups. Twelve tracers were selected for Trial 1 (in order of decreasing discriminatory power): K, Rb, Cr, Cs, Mg, Li, LOI-2*TOC, Ba, Sr, U, Sc, and Y (Appendix Table 15.6.4.2). The twelve tracers selected for Trial 2 were: Hf, Zn, Mg, Li, Cs, Nb, LOI-2*TOC, $\delta^{15}N$, Mn, Ga, Cr, and Sr (Appendix Table 15.6.4.6). Six tracers (Cr, Cs, Mg, Li, LOI-2*TOC, and Sr) were selected for both trials. Significant differences were found among source groups using ANOVA for nearly all of the selected tracers (Tables 6.4.5 and 6.4.6; Figures 6.4.9 through 6.4.14 and Appendix Figures 15.6.4.1 through 15.6.4.6). The differences in tracer concentrations among source groups are mostly attributed to spatial variations in geological rock type (Figure 6.4.4 and Appendix Table 15.6.4.1).

Results of HSPF simulations (section 6.3) agree with Sed_SAT results regarding the two largest sources of sediment to Clear Lake: Scotts Creek and Middle Creek. The models diverge regarding the influence of Kelsey Creek. HSPF results indicate that Kelsey Creek is a strong third-place contributor of sediment, whereas Sed_SAT modeling (which combined Cole Creek with Kelsey Creek in Trial 1) indicates a much smaller contribution. The area of Cole and Kelsey Creeks (source group 2 in Sed_SAT Trial 1) was the only one of the four source groups to have experienced no burning in 2018. According to results from both Sed_SAT and the HSPF model, this area produced less sediment than the other source groups per unit area. Wildfire history is but one of many factors that may have influenced sediment yield in the study area.

Concentrations of P and TON were determined in tributary soils and sediment and in lake sediments. These constituents were higher in concentration in lake sediments than in the tributary sediments; this non-conservative behavior precluded their use as tracers in sediment fingerprinting analysis.

Species of nutrients (forms of P and N) were evaluated in 72 streambed samples from tributaries and 29 lakebed sediment samples. Of the four forms of P evaluated, Fe-Al-associated P and loosely-bound P are the forms most susceptible to mobilization as soluble reactive phosphorus (SRP) during anoxic bottom-water conditions, which can stimulate harmful algal blooms (Swann et al., 2024). Very low concentrations of loosely-bound P were detected in the tributary and lakebed samples. Concentrations of Fe-Al-associated P account for about 20–25% of total P in lakebed sediments. The proportion of Fe-Al-associated P in tributary streambed sediments ranged from 4% in Kelsey Creek to 17% in Cole Creek. Other tributaries with greater than about 10% Fe-Al-associated P were Burns Valley and Molesworth Creek, Manning Creek, Schindler Creek, and Scotts Creek.

Total mercury concentrations in soils and sediments (n = 418) sampled in Clear Lake tributaries were nearly all (98%) less than 1 mg/kg. In contrast, mercury concentrations in lakebed samples (n = 28) were nearly all greater than 1 mg/kg. As expected from previous studies (e.g., Suchanek et al., 2008), mercury concentrations in lake sediments were higher in the Oaks Arm (median of 26 mg/kg) than in the other two arms (median values of 2 to 3 mg/kg). This supports the hypothesis that the dominant source of mercury to Clear Lake is the Sulphur Bank Mercury Mine, located on the eastern shore of the Oaks Arm. The distribution of elevated mercury concentrations in all three arms of Clear Lake is evidence of inter-basin mixing by lake currents. The non-conservative behavior of mercury made it unsuitable for use a tracer in the sediment source analysis. Concentrations of mercury in mine waste at Sulphur Bank Mercury Mine are typically 500 to 5000 mg/kg (McVey et al., 2023). Given the observed concentrations in lake sediment sampled for this study, using only mercury as a tracer, the mine waste could represent 0.5 to 10% of the sediment in the Oaks Arm, and 0.1 to 1% of the sediment in the Upper and Lower Arms.

In summary, this study investigated the relative contributions of sediment from various source watersheds in the Clear Lake basin based on sediment and soil geochemistry and stable isotope tracers. Study results regarding the spatial variability of characteristics of sediment from different tributary watersheds may be used to inform restoration strategies and to develop targeted management strategies to reduce sediment inputs from specific sources, with the goal of improving water quality in Clear Lake.

7 In-Lake Monitoring (UCD-TERC)

Data presented in this section is available through the Environmental Data Initiative portal (Cortés et al. 2025)

7.1 Inflow Water Quality

7.1.1 Methods

We installed high-frequency continuous turbidity and temperature stations with independent Campbell Scientific dataloggers co-located with Department of Water Resources (DWR) gauging stations at three locations on inflowing creeks: Middle Creek, Scotts Creek, and Kelsey Creek (Table 7.1.1, Figure 7.1.1). Lake level and rainfall from those gauging stations are available at the California Nevada River Forecast Center website (https://www.cnrfc.noaa.gov). Each station had an FTS DTS-12 SDI turbidity sensor equipped with a wiper (Figure 7.1.1) sampling at 20 Hz and transmitting data every 10 minutes. We collected data between 2019 and 2024. Each summer, turbidity sensors were removed from the creeks and sent back to the manufacturer for calibration before their reinstallation for the rainy season was initiated (~October).

The turbidity sensor has a range of 0-1,500 NTU, a resolution of 0.01 NTU, an accuracy of 2% of full-scale reading in the range of 0-500 NU, and 4% of full-scale reading in the range of 500-1500 NTU. Temperature accuracy is +/- 0.1 deg. C. Data has been uploaded via modem to a server in the Department of Civil and Environmental Engineering at the University of California, Davis (UC Davis). Then, data was stored on an Amazon Web Services (AWS) account, which provided redundant storage and accessibility through the UC Davis Clear Lake website.

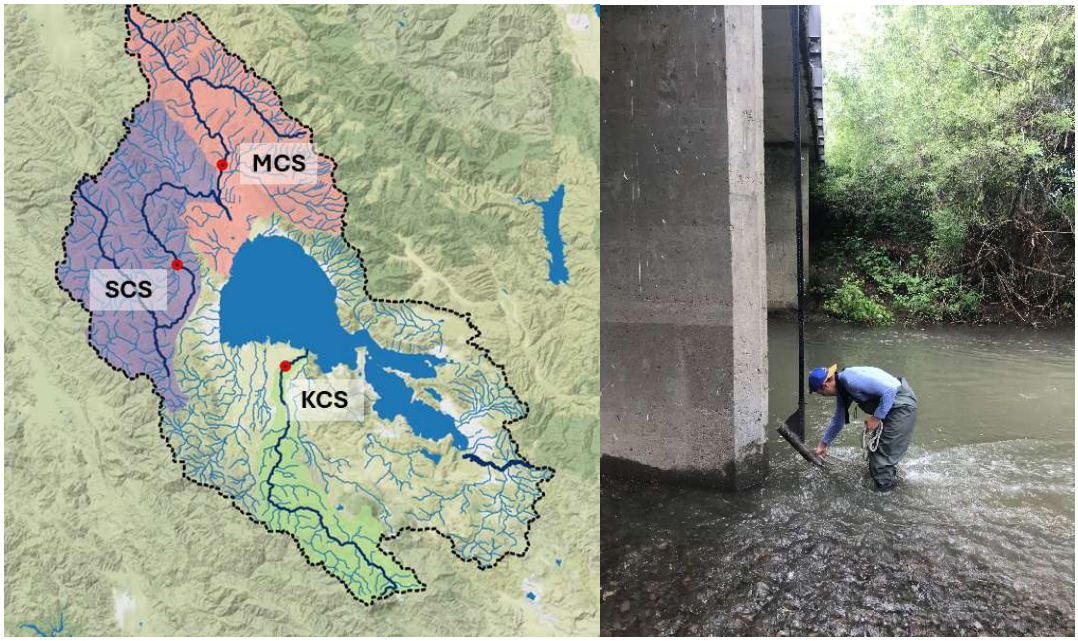

Figure 7.1.1. (left) Map showing the location of the FTS turbidity stations. (right) FTS digital turbidity DTS-12 sensor at Scotts Creek

Table 7.1.1. Details of FTS turbidity stations and data availability

ID	Creek	Road/ Near by	GPS coordinates	Stage and Rain Website
MCS	Middle Creek	Rancheria Road	39.18° N, 122.91° W	https://www.cnrfc.noaa.gov/graphicalRVF.php?id=MUPC1
SCS	Scotts Creek	Eickhoff Rd	39.10° N, 122.96° W	https://www.cnrfc.noaa.gov/graphicalRVF.php?id=SKPC1
KCS	Kelsey Creek	Kelsey Creek Dr.	38.93° N, 122.84° W	https://www.cnrfc.noaa.gov/graphicalRVF.php?id=KCVC1

7.1.2 Results

Time series of stream turbidity and flow measured at Middle, Scotts, and Kelsey Creeks show the interannual variability of the water years between 2019 and 2024. Dry years occurred in 2020, 2021, and 2022, while we experienced wet years in 2019, 2023, and 2024 (Figure 7.1.2). Peak flows in wet years at Middle Creeks reached values of 8,000 cfs (250 m^3/s), and only 2,000-3,000 cfs (55-85 m^3/s) in Scotts Creek and Kelsey Creeks, respectively. We measured mean turbidity values of ~1,000 NTU in all streams, with a tendency to higher values in Scotts Creek.

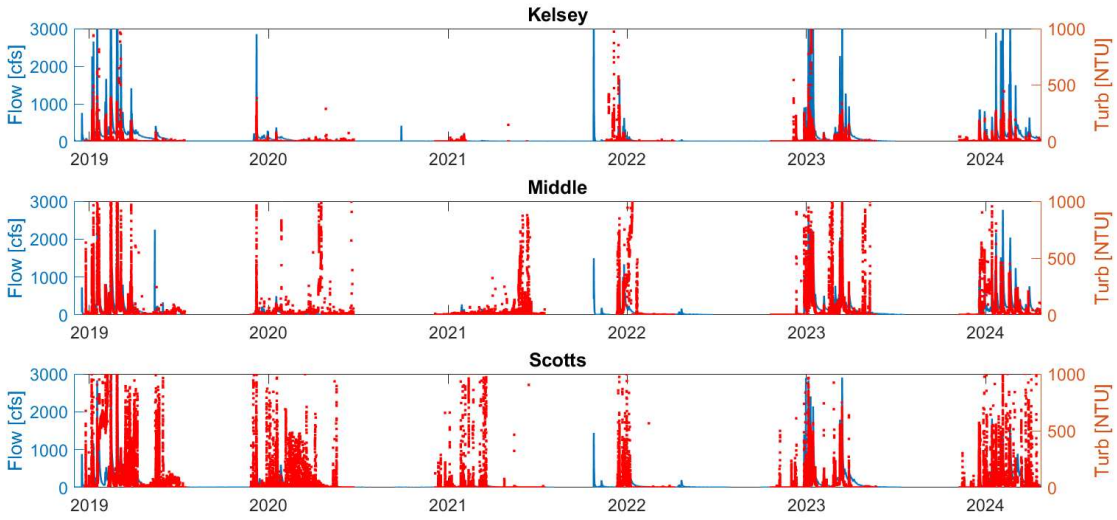

Figure 7.1.2. Time series of stream turbidity (NTU) and flow (cfs) measured at Kelsey, Middle, and Scotts Creeks between 2019 and 2014.

We developed stream-specific linear regressions relating discharge to TP, derived from routine stream monitoring data collected by the Lake County Department of Water Resources from 2014-2018 (Figure 7.1.3). Samples from 2019 – 2021 were excluded due to the large variability in concentrations and the limited number of samples collected during this time frame. Additional information comparing these stream samples can be found in Appendix 15.7.1.

Another potential product of this data set is the development of stream-specific linear regressions relating turbidity and TP/TN between 2022 and 2024 using nutrient concentrations quantified by the USGS stream water quality program.

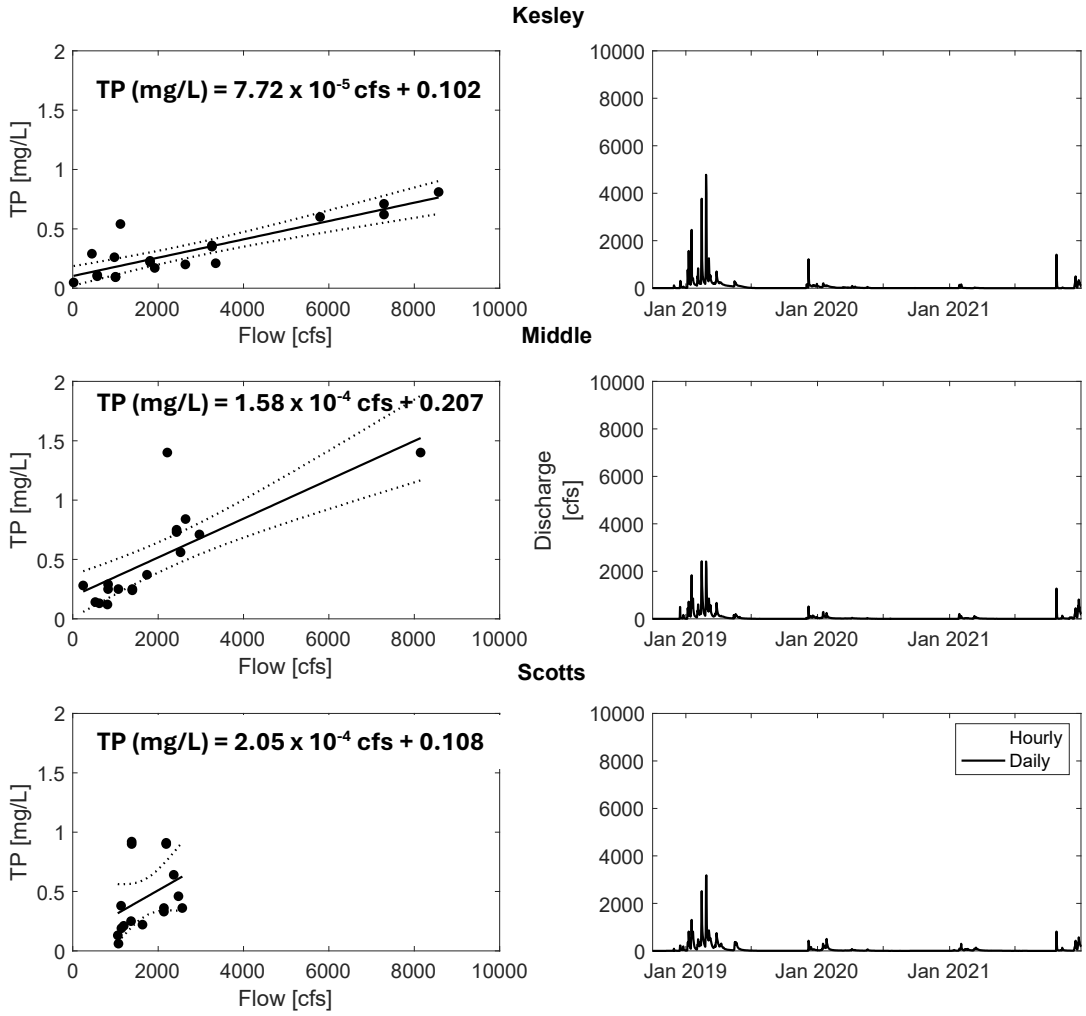

Figure 7.1.3. Left) Discharge vs TP curves based on Lake County stormwater monitoring data (2014-2018). The dotted lines indicate 95% confidence interval. Right) Hourly and daily stream hydrographs for gaged tributaries

7.2 Meteorological Stations and Lake Surface Temperatures

7.2.1 Methods

Seven meteorological stations were installed around the shoreline of Clear Lake on private docks and buildings to characterize the spatially and temporally varying meteorology around the lake (Figure 7.2.1). The selected locations were: Buckingham Point (BKP), Konocti Bay (KNB), Beakbane Island (BBI), Clearlake Oaks (CLO), Nice (NIC), North Lakeport (NLP), and Big Valley Rancheria (BVR). (Table 7.2.1). Note that BVR meteorological station was at an in-land location away from the shore. The wind field is a key input to a spatially variable (three-dimensional) hydrodynamic in-lake model and thus critical to characterize properly. The complex surrounding topography at Clear Lake

contributes to the variability of the wind magnitude and direction across the lake. Data from the meteorological stations will be interpolated to obtain time-varying, spatially distributed wind fields for the in-lake model.

We used Davis Instruments *Wireless Vantage Pro2 Plus* meteorological stations (https://www.davisinstruments.com/solution/vantage-pro2/), which recorded wind speed and direction, rain, solar radiation, air temperature, and relative humidity every 15 min. A Vantage Connect system sent the data to the WeatherLink Cloud using a cell modem every hour (Figure 7.2.2). From the WeatherLink Cloud, the data can be accessed via smartphone with the WeatherLink Mobile App (iOS and Android). The data was also archived on our Amazon Web Services (AWS) account. Data are publicly available via the TERC-Clear Lake website (clearlakerehabilitation.ucdavis.edu).

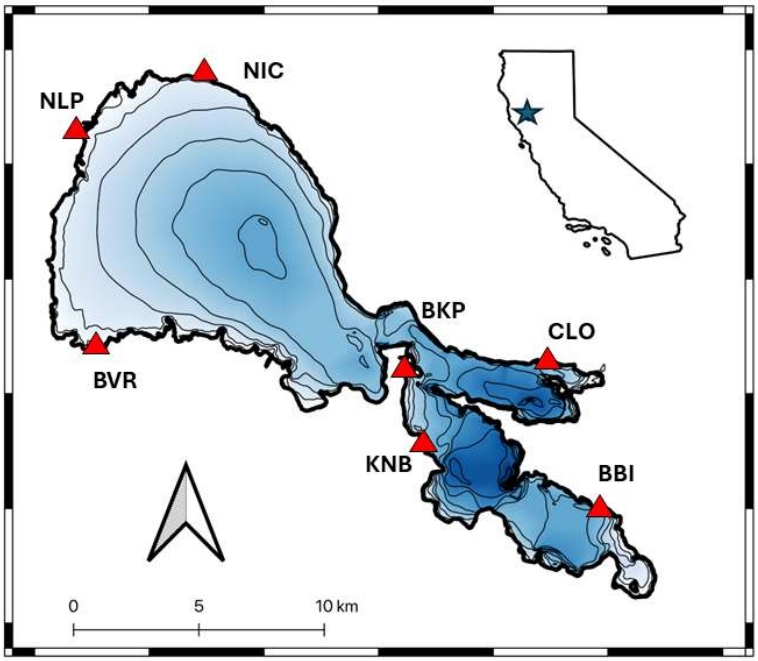

Figure 7.2.1. Location of the meteorological stations on the shoreline of Clear Lake

Table 7.2.1. GPS location of the seven UC Davis meteorological stations at Clear Lake

Location	ID	Latitude (°)	Longitude (°)
Beakbane Island	BEK	38.949779	-122.64555
Buckingham Point	BKP	39.016991	-122.75053
Big Valley Rancheria	BVR	39.025291	-122.88712
Clearlake Oaks	CLO	39.018989	-122.67577
Konocti Bay	KNB	38.99276	-122.74281
Nice	NIC	39.12188	-122.85102
North Lakeport	NLP	39.095301	-122.89978

Figure 7.2.2. Weather station equipment (left-center) Davis Instruments Vantage Pro 2, and (right) Vantage Connect.

Surface inshore temperatures were measured with Hobo Water Temp Pro V2 temperature loggers (accuracy +/- 0.2 deg C and resolution +/- 0.02 deg C) sampling every 10 min and located at the 6 docks where meteorological stations were located around the lake. Loggers were protected by a PVC caging slide inside a ~3 ft perforated PVC pipe attached to a floating dock (Figure 7.2.3). Data from the temperature inshore loggers was downloaded every 4-6 months. All raw data files were stored in a cloud-based storage (AWS), and processed data was uploaded to the SQL database.

Figure 7.2.3. PVC pipe attached to a floating dock to protect the inshore temperature logger. (Right) Caging containing the inshore temperature logger

7.2.2 Results

Meteorological forcing at Clear Lake presented seasonal changes typical of a Mediterranean climate over a given year.

Figure 7.2.4 shows daily meteorological attributes measured at Buckingham Point station between 2019 and 2023. We computed running averages over 10 days and compared records for each variable between years to evaluate interannual variability (Figure 7.2.5). We also computed mean and standard deviation for all variables during the summer (June-Aug) of the five studied years.

Clear skies and maximum daytime incoming shortwave radiation of ~380 W m^{-2} were characteristic during spring and summer (June-Aug), while a greater number of cloudy days with half of that solar input occurred during winter (Dec-Feb). Air temperatures varied between 0°C and 38°C while the lake surface temperature only oscillated between 8.2°C and 29.8°C. Differences between both temperatures at a given time changed seasonally, ranging from a couple of degrees in spring and winter to up to ~8°C in summer and fall. Daily variability of air temperatures ranged between 4°C in cold months to more than 12°C in warm months, while day-night lake surface temperatures only changed ~0.5°C and 2°C, respectively. Cold and wet fronts occurred during the whole year. Relative humidity was ~85-100% and air temperatures dropped more than 8°C during those events. Multiple fronts of dry and warm air were observed in spring and summer when relative humidity dropped below 30% and air temperature increased above 30°C. On average, relative humidity was ~90% in winter and relatively stable in 24 hours, while it was ~60% during the rest of the year, being lower during the day (~35%) and higher at night (~85%). Wind speeds and daily maxima changed between 2 m s^{-1} and 10 m s^{-1}. We observed high winds during cold and wet fronts, while warm and dry fronts tended to be associated with low winds. The wind regime has a diurnal periodicity, with predominant winds from the northwest being low between midnight and early morning and reaching peak values in the afternoon.

Table 7.2.2. Average and standard deviation of summer (June-Aug) meteorological variables measured between 2019 and 2023 at Buckingham Point. We show incoming shortwave radiation (SWin), surface lake temperature (SurfT), air temperature (AirT), relative humidity (RH), wind speed (WS).

Variables	2019	2020	2021	2022	2023
SWin (mean)	315.7	294.9	304.3	299.8	299.2
SWin (std)	15.5	14.6	14.3	19.8	19.2
AirT (mean)	24.4	24.9	25.7	24.1	24.2
AirT (std)	4.8	5.4	5.6	5.6	5.4
SurfT (mean)	24.8	24.7	25.2	24.0	25.0
SurfT (std)	1.9	2.2	2.3	2.5	2.0
RH (mean)	54.5	52.4	49.5	55.8	57.0
RH (std)	15.5	15.9	15.0	16.4	15.6
WS (mean)	2.3	1.9	2.7	3.0	2.3
WS (std)	2.1	2.0	2.6	2.4	2.3

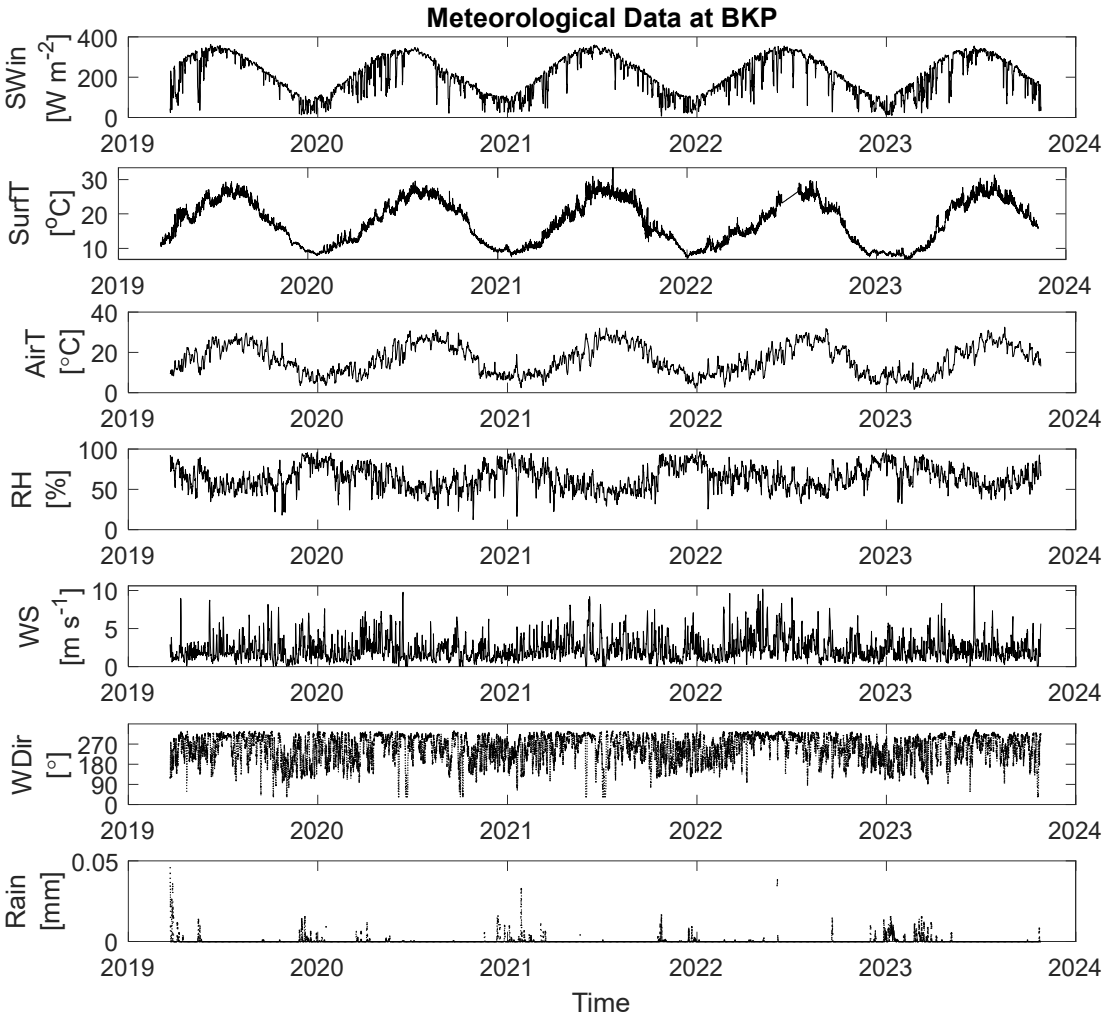

Figure 7.2.4. Time series of meteorological conditions at Buckingham Point between 2019 and 2023. We show incoming shortwave radiation (SWin), surface lake temperature (SurfT), air temperature (AirT), relative humidity (RH), wind speed (WS), wind direction (WDir), and rain (Rain).

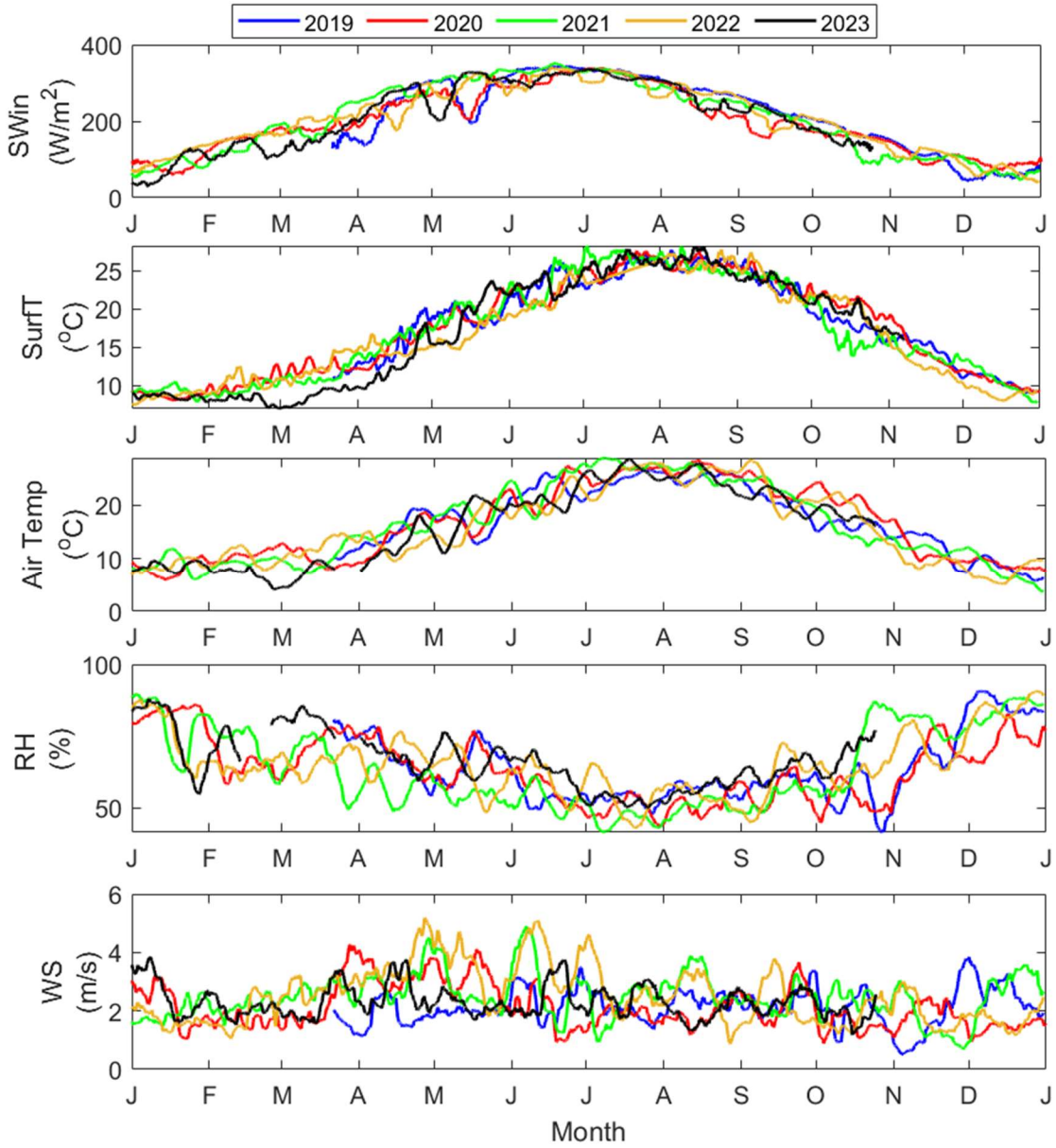

Figure 7.2.5. Time series of 10-day running averages of meteorological conditions at Buckingham Point between 2019 and 2023. We show incoming shortwave radiation (SWin), surface lake temperature (SurfT), air temperature (AirT), relative humidity (RH), and wind speed (WS).

Wind direction and magnitude changed significantly **across the lake**, while other variables experienced only subtle changes between basins (see Appendix 15.7.2). On average, air and lake surface temperatures, relative humidity, and incoming solar varied across the lake only 0.8°C, 0.3°C, 5%, and 20 W m^{-2}, respectively. Differences were larger in summer and fall. Maximum wind values in the Upper Arm were half those measured in the other two basins. Wind direction was predominately north to northwest in the windier basins (Oaks and Lower Arm), while that was not obvious at the stations in the Upper Arm (Figure 7.2.6). Sheltering and inland effects may have yielded low wind measurements at some locations around the lake (BVR station).

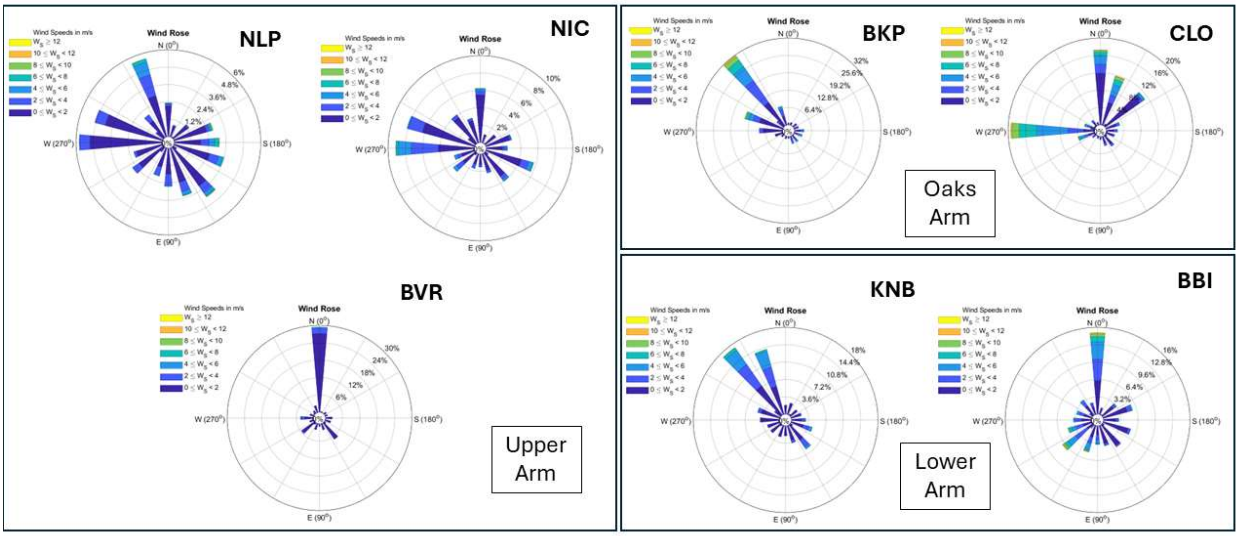

Figure 7.2.6. Wind roses showing the predominant magnitude and direction of the wind recorded by the seven meteorological stations at Clear Lake grouped by Arm: [Upper] North Lakeport (NLP), Nice (NIC), Big Valley Rancheria (BVR), [Oaks] Buckingham Point (BKP), Clearlake Oaks (CLO), [Lower] Konocti Bay (KNB), Beakbane Island (BBI)

7.3 Permanent Mooring Stations

7.3.1 Methods

Six semi-permanent water quality stations (or moorings) were deployed in Clear Lake to measure continuously water temperature and dissolved oxygen concentrations at multiple depths (Figure 7.3.1, Table 7.3.1). These stations did not have surface expression to reduce the chances of theft or vandalism. They each have a 100 lb steel anchor, making it extremely difficult for a recreational fisherman to disturb if accidentally snagged.

Each station consists of up to 12 RBRsolo^3 temperature loggers spaced about 1 m (accuracy ±0.002 deg C and resolution ±0.00005 deg C). The stations also had 1 or 2 RBRvirtuoso^3 dissolved oxygen (DO-RBR) sensors (accuracy maximum of ±8µM or ±5% and resolution <1µM or saturation 0.4%) 0.5 m and 2 m off the bottom. Only the three deepest stations had two near-sediment DO sensors (UA-06, OA-04, LA-03). In addition, those deep arrays had an epilimnetic dissolved oxygen sensor from PME (miniDOT) 3.5 m below the surface (accuracy of 5% of measurement or 0.3 mg L^{-1}, whichever is larger, and resolution

of 0.01 mg L^{-1}). The moorings were deployed at locations shown in Figure 7.3.1. An Onset HOBO U20-001-01water depth sensor was installed on each mooring line to allow for the precise depth of each logger to be known and allowance for changing water levels to be made during the data processing. These sensors have a 10 m depth range, are accurate to 0.5 cm, and have a resolution of 0.21 cm. A Sonotronics-coded acoustic pinger was attached to each mooring line. This assisted with retrieval. Data are publicly available via the TERC-Clear Lake website (clearlakerehabilitation.ucdavis.edu).

Table 7.3.1. GPS locations and nominal depths of moorings

Station #	Latitude (deg. N)	Longitude (deg. W)	Depth (m)
UA-01	39.024	122.788	8
UA-06	39.061	122.817	9
UA-08	39.094	122.847	6
NR-02	39.028	122.745	9
OA-04	39.0127	122.699	12
LA-03	38.983	122.717	13

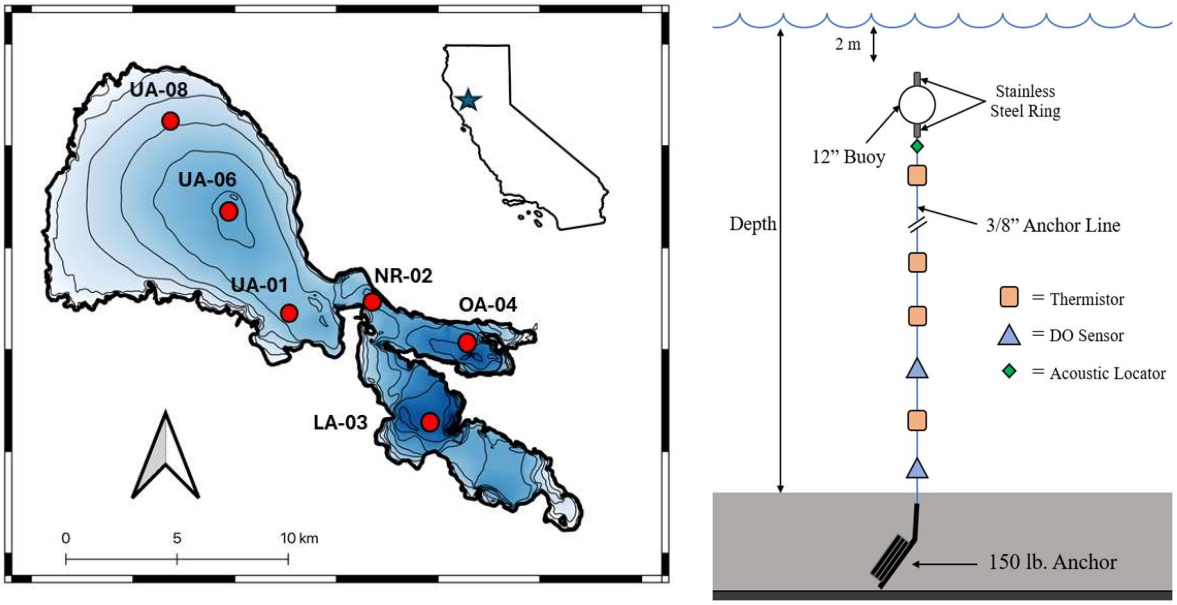

Figure 7.3.1. (left) Mooring locations (red dots) in Clear Lake; (right) Mooring arrangement. This mooring layout does not allow temperature measurements in the top 2-3 m surface

The frequency of instrument retrieval and data downloading was every 4-6 months (90 - 180 days). The sampling frequency for the RBR T and DO sensors was 10 and 30 seconds, respectively. The DO-miniDOT sensor sampled every 1-10 min. The DO wiper (for removing bio-fouling) was programmed to wipe every 3 hours. The pressure sensors were programmed to sample at 1 h intervals. The nominal mooring layout is shown in Figure 7.3.1. The instruments were cable tied and taped to 3/8" double braid polyester yacht

braid. This rope has a working strength of 4200 lb, and has low stretch properties. The buoy was a 12" trawl float with 27 lb of buoyancy.

7.3.2 Results

Lake temperatures in each basin varied seasonally (~28◦C in summer and ~8◦C in winter) and monthly during spring, summer, and fall as a result of multiple stratification and mixing events that occurred almost simultaneously across the lake (Figure 7.3.2 shows data from the three deep moorings). As a result, the strength of the stratification changed rapidly. We use an index called buoyancy frequency (N) to characterize the strength of the stratification as follows:

$$N = \sqrt{\frac{g}{\rho}\frac{\Delta\rho}{\Delta z}}$$

Where ρ is the mean density of the water column, Δz in the change is depth when we observe a density gradient of $\Delta\rho$, g is the acceleration of gravity. The water column was weakly stratified in winter (Dec-Feb) with a mean buoyancy frequency of $N < 0.005$ s^{-1}, while values increased up to 0.01 s^{-1} during fall (Sep-Nov) and spring (Mar-May). Stratification became stronger in the summer (June-Aug), with $N > 0.015$ s^{-1} for 2-3 weeks, normally followed by a mixing event. Temperature gradients in depth tended to be stronger in the Upper Arm than in the Oaks and Lower Arms during summer and fall (Figure 7.3.3). Summer stratification in 2019 and 2020 had multiple cycles of stratification and mixing (4-5 events), while 2021 and 2022 were characterized by a longer and stronger stratified period in the middle of the summer (June-July). Summer of 2023 showed longer than usual stratified periods (~4 weeks) followed by very short periods of mixing (< 1 week).

The strength of the stratification was inversely related to dissolved oxygen (DO) concentrations near the sediments across the lake (Figure 7.3.4). We were not always able to characterize the gradient of DO in the water column because some sensors malfunctioned during our deployments. That was obvious in the Upper Arm, where the shallow depths and high nutrient concentration tended to damage our sensors more often. During spring and summer, near-bottom DO concentrations were progressively depleted for 10–15 days after the onset of stratification or $N > 0.01$ s^{-1}. If the near-sediment water column remained isolated for at least one week, hypoxic conditions (DO<3.5 mg/L) developed next to the sediment-water interface (Figure 7.3.5). As for the stratification, multiple cycles of hypoxia and oxygenation occurred in 2019 and 2020, while more prolongated hypoxic periods were observed between 2021 and 2023, lasting 4 weeks or more during the summer.

Both Figure 7.3.3 and Figure 7.3.5 show a good synchronism in stratification and development of hypoxia across the lake. In general, stronger density gradients and longer periods of hypoxia were observed in the shallow Upper Arm, but the differences are very small. Table 7.3.2 shows the days that each basin remained hypoxic each year across the three basins. Overall, all basins tend to have between 3 to 5 months of hypoxia, and this period has increased by a week or two since 2019, probably as a result of the prolongated drought period (2020-2022), which has not shown an improvement during the wet year we had in 2023.

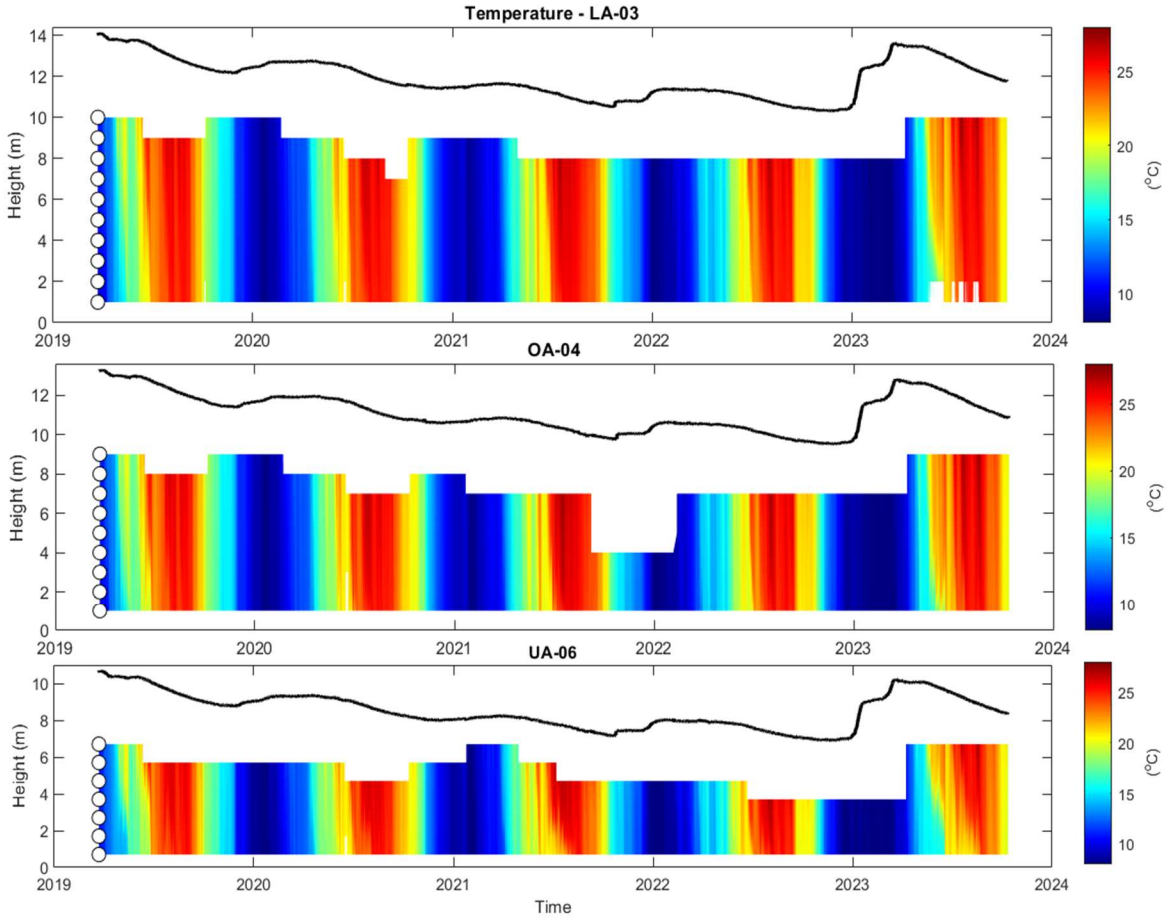

Figure 7.3.2. Time series in depth (as a function of distance from the bottom) of hourly lake temperature at multiple depths between 2019 and 2023. Each subplot shows data from a different mooring: (top) LA-03, (middle) OA-04; (bottom) UA-06. The white circles mark the location where we had instruments measuring temperature continuously. The top black line indicates the changes in lake level.

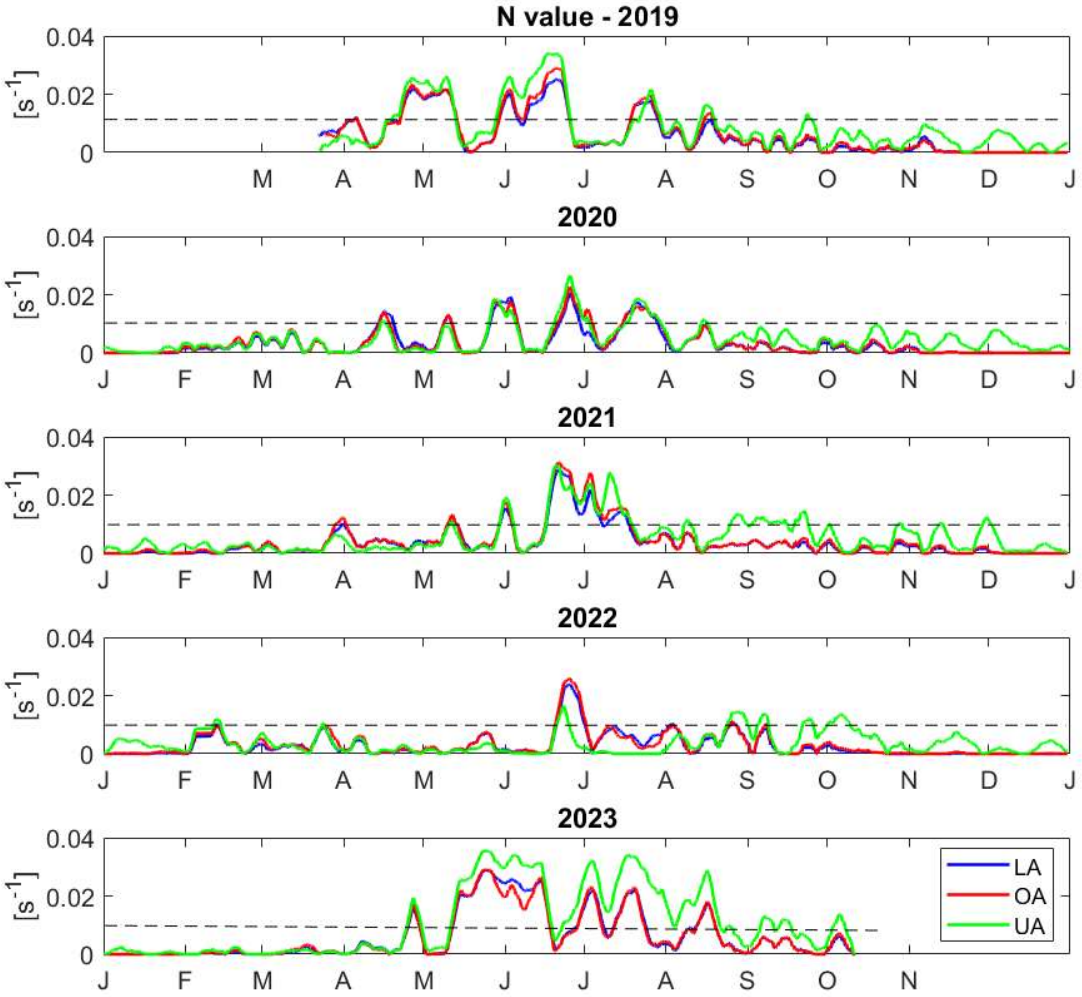

Figure 7.3.3. Time series of 5-day averaged buoyancy frequency as an index of stratification (N) at the three deep moorings, representing each basin: Lower Arm (LA), Oaks Arm (OA), and Upper Arm (UA). Each subplot shows the data from a different year between 2019 and 2023.

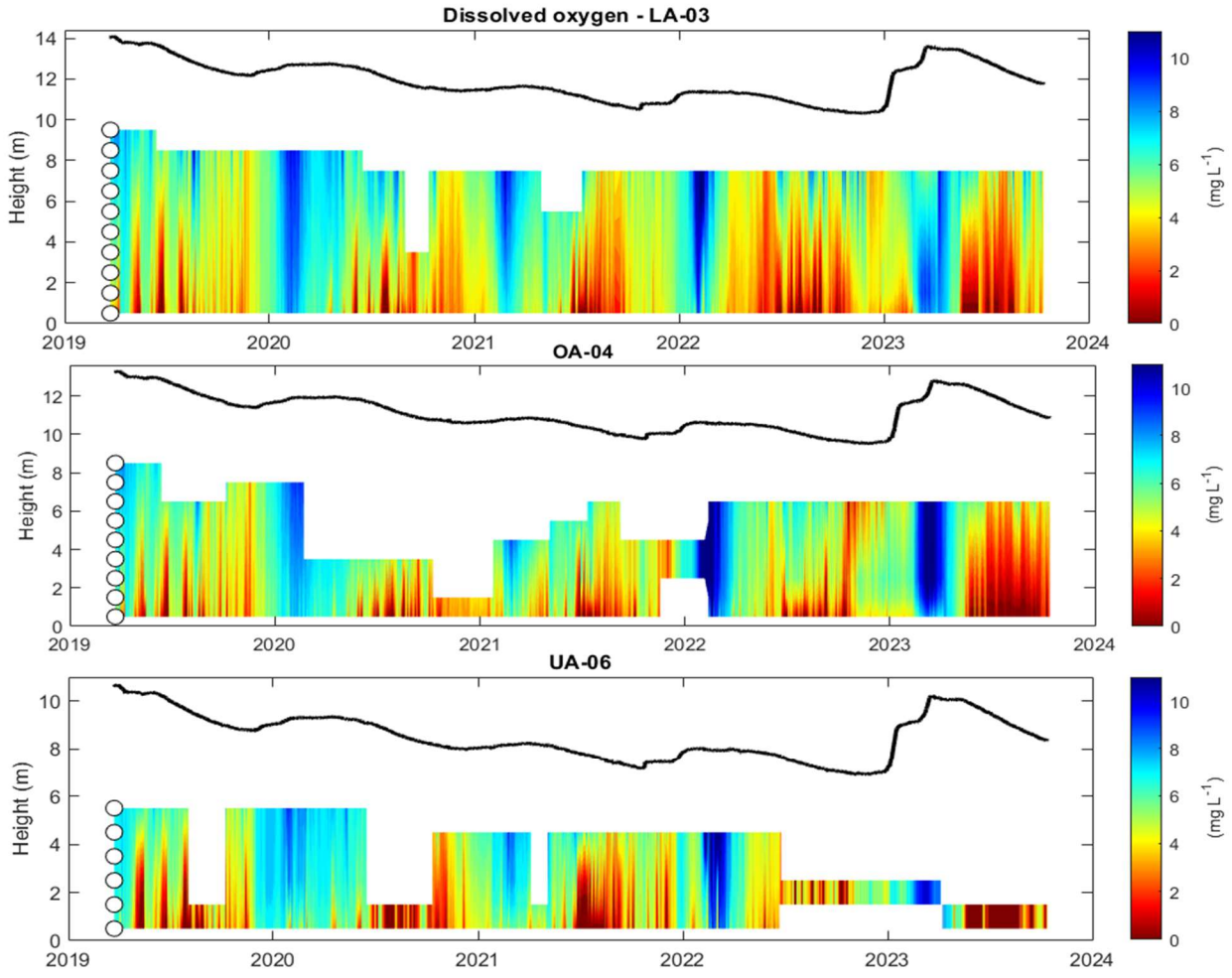

Figure 7.3.4. Time series in depth (as a function of distance from the bottom) of hourly dissolved oxygen at multiple depths between 2019 and 2023. Each subplot shows data from a different mooring: (top) LA-03, (middle) OA-04; (bottom) UA-06. The white circles mark the location where we had instruments measuring temperature continuously. The top black line indicates the changes in lake level.

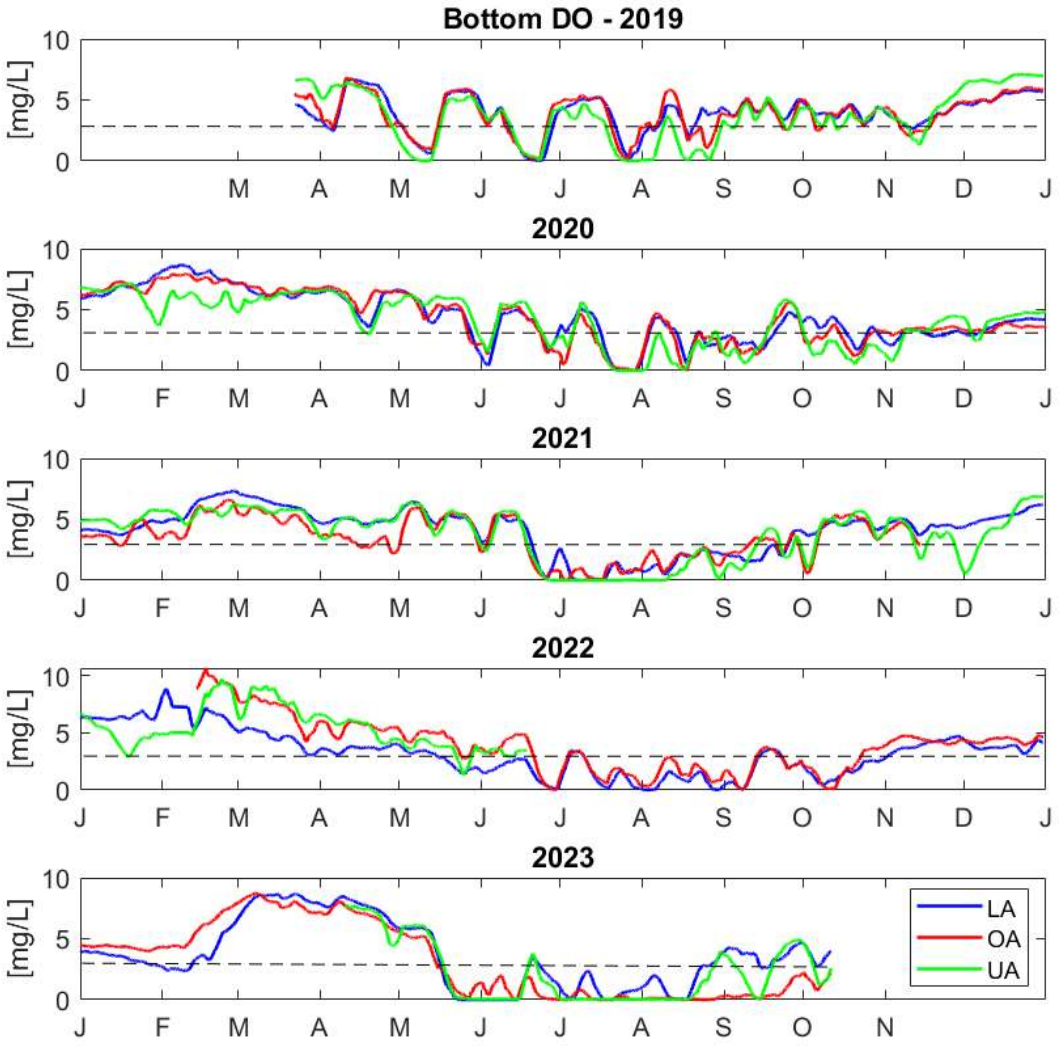

Figure 7.3.5. Time series of 5-day averaged bottom dissolved oxygen (DO) at the three deep moorings, representing each basin: Lower Arm (LA), Oaks Arm (OA), and Upper Arm (UA). Each subplot shows the data from a different year between 2019 and 2023.

Table 7.3.2. Number of hypoxic days (DO < 3.5 mg/L) at the three deep sites (Lower Arm, Oaks Arm, and Upper Arm) between 2019 and 2023.

	2019	2020	2021	2022	2023
LA	92	136	102	200	152
OA	108	148	148	133	151
UA	128	147	132	-	130

We observed strong interannual variability in stratification and hypoxia in all basins (Figure 7.3.6, Figure 7.3.7, Figure 7.3.8). Depth-averaged lake temperatures changed by 2-3°C in spring and fall between 2019 and 2023, while summer depth-averaged lake temperatures were very similar in summer of all years. Patterns of stratification and hypoxia had very different timing each year. However, the strong stratification hypoxic season was coincident with the summer (mid-May to min-August).

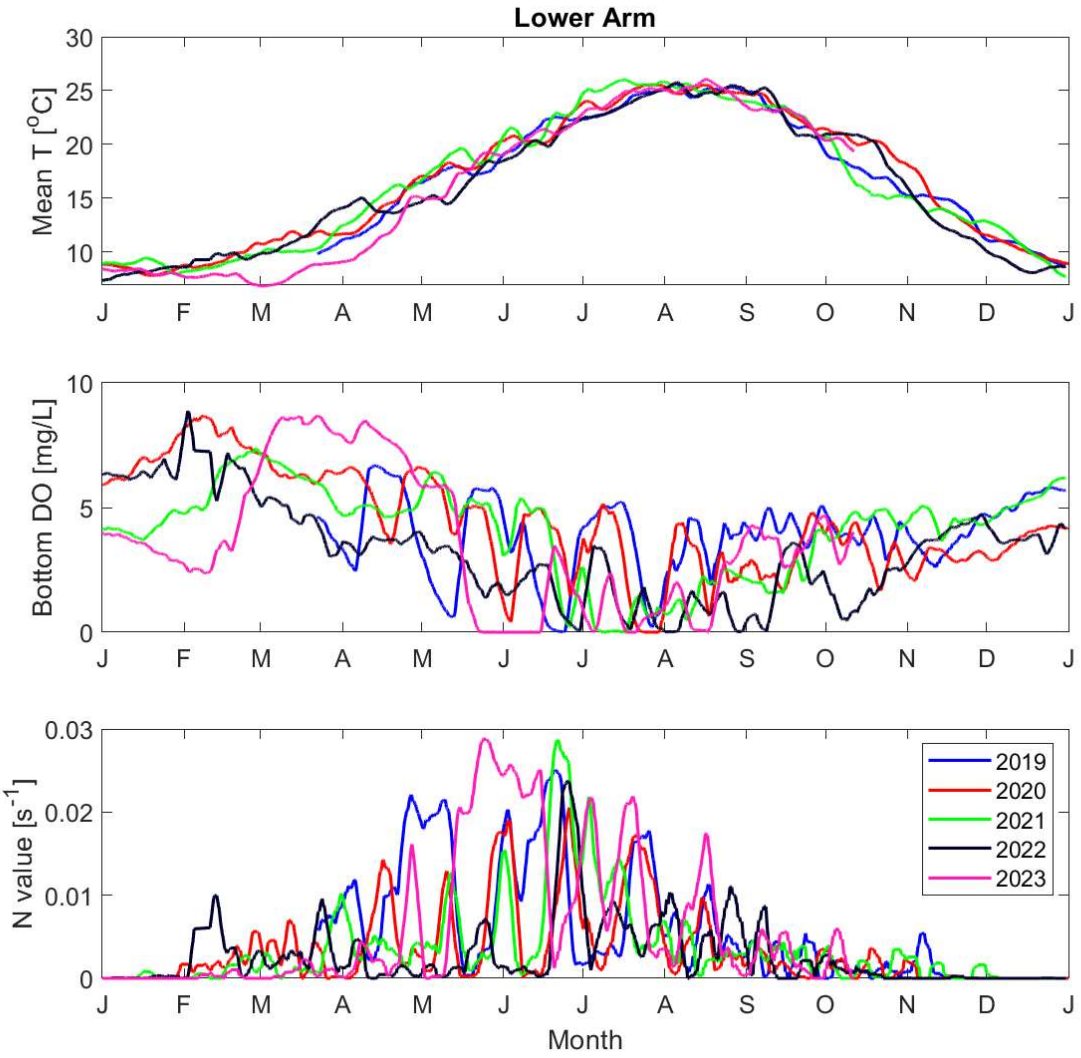

Figure 7.3.6. Time series in the Lower Arm deep mooring of (top) mean lake temperature; (middle) bottom dissolved oxygen (DO), and (bottom) buoyancy frequency or index of stratification (N). Each line corresponds to a different year between 2019 and 2023.

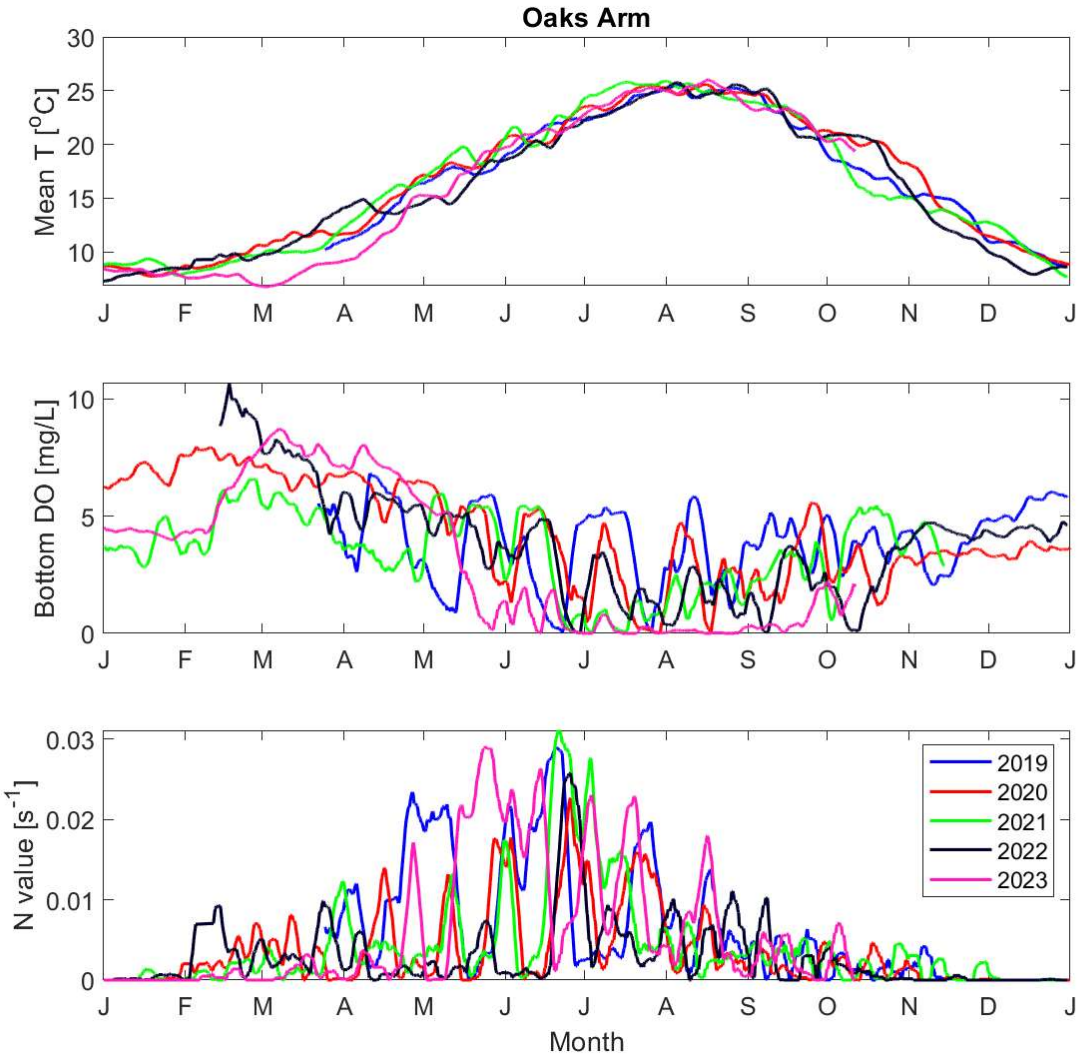

Figure 7.3.7. Time series in the Oaks Arm deep mooring of (top) mean lake temperature; (middle) bottom dissolved oxygen (DO), and (bottom) buoyancy frequency or index of stratification (N). Each line corresponds to a different year between 2019 and 2023.

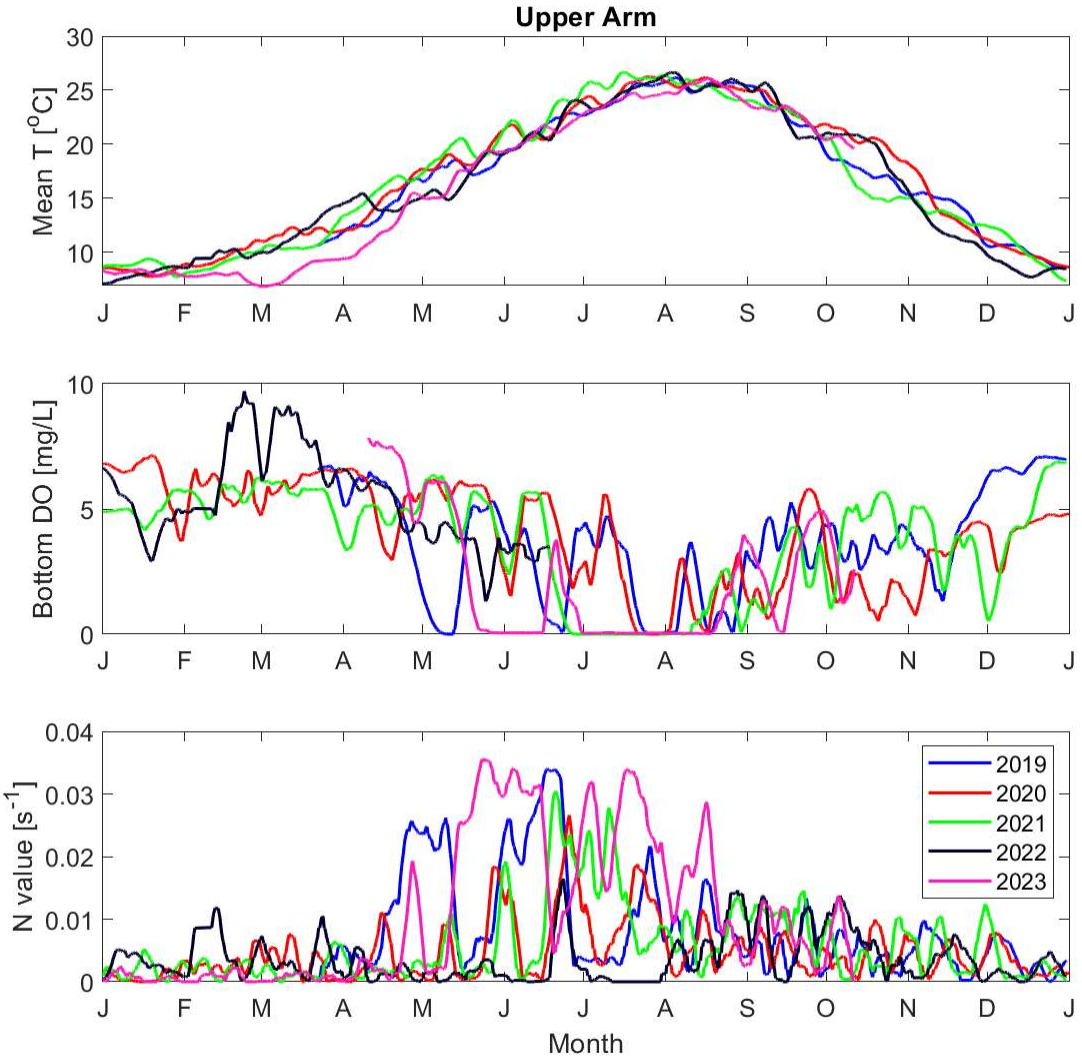

Figure 7.3.8. Time series in the Upper Arm deep mooring of (top) mean lake temperature; (middle) bottom dissolved oxygen (DO), and (bottom) buoyancy frequency or index of stratification (N). Each line corresponds to a different year between 2019 and 2023.

We found that the time series in the other three sites we sampled across the lake (UA-08, UA-01, and NR-02) were informative but did not add extra conclusions to our analysis. The time series of lake temperature and dissolved oxygen are shown in Appendix 15.7.3.

7.4 Physico-biogeochemical Lake Profiles

7.4.1 Methods

We collected lake profiles at 6-week intervals using a Seabird SBE-19 profiler. The SBE-19 was sampled at 4 Hz. When lowered at 0.5 m/s, this will produce a profile with 12.5 cm vertical resolution. The profiler measured temperature, conductivity, depth, turbidity, and

DO. We also measured pH profiles with a YSI Pro10. Measurements of photosynthetically active radiation (PAR) were made throughout the water column using a LiCOR L1400 light meter and used to compute attenuation coefficients. We also measured Secchi depths while collecting PAR profiles to evaluate lake clarity. Profiles were collected adjacents to the six moorings. Table 7.4.1. shows the model, accuracy, and resolution of the different high-resolution sensors used in these profilers. Data are publicly available via the TERC-Clear Lake website (clearlakerehabilitation.ucdavis.edu).

Table 7.4.1. Seabird SBE-19plus vertical profiler and LiCOR L1400 accuracy and resolution of the different sensors

Variable	Model	Accuracy	Resolution
Temperature	ITS-90	0.005 °C	0.0001 °C
Conductivity	SBE 19p cell	0.5 mS/m	0.01 mS/m
Depth	SBE 19p	0.1% of the reading	0.02% of the reading
Oxygen	SBE 43	2% of saturation	0.5% of saturation
Chlorophyll	Turner Cyclops-7	0.3 µg/L	0.5% of the reading
Turbidity	Seapoint	5 % of the reading	0.2% of the reading
Photosynthetically active radiation	Licor L1400	0.5 % of the reading	0.15 % of the reading

7.4.2 Results

High-resolution profiles allowed us to confirm the seasonal patterns shown in the mooring data but added extra information from more variables and across the whole water column (not only a few depths). For example, Figure 7.4.1 shows the warming and cooling of the lake temperature in summer and fall, and develop of oxygen gradients in depth due to density gradients. In addition, these profiles allowed us to visualize the distribution of chlorophyll-a in-depth, confirming that concentrations tend to be uniform throughout the whole water column as long as there is enough oxygen to sustain phytoplankton growth. Similar patterns were observed in other sites across the lake.

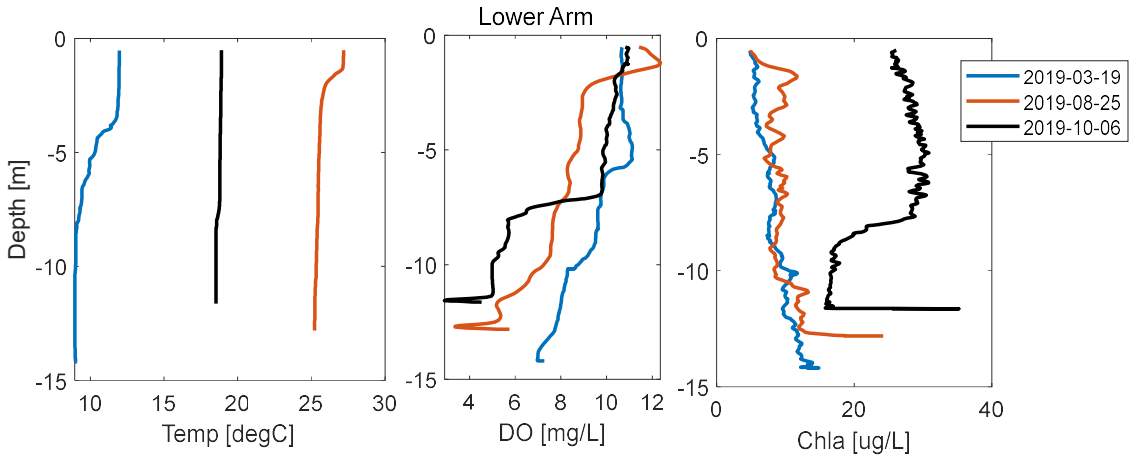

Figure 7.4.1. High-resolution profiles in the Lower Arm during three different sampling events in 2019 (spring, summer, and fall). Each subplot shows values of lake temperature, dissolved oxygen, and chlorophyll-a

PAR profiles allowed us to compute attenuation coefficients following Beer's law: $I(z) = I(0)\ exp(kz * z)$, where I(z) is PAR in-depth (z), I(0) is PAR at the surface, *kz* is attenuation

coefficient (1/m). The average *kz* across all sites ranged between 1.2-1.5 1/m, with minimum values in winter/early spring (~0.5 1/m, Secchi depth ~3 m), and maximum values in summer/fall (~2 1/m, Secchi depth ~ 1 m). We also observed peak values of kz during very high productive periods in summer/fall 2022 and 2023 reaching values of ~3.5 1/m which indicated minimal penetration of light (Secchi depth ~0.25 m) (Figure 7.4.2)

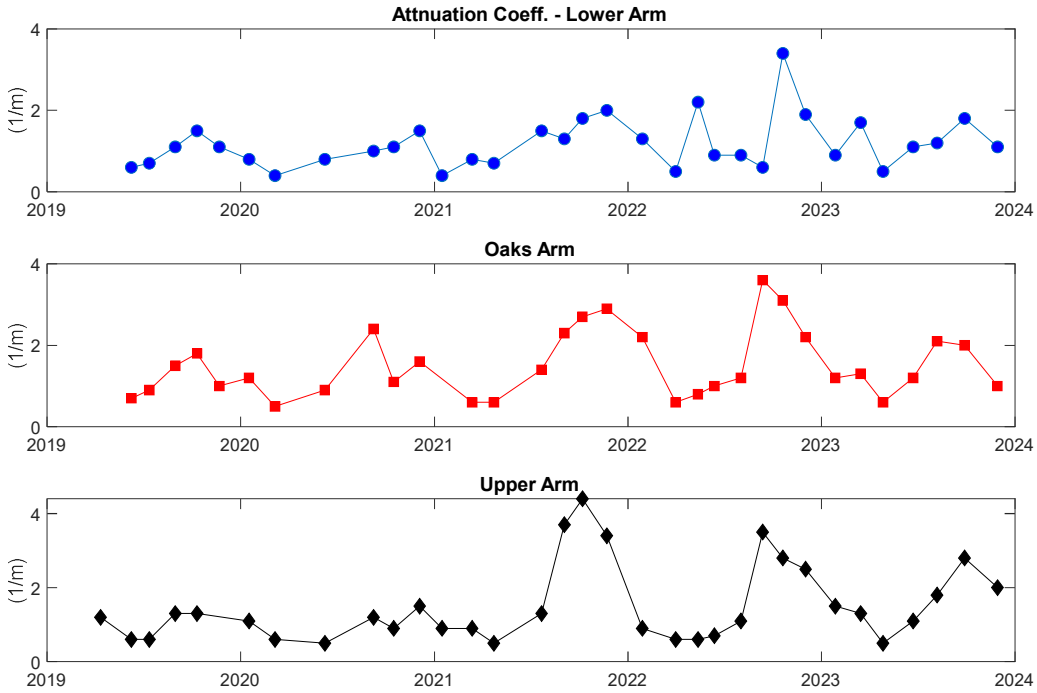

Figure 7.4.2. Time series of attenuation coefficient values (kz) between 2019 and 2023 across the three basins

Depth averaged values of pH range between 7.28 and 10.20, with lower values in the winter and higher values in late summer, and fall. Values of pH changed ~0.3-0.5 in depth (maximum values near the surface), and less than 0.4 across all sites.

7.5 Prediction of Hypoxia in Clear Lake

Historical monitoring data and more recent monitoring have shown that periods of low dissolved oxygen (hypoxia) occurring in the summer/fall when the lake develops temperature gradients in depth (i.e. stratification) is a major explanatory factor in the poor water quality and ecological health of Clear Lake since it controls the nutrient availability for phytoplankton growth (Figure 7.5.1). We developed a simple method to predict when and for how long low dissolved oxygen levels occur in the lake using basic meteorological information such as air temperature, relative humidity, solar radiation, wind speed, and lake surface temperature (Figure 7.5.2). Recent results show this method to be highly accurate when predicting the timing of hypoxia without computing actual lake oxygen values. Our results endorse the newly developed method as a cost-effective tool for predicting the timing of hypoxic events. We believe this method can turn into a

compelling decision-making tool for management actions when aquatic ecological challenges due to hypoxia get accentuated. Peer-reviewed publication here (Cortés et al. 2021).

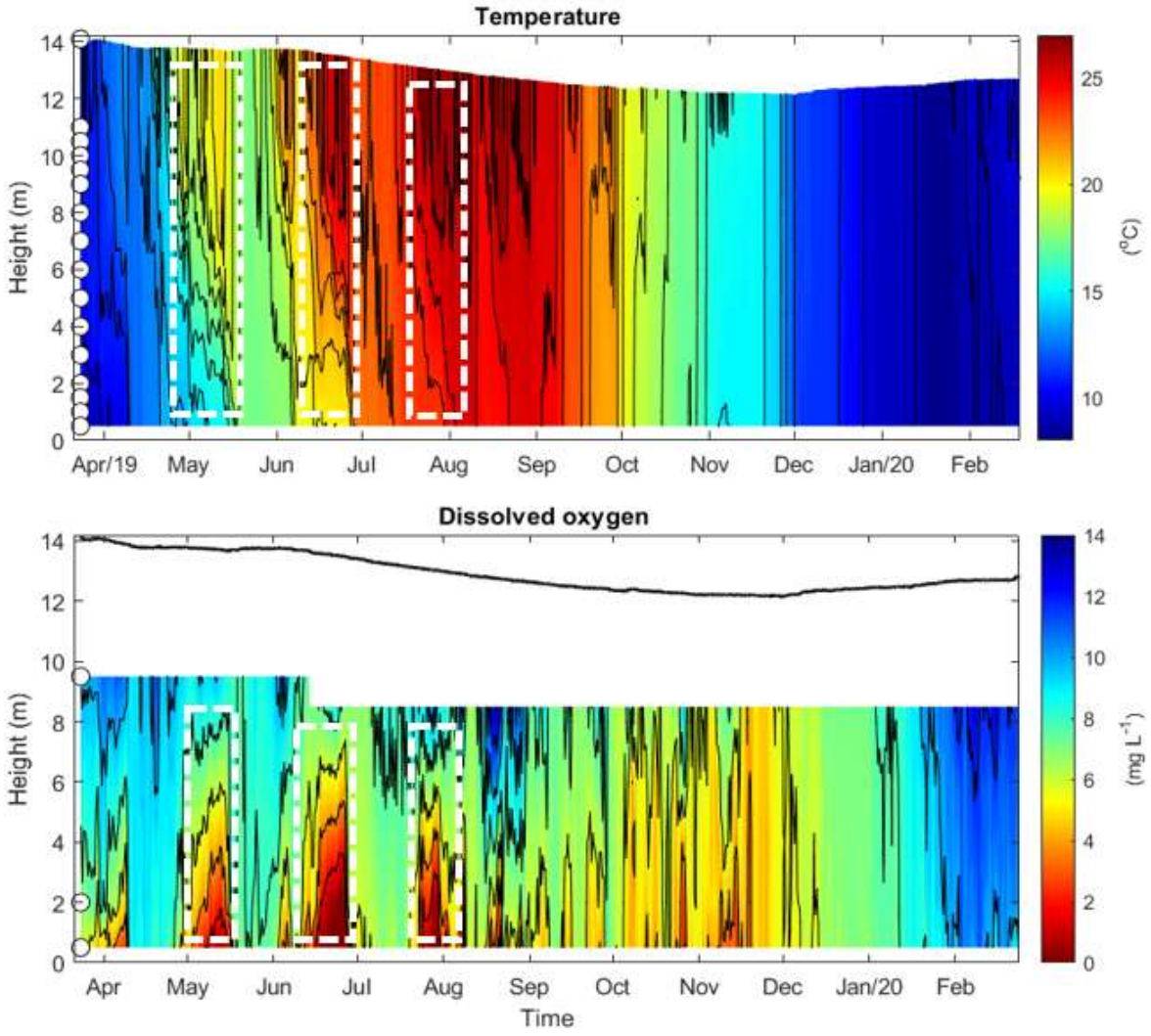

Figure 7.5.1. Time series in depth of the lake temperatures (top) and dissolved oxygen (bottom) in the Lower Arm in 2019. The white boxes highlight the relationship between strong stratification and bottom hypoxia. The black line indicates changes in lake level

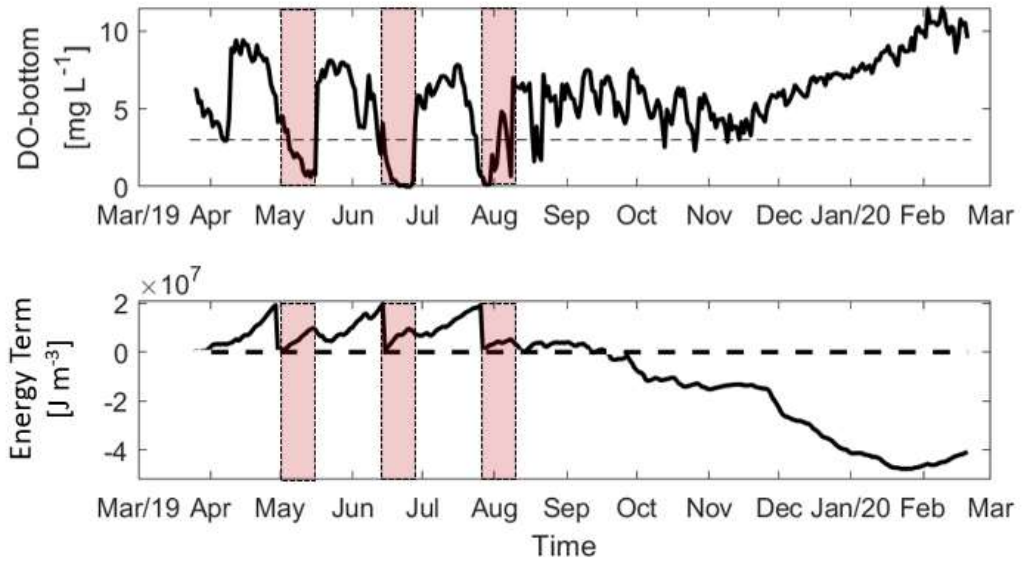

Figure 7.5.2. Analytical model developed by TERC researchers to predict the timing of hypoxia in Clear Lake from an energy term calculated with meteorological data

7.6 Water Quality Sampling

7.6.1 Methods

Field methods

Discrete water samples (4 L minimum volume) were taken with a peristaltic pump at 4 depths at each mooring station: 0.5 m below the surface at 1 m, 2 m, and 4 m off the bottom. All water samples will be collected and decanted into acid-washed bottles that were triple-rinsed with ambient water at the time of collection. For phytoplankton analysis, an aliquot of 100 ml of surface water was collected in clear glass bottles and immediately preserved with 1 ml of Lugol's iodine solution. An air space will be left between the top fill line and lid, and the sample bottles will be kept in the dark on ice in a cooler. Thus, we collected 24 discrete water samples at each mooring during each water quality sampling campaign. The water samples were analyzed for the following nutrients and water quality constituents shown in Table 7.6.1.

Laboratory methods

Samples were transported from the field to UC Davis stored on ice in coolers within 24 hours of collection and filtered upon arrival. Filtered samples were transported by next-day Fedex to the TERC analytical laboratory within 1 day of arrival at UC Davis. All dissolved nutrients, particulate C, N, and P, and Chlorophyll-a samples were filtered through pre-combusted (500 °C for 2h) Whatman GF/F filters (0.7 µm nominal pore size).

Table 7.6.1. Constituents to be sampled for and analyzed for lake water.

	Constituent	Description	Detection level
Nutrients	NO_3+NO_2	Dissolved Nitrite + Nitrate Nitrogen	0.002 mg/L
	NH4	Ammonium	0.002 mg/L
	SRP	Dissolved Orthophosphate Phosphorus (PO4), Soluble reactive phosphorus	0.001 mg/L
	DKN	Dissolved Kjeldhal Nitrogen	0.002 mg/L
	TDP	Total Dissolved Phosphorus	0.002 mg/L
Organic matter	PC	Particulate Carbon	0.01 mg/L
	PP	Particulate Phosphorus	0.002 mg/L
	PN	Particulate Nitrogen	0.01 mg/L
	DOC	Dissolved Organic Carbon	0.05 mg/L
Chlorophyll	Chl-a	Chlorophyll-a	0.5 µg/L
Phytoplankton	Phyto	Identification and enumeration	
QA/QC	Blanks	Source and Field blanks	
	Replicates	Replicates	

Stoichiometric analysis of particulate organic matter (PC, PN, and PP) was used as a broad assessment of overall organic matter quality. Soluble reactive phosphorus and nitrate+nitrite were determined on a flow-through discrete analyzer. Oxidative reduction (Valderrama 1981) was used for dissolved nutrients (TDP) and particulate phosphorus determinations. DIN: SRP and PN: PP ratios were used as indicators of nutrient limitation status. Particulate carbon and nitrogen concentrations were determined using a Costech Elemental Analyzer. Dissolved organic carbon (DOC) was measured on a Shimadzu TOC/TON analyzer. Chlorophyll-a samples were measured on a Turner 10-AU fluorometer after 24 h extraction in 90% methanol and chlorophyll-a was used to model phytoplankton biomass.

Phytoplankton samples were sent to BSA Ltd for enumeration and identification. Cell numbers of all identified Phytoplankton taxa will be quantified on a per milliliter basis using either the Utermohl method (Lund et al. 1958) or the membrane filtration technique (McNabb,1960) following the American Public Health Association Standard Method 10200 (Standard Methods For the Examination of Water and Wastewater, 22nd Edition 2012). These techniques will preserve cell structure and provide good resolution. Samples will be thoroughly mixed before subsampling an aliquot to ensure that the organisms will be evenly distributed. Various aliquots are measured and delivered into custom Utermohl chambers and the organisms are allowed to settle in darkness undisturbed for at least 20 hours within an enclosure protected from vibration and temperature alteration (Burkholder and Wetzel 1989). Utermohl counts are performed on a LEICA DMiL or DMi1 inverted microscope at 800X. The abundance of common taxa will be estimated by random field counts. 400 natural units (colonies, filaments, unicells) or 50 random fields will be enumerated to the lowest possible taxonomic level from each sample. If Cyanobacteria taxa are not encountered in the random fields analysis, a transect analysis will be performed for Cyanobacteria taxa. Cell biovolumes of all identified phytoplankton taxa will be quantified on a per-liter basis. Biovolumes will be estimated using formulae for solid geometric shapes that most closely match the cell shape (Hillebrand et al., 1999). BSA has an extensive hard copy and digital reference library, which includes thousands of taxonomic references and keys. Our literature collection is continually expanding as new sources of information become available. In addition,

BSA's location allows immediate access to several university libraries. Taxonomy will follow accepted nomenclature according to Algaebase.org unless specifically requested otherwise.

At least 48 hours before each lake sampling trip, we contacted the Big Valley Rancheria cyanobacterial sampling program, to arrange to pick up sample bottles for taking surface water samples for their cyanobacterial sampling program. Contact information is as follows: Big Valley Rancheria Environmental Director Sarah Ryan: ryan@big-valley.net

QA/AC for the Clear Lake project followed the TERC QA/QC manual. For every sampling event, one field duplicate was collected, one field blank was collected (while filtering samples) and one source blank was collected at the time of bottle cleaning. We also collected filter blanks with nothing added to the filter and filters with DI water passed through them. In the lab, SOPs were followed, lab duplicates and lab spikes were added to each run for every 10 samples on a run as well as two laboratory DI blanks per run. Each chemistry run went through our rigorous QA/QC standards to ensure accurate data is produced. Data were maintained in an SQL database that is stored and backed up on the cloud using AWS. Data are publicly available via the TERC-Clear Lake website (clearlakerehabilitation.ucdavis.edu).

Calculations: Phytoplankton Carbon biomass

The phytoplankton biovolume expressed as carbon was determined from recorded abundances (cell counts) of phytoplankton and calculated biovolumes. Conversion of the phytoplankton cell counts to carbon was based on species-specific cell volume (biovolume) using the following equation for freshwater algal species (Rocha and Duncan 1985):

$$Phytoplankton\ Carbon\ \left(\frac{\mu g}{L}\right) = Cell\ count\ \left(\frac{cell}{L}\right) \cdot\ [a\ \cdot CellBiovolume\ (\mu m^3)]^b\ \cdot\ 10^{-6}\left(\frac{\mu g}{cell}\right) \quad (7\text{-}1)$$

Here *a* and *b* are the coefficients of a regression whose values are 0.1204 and 1.051, respectively (Figure 7.6.1). Calculations were made either for the entire phytoplankton assemblage or as the contribution of each division.

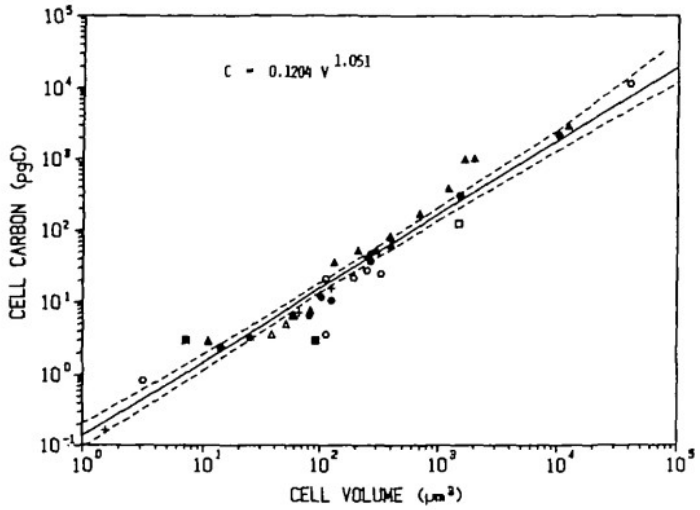

Figure 7.6.1. Relationship between cell carbon and cell volume of freshwater species of algae. For more details, see Figure 1 in Rocha and Duncan (1985).

7.6.2 Results

The water quality sampling conducted between 2019 and 2023 shows the seasonal and interannual variability of nutrients and phytoplankton concentrations at Clear Lake. The reader can find the time series in-depth for all constituents, sampling events, and the 4 sampled depths (surface, [1,2,4] m off the bottom) in the Appendix (Figure 15.7.4.1, Figure 15.7.4.2, Figure 15.7.4.3). However, to better describe the patterns, we have averaged the concentration of the different variables in two layers: (A) the epilimnion, defined as the top layer that runs from the surface to 4 m off the lake bottom; and (B) the hypolimnion characterized as the bottom layer that goes from the sediments to 3 m off the bottom (Figure 7.6.3, Figure 7.6.4 and Figure 7.6.5).

Carbon forms in Clear Lake present a seasonal pattern, with higher values in the summer and lower values in the winter (Figure 7.6.3). Overall, maximum values of particulate and dissolved organic carbon had similar order of magnitude for a given year and season. the time series of carbon-related nutrients showed an increase in different forms associated with the drought between 2020 and 2022. Values of DOC increased by a factor of two in the summer of 2021 across the lake and remained high after the wet year in 2023. We observed peaks of PC in late summer/fall in 2021 and 2022 across the lake, but more significantly in the Upper Arm. Peak values of chlorophyll-a (>100 µg/L) occurred across the whole in summer 2022 but were also observed only in the Oaks and Upper Arms in 2021. Overall, we only found up to 18% differences between carbon-related concentrations in the epilimnion and hypolimnion, with surface values slightly higher than bottom values in some seasons, particularly summer and fall.

Total, particulate, and dissolved organic nitrogen presented minimum values in the winter, and maximum values in the summer and fall due to high phytoplankton biomass (Figure 7.6.4). Overall, maximum values of total and dissolved organic nitrogen had similar order of magnitude in the winter, which suggests that most of the nitrogen in Clear Lake is in a dissolved organic form during this season. Particulate nitrogen only showed peak values during the summer. The time series of nitrogen-related nutrients showed seasonal patterns that were also accentuated with the drought period. The warm season of 2021 and 2022 were particularly rich in nitrogen forms, which was less obvious in the Lower Arm. Ammonium tends to peak in late summer and fall, associated with the anoxic periods and thus release of nutrients from the sediments. On the other hand, nitrate showed spikes during the rainy season (winter) which points to external load as the most likely source of this nitrogen form.

The magnitude of the total, dissolved and dissolved inorganic phosphorus (soluble reactive phosphorus, SRP) had very similar values, which confirms the predominance of dissolved inorganic phosphorus as the main form of P in Clear Lake (Figure 7.6.5). Particulate phosphorus was only 10% of the total P measured in the lake. Maximum values of SPR were measured in the summer/fall while minimum values were recorded in the winter. In the summer, hypolimnetic values of SRP tended to be higher than epilimnetic values, which confirms the source of P from the sediments during the warm anoxic period. Concentrations of SRP increased during the summer of drought years (2020-2022), which also tended to have higher values of particulate phosphorus. Overall, we measured higher concentrations of P in the Upper Arm compared to the other two arms.

Time series of phytoplankton biovolume expressed as carbon shows how diatoms dominate the lake in the winter and spring, while green algae, cryptomonads, and cyanobacteria co-exist during summer and fall (Figure 7.6.6). We also observed how the total biomass increased by the end of the drought period we sampled (2021-2022), and the cyanobacteria became the dominant division during the growing season of those years. Phytoplankton biovolume as carbon was only a third in the Upper Arm of what we measured in the eastern arms during the warm season of 2021 and 2022.

The time series of cyanobacteria biovolume showed some peaks in the summer of 2021 but consistently high values during a longer period in the summer of 2022 (Figure 7.6.7). Mycrocistis, Limnoraphis, and Aphanizomenon tended to be the dominant cyanobacterial genera when peaks in biomass occurred. Overall, cyanobacteria biomass tended to be higher in the Oaks and Lower Arm than in the Upper Arm, which is consistent with the remote sensing observations displayed by the SFEI HABs online tool Figure 7.6.2.

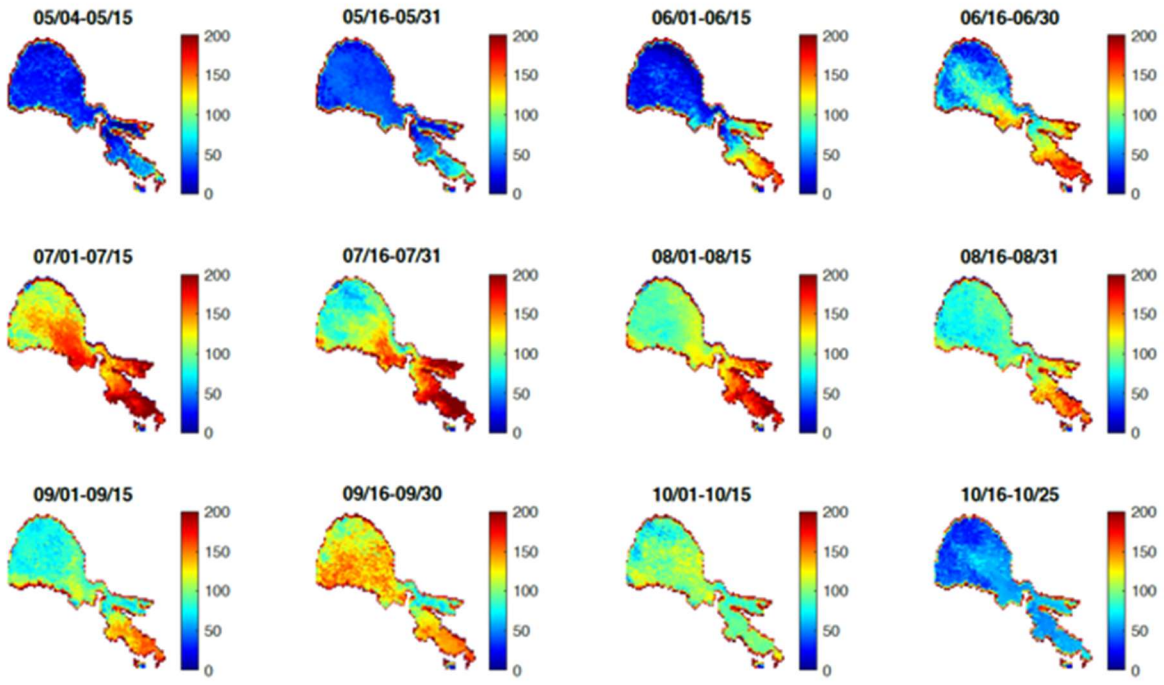

Figure 7.6.2. Bi-weekly averaged modified Cyanobacteria Index across Clear Lake from May to October 2003-2021 (SFEI)

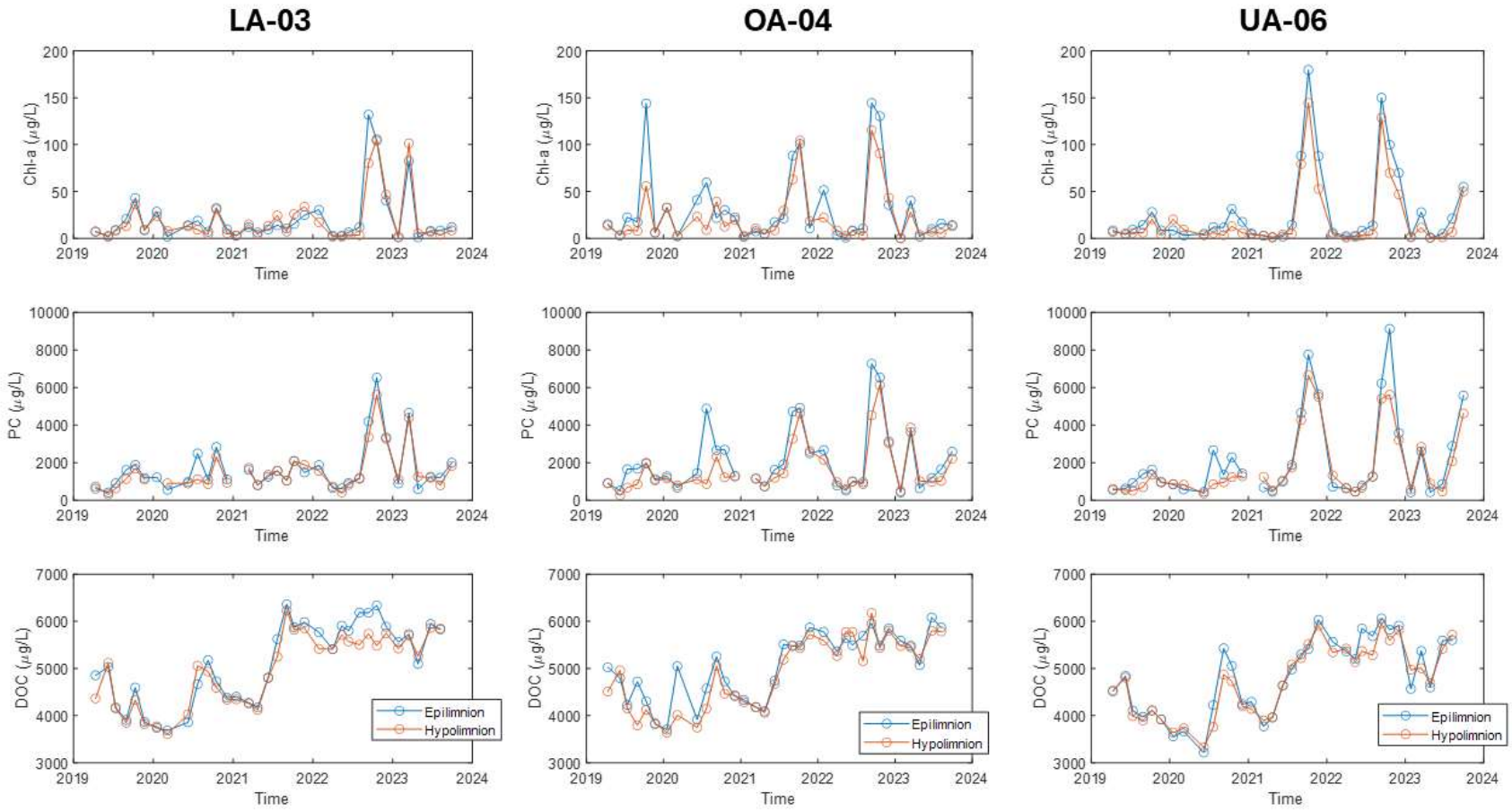

*Figure 7.6.3. Time series of water quality constituents in the epilimnion (surface to 4 m off the bottom) and hypolimnion (averaged in the 3 m layer near the sediments) related with **carbon** measured at four depths between 2019 and 2023 during our sampling events conducted every 6-8 weeks. Each row shows a different constituent: chlorophyll-a (chl-a), particulate carbon (PC), and dissolved organic carbon (DOC). Each column shows data from a different lake site: (left) LA-03, (middle) OA-04; (center) UA-06.*

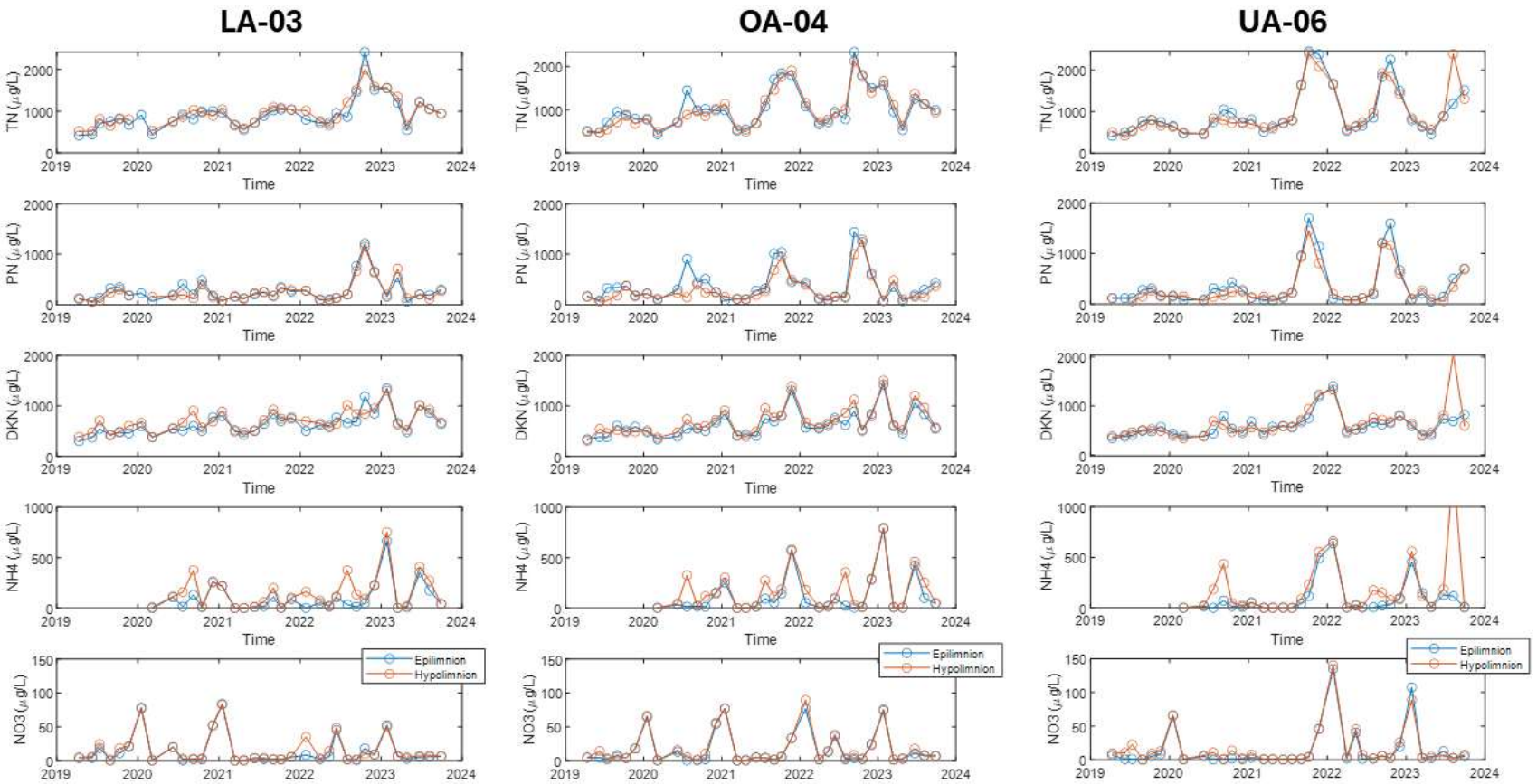

*Figure 7.6.4. Time series of water quality constituents in the epilimnion (surface to 4 m off the bottom) and hypolimnion (averaged in the 3 m layer near the sediments) related with **nitrogen** measured at four depths between 2019 and 2023 during our sampling events conducted every 6-8 weeks. Each row shows a different constituent: total nitrogen (TN), particulate nitrogen (PN), dissolved Kjeldhal nitrogen (DKN), ammonium (NH4), and nitrate (NO3).*

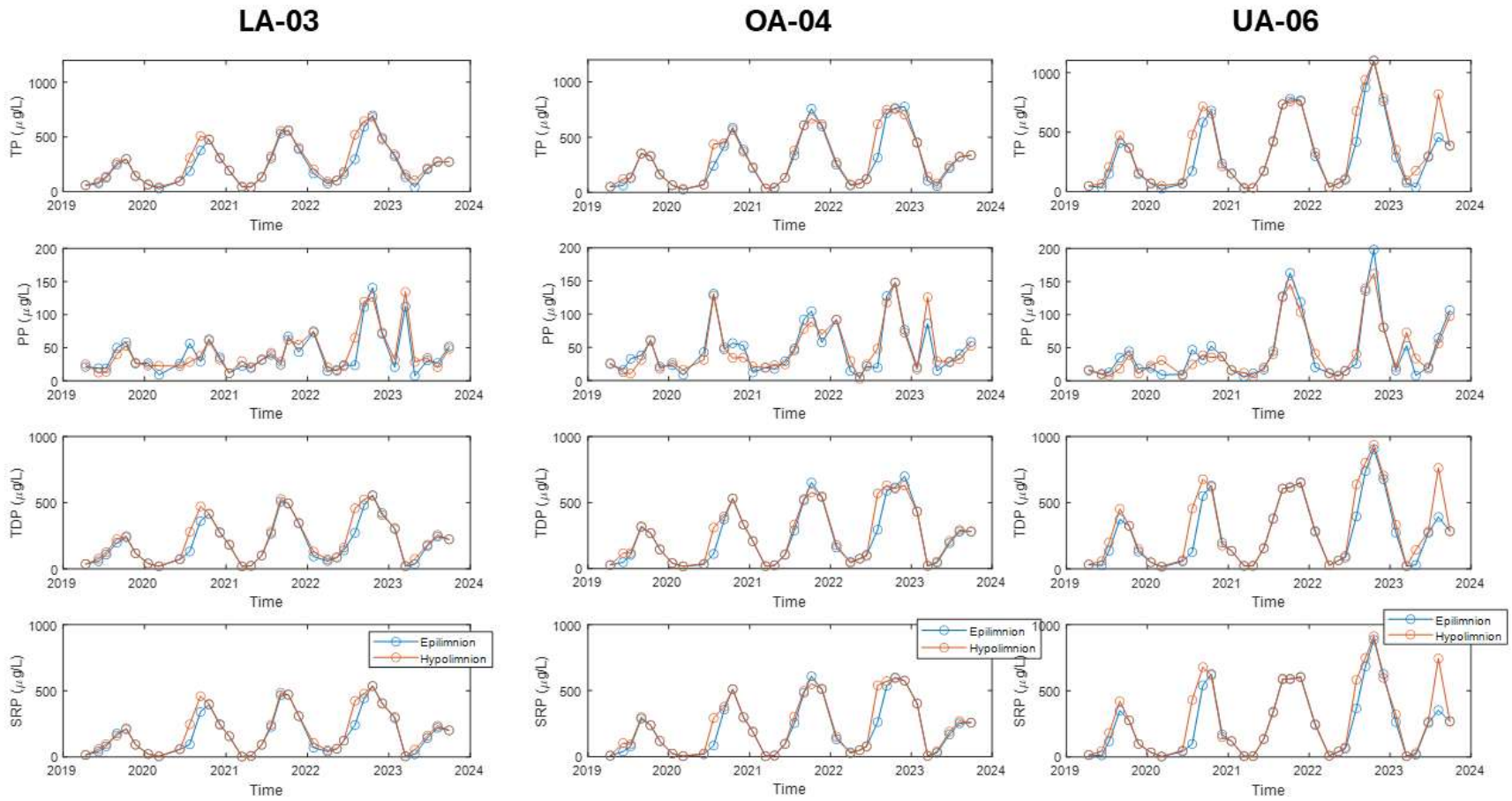

*Figure 7.6.5. Time series of water quality constituents in the epilimnion (surface to 4 m off the bottom) and hypolimnion (averaged in the 3 m layer near the sediments) related with **phosphorus** measured at four depths between 2019 and 2023 during our sampling events conducted every 6-8 weeks. Each row shows a different constituent: total phosphorus (TP), particulate phosphorus (PP), total dissolved phosphorus (TDP), and Orthophosphate Phosphorus PO_4, Soluble reactive phosphorus (SRP). Each column shows data from a different lake site: (left) LA-03, (middle) OA-04; (center) UA-06.*

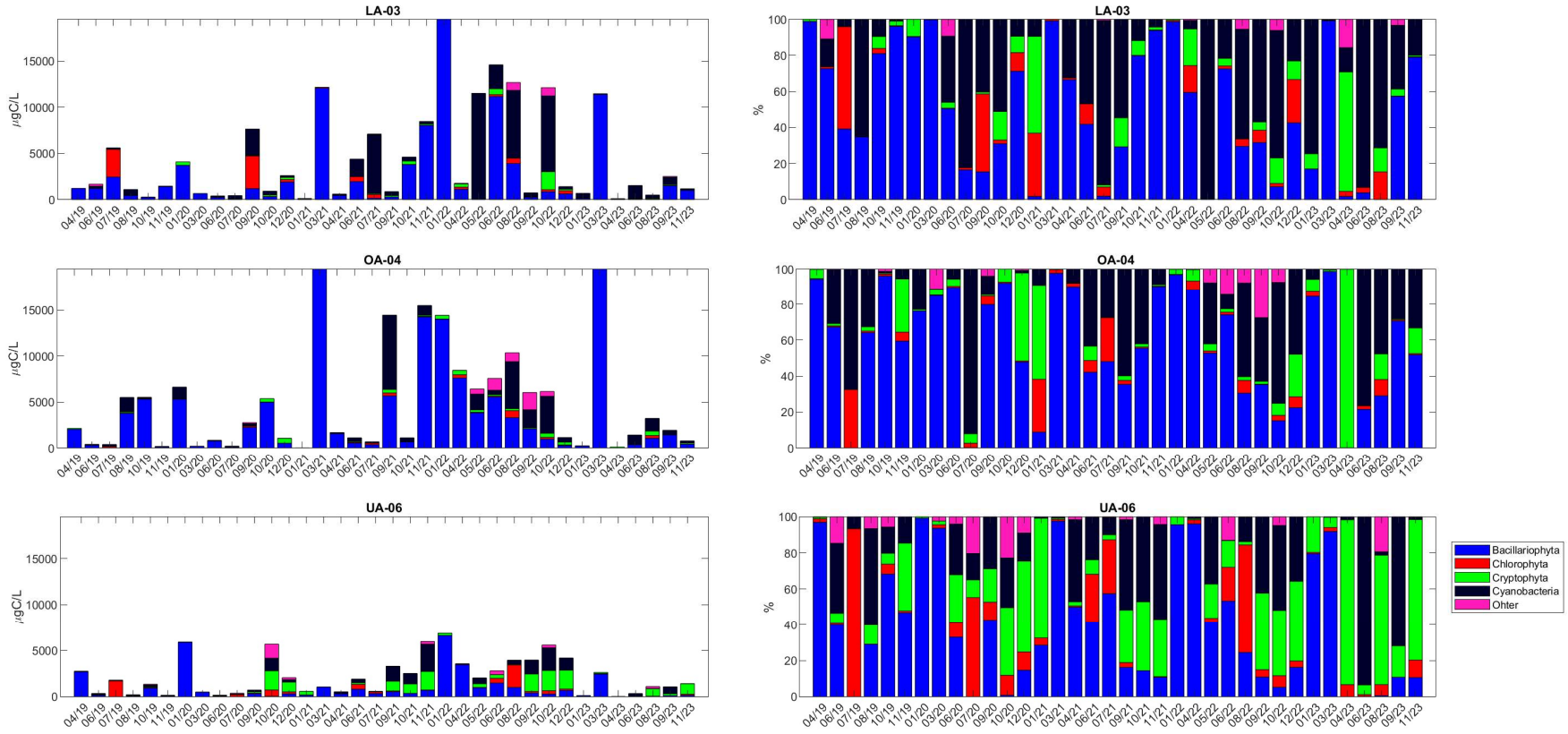

Figure 7.6.6. ***Phytoplankton*** *biovolume expressed as concentration of carbon (left) and percentage of the total biovolume per sampling (right) for the four main divisions of phytoplankton encountered at Clear Lake during our sampling between 2019-2023. The four main divisions are Bacillariophyta (diatoms), Chlorophyta (green algae), Cryptophyta (cryptomonads), and Cyanobacteria. Each row shows data from a a different lake site: (top) LA-03, (middle) OA-04; (bottom) UA-06.*

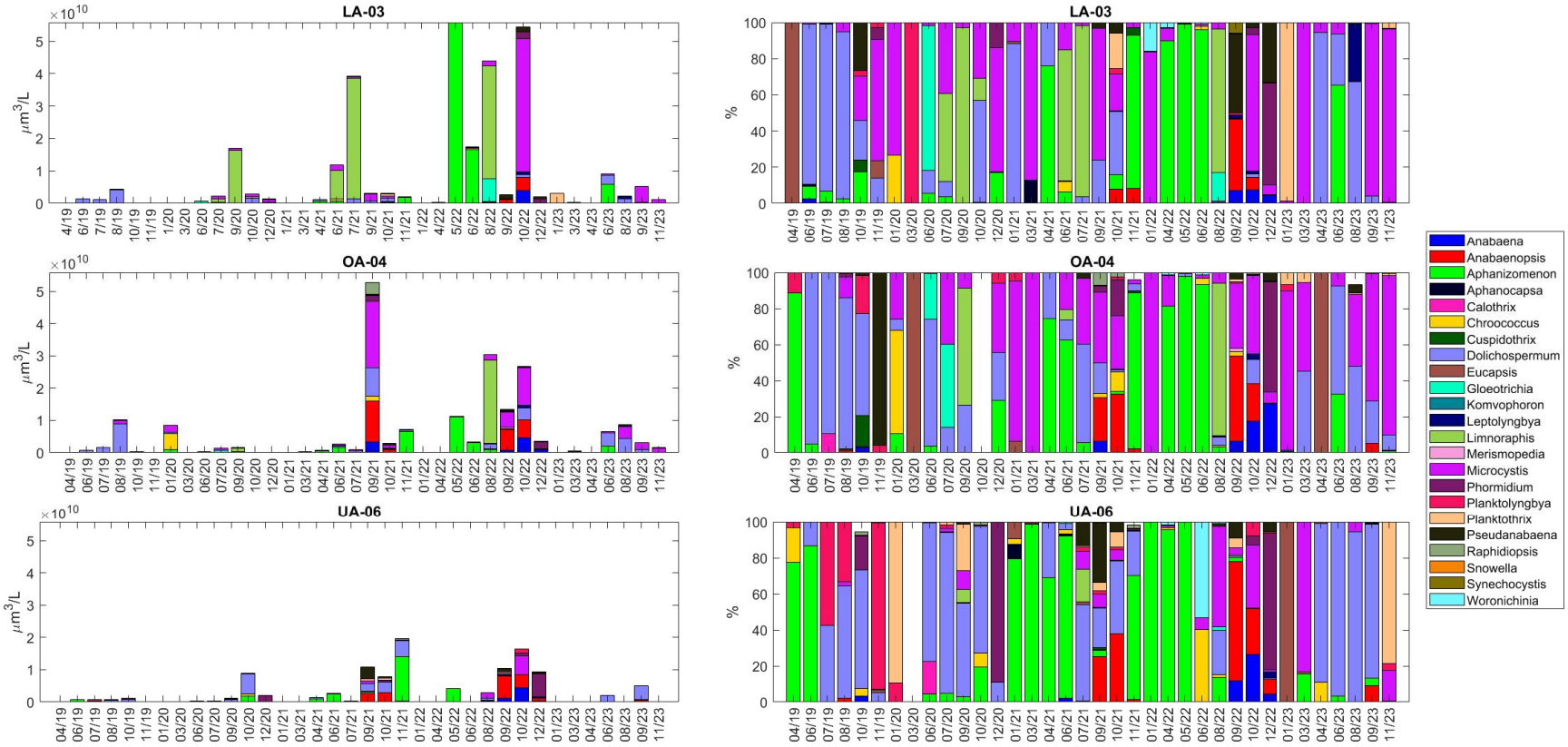

Figure 7.6.7. ***Cyanobacteria*** *biovolume expressed as concentration (left) and percentage of the total biovolume per sampling (right) for the main Cyanobacteria genus encountered at Clear Lake during our sampling between 2019-2023. Each row shows data from a a different lake site: (top) LA-03, (middle) OA-04; (bottom) UA-06.*

7.7 Sediment Incubation Experiments

7.7.1 Methods

Phosphorus (P) fluxes were measured from sediments collected in November 2019 from 6 sites coincident with the location of our permanent moorings across the lake (UA-01, UA-06, UA-08, NR-02, OA-04, LA-03, Figure 7.3.1), using a gravity corer and polycarbonate tubes. At each site, 4 replicate cores were collected and capped with overlaying water to minimize disturbance to the sediments. Cores were stored in coolers in the dark at ambient temperatures and transported to the lab within 6 hours of collection. A total of 20 L of ambient water was collected from each site in high-density polyethylene carboys to use during laboratory incubations. Sediment cores were incubated directly within the polycarbonate tubes in which they were collected from the field. The overlaying water in each core incubation chamber was removed by siphoning and replaced with 1.0 µ filtered (Whatman GF/F) and oxygenated ambient water. Samples were allowed to rest in the dark at ambient temperatures for 12-24 hours before the start of incubations. Cores were incubated at ambient 15°C for 30 days. We oxygenated 2 cores from each site by bubbling with air and the remaining 2 cores were kept anoxic by bubbling with N2 gas (Figure 7.7.1). Sediment P flux was determined by measuring changes in concentration within the overlaying water within each incubation chamber and evaluated to rates of oxygen demand and/or changes in redox potential measured every 3 days. Dissolved oxygen within the overlaying water of each chamber was measured non-invasively using a PreSens optical dissolved oxygen system (Fibox4) and a redox was measured using a Mettler/Toledo redox probe. After each incubation, sediment samples were collected from each core and analyzed for PC and PN, and three forms of bound Phosphorus (Loosely Bound, Iron Bound, and Calcium Bound phosphorus). Nutrient flux rates from sediment incubations were scaled up for each basin to estimate internal P loading rates for the entire lake.

Figure 7.7.1. Sediment core and laboratory setup for the sediment incubation experiment

7.7.2 Results

Results from the sediment incubations allowed us to quantify the soluble reactive phosphorus (SRP) fluxes from the sediments. Anoxic cores (red lines) exhibit the highest rates of SRP flux with values ranging from 8.8 to 26.7 mg/m^2/d. Oxic cores (blue lines) exhibit much lower rates with values ranging from -0.14 to 1.16 mg/m^2/d. Site NR-02 has the highest SRP flux rates (>3 times the rate of site UA-08) (Figure 7.7.2 and Figure 7.7.3).

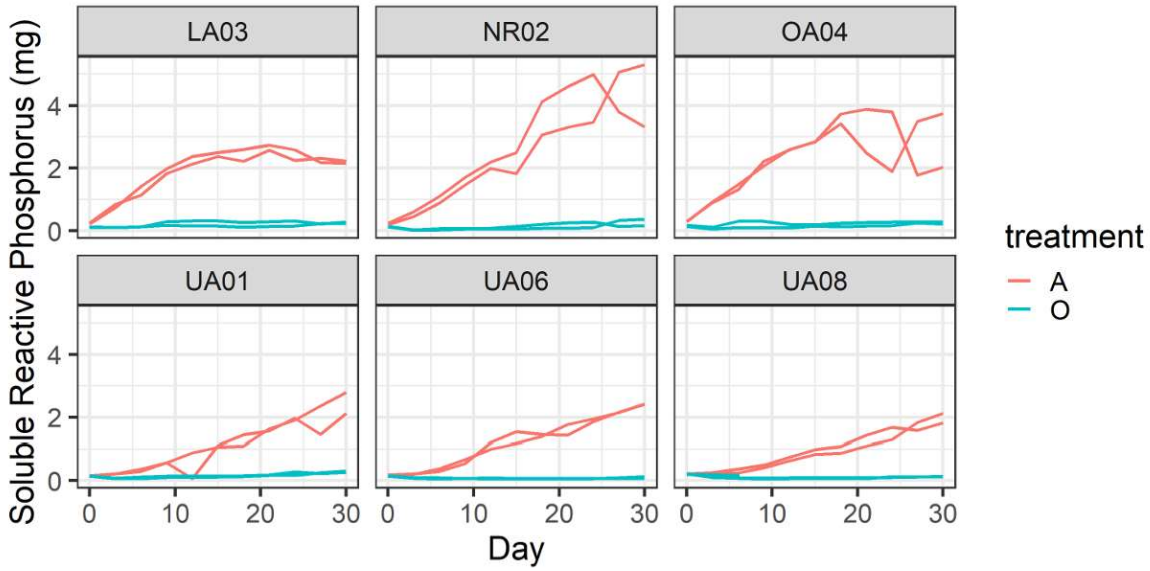

Figure 7.7.2. Time series of soluble reactive phosphorus (SRP) mass (mg) in individual cores taken from each of the 6 sites during the November 2019 experiment

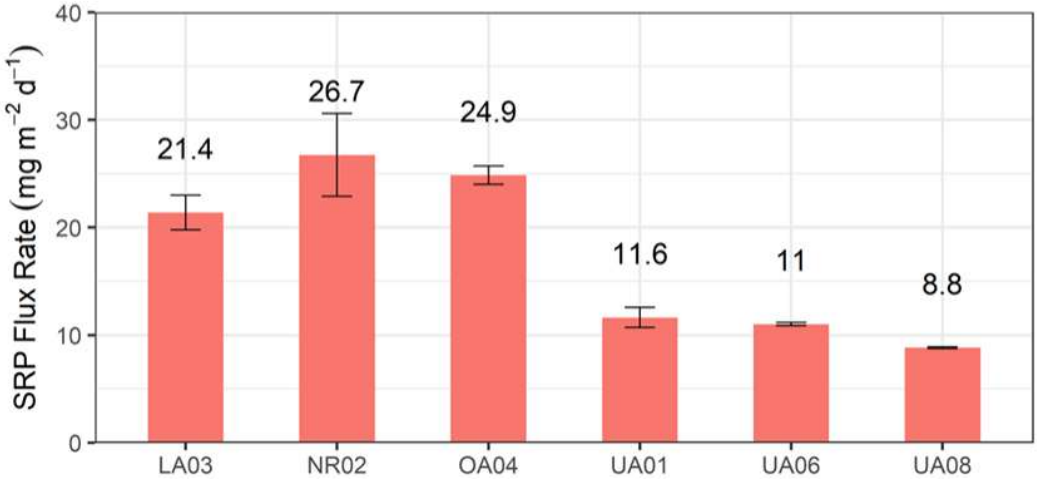

Figure 7.7.3. Soluble reactive phosphorus (SRP) flux rates obtained during the November 2019 experiment

7.8 Internal Loading Characterization

Clear Lake has had recurring cyanobacteria harmful algal blooms (CHABs) for over a century despite reductions in external phosphorus (P) loadings. Internal P loadings from lake sediments can also alter nutrient availability, but these changes are rarely quantified or compared with external loads. We quantified both external watershed P loads and internal P loads from 2019-2023. We combined high-frequency measurements of water temperature and dissolved oxygen, discrete grab sampling for nutrient chemistry, and remote sensing to explore the potential drivers of the observed variability and provide a comprehensive view of the spatiotemporal dynamics of CHABs. Comparative estimates of external and internal phosphorus loading indicate that internal sources accounted for 70 – 95% of the total P input into the system during the study period (Figure 7.8.1). Contrary to other lakes, the intensity of the summer bloom season was correlated to the timing and duration of anoxia rather than the magnitude of spring runoff. Internally released P shifted the system from phosphorus to nitrogen limitation during the summer, potentially favoring the proliferation of nitrogen-fixing cyanobacteria. Peer-reviewed publication here (Swann et al. 2024).

We also produced "The phosphorus (P) budget for the Clear Lake watershed from 2019 - 2022", published on our website (Swann et al. 2023). Clear Lake's P budget demonstrates that the annual cycling of P in the system is largely controlled by internal fluxes between lake sediments and the water column. The overwhelming influence of the internal process on P cycling in Clear Lake suggests that focusing on controlling in-lake internal P loading will be crucial to mi ga ng cyanobacteria blooms in the future.

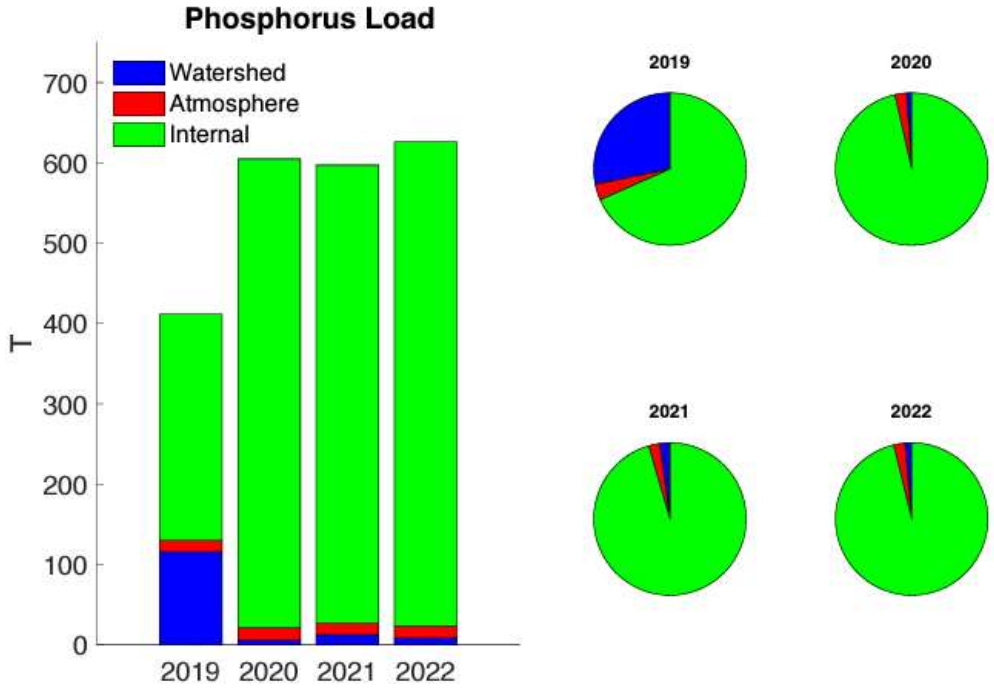

Figure 7.8.1. Clear Lake total phosphorus load allocations (2019-2022). Pie charts show the relative contribution of external, internal, and atmospheric loads (credit to Micah Swann)

7.9 Spatial and Temporal Variability of CHABs

Cyanobacteria measurements are intrinsically complicated due to the high spatial and temporal variability of the blooms. Understanding the spatial and temporal variability of these blooms helps design adequate sampling plans that inform lake managers and local communities about their ability to rely on the lake for key water uses (Figure 7.9.1).

Figure 7.9.1. Cyanobacteria blooms in Soda Bay, une 2020; (right) Cyanobacteria bloom in the Narrow, June 2023

We studied the spatial heterogeneity of cyanobacteria blooms in Clear Lake by collecting coincident measurements at varying scales and resolutions. We collected discrete boat-based measurements (in situ spectroscopy and water samples), Autonomous Underwater Vehicle (AUV) optical measurements, multispectral imagery from small Unmanned Aerial System (sUAS) flights; and multispectral imagery from the Ocean and Land Color Instrument (OLCI) sensor on the Sentinel-3a satellite. A semivariogram analysis of the high-resolution AUV and sUAS data found the Critical Scale of Variability for cyanobacterial blooms to range from 70 to 175 m, which is finer than what is resolvable by the satellite data. We thus observed high spatial variability within each 300 m satellite pixel. Peer-reviewed publication here (Sharp et al. 2021). We also used the data collected for this study and from our 5-year water quality monitoring program dataset to evaluate the Cyanobacteria Index (CI) remote sensing algorithm, which estimates cyanobacteria abundance from the top portion of the water column from OLCI data, and it is publicly available from https://fhab.sfei.org/. The CI tool is valuable because it provides near-daily measurements of cyanobacteria abundance across the entire lake. Our validation found the current version of the CI algorithm is not effective for Clear Lake and found better performance with the original CI algorithm (Figure 7.9.2).

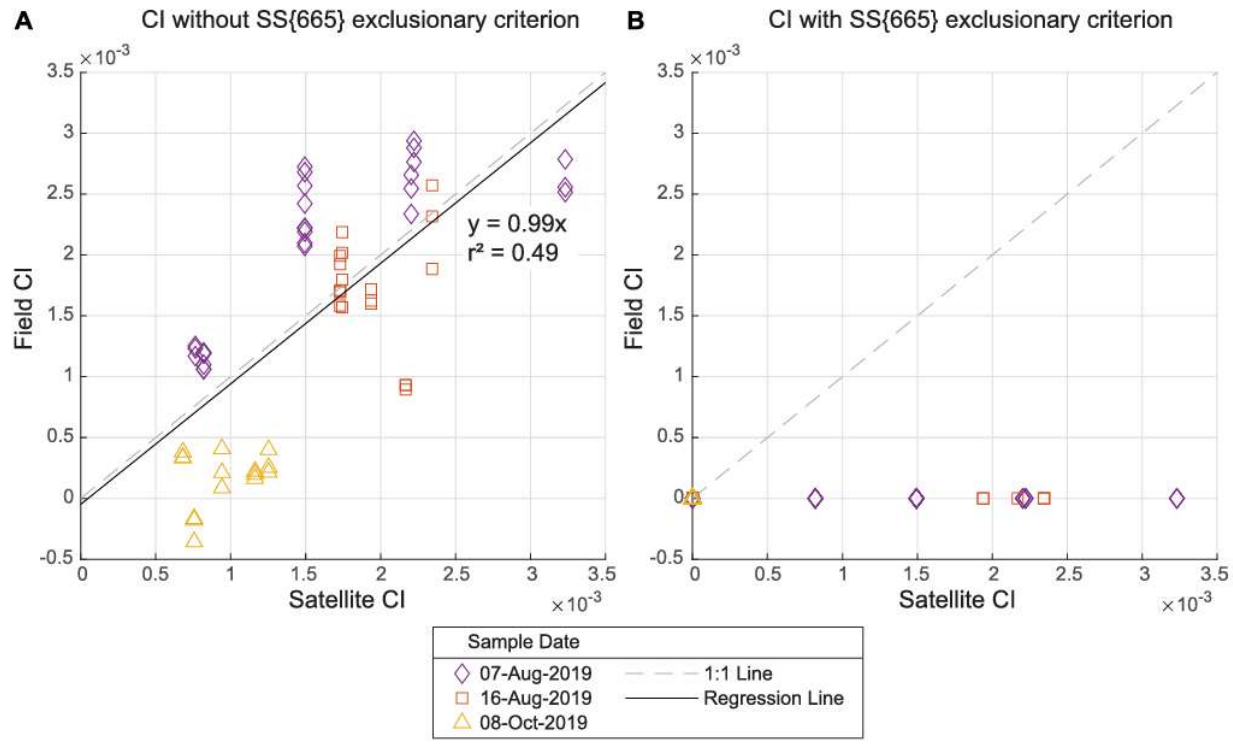

Figure 7.9.2. A) CI without exclusionary criterion (original CI algorithm); and B) CI with exclusionary criterion (current CI algorithm available online) for field spectroradiometer measurements (y-axis) and the Sentinel-3 measurements (x-axis) for the same sampling dates. Not using the exclusionary criterion demonstrates the best correlation between the field and satellite CI (Credit to Samantha Sharp)

7.10 Seasonal Velocity Measurements

7.10.1 Methods

We used an Acoustic Doppler Current Profiler (ADCP), Model Signature1000 from Nortek to characterize the seasonal patterns of currents in Clear Lake. This instrument was bottom mounted, upward looking in the deep hole of the Upper Arm (Figure 7.10.1). Deployments lasted ~2-3 months in winter and summer. Velocity profiles extended from 0.1 m away from the instrument head to ~0.2 cm below the surface (~8 m of water column). Cell size was 0.2 m. We used a continuous sampling plan with an average interval of 90 seconds, sampling every 5 seconds, and achieved a horizontal precision of ~ 0.01 m/s.

7.10.2 Results

Time series in depth of east-west (U) and north-source (V) velocities in the Upper Arm in winter 2021 showed that the water column was fully mixed and the currents experienced shifts in their direction depending on the predominant winds (Figure 7.10.2).

Figure 7.10.1. Field work photos during the deployment of an ADCP at Clear Lake

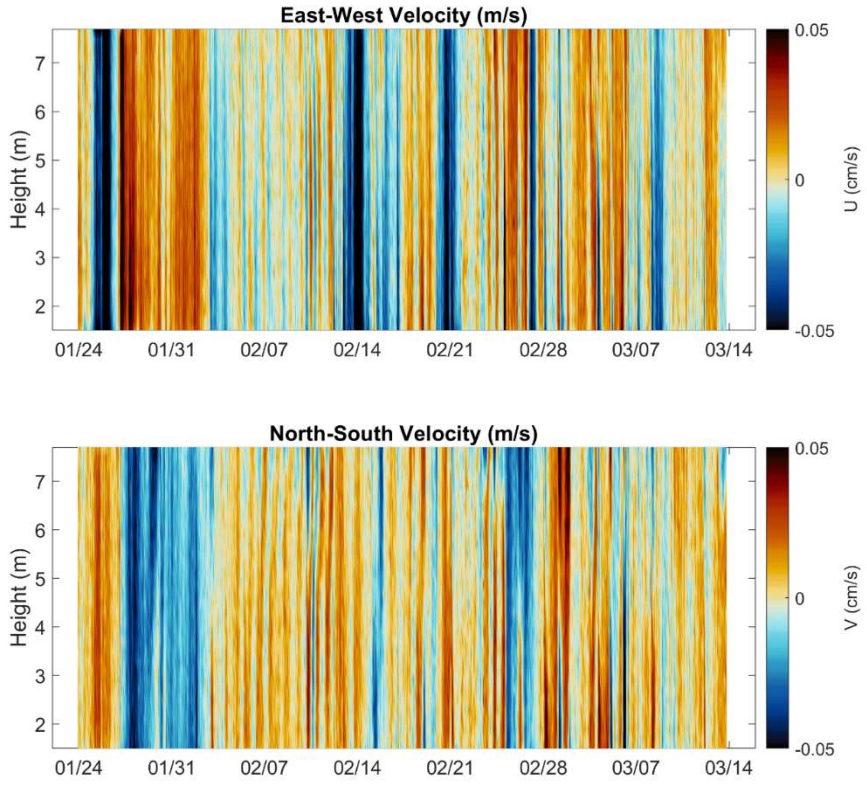

Figure 7.10.2. Time series in depth of east-west (U) and north-source (V) velocities in the Upper Arm in winter 2021

Time series in depth of east-west (U) and north-source (V) velocities in the Upper Arm in spring/summer 2021 showed that the water column had two to three layers with currents flowing in opposite directions at a given time. This structure was driven by the water column stratification and favored faster exchange in spring/summer than during the winter (Figure 7.10.3).

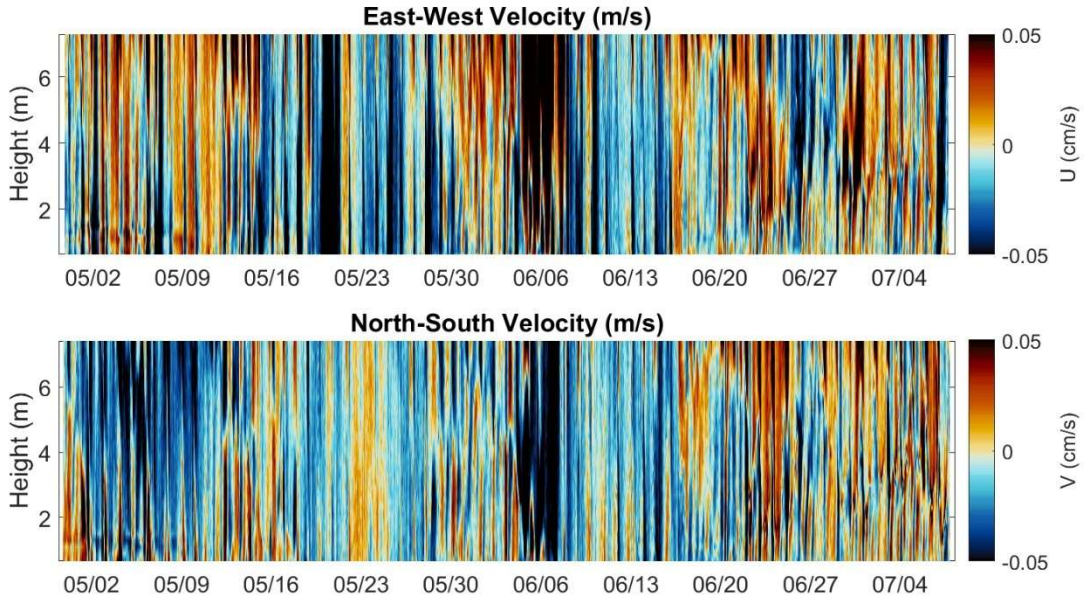

Figure 7.10.3. Time series in depth of east-west (U) and north-source (V) velocities in the Upper Arm in spring/summer 2021

7.11 Characterization of Flows at the Confluence

7.11.1 Methods

We collected high spatial and temporal resolution water velocity and temperature measurements at the confluence of the three basins to evaluate both the quantity (flow partition) and the properties (driven mechanisms) of the flow field at this location. We selected three cross-sections at which water from each individual basin starts mixing with water from the other two basins: Narrows (NR), Oaks Arm (OA), and Lower Arm (LA) (Figure 7.11.1). We conducted this experiment between August and October 20223 for six weeks.

We used two chains of thermistors and two upward-looking bottom-mounted Acoustic Doppler Current Profilers (ADCPs) at each cross-section to characterize the transverse variability of the flow, making a total of 6 moorings at the confluence (Figure 7.11.1). We named those moorings by their cross-section and their location in the cross-section (NRN, NRS, OAN, OAS, LAW, LAE). In addition, we also deployed another pair of temperature

and velocity mooring in the Upper Arm 3 km away from the confluence (UAJ) to fill the gap between our long-term mooring and the instrumentation deployed at the Narrows.

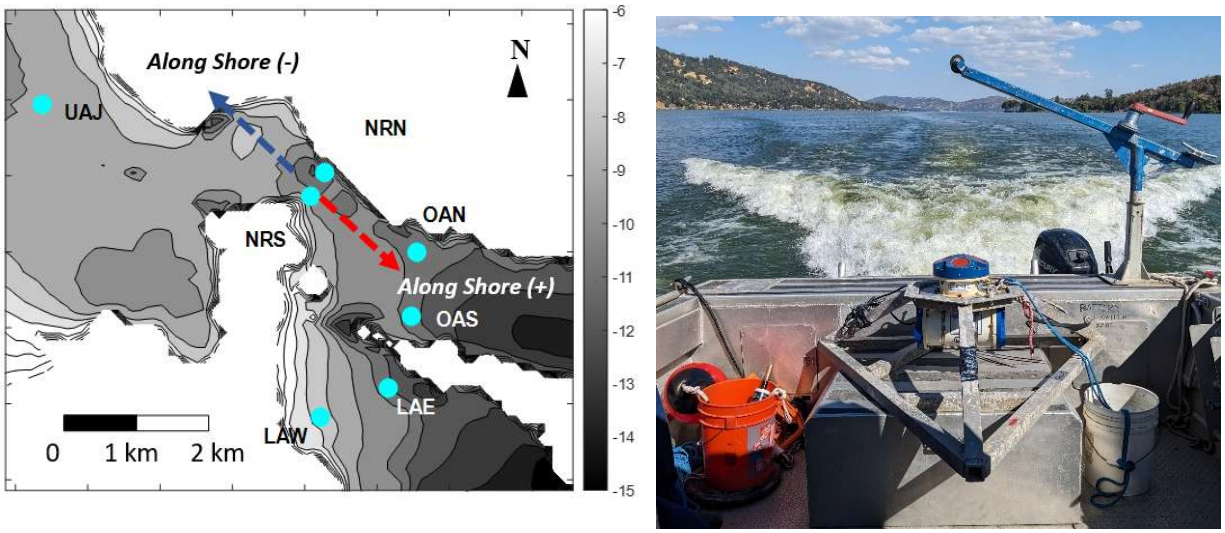

Figure 7.11.1. (Left) Map showing the location of temperature and velocity moorings at the confluence of Clear Lake during our experiment; (right)ADCP and frame ready for deployment at Clear Lake.

7.11.2 Results

One of the main insights that our field measurements provided was the daily surface flow pathways at the confluence. While the northwest winds were blowing, surface flow from the Narrows split in two and they entered the OA and LA. Due to the shape of these basins and rotational effects, we observed a return flow when the wind died at the surface, which passed through the Narrows again, but this time as a bottom current (Figure 7.11.2).

We also studied time series of wind, lake temperature, and along shore velocities both at the south and north shore of the Oaks arm over two days. We observed similar wind forcing with strong winds in the afternoon that died at night, but different stratification conditions. For the example on the left of Figure 7.11.3, we observed a residual stratification at night (mode 1), while the water column was homogenous at that time for the second case shown on the right of this figure (mode 2). As a result, during the wind forcing phase, we observed flow moving to the east at the surface in the south shore for both modes, but once the wind died, the return flow at the surface set up immediately thanks to the residual stratification in mode 1, while that only happened once the stratification set up the following day in mode 2. As a result, we identified two different modes of exchange, one with immediate flow return and the second one with delayed return flow. The delayed mode described here may be important for water quality because it entrains deep water into the surface waters which are sent out of the Oaks Arm to somewhere else (e.g. Upper or Lower Arms).

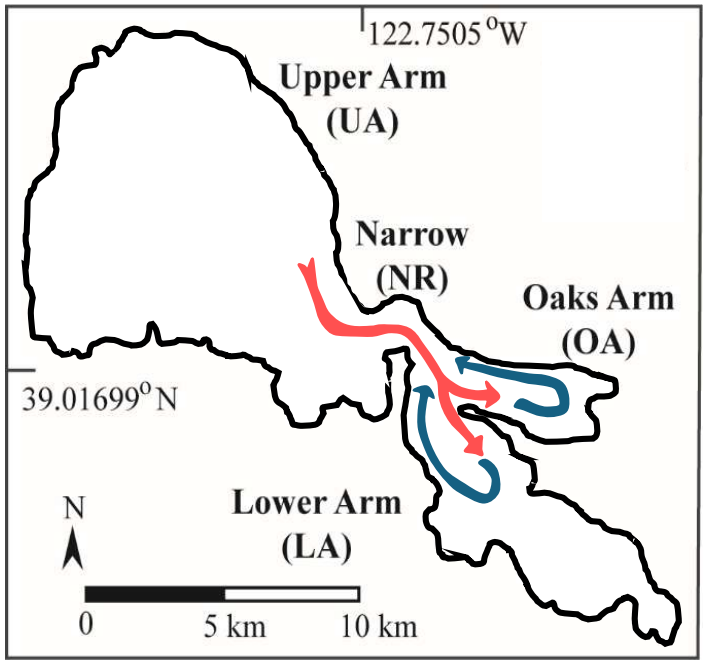

Figure 7.11.2. Daily surface flow pathways at the confluence of Clear Lake

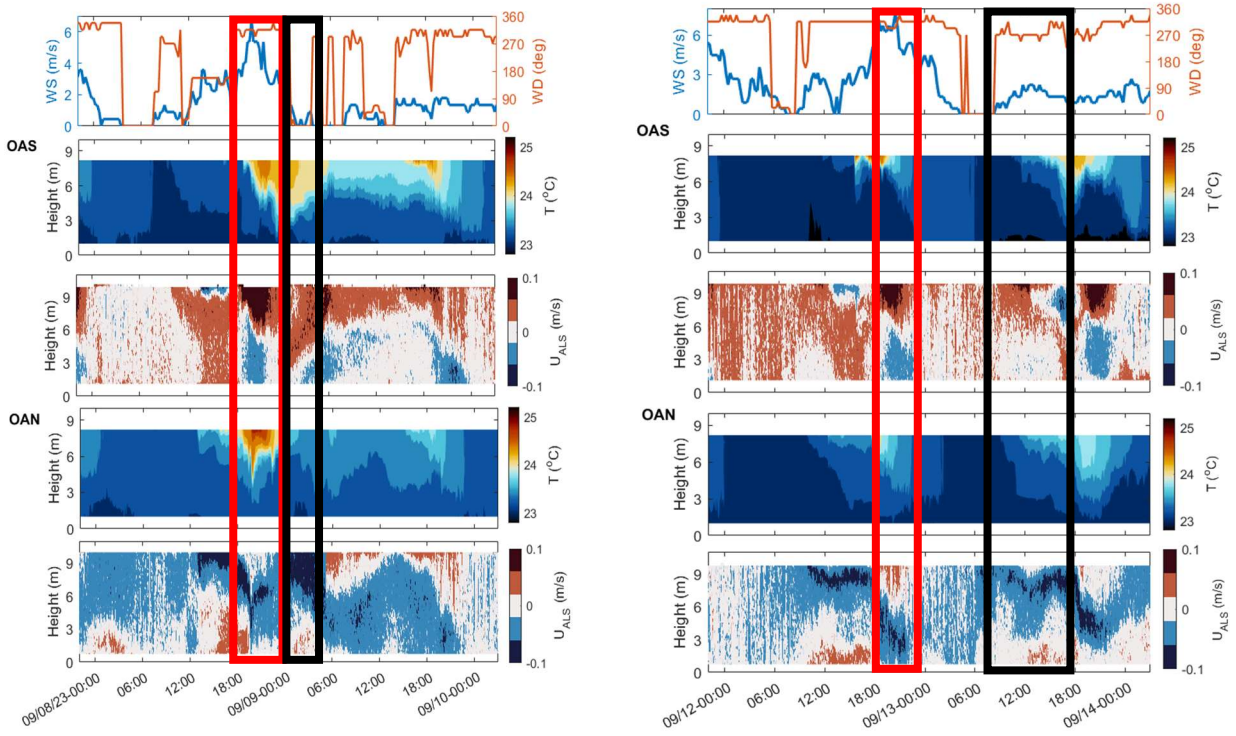

Figure 7.11.3. Time series of wind, lake temperature, and along shore velocities both at the south and north shore of the Oaks arm over two days

8 In-Lake Modeling (UCD-TERC)

8.1 Overview of the Lake Model

Models are representations of real systems. The need for in-lake water quality modeling in Clear Lake has arisen as a result of the increased need to (1) predict lake responses, (2) understand the processes that are causing the poor water quality, and (3) inform and optimize regulation and management decisions. Clear Lake faces numerous water quality challenges, but the greatest barrier to improvement is the absence of quantitative data on the response of the system to investments in specific restoration projects. Acquiring quantitative data requires completing three fundamental tasks:

a) Quantifying the processes that contribute to poor water quality (in-lake monitoring, see Section 7).
b) Accurately predicting the lake response to environmental forcings, including the extent of the current water quality challenges, i.e. model development.
c) Quantitatively evaluating the impacts, and unintended consequences of implementing particular restoration projects or strategies, i.e. scenario development.

A broad variety of in-lake models are available, which can be grouped into two categories: (1) data-driven, empirical, or statistical models, that rely on observations rather than theory, and (2) processed-based models, that use mathematical equations based on theory to characterize/represent a system. Empirical models for lakes have been used broadly, particularly now with the widespread use of Machine Learning and Artificial Intelligence (AI), which mostly use "trained" empirical models. However, the need for long (>30 years) and complex data sets to use AI, made us suggest the development of a "process-based" or "mechanistic" model for this project, in which theory sets the basics of a successful model.

Multiple shortcomings have been adopted when developing mechanistic water quality models. First, in ecological water quality models, the physical processes of transport and mixing within the water body (i.e., how the water moves) have generally been oversimplified, with assumptions of continuously stirred being common. However, the predictive ability of these models is compromised since temporal variability of the transport is lacking and it yields wrong effects in the water quality. Second, the dimensionality of the system representation is particularly important in systems with complex bathymetry such as multi-basin lakes, where the assumption of horizontal or lateral mixing (one- or two- dimensional) is rarely observed. Three-dimensional models are more appropriate for systems with complex topography, such as Clear Lake, because they consider changes both in the horizontal and vertical directions.

Thus, we have developed an in-lake three-dimensional (3D) processed-based model for Clear Lake. The processes the model simulates are organized into two groups: those that characterize how the water moves (i.e. hydrodynamic) and those that modify nutrients and algae in the lake (i.e. water quality or biogeochemical-ecological) (Figure 8.1.1).

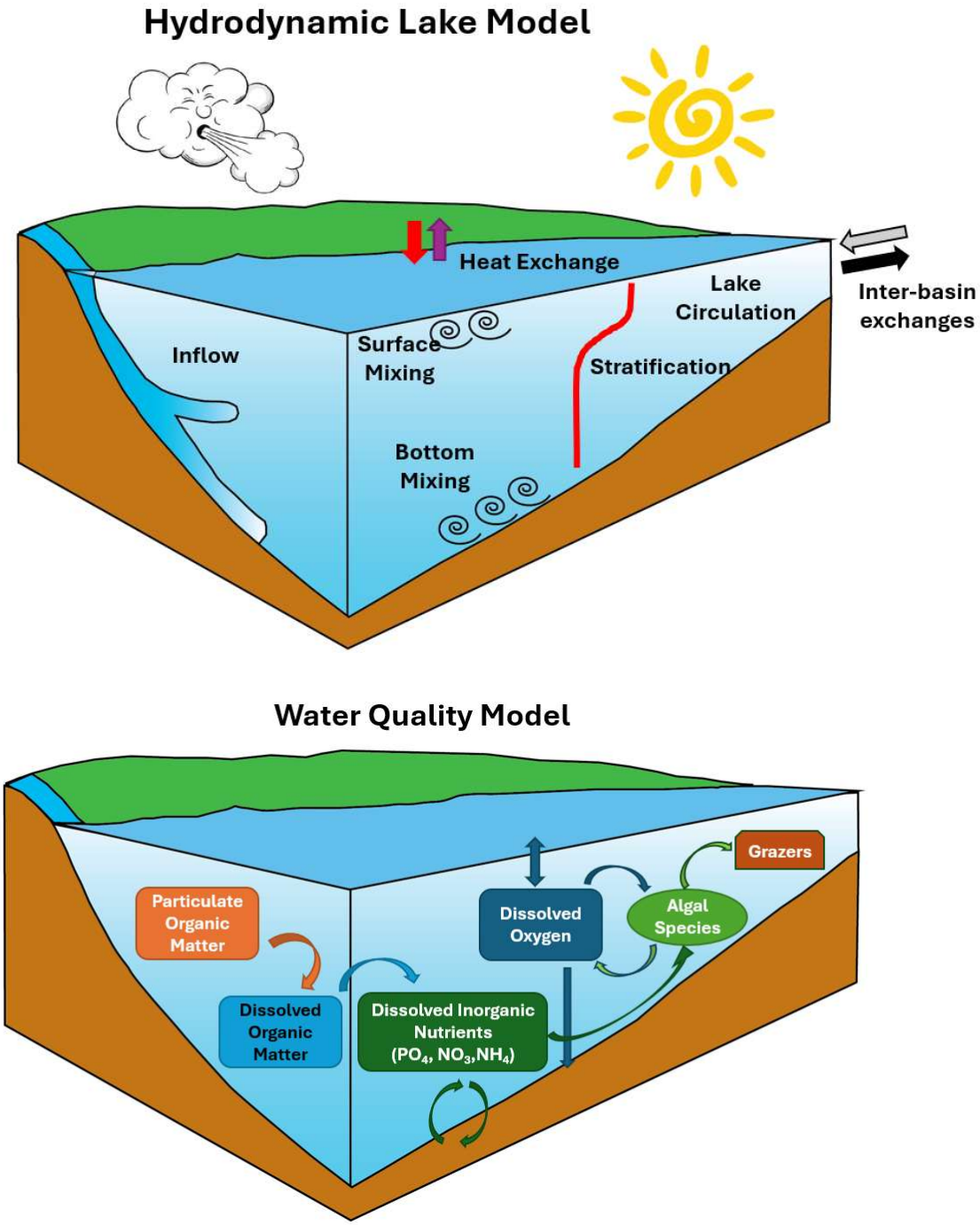

Figure 8.1.1. Conceptual models of the hydrodynamic (top) and water quality (bottom) models developed for Clear Lake

8.2 Hydrodynamic Lake Model: Si3D

8.2.1 Hydrodynamic Model Description

Si3D is the semi-implicit, 3D, free-surface hydrodynamic numerical model (Si3D) originally developed to address estuarine circulation (Smith, 2006) and extended to analyze lake hydrodynamics by Rueda (2001). The hydrodynamic model solves using a finite difference scheme the continuity equation for incompressible fluids, the hydrostatic Reynolds-averaged form of the Navier-Stokes equations (the weight of the fluid balances the pressure), and assumes negligible density fluctuations except for the buoyancy term (i.e., the Boussinesq approximation). The numerical model also includes a transport equation for temperature, and an equation of state relating temperature, salinity, and pressure to fluid density (Rueda and Schladow 2003).

Si3D solves the layer-averaged form of the above equations for stratified flows using a semi-implicit leapfrog-trapezoidal finite difference numerical scheme formulated on a staggered cartesian grid. Temperature is modeled with the advection-diffusion equation following a flux-limiter numerical scheme. Turbulence in the vertical direction is parameterized using the turbulence closure model Mellor-Yamada 2.5, to calculate the vertical turbulent kinetic energy (TKE) and a turbulent macroscale (l). In the horizontal plane, the turbulence is described following the eddy-viscosity method by either specifying constant values or by parameterizing the horizontal eddy coefficients following Blumberg (1986).

Since Si3D uses the hydrostatic and Boussinesq approximations, it is not able to predict nonlinear internal wave motions and high-frequency internal waves, which normally require non-hydrostatic formulations (e.g., MITgcm: Dorostkar et al. 2017). However, computational requirements of non-hydrostatic 3D numerical models and common simulation periods considered in 3D lake models (often on the order of weeks or months) are extremely high, and likely unfeasible in a timely manner considering today's technology. In particular, Si3D has been used in Clear Lake, Lake Tahoe, and other lakes with reasonable results (e.g., Rueda and Schladow 2003; Rueda et al. 2005; Rueda and MacIntyre 2009; Valbuena. et al. 2021).

Numerical simulations with Si3D require an initial temperature profile that describes the conditions of the lake at the beginning of the study period and a time series of meteorological conditions that include: the wind speed, wind direction, atmospheric pressure, air temperature, shortwave net radiation, incoming longwave radiation, relative humidity, and light attenuation. The initial condition of the velocity field of the numerical model is characterized as a stagnant fluid (i.e., $U = 0$) thus requiring a spin-up time of 3-4 days at the beginning of each simulation.

8.2.2 Hydrodynamic Model Set-up: Initial and Boundary Conditions

The set-up of the hydrodynamic model requires the following elements: (1) profile of lake water *initial conditions* of the different properties of interest (e.g., lake temperature); (2) the shape of the lake or *lake morphometry* obtained from bathymetrical maps; (3) *boundary conditions* that characterize the external forcing, such as meteorological conditions or inflows into the lake; and (4) *model parameters*.

The initial condition for the temperature field is specified as uniform in the horizontal plane and variable in the vertical direction using the spatially averaged high-resolution vertical profile measured during our monitoring program at the start date of the simulation.

Lake bathymetry was determined using two different surveys. First, we used the bathymetrical map obtained in 2002 by ReMetrix and the one produced by UC Davis TERC under this project in 2024. We adopted a dx = 100 m horizontal grid resolution for the hydrodynamic model and dz = 0.5 m vertical resolution. We selected this grid cell size through a convergence analysis, that consisted of selecting the grid size in which the model solution converged with the finer grid size tested.

Following the Courant–Friedrichs–Lewy condition ($C = u\Delta t/\Delta x$), the time step of the simulations was defined as $\Delta t = 20\,sec$ to guarantee convergence on the numerical solution to the governing equations.

We used the meteorological conditions measured by our network of meteorological stations on the lake shore as surface boundary conditions for Si3D (see Section 7.2). We defined spatially variable surface boundary conditions across the lake with air temperature, relative humidity, incoming short radiation, wind speed, and wind direction time series. Monthly PAR measurements were used to estimate the time series of time variable light attenuation coefficient following Beer's law. The incoming longwave (Lwin) input was estimated using Equation (8-1), using vapor pressure (ea), relative humidity as a fraction (RH), air temperature (AirT), the emissivity of air (EmAir), and cloud cover (cc) estimations following Martin & McCutcheon (1999),

$$ea = (2.1718 \times 10^{10}) \times e^{(-4157/(AirT-33.91+273))} \times RH,$$

$$EmAir = 0.642 \times \left(\frac{ea}{AirT + 273}\right)^{0.1428} \times (1 + 0.17 \times cc^2),$$

$$LW_{in} = EmAir \times 5.67e^{-8} \times ((AirT + 273.16)^4) \qquad (8\text{-}1)$$

Also, we were able to collect LWin for 1.5 years between June 2021 and July 2023. We used this in-situ data to develop seasonal correction factors of the estimated LWin with Equation (8-1). Correction factors ranged between [-130; -80] W/m^2 in summer and winter, respectively. We corrected the wind speed (WS) to be measured at 10 m instead of the actual z=2 m height using the Law-of-wall: $U(10m) = U_* / [0.41 \times \log(10/z_o)]$, where z_o is the surface roughness for water = 0.01 (1/m) and U_* is the friction velocity calculated as $U_* = WS(z) \times 0.41 / [\log(z/z_o)]$. We also used on-shore and off-shore factors to correct the wind magnitude depending on the wind direction. Wind drag was estimated using Amorocho Devries (1980) equation.

Our simulations included Coriolis effects, and the factor was estimated as 9.1 x 10^{-5} according to the Clear Lake latitude.

8.2.3 Statistical Metrics of Model Performance

We verified the agreement between measured and simulated velocity values by estimating the Root Mean Square Error (RMSE), and also the Model Skill Score (SS) (Murphy and Epstein 1989) for temperatures, following the equations:

$$SS = 1 - \frac{\sum_{j=1}^{N}\left(x_{obs_j} - x_{sim_j}\right)^2}{\sum_{j=1}^{N}\left(x_{obs_j} - \underline{x_{obs_j}}\right)^2}, \quad (8\text{-}2)$$

$$RMSE = \sqrt{\frac{\sum_{j=1}^{N}\left(x_{sim_j} - x_{obs_j}\right)^2}{N}}, \quad (8\text{-}3)$$

where x_{obs} are the field observations, $\underline{x_{obs}}$ is the mean value of all field data points, x_{sim} are the simulated results, and N is the number of data records.

8.2.4 Hydrodynamic Model Calibration

Model calibration is the process of adjusting the model parameters and forcing within the margins of the uncertainties to obtain a good representation of the processes of interest by matching measured and modeled results of key modeled variables (e.g., lake temperature and velocities).

We selected winter 2021 (Feb-March) as the calibration period of our hydrodynamic model since high-frequency lake currents (velocity) and temperatures were measured simultaneously during that period. The initial temperature profile for the simulation had a uniform temperature top to bottom of 7.6°C and the the surface boundary conditions for heat and wind forcing (meteorology) are shown in Figure 8.2.1 and Figure 8.2.2.

The key parameters we adjusted during the calibration were the attenuation coefficient, horizontal diffusivity, and bottom drag coefficient (C_d). Figure 8.2.3 shows the parameter values we tested and how the selected values yielded the lowest RMSE, both when using velocities and temperatures. We obtained RMSE < 2 cm/s and 0.5°C for lake currents and temperatures, respectively. These values represented a Score Skill (SS) > 80% for temperature, graded as very good model performance. As a result, our simulations have used an attenuation coefficient equal to 0.5 1/m, horizontal diffusivity equal to 10^{-2} m^2/s, and bottom drag coefficient equal to 0.002.

Wind forcing was also evaluated in the calibration to improve the performance of the hydrodynamic lake model. We run multiple simulations using (a) different number of meteorological stations to create a spatially variable wind field, and (b) different onshore and offshore values [1.1-1.3]. Statistical metrics of model performance for velocity and temperature results showed that wind field from *5 meteorological stations* (Buckingham Point (BKP), Konocti Bay (KNB), Beakbane Island (BBI), Clearlake Oaks (CLO), Nice (NIC)) and fOFF = 1.2 yielded the best model results, with RMSE < 2 cm/s and 0.5°C for lake currents and temperatures, respectively, and SS > 80% for temperature (very good model performance) (Figure 8.2.4).

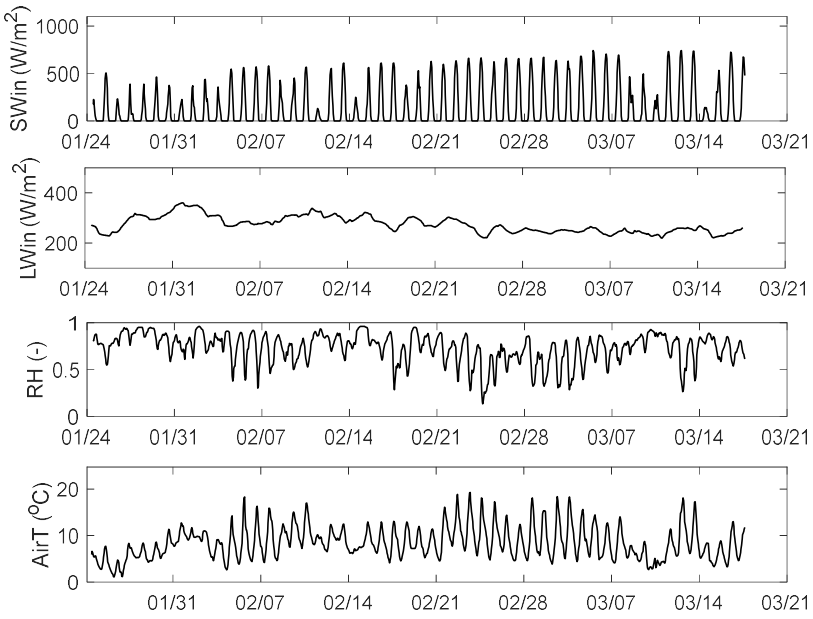

Figure 8.2.1. Time series of heat-related meteorological variables (incoming short wave radiation SWin, incoming longwave radiation LWin, relative humidity RH, and air temperature, AirT) at Clear Lake used for the model calibration during winter 2021. Values are averaged across the lake.

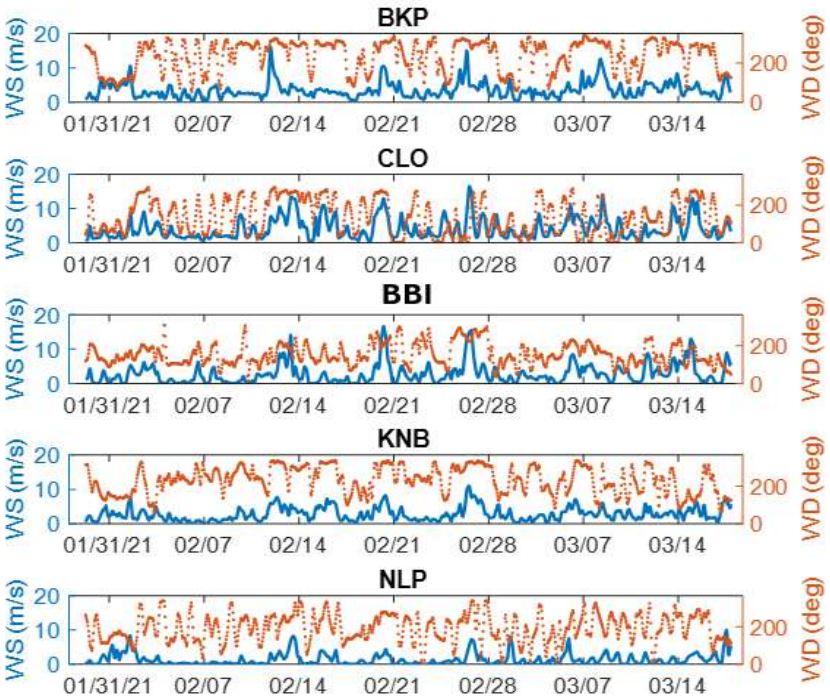

Figure 8.2.2. Time series of wind conditions (magnitude WS and direction WD) at Clear Lake used for the model calibration during winter 2021 at five stations across the lake: Buckingham Point (BKP), Konocti Bay (KNB), Beakbane Island (BBI), Clearlake Oaks (CLO), Nice (NIC)

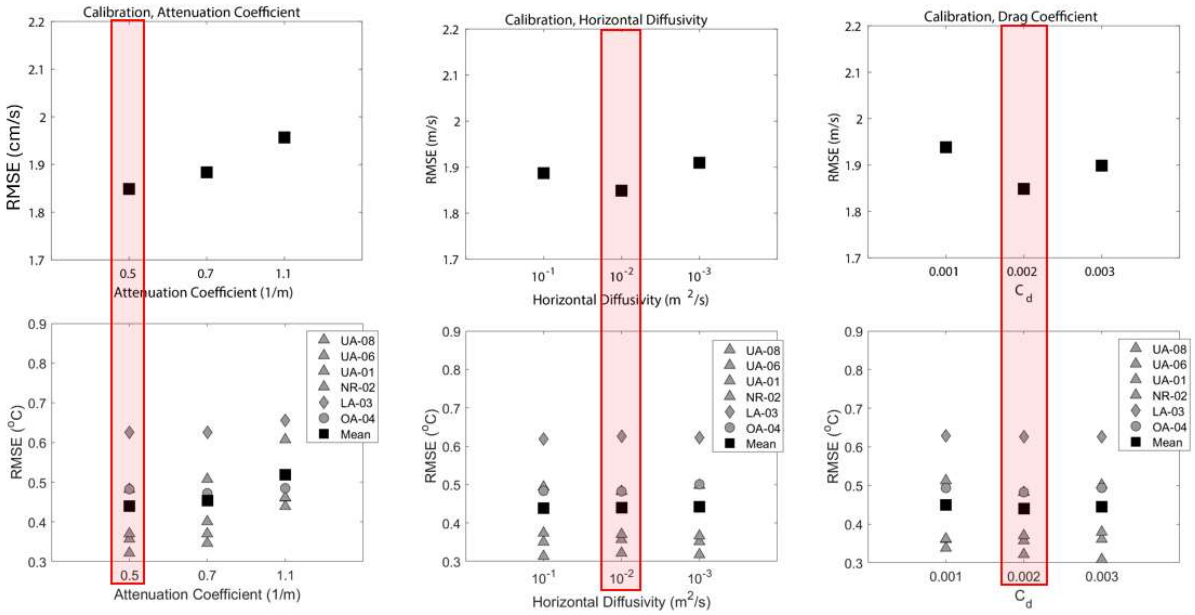

Figure 8.2.3. Root mean square errors calculated using measured and modeled velocity (top) and temperature (bottom) from winter 2021 in the Upper Arm. The calibration runs aimed to select the best values (marked with a red rectangle) of three parameters: attenuation coefficient, horizontal diffusivity, and bottom drag coefficient (C_d)

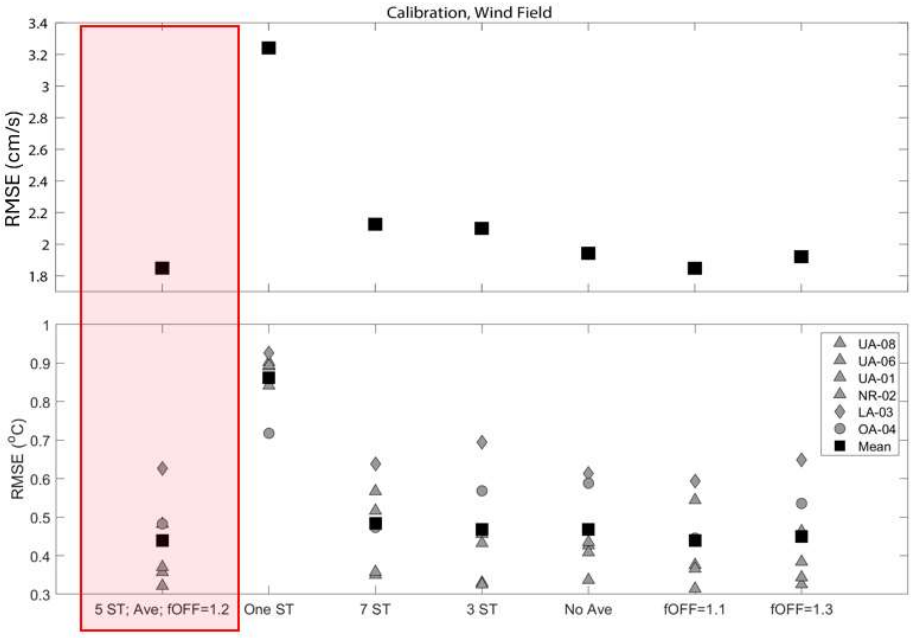

Figure 8.2.4. Root mean square errors calculated using measured and modeled velocity (top) and temperature (bottom) from winter 2021 in the Upper Arm. The calibration runs aimed to select the optimal combination of meteorological stations (marked with a red rectangle) and fOFF factor

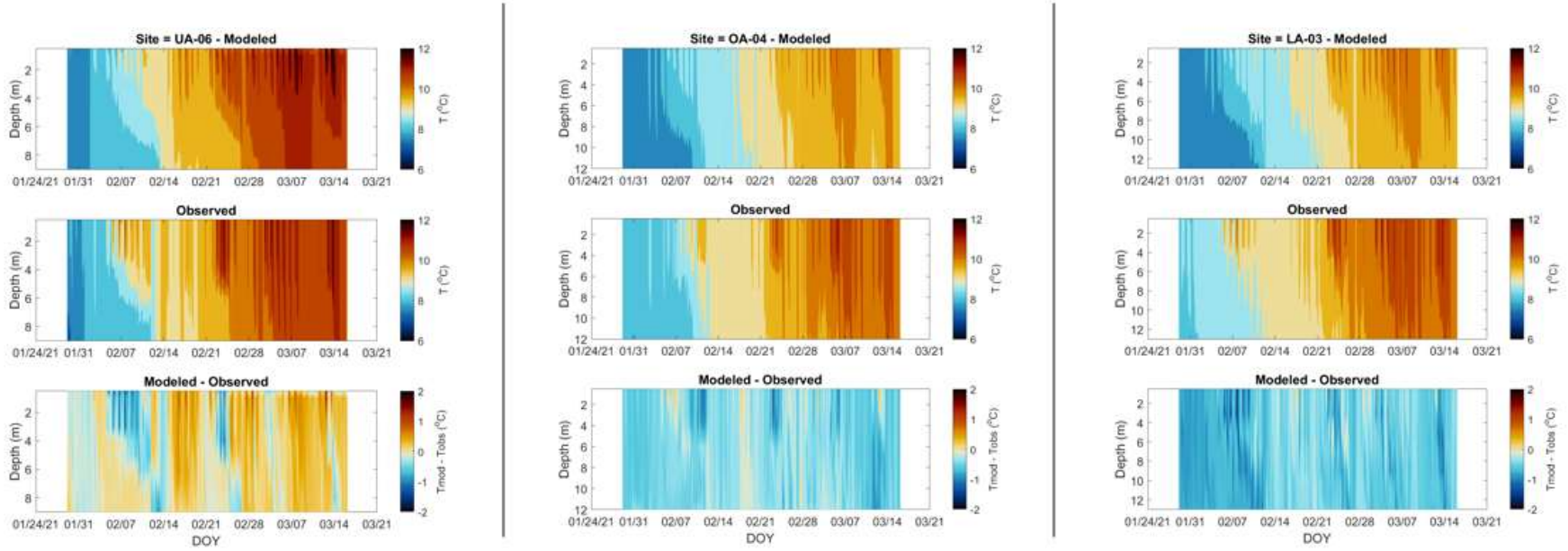

Figure 8.2.5. Time series of lake temperatures in depth of (top) modeled, (middle) observed, and (bottom) temperature differences between the two for the three deep monitoring locations at Clear Lake: (left) Upper Arm, (center) Oaks Arm, and (right) Lower Arm during the winter 2021 calibration period.

A comparison of modeled and observed temperatures and velocities during the calibration period in winter 2021 confirms the good performance of the Clear Lake hydrodynamic model (Figure 8.2.5 and Figure 8.2.6). The difference between the modeled and observed temperatures in depth was ~+/-2°C across the 3 basins, with warmer modeled temperatures than observed in the Upper Arm, and colder modeled temperatures than observed in the other two basins. The comparison of modeled and observed lake currents yielded differences of ~2 cm/s, which were even smaller when comparing bottom currents.

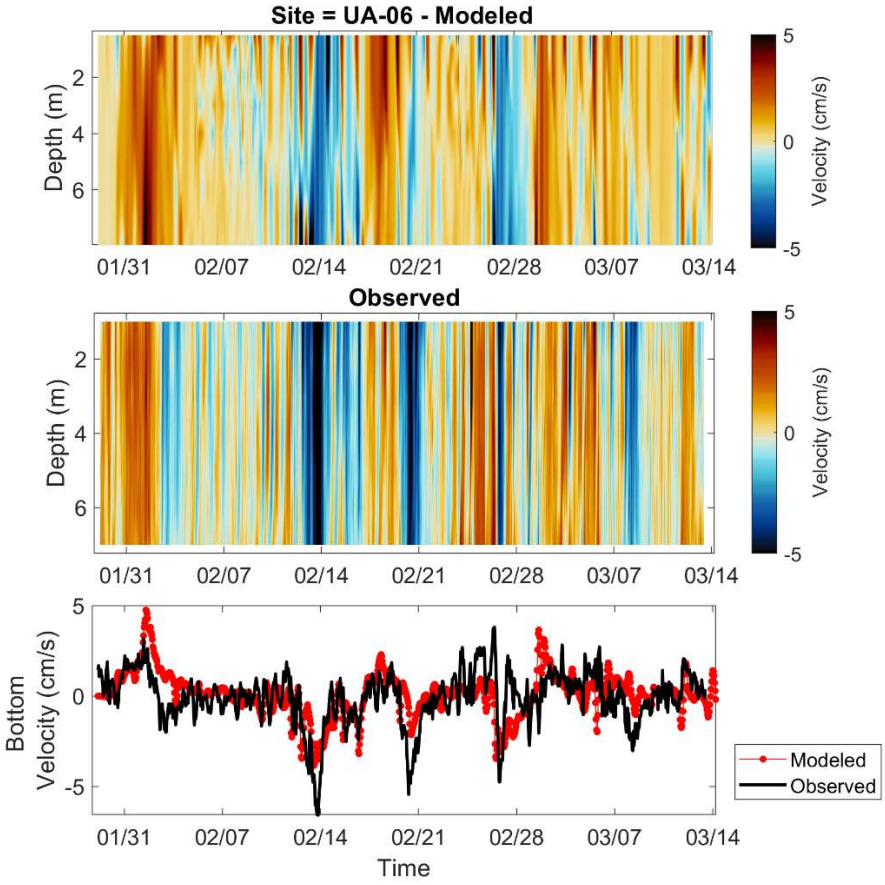

Figure 8.2.6. Time series of lake currents in depth of (top) modeled, and (middle) observed values in the Upper Arm. The bottom panels show the comparison of the bottom modeled and observed currents during the winter 2021 calibration period.

8.2.5 Hydrodynamic Model Validation

Once the Clear Lake hydrodynamic model was successfully calibrated for winter 2021, we used the same model parameters and assumptions when creating surface boundary conditions to run a simulation during a different period of time and confirm that our hydrodynamic model is robust and reliable. We run a 2-year simulation between April 2019 and March 2021 as our validation scenario.

Modeled lake temperatures during the validation run reproduce the same patterns as observed in the field across different sites (Figure 8.2.7). Temperature differences between modeled and observed values were still below 2°C, which indicates a very good performance of the Clear Lake hydrodynamic model.

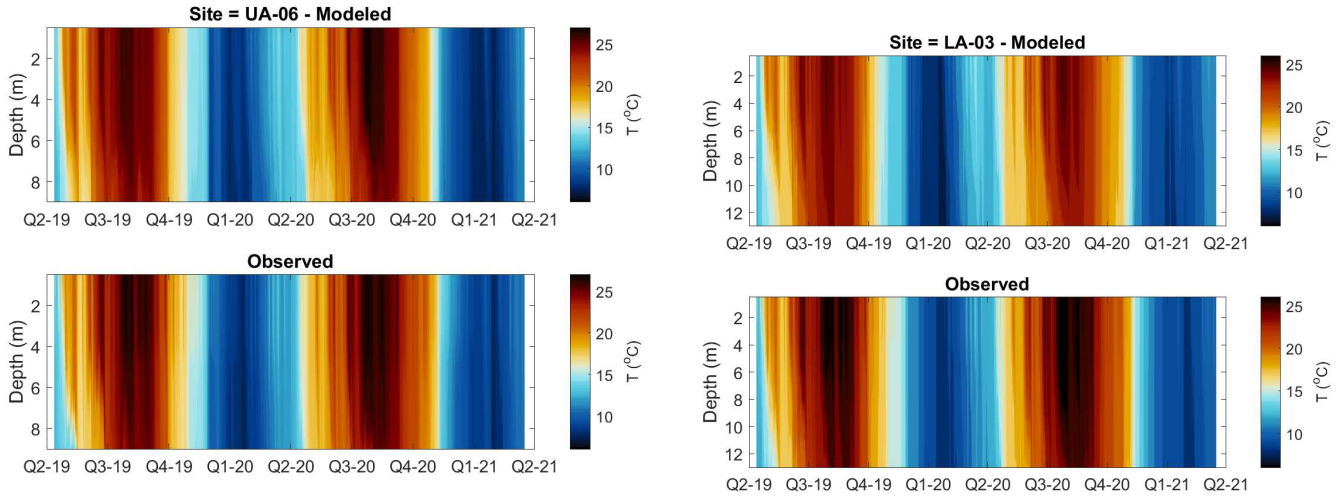

Figure 8.2.7. Time series of lake temperatures in depth of (top) modeled, and (bottom) observed values at two deep monitoring locations at Clear Lake: (left) Upper Arm, and (right) Lower Arm between April 2019 and March 2021(validation period).

8.3 Water Quality Lake Model: Si3D-AEM

8.3.1 Water Quality Model Description

We have implemented a coupled Aquatic Ecological Model (AEM) to the hydrodynamic Si3D numerical model described in section 8.2. For this project, we will refer to the newly developed coupled **3-D hydrodynamic Aquatic Ecological Model** as **Si3D-AEM**. A similar water quality model has been applied previously using both a one-dimension framework such as MINLAKE (Riley and Stefan 1988) and DYRESM-WQ (Hamilton and Schladow 1997; Schladow and Hamilton 1997), and a three-dimension framework such as ELCOM-CAEDYM (Hodges et al. 2000; Hipsey et al. 2019). Coupled hydrodynamic-ecological models are used as a management tool in a variety of lakes such as Lake Erie (Boegman et al. 2008, Leon et al. 2011, Wang and Boegman 2021), Lake Kinneret, (Bruce et al. 2006), Lake Michigan (Chen et al. 2002), and Lake Champlain (Marti et al. 2019), among others (Bruce et al. 2018). In all these coupled models, ecological processes are updated after each hydrodynamic model time step. In Si3D-AEM the aquatic ecological model uses the temperature and velocity solved in the hydrodynamic module *every hour* to simulate the advective and diffusive transport of active scalars or state variables. Active scalars will change due to transport in each time step and due to chemical and biological processes quantified using source-sink equations. These source-sink equations follow the parameterizations described by Hipsey et al. (2013) and summarize in the next sub-sections.

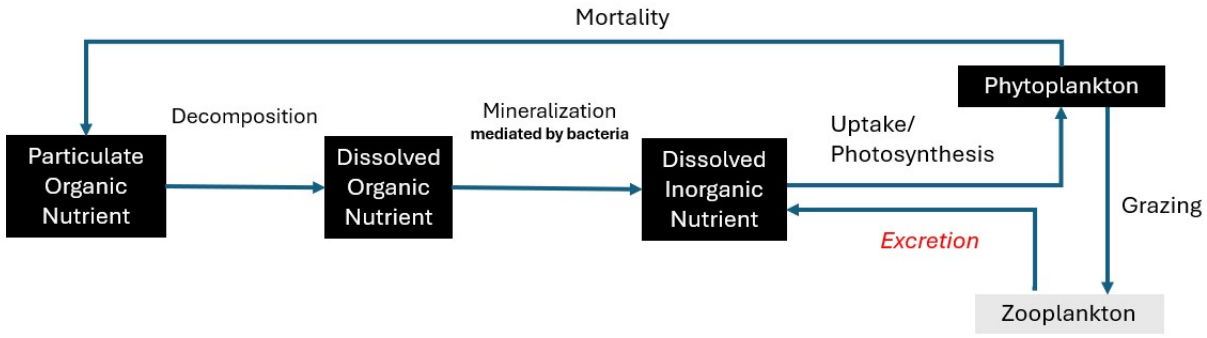

Figure 8.3.1. Generic diagram of the main state variables and processes modeled in Si3D-AEM. State variables in black are explicitly modeled (particulate organic matter, dissolved organic matter, dissolved inorganic matter, and phytoplankton), while state variables in gray are not modeled (zooplankton). Processes in red have not been parameterized but are included in this figure for completeness.

For this project, the AEM includes the cycling of carbon (C), nitrogen (N), and phosphorus (P), along with dissolved oxygen (DO) and phytoplankton dynamics including growth, respiration, and grazing by zooplankton. Figure 8.3.1 is a generic diagram of the main state variables and processes modeled in Si3D-AEM. Each state variable or active scalar has a source-sink equation associated with quantifying its rate of change in each time step. State variables in black are explicitly modeled (particulate organic matter, dissolved organic matter, dissolved inorganic matter, and phytoplankton as four individual functional groups), while state variables in gray are not explicitly modeled (zooplankton) but their impact on the other state variable is accounted for. Processes shown in red have not been parameterized but are included in this figure for completeness.

The model accounts for the source and sink terms of each state variable:

- Nitrogen forms: particulate organic nitrogen (PON), dissolved organic nitrogen (DON), ammonium (NH_4), and nitrate plus nitrite (NO_3)
- Phosphorus forms: particulate organic phosphorus (POP), dissolved organic phosphorus (DOP), and soluble reactive phosphorus (SRP)
- Four phytoplankton groups (ALG1, ALG2, ALG3, ALG4), as carbon units. We model particulate organic carbon (POC) and dissolved organic carbon (DOC). According to our monitoring network, the four main divisions we have modeled are diatoms, green algae, cryptomonads, and cyanobacteria.

The main features of Si3D-AEM include:

- Phytoplankton represented as carbon concentrations (PhytoC, µg/L = mg/m^3)
- Four phytoplankton divisions (diatoms, green algae, cryptomonads, and cyanobacteria)
- Nutrient regeneration (C, N, P)
- Dissolved oxygen dynamics (DO)

- The coupled model operates on any sub-daily time step to resolve algal processes. Due to the large computational resources (time and space) required to save 3D outputs, we produced model results every 4 hours.
- Sink-source terms in the active scalar transport equation must have units of flux. For consistency, we used the following units of flux: [mg m^{-2} s^{-1}]. Thus, active scalar concentrations are in [mg m^{-3}] = [µg L^{-1}]

In the next sections, we will present the following:

- Overview of the phytoplankton, dissolved oxygen, and nutrient dynamics, including conceptual models, equations, and model parameters/constants.
- Water quality model calibration in summer 2020.
- Water quality model validation in summer 2022.

8.3.2 Phytoplankton, Dissolved Oxygen, and Nutrient Dynamics: Conceptual Models, Equations and Parameters

The equations and parameters described below are adapted from the following sources: Hamilton and Schladow (1997), and Hipsey et al. (2013).

- **Phytoplankton**

Phytoplankton biomass is represented as particulate carbon (PhytoC, mg/m^3) and we currently model four phytoplankton groups arranged by division (diatoms, green algae, cryptomonads, and cyanobacteria). For each phytoplankton group, the source-sink equation that models the rate of change of phytoplankton carbon concentration, [d[PhytoC]/dt], includes three processes: growth, resuspension (sources), mortality, grazing, and settling (sinks).

$$\frac{d[Phyt\quad]}{dt}\left[\frac{mg}{m^2 d}\right] = \ Growth\ - Mortality - Grazing - Settling + resuspension \qquad (8\text{-}4)$$

Phytoplankton Growth: The rate of change of phytoplankton biomass (*Growth*) is proportional to the phytoplankton biomass in the previous time step (*PhytoC*) and the product of a series of constants. The daily maximum potential growth (μ_{max}) rate is multiplied by a temperature function (f_T) and the minimum value of expressions for limitation by light (f_L), nitrogen (f_N), and phosphorus (f_P), and *h* is the thickness of each modeled layer, as follows,

$$Growth\ \left[\frac{mg}{m^2 d}\right] = \ \mu_{max}\ [d^{-1}]\ \cdot MIN(f_L, f_N, f_P)\ \cdot f_T\ \cdot PhytoC[mg/m^3] \cdot h[m] \qquad (8\text{-}5)$$

Light limitation on phytoplankton growth is configured to be subject to photoinhibition, following the P-I curve described by Steele's (1982) equation:

$$f_L = \frac{I}{I_{sat}} \cdot e^{\left(1-\frac{I}{I_{sat}}\right)} \qquad (8\text{-}6)$$

where *I* is the photosynthetically active radiation (PAR) reaching a certain depth, I_{sat} is the PAR saturation value (µE/m^2/s). To compute PAR, we are using the incoming shortwave radiation values from the hydrodynamic model (SWin) and converted as PAR = 0.47 SWin

Table 8.3.1. List of selected parameters used in Si3D-AEM simulations, with their symbols, units, and assigned values based on calibration and values from the literature.

Biological rates/velocities	**Symbols**	**Units**	**Assigned values**	**Values from literature**
Maximum growth rate of phytoplankton	μ_{max}	d^{-1}	0.5	0.2-4.5[a,b]
Mortality rate of phytoplankton	R_{mort}	d^{-1}	0.08	0.03-0.2[f,g]
Grazing rate of zooplankton on phytoplankton	R_{graz}	d^{-1}	0.00	0-0.2
Settling velocity	V_{settl}	$m\,d^{-1}$	0.001	0-0.5
Resuspension velocity	v_{resusp}	$m\,d^{-1}$	0.00	0-0.05
Reaeration rate	R_{reaer}	$m\,d^{-1}$	0.05	0.01-0.1
Biological constants	**Symbols**	**Units**	**Assigned values**	**Values from literature**
PAR saturation value	I_{sat}	µE/m²/s	40	40-500[c,d]
Half-saturation constant for nitrogen	K_{SN}	mg/m³	70	10-35[e,f]
Half-saturation constant for phosphorus	K_{SP}	mg/m³	20	3-11[e,f]
Ratio of nitrogen to carbon	rnc	-	0.151	16:106[l]
Ratio of phosphorus to carbon	rpc	-	0.01	1:106[l]
Ratio of oxygen to carbon	roc	-	1.0	16:12[l]
Ratio of oxygen to nitrogen	ron	-	1.0	16:14[l]
Algae preference factor for NH_4	f_{NH4}	-	0.25	0.2-0.25[f,g]
Optimal temperature for growth	T_{opt}	°C	25	Calibration
Temperature correction constant for mortality/grazing	θ	-	1.05	1-1.1[a,i]
Chemical rates and constants	**Symbols**	**Units**	**Assigned values**	**Values from literature**
PON decomposition rate	R_{dcn}	d^{-1}	0.08	0.01-0.03[a,f,h]
DON mineralization rate	R_{mn}	d^{-1}	0.015	0.001-0.005[a,f,i]
Nitrification rate	R_n	d^{-1}	0.015	0.01-0.02[f,d,j]
POP decomposition rate	R_{dcp}	d^{-1}	0.05	0.01-0.1[f,k]
DOP mineralization rate	R_{mp}	d^{-1}	0.10	0.001-0.1[f,k]
POC decomposition rate	R_{dcc}	d^{-1}	0.05	0.01-0.2[f]
DOC mineralization rate	R_{Mc}	d^{-1}	0.001	0.001-0.2[f]
Half-saturation constant for DO inhibition of chemical reactions	K_{DO}	mg/m³	1.0	
Temperature correction constant for decomposition/mineralization/nitrification	θ	-	1.08	1-1.1[a,i]
Temperature correction constant for sediment nutrient fluxes/sediment oxygen demand	θ	-	1.05	1-1.08[a,d]
Fluxes (atmospheric and sediments)	**Symbols**	**Units**	**Assigned values**	**Values from literature**
Sediment oxygen demand rate	R_{SOD}	$mg\,m^{-2}d^{-1}$	0.8	field value
Atmospheric deposition rate of DON	ATM_{DON}	$mg\,m^{-2}d^{-1}$	0.0	
Atmospheric deposition rate of NH4	ATM_{NH4}	$mg\,m^{-2}d^{-1}$	0.0	
Atmospheric deposition rate of NO3	ATM_{NO3}	$mg\,m^{-2}d^{-1}$	0.0	
Atmospheric deposition rate of DOP	ATM_{DOP}	$mg\,m^{-2}d^{-1}$	0.0	
Atmospheric deposition rate of PO4	ATM_{PO4}	$mg\,m^{-2}d^{-1}$	0.0	
Atmospheric deposition rate of DOC	ATM_{DOC}	$mg\,m^{-2}d^{-1}$	0.0	
Sediment release rate of DON	SED_{DON}	$mg\,m^{-2}d^{-1}$	0.0	
Sediment release rate of NH4	SED_{NH4}	$mg\,m^{-2}d^{-1}$	0.1	Calibration
Sediment release rate of NO3	SED_{NO3}	$mg\,m^{-2}d^{-1}$	0.0	
Sediment release rate of DOP	SED_{DOP}	$mg\,m^{-2}d^{-1}$	0.0	
Sediment release rate of PO4	SED_{PO4}	$mg\,m^{-2}d^{-1}$	0.1	Calibration
Sediment release rate of DOC	SED_{DOC}	$mg\,m^{-2}d^{-1}$	0.0	

[a]Bowie et al (1985); [b]Pollingher and Berman (1982); [c]Schladow & Hamilton (1997); [d]Chapra (1997); [e]Bruce et al (2006); [f]Losada 2001; [G]Chen et al (2002); [h]Hipsey et al (2006); [i]Missaghi and Hondzo (2010); [j]Romero et al (2004); [k]Leon et al (2011); [l]Redfield (1958)

Michaelis-Menten equations are used to model nutrient limitation on the growth (f_N for nitrogen, and f_P for phosphorus). In addition, a temperature correction factor (f_T) is used to account for maximum, minimum and optimal temperature (T_{max} = 30°C, T_{min} = 5°C, T_{opt}) on the growth rate, being the optimal temperature specific for each phytoplankton division:

$$f_N = \frac{[NO_3 + NH_4]}{[NO_3 + NH_4] + K_{SN}} \quad (8\text{-}7)$$

$$f_P = \frac{[PO_4]}{[PO_4] + K_{SP}} \quad (8\text{-}8)$$

$$f_T = \frac{(T - T_{min})}{(T_{opt} - T_{min})} if\ T_{min} < T < T_{opt};\ f_T = \frac{(T_{max} - T)}{(T_{max} - T_{opt})} if\ T > T_{opt};\ f_T = 0\ if\ T < T_{min} \quad (8\text{-}9)$$

where K_{SN} and K_{SP} are a half-saturation constant for N and P, respectively.

Phytoplankton Mortality: This term is assumed to be proportional to the daily rate of mortality (R_{mort}), and phytoplankton biomass in the previous time step, corrected by temperature as follows,

$$Mortality\ \left[\frac{mg}{m^2 d}\right] = R_{mort}\ [d^{-1}] \cdot f_T \cdot PhytoC[mg/m^3] \cdot h[m] \quad (8\text{-}10)$$

$$f_T = \vartheta^{(T-20)}$$

where Arrhenius factor (f_T) is used to account for temperature correction, with θ as a temperature correction constant and T as water temperature.

Zooplankton Grazing: This term is assumed to be proportional to the daily rate of grazing (R_{graz}), and phytoplankton biomass in the previous time step, corrected by temperature as follows,

$$Grazing\ \left[\frac{mg}{m^2 d}\right] = R_{grz}\ [d^{-1}] \cdot f_T \cdot PhytoC[mg/m^3] \cdot h[m] \quad (8\text{-}11)$$

Settling and resuspension:These processes are quantified as the product between the characteristic velocity of each process (v_{settl} and v_{resusp}) multiplied by the phytoplankton concentration as follows:

$$Settling/Resuspension\ \left[\frac{mg}{m^2 d}\right] = v_{settl-resusp}\ \left[\frac{m}{d}\right] \cdot PhytoC[mg/m^3] \quad (8\text{-}12)$$

Table 8.3.1 has a full description of all constants and their values assigned during the model calibration. We also included the ranges of values found in the literature for those parameters. Biological rates and constants for phytoplankton shown in this table assume that all phytoplankton division are lamped into one group (i.e., total biomass of phytoplankton. Table 8.3.2 shows the biological rates and constants for the four phytoplaknto divisions modeled for Clear Lake.

Table 8.3.2. List of selected biological rates and constants selected in Si3D-AEM simulations, with their symbols, units, assigned values based on calibration and values from the literature when 4 different phytoplankton divisions were modeled.

	Biological rates and constants	Symbols	Units	Assigned values	Values from literature
Diatoms (1)	Maximum growth rate of phytoplankton	μ_{max}	d^{-1}	0.65	0.2-4.5[a,b]
	Mortality rate of phytoplankton	R_{mort}	d^{-1}	0.09	0.03-0.2[f,g]
	Grazing rate of zooplankton	R_{graz}	d^{-1}	0.00	0-0.2
	PAR saturation value	I_{sat}	µE/m²/s	40	40-500[c,d]
	Optimal temperature for growth	T_{opt}	°C	13.5	Calibration
Green Algae (2)	Maximum growth rate of phytoplankton	μ_{max}	d^{-1}	0.31	0.2-4.5[a,b]
	Mortality rate of phytoplankton	R_{mort}	d^{-1}	0.03	0.03-0.2[f,g]
	Grazing rate of zooplankton	R_{graz}	d^{-1}	0.00	0-0.2
	PAR saturation value	I_{sat}	µE/m²/s	80	40-500[c,d]
	Optimal temperature for growth	T_{opt}	°C	18	Calibration
Crypto-monads (3)	Maximum growth rate of phytoplankton	μ_{max}	d^{-1}	0.15	0.2-4.5[a,b]
	Mortality rate of phytoplankton	R_{mort}	d^{-1}	0.02	0.03-0.2[f,g]
	Grazing rate of zooplankton	R_{graz}	d^{-1}	0.00	0-0.2
	PAR saturation value	I_{sat}	µE/m²/s	95	40-500[c,d]
	Optimal temperature for growth	T_{opt}	°C	20	Calibration
Cyano-bacteria (4)	Maximum growth rate of phytoplankton	μ_{max}	d^{-1}	0.5	0.2-4.5[a,b]
	Mortality rate of phytoplankton	R_{mort}	d^{-1}	0.08	0.03-0.2[f,g]
	Grazing rate of zooplankton	R_{graz}	d^{-1}	0.00	0-0.2
	PAR saturation value	I_{sat}	µE/m²/s	45	40-500[c,d]
	Optimal temperature for growth	T_{opt}	°C	28	Calibration

[a]Bowie et al (1985); [b]Pollingher and Berman (1982); [c]Schladow & Hamilton (1997); [d]Chapra (1997); [e]Bruce et al (2006); [f]Losada 2001; [G]Chen et al (2002);

- **Dissolved Oxygen**

The main processes involved in dissolved oxygen (DO)fate in the water column are:

Exchange to and from the air-water interface (reaeration): We computed the DO saturation of dissolved oxygen at 1 atm (DO_{ss}), equilibrium DO at non-standard pressure (DO_s), and partial pressure of water vapor (p_{wv}) following Chappra (1997). The transfer of DO across the air-water interface is modeled as,

$$Reaeration\ \left[\frac{mg}{m^2 d}\right] = R_{reaer}\ \left[\frac{m}{d}\right] \cdot (DO_s - DO)[mg/m^3] \quad (8\text{-}13)$$

Where R_{reaer} is the velocity of DO exchange at the air-water interface (constant only at the top layer), and DO is the modeled dissolved oxygen concentration in the previous time step.

Sediment oxygen demand (SOD): It represents the utilization of DO at the sediment-water interface (only the bottom layer). We use a simple sediment oxygen demand flux (R_{SOD}) that varies as a function of the overlying water temperature and dissolved oxygen levels as,

$$SOD\ \left[\frac{mg}{m^2 d}\right] = R_{SOD}\ \left[\frac{mg}{m^2 d}\right] \cdot f_{DO} \cdot \vartheta^{(T-20)} \quad (8\text{-}14)$$

Where f_{DO} is a function that controls DO inhibition and follows a Michaelis-Menten equation: f_{SOD} = DO / (K_{SOD} + DO), K_{SOD} is the half-saturation constant for sediment oxygen demand.

Water column biological oxygen demand: It is the DO consumption by mineralization of DOC (bacterial respiration) and we modeled it as,

$$Bio\ Oxygen\ Demand\ \left[\frac{mg}{m^2 d}\right] = R_{mc}\ [d^{-1}] \cdot f_{DO} \cdot \vartheta^{(T-20)} \cdot DOC[mg/m^3] \cdot h[m] \quad (8\text{-}15)$$

Where R_{mc} is the rate of mineralization of DOC. The term "bio oxygen demand" is expressed in oxygen units by [*bio oxygen demand x roc]*, where *ron* is the ratio O:C

Consumption by nitrification: This is the utilization of oxygen during the oxidation of reduced element and we modeled it as,

$$Nitrification\ \left[\frac{mg}{m^2 d}\right] = R_n\ [d^{-1}] \cdot f_{DO}\ \cdot \vartheta^{(T-20)} \cdot NH_4[mg/m^3] \cdot h[m] \quad (8\text{-}16)$$

Where R_n is the rate of nitrification of NH_4. The term "nitrification" is expressed in oxygen units by [*nitrification x ron]*, where *ron* is the ratio O:N.

Oxygen production and consumption by phytoplankton: It refers to the change in oxygen concentration due to photosynthesis and respiration, modeled as,

$$DO\ photosyntesis\ \left[\frac{mg}{m^2 d}\right] = roc\ \times growth\left[\frac{mg}{m^2 d}\right] \quad (8\text{-}17)$$

$$DO\ respiration\ \left[\frac{mg}{m^2 d}\right] = roc\ \times mortality\left[\frac{mg}{m^2 d}\right] \quad (8\text{-}18)$$

Table 8.3.1 has a full description of all constants and their values assigned during the model calibration. We also included the ranges of values found in the literature for those parameters.

- **Carbon**

Carbon is considered the "primary currency" within AEM and the carbon cycle forms the backbone upon which the other elemental cycles are based. The carbon state variables of AEM carbon cycling are phytoplankton carbon (PhytoC), particulate organic carbon (POC), dissolved organic carbon (DOC), dissolved inorganic carbon (DIC), zooplankton and bacteria. The last three state variables have not been modeled in the current version of AEM due to lack of data, but are included in our conceptual diagram for completeness (Figure 8.3.2).

The main processes involved in carbon fate in the water column are:

- Biological uptake of DIC by phytoplankton (photosynthesis) - no modeled
- Respiration of living organisms into DIC (no modeled)
- Mortality of phytoplankton into POC
- Decomposition of POC into DOC
- Mineralization of DOC into inorganic nutrients (P, N) mediated by bacteria
- Atmospheric deposition of DOC (fixed flux into the surface layer)
- Settling and resuspension of phytoplankton and POC
- Dissolved sediment flux of DOC (only at the bottom layer)
- Grazing of phytoplankton, and POC by zooplankton

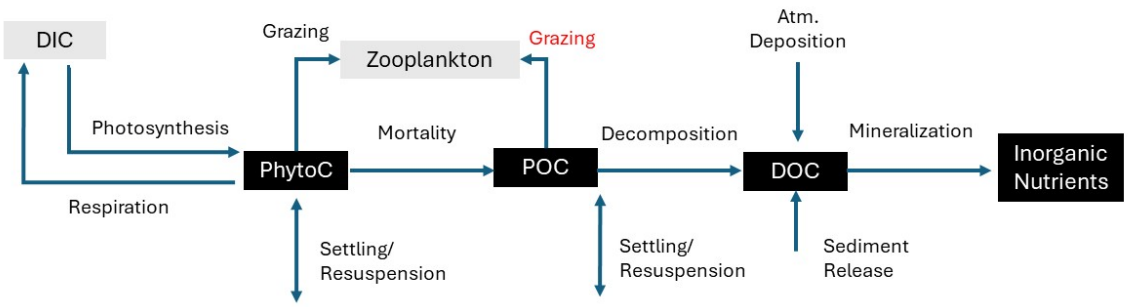

Figure 8.3.2. Carbon cycling conceptual model, including state variables and processes modeled in PSi3D-AEM. State variables in black are explicitly modeled (particulate organic carbon, dissolved organic carbon, and phytoplankton carbon), while state variables in gray are not modeled (zooplankton, bacteria, and dissolved inorganic carbon). Processes in red have not been parameterized but are included in this figure for completeness.

Due to the lack of input data and limited literature values to parameterize some of the above-described ecological processes in Clear Lake, only three carbon state variables have been modeled (PhytoC, POC, DOC), which are marked in black in Figure 8.3.2. Similarly, processes in red in this figure have not been parameterized. The source-sink equation showing the rate of change PhytoC has been described in detail in the sub-section above. Source-sink equations for POC and DOC are as follows,

$$\frac{d[POC]}{dt}\left[\frac{mg}{m^2 d}\right] = \underbrace{R_{mort}\,[d^{-1}] \cdot \vartheta^{(T-20)} \cdot PhytoC\left[\frac{mg}{m^3}\right] \cdot h[m]}_{Phytoplankton\ Mortality} - \underbrace{k_{dcc}\,[d^{-1}] \cdot f_{DO} \cdot \vartheta^{(T-20)} \cdot POC\left[\frac{mg}{m^3}\right] \cdot h[m]}_{Decomposition} \pm \underbrace{v_{settl/resusp}\left[\frac{m}{d}\right] \cdot POC\,[mg/m^3]}_{Settling/Reuspension} \quad (8\text{-}19)$$

Where k_{dcc} is the rate of POC decomposition, f_{dcc} is a function that controls DO inhibition of decomposition, and θ_{dccf} is a temperature correction constant for decomposition.

$$\frac{d[DOC]}{dt}\left[\frac{mg}{m^2 d}\right] = \underbrace{k_{dcc}\,[d^{-1}] \cdot f_{DO} \cdot \vartheta^{(T-20)} \cdot POC\left[\frac{mg}{m^3}\right] \cdot h[m]}_{Decomposition} - \underbrace{R_{mc}\,[d^{-1}] \cdot f_{DO} \cdot \vartheta^{(T-20)} \cdot DOC\left[\frac{mg}{m^3}\right] \cdot h[m]}_{Mineralization} + \underbrace{SED_{DOC}\left[\frac{mg}{m^2 d}\right] \cdot f_{DO} \cdot \vartheta^{(T-20)}}_{Sediment\ flux} + \underbrace{ATM_{DOC}\left[\frac{mg}{m^2 d}\right]}_{Atmospheric\ deposition} \quad (8\text{-}20)$$

Table 8.3.1 has a full description of all constants and their values assigned during the model calibration. We also included the ranges of values found in the literature for those parameters.

- **Nitrogen**

The nitrogen forms modeled in AEM are particulate organic nitrogen (PON), dissolved organic nitrogen (DON), ammonium (NH_4), and nitrate plus nitrite (NO_3+NO_2). The conceptual diagram of the processes is shown in Figure 8.3.3. The main processes involved in nitrogen fate in the water column are:

- Biological uptake of NO_3 and NH_4 by phytoplankton

- Biological mortality of phytoplankton into PON
- Biological excretion of NH_4 by zooplankton (no modeled)
- Mineralization of DON to NH_4
- Nitrification of NH_4 to NO_3 (consumes oxygen)
- Denitrification and nitrogen fixation (no modeled)
- Settling and resuspension of PON
- Dissolved sediment flux release of DON, NO_3 and NH_4
- Atmospheric deposition of DON and NH_4

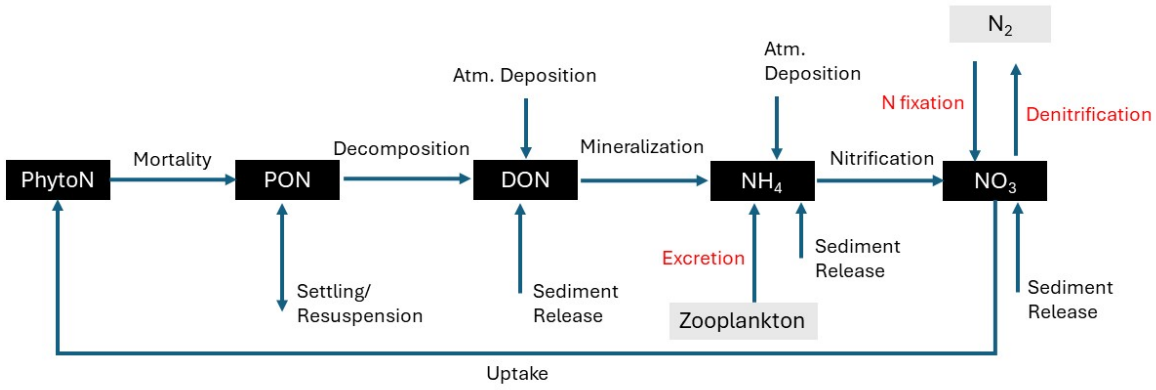

Figure 8.3.3. Nitrogen cycling conceptual model, including state variables and processes modeled in Si3D-AEM. State variables in black are explicitly modeled (particulate organic nitrogen, dissolved organic nitrogen, ammonium, and nitrate), while state variables in gray are not modeled (phytoplankton and N_2). In addition, processes in red have not been parameterized but are included in this figure for completeness.

Due to the lack of input data and limited literature values to parameterize some of the above-described ecological processes in Clear Lake, processes in red in Figure 8.3.3 have not been parameterized. The source-sink equation equations for PON, DON, NH_4, and NO_3 are as follows,

$$\frac{d[PON]}{dt}\left[\frac{mg}{m^2 d}\right] = \underbrace{rnc \cdot R_{mort}\,[d^{-1}] \cdot \vartheta^{(T-20)} \cdot PhytoC\left[\frac{mg}{m^3}\right] \cdot h[m]}_{Phytoplankton\ Mortality} - \underbrace{R_{dcn}\,[d^{-1}] \cdot f_{DO} \cdot \vartheta^{(T-20)} \cdot PON\left[\frac{mg}{m^3}\right] \cdot h[m]}_{Decomposition} \pm \underbrace{v_{settl/resusp}\left[\frac{m}{d}\right] \cdot PON\,[mg/m^3]}_{Settling/Reuspension} \quad (8\text{-}21)$$

$$\frac{d[DON]}{dt}\left[\frac{mg}{m^2 d}\right] = \underbrace{R_{dcn}\,[d^{-1}] \cdot f_{DO} \cdot \vartheta^{(T-20)} \cdot PON\left[\frac{mg}{m^3}\right] \cdot h[m]}_{Decomposition} - \underbrace{R_{mn}\,[d^{-1}] \cdot f_{DO} \cdot \vartheta_{miner}{}^{(T-20)} \cdot DON\left[\frac{mg}{m^3}\right] \cdot h[m]}_{Mineralization} + \underbrace{SED_{DON}\left[\frac{mg}{m^2 d}\right] \cdot f_{DO} \cdot \vartheta^{(T-20)}}_{Sediment\ flux} + \underbrace{ATM_{DON}\left[\frac{mg}{m^2 d}\right]}_{Atmospheric\ deposition} \quad (8\text{-}22)$$

$$\frac{d[NH_4]}{dt}\left[\frac{mg}{m^2 d}\right] = \underbrace{R_{mn}\,[d^{-1}]\,f_{DO}\cdot\vartheta^{(T-20)}\cdot\ DON\left[\frac{mg}{m^3}\right]\cdot h[m]}_{Mineralization} -$$

$$\underbrace{R_{nitrif}\,[d^{-1}]\cdot f_{DO}\cdot\vartheta^{(T-20)}\cdot NH_4[mg/m^3]\cdot h[m]}_{Nitrification} -$$

$$\underbrace{rnc\cdot f_{NH}\ \cdot\mu_{max}\,[d^{-1}]\cdot MIN(f_L,f_N,f_P)\cdot f_T\cdot PhytoC[\frac{mg}{m^3}]\cdot h[m]}_{Phytoplankton\ uptake} +$$

$$\underbrace{SED_{NH4}\left[\frac{mg}{m^2 d}\right]\cdot f_{sedflux}\cdot\vartheta^{(T-20)}}_{Sediment\ flux} + \underbrace{ATM_{NH4}\left[\frac{mg}{m^2 d}\right]}_{Atmospheric\ deposition} \quad (8\text{-}23)$$

$$\frac{d[NO_3]}{dt}\left[\frac{mg}{m^2 d}\right] = \underbrace{R_{nitrif}\,[d^{-1}]\cdot f_{DO}\cdot\vartheta^{(T-20)}\cdot NH_4[mg/m^3]\cdot h[m]}_{Nitrification} -$$

$$\underbrace{rnc\cdot(1-f_{NH}\ )\cdot\mu_{max}\,[d^{-1}]\cdot MIN(f_L,f_N,f_P)\cdot f_T\cdot PhytoC\left[\frac{mg}{m^3}\right]\cdot h[m]}_{Phytoplankton\ uptake} +$$

$$\underbrace{SED_{NO3}\left[\frac{mg}{m^2 d}\right]\cdot f_{DO}\cdot\vartheta^{(T-20)}}_{Sediment\ flux} \quad (8\text{-}24)$$

Table 8.3.1 has a full description of all constants and their values assigned during the model calibration. We also included the ranges of values found in the literature for those parameters.

- **Phosphorus**

The phosphorus forms modeled in AEM are particulate organic phosphorus (POP), dissolved organic phosphorus (DOP), and soluble reactive phosphorus (SRP). The conceptual diagram of the processes is shown in Figure 8.3.4. The main processes involved in phosphorus fate in the water column are:

- Biological uptake of SRP by phytoplankton
- Biological mortality of phytoplankton into POP
- Biological excretion of SRP by zooplankton (no modeled)
- Decomposition of POP to DOP
- Mineralization of DOP to SRP
- Settling and resuspension of POP
- Dissolved sediment flux of DOP and SRP
- Atmospheric deposition of DOP and SRP

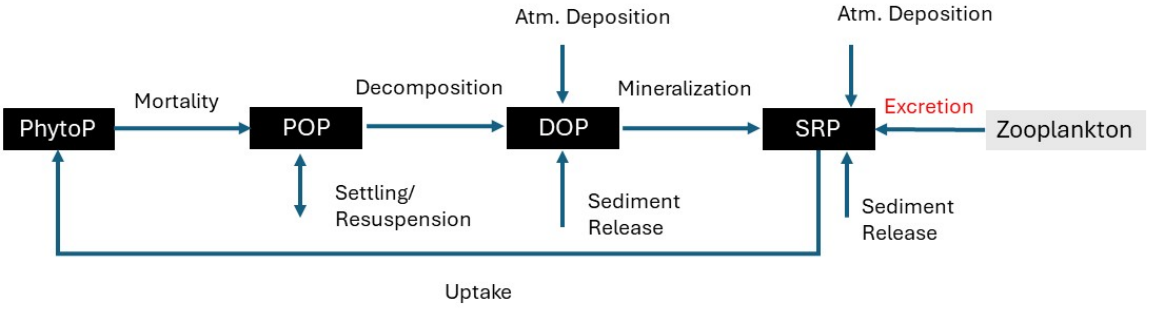

Figure 8.3.4. Phosphorus cycling conceptual model, including state variables and processes modeled in Si3D-AEM. State variables in black are explicitly modeled (particulate organic phosphorus, dissolved organic phosphorus, and soluble reactive phosphorus), while state variables in gray are not modeled (phytoplankton P). In addition, processes in red have not been parameterized but are included in this figure for completeness.

Due to the lack of input data and limited literature values to parameterize some of the above-described ecological processes in Clear Lake, processes in red in Figure 8.3.4 have not been parameterized. The source-sink equation equations for POP, DOP, and SRP are as follows,

$$\frac{d[POP]}{dt}\left[\frac{mg}{m^2 d}\right] = \underbrace{rpc \cdot R_{mort}\,[d^{-1}] \cdot \vartheta^{(T-20)} \cdot PhytoC\left[\frac{mg}{m^3}\right] \cdot h[m]}_{Phytoplankton\ Mortality} -$$

$$\underbrace{R_{dcp}\,[d^{-1}] \cdot f_{DO} \cdot \vartheta^{(T-20)} \cdot POP\left[\frac{mg}{m^3}\right] \cdot h[m]}_{Decomposition} \pm \underbrace{v_{settl/resusp}\left[\frac{m}{d}\right] \cdot POP\,[mg/m^3]}_{Settling/Reuspension} \quad (8\text{-}25)$$

$$\frac{d[DOP]}{dt}\left[\frac{mg}{m^2 d}\right] = \underbrace{R_{dcp}\,[d^{-1}] \cdot f_{DO} \cdot \vartheta^{(T-20)} \cdot POP\left[\frac{mg}{m^3}\right] \cdot h[m]}_{Decomposition} -$$

$$\underbrace{R_{mp}\,[d^{-1}] \cdot f_{DO} \cdot \vartheta^{(T-2\ )} \cdot DOP\left[\frac{mg}{m^3}\right] \cdot h[m]}_{Mineralization} + \underbrace{SED_{DOP}\left[\frac{mg}{m^2 d}\right] \cdot f_{DO} \cdot \vartheta^{(T-20)}}_{Sediment\ flux} + \underbrace{ATM_{DOP}\left[\frac{mg}{m^2 d}\right]}_{Atmospheri\ \ deposition} \quad (8\text{-}26)$$

$$\frac{d[SRP]}{dt}\left[\frac{mg}{m^2 d}\right] = \underbrace{R_{mp}\,[d^{-1}] \cdot f_{DO} \cdot \vartheta^{(T-20)} \cdot DOP\left[\frac{mg}{m^3}\right] \cdot h[m]}_{Mineralization} -$$

$$\underbrace{rpc \cdot \mu_{max}\,[d^{-1}] \cdot MIN(f_L, f_N, f_P) \cdot f_T \cdot PhytoC\left[\frac{mg}{m^3}\right] \cdot h[m]}_{Phytoplankton\ uptake} +$$

$$\underbrace{SED_{SRP}\left[\frac{mg}{m^2 d}\right] \cdot f_{DO} \cdot \vartheta^{(T-2\ )}}_{Sediment\ flux} + \underbrace{ATM_{SRP}\left[\frac{mg}{m^2 d}\right]}_{Atmospheric\ deposition} \quad (8\text{-}27)$$

Table 8.3.1 has a full description of all constants and their values assigned during the model calibration. We also included the ranges of values found in the literature for those parameters.

8.3.3 Water Quality Model Calibration

The calibration of the water quality lake model (AEM) followed the same procedure as the hydrodynamic lake model (Si3D), but in this case, adjusting biological and chemical rates and constants (Table 8.3.1) within the margins of the uncertainties to obtain a good representation of the processes of interest. As a result, we were looking for the best match between the modeled and observed results of biogeochemical variables, such as nutrients (C, N, P) and phytoplankton biomass. As shown in Table 8.3.1, the number of parameters involved in the water quality lake model calibration is higher than for the hydrodynamic lake model due to the complex nature of the biogeochemical processes. In addition, we have not available continuous time series of nutrients and phytoplankton concentrations. Hence, our calibration procedure consists of comparing profiles of the different modeled variables by the end of the calibration period.

The additional element required to run water quality simulations consists of profiles of lake water initial conditions of the different active scalars (phytoplankton and nutrients) we are aiming to model. Also, as shown in the previous sub-section, those active scalars do not match the nutrient forms we measured in the field (see Section 7.6). Hence, we will be doing the following conversions to produce the initial condition profiles that the water quality model requires:

- POC = PC - PhytoC
- DOC = directly measured
- PON = PN - (PhytoC * rnc)
- DON = DKN - NH4
- NH4 and NO3 directly measured
- POP = PP - (PhytoC * rpc)
- DOP = TDP - SRP
- SRP or PO4 = directly measured

We selected June-July 2020 as the calibration period of our water quality model (AEM). Lake profiles of the initial conditions are shown in Appendix Figure 15.8.1.1 and Figure 15.8.1.2, and surface boundary conditions (meteorology) are shown in Figure 15.8.1.3 and Figure 15.8.1.4.

A comparison of modeled and observed nutrient and phytoplankton concentration profiles by the end of the calibration period (July 22, 2020) confirms the good performance of the Clear Lake water quality lake model (Figure 8.3.5 and Figure 8.3.6). Overall, we can reproduce the patterns in the different variables and modeled values are within the same order of magnitude as the measured values. Due to the spatial variability of the nutrient and phytoplankton concentrations across the lake, we have focused on reproducing the conditions in the Upper Arm for this calibration exercise.

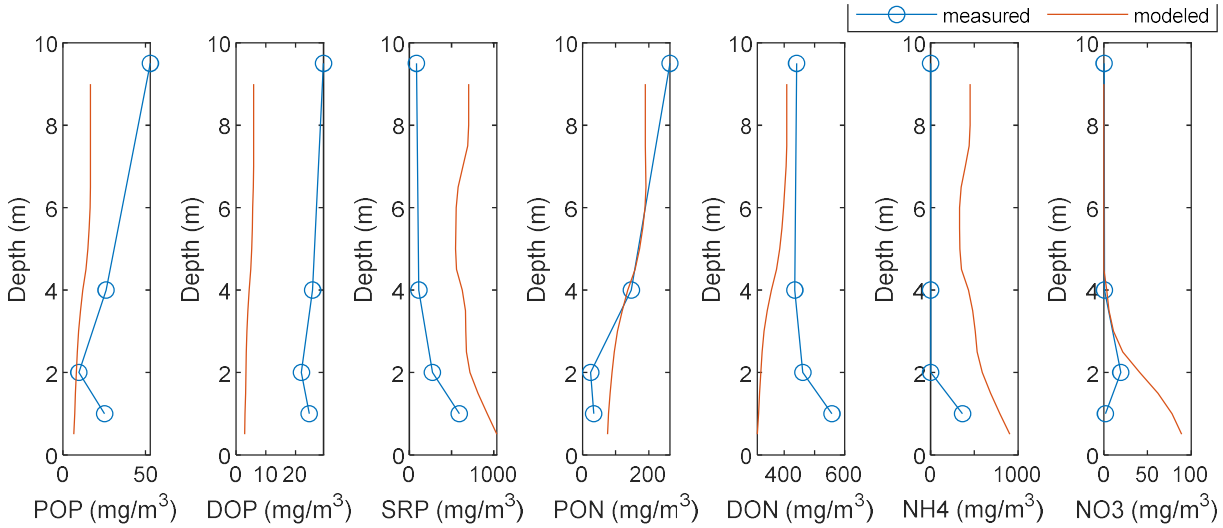

Figure 8.3.5. Profiles comparing measured and modeled results of nitrogen and phosphorus forms in Clear Lake (Upper Arm) by the end of the calibration period (22 July 2020).

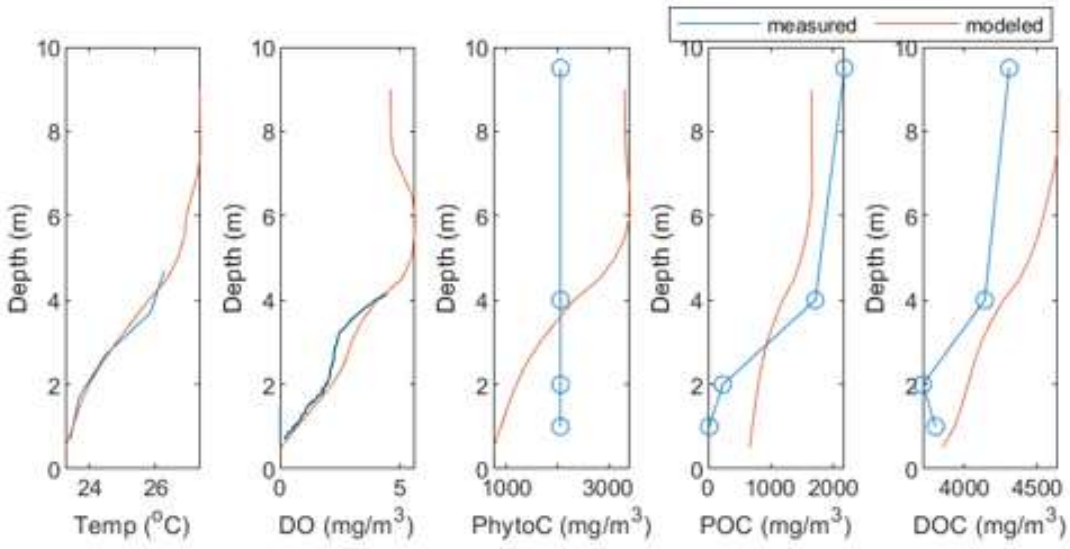

Figure 8.3.6. Profiles comparing measured and modeled results of temperature, dissolved oxygen, and carbon forms (including phytoplankton) in in Clear Lake (Upper Arm) by the end of the calibration period (22 July 2020).

As a result, modeled results of water quality parameters provide a higher temporal resolution of the changes in nutrients and phytoplankton in Clear Lake. For example, model results confirm the phosphorus release from the sediments under hypoxic and stratified conditions. In addition, we observed an increase in phytoplankton as a

result of the entrainment of nutrients released from the sediments during mixing events (Figure 8.3.7).

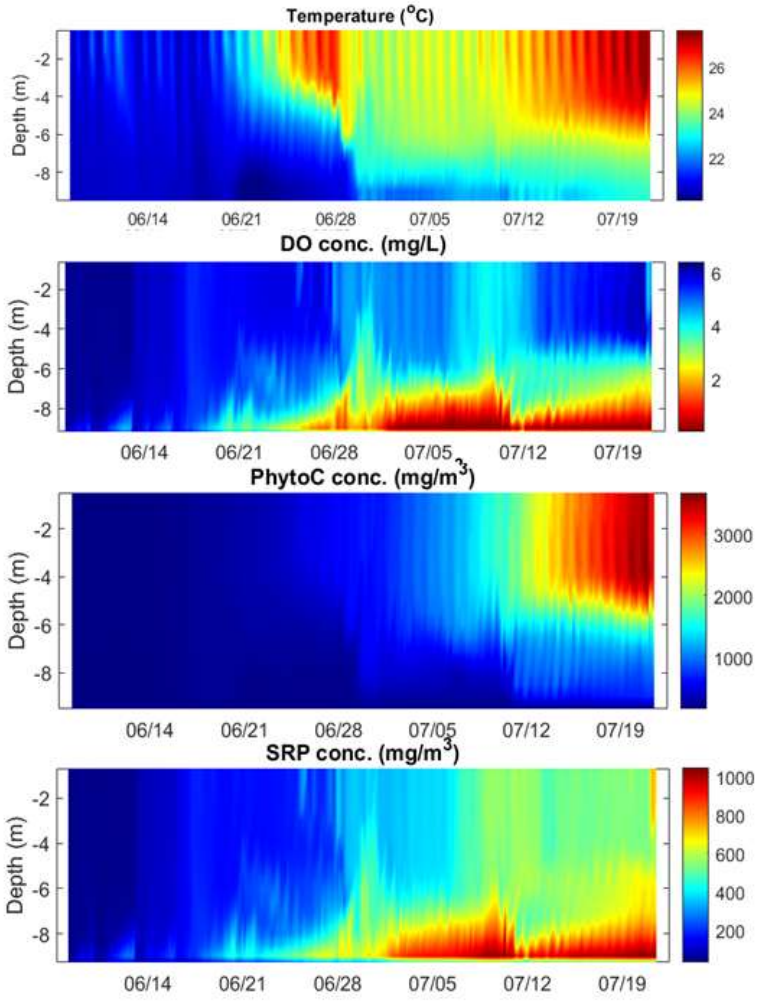

Figure 8.3.7. Modeled time series in depth of key water quality parameters during the calibration period in Clear Lake (Upper Arm)

8.3.4 Water Quality Model Validation

Once the Clear Lake water quality model was successfully calibrated in June-July 2020, we used the same model parameters and assumptions to run a simulation during a different period of time and confirm that our water quality model is robust and reliable. We selected July 2022 as the calibration period of our water quality model (AEM). Lake profiles of the initial conditions are shown in Appendix Figure 15.8.1.5 and Figure 15.8.1.6, and surface boundary conditions (meteorology) are shown in Figure 15.8.1.7 and Figure 15.8.1.8.

A comparison of modeled and observed nutrient and phytoplankton concentration profiles by the end of the validation period (August 4, 2022) confirms the good

performance of the Clear Lake water quality lake model (Figure 8.3.8 and Figure 8.3.9).

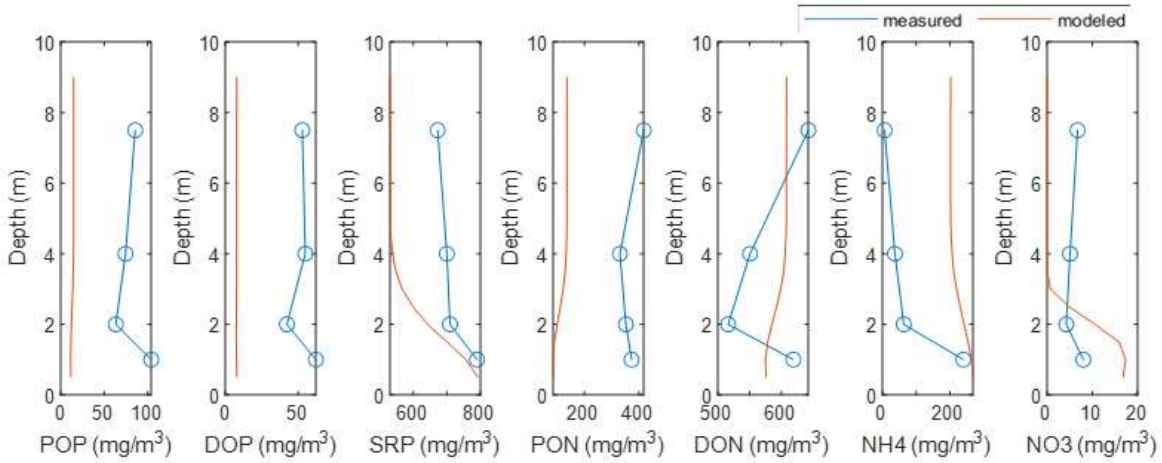

Figure 8.3.8. Profiles comparing measured and modeled results of nitrogen and phosphorus forms in in Clear Lake (Upper Arm) by the end of the validation period (4 August 2022).

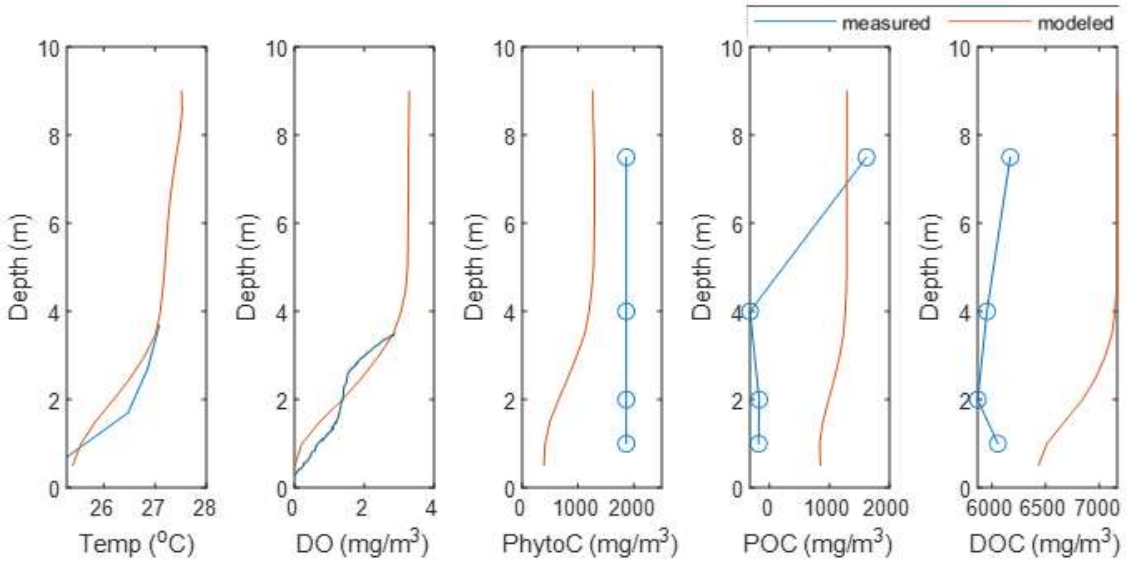

Figure 8.3.9. Profiles comparing measured and modeled results of temperature, dissolved oxygen, and carbon forms (including phytoplankton) in in Clear Lake (Upper Arm) by the end of the validation period (4 August 2022).

8.4 Model Scenarios: Remediation Strategies to Mitigate CHABs

Lake **restoration strategies to mitigate CHABs** can be grouped into physical (dredging of the sediment, weed removal, water drawdown, harvesting of algae/nutrients, aeration, oxygenation, ozonation, water mixing, water shading, sediment capping, flocculants/nutrient sequestration, ultrasonic exposure, UV exposure), chemical (cooper/peroxide based algaecides, organic algaecides), and biological (microbial/food web manipulations, barley/rice straws, wetland restoration, shoreline stabilization) strategies. Between 2022 and 2023, pilot projects to test four lake restoration strategies at Clear Lake have been recommended and approved by the Blue Ribbon Committee. Those restoration strategies include **dissolved oxygen enhancement (e.g., hypolimnetic oxygenation), algae and nutrient harvesting, ultrasonic algae control, and sediment phosphorus (P) sequestration**. All these techniques have proved to improve the water quality of the sites where they have been previously tested. However, Clear Lake is a unique system with a large surface area, very strong currents, high nutrient and algae concentrations, and a highly dynamic mixing regime. Thus, we have used the newly developed in-lake model to evaluate the effects of the recommended pilot projects on Clear Lake's water quality. Scenario testing has allowed us to identify key variables in the design of the different pilot restoration projects that should be further explored and carefully quantified before the projects move into the implementation phase. This modeling exercise points out the technologies that only provide localized benefits for the water quality and those whose implementation can be challenged due to the dynamic nature of Clear Lake (strong currents). A detailed cost-benefit analysis should be performed to evaluate if the capital investment and maintenance costs of the strategies are worth the water-quality improvement obtained.

8.4.1 Hypolimnetic Oxygenation System (HOS)

- ***Context and remediation strategy introduction***

The Tahoe Environmental Research Center (TERC) researchers have conducted an extensive in-lake monitoring (in-situ measurement) and modeling (predictions) program between 2019 and 2023 that have shown that periods of **low dissolved oxygen** (DO) next to the lakebed sediments are a major factor driving the **poor water quality and ecological health of Clear Lake**. These periods of depleted DO occur when the lake thermally stratifies in summer (i.e., the lake surface gets warmer than the bottom), typically June to September, but occasionally May to November. The absence of DO during the summer months leads to the release of sediment-bound phosphorus (internal loading) in Clear Lake, a major factor driving the formation of cyanobacteria harmful algal blooms (CHABs); the production of methylmercury; and the loss of fish habitat with the potential of summer fish kills, among other environmental problems. A Hypolimnetic Oxygenation System (HOS) is a technology that has been used nationwide (and in California) to augment oxygen at the bottom of lakes during periods of depleted DO. It entails the **direct**

injection of pure oxygen into the lake's hypolimnion (the lower stratum of the lake) via a set of diffusers installed at the bottom of the lake from an external oxygen supply onshore (Figure 8.4.1.1 and Figure 8.4.1.2). Appendix 15.8.1 provides background details about the HOS technology.

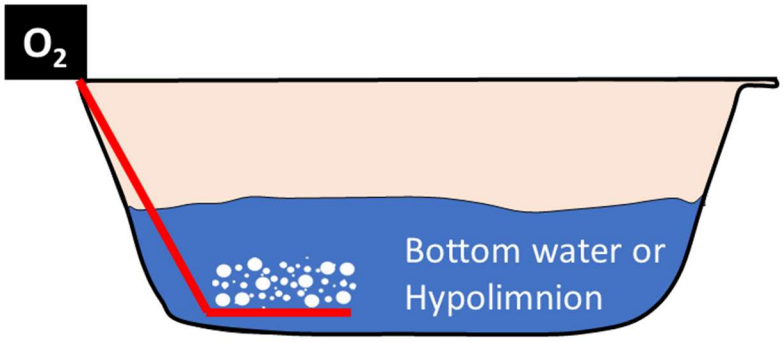

Figure 8.4.1.1. Schematic of a Hypolimnetic Oxygenation System (HOS)

While many reservoirs are successfully utilizing this technique, Clear Lake has a very large surface area (150 km^2) and is naturally highly productive (hypereutrophic), which results in a very high oxygen demand at the sediment-water interface (approx. 0.9 g O_2/m^2/day). For these reasons, TERC proposed a **pilot project** in the **Oaks Arm** (3,500 acres, 14.1 km^2, 0.125 km^3) to fine-tune the technology for Clear Lake before a whole-lake implementation is designed. This pilot project has the capacity to meet the summer oxygen deficit for the entire Oaks Arm and also add oxygen to the Upper and Lower Arms.

Figure 8.4.1.2. A) Onshore elements of a HOS installed in Loch Lomond, Santa Cruz, CA; B) Pipes connecting the onshore elements with the diffusers in the lake

- ***Project description and goals***

This project consists of the design, construction, oxygen injection (for one summer), monitoring, water testing, and operations testing of HOS in the Oaks Arm of Clear Lake, CA. The Oaks Arm was selected as it is the smallest basin, is affected by long-term mercury issues, and is the site of many of the largest CHAB blooms in Clear Lake. Pure oxygen (five times more effective than air) is injected at low flow rates through a porous diffuser line that is elevated a short distance (~6 in) above the sediments (Figure 8.4.1.3). The released fine bubbles dissolve rapidly in the hypolimnion, without significant lake mixing. Sediment disturbance will also be minimal given the low oxygen flow rates and the suspension of the diffuser above the sediments. This design is self-cleaning, and the whole system need only be floated to the surface in the unlikely event of a line break. This operation can be simply performed on-site if needed.

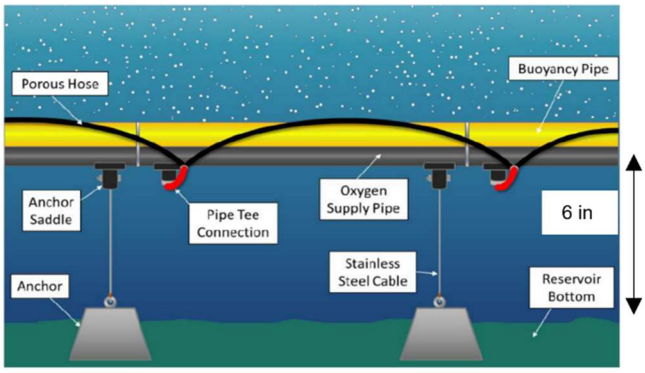

Figure 8.4.1.3. Oxygen diffuser diagram. The thin black pipeline is very porous and it releases fine bubbles creating a crater that removes the sediments that may be covering it. The gray pipe transports the oxygen and the yellow pipe is designed to float and keep the diffuser above the sediments

There are three main objectives for this pilot project: 1) quantify rates at which oxygen is dispersed and taken up after injection (**target near bottom DO > 3.5 mg/L**); 2) quantify the reduction of P-release from sediments (**target mean water SRP (soluble reactive phosphorus) concentration reduced by 20-50%**); and 3) **monitor** the effect of oxygenation on water quality. The success of the pilot project is necessarily more targeted than the eventual lake-wide implementation goal of reducing CHABs. Here, success will be defined as quantifiably increasing DO in bottom waters and having such oxygenation result in a measurable reduction in P-release from sediments, and validating predictions made using our 3D lake model. An important advantage that Clear Lake possesses over smaller lakes is that it has high water current velocities resulting from longer distances winds can blow across the lake. This feature will be utilized through the model-based design to help distribute the oxygen over a larger area in the Oaks Arm and, potentially, into the other two Arms.

An initial estimate of the cost of this pilot project was $2.2 M to complete both the planning and implementation phases. However, this estimate did not include overhead, it was based on good faith estimates from specialized contractors and assuming the reduced COVID-19 pandemic pricing. **New cost estimates for this project** including inflation, updated quotes from experienced contractors and

suppliers, and 15-26% overhead is of the order **~$4M** (including University-levied overheads). The California Natural Resources Agency (CNRA) recently granted $1.1 million of State Funds to TERC for the first phase of this pilot project. The funds were awarded in October 2024. The first phase consists of the design, permitting, outreach activities, and pre-monitoring of the HOS in the Oaks Arm. The second phase of this pilot project will include the construction and installation of the HOS by an engineering contractor, its operation (oxygen injection) for one summer (potentially 2026), and post-monitoring to evaluate the success of the technology. We will collaborate with USGS for the post-monitoring to evaluate how the methyl mercury production will change after the oxygen injection. We have also recently applied for and received a US EPA Community Grant (~$1M). Additional funds for the implementation are being pursued and US EPA is currently a potential sponsor through the Sulfur Bank Mercury Mine Superfund Site program (~$1.25M).

- ***Model setup, assumptions, and sensitivity analysis***

We have compared modeled results from a *control scenario* without an HOS and a *testing scenario* with the injection of pure oxygen at rates related to the system design. We used the validated model scenario between **July-August 2022** described in Section 8.3.4 as our control scenario. This period was selected because we observed 2 weeks of hypoxia/anoxia, SRP increase in the water column, and significant phytoplankton growth. For the testing model scenario, we prescribed the same initial conditions (lake temperature and nutrients), meteorological forcing, grid size, and physical and biogeochemical parameters as the control scenario, and added the injection of continuous pure oxygen (10 mg/L) along **two 4,000 ft (~1 km) diffusers** (recommended for redundancy). Our sensitivity analysis consisted of evaluating **different pure oxygen flow rates at the diffusers**: [250; 350; 500] cfm = [0.12; 0.17; 0.25] m^3/s. We also tested **two locations** of the two 1 km diffusers using a flow rate of 500 cfm at the deepest hole in the Oaks Arm (Figure 8.4.1.4) and a centered location in this arm.

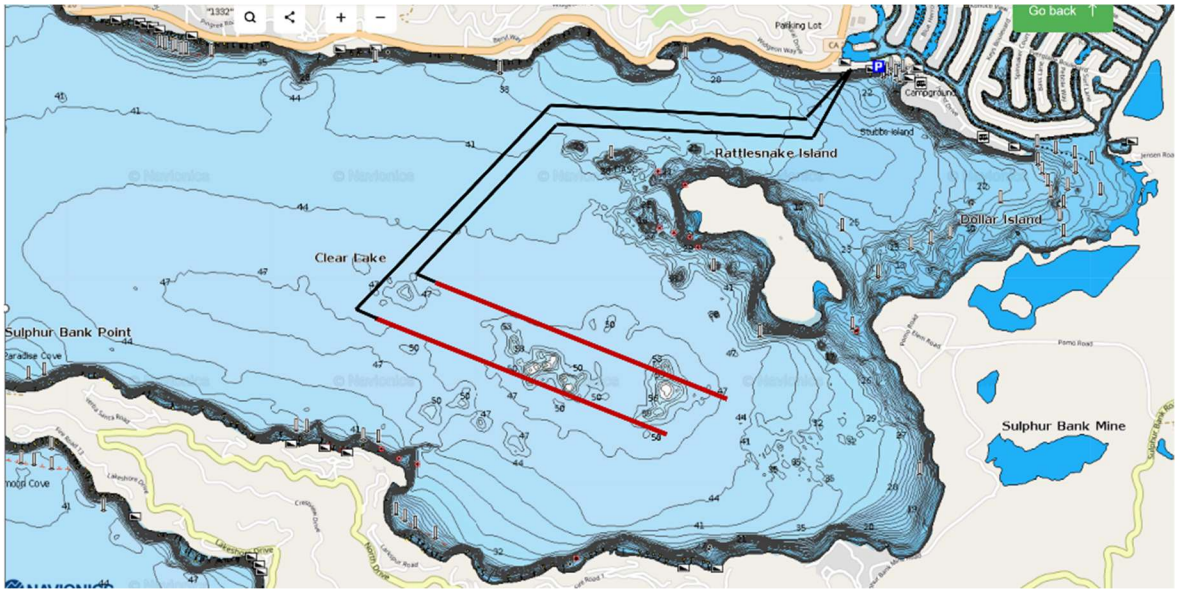

Figure 8.4.1.4. Tentative layout of the diffusers location (red lines) in the deep hole of the Oaks Arm (preferred location according to model results to favor recirculation)

- ***Model results: Scenario testing***

Model results from the control and testing HOS scenarios allowed us to conduct a preliminary evaluation of this remediation strategy impact in the Oaks Arm. Figure 8.4.1.5 shows the modeled spatial distribution of the mean near-bottom (2 m layer) dissolved oxygen (DO) concentration across this basin for the scenarios without and with DO injection (top and bottom, respectively). Shortly after the beginning of the DO injection using a flow rate of 500 cfm, the DO concentrations in the near-bottom eastern arm started showing DO > 3.5 mg/L (target), and after two weeks of injection, ~93% of the basin had near-bottom above this target DO concentration > 3.5 mg/L (see bottom panels, Figure 8.4.1.5).

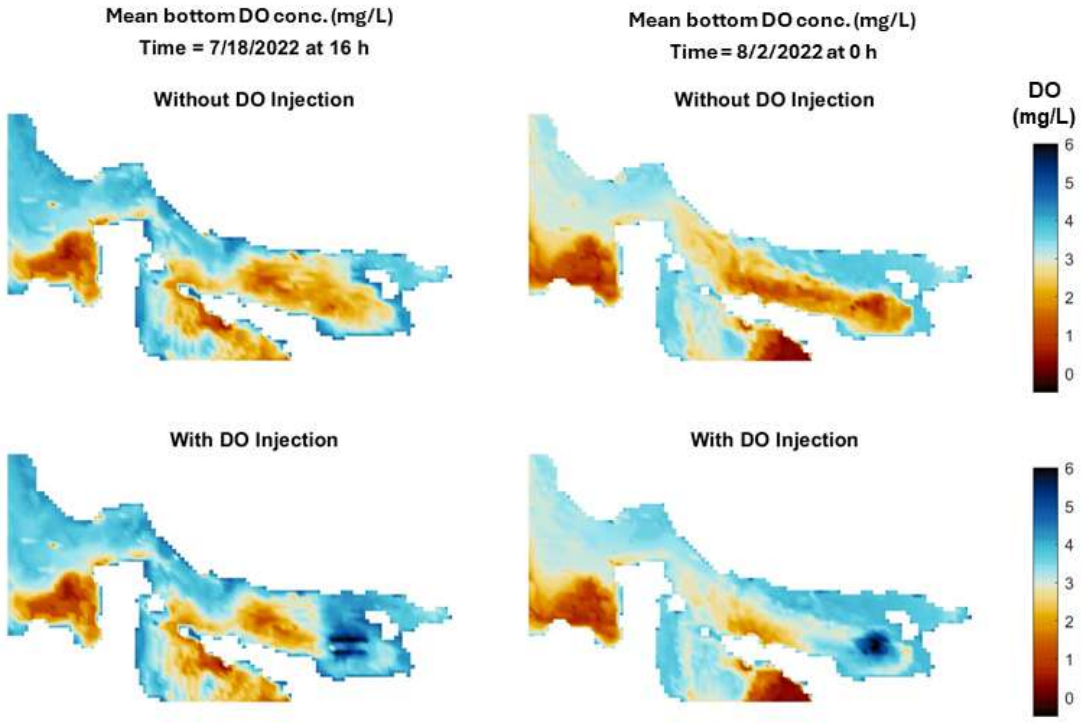

Figure 8.4.1.5. Modeled spatial distribution of the mean near-bottom (2 m layer) dissolved oxygen (DO) concentration across the Oaks Arm for the control scenario (top, without DO injection) and the testing scenario (bottom, with DO injection). Model results on the left column are from mid-July 2022 and on the right from early August 2022 (~2 weeks apart)

Figure 8.4.1.6 shows the modeled time series in depth of lake temperature, dissolved oxygen (DO) concentration, SRP (soluble reactive phosphorus) concentrations and phytoplankton carbon (PhytoC) averaged across the Oaks Arm (14.1 km^2) for the control scenario (left, without DO injection) and the testing scenario (right, with DO injection). The DO injection did not affect the lake stratification but it dramatically changed the DO concentration in the water column, maintaining it at ~5 mg/L. That impacted the SPR concentrations in the water column, which dropped from 700 mg/m^3 without DO injection to 350 mg/m^3 with DO injection as mean values in depth

and space. Thus, we achieved the target reduction of SRP by 50% compared to the control scenario (no DO injection). In addition, phytoplankton carbon showed a modest decrease in maximum concentrations from 1,500 mg/m^3 to 1,200 mg/m^3 (20% reduction).

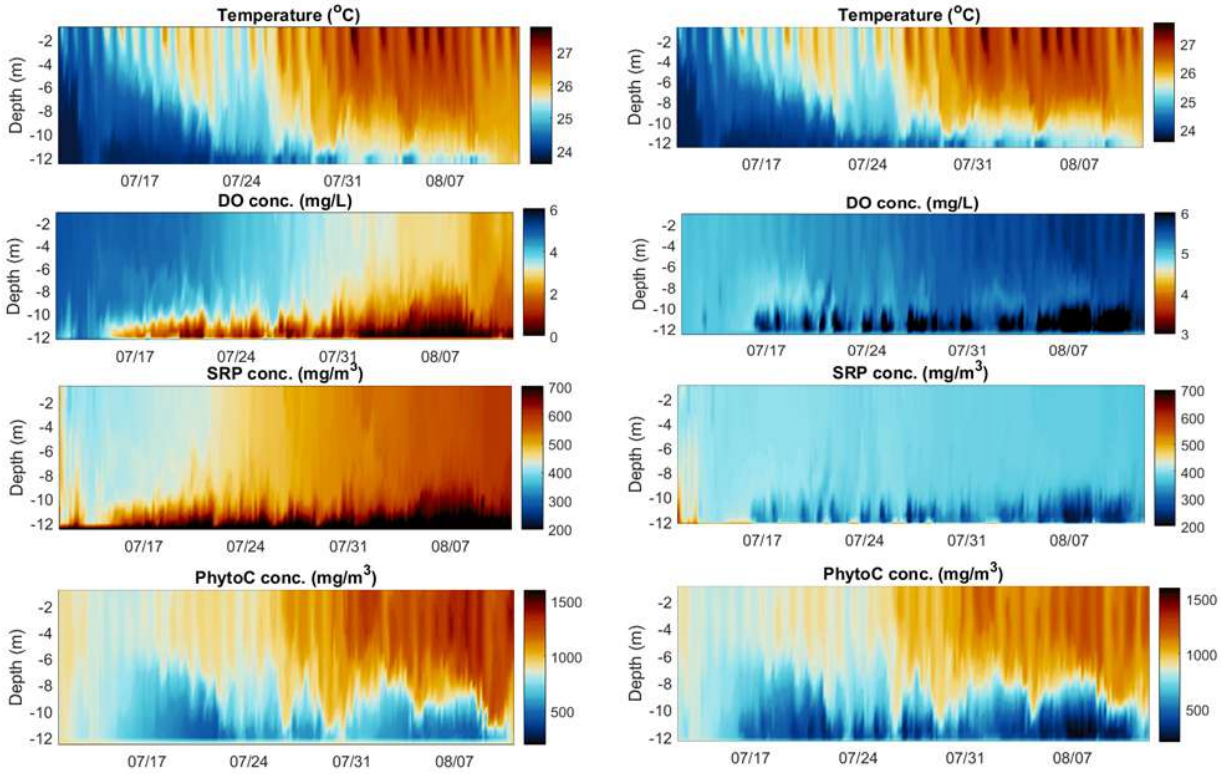

Figure 8.4.1.6. Modeled time series in the depth of lake temperature, dissolved oxygen (DO) concentration, SRP concentrations, and phytoplankton carbon (PhytoC) averaged across the Oaks Arm for the control scenario (left, without DO injection) and the testing scenario (right, with DO injection).

Figure 8.4.1.7 shows the modeled time series of near-bottom dissolved oxygen (DO) concentration, and depth-averaged SRP concentrations and phytoplankton carbon (PhytoC) spatially averaged across the Oaks Arm for the control scenario, and the testing scenarios. DO concentrations remained above our target (3.5 mg/L) and SRP concentrations were reduced by 50% when **Q = 500 cfm**. Changing the location of the diffusers mostly affected the spatial distribution of the DO, but not the overall performance of the HOS (Figure 8.4.1.8).

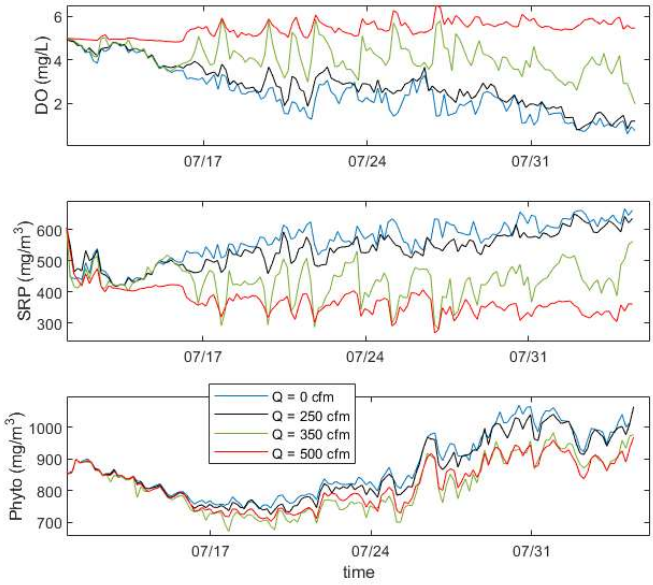

Figure 8.4.1.7. Modeled time series of spatially averaged (top) near-bottom dissolved oxygen (DO) concentration, and depth-averaged values of (middle) SRP concentrations and (bottom) phytoplankton carbon (PhytoC). Time series show average values across the Oaks Arm basin in the control scenario (no injection of DO), and the testing scenarios where DO injection Q = [250; 350; 500] cfm. Diffusers were in the deep hole for the testing scenarios.

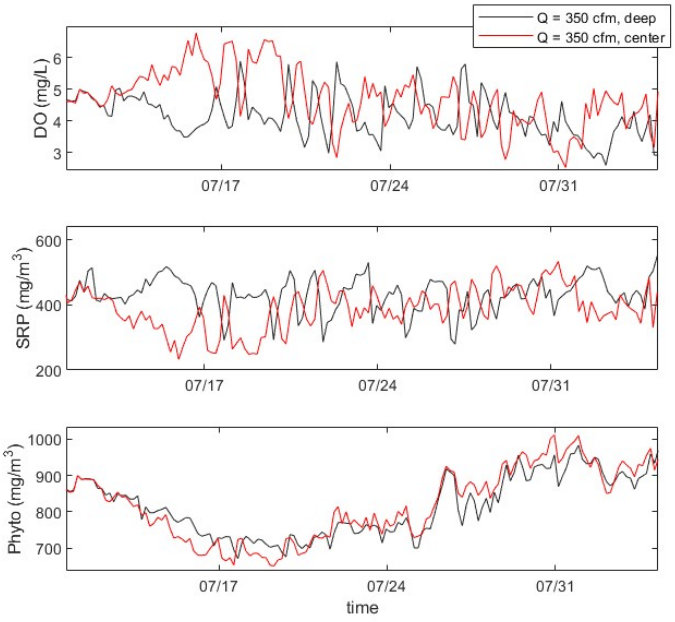

Figure 8.4.1.8 Modeled time series of spatially averaged (top) near-bottom dissolved oxygen (DO) concentration, and depth-averaged values of (middle) SRP concentrations and (bottom) phytoplankton carbon (PhytoC). Time series show average values across the Oaks Arm basin for the testing scenario of an injection flow of 350 cfm with diffusers located at the deep hole (black) and the center of the basin (red)

The conclusions from our lake model results to assist the HOS design in the Oaks Arm are:

- **Diffuser flow rate**: We recommend **500 cfm** (0.25 m^3/s). This flow will allow to injection of ~20 tons/day, equivalent to ~3,500 gallons of liquid oxygen (LOX)/day. These results match recommendations from experienced HOS contractors for the preliminary design of the HOS considering Oaks Arm sediment surface area 1.4 x 10^7 m^2, maximum depth 14 m, volume 1.25 x 10^8 m^3, and sediment oxygen demand (SOD) ~0.9 $g/m^2/day$.
- **Location of the diffusers**: We recommend the **easter location** of the diffusers (**deep hole**) because this area is the more susceptible to hypoxia/anoxia and added oxygen gets distributed across the basin through an anticlockwise gyre formed due to Coriolis and temperature gradients across the basin.

These preliminary results allow us to make some suggestions to the specialized contractor designing the HOS in the Oaks Arm:

- The system will require 1-2 tanks of 15,000 gallons of liquid oxygen (LOX) to be installed on land (expected footprint: 60 ft x 40 ft for the two tanks when placed horizontally). LOX tanks on the ground should be installed on top of a concrete pad, to prevent hazardous conditions.
- LOX tanks will be refilled once a week with 2-3 trucks that can deliver ~4,500 gallons of LOX per truck.
- The power requirements for this system will be covered with a small solar panel to be installed by the pilot project.
- There will be no noise from generators or pumps. Liquid oxygen will be converted to gas with a vaporizer, and the gas will be regulated with a control panel into the diffusers running along the lake bottom.

To sum up, model results have allowed us to quantify rates at which oxygen is dispersed and taken up after injection, achieving our **target near bottom DO > 3.5 mg/L** when the **flow rate of the diffusers** is above **500 cfm**. In addition, model results have allowed us to quantify the reduction of P-release from sediments, achieving our **target mean water P concentration reduction of 20-50%.** This would represent a **successful HOS pilot project in the Oaks Arm**, which will treat ~**10% of the lake water using $4M funding** (planning and implementation).

- ***Upscaling HOS to the whole lake***

The model results from our scenario testing showed that we could successfully oxygenate 10% of Clear Lake (the Oaks Arm) with an investment of ~$4M. This suggests that approximately 5 more HOS facilities will be required to oxygenate the entire lake. Figure 8.4.1.9 shows the modeled spatial distribution of the mean near-bottom (2 m layer) dissolved oxygen (DO) concentration across lake for the scenarios without and with DO injection (top and bottom, respectively) using **six HOS facilities (three in the Upper Arm, two in the Lower Arm, and one in the Oaks Arm)**. The exact locations and sizes of the individual installations would need to be refined based on the results of the Oaks Arm pilot project.

Costs for the design and permitting of the lake-wide system may be reduced because of the lessons learned and communications established during the pilot project. Thus, we estimate that the capital investment for **lake-wide HOS implementation is likely to cost ~$20-30 M**. Annual operation, management, and monitoring (O&M&M) for 10 years of the full lake HOS facilities may cost ~$25 M. As a result, the total capital investment plus O&M&M for 10 years of the full lake HOS may be of the order ~50 M.

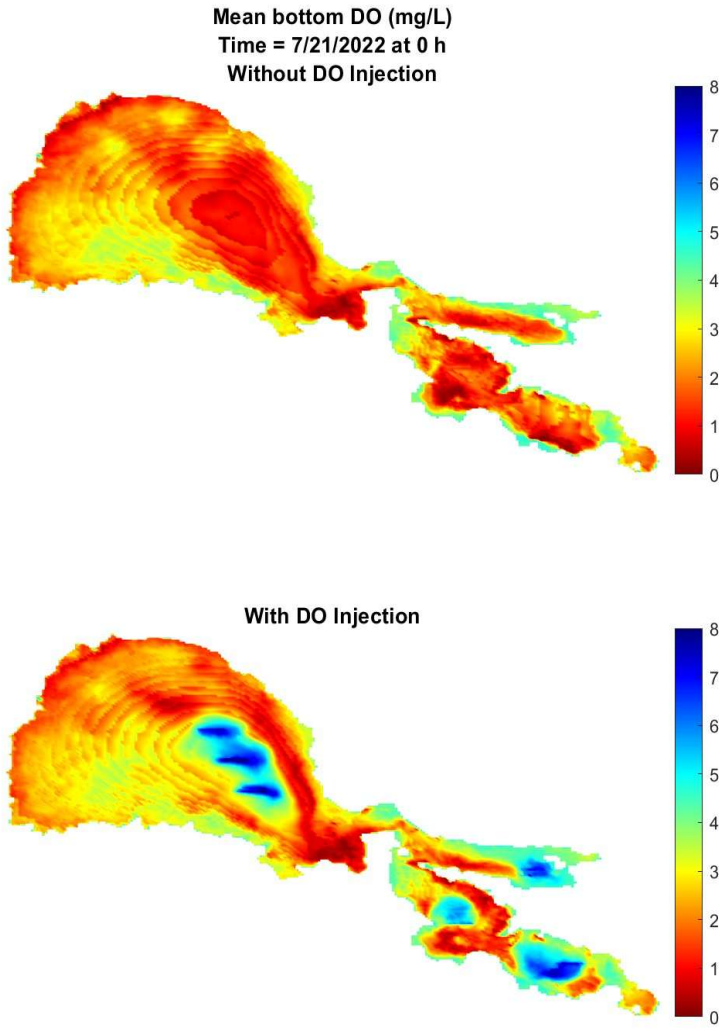

Figure 8.4.1.9. Modeled spatial distribution of the mean near-bottom (2 m layer) dissolved oxygen (DO) concentration across the whole lake without any HOS installed (top) and the testing scenario (bottom) with six HOS installed across the lake. Model results on the two snapshots were obtained after two weeks of simulation (without and with DO injections).

8.4.2 Algae and Nutrient Harvesting

- ***Project description and goals***

AECOM, Aquatic EcoTechnologies, Central Valley Regional Water Quality Control Board, the City of Clearlake, and tribal representatives are supporting a pilot project to test algae harvesting technology. An algae harvester **removes algal biomass, nutrients (phosphorus and nitrogen), and cyanotoxins from the lake** between the inflow water (coming from Clear Lake) and outflow water (clean and oxygenated). The clarified and oxygenated water will be returned to the lake, improving the overall water quality in the treated area.

The pilot study recommended by the project proponents suggests a limited treated area of **~0.5 acres** (0.002 km^2, Figure 8.4.2.1) over 3 weeks with a 1 million gallons per day (MGD) system. **This area represents 0.001% of the total lake surface** but can help to **control CHABs near Redbud Park (Lower Arm).** A turbidity curtain will be installed west of the effluent to prevent polluted water from entering the treated area. A restoration target for the algae harvesting pilot project would need to be developed. As an example, the project proponents suggested reducing total phosphorus (TP) by ~0.04 mg/L, from 0.16 mg/L to 0.12 mg/L, based on averaged historical TP values. However, project proponents consider "it would be beneficial to use UC Davis' water quality model to develop an appropriate nutrient reduction target for the lake and use results from the pilot project to confirm calculations and goals". Recent monitoring data gathered by UC Davis has shown that the summer concentrations of TP in the lake are in the order of 1 mg/L (Figure 7.6.5).

For this pilot project, AECOM is planning to run one 1-million-gallon per day (MGD, **700 GPM, 0.04 m^3/s) harvester for 3 weeks** in mid-summer to early fall. This pilot aims to determine the nutrient and algal removal efficiency. **The pilot project will cost $1.3M, and includes, planning, testing, monitoring, reporting/presentation**. Proposal leaders estimate that each harvester costs ~$1.5 M. The 3 weeks pilot project will be sufficient to collect the necessary data to confirm the nutrient removal efficiency of the algae harvester and support the development of a full-scale treatment plant. We anticipate that water quality benefits will be observed in the mesocosm enclosure during this 3 week period. The pilot test is not sized to realize significant benefits outside the enclosure.

For lake restoration, a larger system would be operated continuously throughout the year to achieve water quality targets. The size of the system will depend on the water quality target and available funds. For example, we anticipate that a **5 MGD system** would be able to treat approximately **250 acres** in the lower arm of Clear Lake **over an extended period** removing more than 2 tons of phosphorus per year. The data we collect from the pilot test will allow the project leads to design a larger-scale system that can be used to achieve a reduction in the nutrient concentrations that are driving the production of HABs. This will allow them to design options for a larger-scale system and take into account budgets, technologies, synergistic benefits, and remedial targets.

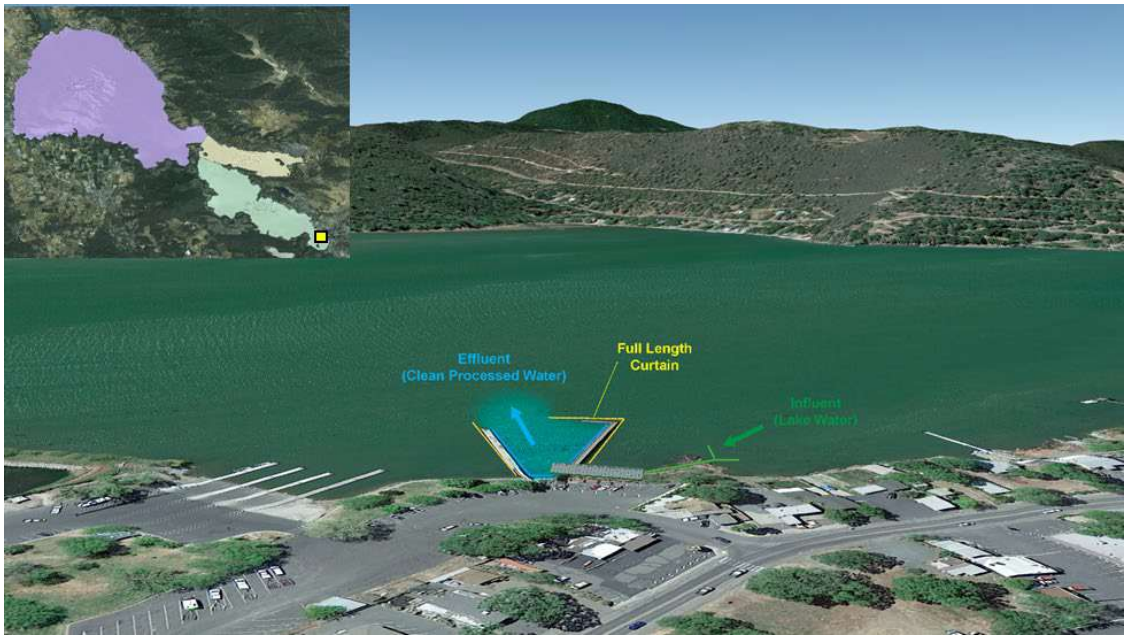

Figure 8.4.2.1. Proposed location and illustration of the algae harvester deployment for AECOM pilot project, near Redbud Park, Clear Lake

- ***Model setup and assumptions***

We have compared modeled results from a *control scenario* without harvesting technology and a *testing scenario* with harvesting technology. We used the validated model scenario between **July and August 2022** described in Section 8.3.4 as our control scenario. The model setup for the testing scenario required some extra information from the leaders of this proposal, who provided valuable information to develop initial model assumptions:

- Treated area: Water will be collected just below the surface from the location indicated in green in Figure 8.4.2.1.
- Treatment efficacy: The algae harvester achieves a total phosphorus concentration of 0.01 mg/L regardless of the influent (lake water) concentration. The system also removes approximately 80% of total nitrogen. The treated water is fully oxygenated (100% saturation).
- Flow rate at the intake and effluent: The algae harvester is a flow-through solid/liquid separation process. The influent (intake of dirty water) will be approximately 700 gpm, and the effluent (discharge of clarified clear water) will be approximately 700 gpm.

Thanks to the project proponents feedback, we have made the following assumptions in our model runs: (1) water from the lake will be drawn at the top 50 cm (surface), with an average flow rate of 0.04 m^3/s (700 gpm), assuming a treatment efficiency of 100% (ideal scenario); (2) the return flow will be equivalent to the drawdown (0.04 m^3/s), but the water will have a total phosphorus concentration of ~0.01 mg/L and be fully oxygenated; (3) we run a model simulation with these conditions for 3 weeks in July 2022 to reproduce the conditions of the pilot project.

- ***Model results: Scenario testing***

Figure 8.4.2.2 shows the modeled time series of depth-averaged dissolved oxygen (DO) concentration, SRP concentrations, and phytoplankton carbon (PhytoC) spatially averaged across a surface area of 2.5 acres (100 m x 100 m) next to the harvester intake in the Lower Arm (Redbud Park) for the control scenario and the testing scenario. Due to the spatial resolution of our model, we are not capable of testing results in a smaller domain (e.g. 0.5 acres). Model results showed that the testing scenario of 2.5 acres described above did yield **improvements in key water quality variables**: DO ~ 6 mg/L; SRP concentration remained ~350 mg/m^3; and the algae concentrations were reduced ~10% by the end of the 3-week study period.

We initially tested this technique in a larger domain (~50 acres), and results showed limited improvement in the water quality variables due to the **continuous transport of nutrient and algae-rich water from outside the control area**.

Project proponents recommended that the model should be run on an annual basis as the action of algae harvesting to remove nutrients is cumulative over time. They believe it would be beneficial to meet with the UC Davis team to discuss the model input parameters and run scenarios.

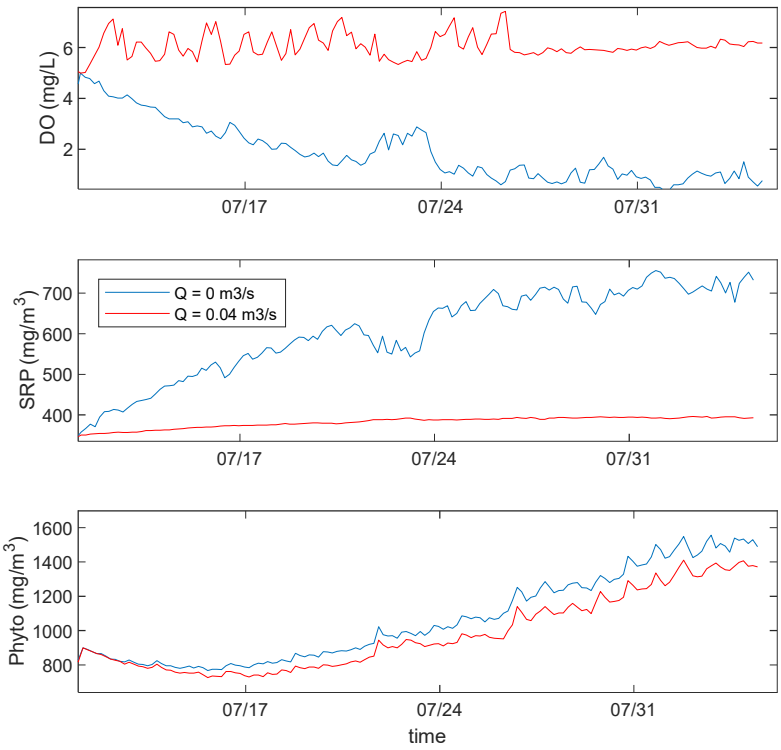

Figure 8.4.2.2. Depth averaged concentrations spatially averaged in a surface area of 2.5 acres for the control and testing scenario assuming 1 harvester over 3 weeks.

8.4.3 LG Sonic MPC Buoy

- ***Project description and goals***

LG Sonic is suggesting a pilot project in Clear Lake to implement a cyanobacteria harmful algal bloom (CHAB) control system. The LG Sonic will deploy a set of MPC Buoys, which use ultrasonic waves to form continuous pressure around algal cells, preventing their growth (Figure 8.4.3.1). Each buoy is about 2 m x 2 m in size, powered with solar panels, and treats a surface area of 50 acres (0.2 km^2), equal to 0.1% of the lake surface.

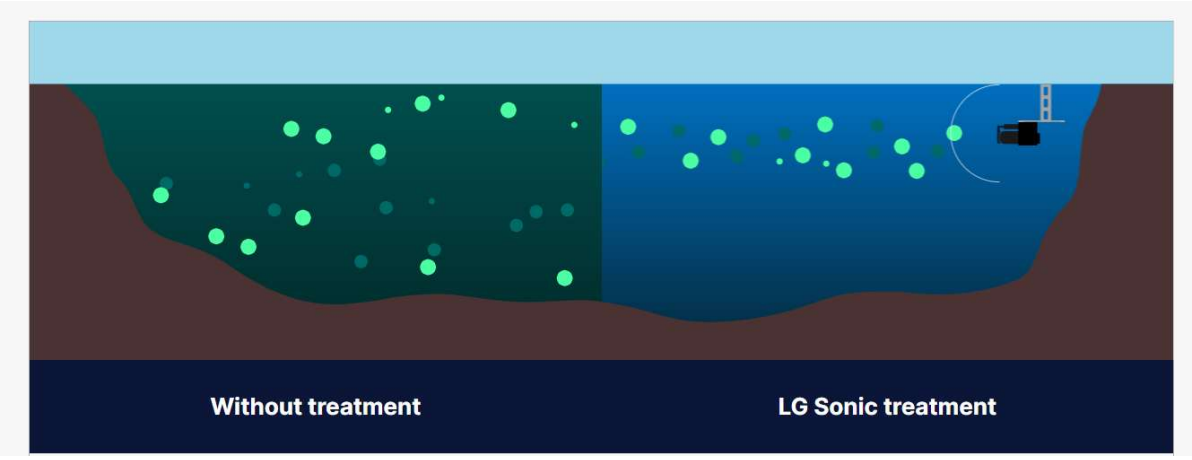

Figure 8.4.3.1. Diagram describing the LG Sonic treatment (https://www.lgsonic.com/ultrasonic-algae-control/)

The main outcome of this technology is the prevention of algae growth (Figure 8.4.3.2), and hence, reducing organic build-up in the sediments.

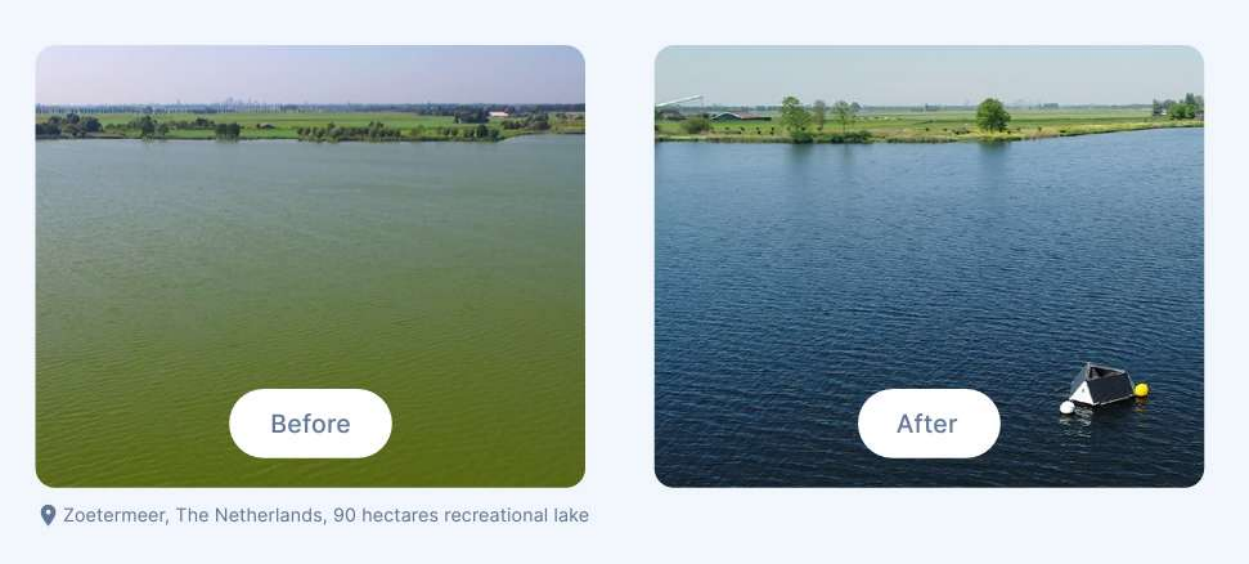

Figure 8.4.3.2. Example of preventive algae growth by LG MPC boys

For their pilot project, LG Sonic will deploy 16 buoys to control CHABs near Redbud Park (Lower Arm) covering a confined area between this park and Cache Creek

Dam, which historically has been very severely affected by CHABs. Thus the total area to be treated will be ~800 acres (~3 km^2, ~2% of the total lake surface area). For modeling purposes, we are simulating the effects of **one buoy on 50 acres**. The different tasks of the suggested pilot project include planning, permitting, outreach, equipment purchase/shipping, monitoring and maintenance, and reporting, with a total **cost of $1.2M**. The project will last 4 years, and the system will run the **treatment and monitoring for about 2.5 years**.

- ***Model setup and assumptions***

We have compared modeled results from a *control scenario* without the LG Sonic buoy and a *testing scenario* with the LG Sonic buoy, assuming phytoplankton growth equal to zero in a four-meter layer at the lake surface. We used the validated model scenario between **July-August 2022** described in Section 8.3.4 as our control scenario. The model setup for the testing scenario required some extra information from the proposal proponents. We contacted them, and they provided some information, but some key questions remain:

1. How **effective** is the ultrasonic technology in **preventing algae growth in depth**? In other words, how **deep and thick is the layer** where the **ultrasonic treatment** prevents algae growth? That is, if the system is installed at 2 m deep, how strong would the ultrasonic signal be at 4 m? Monitoring data at Clear Lake shows that algae are not only at the surface, and they can thrive in depth (> 6 m)
2. How would the technology deal with the **strong currents** at Clear Lake? Project proponents indicated that the technology does not kill algae, it only prevents their growth. Hence, what would your MPC-Buoy do if a patch of algae comes from an area outside your confined segment? Currents in Clear Lake are strong, and rapid transport is one of the characteristics of this system.
3. LG Sonic indicated that the technology has an immediate effect on preventing algae growth, but how does the technology help when algae enter the control area due to **horizontal transport and vertical mixing**? How long does it take for your ultrasonic waves to treat (control) the algae?

Model results: Scenario testing

Figure 8.4.3.3 shows the modeled time series of depth-averaged dissolved oxygen (DO) concentration, P concentrations, and phytoplankton carbon (PhytoC) spatially averaged across a surface area of 50 acres near the LG Sonic Buoy in the Lower Arm (Redbud Park) for the control scenario and the testing scenario. Model results showed that the testing scenario described above did not yield any significant change in key water quality variables. We relate this **limited improvement** in the water quality variables to the **continuous transport of nutrient and algae-rich water** from the west to the control area. It is important to note that algae biomass decreased by 10% when measured directly underneath the buoy, but its concentration did not change significantly when averaging the effects across the 50-acre treated area.

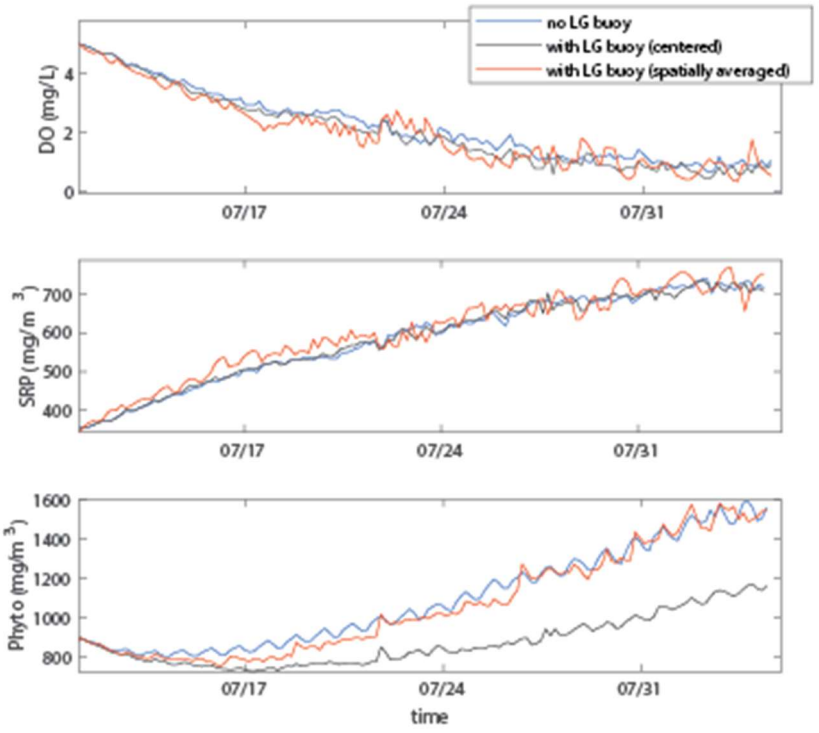

Figure 8.4.3.3. Depth averaged concentrations spatially averaged in a surface area of 50 acres (treated area by 1 LG Sonic buoy). Minimal effects are shown for DO, SRP, and algae biomass when concentrations are spatially averaged. We only observed a reduction in algae biomass of 10% when measuring the changes right underneath the LG Sonic Buoy.

8.4.4 Sediment Phosphorus Sequestration

- ***Project description and goals***

The phosphorus-locking technology EutroSORB® G is a chemically enhanced clay known as lanthanum-modified bentonite (LMB). This LMB is distributed over the surface of a water body. LMB settles through the water column and integrates into the lakebed *over weeks-months* permanently binding mobile phosphorus from the surficial sediments thereby reducing phosphorus (P) release from lake sediments. **EutroPHIX** proposes performing a detailed assessment of mobile and bound sediment phosphorus across Clear Lake sediments (~ 4 months) and an initial field demonstration (~2 years, including monitoring) which will cost in **total of $3.38M**. This project will be used to better determine long-term implementation costs and build a comprehensive plan for In-lake adaptive management of phosphorus. For the pilot project at a small scale, EutroPHIX proposes an **application of 725,000 lbs (330,000 kg) of EutroSORB G to an area** up to 2,900 acres (~10 km^2, **7% of the Clear Lake surface**) or smaller. The goal of this approach is to reduce the concentration of mobile P in the surficial sediments and reduce the internal loading of P to levels that support beneficial uses of Clear Lake.

The LMB transport within Clear Lake can be modeled as a suspended sediment with a specific density and diameter. LMB physical characteristics vary and range between $2\ \mu m - 50\ \mu m$ for the sediment diameter and $900\ kg/m^3 - 1200\ kg/m^3$ for the sediment density. For instance, Haghseresht et al. (2009) report an average particle diameter of $22\ \mu m$ and a bulk density of $910 - 960\ kg/m^3$ for Phoslock, an LMB for phosphate removal. Furthermore, bentonites are composed of clays, sediments known to have a bulk density between $2000\ kg/m^3\ and\ 2500\ kg/m^3$. LMB applied to the lake also has been shown to increase the cohesiveness of the sediment and improve sediment stability (Egemose, 2010), although more work would be needed to parameterize for modeling purposes. EutroPHIX estimates "*a 5-50 µm size diameter after the product has been applied. They measured EutroSORB particle density as 1480 kg/m*^{3}, which confirms our initial model assumptions.

- ***Model development and assumptions***

TERC in-lake model Si3D also includes a Suspended Sediment Module (SSM) that uses sediment characteristics and water currents to predict the transport of suspended particles within the water column, the deposition of such sediments into the benthic layer, and the entrainment of particles into the water column. It is necessary to know the **sediment characteristics** such as density, mean diameter, and cohesiveness to predict the sediment transport within a water body, which is then used to estimate the balance between the gravitational and lift forces, estimating whether sediments deposit or entrain into suspension given the transient lake currents and surface waves.

After our interactions with EutroPHIX, **we assumed $50\ \mu m$ and $1200\ kg/m^3$** to be the sediment diameter and density, and average cohesiveness of 1 Pa typical for clay-rich sediments.

- ***Model results: Scenario testing***

Three models were developed to predict the sediment transport of LMB at Clear Lake, CA, and the results presented in Figure 8.4.4.1, Figure 8.4.4.2, and Figure 8.4.4.3 predict the sediment transport using the assumptions above. All models were run for 5 days as a spin-up time to accurately represent the flow conditions before the suspended sediment's initial conditions were set in the lake. Since the phosphorus sequestration means that the LMB integrates into superficial sediment lakebed by natural processes over months and binds mobile P as it is released, the product requires a calm environment at shorter time scales (e.g. days) to ensure the applied dose reaches the target area and the integration is successful. Thus, we have run our models for 5-day runs to evaluate the efficacy of the P sequestration. In addition, all models were run in the Oaks Arm. We selected this application area instead of those proposed by EutroPHIX in their proposal to the BRC for being the smallest and confined basin of the lake, hence, reducing the risk of undesired spreading of the applied product to different target areas. Also, even if winds in the Oaks Arm tend to be 10-15% stronger than other basins, lake currents across the whole lake are on average 10-20 cm s^{-1}. Our model runs are testing the impact on sequestration materials when currents are above 10 cm s^{-1}, which occurs in all basins at Clear Lake.

The following is a description of the scenarios tested:

- **Scenario 1**: This model represents an application of LMB at the lake surface within the Oaks Arm. The sediment concentration at the benthic layer was set at $0\ kg/m^3$. This model assumes the **lake forcing to be negligible**, and thus, no currents are expected within the lake. Thus, the results shown in Figure 8.4.4.1 predict the vertical settling of the applied LMB *under the ideal scenario* in which the treated area is vertically aligned with the area of LMB applied at the surface.
- **Scenario 2**: This model predicts the **settling of LMB** applied at the lake surface within the Oaks Arm considering the lake is forced by wind and solar conditions experienced in Clear Lake during the summer of 2020. The sediment concentration at the benthic layer is set to $0\ kg/m^3$ to characterize sediment accumulation at the lakebed. The results from this model, presented in Figure 8.4.4.2, show the transport of the LMB induced by the lake's currents. Nonetheless, the entrainment caused by the currents is always assumed to be negligible. Thus, the model predicts the **horizontal dispersion of LMB** and how the product settles and accumulates at the lake bottom at locations that differ from the initial surface coverage of the LMB application.
- **Scenario 3**: The model represents a lake without suspended sediment in the water column as the initial condition, and it is forced using Clear Lake wind and solar conditions observed during the summer of 2020. This model shows the potential of Clear Lake currents to **resuspend the LMB integrated into the sediments** (Figure 8.4.4.3) and exemplifies the potential pickup of the LMB material from the lakebed from being carried horizontally by the lake currents preventing the material to bind the P released from the sediments.

The ideal Model 1 predicts a vertical transport of the applied LMB material with minimal horizontal transport. Results show that the application area of the P sequestration material is equivalent to the lakebed area where the LMB will integrate the surface of the sediments. This suggests that the application and treated area are expected to be aligned and have the same extent. However, compared to Model 2, **lake currents in Clear Lake can transport the LMB to untargeted locations, decreasing the dose of LMB for sediment integration in a target area**. The transport of the particles was observed in both horizontal directions (as shown by the top view snapshots in Figure 8.4.4.2). The cross-section plots of Oaks Arm in Figure 8.4.4.2 exemplify the potential horizontal transport and indicate that along the Oaks Arm transect (gray line in Figure 8.4.4.2), particles are dispersed over a swath of $\pm 6\ km$ rather than the $\pm 2\ km$ in which the LMB was applied. The results from Model 2 also suggest that lake **currents delay the settling of the applied LMB, compromising its integration into the superficial sediment lakebed**. While results from Model 1 show that all the LMB can reach the lake bottom within $\pm 24\ hrs$, the Model 2 results show a significant amount of suspended LMB after the same period. Also, due to the polymictic nature of Clear Lake (i.e., the lake mixes every week or two), the settling of the release LMB may not reach a steady state which may compromise the effectiveness of application to targeted areas.

Model 3 was developed to exemplify the potential entrainment that Clear Lake can experience under common wind forcing and for the assumption of LMB with a density of $1200\ kg/m^3$ and grain size $50\ \mu m$. Winds generate currents and waves, both mechanisms capable of causing **sediment resuspension**. Despite currents and waves that can pick up sediment from the lakebed and into the water column, our

model only considers the stress induced by the currents. Thus, sediment entrainment is expected to be higher when both currents and waves are considered. The model results suggest that **LMB material can be resuspended during windy days**. This material can then be transported horizontally with the lake currents and settle down to the lakebed at a different location. This entrainment and subsequent horizontal transport can redistribute LMB and expose sediment with higher mobile phosphorus to the water interface, inducing higher phosphorus release. The results suggest that LMB is resuspended by the currents and can reach the surface, implying that suspended LMB concentrations in the extent of the water column increase during these high-speed wind events. Concentrations of ~ $0.05\ kg/m^3$ were observed throughout the water column and transported horizontally before redepositing at a different horizontal location. The resuspension event recorded within Model 3 **lasted for over $36\ hrs$**, increasing the probability of resuspended sediment being transported longer distances and entering the Upper Arm and Lower Arm basins, ultimately decreasing the mass of LMB material deposited in the Oaks Arm as a remediation strategy.

- ***Model Conclusions***

We have used the in-lake model to test aspects of the sediment phosphorus sequestration remediation pilot project recommended by EutroPHIX. The numerical model considers the **dispersion, settling, and resuspension** of suspended particles with physical characteristics of the lanthanum-modified bentonite (LMB). Our model results indicate:

- Clear Lake currents can transport the applied LMB to untargeted locations (**dispersion**) and **delay the settling**, potentially reducing the application efficiency to targeted areas. These processes increase the **uncertainty of the amount of product** required to reduce internal P loading from the sediments. Methods to account for this should be taken into account in dosing calculations.
- Clear Lake currents and waves can **resuspend sediments from the lakebed** during windy days, which may lead to the horizontal redistribution of the **deposited LMB**. While this may benefit sequestering phosphorous at different locations on the lake until material's capacity is reached, the resuspension of the deposited LMB and subsequent transport may lead to lower efficiency of treatment at targeted locations. Thus, the transport and resuspension of sediments at Clear Lake must be considered when defining the areas to be treated and designing the dosing required to treat the targeted area.

EutroPHIX has suggested an estimated cost for the lake-wide treatment using sediment capping, which is of the order of $100M. However, due to the site-specific challenges associated with this technique (LMB dispersion, settling, resuspension), the leaders of this proposal need to perform their suggested pilot project to evaluate their cost estimates and include the uncertainties listed in this section.

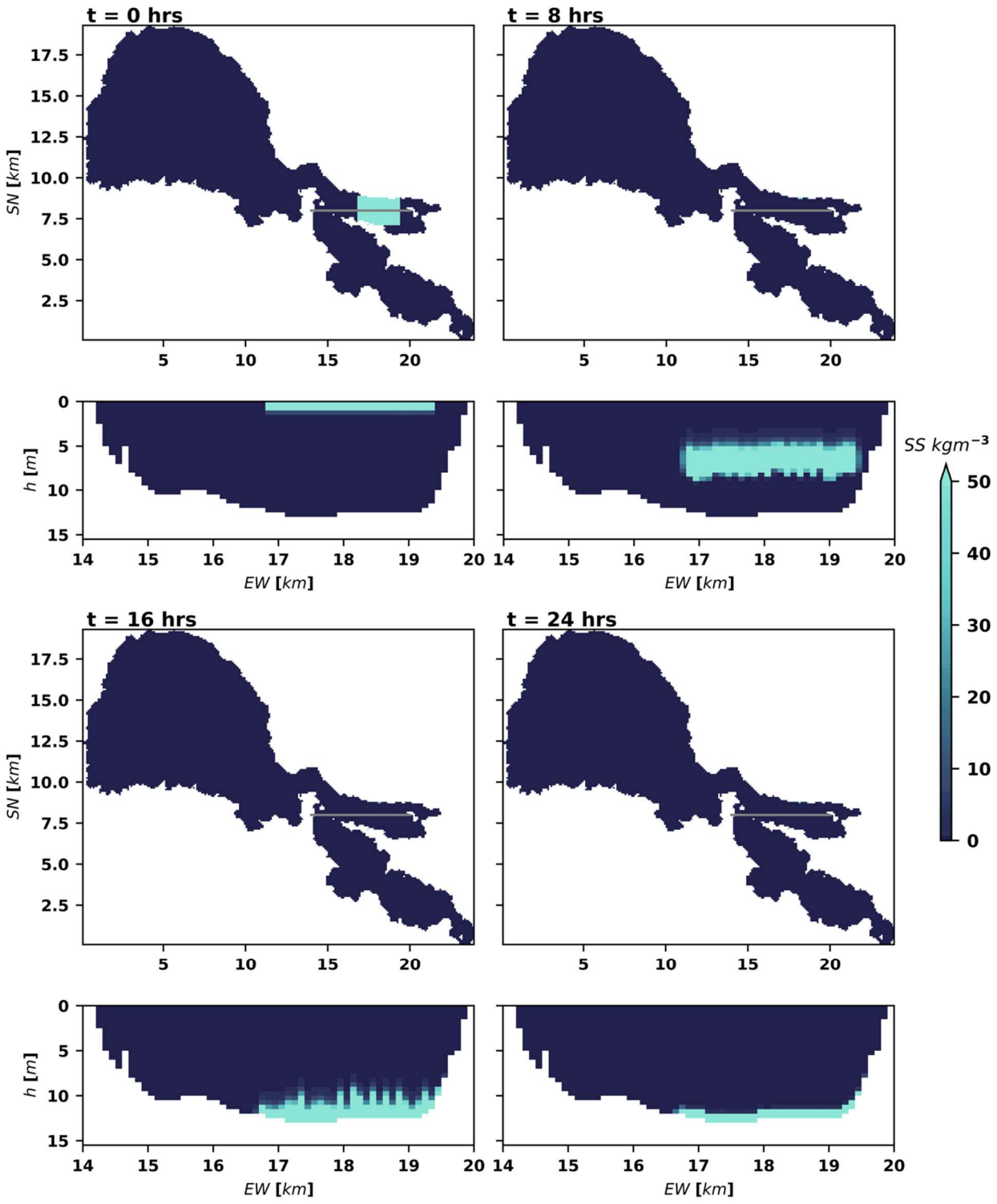

Figure 8.4.4.1. Snapshots characterizing the transport of suspended sediment under Model 1 at Clear Lake, CA. The horizontal gray line on the top view of each snapshot represents the horizontal location of the cross-section shown below as a profile view (Oaks Arm cross-section).

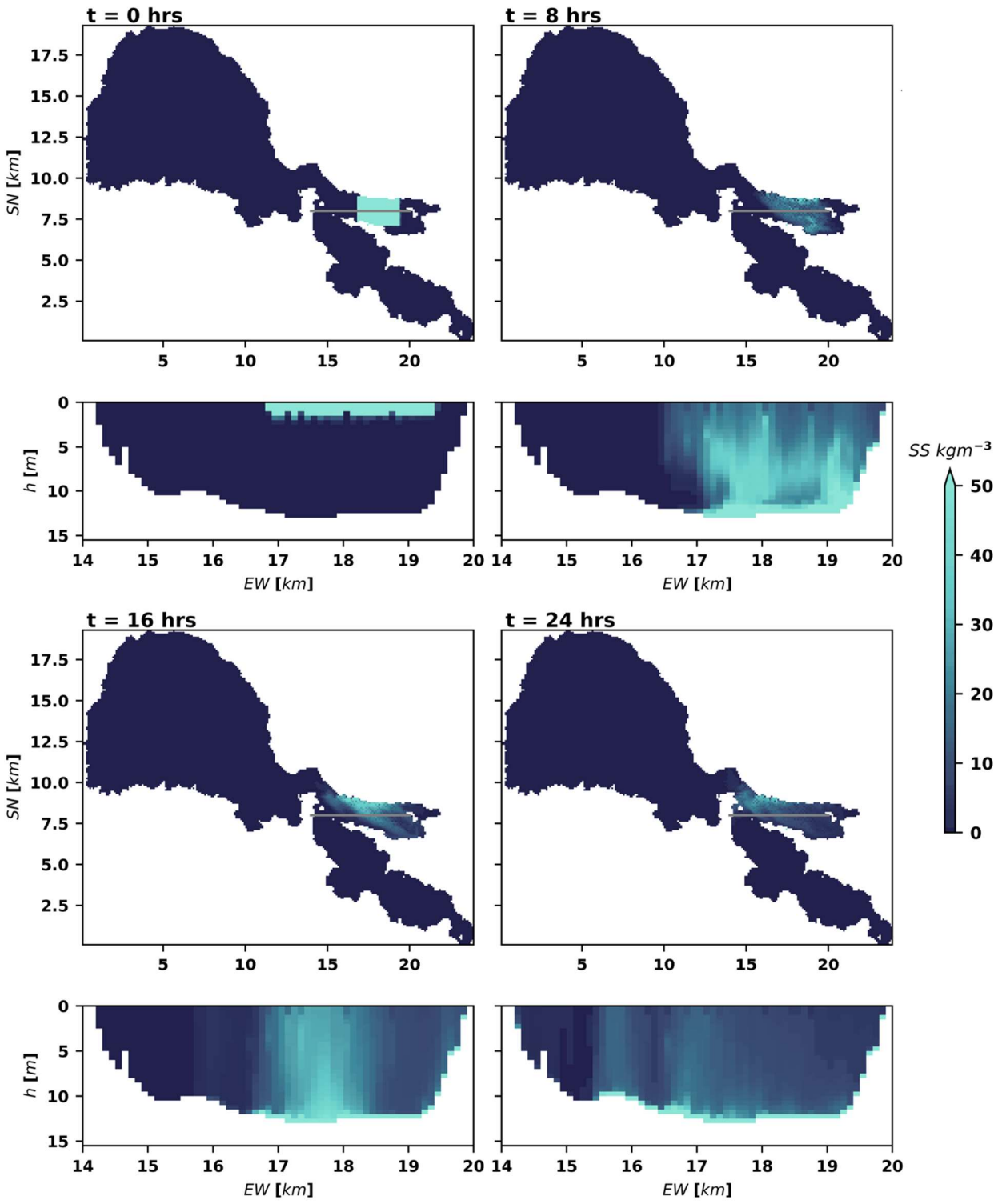

Figure 8.4.4.2. Snapshots characterizing the transport of suspended sediment under Model 2 at Clear Lake, CA. The horizontal gray line on the top view of each snapshot represents the horizontal location of the cross-section shown below as a profile view (Oaks Arm cross-section).

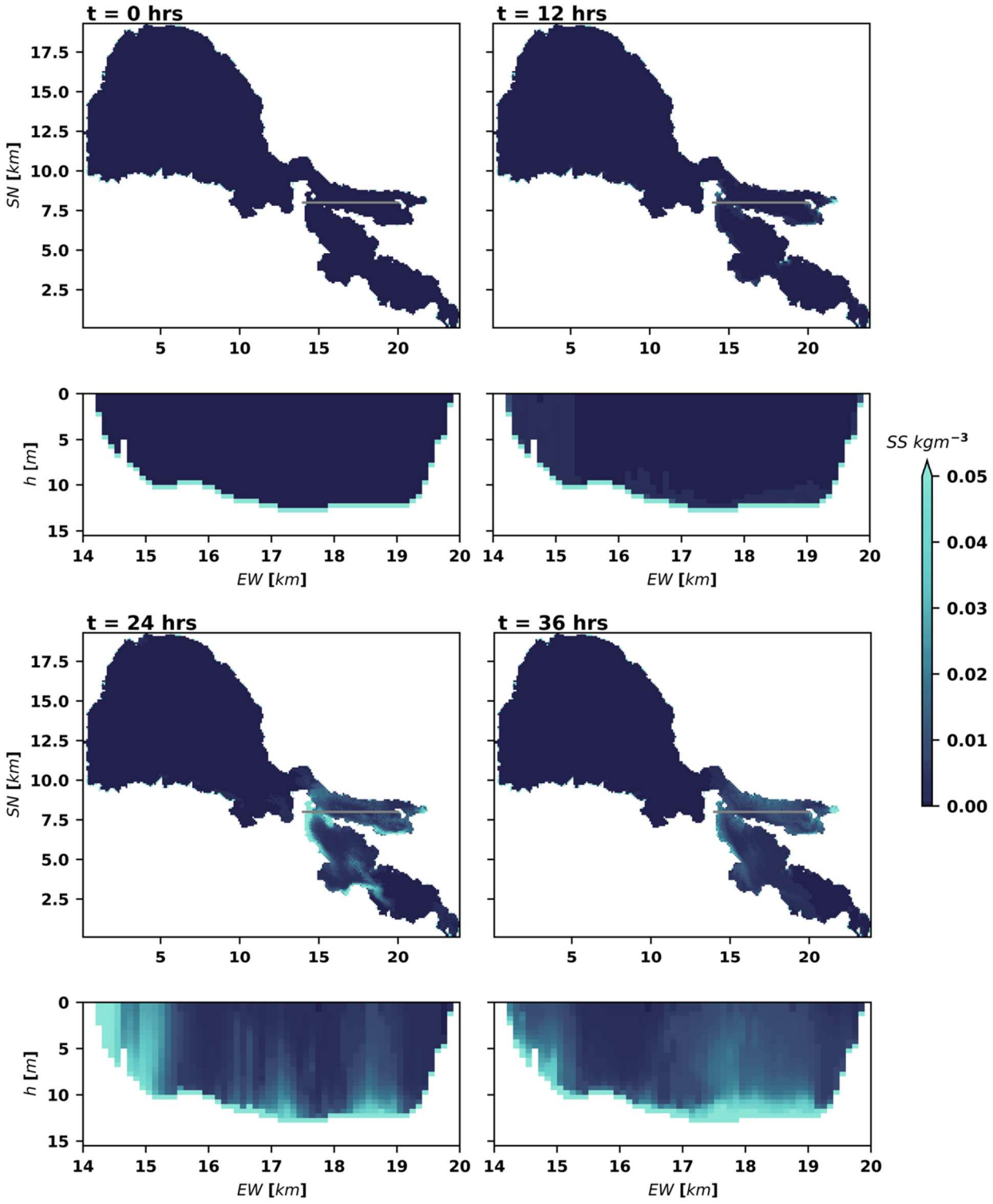

Figure 8.4.4.3. Snapshots characterizing the transport of suspended sediment under Model 3 at Clear Lake, CA. The horizontal gray line on the top view of each snapshot represents the horizontal location of the cross-section shown below as a profile view (Oaks Arm cross-section).

9 In-Lake Bathymetric Survey (UCD-TERC)

Three-dimensional hydrodynamic models are necessary to predict the mixing and transport of contaminants and particulate matter in lakes. Their accuracy is dependent on the resolution of bathymetry data used to create the model grid. In Clear Lake, CA, where periods of warm temperatures and strong vertical gradients of temperature and oxygen can drive the formation of cyanobacterial harmful algal blooms (CHABs), there is a critical need to be able to better predict when these events may occur. Publicly available bathymetric data based on a 2002 survey had a relatively coarse resolution of 100 m that degraded model results by causing numerical instabilities. Using a boat-mounted interferometric sonar mapping system, a finer horizontal resolution of 1 m was achieved in 2024 for this relatively large (31 km x 13 km) and complex lake (three main interconnected basins). The model results describing the complex exchange flows between the three individual basins were far better resolved with the implementation of the new survey data.

Understanding inter-basin flows in this system is important as the addition of a hypolimnetic oxygen system (HOS) is being currently explored as a form of treatment to reduce CHABs in Clear Lake. Quantifying the efficacity of this, or any, treatment methodology requires the model to be running well. In addition to helping refine flow models, a combination of both bathymetric and side scan sonar data better characterizes the lakebed substrate for the installation of HOS to avoid unstable or inappropriate locations. These locations could be where the underlying substrate is too soft (e.g. prone to resuspension) for the addition of diffusers, or areas of natural, active bubble degassing. These natural bubble vents were charted in each of the three basins of the lake. The hydrographic products from the mapping of Clear Lake will provide information to a broad range of stakeholders working on the lake and help reduce the cost of the implementation of restoration strategies.

9.1 Methods

Hydroacoustic data was collected using a combined, fully-integrated, swath bathymetry and dual frequency side scan sonar system operating at 550 (bathymetry) and 1600 (side scan) kHz coupled with an inertial navigation system (INS) for navigation and attitude corrections. The survey was completed between January 2023 and June 2024 due to delays caused by low lake levels and research vessel malfunctions. Swath bathymetry and side scan data were collected and processed using hydrographic survey (SonarWiz) and GIS (QGIS) software. Maps were produced at a 1-meter horizontal resolution.

Fluctuations in lake level during the 1.5-year survey period were accounted for via 15-minute interval lake level measurements from USGS gauge 11450000 (Rumsey gauge). Sound velocity profiles were calculated from temperature profiles acquired with a high-precision temperature logger (RBR SoloT, ±0.002°C) using an empirical temperature-to-sound velocity relationship,

$$SV = 3.8514\,T + 1405.8 \qquad (9\text{-}1)$$

Where SV is the sound velocity (m/s) and T is the temperature (°C). This relationship was derived from a table of sound velocity measurements in fresh water at varying temperatures.

Volume and area calculations were produced in GIS software and python packages. A pixel-based approach was applied, where area and volume are calculated by summing the area or volume of all the pixels present at a given depth in the lake.

High-resolution LIDAR of the surrounding landscape was combined with bathymetry so that bathymetry data could be interpolated to the reference datum. A reference datum of 0m on the Rumsey gauge was chosen for comparisons with bathymetry collected in 2002, and a reference datum of +2.3m on the Rumsey gauge (full lake) was selected for model grid creation.

9.2 Lake Bottom Topography

This new, high-resolution bathymetry provides a valuable update to the previous survey of Clear Lake in 2002 (Figure 9.2.1 and Figure 9.2.2). The 2002 survey's 1,000-meter horizontal resolution resulted in small-scale features (gas vents, inflow mouths) being omitted, limiting model accuracy and overall understanding of the system. The updated survey enables higher-resolution model results (1-meter resolution) and a new understanding of the spatial distribution of gas vents and inflow features in Clear Lake. The benefits of this improved and refined representation of the lake bottom topography also include the capability to resolve fine-scale processes such as the fate of inflows (i.e., where does the inflow water go?), their impacts, and changes with restoration strategies. This product provides information to a broad range of stakeholders working on the lake and helps reduce the cost of the implementation of restoration strategies.

Although the maximum depth of Clear Lake appears to have increased by 4 m between 2002 and 2024 (Lower Arm), this is not necessarily the case and is highly unlikely from a physical sense. Instead, greater mapping resolution allows for the detection of deep features on a sub-100 m scale, giving the appearance of a deeper lake. Those deep features were there in 2002 but were not resolved due to the relatively coarse resolution of the collected data.

Relative to a reference datum of 0 m on the Rumsey gauge, the 2002 bathymetry has a total volume and surface area of 1.06 km^3 and 159.24 km^2, respectively. The 2024 bathymetry shows a slight reduction in both volume (-0.07 km^3) and surface area (-3.85 km^2), containing 0.99 km^3 and 155.39 km^2 below 0m on the Rumsey gauge. This slight reduction potentially results from sediment loading between the two survey times but is more likely to be the discrepancy between the different survey techniques. Data collected in this study is better able to resolve features in the water as well the shoreline. The storage and hypsographic curves are very similar in shape between the two surveys but exhibit a slight vertical offset (1-2 m) (Figure 9.2.3).

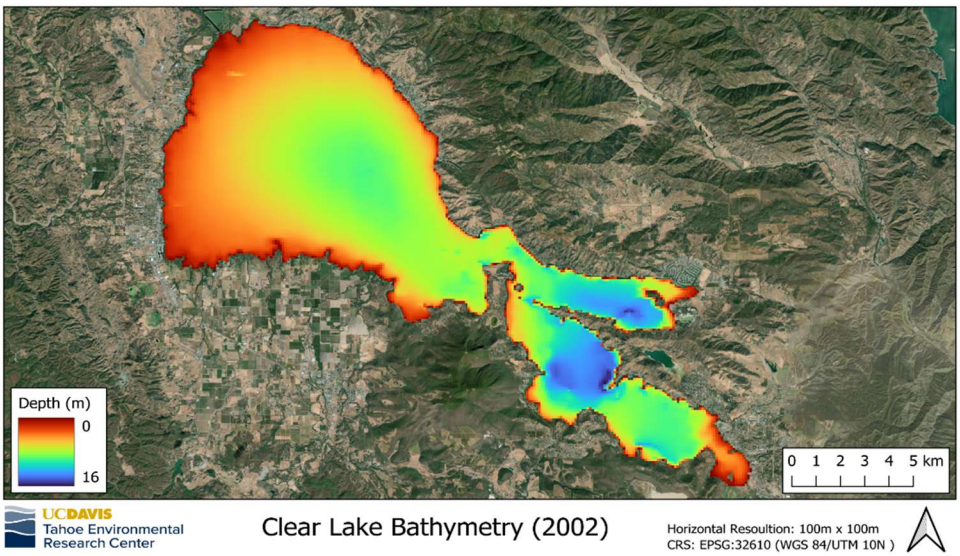

Figure 9.2.1. Visualization of a bathymetric survey of Clear Lake completed in 2002 by ReMatrix at a horizontal resolution of 100m. The overall topography of the lake is visible, but fine-scale details are lost due to pixel size. Depths are presented below 0m on the Rumsey gauge (1318.33 ft asl)

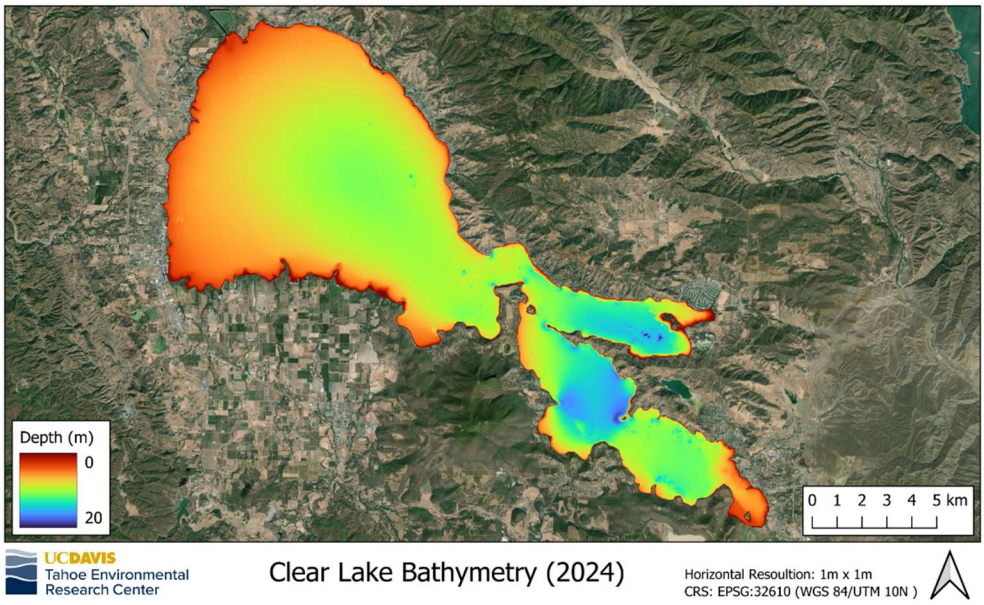

Figure 9.2.2. Visualization of an updated bathymetric survey of Clear Lake completed in 2024 by UCD at a horizontal resolution of 1m. In addition to large-scale lake topography, fine-scale features (gas vents) are resolved. Depths are presented below 0m on the Rumsey gauge (1318.33 ft asl)

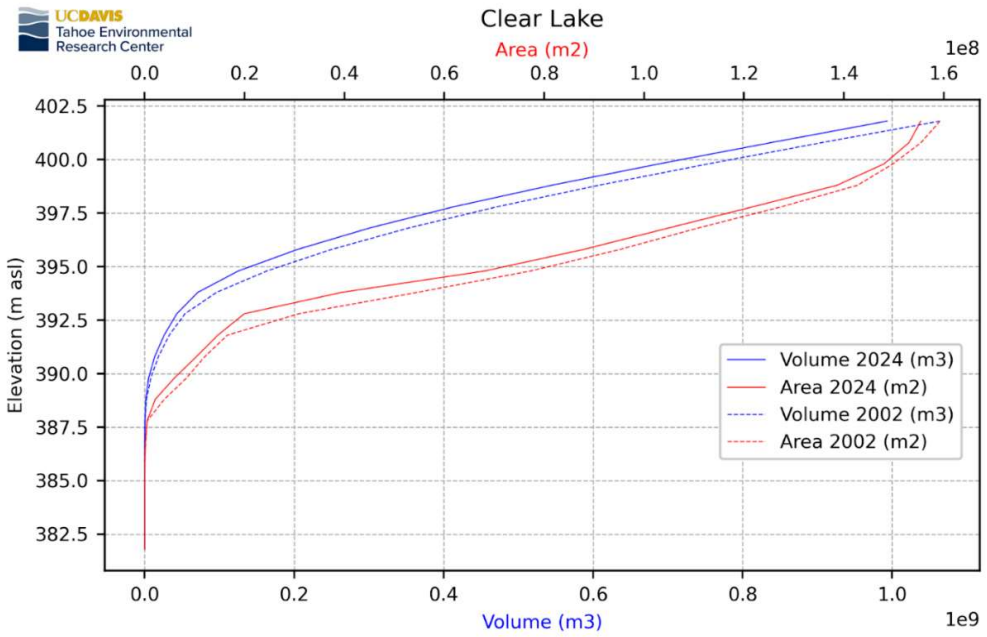

Figure 9.2.3. Storage curves for 2024 (blue) and 2002 (red) bathymetry at Clear Lake, CA. 2002 bathymetry has a total volume and surface area of 1.06 km^3 and 159.24 km^2, respectively. The 2024 bathymetry shows a slight reduction in both volume (-0.07 km3) and surface area (-3.85 km2), containing 0.99 km^3 and 155.39 km^2 below 0m on the Rumsey gauge. Curves are presented below 0m on the Rumsey gauge (1318.33 ft asl)

9.3 Side-scan Maps/Targets

Sidescan (e.g. acoustic backscatter) is a type of sonar used for imaging objects on the bottom of a body of water. Rather than measuring depth, sidescan measures the amplitude of the returning sound wave, which is dependent on the density of the surface it is reflected from. Sidescan sonar is a complementary dataset to bathymetry, allowing better target acquisition and understanding of the substrate versus bathymetry.Figure 9.3.3 provides an overview of sidecan imagery gridded at 1 m for the entirety of Clear Lake. As is readily apparent from the dominantly red colors, the majority of the lakebed is dominated by less dense material (e.g. mud). The slight color differences in the Upper Arm are the result of data being collected over multiple survey days and the color balancing required during processing but don't represent real variations in the substrate. Having this amount of less dense material corresponds well to both the age of the lake and known sedimentation rates. Future remediation strategies also need to include the substrate in the design. Less dense materials will have a greater tendency of sediment resuspension during wind mixing events but they will also be less supportive for installed equipment in the lake. From the data collected, the depth of this material layer is unknown, and further surveys with subbottom profiling equipment (e.g. Chirp) would be required.

In addition to the large areal extent of mud within the lake, limited amounts of denser material (e.g. rock) around the edges and in occasional areas where rocks are exposed. The greatest extent of the lake where this is evident is at the end of Lower Arm near Luebow Point and, to a lesser extent, around Monitor Point. Areas where this is evident tend to be around steeper shorelines.

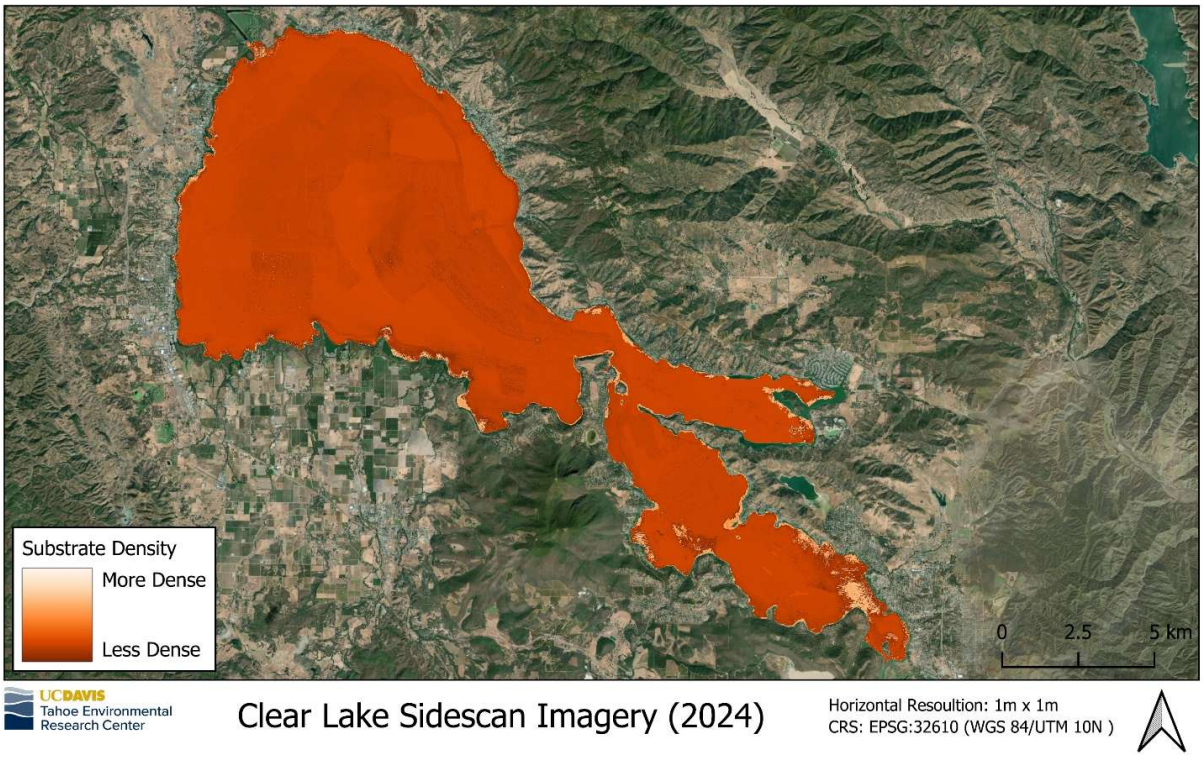

Figure 9.3.1. Sidescan sonar imagery of all of Clear Lake at 1m horizontal resolution. Yellow represents areas of more dense substrate, red indicates areas of less dense substrate. The majority of the lake is dominated by less dense substrate (i.e., mud), with more dense substrate (i.e., rocks) along the shoreline, especially in the southwest part of the bay

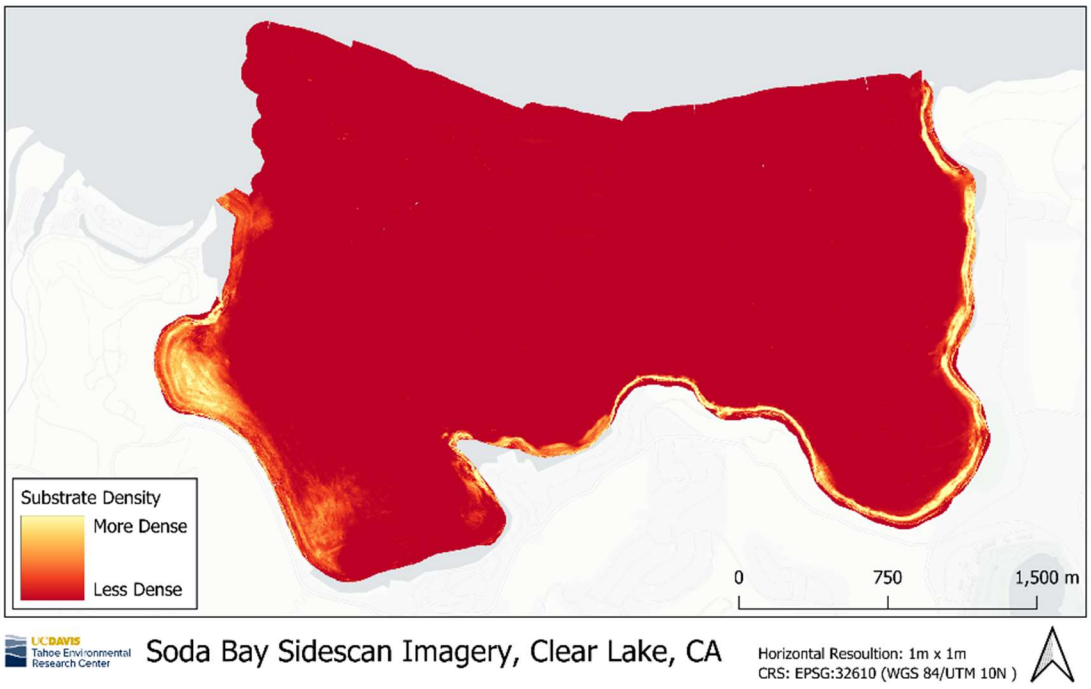

Figure 9.3.2. Sidescan sonar imagery of Soda Bay at 1m horizontal resolution. Yellow represents areas of more dense substrate, red indicates areas of less dense substrate. Overall, Soda Bay is dominated by less dense

substrate (i.e., mud), with more dense substrate (i.e., rocks) along the shoreline, especially in the southwest of the bay.

Figure 9.3.2 and Figure 9.3.3. provide two examples of sidescan imagery from Soda Bay and Oak's Arm. In these images, the dark red color represents less dense (e.g. mud) and the yellow color represents denser (e.g. rocks). In the Soda Bay example, the detail of the shoreline on the eastern side is clearly shown. On the western side, rocks are shown to extend into the water. The same story is evident in the Oak's Arm example; however, it is interesting to note that there is more denser material just offshore of the Herman Impoundment directly south of Rattlesnake Island. This is likely mining materials that were deposited in the lake.

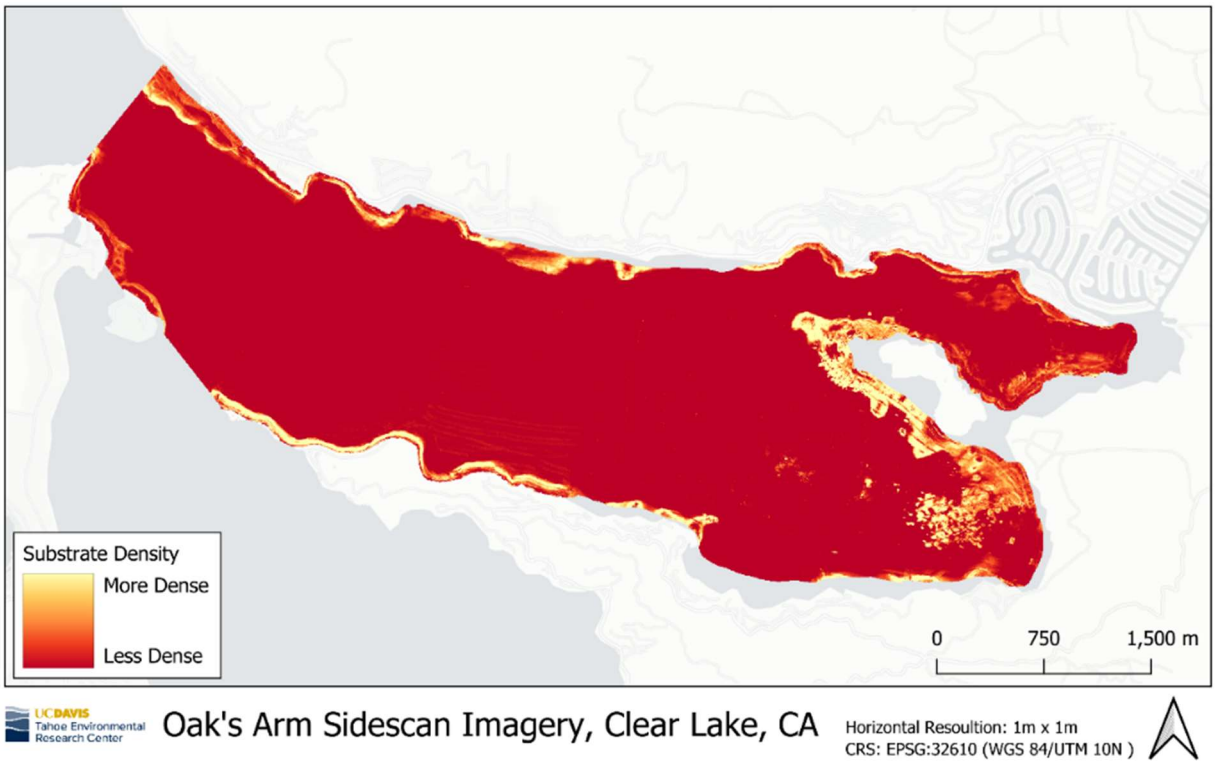

Figure 9.3.3. Sidescan sonar imagery of the Oak's Arm at 1m horizontal resolution. Yellow represents areas of more dense substrate, red indicates areas of less dense substrate. Overall, the Oak's Arm is dominated by less dense substrate (i.e., mud), with more dense substrate (i.e., rocks) along the shoreline. Areas of denser substrate also stand out around Rattlesnake Island and offshore of the southeast end of the arm, near the Herman Impoundment.

9.4 Bubbles, CO_2 Fluxes & USGS Collaboration

In addition to rock, bubbles and gas fluxes are also acoustically dense in the sidescan data and are a characteristic feature of the Clear Lake bottom. We have started conversations with the Volcanologist Department at UGSG to better understand the temporal and spatial variations in gas and heat emissions at Clear Lake. These natural bubble vents were charted in each of the three basins of the

lake. As an example, the side-scan sonar cross section near the deep hole in the Oaks Arm showed a very active gas vent (Figure 9.4.1). While this figure was collected in a region that is predominantly mud, the data extracted from one line does show variation (Figure 9.4.1). Generally, locations where bubble plumes were identified were in depressions where the mud had been scoured away leaving the underlying rock exposed. These bubble vents do not have direct implications for the remediation of the lake but are certainly of interest to those trying to understand gas flux in the system. USGS has conducted a 2024 CO_2 flux survey in the Oaks Arm and has further work planned to understand gas fluxes. The identification of gas vents by our sonar survey informed their sampling strategy.

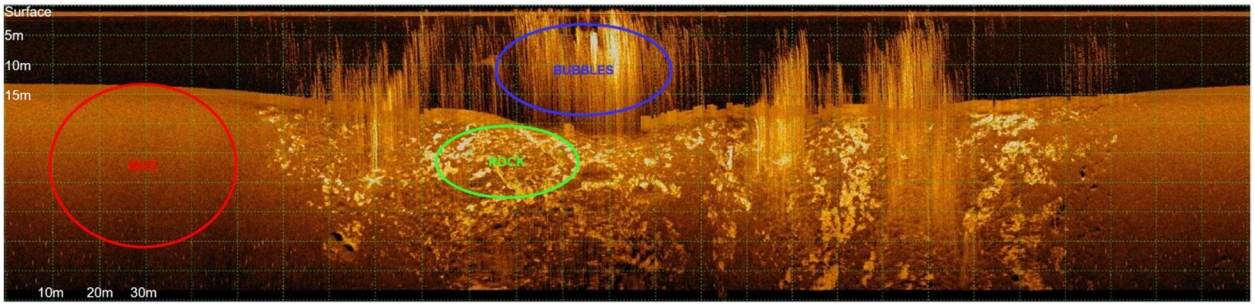

Figure 9.4.1. Sidescan sonar cross-section of gas vents in the Oak's Arm. Gas vents are characterized by a texture transition in the substrate from less dense (mud) to more dense (rocky) and visible bubble plumes rising from depressions 1-4m deep and 1-4m wide. Sidescan imagery and field observations indicate that these bubble plumes are not always visible from the surface, especially on windy days

10 Coupling of Upper Watershed and In-Lake Modeling (UCD-TERC)

This section outlines our initial attempt to couple the results from the upper watershed and in-lake modes developed by USGS and TERC, respectively. These results are preliminary, but promising. We used modeled discharge and temperature from HSPF and nutrient loads from LOADEST at the three main watersheds, which yielded a total of three river mouths numbered 1, 2, and 4 in Figure 10.1. These river mouths are linked to the following creeks and sampling locations:

- Mouth 1: Scotts, Middle, Clover Creeks (SCS, MCS, ACS)
- Mouth 2: Kelsey, Cole Creeks (KCS, CCK)
- Mouth 4: Adobe Creek (ADD, with KCS nutrients)

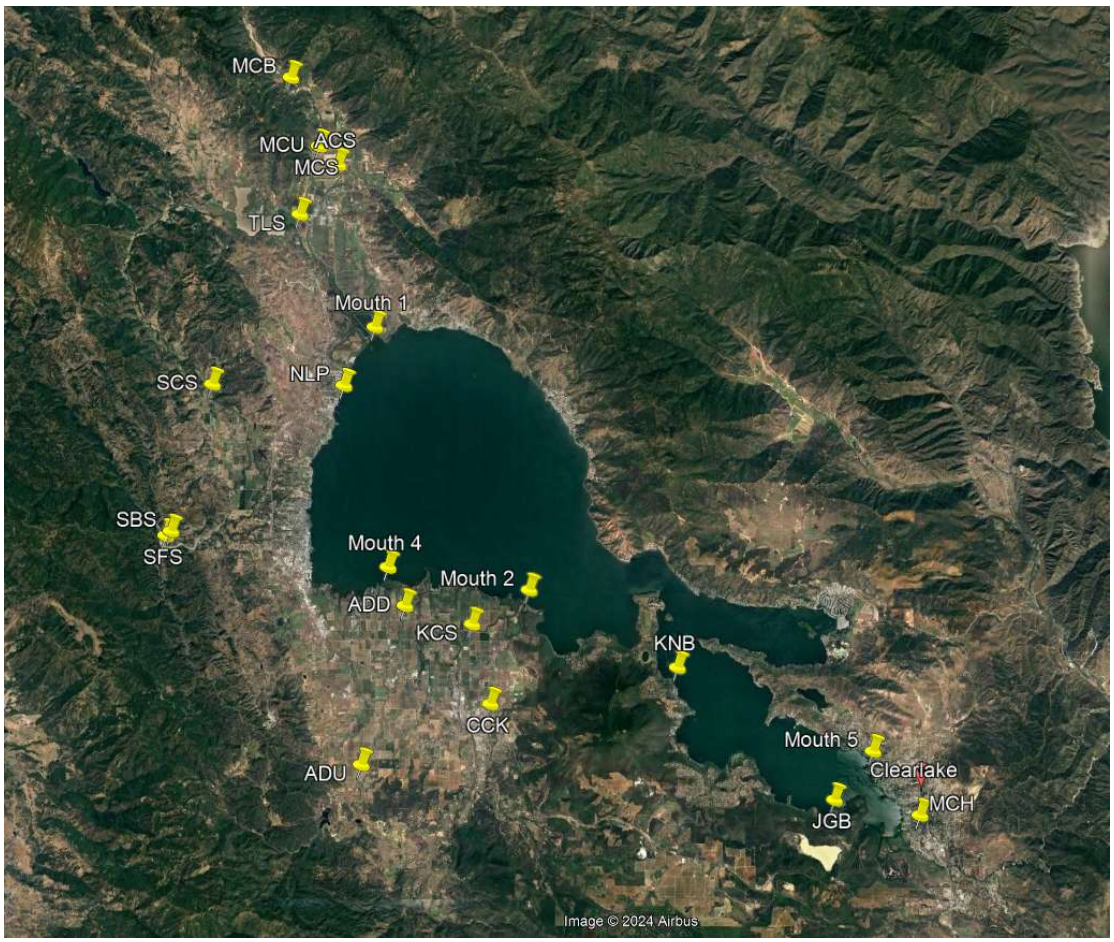

Figure 10.1 Map of the stream locations where USGS collected water quality data and flow is also available. We also marked the location of the three mounts (Scotts, Middle, Clover Creeks = 1; Kelsey, Cole Creeks = 2; Adobe = 3) modeled when coupling the watershed and lake models

Model results showing the mean nitrate concentrations in the lake bottom (~3 m) during the rain events occurring in the water year 2022-23 (Dec 15, 2022, to Feb 15, 2023) showed the spatial and temporal distribution of this nutrient as the creeks entering the lake (Figure 10.2).

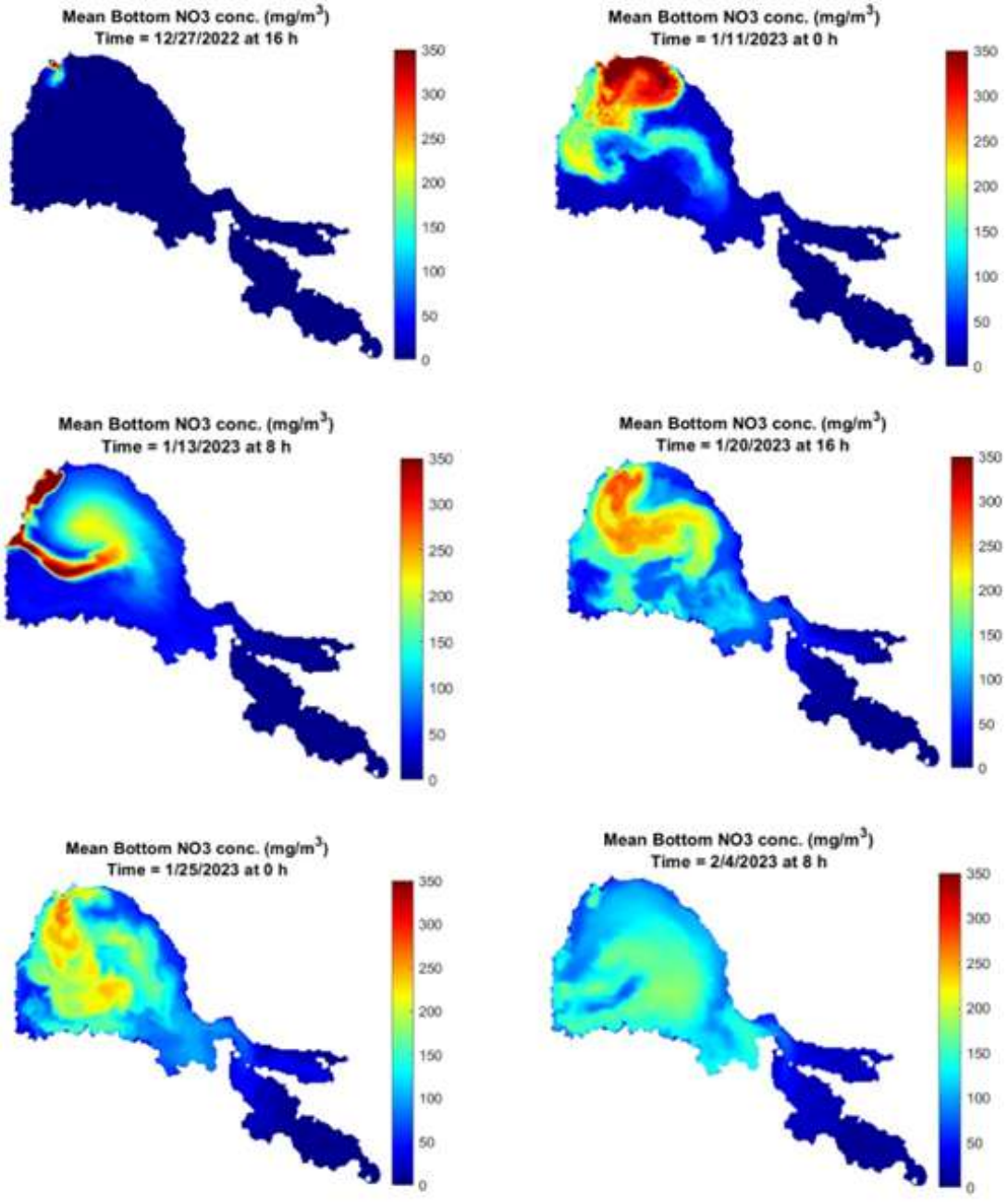

Figure 10.2. Snapshots of the mean bottom concentrations (3 m layer) of nitrate (NO_3) in Clear Lake as a result of the rain events occurring between December 2022 and February 2023 (wet year). This sequence of images shows the spatial and temporal distribution of this nutrient as the creeks entered the lake

11 Conclusions

The monitoring and modeling work conducted at the Clear Lake watershed and within the lake has allowed us to develop the following conclusions:

USGS Watershed Monitoring and Modeling

- Adding four USGS stream gages to the **watershed monitoring** network provided important data for stream flow, temperature, and turbidity that were essential for calibration of the SPARROW and HSPF watershed models.
- The following summary observations were made from the nutrient modeling data:
  - On average, concentrations of filtered soluble reactive phosphorus (SRP) were about a quarter or less of unfiltered (total) P concentrations (TP), except for urban locations where the amount of SRP accounted for almost 50% of the TP.
  - Nitrate (NO_3^-) in filtered samples accounted for about 30% of total N (TN) in unfiltered samples.
  - The remainder of N was mainly organic; concentrations of ammonia (NH_3) and ammonium (NH_4^+) were typically low in the tributaries.
  - Molesworth Creek and the storm drains, representing urbanized areas in the Clear Lake basin, had the highest concentrations of N and P species, turbidity, and suspended sediment among monitored tributaries, but relatively low discharge.
- The **SPARROW** model identified source areas and land uses contributing total nitrogen and total phosphorus within the watershed. Runoff from undeveloped areas sourced total nitrogen and total phosphorus from shrublands and forested land and contributed total phosphorus from geological background and stream channels. Agricultural practices were also a source of total nitrogen and total phosphorus and were mostly important in watersheds with a significant amount of agricultural land such as Middle and Clover Creeks, Adobe Creek, and Kelsey Creek (Big Valley region). **Although agriculture was determined to be a significant source of phosphorus, it was found that 90% of the phosphorus applied as fertilizer was not transported off the landscape to the lake. The proportion of phosphorus load from agriculture in Middle and Clover Creeks was found to be the highest from SPARROW modeling; this is a source that potentially could be mitigated**.
- A comprehensive **watershed discharge and sediment model** (HSPF) has been developed for each main tributary draining to Clear Lake.
  - Hydrologic calibration results range from "good to "excellent", allowing a direct comparison between tributaries and adding crucial information about ungaged locations and during data gaps.
  - Sediment calibrations resulted in a good representation of daily sediment loads and instantaneous suspended sediment concentrations.
  - According to the HSPF model results, Scotts Creek contributes 52% of the

streamflow and 34% of the sediment loads to Clear Lake; Middle Creek contributes 17% of the streamflow and 27% of the sediment; and Kelsey Creek contributes 10% of the streamflow and 15% of the sediment.

- Tule Lake reduces sediment loads from Scotts Creek by ~36% on average.
- Continued monitoring is essential to capture a range of hydrologic conditions for accurately representing sediment and nutrient loads through time. Filling data gaps, especially in ungaged watersheds, will reduce uncertainty in future modeling efforts.
- In addition, a much better understanding of the interactions between surface water and groundwater is needed for better management decisions, especially on water use, and how that affects fish populations, especially Hitch, that use the watershed for reproduction.

- **Sediment source analysis** was done using new data for several hundred soil and sediment samples collected during 2021–23 from Clear Lake tributaries and 28 bed sediment samples from Clear Lake. The samples were sieved to < 0.063 mm and analyzed for major elements, trace elements, organic carbon, carbon and nitrogen isotopes, and particle-size distribution. Statistical techniques were used to compute mixing relationships for target sediments, including 25 locations in Clear Lake (representing all three arms) and three locations in Rodman Slough delta, which receives sediment from Scotts Creek, Middle Creek, and Clover Creek.
- Results of Linear Discriminant Analysis (LDA) indicate **distinct geochemical signatures for four tributary source groups**: 1) Adobe Creek, Manning Creek, and Scotts Creek, 2) Cole and Kelsey Creeks, 3) Burns Valley, Molesworth Creek, and Schindler Creek, and 4) Clover Creek and Middle Creek. Source group 1 is the dominant source of sediment to Clear Lake, representing about 60% based on target samples distributed in all three arms of the lake. Source group 3 is the source of about 25% of Clear Lake sediment, predominantly in the Lower Arm and Oaks Arm. Source Group 4 is the source of about 15% of Clear Lake sediment, predominantly in the Upper Arm. A separate set of calculations showed **a distinct geochemical signature for upper Scotts Creek (South Cow Mountain area)** compared with middle and lower Scotts Creek and the Clover Creek and Middle Creek source group.

UCD-TERC In-lake Monitoring and Modeling

- Periods of **warm water temperature and low dissolved oxygen (hypoxia**) occurring in the summer/fall, when the lake develops temperature gradients with depth (i.e. stratification), are the major explanatory factors in the poor water quality and ecological health of Clear Lake because they control the **availability of a limiting nutrient** (phosphorus, P) for phytoplankton growth, particularly **cyanobacteria harmful algal blooms (CHABs)**.
- We developed a simple cost-effective decision-making tool to **predict when and for how long low dissolved oxygen (DO) levels occur** in the lake using basic meteorological information.
- In contrast to many other lakes, the intensity of the summer CHAB season in Clear

Lake was correlated to the timing and duration of hypoxia rather than the magnitude of spring runoff because of the release of nutrients (P) from the sediments (internal loading). Comparative estimates of external and internal phosphorus loading indicate that **internal sources accounted for 70 – 95% of the total phosphorus input** into the system.

- The release of P during hypoxic periods shifted the system towards **nitrogen (N) limitation**, favoring the proliferation of CHABs, which can fix atmospheric nitrogen. N-fixing cyanobacteria input additional N to the lake throughout the summer, facilitating the subsequent growth of non-N-fixing toxin-producing cyanobacteria, including Microcystis, in the fall. As a result, **the two major factors predicting CHABs are the ratio TN:TP and lake temperature.**
- Cyanobacteria measurements at Clear Lake are intrinsically complicated due to the high spatial and temporal variability of the blooms. **Critical Scale of Variability for cyanobacterial blooms ranges from 70 to 175 m**, which is finer than what is resolvable by currently available satellite data (300 m). The current version of the **cyanobacteria index (CI)** algorithm publicly available from fhab.sfei.org/ is not effective for Clear Lake and we found **better performance with the original CI algorithm**.
- The **new bathymetric map** (2024) of the lake's bottom topography with a horizontal resolution of 1 m allows more robust model predictions and **the capability to resolve fine-scale processes** such as the fate of creeks, and their impacts on the lake, and to predict changes with restoration strategies. This information serves a broad range of stakeholders working on the lake and helps **reduce the cost** of the implementation of restoration strategies.
- Lake **restoration strategies** to mitigate CHABs can be grouped in physical (dredging of the sediment, weed removal, water drawdown, harvesting of algae/nutrients, aeration, oxygenation, ozonation, water mixing, water shading, sediment capping, flocculants/nutrient sequestration, ultrasonic exposure, UV exposure), chemical (copper/peroxide based algaecides, organic algaecides), and biological (microbial/food web manipulations, barley/rice straws, wetland restoration, shoreline stabilization) strategies. Between 2022 and 2023, **pilot projects** to test four lake restoration strategies at Clear Lake have been recommended and approved by the Blue Ribbon Committee. Those restoration strategies include **dissolved oxygen enhancement (i.e., hypolimnetic oxygenation), algae and nutrient harvesting, ultrasonic algae control, and sediment phosphorus (P) sequestration**. All of these techniques have proved to improve the water quality of the sites where they have been previously tested. However, Clear Lake is a unique system with a large surface area, very strong currents, high nutrient and algae concentrations, and a highly dynamic mixing regime. Thus, we have used the newly developed **in-lake model to evaluate the effects** of the recommended pilot projects on Clear Lake's water quality. Scenario testing has allowed us to identify key variables in the design of the different pilot restoration projects that should be further explored and carefully quantified before the projects move into the implementation phase. This modeling exercise also points out the technologies that provide localized benefits, and those that can be challenged due to the dynamic nature of Clear Lake. A detailed cost-

benefit analysis should be performed to evaluate if the capital investment and maintenance costs of the strategies are worth the water-quality improvement obtained. Model results of the four pilot restoration projects are summarized here:

- *Hypolimnetic oxygenation*: Direct addition of DO to the bottom of the Oaks Arm (3,500 acres, 14.2 km^2) allowed DO concentrations to remain above 3.5 mg/L across the basin after 2 weeks of treatment during summer. Model results showed a ~50 % reduction in P concentrations and a ~20% reduction in algae biomass compared to the model scenario without oxygen injection. We obtained these results using an injection flow of 500 cubic feet per minute (cfm). About 10% of the lake surface can be treated using approximately $4M funding using 2022 estimates.
- *Algae and nutrient removal*: The use of an algae and nutrient harvester to treat a lake area of 0.5 acres (0.002 km^2) in the Lower Arm aimed to pump out nutrient and algae-rich water and return clarified and oxygenated water back to the lake. Model results showed that this pilot project yielded improvements in key water quality variables (DO, P, algae biomass) when using a flow rate of 1 million gallons per day (pilot project cost of $1.3M), but not for larger areas due to the continuous transport of nutrient and algae-rich water from outside the control area.
- *Ultrasonic algae control*: The deployment of an LG Sonic MPC Buoy to treat a lake area of 50 acres (0.2 km^2, 0.1% of the lake surface), in the Lower Arm aimed to prevent algae growth via ultrasonic waves ($1.5 M). Model results showed limited improvement in key water quality variables. We observed a reduction in algae grown by only 10% underneath the buoy, and less than 1% algae biomass reduction when evaluating spatially averaged results in the control area.
- *Sediment phosphorus sequestration:* We have identified processes that may reduce the efficacy of this technology. Clear Lake currents can transport the applied lanthanum-modified bentonite (LMB) to untargeted locations (dispersion) and delay the settling, potentially reducing the application efficiency to targeted areas. These processes increase the uncertainty of the amount of product required to reduce internal P loading from the sediments. Methods to account for this should be taken into account in dosing calculations. Clear Lake currents and waves can resuspend sediments from the lakebed during windy days, which may lead to the horizontal redistribution of the deposited LMB. Although this may benefit sequestering phosphorus at different locations on the lakebed until the material's capacity is reached, the resuspension of the deposited LMB and subsequent transport may lead to lower efficiency of treatment at targeted locations. Thus, the transport and resuspension of sediments at Clear Lake must be considered when defining the areas to be treated and designing the dosing required to treat the targeted area.

Coupled watershed and in-lake results

- The main source of **total phosphorus (TP)** in the lake in the **short-term** is the sediments, as **summer** hypoxia and stratification are triggering internal loading

through release of P from sediments. As a result, TP is higher in the lake when the creeks are not flowing. On a **long-term** basis, TP in the lake is higher during summer in **dry years**, when the watershed inputs are minimal.

- On the other hand, the main source of **nitrate** (NO_3^-) in the lake in the **short-term** is the creeks during the **wet season**, showing that the availability of NO_3^- in lake water is directly correlated with the creek loads. NO_3^- availability in the lake is higher in **wet years in the long term**.
- Preliminary estimates of the magnitude of nutrient reduction required to improve lake water quality indicate that a ~50% reduction of P concentrations in the lake translates into a ~20% reduction of algae. Because the P loads in the lake are not directly linked to the creeks in the short term, any reduction in the P loads in the creeks will only reduce the available P concentration in the sediments to move into the water column during the warm, dry season.
- Potential restoration strategies:
    - *Watershed strategies*: The upper portion of the Scotts Creek sub-watershed (South Cow Mountain area), location of an off-highway vehicle recreation area, was found to be a source of total phosphorus from eroding geological material. Identification of the most problematic areas subject to erosion represents a good short-term solution to a reduction of watershed phosphorus loads. The combined flow of Middle and Clover Creeks was found to be a relatively large source of agriculturally derived total phosphorus. The Middle Creek restoration project (a longer-term solution) should greatly reduce that loading by restoring wetlands. Watershed restoration activities in Scotts Creek, Middle Creek, and Kelsey Creek would have the biggest impact on sediment and nutrient loadings to Clear Lake and would limit the availability of in-lake nutrients that fuel harmful algal blooms in the short- and long-term. The Tule Lake restoration has resulted in reducing sediment loads by ~36% from Scotts Creek, and a similar restoration below the confluence of Scotts Creek, Middle Creek, and Clover Creek would likely reduce the sediment and nutrient loadings to Clear Lake significantly. Challenges with acquiring the privately owned land to complete the Rodman Slough restoration have resulted in long delays and uncertainty in the timeline for completing this work.
    - *In-lake strategies*: Because the seasonal lack of dissolved oxygen in the lake's water column is the root cause of the CHAB problem, **hypolimnetic oxygenation** has proved to be the most cost-effective and practical solution to improving Clear Lake's water quality. Hypolimnetic oxygenation is also the most economical and viable solution in the short and long term due to its ability to treat the full lake with a feasible number of facilities as it takes advantage of the highly dynamic environment. The overall conclusions from our in-lake model results are that by maintaining the oxygenated conditions near the lake bottom, P concentrations may be capped to typical winter values (~100 mg/m^3) preventing the excessive P loads that cause a shift in nutrient limitation (P >> N), and thus a relative deficit in nitrogen for all algae.

12 Recommendations

1. Management implications
   - Our study shows that the key remediation goal should focus on **increasing dissolved oxygen** at the lake bottom to **reduce the release of nutrients from the sediment** during the warm dry season (**summer**). Nutrient reduction (**particularly P**) will prompt the **reduction of CHABs**.
   - Preliminary estimates of the **magnitude of nutrient reduction** required to improve water quality indicate that a ~50% reduction of P concentrations in the lake translates into a 20% reduction of algae. Because the P loads in the lake are not directly linked to the creeks in the short term, any reduction in the P loads in the tributary creeks will only reduce the available P concentration in the sediments to move into the water column during the warm, dry season.
   - Despite the need to focus on the reduction of nutrients in the summer to mitigate CHABs, monitoring and modeling efforts conducted in this project showed the importance of a multidisciplinary approach to improving the lake's water quality that combines **in-lake restoration strategies in the short term (seasonal scale) and watershed restoration strategies in the long term (annual to multi-year scale).**
2. Potential remediation strategies
   a. **Stream** remediation strategies include **reducing erosion** through best management practices, especially in areas with high phosphorus sources. The **upper Scotts Creek** watershed (South Cow Mountain area) was found to release a large amount of total phosphorus from erodible soils, unpaved roads, and/or stream banks. Identification of suitable areas for erosion control should be a high priority. On a longer time scale, the **Middle Creek** restoration project will help to reduce the phosphorus loading from agricultural and other sources in that region. Support for local **best management practices** is recommended in the lower portion of most tributary creeks will help to reduce erosion from high-clay-content soils that are easily eroded.
   b. **Lake** restoration strategies to mitigate CHABs can be grouped in physical (dredging of the sediment, weed removal, water drawdown, harvesting of algae/nutrients, aeration, oxygenation, ozonation, water mixing, water shading, sediment capping, flocculants/nutrient sequestration, ultrasonic exposure, UV exposure), chemical (copper/peroxide based algaecides, organic algaecides), and biological (microbial/food web manipulations, barley/rice straws, wetland restoration, shoreline stabilization) strategies. During 2022 and 2023, pilot projects to test four lake restoration strategies at Clear Lake were **recommended and approved by the Blue Ribbon Committee**. Those restoration strategies include **dissolved oxygen enhancement (i.e., hypolimnetic oxygenation), algae and nutrient harvesting, ultrasonic algae control, and sediment phosphorus (P)**

sequestration. All of these techniques have proved to improve the water quality of the sites where they have been previously tested. However, **Clear Lake is a unique system** with a large surface area, very strong currents, high nutrients, and algae concentrations, and a highly dynamic mixing regime. Thus, we have used the newly developed in-lake model to evaluate the effects of the recommended pilot projects on Clear Lake's water quality. Scenario testing has allowed us to identify key variables in the design of the different pilot restoration projects that should be further explored and carefully quantified before the projects move into the implementation phase. This modeling exercise also points out the technologies that provide localized benefits, and those that can be challenged due to the dynamic nature of Clear Lake. A detailed cost- benefit analysis should be performed to evaluate if the capital investment and maintenance costs of the strategies are worth the water-quality improvement obtained. However, because the lack of dissolved oxygen is the root cause of the problem, hypolimnetic oxygenation has proved to be the most appropriate solution to Clear Lake's water quality. Hypolimnetic oxygenation is also the most economical and viable solution in the short and long term due to its ability to treat the full lake with a feasible number of facilities as it takes advantage of the highly dynamic environment. The overall conclusions from our in-lake model results are that by maintaining the oxygenated conditions near the lake bottom, P concentrations may be capped to winter values (~100 mg/m^3) preventing the excessive P loads that cause a shift in nutrient limitation (P >> N), and thus a relative deficit in nitrogen for all algae.

3. Develop a sustained, long-term, science-based, community-led monitoring program at Clear Lake and its basin

   Results from this work highlight the need for continuing with the monitoring of Clear Lake and its basin for multiple reasons:

   - Evaluate standards for drinking water supply, and cultural and recreational uses;
   - Niche for several endangered wildlife species;
   - Evaluate the effects of restoration projects; and
   - Continue improving our understanding of long-term changes in the watershed and the lake under natural and anthropogenic stressors (e.g. climate change, land uses)

   Members from the UC Davis project team led a series of four conversations between representatives from the community and local, state, and federal agencies during March to May 2024. This task force concluded that a **sustained, long-term monitoring and science program** at Clear Lake needs to be a **cooperative** effort with a well-defined **science-based** framework that provides an opportunity for the community to lead the efforts, ensure **technology transfer, capacity building** for the local communities, and the development of an engaged science community at Clear Lake, with guidance from regional expertise.

This group also identified **six monitoring categories**: stream, lake, municipal water (intakes), shoreline, groundwater, and special studies monitoring. Table 12.1 shows a list of the monitoring activities we identified, including tentative locations, sampling frequency and variables to be measured for each activity.

Figure 12.1. List of monitoring activities organized by category (stream monitoring, lake monitoring, municipal water monitoring or intakes, shoreline monitoring, groundwater monitoring, special studies), with tentative locations, frequency and potential environmental variables to be measured

Category	Activity (What?)	Location (Where?)	Frequency (When?)	Measured variables
Stream Monitoring	Discrete water samples for chemistry analysis	[TENTATIVE] Middle (MCS), Scotts Creek (SCS, TLS), Clover Creek Bypass (ACS); Adobe, Kelsey (KCS, KCU), Manning, Cole, Hill	During storms	Total Nutrients (TN, TKN, TP), NO3, Total Suspended Solids (TSS) + profile (Temp, DO, pH, Conductivity, TDS) (first flush with metals and TOC)
	Gaging stations of continuous variables	ACS, TLS, Cole Creek near Mt. Konocti, Burns Valley Creek (4 new stations), MSC, SCS, KCS, Adobe	15 min	Temperature, flow, turbidity
	Fish surveys & tagging; Fish habitat assessment			
Lake Monitoring	Discrete water samples for biogeochemical analysis & profiles	3 sites, 3 depths, and profiles	10-11 times/year	Total Nutrients (TN, TKN, TP), NO3, NH4, PO4, DOC, Total Suspended Solids (TSS) (Metals and alkalinity quarterly) & chl-a
	Continuous lake properties	3 sites, multiple depths (6-10 depths depending on each site)	10 min	temperature and dissolved oxygen
	Discrete water samples for phytoplankton & zooplankton identification and enumeration	3 sites, surface for phyto, integrated sample for zoop	7-9 times/year	Phytoplankton, zooplankton
	HABs toxin sampling	20-22 sites plus offshore locations	~2 weeks during HABs season	levels of microcystin cyanotoxins
	Continuous littoral lake properties	3 sites (water treatment plants): Clearlake Oaks, Riviera, Highlands (Lucerne). Mostly surface (some 3 m deep sensors)	Every hour	Temperature, dissolved oxygen, fluorescence (chl-a, phyto)
	Sediment cores	3 sites	10 times/year	Nutrients in the top 10 cm (TP, TN, TKN, NO3, and P speciation)
	Invasive species monitoring	16-20 sites	2-4 times/year	Invasive species enumeration and identification

Category	Activity (What?)	Location (Where?)	Frequency (When?)	Measured variables (What?)
Municipal Water Monitoring (intakes)	Discrete water samples for chemistry analysis at Culverts (MS4)	MS4 - Culverts - 12 sites	During storms?	Total Nutrients (TN, TKN, TP), NO3, Total Suspended Solids (TSS) + profile (Temp,-DO, pH,-Conductivity, TDS, Turbidity) (first flush with metals only 4 sites)
	Cal-WATCH drinking water	Private intakes and wells (locations)		Toxins, metals, pesticides
Shoreline Monitoring	Continuous meteorological data on the shoreline	5 sites in the shoreline (NLP, CLO, BBI, KNB, BKP)	15 min	Air temperature, relative humidity, solar radiation, wind speed and direction, precipitation
	Cal-WATCH drinking water	Private intakes and wells (locations)		Toxins, metals, pesticides
	Cultural burns and biological monitoring	Shoreline, near cultural burns		Biological monitoring
Groundwater Monitoring	Continuous groundwater level	Adobe Creek, Kelsey Creek, other locations?	Every hour or 15 min	Pressure sensors
Special Studies	Fish surveys for abundance			Fish counts
	Fish tissue monitoring		2 times/year (spring and fall)	Toxins, metals, pesticides

The **next steps** include: (1) identifying leaders for each activity, which will allow the development of a budget; (2) selecting mentors to coordinate activities of the scientific program led by the communities; (3) developing protocols; (4) maintain a centralized open-access data repository of data collected; (5) conducting data analysis and interpretation as frequently as possible; (6) using the new data to keep the community informed about water-quality standards, update predictive tools for the lake and load calculations for the creeks, and use these outcomes to guide science-based management decisions.

4. <u>Continue using the newly developed predictive tools for the watershed and in-lake</u>

   The novelty of this project focuses on the **newly developed models** to (1) accurately **anticipate or predict** the creeks and lake, and their combined response to the environmental changes, which will inform lake managers and stakeholders of recurrent or new water-quality challenges; and (2) quantitatively **evaluate** the effectiveness, impacts, and potential unintended consequences of implementing particular restoration strategies. This project represents the initial effort in the development and use of those predictive tools. However, we recommend to **continue using** the newly developed watershed and in-lake models in Clear Lake as we move forward in the task of rehabilitating the lake, which will be facing **new challenges** due to changes in climate and land use, but also to **update their predictive capabilities** by updating model calibration as new monitoring data become available. As an example, the California Natural

Resources Agency has recently funded a modeling effort to couple a mercury model to the water-quality model. This expansion of the Clear Lake's predictive tools will enable State and Federal Agencies to explore lake remediation strategies that ameliorate mercury concentrations accumulated in the lake water and the sediments, that ultimately move to the biota.

5. Improve the biogeochemical water-quality in-lake model to include more complex processes which may be key to correctly predicting cyanobacteria blooms
   - Incorporate dynamic intracellular storage of nutrients for algae dynamics: The current model uses a constant-used defined concentration of nutrients (nitrogen and phosphorus) following a Michaelis-Menten equation. However, we could also test the performance of a dynamic internal nutrient model that allows the phytoplankton to have variable internal nutrient concentrations. Under this model also referred to as "luxury uptake", the user needs to define the upper and lower boundaries of the internal nutrient concentrations for each phytoplankton group.
   - Include nitrogen fixation as part of the nitrogen cycle to contribute to the pool of nitrate when N is the limiting nutrient of phytoplankton growth during the summer.
   - Incorporate dynamic modeling of the sediment fluxes in the sediments, where the mass balance of nutrients are computed in a sediment layer and first-order flux equations are used based on available nutrients at the sediment layer, instead of using fixed sediment nutrient release for any given time.
   - Include the effects of the microbial community dynamics in the sediments on cyanobacteria harmful algal blooms (CHABs). The development of this model component will require the exploration of the structural changes, diversity, and co-occurrence patterns of microbial communities during cyanobacterial blooms.

13 Acknowledgments

We are deeply grateful for the funding received for this study. It was initially (2019-2021) provided by the California Department of Fish and Wildlife (Grant Agreement # P1720013), with further support by the California Natural Resources Agency (Grant Agreement # GF2141-0) between 2021 and 2024. Partial matching funds for Grant GF2141-0 were provided by the U.S. Geological Survey (USGS) Cooperative Water Program. Funds provided to USGS through an inter-agency agreement with the Bureau of Land Management supported some of the sample collection, laboratory analyses, and modeling activities.

We are thankful for the continued support and advice from the Blue Ribbon Committee for the Rehabilitation of Clear Lake, created by Assembly Bill 707 (Aguiar-Curry, Ch. 842, Statutes of 2017) includes representatives from tribes, Lake County, UC Davis, and the Central Valley Regional Water Quality Control Board. It also includes four members appointed by Lake County with expertise in agriculture, economics, environment, and public water supplies.

We are grateful to the Clear Lake Native American tribes who live in the basin to allow us to conduct work on their land: Big Valley Band of Pomo Indians, Scotts Valley Band of Pomo Indians, Habematolel Pomo of Upper Lake, Middletown Rancheria of Pomo Indians, Robinson Rancheria of Pomo Indians, Elem Indian Colony, and Koi Nation of Northern California.

Guidance, advice, and support from members of different Lake County Departments have been also essential. Some examples are Economic Development, Water Resources Department, Agricultural Department, Environmental Health, Public Health, and Vector Control District.

The assistance and support from local stakeholders and water treatment plants have played a significant role in our project: Riviera West Homeowners Assoc Water Treatment Plan, Highlands Water Company, Recycling Center, Nice Mutual Water Co, Worldmark Resort, Clearlake Oaks County Water District, Buckingham Park Water District, Braito's Buckingham Marina, and many others.

We are thankful to all the contributors from the University of California for producing this final report: Micah Swann, Misa W. Terrell, Samantha Sharp, Kanarat Pinkanjananavee, Ruth Thirkill, Nick T. Framsted, Drew Stang, Anne M. Liston, Steven M. Sesma, Keeley C. Martinez, Tina Hammell, Helen Fillmore, Aaron. L. Vanderpool, Lindsay E. Vaughan, Lidia Tanaka, Brandon Berry, Brant Allen, Raph Townsend, Katie Senft, Erik W. Young, Michael Cane, and Shohei Watanabe at UC Davis. We also thank our Business Managers, Carmen Woods and Fatima Garcia.

14 References

14.4 Introduction

Horne, A.J., 1975, The Ecology of Clear Lake Phytoplankton. Lakeport: Clear Lake Algal Research Unit. 116 pp.

Goldstein, J.J., and Tolsdorf, T.N., 1994, An Economic Analysis of Potential Water Quality Improvement in Clear Lake: Benefits and Costs of Sediment Control, Including a Geological Assessment of Potential Sediment Control Levels, USDA Soil Conservation Service Davis and Lakeport Offices.

Richerson, P., and Suchanek, T., 1994, The causes and control of algal blooms in Clear Lake. Clean Lakes Diagnostic/Feasibility Study For Clear Lake, California.

Richerson, P.J., Suchanek, T.H., Zierenberg, R.A., Osleger, D.A., Heyvaert, A.C., Slotton, D.G., Eagles-Smith, C.A., Vaughn, C.E., 2008, Anthropogenic Stressors and Changes in the Clear Lake Ecosystem as Recorded in Sediment Cores: Ecol. Appl., v.18, p. A257–A283. https://doi.org/10.1890/06-1458.1

Suchanek, T.H., 2008, Mercury cycling and bioaccumulation in a mine-dominated aquatic ecosystem: Clear Lake, California: Ecological Applications, v. 18(8). https://www.jstor.org/stable/i27645923

Tetra Tech, 2004, Total Maximum Daily Load for Nutrients in Clear Lake, Lake County, California, Technical Report (Draft). Prepared for the Central Valley Regional Water Quality Control Board http://www.waterboards.ca.gov/centralvalley/programs/tmdl/ClearLake/ClkDraftTechTMDL.pdf

Thirkill, R., Forrest, A. L., Schladow, S. G., and Sadro, S., 2021, Trends in nitrogen and phosphorus across decades in Clear Lake, CA. Water quality report.

Winder, M., Reuter, J., and Schladow, S. G., 2010, Clear Lake Historical Data Analysis.

14.5 Upper Watershed Monitoring (USGS)

Stream Discharge

Richerson, P., Suchanek, T., and Why, S.J., 1994, The causes and control of algal blooms in Clear Lake—Clean Lakes Diagnostic/Feasibility Study For Clear Lake, California: Lake County Flood Control and Water Conservation District, California State Water Resources Control Board, and U.S. Environmental Protection Agency, prepared by authors under contract, 182 p., http://www.des.ucdavis.edu/Faculty/richerson/CleanLakesReport1994.pdf.

Smith, P.E., 2006, A Semi-Implicit, Three-Dimensional Model for Estuarine Circulation: U.S Geological Survey Open-File Report 2006-1004, 176 p. https://pubs.usgs.gov/of/2006/1004/

Turnipseed, D.P., and Sauer, V.B., 2010, Discharge measurements at gaging stations: U.S. Geological Survey Techniques and Methods book 3, chap. A8, 87 p., https://doi.org/10.3133/tm3A8

U.S. Geological Survey, [2024], USGS water data for the Nation: U.S. Geological Survey National Water Information System database, accessed [April 8, 2024], at https://doi.org/10.5066/F7P55KJN

Wahl, K.L., Thomas, W.O., Jr., and Hirsch, R.M., 1995, Data-collection process, in Stream-gaging program of the U.S. Geological Survey: U.S. Geological Survey Circular 1123, https://pubs.usgs.gov/circ/circ1123/collection.html

Water Quality

Fishman, M.J., ed., 1993, Methods of analysis by the U.S. Geological Survey National Water Quality Laboratory—Determination of inorganic and organic constituents in water and fluvial sediments: U.S. Geological Survey Open-File Report 93-125, 217 p., accessed October 1, 2021, at https://doi.org/10.3133/ofr93125

Fishman, M.J., and Friedman, L.C., 1985, Methods for the determination of inorganic substances in water and fluvial sediments: U.S. Geological Survey Open-File Report 85-495, 709 p.,

https://doi.org/10.3133/ofr85495

Kamphake, L.J., Hannah, S.A., and Cohen, J.M., 1967, Automated analysis for nitrate by hydrazine reduction: Water Research, v. 1, p. 205–219.

Kempers, A.J., and Luft, A.G., 1988, Re-examination of the determination of environmental nitrate as nitrite by reduction with hydrazine: Analyst, v. 113, p. 3–6.

Liddicoat, M.I., Tibbits, S., and Butler, E.I., 1975, The determination of ammonia in seawater: Limnology and Oceanography, v. 20, p. 131–132.

Murphy, J., and Riley, J.P., 1962, A modified single-solution method for the determination of phosphate in natural waters: Analytica Chemica Acta, v. 27, p. 31–36.

Redfield, A.C., 1958, The biological control of chemical factors in the environment: American Scientist, v. 46, p. 205–221.

Solorzano, L., 1969, Determination of ammonia in natural waters by the phenolhypochlorite method: Limnology and Oceanography, v. 14, p. 799–801.

Strickland, J.D.H., and Parsons, T.R., 1972, A Practical Handbook of Seawater Analysis (2nd ed.): Ottawa, Ontario, Canada, Fisheries Research Board of Canada Bulletin 168., 310 p.

Sushch, D., Alpers, C.N., Watanabe, P.T., Bennett, P.A., Brewster, G.D., Hansen, A., Le, A.K., Marvin-DiPasquale, M.C., Agee, J.L., Kieu, L., Kakouros, E., DePalma-Dow, A., Beaton, J., Liston, A.M., Sesma, S.M., Martinez, K.C., Cortes, A., and Schladow, S.G., 2025, Geochemical data for selected streams in the Clear Lake basin, Lake County, California: U.S. Geological Survey data release, https://doi.org/10.5066/P9AKO3CG

U.S. Geological Survey, [2024], USGS water data for the Nation: U.S. Geological Survey National Water Information System database, accessed [April 8, 2024], at https://doi.org/10.5066/F7P55KJN

14.6 Upper Watershed Modeling (USGS)

LOADEST

Hurvich, C.M., and Tsai, C.-L., 2019, Regression and time series model selection in small samples: Biometrika, v. 76, p. 297-307. https://doi.org/10.1093/biomet/76.2.297

Jain, S.K. and Sudheer, K.P., 2008, Fitting of Hydrologic Models: A Close Look at the Nash-Sutcliffe Index, Journal of Hydrologic Engineering, 13:981-986, https://doi.org/10.1061/(ASCE)1084-0699(2008)13:10(981)

Runkel, R., Crawford, C.G., and Cohn, T.A., 2004, Load Estimator (LOADEST): A FORTRAN Program for Estimating Constituent Loads in Streams and Rivers, U.S. Geological Survey, Techniques and Methods Book 4, Chapter A5. https://pubs.usgs.gov/publication/tm4A5

Saleh, D.K., and Alpers, C.N, 2025, Modeling of nutrient and sediment concentrations and loads for Clear Lake CA, using RLOADEST, U.S. Geological Survey data release, https://doi.org/10.5066/P1MHGVGR

Sushch, D., Alpers, C.N., Watanabe, P.T., Bennett, P.A., Brewster, G.D., Hansen, A., Le, A.K., Marvin-DiPasquale, M.C., Agee, J.L., Kieu, L., Kakouros, E., DePalma-Dow, A., Beaton, J., Liston, A.M., Sesma, S.M., Martinez, K.C., Cortes, A., and Schladow, S.G., 2025, Geochemical data for selected streams in the Clear Lake basin, Lake County, California: U.S. Geological Survey data release, https://doi.org/10.5066/P9AKO3CG

Wetzel, R.G., 2001, Limnology, Lake and River Ecosystems, Third Edition, Academic Press, 1006 p.

SPARROW

Alexander, R.B., Schwarz, G.E., and Boyer, E.W., 2019, Advances in quantifying streamflow variability across continental scales: 1. Identifying natural and anthropogenic controlling factors in the USA using a spatially explicit modeling method, Water Resources Research, 55,

https://doi.org/10.1029/2019WR025001.

Alexander, R.B., Schwarz, G.E., Boyer, E.W., Nolan, J.V., and Brakebill, J.W., 2008, Differences in phosphorus and nitrogen delivery to the Gulf of Mexico from the Mississippi River basin, Journal of Environmental Science and Technology, 42, 3, pp. 647-976, https://doi.org/10.1021/es0716103

De Palma-Dow, A., McCullough, I.M., and Brentrup, J.A., 2022, Turning up the heat: Long-term water quality responses to wildfires and climate change in a hypereutrophic lake, Ecosphere https://doi.org/10.1002/ecs2.4271

Falcone, J.A., 2021, Estimates of county-level nitrogen and phosphorus from fertilizer and manure from 1950 through 2017 in the conterminous United States: U.S. Geological Survey Open-File Report 2020-1153, 20 p., https://doi.org/10.3133/ofr20201153

Gronberg, J.M., and Arnold, T.L., 2017, County-level estimates of nitrogen and phosphorus from animal manure for the conterminous United States, 2007 and 2012: U.S. Geological Survey Open-File Report 2017–1021, 6 p., https://doi.org/10.3133/ofr20171021

Gronberg, J.M., and Spahr, N.E., 2012, County-level estimates of nitrogen and phosphorus from commercial fertilizer for the conterminous United States, 1987–2006: U.S. Geological Survey Scientific Investigations Report 2012-5207, 20 p., https://doi.org/10.3133/sir20125207

Horne, A.J., and Goldman, C.R., 1972, Nitrogen fixation in Clear Lake California. I. Seasonal variation and the role of heterocysts, Limnology and Oceanography, v. 17(5), p. 678–692, https://doi.org/10.4319/lo.1972.17.5.0678

Miller, O.L., Putnam, A.L., Alder, J., Miller, M., Jones, D.K., and Wise, D.R., 2021a, Changing climate drives future streamflow declines and challenges in meeting water demand across the southwestern United States, Journal of Hydrology X, 11, article 100074, https://doi.org/10.1016/j.hydroa.2021.100074

Miller, O.L., Miller, M.P., Longley, P.C., Alder, J.R., Bearup, L.A., Pruitt, T., Jones, D.K., Putman, A.L., Rumsey, C.A., and McKinney, T., 2021b, How will base flow respond to climate change in the Upper Colorado River Basin? GeophysicalResearch Letters, 48, article e2021GL095085, https://doi.org/10.1029/2021GL095085

Dewitz, J., and U.S. Geological Survey, 2021, National Land Cover Database (NLCD) 2019 Products (ver. 3.0, February 2024): U.S. Geological Survey data release, https://doi.org/10.5066/P9KZCM54

Schmadel, N.M., and Peterman-Phipps, C.L., 2023, Monthly inorganic nitrogen atmospheric wet deposition estimates for the conterminous United States, 1999 through 2020: U.S. Geological Survey data release, https://doi.org/10.5066/P9ZLKCD2

Saleh, D.K., 2025, SPARROW model inputs and simulated Total Nitrogen and Total Phosphorus loads in the Clear Lake watershed, California: U.S. Geological Survey data release, https://doi.org/10.5066/P1HJP5XJ

Schwarz, G.E., Hoos, A.B., Alexander, R.B., and Smith, R.A., 2006, The SPARROW surface water-quality model—Theory, applications and user documentation: U.S. Geological Survey Techniques and Methods, book 6, chap. B3, 248 p., CD-ROM and at https://pubs.usgs.gov/tm/2006/tm6b3/

Schwarz, G.E., and Wieczorek, M.E., 2018, Database of modified routing for NHDPlus version 2.1 flowlines: ENHDPlusV2_us: U.S. Geological Survey data release, https://doi.org/10.5066/P9PA63SM

Smith, R.A., Schwarz, G.E., and Alexander, R.B., 1997, Regional interpretation of water-quality monitoring data, Water Resources Research, 33:2781-2798, https://doi.org/10.1029/97WR02171

White, D.A., Smith, R.A., Price, C.V., Alexander, R.B., and Robinson, K.W., 1992, A spatial model to aggregate point-source and nonpoint-source water-quality data for large areas, Computers and Geosciences, 18:1055-1073, https://doi.org/10.1016/0098-3004(92)90021-I

Wieczorek, M.E., Staub, L.E., and Schwarz, G.E., 2024, Attributes for NHDPlus Version 2.1 catchments and modified routing of upstream watersheds for the conterminous United States; riparian National Land Cover Data for 2019 versions for the years 2001, 2004, 2006, 2008, 2011, 2013, 2016, and 2019: U.S.

Geological Survey data release, https://doi.org/10.5066/P9529PKE

Wieczorek, M.E., Jackson, S.E., and Schwarz, G.E., 2018, Select attributes for NHDPlus Version 2.1 reach catchments and modified network routed upstream watersheds for the conterminous United States (ver. 4.0, August 2023): U.S. Geological Survey data release, https://doi.org/10.5066/F7765D7V

Wise, D.R., 2019, Spatially referenced models of streamflow and nitrogen, phosphorus, and suspended-sediment loads in streams of the Pacific region of the United States, U.S. Geological Survey Scientific Investigations Report 2019-5112, 64 p., https://doi.org/10.3133/sir20195112

HSPF

Bicknell, B.R., Imhoff, J.C., Kittle, J.L., Jr., Donigian, A.S., Jr., and Johanson, R.C., 2001, Hydrologic Simulation Program—FORTRAN, User's Manual for Version 12: AQUA TERRA Consultants, Mountain View, CA, USA, 845 p.

Bond, S., and Curtis, J.A., 2024, Geospatial mapping products derived from 2018, 2020, and 2022 NAIP aerial imagery for the Scotts Creek Watershed, Lake County, CA: U.S. Geological Survey data release, https://doi.org/10.5066/P13VNUF7.

Ewing, B., 2014, Upper Blue Lake General Fish Survey, Spring: California Department of Fish and Wildlife, https://www.nrm.dfg.ca.gov/FileHandler.ashx?DocumentID=91244.

Jennings, C.W., with modifications by Gutierrez, C., Bryant, W., Saucedo, G., and Wills, C., 2010, Geologic map of California: California Geological Survey, Geologic Data Map No. 2, scale 1:750,000.

Krantz, W., Pierce, D., Goldenson, N. and Cayan, D., 2021, Memorandum on evaluating global climate models for studying regional climate change in California: California Energy Commision, Electric Program Investment Charge (EPIC) Program, 24 p.

Rahimi, S., Huang, L., Norris, J., Hall, A., Goldenson, N., Krantz, W., Bass, B., Thackeray, C., Lin, H., Chen, D. and Dennis, E., 2023, An overview of the western united states dynamically downscaled dataset (wus-d3): Geoscientific Model Development Discussions, p. 1–56.

Richerson, P.J., Suchanek, T.H., and Why, S.J., 1994, The causes and control of algal blooms in Clear Lake, Final report: University of California, Davis, 182 p.

Singer, M.B., Asfaw, D.T., Rosolem, R., Cuthbert, M.O., Miralles, D.G., MacLeod, D., Quichimbo, E.A., and Michaelides, K., 2021, Hourly potential evapotranspiration at 0.1 resolution for the global land surface from 1981-present: Scientific Data, v. 8, no. 1, 224 p.

Soil Survey Staff, Natural Resources Conservation Service, United States Department of Agriculture. Web Soil Survey. Available online at https://websoilsurvey.nrcs.usda.gov/

Stern, M., Flint, L., Minear, J., Flint, A., and Wright, S., 2016, Characterizing changes in streamflow and sediment supply in the Sacramento River Basin, California, using hydrological simulation program—FORTRAN (HSPF): Water, v. 8, no. 10, 432 p.

Stern, M.A., 2025, Historical and future simulated streamflow and sediment loads from Clear Lake tributaries in California: U.S. Geological Survey data release, https://doi.org/10.5066/P13ZPMAD

Sushch, D., Alpers, C.N., Watanabe, P.T., Bennett, P.A., Brewster, G.D., Hansen, A., Le, A.K., Marvin-DiPasquale, M.C., Agee, J.L., Kieu, L., Kakouros, E., DePalma-Dow, A., Beaton, J., Liston, A.M., Sesma, S.M., Martinez, K.C., Cortes, A., and Schladow, S.G., 2025, Geochemical data for selected streams in the Clear Lake basin, Lake County, California: U.S. Geological Survey data release, https://doi.org/10.5066/P9AKO3CG

Tetra Tech, 2004, Total Maximum Daily Load for Nutrients in Clear Lake, Lake County, California Technical Report: Prepared for Central Valley Regional Water Quality Control Board, 98 p.

U.S. Environmental Protection Agency [EPA], 2024, Basins Framework and Features: U.S. Environmental Protection Agency, accessed December 4, 2024, at https://www.epa.gov/hydrowq/basins-framework-and-features

U.S. Environmental Protection Agency [EPA], 2006, Sediment Parameter and Calibration Guidance for HSPF; EPA BASINS Technical Note 8: Office of Water, Washington, DC, 43 p.

U.S. Environmental Protection Agency [EPA], 2000, Estimating Hydrology and Hydraulic Parameters for HSPF; EPA BASINS Technical Note 6: Office of Water, Washington, DC, 32 p.

U.S. Geological Survey, [2024a], 3D Elevation Program 1/3 Arc Second Resolution Digital Elevation Model, accessed October 29, 2022 at URL https://www.usgs.gov/the-national-map-data-delivery

U.S. Geological Survey, [2024b], National Hydrography Dataset (ver. USGS National Hydrography Dataset Plus V2 (NHDPlus V2), accessed April 23, 2022 at URL https://www.epa.gov/waterdata/get-nhdplus-national-hydrography-dataset-plus-data

Xia, Y., Mitchell, K., Ek, M., Sheffield, J., Cosgrove, B., Wood, E., Luo, L., Alonge, C., Wei, H., Meng, J. and Livneh, B., 2012, Continental-scale water and energy flux analysis and validation for the North American Land Data Assimilation System project phase 2 (NLDAS-2); 1. Intercomparison and application of model products: Journal of Geophysical Research Atmospheres, v. 117, no. D3.

Sediment Fingerprinting

Babyak, M.A., 2004, What you see may not be what you get: A brief, nontechnical introduction to overfitting in regression-type models: Psychosomatic Medicine, v. 66, no. 3, p. 411-421.

Beckman Coulter Inc., 2019, User's Manual, LS 13–320 Laser diffraction particle size analyzer: PN B05577AD, Brea, Calif., Beckman Coulter Inc., 266 p. https://www.beckman.com/particle-size-analyzers/ls-13-320

Carter, J., Owens, P.N., Walling, D.E., and Leeks, G.J.L., 2003, Fingerprinting suspended sediment sources in a large urban river system: Science of the Total Environment, v. 314-316, p. 513-534. https://doi.org/10.1016/S0048-9697(03)00071-8

Cashman, M.J., Gellis, A., Gorman Sanisaca, L., Noe, G.B., Cogliandro, V., and Baker, A., 2018, Bank-derived material dominates fluvial sediment in a suburban Chesapeake Bay watershed: River Research and Applications, v. 34, p. 1032-1044. https://doi.org/10.1002/rra.3325

Collins, A.L., Blackwell, M., Boeckx, P. et al., 2020, Sediment source fingerprinting: benchmarking recent outputs, remaining challenges and emerging themes. Journal of Soils and Sediments, v. 20, p. 4160–4193. https://doi.org/10.1007/s11368-020-02755-4

Collins A.L., Zhang, Y.S., Walling, D.E., and Black, K., 2010, Apportioning sediment sources in a grassland dominated agricultural catchment in the UK using a new tracing framework. In: Banasik, K., Horowitz, A.J., Owens, P.N., Stone, M., Walling, D.E. (eds.) Sediment dynamics for a changing future. IAHS Publication 337, IAHS Press, Wallingford, p. 68

Collins A.L., Zhang Y.S., Duethmann, D., Walling, D.E., and Black, K., 2013, Using a novel tracing-tracking framework to source fine-grained sediment loss to watercourses at sub-catchment scale: Hydrological Processes, v. 27, p. 959–974. https://doi.org/10,.1002/hyp.9652

Collins, A., Zhang, Y., McChesney, D., Walling, D.E., Haley, S.M., and Smith, P., 2012, Sediment source tracing in a lowland agricultural catchment in southern England using a modified procedure combining statistical analysis and numerical modelling: Science of the Total Environment, v. 414, p. 301–317. https://doi.org/10.1016/j.scitotenv.2011.10.062

Collins, A.L., Pulley, S., Foster, I.D.L., Gellis, A., Porto, P., and Horowitz, A.J., 2017, Sediment source fingerprinting as an aid to catchment management: A review of the current state of knowledge and a methodological decision-tree for end-users: Journal of Environmental Management, v. 194, p. 86-108. https://doi.org/10.1016/j.jenvman.2016.09.075

Cooper, R.J., Krueger, T., Hiscock, K.M., and Rawlins, B.G., 2014, Sensitivity of fluvial sediment source apportionment to mixing model assumptions: A Bayesian model comparison: Water Resources Research, v. 50, no. 11, p. 9031-9047. https://doi.org/10.1002/2014WR016194

Cotrufo, M.F., Boot, C., Abiven, S., Foster, E.J., Haddix, M., Reissner, M., Wurster, C.M., Bird, M.I., and Schmidt, M.W.I., 2016, Quantification of pyrogenic carbon in the environment: An integration of analytical

approaches: Organic Chemistry, v. 100, p. 42-50. https://doi.org/10.1016/j.orggeochem.2016.07.007

Curtis, J.A., Flint, L.E., Alpers, C.N., and Yarnell, S.M., 2005, Conceptual model of sediment processes in the upper Yuba River watershed, Sierra Nevada, CA: Geomorphology, v. 68, p. 149–166. http://doi.org/10.1016/j.geomorph.2004.11.019

De Palma-Dow, A., McCullough, I.M., and Brentrup, J.A., 2022, Turning up the heat: Long-term water quality responses to wildfires and climate change in a hypereutrophic lake: Ecosphere, v. 13, e4271. https://doi.org/10.1002/ecs2.4271

Dewitz, J., 2023, National Land Cover Database (NLCD) 2021 Products: U.S. Geological Survey data release, https://doi.org/10.5066/P9JZ7AO3

East, A.E., Logan, J.B., Dartnell, P., Dow, H.W., Lindsay, D.N., and Cavagnaro, D.B., 2025, Post-fire sediment yield from a western Sierra Nevada watershed burned by the 2021 Caldor fire: Earth and Space Science, v. 12, e2024EA003939. https://doi.org/10.1029/2024EA003939

East, A.E., Logan, J.B., Dow, H.W., Smith, D.P., Iampietro, P., Warrick, J.A., Lorenson, T.D., Hallas, L., and Kozlowicz, B., 2024, Post-Fire sediment yield from a central California watershed: field measurements and validation of the WEPP model: Earth and Space Science, v.11, e2024EA003575. https://doi.org/10.1029/2024EA003575

Essene, E.J., Fyfe, W.S., and Turner, F.J., 1965, Petrogenesis of Franciscan glaucophane schists and associated metamorphic rocks, California: Beiträge zur Mineralogie und Petrographie. v. 11, p. 695–704. https://doi.org/10.1007/BF01128709

Evrard, O., Poulenard, J., Némery, J., Ayrault, S., Gratiot, N., Duvert, C., Prat, C., Lefévre, I., Bonté, P., and Esteves, M., 2013, Tracing sediment sources in a tropical highland catchment of central Mexico by using conventional and alternative fingerprinting methods: Hydrological Processes, v. 27, p. 911–922. https://doi.org/10.1002/hyp.9421

Feyrer, F., Whitman, G., Young, M., and Johnson, R.C., 2019, Strontium isotopes reveal ephemeral streams used for spawning and rearing by an imperilled potamodromous cyprinid Clear Lake hitch Lavinia exilicauda chi: Marine and Freshwater Research, v. 70, p. 1689–1697. https://doi.org/10.1071/MF18264

Gelhardt, L., Kuch, B., Dittmer, U., and Welker, A., 2021, Granulometric distribution of metals in road-deposited sediments by using different sieving methods: Environmental Advances, v. 5, 100094. https://doi.org/10.1016/j.envadv.2021.100094

Gellis, A.C., Fitzpatrick, F., and Schubauer-Berigan, J., 2016, A manual to identify sources of fluvial sediment: U.S. Environmental Protection Agency report. EPA/600/R-16/210, 106 p., accessed July 29, 2024, at https://clu-in.org/download/contaminantfocus/sediments/Sediment-sources-600R16210.pdf

Gellis, A.C., Gorman Sanisaca, L.E., and Cashman, M.J., 2018, Sediment source assessment using sediment fingerprints. U.S. Geological Survey Fact Sheet 2018-3008. https://pubs.usgs.gov/fs/2018/3008/fs20183008.pdf

Gellis, A.C., Noe, G.B., Clune, J.W., Myers, M.K., Hupp, C.R., Schenk, E.R., and Schwarz, G.E., 2015, Sources of finegrained sediment in the Linganore Creek watershed, Frederick and Carroll Counties, Maryland, 2008–10: U.S. Geological Survey Scientific Investigations Report 2014–5147, 56 p. http://dx.doi.org/10.3133/sir20145147

Gorman Sanisaca, L.E., Gellis, A.C., and Lorenz, D.L., 2017, Determining the sources of fine-grained sediment using the Sediment Source Assessment Tool (Sed_SAT): U.S. Geological Survey Open File Report 2017–1062, 104 p. https://doi.org/10.3133/ofr20171062

Green, S.B., 1991, How many subjects does it take to do a regression analysis: Multivariate Behavioral Research, v. 26, no. 3, p.499-510. https://doi.org/10.1207/s15327906mbr2603_7

Hammersley, L., and DePaolo, D.J., 2006, Isotopic and geophysical constraints on the structure and evolution of the Clear Lake volcanic system: Journal of Volcanology and Geothermal Research, v. 153, p. 331-356. https://doi.org/10.1016/j.jvolgeores.2005.12.003

Harrell, F.E., Jr., 2001, Regression Modeling Strategies-With Applications to Linear Models,

Logistic Regression, and Survival Analysis: Springer, New York, 568 p.

Hearn, B.C., Donnelly-Nolan, J.M., and Goff, F.E., 1995, Geologic map and structure sections of the Clear Lake Volcanics, northern California: U.S. Geological Survey Miscellaneous Investigations Map I-2362, 3 sheets, scale 1:24,000. https://pubs.usgs.gov/imap/2362/

Helsel, D.R., Hirsch, R.M., Ryberg, K.R., Archfield, S.A., and Gilroy, E.J., 2020, Statistical methods in water resources: U.S. Geological Survey Techniques and Methods, book 4, chapter A3, 458 p. https://doi.org/10.3133/tm4a3

Horowitz, A.J., and Elrick, K.A., 1987, The relation of stream sediment surface area, grain size, and composition to trace element chemistry: Applied Geochemistry, v. 2, p. 437–451. https://doi.org/10.1016/0883-2927(87)90027-8

Horowitz, A.J., Stephens, V.C., Elrick, K.A., and Smith, J.A., 2012, Annual fluxes of sediment-associated trace/major elements, carbon, nutrients, and sulfur from US coastal rivers, in Erosion and Sediment Yields in the Changing Environment: proceedings of the 2012 International Commission on Continental Erosion International Symposium, Chengdu, China, 11-15 October 2012, International Association of Hydrological Sciences, publication 356. https://iahs.info/uploads/dms/15790.10-39-48-356-04-ICCE2012_Arthur-J.-Horowitz--2--Corr.pdf

Ingre, M., 2013, Why small low-powered studies are worse than large high-powered studies and how to protect against "trivial" findings in research: Comment on Friston (2012). NeuroImage: 81, p. 496–498. https://doi.org/10.1016/j.neuroimage.2013.03.030

Kalra, I., Stewart, B.P., Florea, K.M., Smith, J., Webb, E.A., and Caron, D.A., 2025, Temporal and spatial dynamics of harmful algal bloom-associated microbial communities in eutrophic Clear Lake, California: Applied and Environmental Microbiology, v. 91, e00011-25. https://doi.org/10.1128/aem.00011-25

Linn, A.M., DePaolo, D.J., Ingersoll, R.V., 1992, Nd–Sr isotopic, geochemical, and petrographic stratigraphy and paleotectonic analysis—Mesozoic Great Valley fore-arc sedimentary rocks of California: Geological Society of America Bulletin, v. 104, p. 1,264–1,279. https://doi.org/10.1130/0016-7606(1992)104<1264:NSIGAP>2.3.CO;2

Liu, Q., Li, P., Jiang, L., Jin, Z., Liang, X., Zhu, D., Pang, Q., Zhang, R, and Liu, J., 2024, Distinctive volcanic ash–rich lacustrine shale deposition related to chemical weathering intensity during the Late Triassic: Evidence from lithium contents and isotopes: Science Advances, v. 10 (11), https://doi.org/10.1126/sciadv.adi6594

Lundquist, E., and Smythe, T., 2010, Clear Lake Integrated Watershed Management Plan: County of Lake, Department of Public Works, Water Resources Division, prepared for West Lake and East Lake Resource Conservation Districts, Lakeport, California. Accessed July 31, 2024 at: https://www.lakecountyca.gov/1130/Clear-Lake-Integrated-Watershed-Manageme

Marvin-DiPasquale, M.C., Alpers, C.N., Agee, J.L., Kieu, L.H., Kakouros, Evangelos, Sadro, Steven, Framsted, N.T., and Baesman, S.M., 2021, The Geochemistry of Mercury and Other Constituents in Redox Manipulated Sediment Cores from Clear Lake, Lake County, California. U.S. Geological Survey data release. https://doi.org/10.5066/P9REF3QV

McLaughlin, R.J., Moring, B.C., Hitchcock, C.S., and Valin, Z.C., 2018, Framework geologic map and structure sections along the Bartlett Springs fault zone and adjacent area from Round Valley to Wilbur Springs, northern Coast Ranges, California, U.S. Geological Survey, Scientific Investigations Map SIM-3395, 1:100,000. https://doi.org/10.3133/sim3395.

McVey, C.J., 2023, Determining chemical and mineral signatures in mine waste from Sulphur Bank Mercury Mine, Lake County, California. M.Sc. thesis, Department of Geology, California State University, Sacramento, CA. https://hdl.handle.net/20.500.12741/rep:11946

McVey, C.J., Alpers, C.N., Benzel, W.M., Foster, A.L., Whitacre, S., and Basta, N., 2023, Geochemical and

mineralogical data for mine waste from Sulphur Bank Mercury Mine, Lake County, California. U.S. Geological Survey data release. https://doi.org/10.5066/P93EDIQQ

Miller, J.R., and Orbock Miller, S.M., 2007, Contaminated rivers: a geomorphological-geochemical approach to site assessment and remediation. Springer Science & Business Media, Berlin, 418 p.

Miller, J.R., Macklin, G., and Orbock Miller, S.M., 2015, Application of Geochemical Tracers to Fluvial Sediment. Springer Briefs in Earth Science, 142 p. https://link.springer.com/chapter/10.1007/978-3-319-13221-1_2

Monitoring Trends in Burn Severity, 2025, MTBS. https://www.mtbs.gov/ (accessed October 13, 2021)

Mukundan R., Walling, D., Gellis, A., Slattery, M., and Radcliffe, D., 2012, Sediment source fingerprinting: transforming from a research tool to a management tool. Journal of the American Water Resources Association, v. 48, p. 1241–1257. https://doi.org/10.1111/j.1752-1688.2012.00685.x

Nelson, B.K., 1995, Fluid flow in subduction zones: evidence from Nd- and Sr-isotope variations in metabasalts of the Franciscan complex, California: Contributions to Mineralogy and Petrology, v. 119, p. 247-262. https://link.springer.com/content/pdf/10.1007/BF00307285.pdf

Paerl, H.W., Fulton, R.S., Moisander, P.H., and Dyble, J., 2001, Harmful freshwater algal blooms, with an emphasis on cyanobacteria: The Scientific World Journal, v.1, p.76-113. https://doi.org/10.1100/tsw.2001.16

Phan, T.T., Capo, R.C., Stewart, B.W., Macpherson, G.L., Rowan, E.L., and Hammack, R.W., 2016, Factors controlling Li concentration and isotopic composition in formation waters and host rocks of Marcellus Shale, Appalachian Basin: Chemical Geology, v. 420, p. 162-179. https://doi.org/10.1016/j.chemgeo.2015.11.003

Rowan, J.S., Black, S., and Franks, S.W., 2012, Sediment fingerprinting as an environmental forensics tool explaining cyanobacteria blooms in lakes: Applied Geography, v. 32, p. 832-843. https://doi.org/10.1016/j.apgeog.2011.07.004

Ryan, C.E., 2018, Burned Area Emergency Response, Mendocino Complex Fire, Watershed Modeling Report, 12 p. https://www.blm.gov/sites/blm.gov/files/uploads/Programs_Fire_California_Watershed_Modeling_Report-Mendocino-Complex-Fire.pdf

Saucedo, G.J., Bedford, D.R., Raines, G.L., Miller, R.J., and Wentworth, C.M., 2000, Digital Data for the Geologic Map of California by Charles Jennings, California Geological Survey, Digital data

Shelton, L.R., and Capel, P.D., 1994, Guidelines for collecting and processing samples of stream bed and sediment for analysis of trace elements and organic contaminants for the National Water-Quality Assessment Program: U.S. Geological Survey Open-File Report 94–458. http://water.usgs.gov/nawqa/pnsp/pubs/ofr94-458/

Sims, J.D., and White, D.E., 1982, Mercury in the sediments of Clear Lake: U.S. Geological Survey Professional Paper 1141, p. 237-241. https://doi.org/10.3133/pp1141

Small, I.F., Rowan, J.S., Franks, S.W., Wyatt, A., and Duck, R.W., 2004, Bayesian sediment fingerprinting provides a robust tool for environmental forensic geoscience application. In: Pye, K., and Croft, D.J., (eds.) Forensic geoscience: principles, techniques, and applications, v. 232. Geological Society, London, Special Publications, p. 207–213.

Stewart, H.A., Massoudieh, A., and Gellis, A., 2015, Sediment source apportionment in Laurel Hill Creek, PA, using Bayesian chemical mass balance and isotope fingerprinting: Hydrological Processes, v. 29, no. 11, p. 2545-2560, http://dx.doi.org/10.1002/hyp.10364

Stock, B.C., Jackson, A.L., Ward, E.J., Parnell, A.C., Phillips, D.L., and Semmens, B.X., 2018, Analyzing mixing systems using a new generation of Bayesian tracer mixing models: PeerJ Preprints, v. 6, e5096. https://doi.org/10.7287/peerj.preprints.26884v1

Suchanek, T.H., Eagles-Smith, C.A., Slotton, D.G., Harner, E.J., and Adam, D.P., 2008, Mercury in abiotic matrices of Clear Lake, California: human health and ecotoxicological implications: Ecological

Applications, v. 18, no. 8 Supplement, p. A128-A157.

Sun, H., Nelson, M., Chen, F., and Husch, J., 2009, Soil mineral structural water loss during loss on ignition analyses: Canadian Journal of Soil Science, v. 89, p. 603-610. https://doi.org/10.4141/CJSS09007

Sutherland, R.A., 1998, Loss-on-ignition estimates of organic matter and relationships to organic carbon in fluvial bed sediments: Hydrobiologia, v. 389, p. 153-167. https://doi.org/10.1023/A:1003570219018

Swann, M.M., Cortes, A., Forrest, A.L., Framsted, N., Sadro, S., Schladow, S.G., and De Palma-Dow, A., 2024, Internal phosphorus loading alters nutrient limitation and contributes to cyanobacterial blooms in a polymictic lake: Aquatic Sciences, v. 86, 46, 22 p. https://doi.org/10.1007/s00027-024-01045-2

Takeda, A., Kimura, K., and Yamasaki, S., 2004, Analysis of 57 elements in Japanese soils, with special reference to soil group and agricultural use: Geoderma, v. 119, p. 291–307. https://doi.org/10.1016/j.geoderma.2003.08.006

University of California, Davis, Stable Isotope Facility (UCD SIF), 2024, Carbon and Nitrogen in Solids. https://stableisotopefacility.ucdavis.edu/carbon-and-nitrogen-solids (accessed December 9, 2024).

U.S. Environmental Protection Agency, 2023, Sulphur Bank Superfund Site OU-1 Proposed Plan, Fact Sheet, 40 p. https://semspub.epa.gov/work/09/100031865.pdf

U.S. Environmental Protection Agency, 2025, TMDL Support Documents. https://www.epa.gov/tmdl/tmdl-support-documents (Accessed July 2, 2025).

U.S. Geological Survey (USGS), 2022, Analytical Chemistry. https://www.usgs.gov/centers/gggsc/science/analytical-chemistry (accessed December 9. 2024).

Van Gosen, B.S., Verplanck, P.L., and Emsbo, P., 2019, Rare earth element mineral deposits in the United States (ver 1.1, April 15, 2019): U.S. Geological Survey Circular 1454, 16 p., https://doi.org/10.3133/cir1454

Walling, D.W., 2005, Tracing suspended sediment sources in catchments and river systems: Science of the Total Environment, v. 344, p. 159–184. https://doi.org/10.1016/j.scitotenv.2005.02.011

Walling, D.E., and Collins, A.L., 2005, Suspended sediment sources in British Rivers, in Walling, D.E., and Horowitz, A.J. (eds.) Sediment Budgets, v.1, International Association of Hydrological Science Publication 291 Wallingford UK, p. 123–133. https://iahs.info/uploads/dms/13016.19%20123-133%20S11-43%20Walling%20&%20Collins.pdf

Walling, D.W., 2013, The evolution of sediment source fingerprinting investigations in fluvial systems: Journal of Soils and Sediments, v. 13, p. 1658-1675. https://doi.org/10.1007/s11368-013-0767-2

Watanabe, P.T., Alpers, C.N., McVey, C.J., Grechkosey, D., Stern, M., Curtis, J.A., Vanderpool, A.L., Liston, A.M., Sesma, S.M., Martinez, K.C., Cortés, A., and Schladow, S.G., 2025, Geochemical and isotopic data for soils and sediments from the Clear Lake drainage basin, Lake County, California. U.S. Geological Survey data release. (ver. 2.0, August 2025) https://doi.org/10.5066/P1DZUNJN

Williamson, T.N., Fitzpatrick, F.A., and Kreiling, R.M., 2023, Building a library of source samples for sediment fingerprinting – Potential and proof of concept: Journal of Environmental Management, v. 333, 117254. https://doi.org/10.1016/j.jenvman.2023.117254

Xu, Z., Belmont, P., Brahney, J., and Gellis, A.C., 2022, Sediment source fingerprinting as an aid to large-scale landscape conservation and restoration: A review for the Mississippi River Basin: Journal of Environmental Management, v. 324, 116260. https://doi.org/10.1016/j.jenvman.2022.116260

Yang, L., Zhang, Y., Kang, S., Wang, Z., and Wu, C., 2021, Microplastics in freshwater sediment: A review on methods, occurrence, and sources: Science of the Total Environment, v. 754, 141948. https://doi.org/10.1016/j.scitotenv.2020.141948

Zhang, Y.S., Collins, A.I., and Horowitz, A.J., 2012, A preliminary assessment of the spatial sources of contemporary suspended sediment in the Ohio River basin, United States, using water quality data from the NASQAN programme in a source tracing procedure: Hydrological Processes, v. 26, p. 326-334.

https://doi.org/10.1002/hyp.8128

Zimmerman, D.W., 1994, A note on the influence of outliers on parametric and nonparametric tests: Journal of General Psychology, v. 121, no. 4, p. 391–401. https://doi.org/10.1080/00221309.1994.9921213

14.7 In-Lake Monitoring (UCD-TERC)

American Public Health Association, 2012, Standard Methods For the Examination of Water and Wastewater, 22nd Edition. APHA, Washington, DC.

Burkholder, J.M., and Wetzel, R.G., 1989, Epiphytic microalgae on natural substrata in a hardwater lake: seasonal dynamics of community structure, biomass and ATP content: Arch. Hydrobiol., Suppl., v. 83, p. 1-56.

Cortés, A., Forrest, A.L., Sadro, S., Stang, D., Swann, M., Framsted, N.T., Thirkill, R., Sharp, S.L., Schladow, S.G., 2021, Prediction of hypoxia in eutrophic polymictic lakes. Water Resour. Res. 57:e2020WR028693, http://dx.doi.org/10.1029/2020WR028693

Cortés, A., Schladow, S.G., Alpers, C., et al., 2022, Summary on metals and metalloids in Clear Lake based on historical data. A report to the Blue Ribbon Committee for the Rehabilitation of Clear Lake. June 2022. https://clearlakerehabilitation.ucdavis.edu/sites/g/files/dgvnsk12236/files/inline-files/2022_Metals%20in%20Clear%20Lake_final.pdf

Cortés, A., Schladow, S.G., Forrest, A., and Sadro, S., 2025, Clear Lake water quality monitoring data from 2019 to 2023 by the University of California, Davis ver 1, Environmental Data Initiative, https://doi.org/10.6073/pasta/4f803082f7906f764994366a9e69c940

Hillebrand, H., Dürselen, C.D., Kirschtel, D. , Pollingher, U., and Zohary, T., 1999, Biovolume calculation for pelagic and benthic microalgae: Journal of Phycology, v. 35, p. 403-424.

Lund, J. W. G., Kipling, C., LeCren, E. D., 1958, The inverted microscope method of estimating algal numbers and the statistical basis of estimates by counting: Hydrobiologia, v. 11, p. 143-170.

McNabb, C. D., 1960, Enumeration of Freshwater Phytoplankton Concentrated on the Membrane Filter: Limnology and Oceanography, v. 5(1), p. 57-61.

Rocha, O., Duncan, A., 1985, The relationship between cell carbon and cell volume in freshwater algal species used in zooplanktonic studies: Journal of Plankton Research, v. 7(2), p. 279–294. https://doi.org/10.1093/plankt/7.2.279

Sharp, S. L., Forrest, A. L., Bouma-Gregson, K., Jin, Y., Cortés, A., Schladow, S. G., 2021, Quantifying scales of spatial variability of cyanobacteria in a large, eutrophic lake using multiplatform remote sensing tools: Front. Environ. Sci., v. 9, p. 23. http://dx.doi.org/10.3389/fenvs.2021.612934

Swann, M., Cortés, A., Forrest, A. L., Framsted, N., Sadro, S., DePalma-Dow, A., Schladow, S. G., 2024, Internal phosphorus loading alters nutrient limitation and contributes to cyanobacterial blooms in a polymictic lake: Aquat. Sci., v. 86, p. 46. http://dx.doi.org/10.1007/s00027-024-01045-2

Swann, M., Schladow, S. G., Forrest, A., Sadro, S., Cortes, A., 2023, Clear Lake Phosphorus Budget 2019-22. A report to the Blue Ribbon Committee for the Rehabilitation of Clear Lake. https://clearlakerehabilitation.ucdavis.edu/sites/g/files/dgvnsk12236/files/inline-files/Clear%20Lake%20P%20Budget%202019_2022%20Final-2.pdf

Valderrama, J. C., 1981, The Simultaneous Analysis of Total Nitrogen and Total Phosphorus in Natural Waters: Marine Chemistry, v. 10, p. 109-122. http://dx.doi.org/10.1016/0304-4203(81)90027-X

14.8 In-Lake Modeling (UCD-TERC)

Hydrodynamic Lake Model: Si3D

Amorocho, J., DeVries, J., 1980, A new evaluation of the wind stress coefficient over water surfaces: Journal of Geophysical Research, v. 85(C1). https://doi.org/10.1029/JC086iC05p04307

Blumberg, A., 1986, Turbulent Mixing Processes in Lakes, Reservoirs, and Impoundments. In W. G. Gray (Ed.), Physics-Based Modeling of Lakes, Reservoirs, and Impoundments ASCE, p. 79–104. Mahwah.

Dorostkar, A., Boegman, L., Pollard, A., 2017, Three-dimensional simulation of high-frequency nonlinear internal wave dynamics in Cayuga Lake: Journal of Geophysical Research: Oceans, v. 122(3), p. 2183–2204. https://doi.org/10.1002/2016JC011862

Martin, J. L., McCutcheon, S. C., 1999, Hydrodynamics and transport for water quality modeling. (S. Wood, Ed.), v. 1. Boca Raton: CRC Press. https://doi.org/10.1128/AAC.03728-14

Murphy, A. H., Epstein, E. S., 1989, Skill Scores and Correlation Coefficients in Model Verification: Monthly Weather Review, v. 117(3), p. 572–582. https://doi.org/10.1175/1520-0493(1989)117<0572:SSACCI>2.0.CO;2

Rueda, F. J., 2001, A three-dimensional hydrodynamic and transport model for lake environments. University of California Davis.

Rueda, F. J., Cowen, E. A., 2005, Residence time of a freshwater embayment connected to a large lake: Limnology and Oceanography, v. 50(5), p. 1638–1653. https://doi.org/10.4319/lo.2005.50.5.1638

Rueda, F. J., MacIntyre, S., 2009, Flow paths and spatial heterogeneity of stream inflows in a small multibasin lake: Limnology and Oceanography, v. 54(6), p. 2041–2057. https://doi.org/10.4319/lo.2009.54.6.2041

Rueda, F. J., Schladow, S. G., 2003, Dynamics of Large Polymictic Lake. II: Numerical Simulations: Journal of Hydraulic Engineering, v. 129(2), p. 92–101. https://doi.org/10.1061/(ASCE)0733-9429(2003)129:2(92

Rueda, F. J., Schladow, S. G., Monismith, S. G., Stacey, M. T., 2005, On the effects of topography on wind and the generation of currents in a large multi-basin lake: Hydrobiologia, v. 532(1), p. 139–151. https://doi.org/10.1007/s10750-004-9522-4

Smith, P. E., 2006, A Semi-Implicit, Three-Dimensional Model for Estuarine Circulation: U.S Geological Survey Open-File Report 2006-1004, 176 p. https://pubs.usgs.gov/of/2006/1004/

Valbuena, S. A., Roberts, D. C., Cortés, A., Largier, J. L., Bombardelli, F. A., Forrest, A., Schladow, S.G., 2022, 3D flow structures during upwelling events in rotationally influenced lakes: Water Resources Research, v. 58, p. e2021WR030666. https://doi.org/10.1029/2021WR030666

Water Quality Model: Si3D-AEM

Boegman, L., Loewen, M. R., Culver, D. A., Hamblin, P. F., Charlton, M. N., 2008, Spatial-Dynamic Modeling of Algal Biomass in Lake Erie: Relative Impacts of Dreissenid Mussels and Nutrient Loads: J. Environ. Eng. ASCE, v. 134, p. 456–468.

Bowie, G., Mills, W., Porcella, D., Campbell, C., Pagenkopk, J., Rupp, G., Johnson, K., and others, 1985, Rates, constants, and kinetics formulations in surface water quality modeling. Tetra Tech, Incorporated. U.S. Environmental Protection Agency. 455p.

Bruce, L., Hamilton, D., Imberger, J., Gal, G., Gophen, M., Zohary, T., Hambright, K., 2006, A numerical simulation of the role of zooplankton in C, N and P cycling in Lake Kinneret, Israel: Ecol. Model., v. 193, p. 412-436.

Bruce, L. C., Frassl, M. A., Arhonditsis, G. B., Gal, G., Hamilton, D. P., Hanson, P. C., Hetherington, A. L., Melack, J. M., Read, J. S., Rinke, K., et al., 2018, A multi-lake comparative analysis of the General

Lake Model (GLM): Stress-testing across a global observatory network: Environ. Model. Softw, v. 102, p. 274–291.

Chapra, S. C., 1997, Surface water-quality modeling. McCraw-Hill, New York, 844p.

Chen, C., Ji, R., Schwab, D. J., Beletsky, D., Fahnenstiel, G. L., Jiang, M., Johengen, T. H., Vanderploeg, H., Eadie, B., Budd, J. W., 2002, A model study of the coupled biological and physical dynamics in Lake Michigan: Ecol. Model., v. 152, p. 145–168.

Egemose, S., Reitzel, K., Andersen, F., Flindt, M. R., 2010, Chemical lake restoration products: Sediment stability and phosphorus dynamics: Environmental Science and Technology, v. 44(3), p. 985–991. https://doi.org/10.1021/es903260y

Hamilton, D. P., Schladow, S. G., 1997, Prediction of water quality in lakes and reservoirs. Part I—Model description: Ecol. Model., v. 96, p. 91–110.

Hipsey, M. R., Gal, G., Antenucci, J. P., Zohary, T., Makler, V., Imberger, J., 2006, Lake Kinneret Water Quality Management System.

Hipsey, M., Bruce, L., Hamilton, D., 2013, Aquatic Ecodynamics (AED) Model Library Science Manual; The University of Western Australia Technical Manual: Perth, Australia, v. 34.

Hipsey, M. R., Bruce, L. C., Boon, C., Busch, B., Carey, C. C., Hamilton, D. P., Hanson, P. C., Read, J. S., De Sousa, E., Weber, M., 2019, A General Lake Model (GLM 3.0) for linking with high-frequency sensor data from the Global Lake Ecological Observatory Network (GLEON): Geosci. Model Dev., p. 473–52.

Hodges, B. R., Imberger, J., Saggio, A., Winters, K. B., 2000, Modeling basin scale waves in a stratified lake: Limnol. Oceanogr., v. 45, p. 1603–1620.

Leon, L. F., Smith, R. E., Hipsey, M. R., Bocaniov, S. A., Higgins, S. N., Hecky, R. E., Antenucci, J. P., Imberger, J. A., Guildford, S. J., 2011, Application of a 3D hydrodynamic–biological model for seasonal and spatial dynamics of water quality and phytoplankton in Lake Erie: J. Great Lakes Res., v. 37, p. 41–53.

Losada, J. P., 2001, A deterministic model for lake clarity. Application to management of Lake Tahoe (California-Nevada), USA. Universittat de Girona.

Marti, C. L., Schroth, A. W., Zia, A., 2019, Physical and biogeochemical processes across seasons in Missisquoi Bay, Lake Champlain: Insights from a three-dimensional model. AGU Fall Meeting, 9-13 December 2019, San Francisco, USA. Oral session. H34C-04.

Missaghi, S., Hondzo, M., 2010, Evaluation and application of a three-dimensional water quality model in shallow lake with complex morphometry: Ecol. Model., v. 221, p. 1512-1525.

Pollingher, U., Berman, T., 1982, Relative contributions of net and nano phytoplankton to primary production in Lake Kinneret (Israel): Arch. Hydrobiol., v. 96, p. 33–46.

Redfield, A. C., 1958, The biological control of chemical factors in the environment: Am. Sci., v. 46, p. 205–221.

Riley, M. J., Stefan, H. G., 1988, MINILAKE: A dynamic lake water quality simulation model: Ecol. Model., v. 43, p. 155–182.

Romero, J. R., Antenucci, J. P., Imberger, J., 2004, One-and three-dimensional biogeochemical simulations of two differing reservoirs: Ecol. Model., v. 174, p. 143–160.

Schladow, S. G., Hamilton, D. P., 1997, Water quality in lakes and reservoirs. Part II—model calibration, sensitivity analysis and application: Ecol. Model., v. 96, p. 111–123.

Steele, J. H., 1982, Environmental control of photosynthesis in the sea: Limnol. Oceanogr., v. 7, p. 137-150.

Wang, Q., Boegman, L., 2021, Multi-year simulation of western Lake Erie hydrodynamics and biogeochemistry to evaluate nutrient management scenarios: Sustainability, v. 13, p. 7516.

15 Appendices

15.5 Upper Watershed Monitoring (USGS)

15.5.1 Nutrient Concentrations at Clear Lake Tributary Sites

Plots of nutrient concentrations at Clear Lake Tributary sites. Plots are arranged by concentration versus flow and concentration versus time. Samples were collected by the U.S. Geological Survey during the duration of the project. Gray shaded areas are the 95% percent confidence interval. All data are available from Sushch et al. (2025).

Cole Creek (CCK)

DP

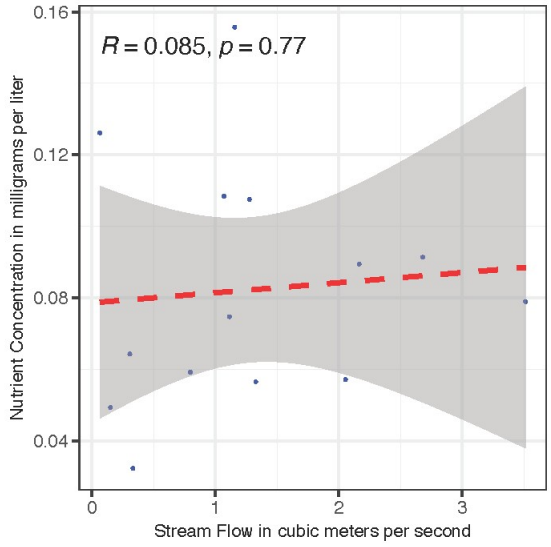

DP

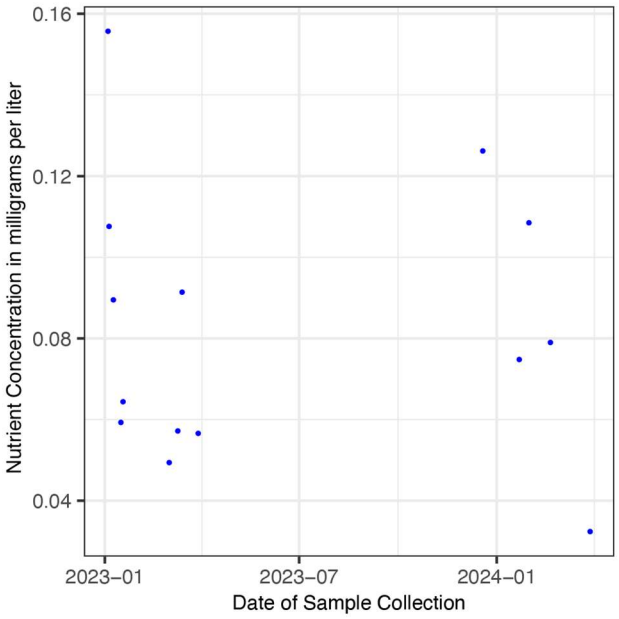

NH4

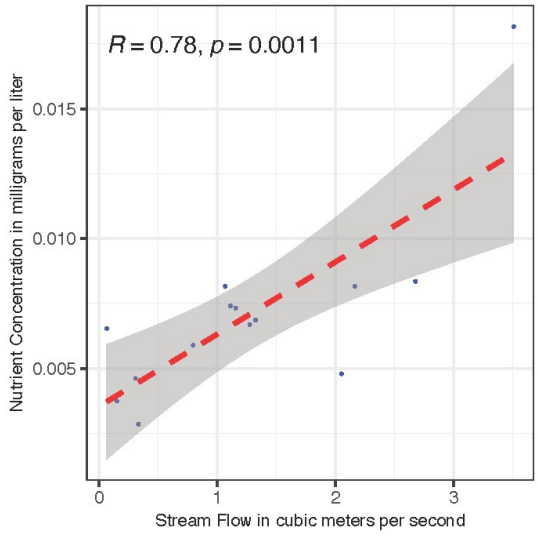

NH4

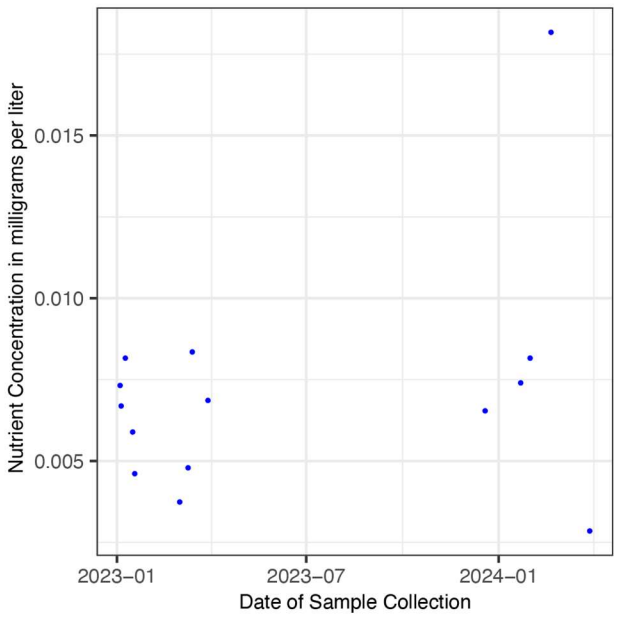

NO3

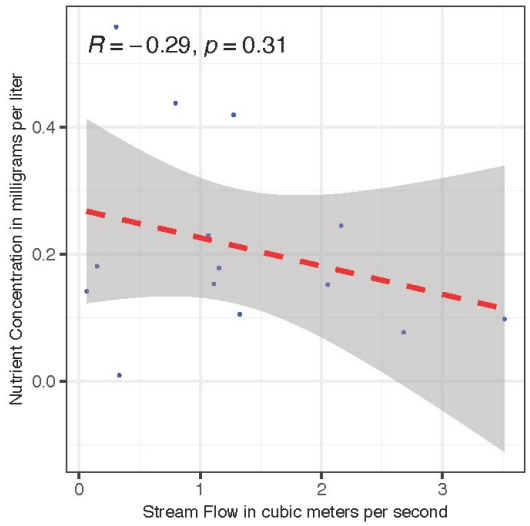

NO3

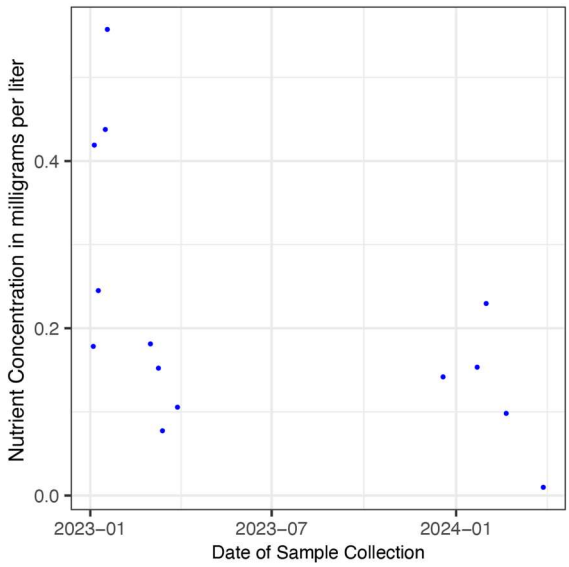

SRP

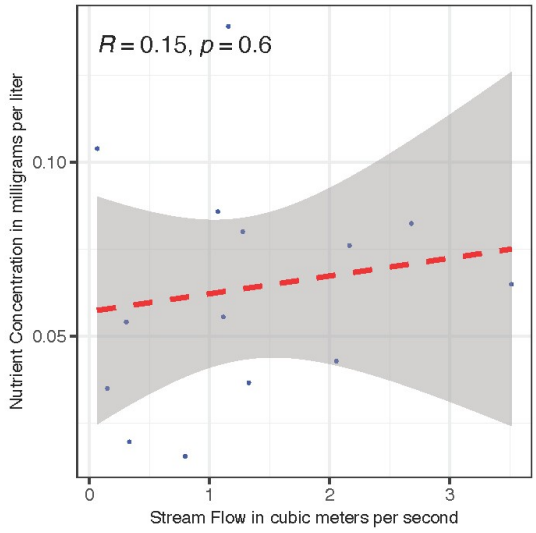

SRP

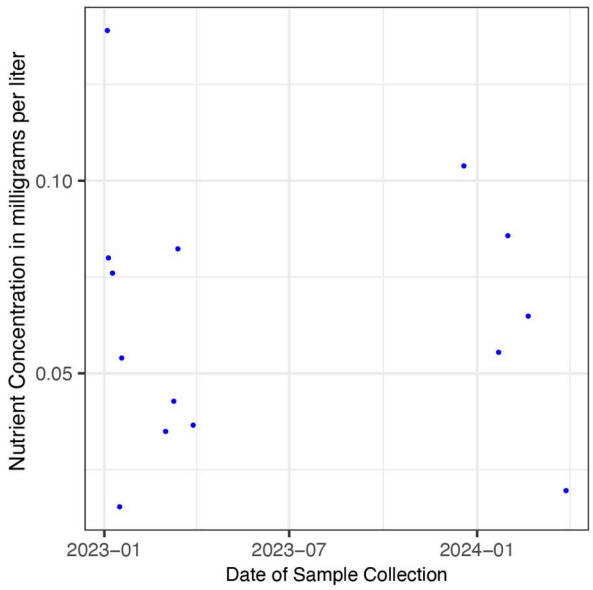

TKN

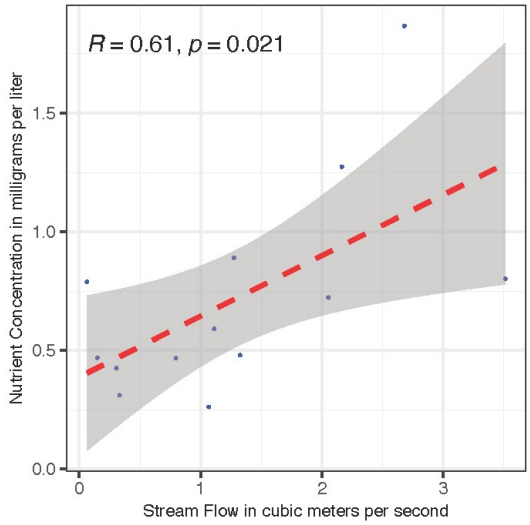

TKN

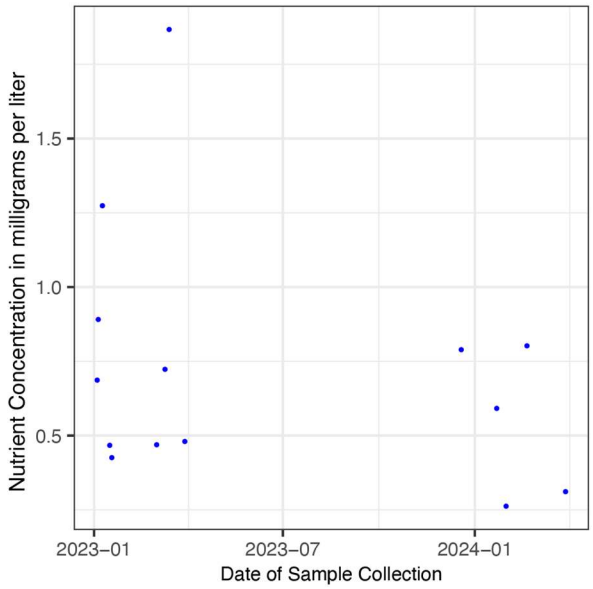

TN

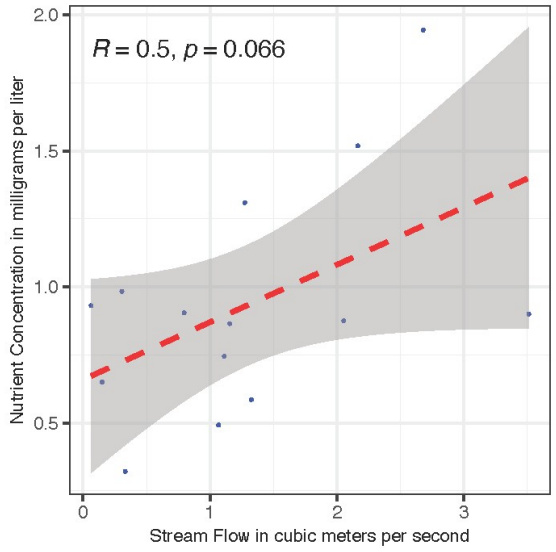
R = 0.5, p = 0.066
Nutrient Concentration in milligrams per liter
Stream Flow in cubic meters per second
2.0
1.5
1.0
0.5
0
1
2
3

TN

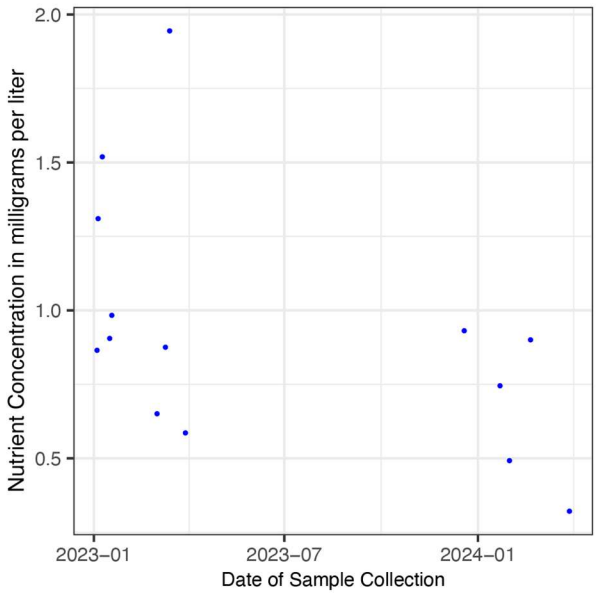
Nutrient Concentration in milligrams per liter
Date of Sample Collection
2.0
1.5
1.0
0.5
2023–01
2023–07
2024–01

TP

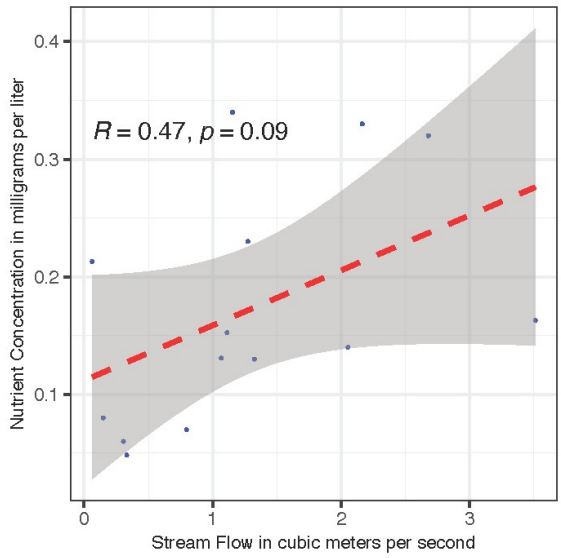
R = 0.47, p = 0.09
Nutrient Concentration in milligrams per liter
Stream Flow in cubic meters per second
0.4
0.3
0.2
0.1
0
1
2
3

TP

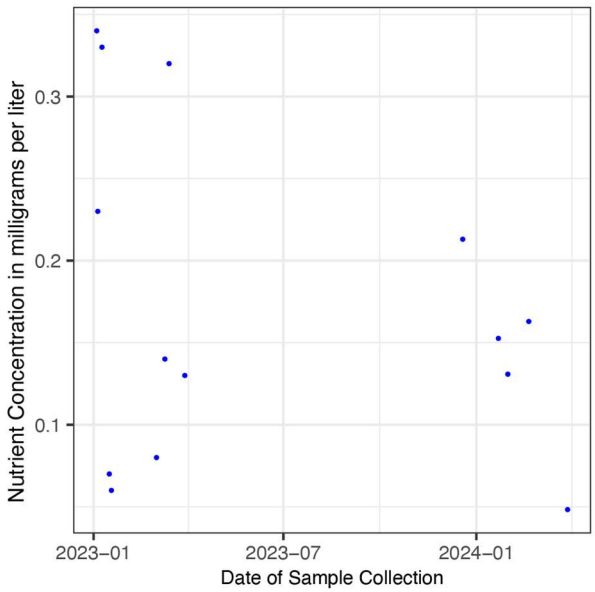
Nutrient Concentration in milligrams per liter
Date of Sample Collection
0.3
0.2
0.1
2023–01
2023–07
2024–01

Scotts Creek at Eickhoff Road near Lakeport (SCS)

DP

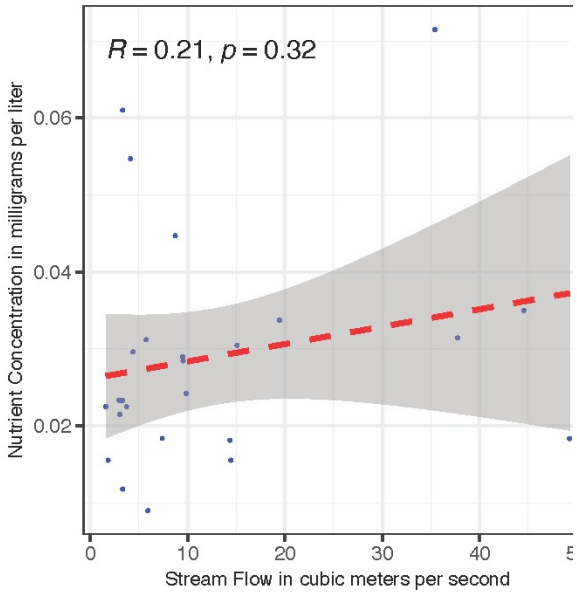

DP

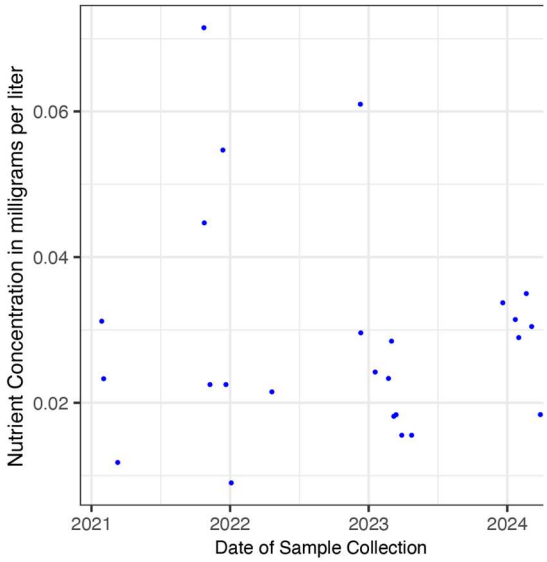

NH4

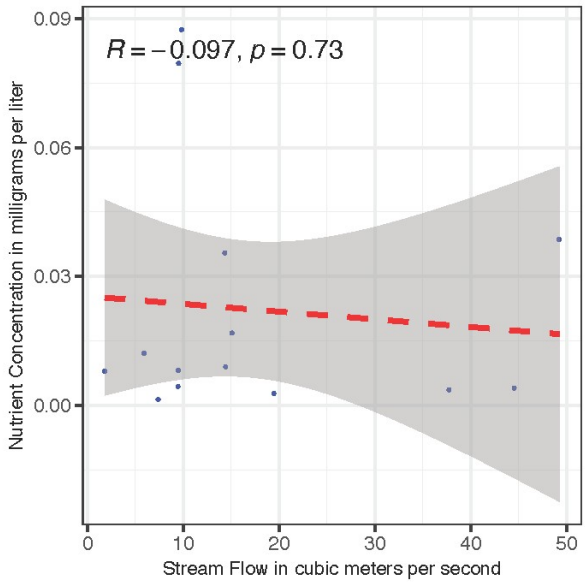

NH4

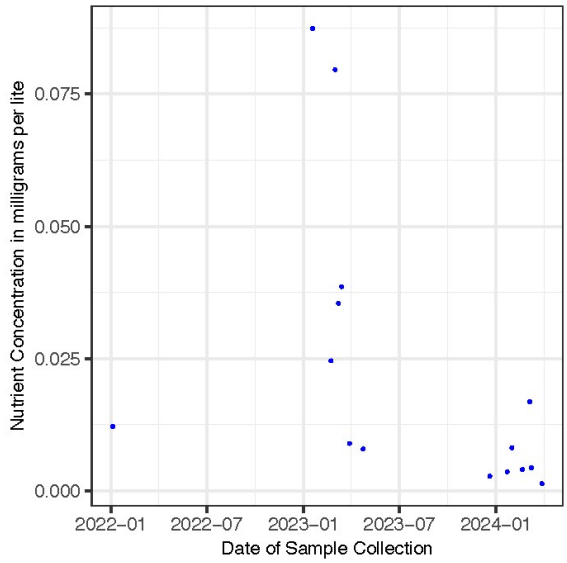

NO3

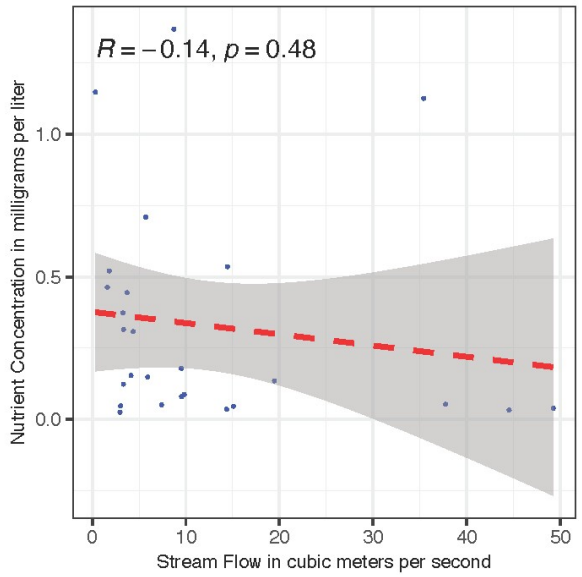

NO3

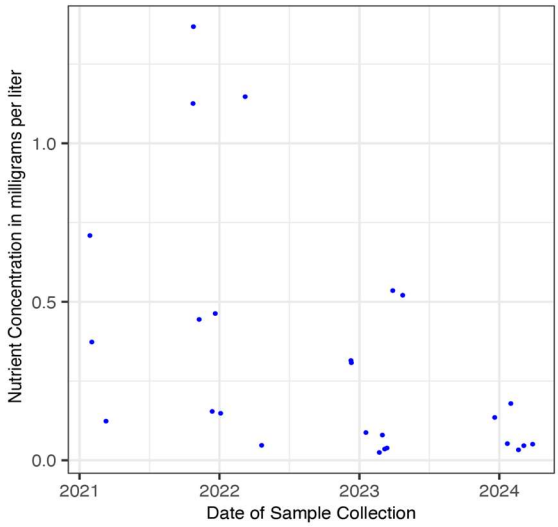

SRP

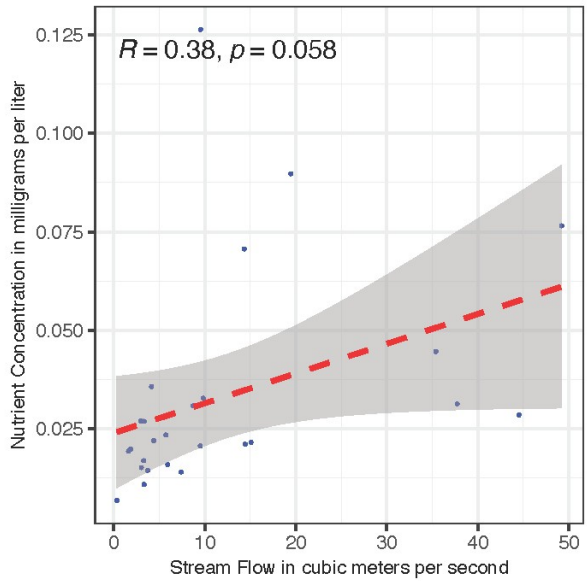

SRP

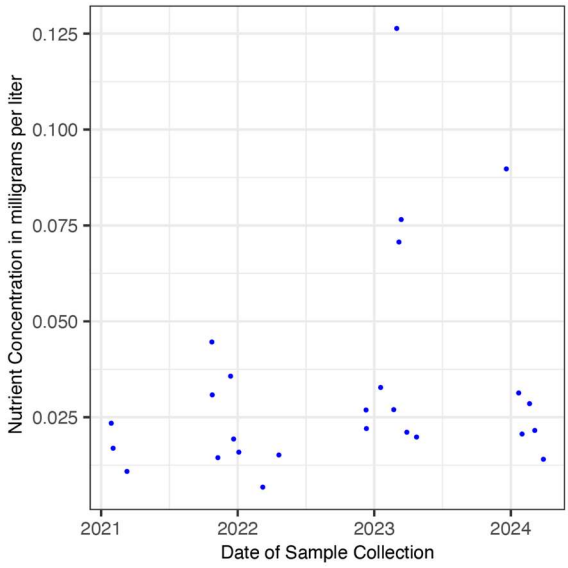

TKN

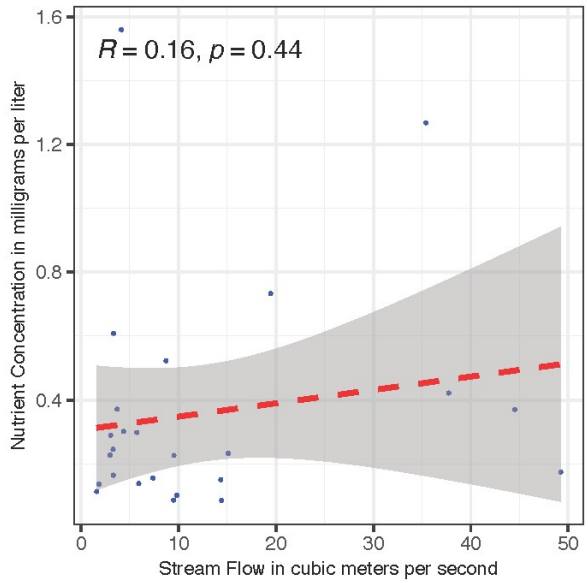
R = 0.16, p = 0.44
Nutrient Concentration in milligrams per liter
Stream Flow in cubic meters per second

TKN

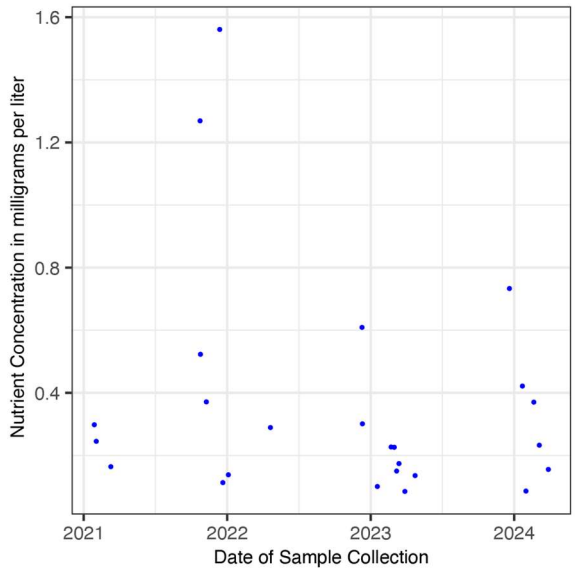
Nutrient Concentration in milligrams per liter
Date of Sample Collection

TN

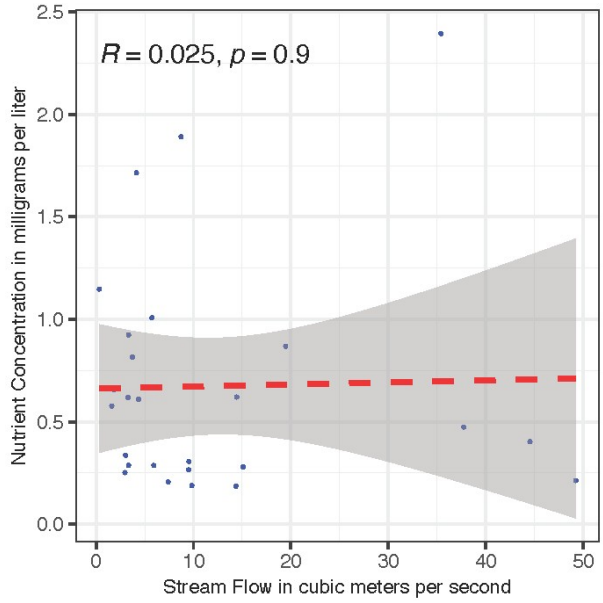
R = 0.025, p = 0.9
Nutrient Concentration in milligrams per liter
Stream Flow in cubic meters per second

TN

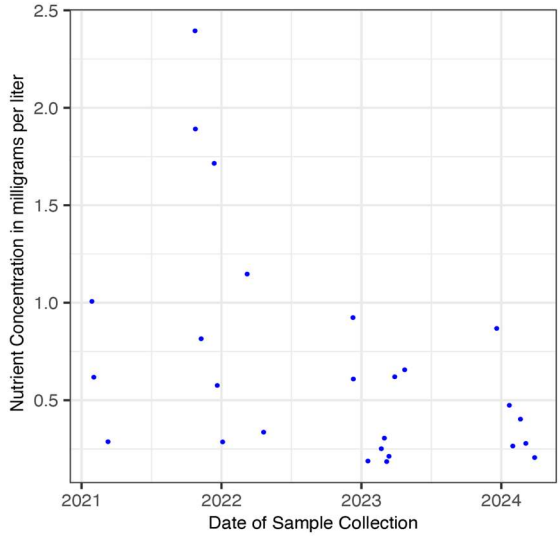
Nutrient Concentration in milligrams per liter
Date of Sample Collection

TP

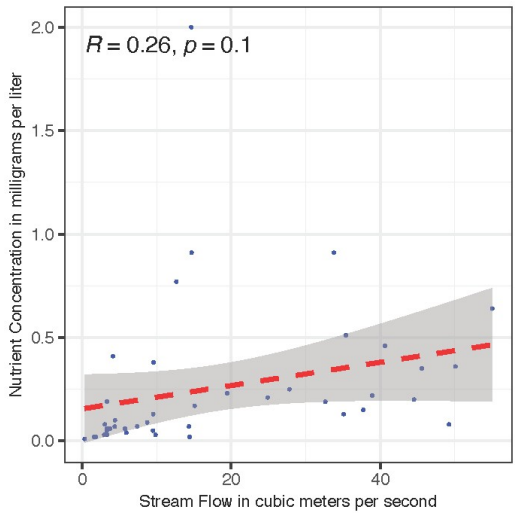
R = 0.26, p = 0.1
Nutrient Concentration in milligrams per liter
Stream Flow in cubic meters per second
0.0
0.5
1.0
1.5
2.0
0
20
40

TP

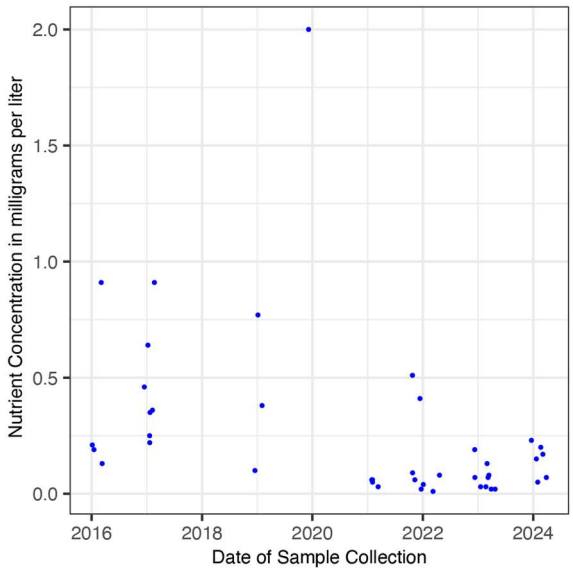
Nutrient Concentration in milligrams per liter
Date of Sample Collection
0.0
0.5
1.0
1.5
2.0
2016
2018
2020
2022
2024

South Fork Scotts Creek near Lakeport (SFS)

DP

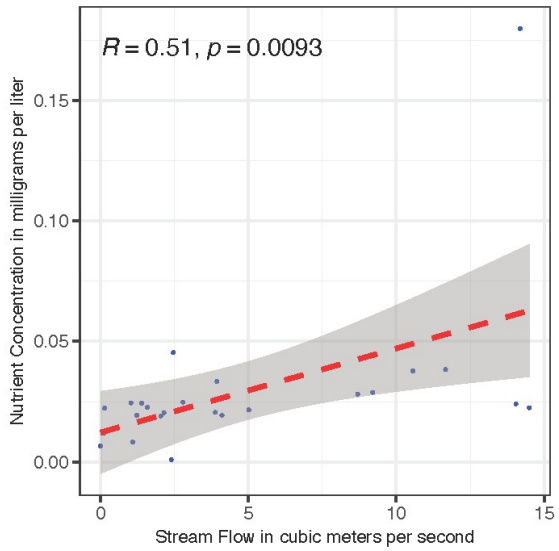

DP

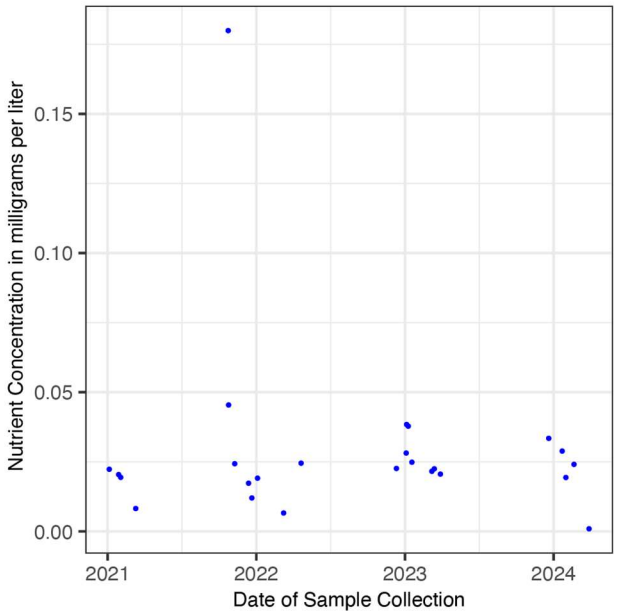

NH4

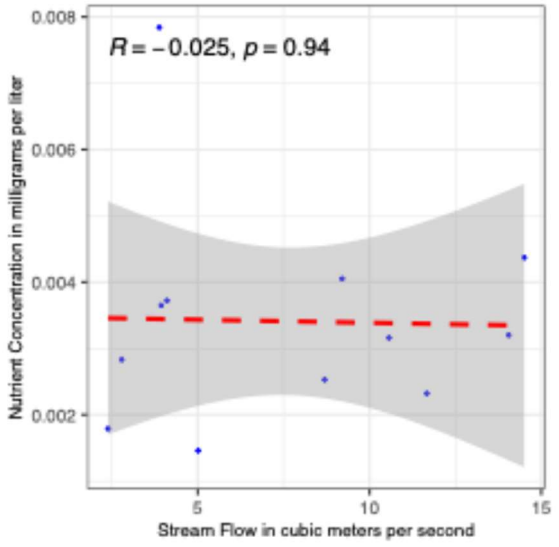

NH4

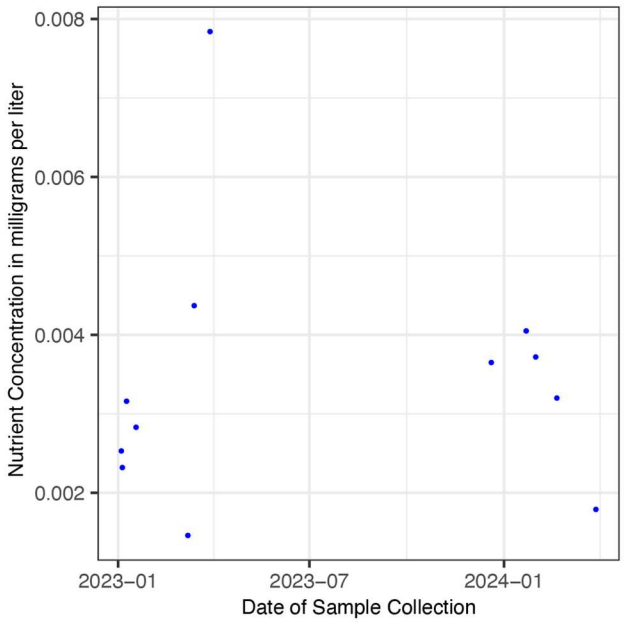

NO3

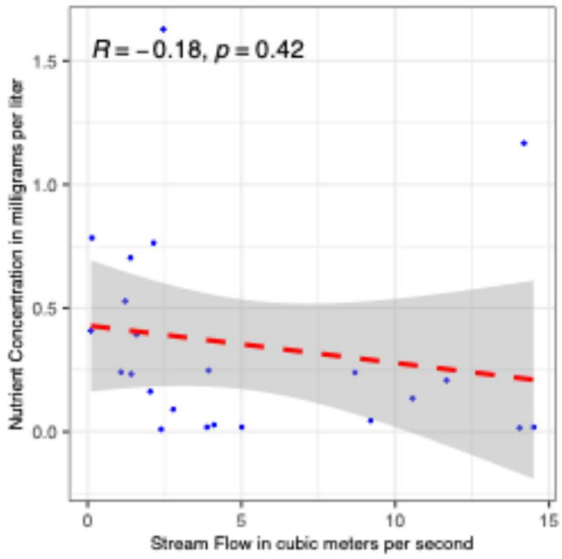

NO3

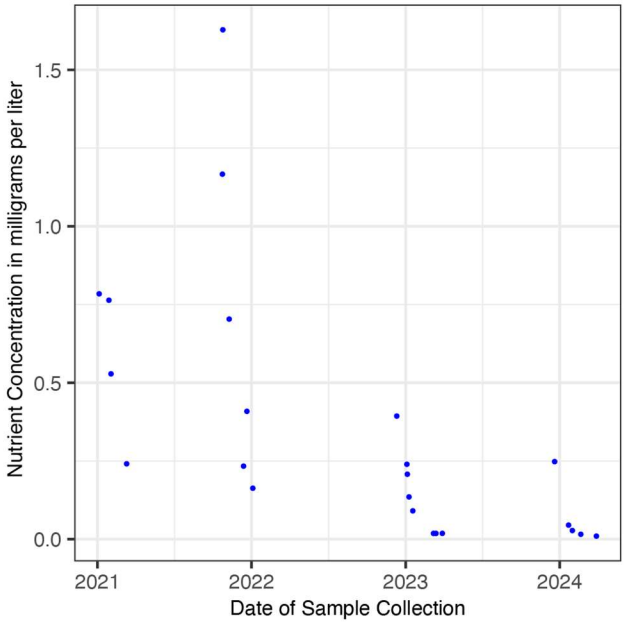

SRP

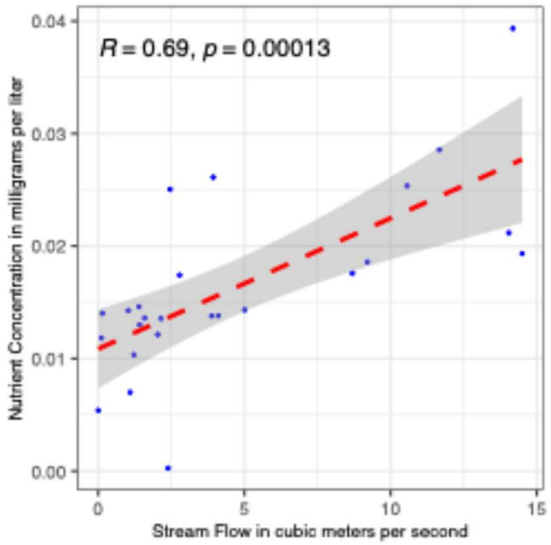

SRP

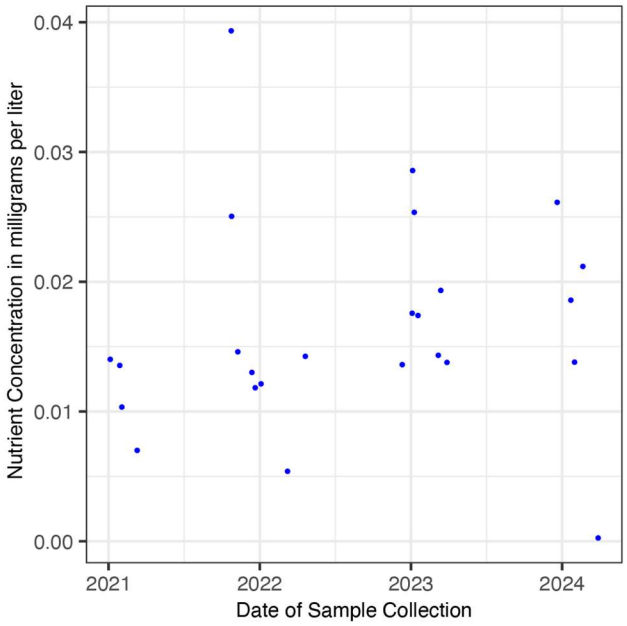

TKN

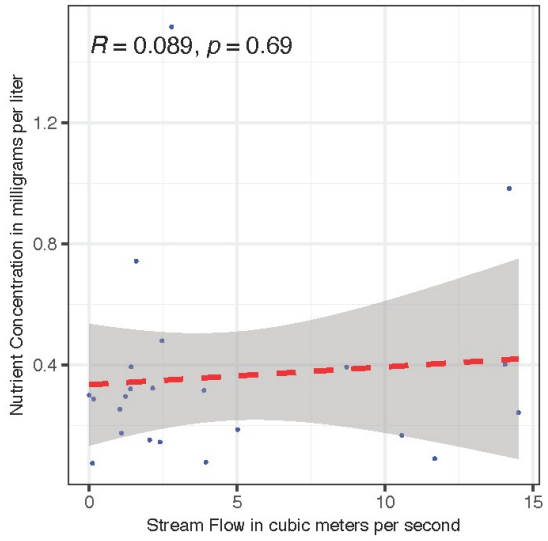
R = 0.089, p = 0.69
Nutrient Concentration in milligrams per liter
1.2
0.8
0.4
0
5
10
15
Stream Flow in cubic meters per second

TKN

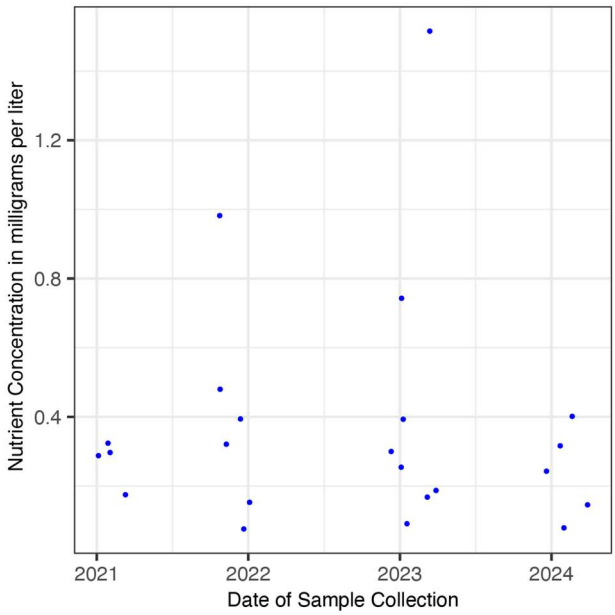
Nutrient Concentration in milligrams per liter
1.2
0.8
0.4
2021
2022
2023
2024
Date of Sample Collection

TN

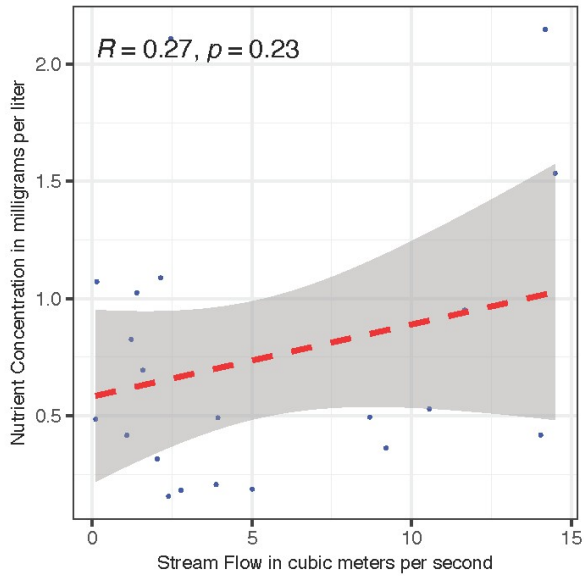
R = 0.27, p = 0.23
Nutrient Concentration in milligrams per liter
2.0
1.5
1.0
0.5
0
5
10
15
Stream Flow in cubic meters per second

TN

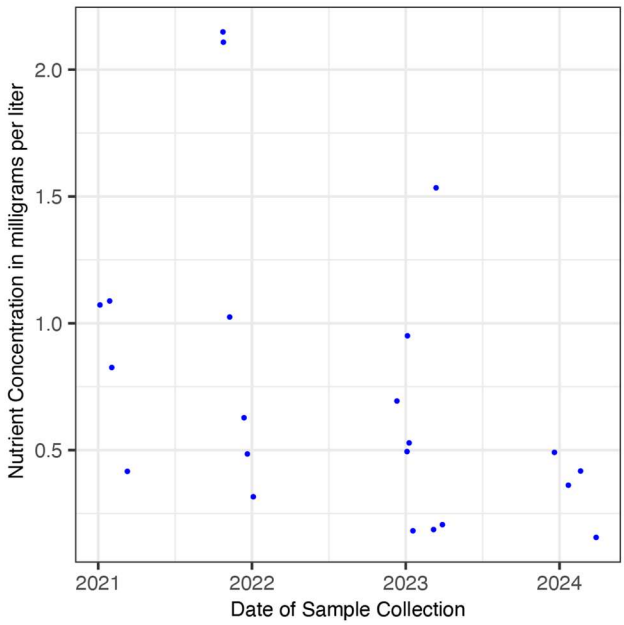
Nutrient Concentration in milligrams per liter
2.0
1.5
1.0
0.5
2021
2022
2023
2024
Date of Sample Collection

TP

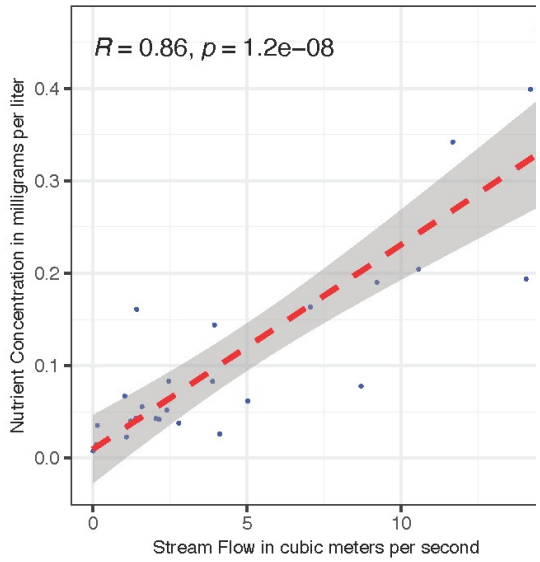
R = 0.86, p = 1.2e−08
Nutrient Concentration in milligrams per liter
0.0
0.1
0.2
0.3
0.4
0
5
10
Stream Flow in cubic meters per second

TP

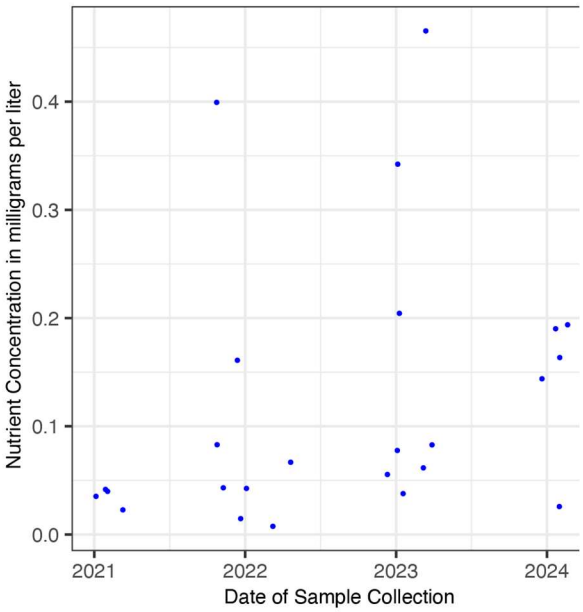
Nutrient Concentration in milligrams per liter
0.0
0.1
0.2
0.3
0.4
2021
2022
2023
2024
Date of Sample Collection

Middle Creek at Rancheria Road near Upper Lake (MCU/MCS)

DP

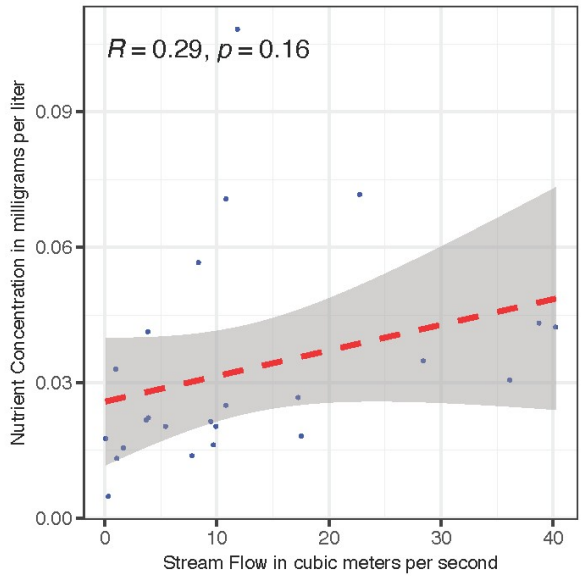

DP

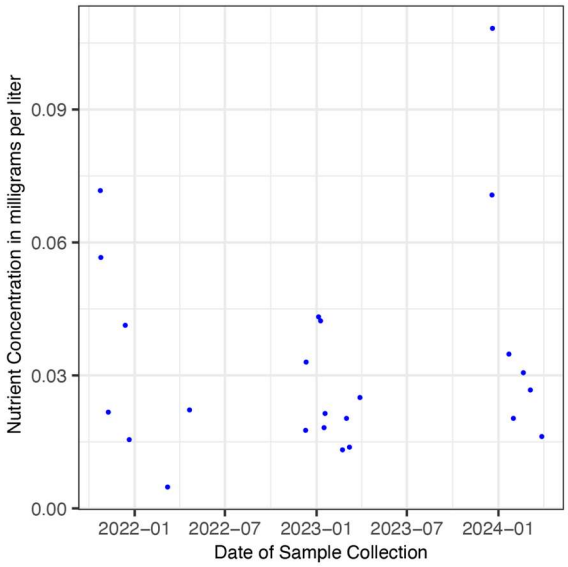

NH4

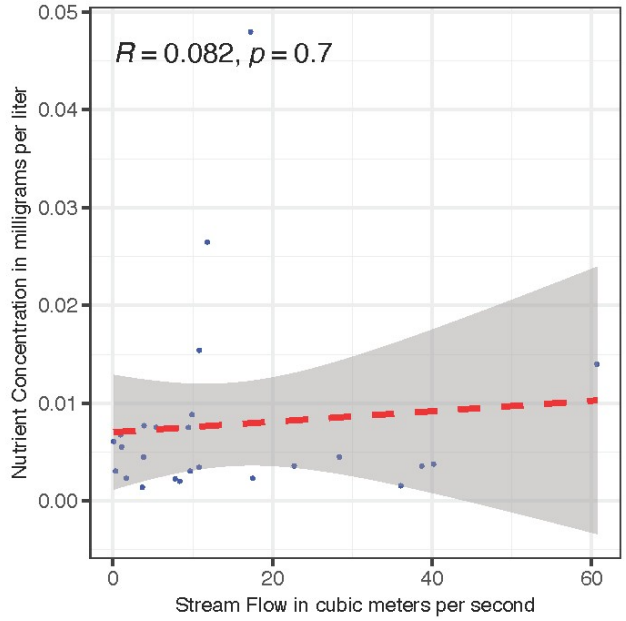

NH4

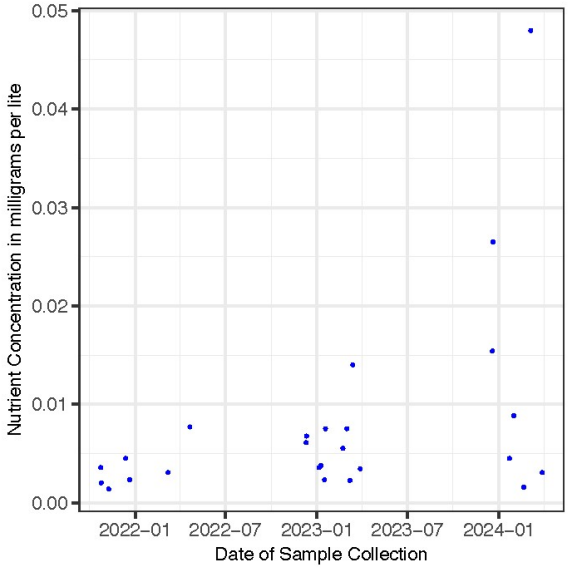

NO3

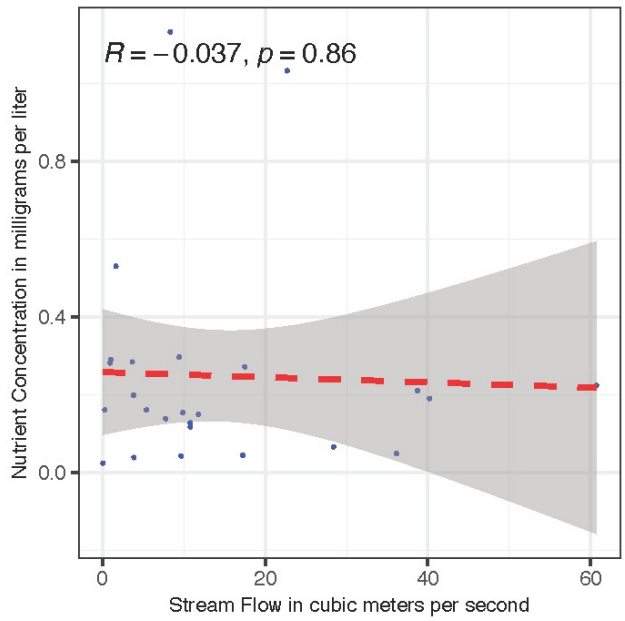

NO3

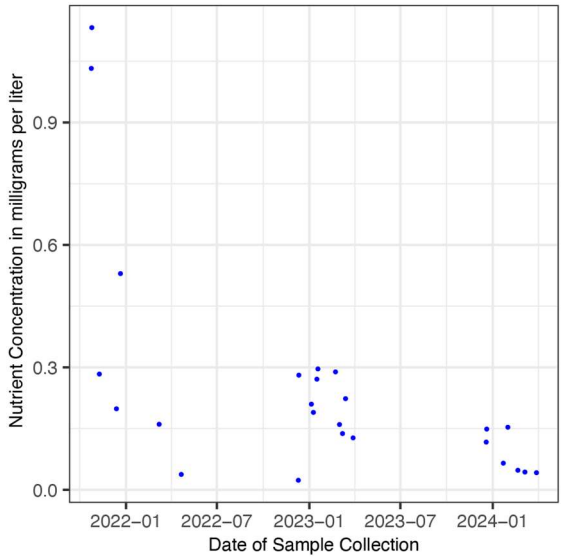

SRP

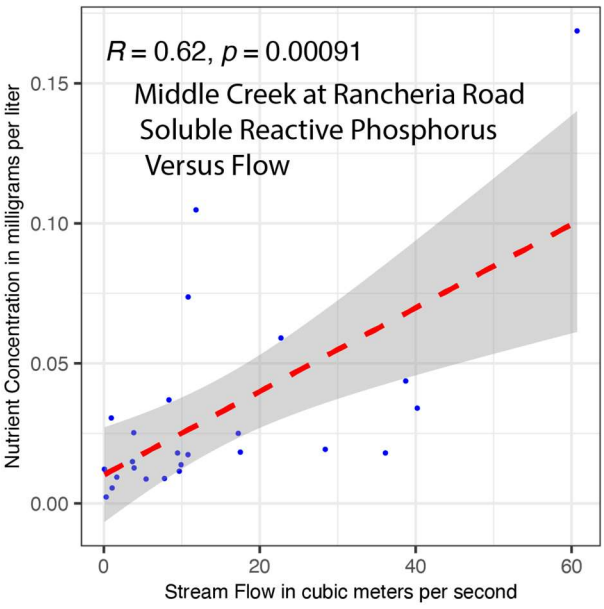

SRP

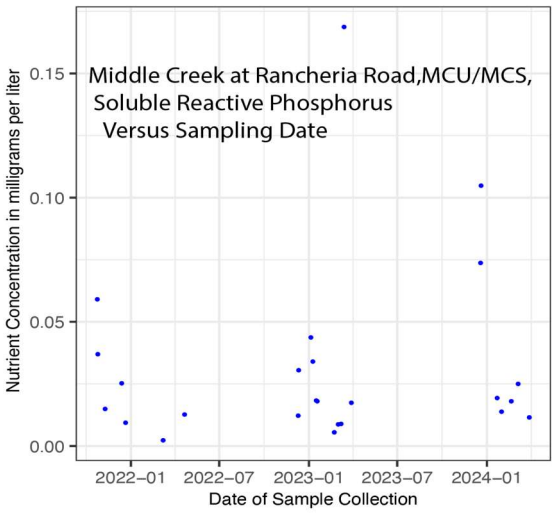

TKN

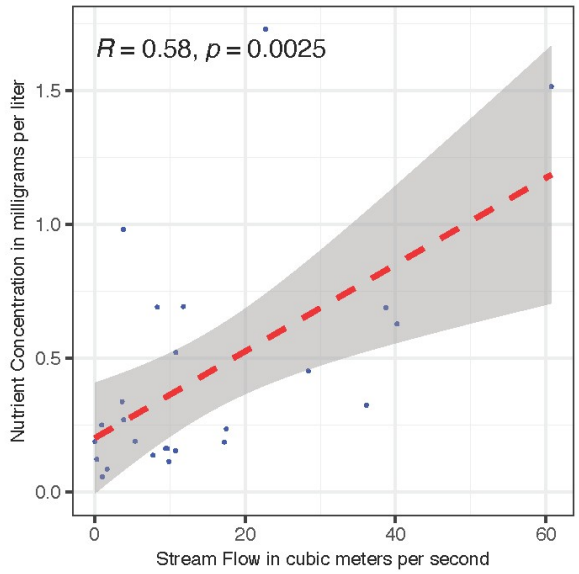
R = 0.58, p = 0.0025
Nutrient Concentration in milligrams per liter
Stream Flow in cubic meters per second
0.0
0.5
1.0
1.5
0
20
40
60

TKN

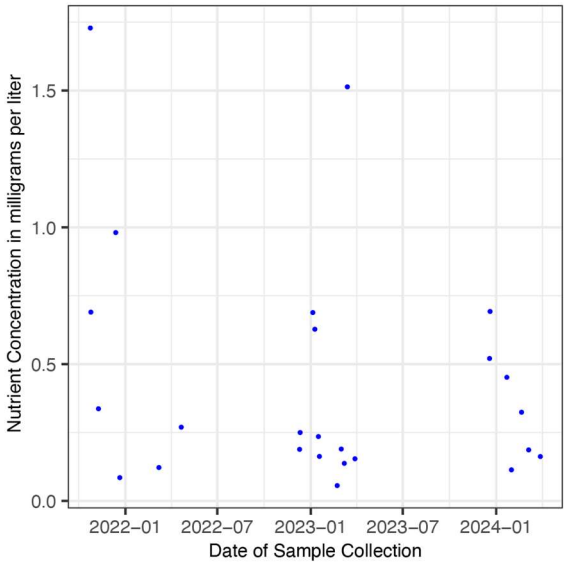
Nutrient Concentration in milligrams per liter
Date of Sample Collection
0.0
0.5
1.0
1.5
2022–01
2022–07
2023–01
2023–07
2024–01

TN

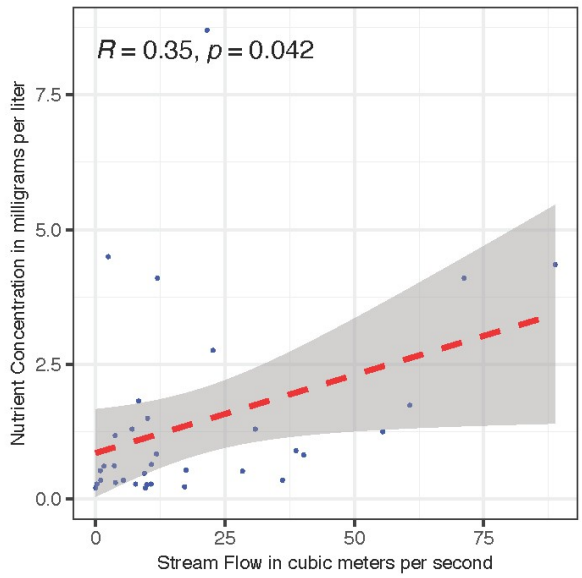
R = 0.35, p = 0.042
Nutrient Concentration in milligrams per liter
Stream Flow in cubic meters per second
0.0
2.5
5.0
7.5
0
25
50
75

TN

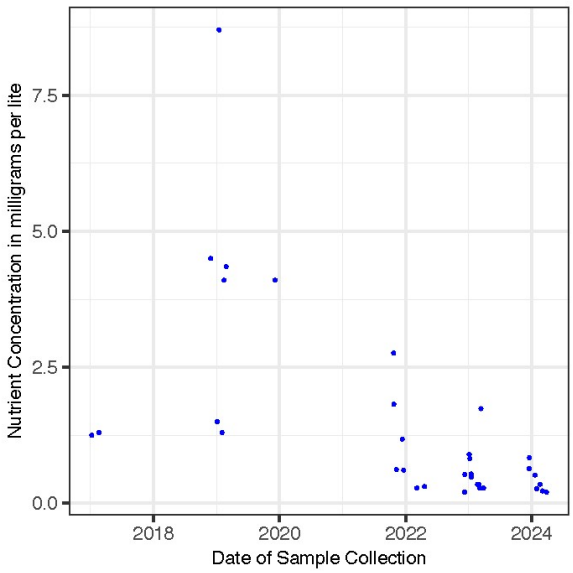
Nutrient Concentration in milligrams per lite
Date of Sample Collection
0.0
2.5
5.0
7.5
2018
2020
2022
2024

TP

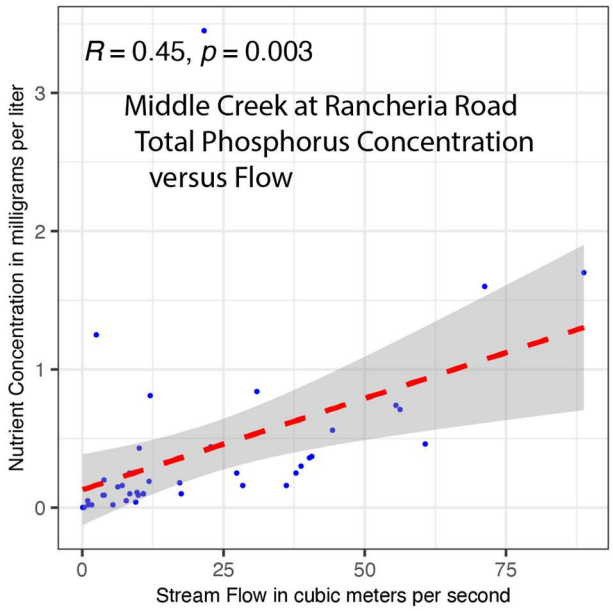
R = 0.45, p = 0.003
Middle Creek at Rancheria Road
Total Phosphorus Concentration
versus Flow
Nutrient Concentration in milligrams per liter
Stream Flow in cubic meters per second
0
1
2
3
0
25
50
75

TP

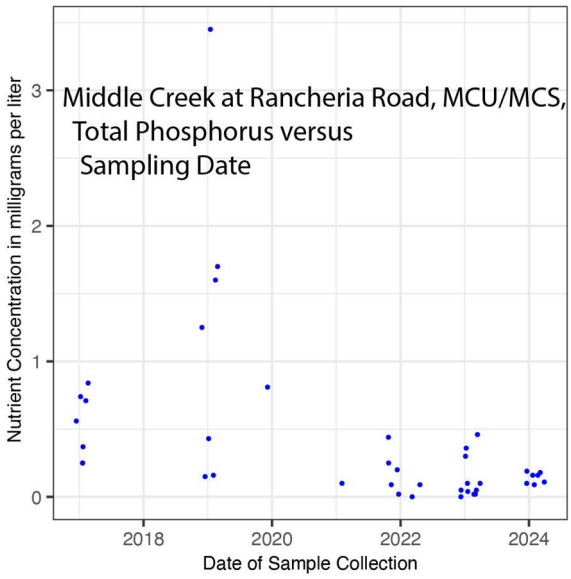
Middle Creek at Rancheria Road, MCU/MCS,
Total Phosphorus versus
Sampling Date
Nutrient Concentration in milligrams per liter
Date of Sample Collection
0
1
2
3
2018
2020
2022
2024

Scotts Creek Below South Fork Scotts Creek near Lakeport (SBS)

DP

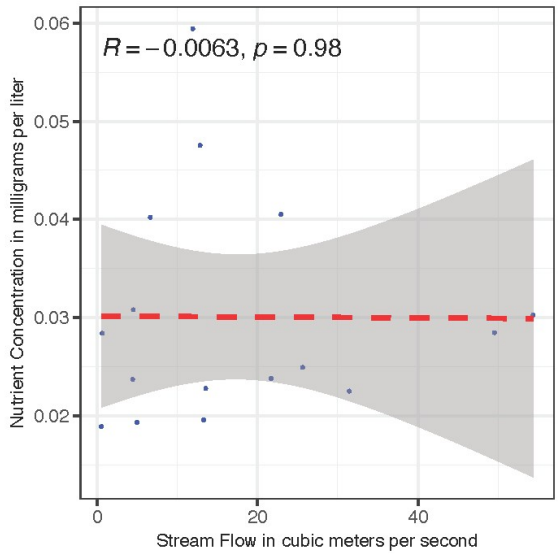

DP

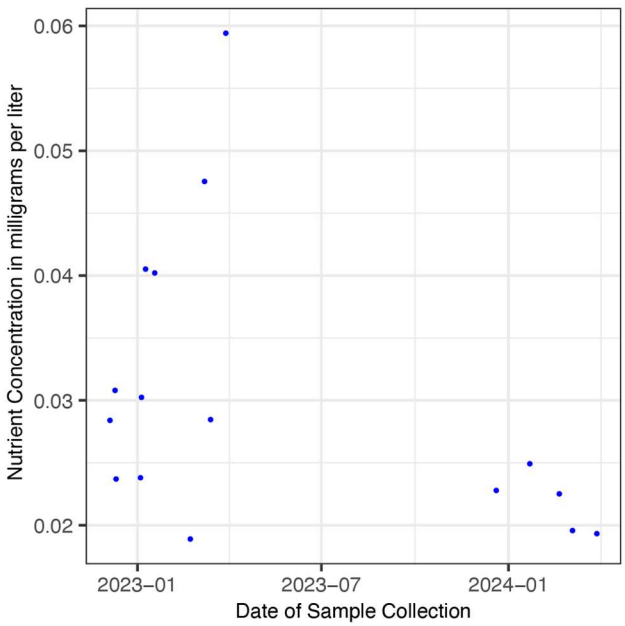

NH4

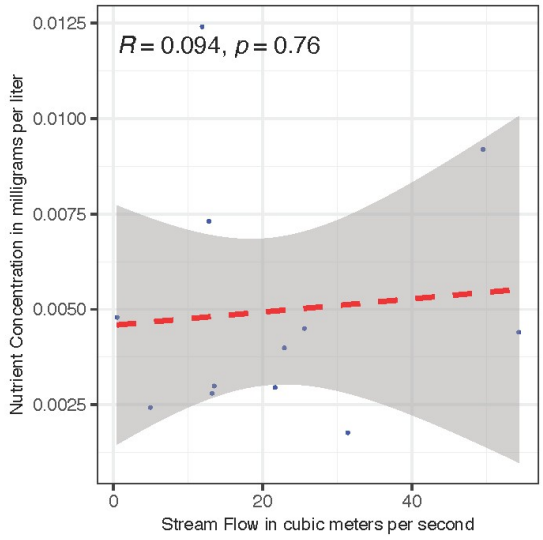

NH4

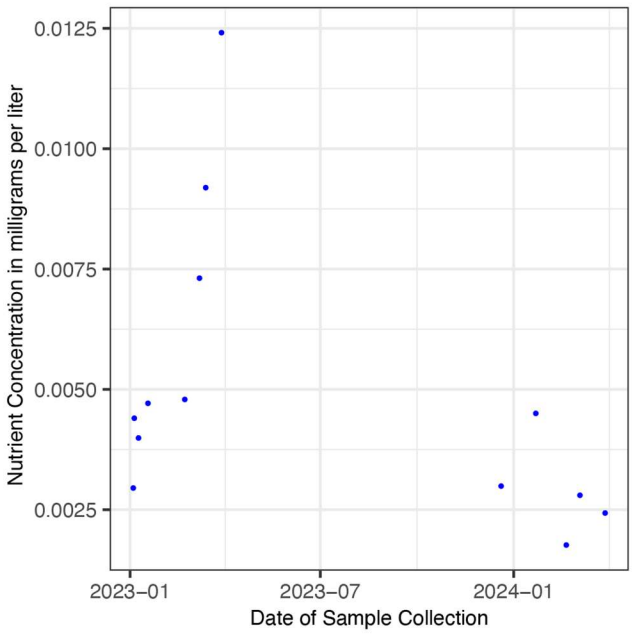

NO3

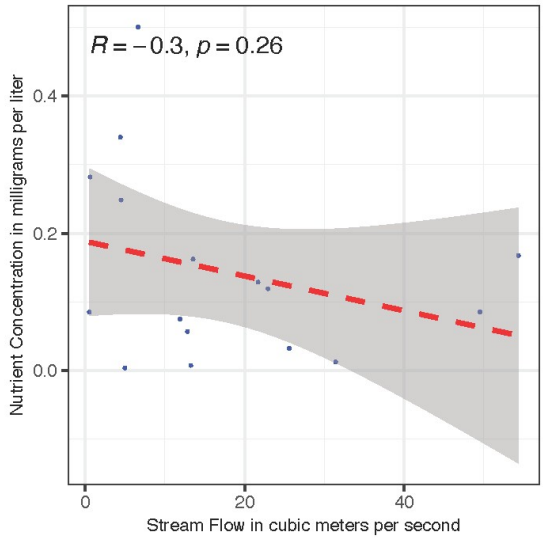

NO3

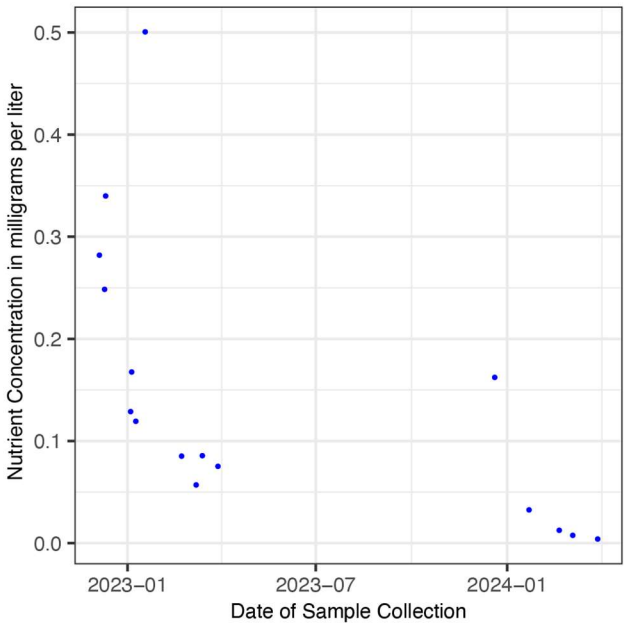

SRP

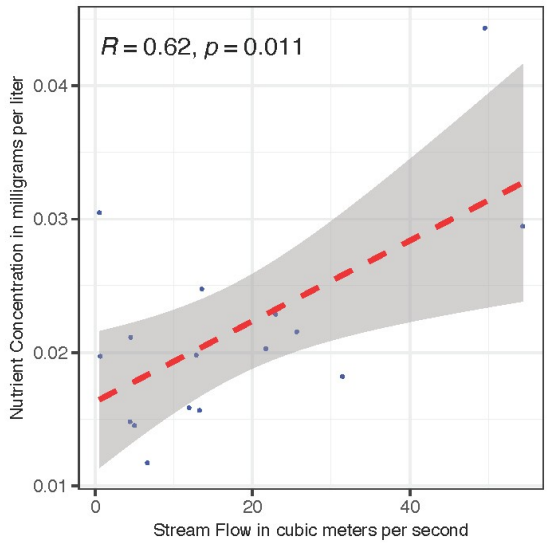

SRP

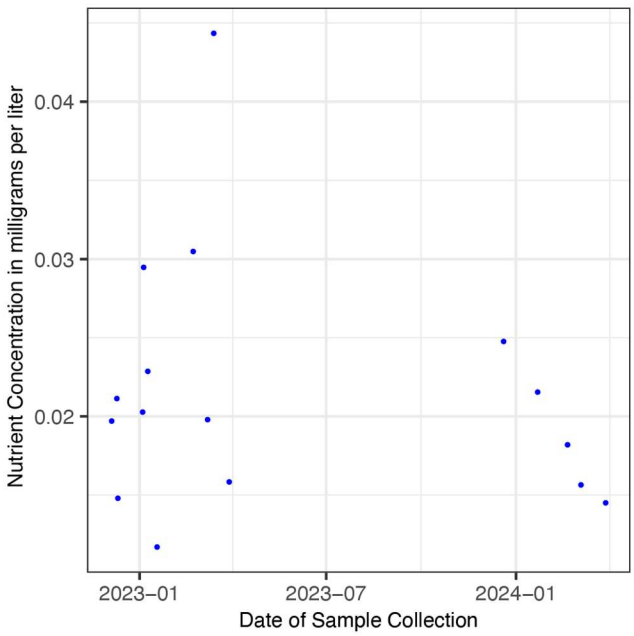

TKN

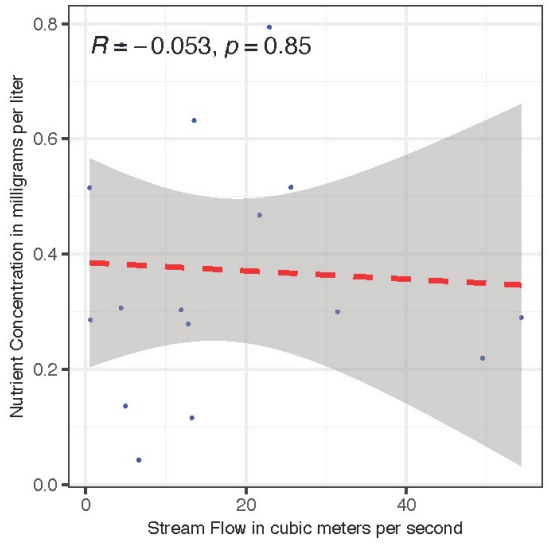
R = −0.053, p = 0.85
Nutrient Concentration in milligrams per liter
0.0
0.2
0.4
0.6
0.8
0
20
40
Stream Flow in cubic meters per second

TKN

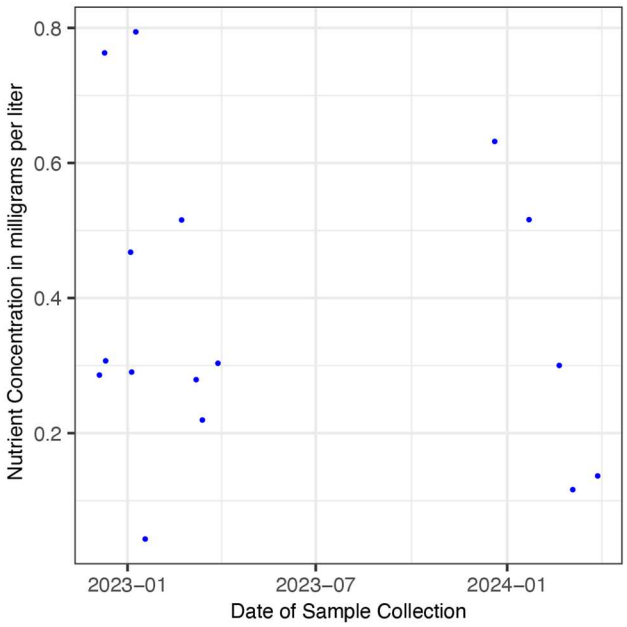
Nutrient Concentration in milligrams per liter
0.2
0.4
0.6
0.8
2023–01
2023–07
2024–01
Date of Sample Collection

TN

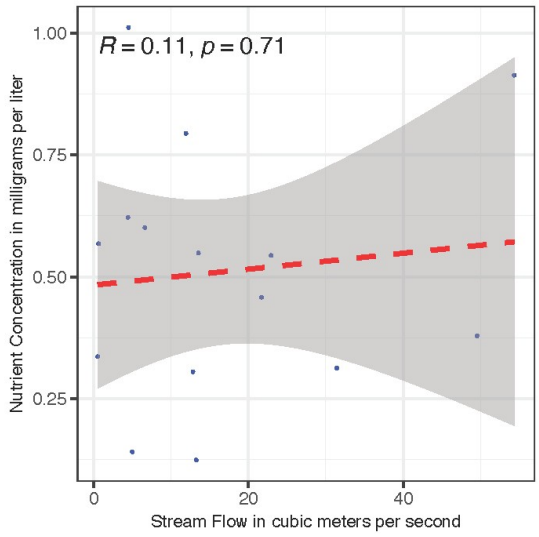
R = 0.11, p = 0.71
Nutrient Concentration in milligrams per liter
0.25
0.50
0.75
1.00
0
20
40
Stream Flow in cubic meters per second

TN

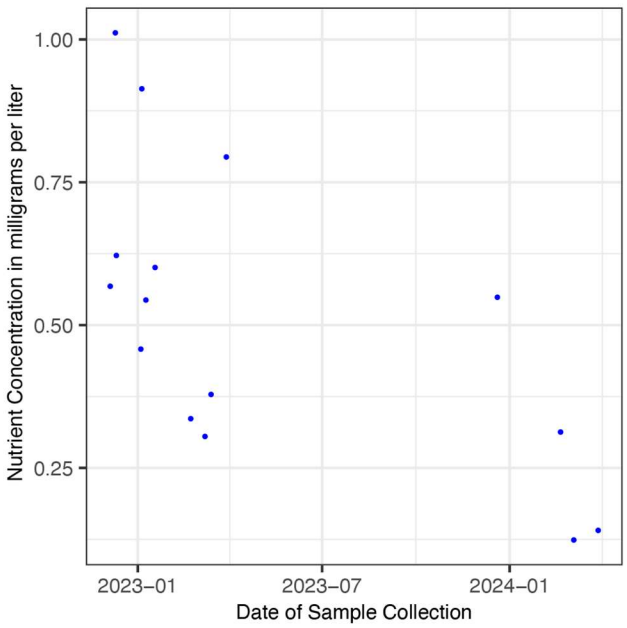
Nutrient Concentration in milligrams per liter
0.25
0.50
0.75
1.00
2023–01
2023–07
2024–01
Date of Sample Collection

TP

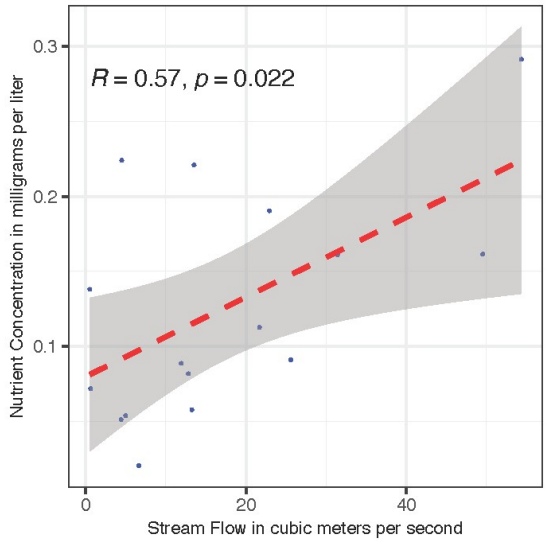
R = 0.57, p = 0.022
Nutrient Concentration in milligrams per liter
0.3
0.2
0.1
0
20
40
Stream Flow in cubic meters per second

TP

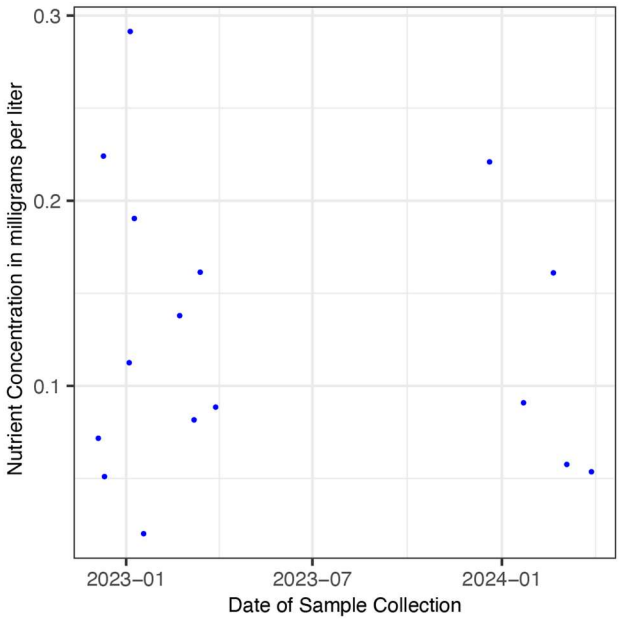
Nutrient Concentration in milligrams per liter
0.3
0.2
0.1
2023–01
2023–07
2024–01
Date of Sample Collection

Scotts Creek Above State Route 29 at Upper Lake (TLS)

DP

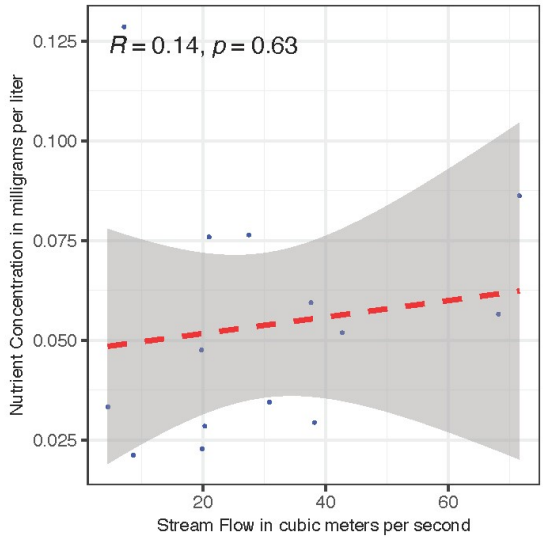

DP

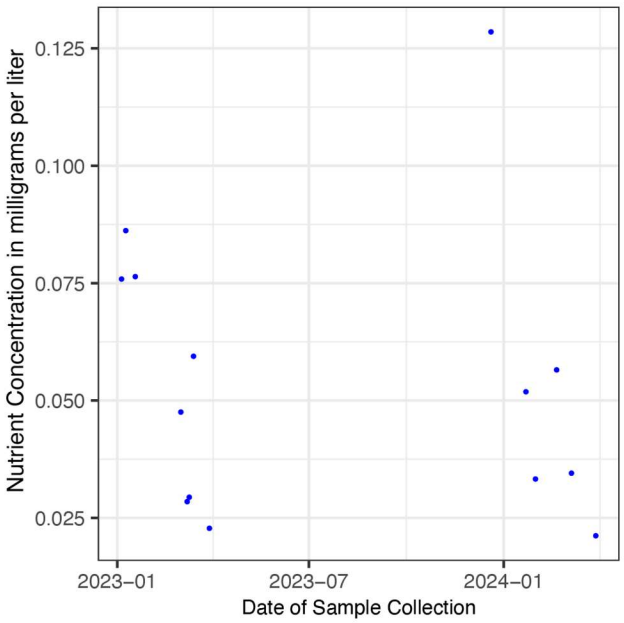

NH4

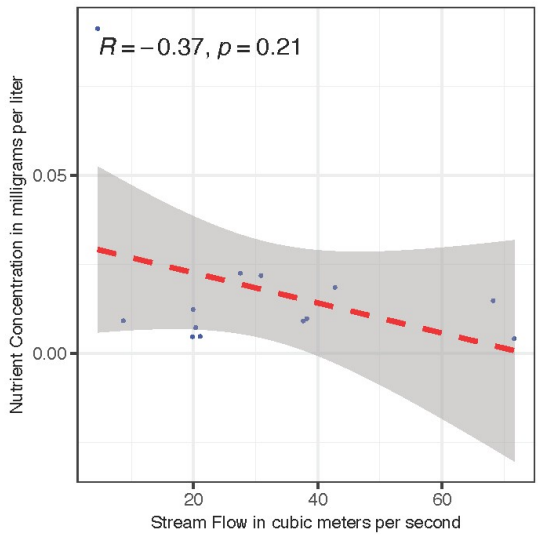

NH4

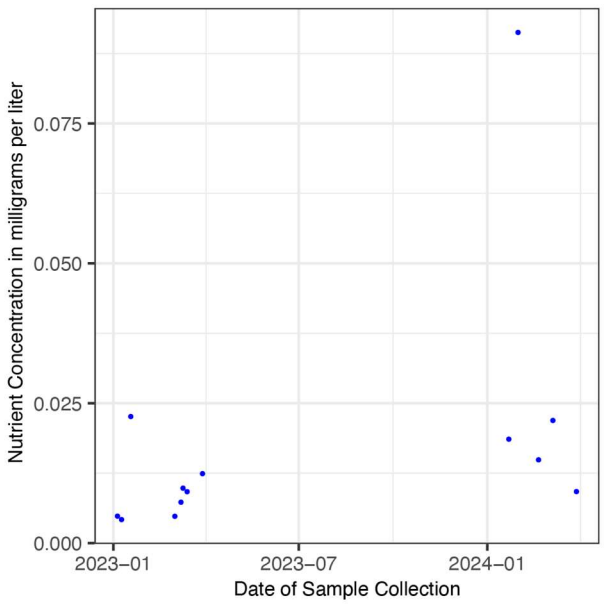

NO3

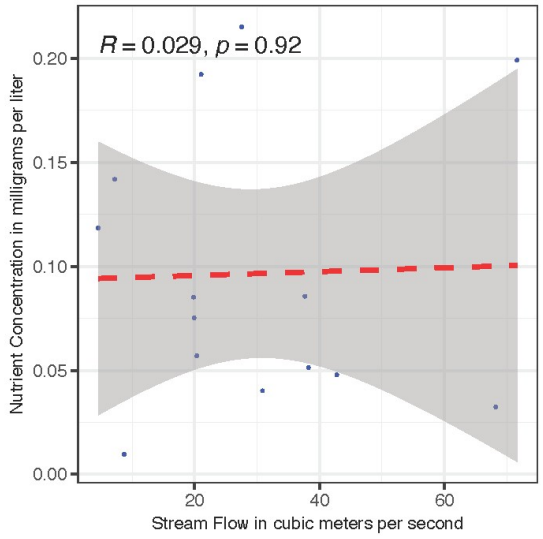

NO3

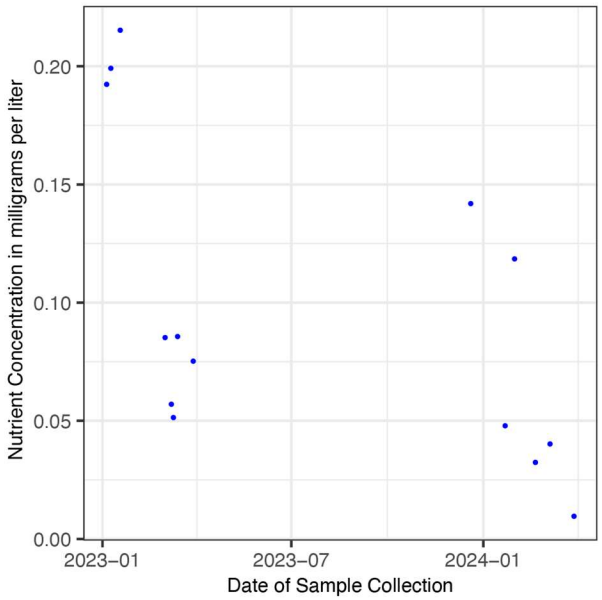

SRP

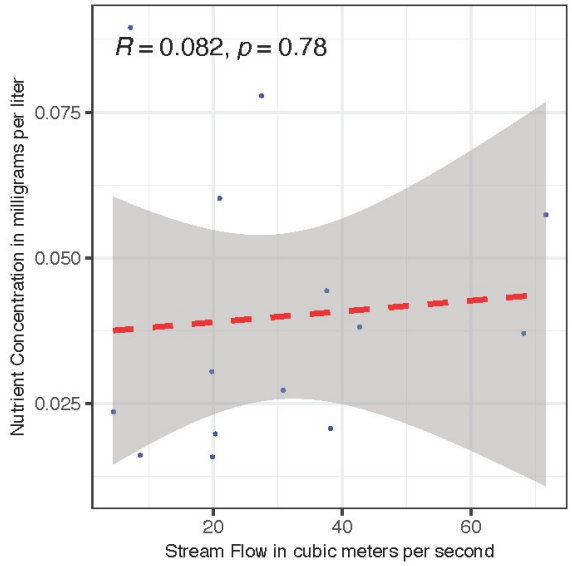

SRP

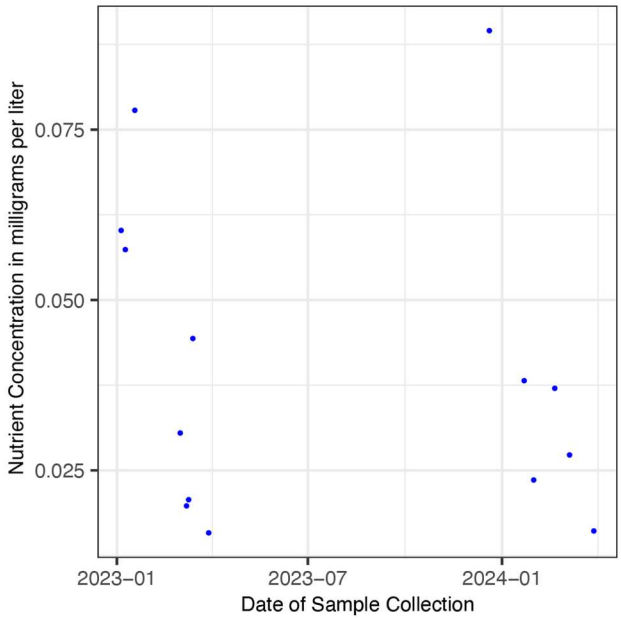

TKN

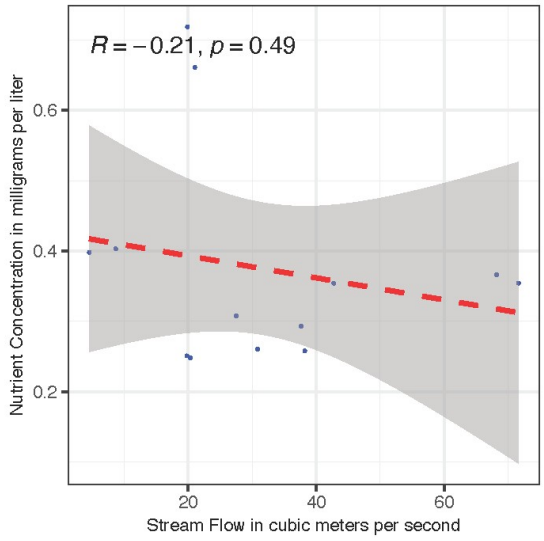
R = −0.21, p = 0.49
Nutrient Concentration in milligrams per liter
0.6
0.4
0.2
20
40
60
Stream Flow in cubic meters per second

TKN

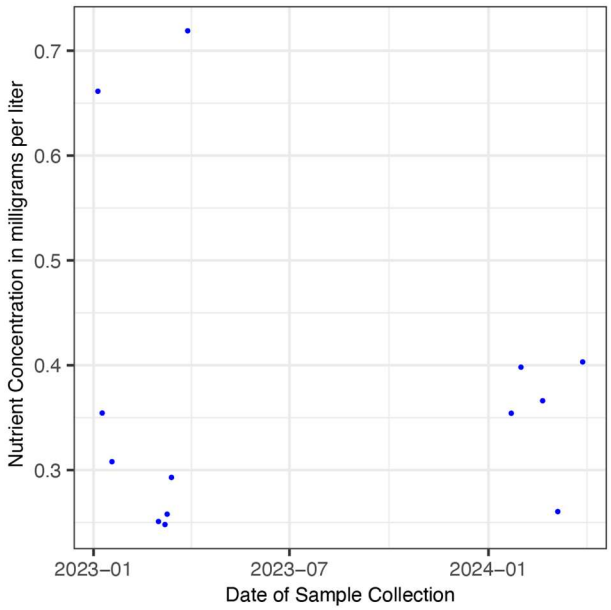
Nutrient Concentration in milligrams per liter
0.7
0.6
0.5
0.4
0.3
2023–01
2023–07
2024–01
Date of Sample Collection

TN

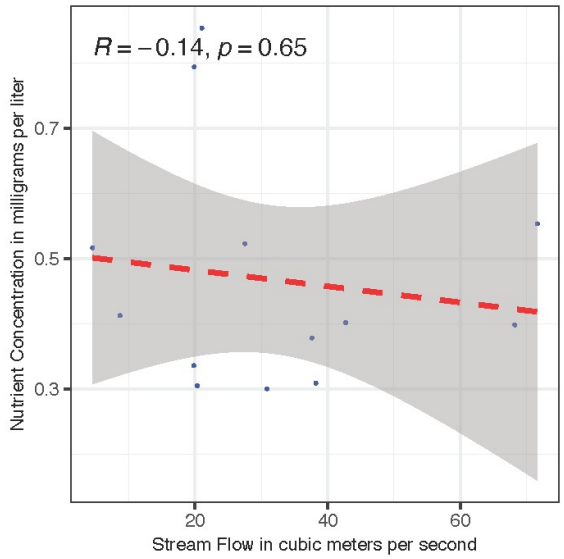
R = −0.14, p = 0.65
Nutrient Concentration in milligrams per liter
0.7
0.5
0.3
20
40
60
Stream Flow in cubic meters per second

TN

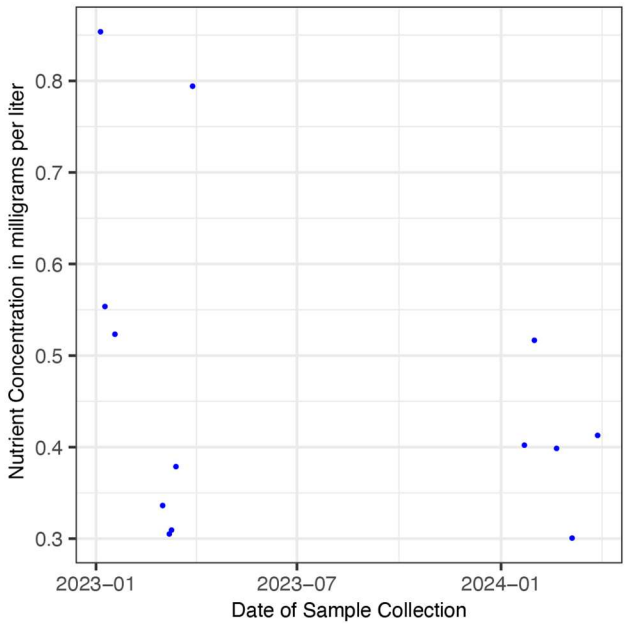
Nutrient Concentration in milligrams per liter
0.8
0.7
0.6
0.5
0.4
0.3
2023–01
2023–07
2024–01
Date of Sample Collection

TP

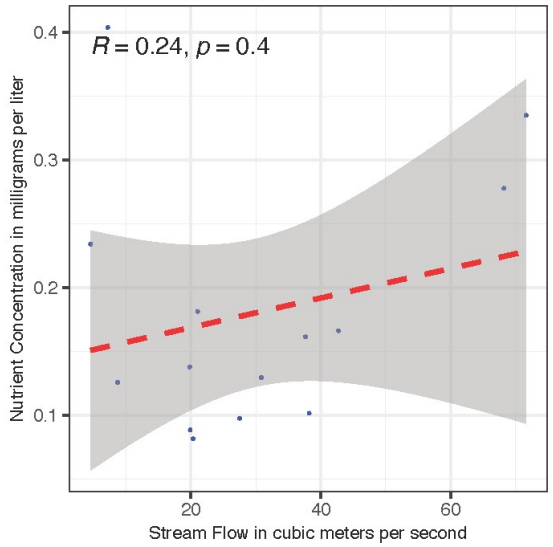
$R = 0.24, p = 0.4$
Nutrient Concentration in milligrams per liter
0.4
0.3
0.2
0.1
20
40
60
Stream Flow in cubic meters per second

TP

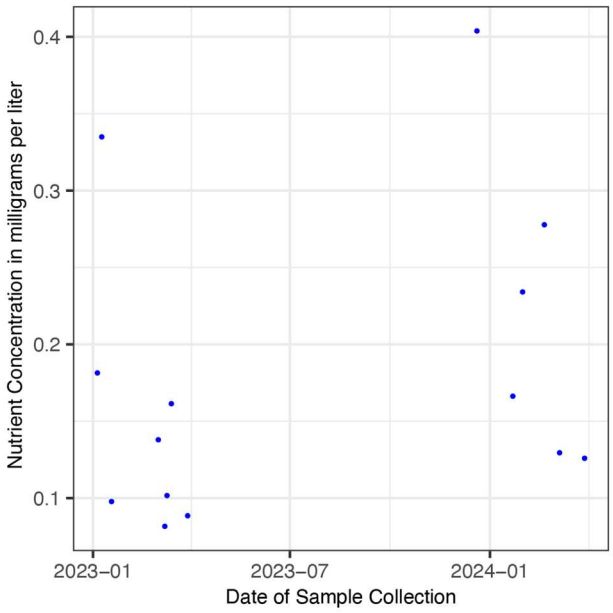
Nutrient Concentration in milligrams per liter
0.4
0.3
0.2
0.1
2023–01
2023–07
2024–01
Date of Sample Collection

Upper Kelsey Creek, Kelsey Creek at Kelseyville (KCU)

DP

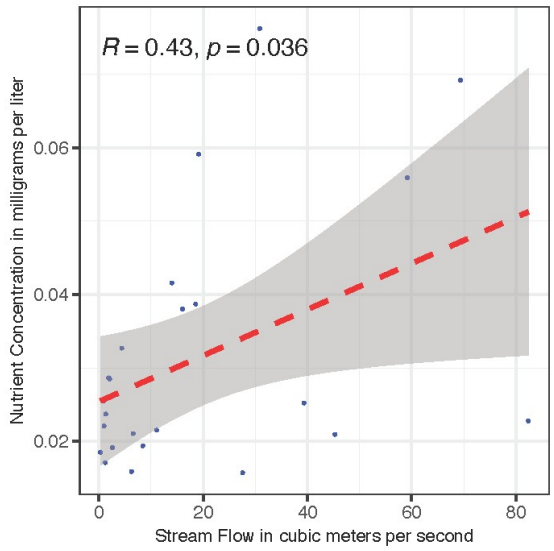

DP

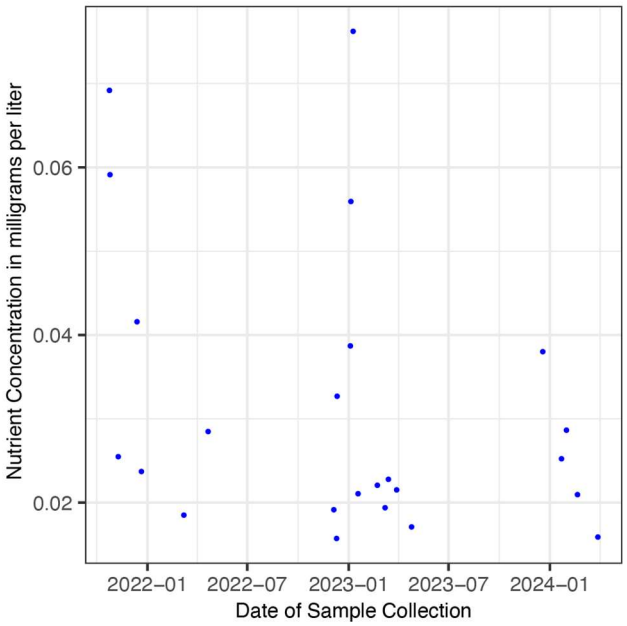

NH4

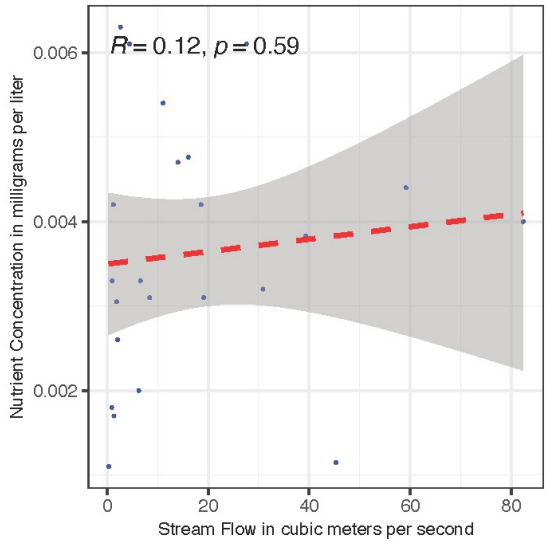

NH4

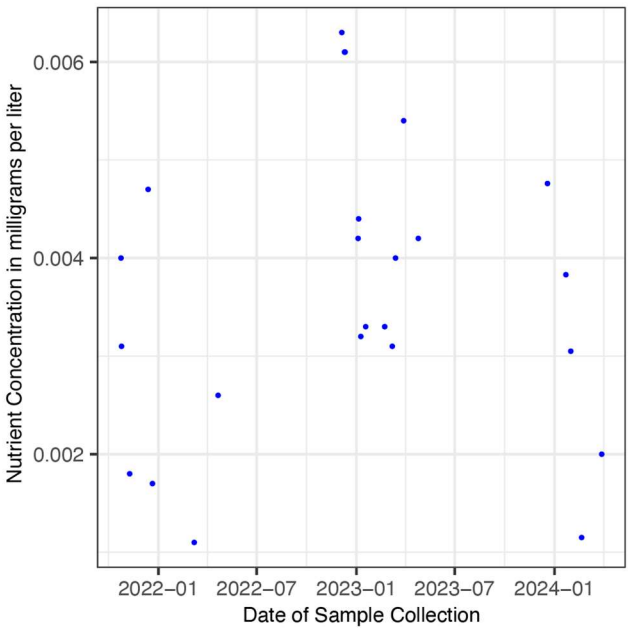

NO3

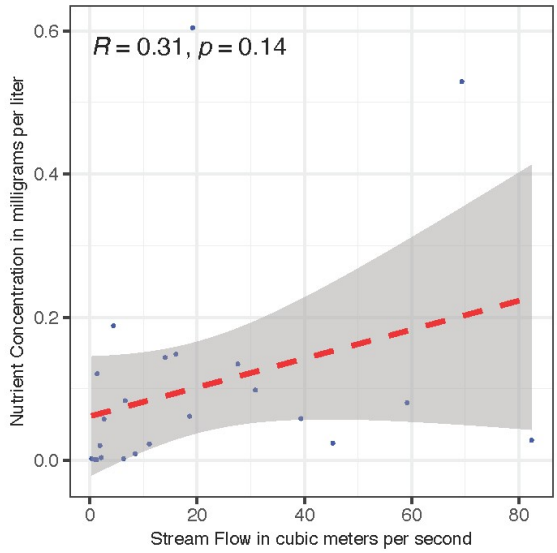

NO3

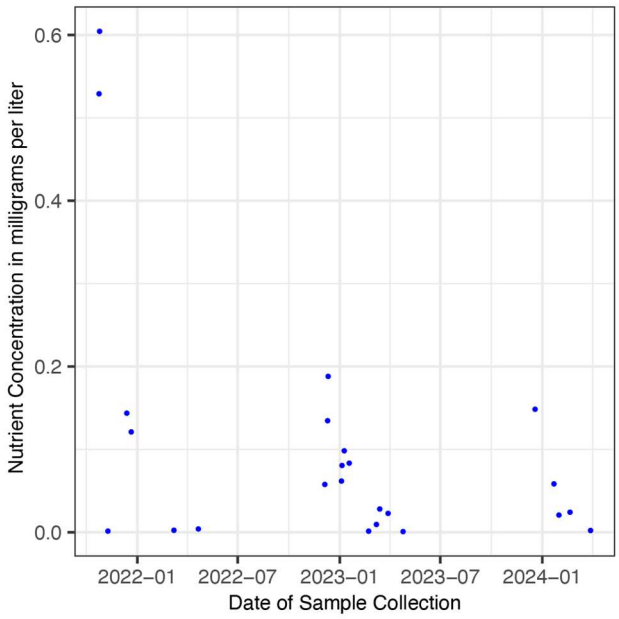

SRP

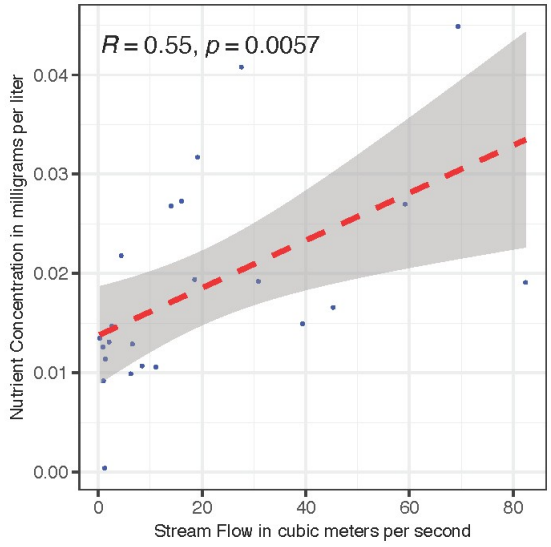

SRP

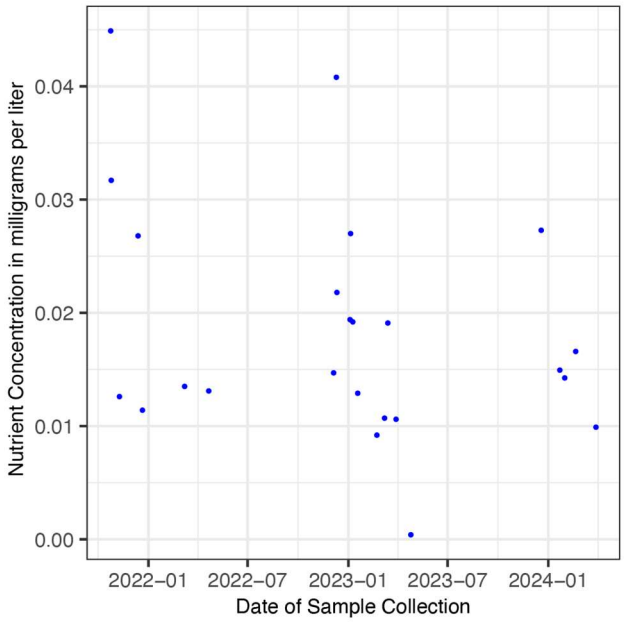

TKN

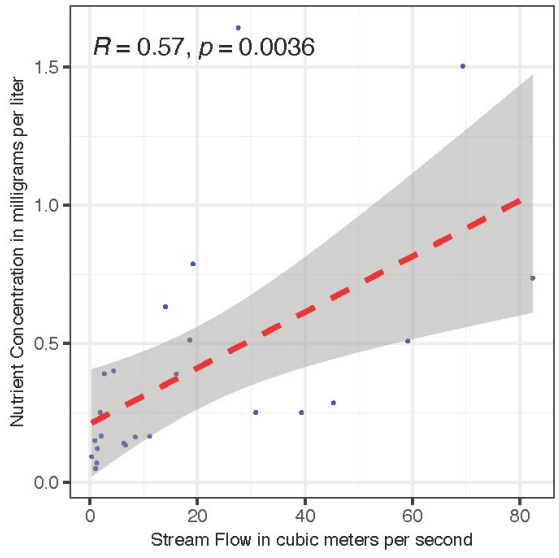
R = 0.57, p = 0.0036
Nutrient Concentration in milligrams per liter
Stream Flow in cubic meters per second
0.0
0.5
1.0
1.5
0
20
40
60
80

TKN

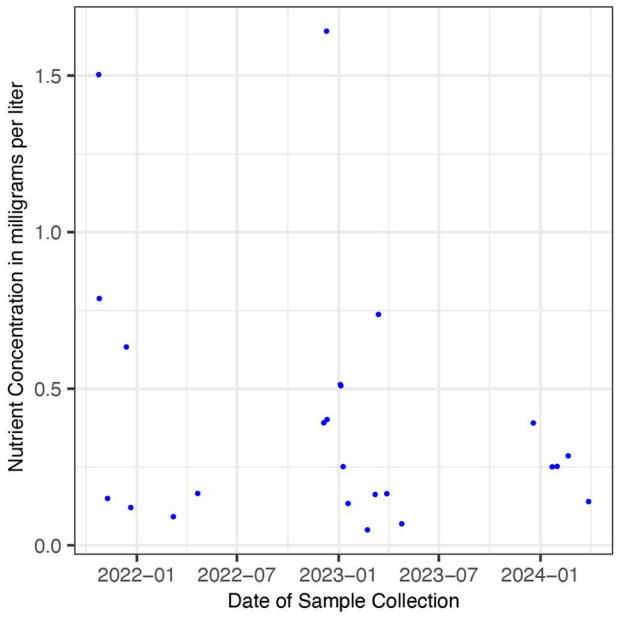
Nutrient Concentration in milligrams per liter
Date of Sample Collection
0.0
0.5
1.0
1.5
2022–01
2022–07
2023–01
2023–07
2024–01

TN

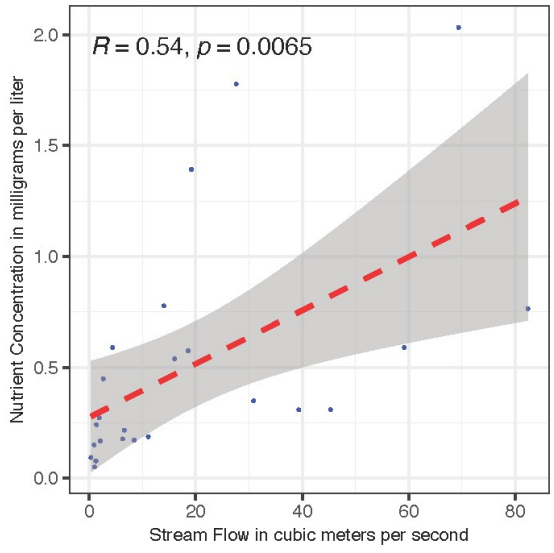
R = 0.54, p = 0.0065
Nutrient Concentration in milligrams per liter
Stream Flow in cubic meters per second
0.0
0.5
1.0
1.5
2.0
0
20
40
60
80

TN

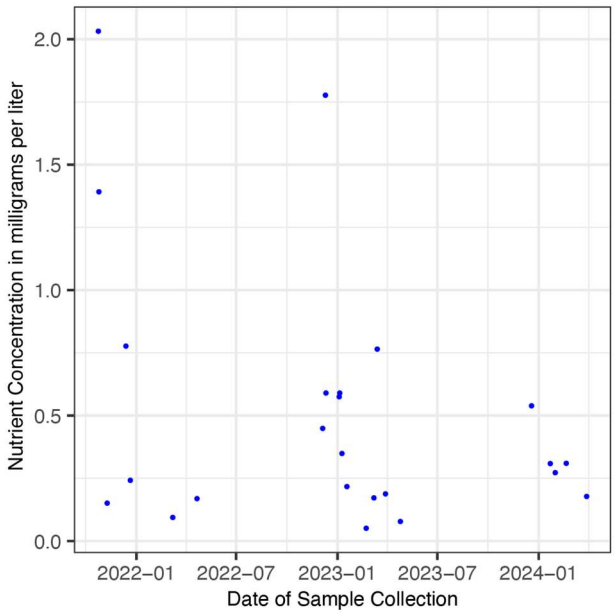
Nutrient Concentration in milligrams per liter
Date of Sample Collection
0.0
0.5
1.0
1.5
2.0
2022–01
2022–07
2023–01
2023–07
2024–01

TP

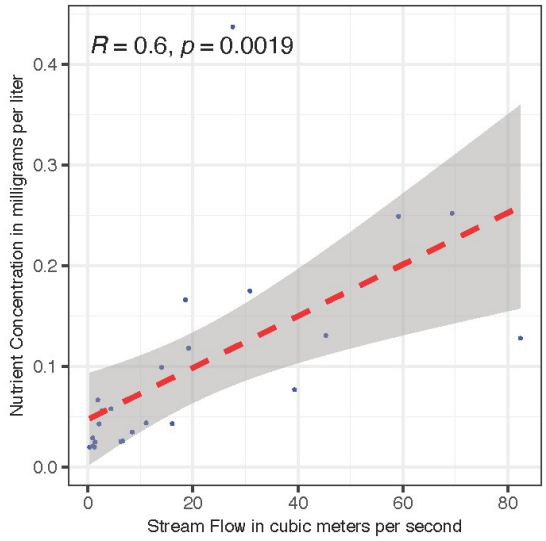
R = 0.6, p = 0.0019
Nutrient Concentration in milligrams per liter
0.0
0.1
0.2
0.3
0.4
0
20
40
60
80
Stream Flow in cubic meters per second

TP

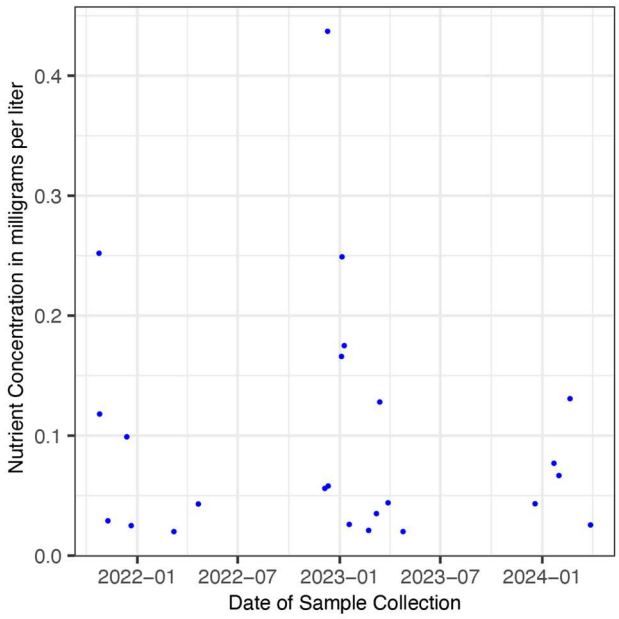
Nutrient Concentration in milligrams per liter
0.0
0.1
0.2
0.3
0.4
2022–01
2022–07
2023–01
2023–07
2024–01
Date of Sample Collection

Lower Kelsey Creek, at Soda Bay Road (KCK/KCS)

DP

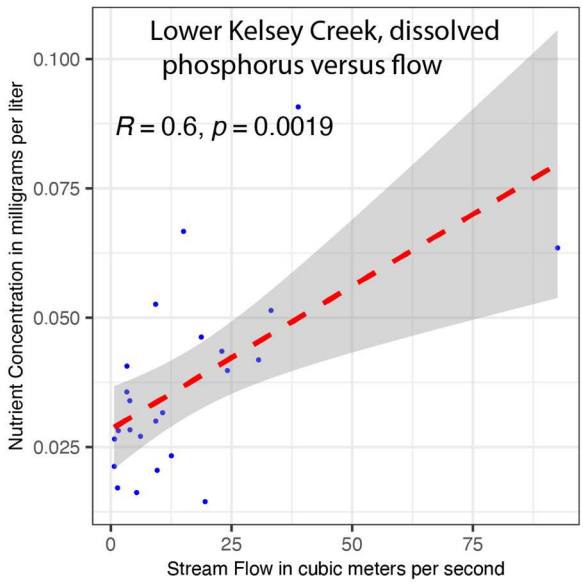

DP

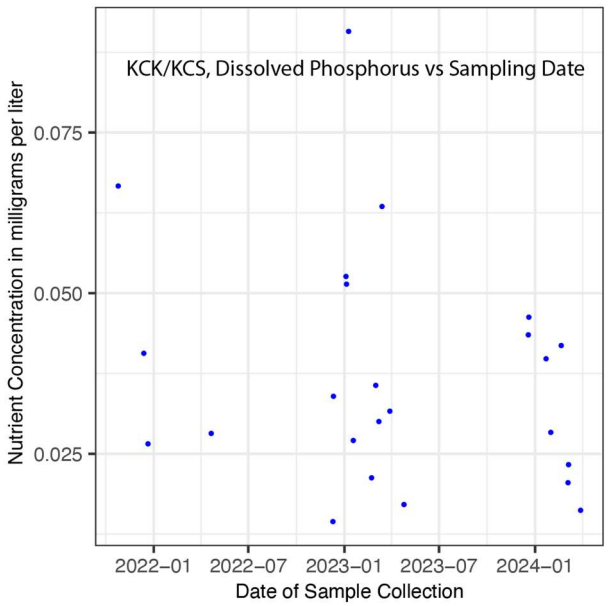

NH4

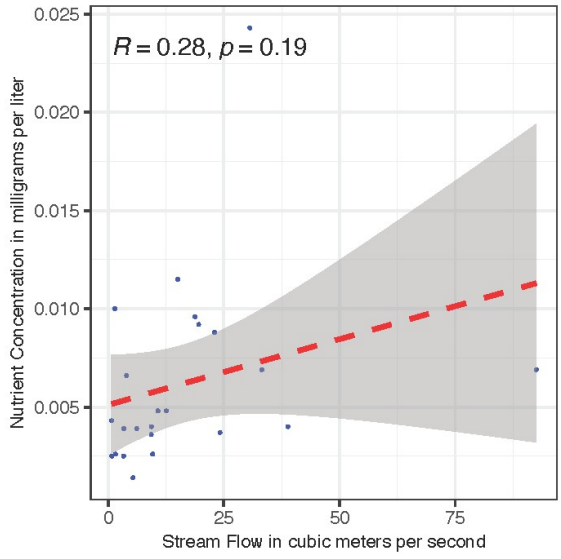

NH4

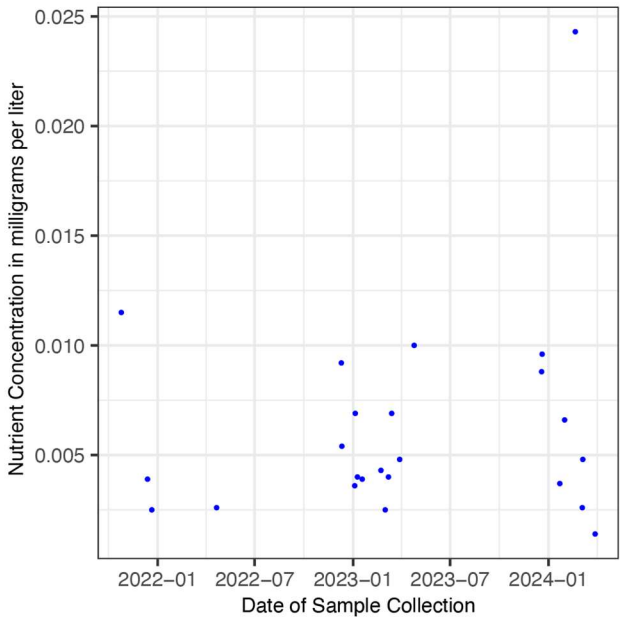

NO3

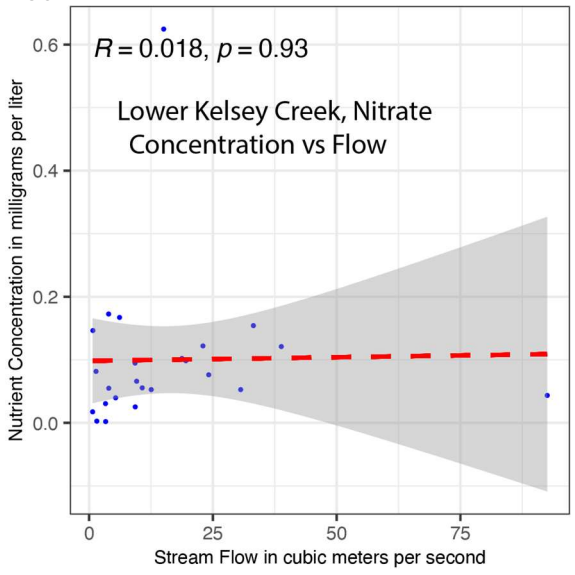

NO3

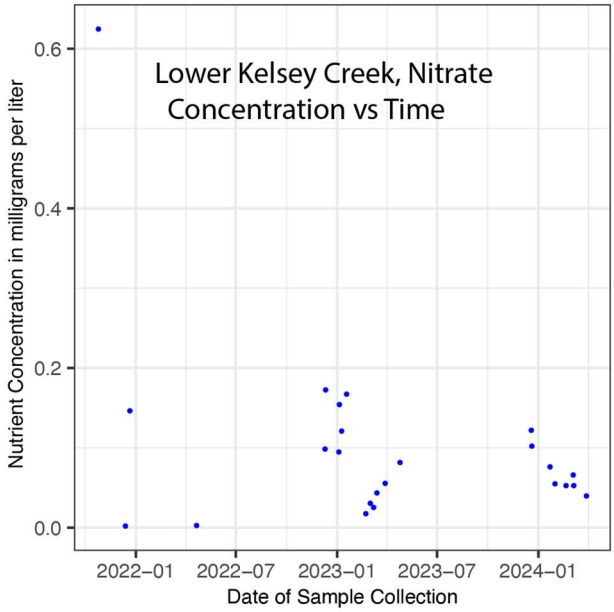

SRP

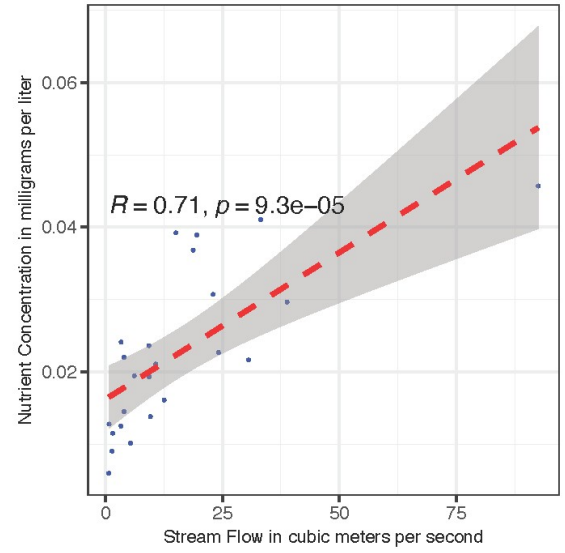

SRP

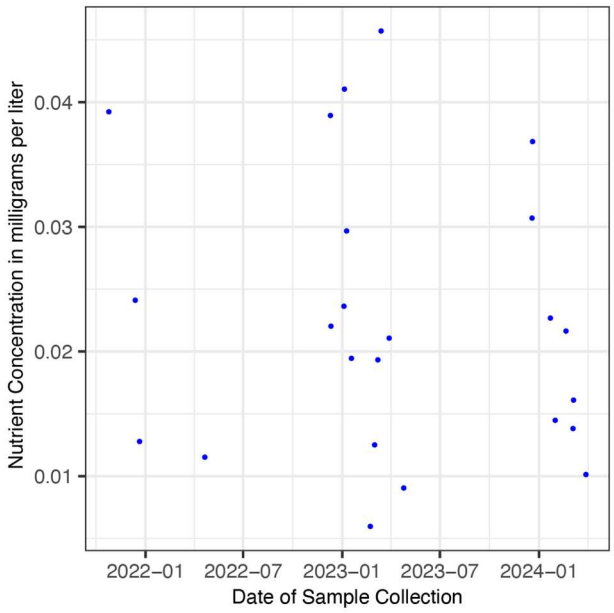

TKN

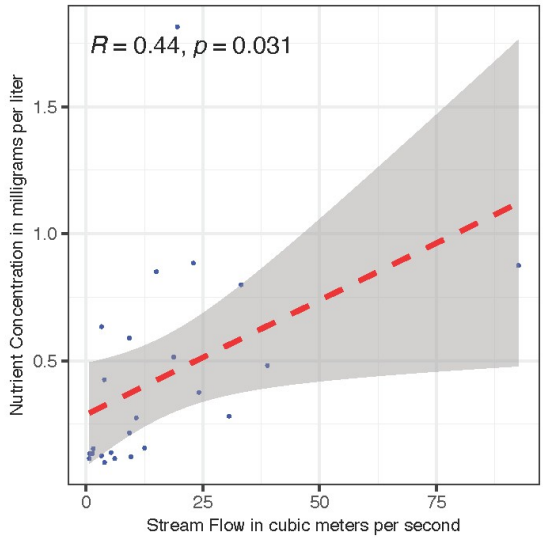
R = 0.44, p = 0.031
Nutrient Concentration in milligrams per liter
1.5
1.0
0.5
0
25
50
75
Stream Flow in cubic meters per second

TKN

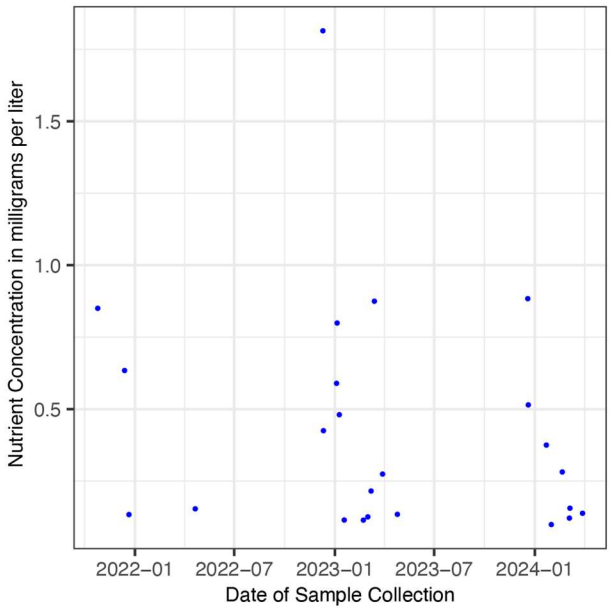
Nutrient Concentration in milligrams per liter
1.5
1.0
0.5
2022–01
2022–07
2023–01
2023–07
2024–01
Date of Sample Collection

TN

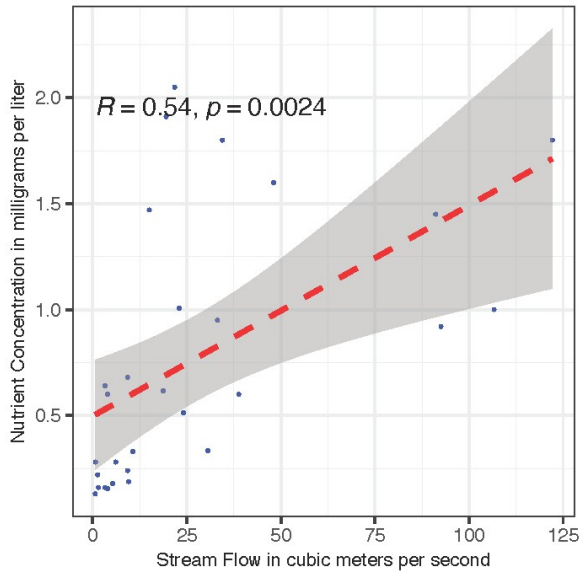
R = 0.54, p = 0.0024
Nutrient Concentration in milligrams per liter
2.0
1.5
1.0
0.5
0
25
50
75
100
125
Stream Flow in cubic meters per second

TN

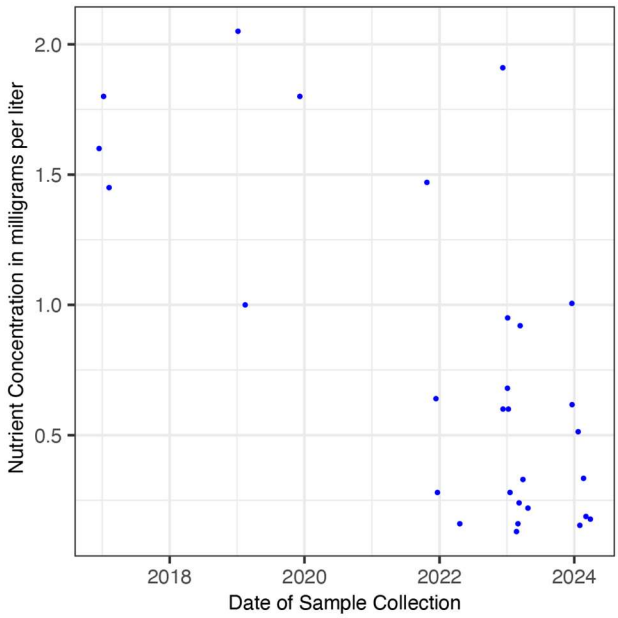
Nutrient Concentration in milligrams per liter
2.0
1.5
1.0
0.5
2018
2020
2022
2024
Date of Sample Collection

TP

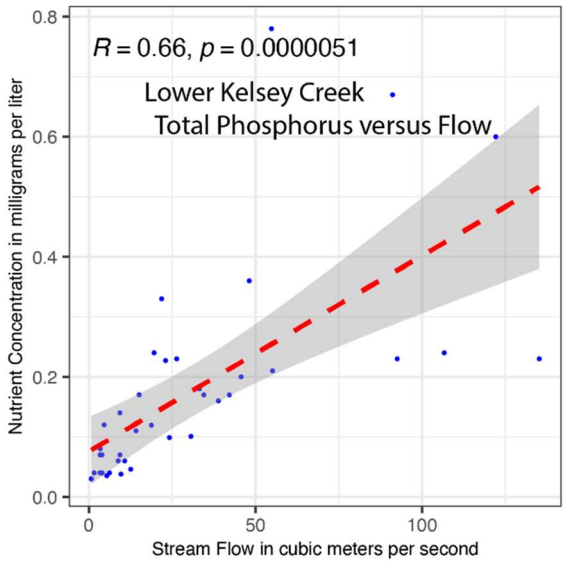
R = 0.66, p = 0.0000051
Lower Kelsey Creek
Total Phosphorus versus Flow
Nutrient Concentration in milligrams per liter
Stream Flow in cubic meters per second
0.0
0.2
0.4
0.6
0.8
0
50
100

TP

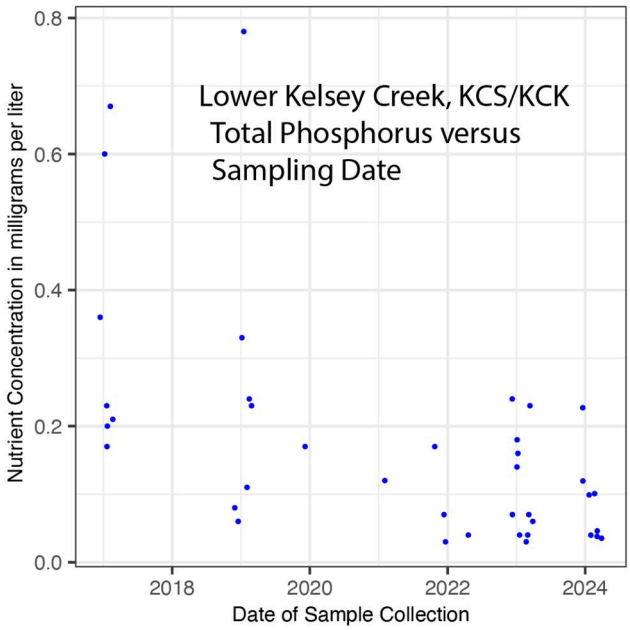
Lower Kelsey Creek, KCS/KCK
Total Phosphorus versus
Sampling Date
Nutrient Concentration in milligrams per liter
Date of Sample Collection
0.0
0.2
0.4
0.6
0.8
2018
2020
2022
2024

Clover Creek (CCK)

DP

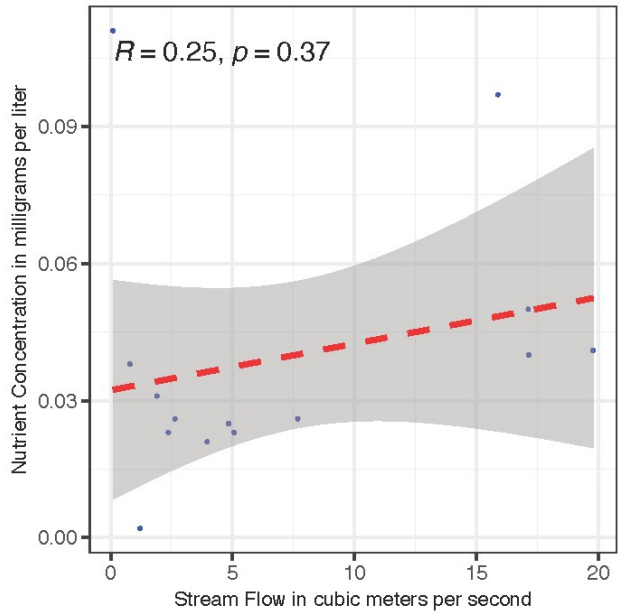

DP

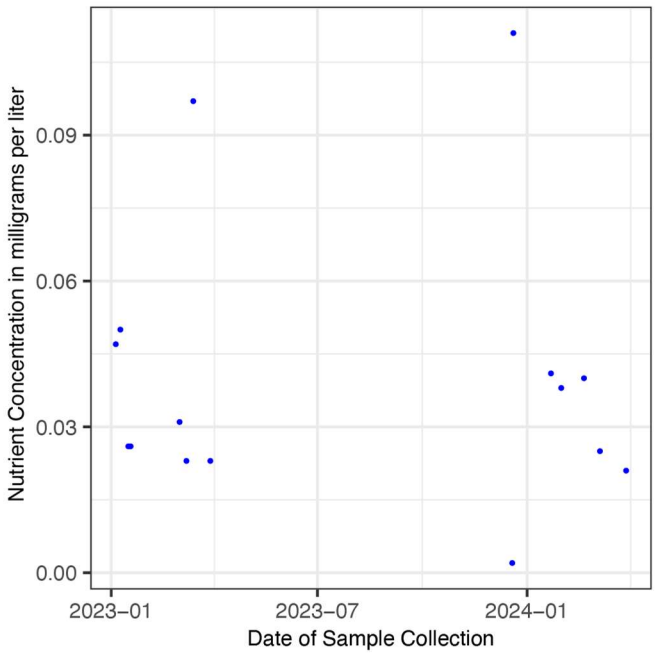

NH4

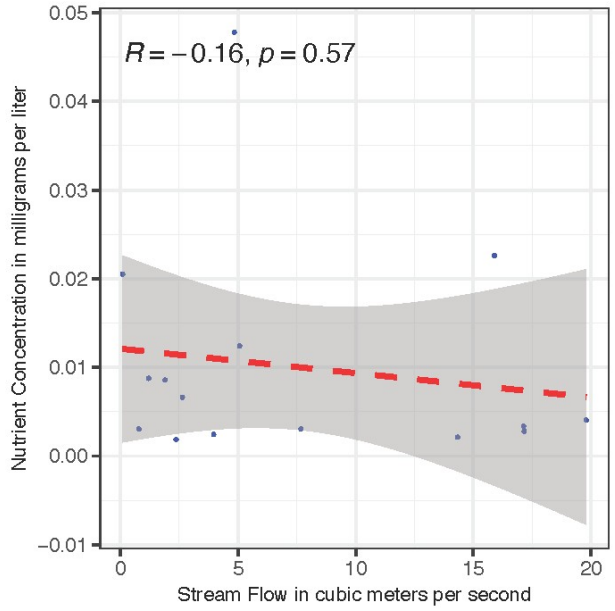

NH4

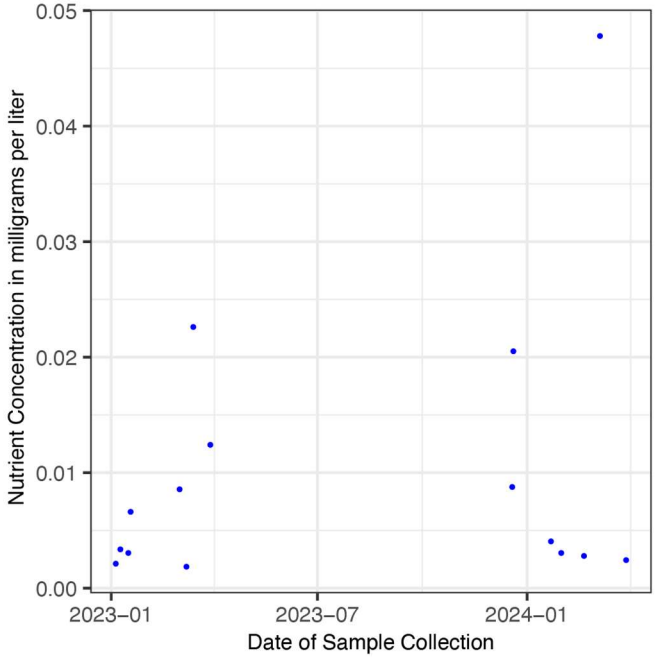

NO3

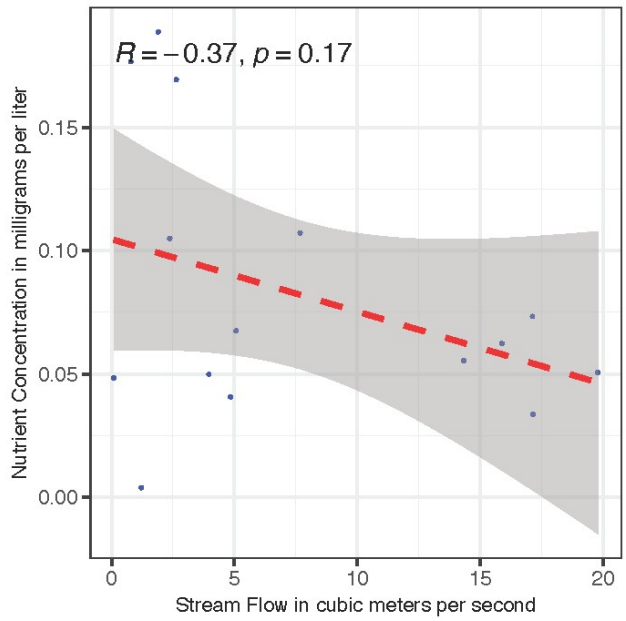

NO3

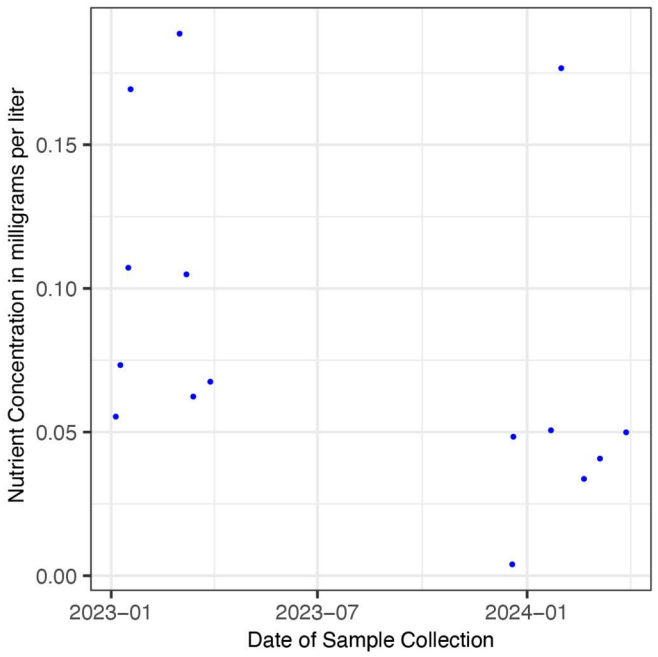

SRP

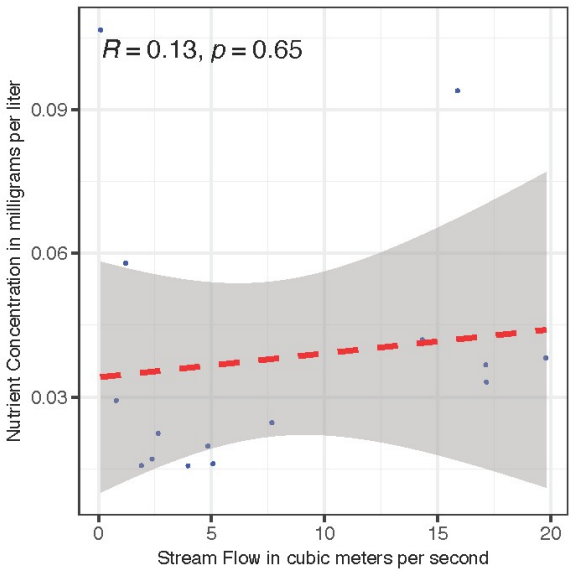

SRP

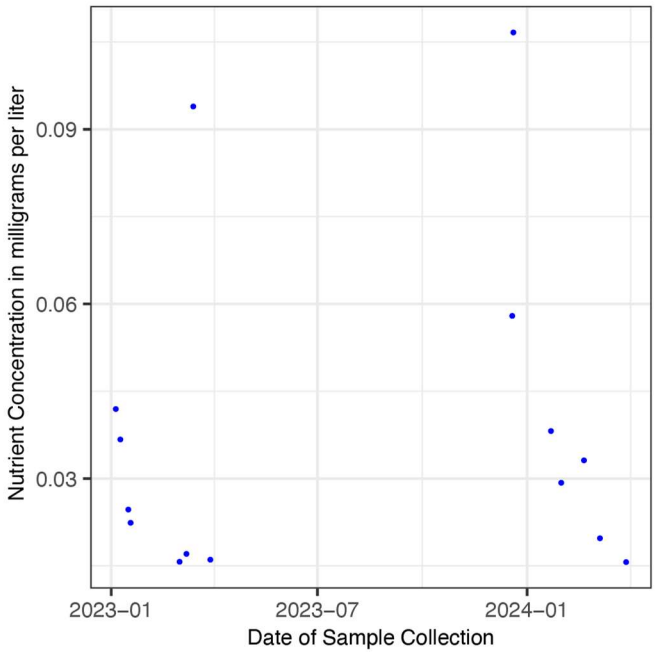

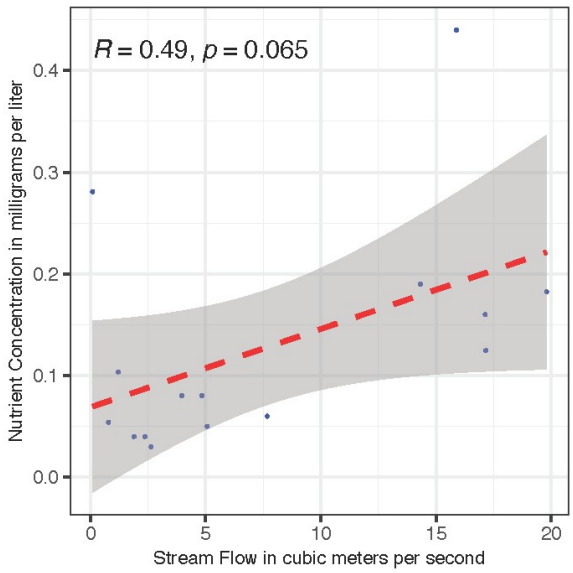
R = 0.49, p = 0.065
Nutrient Concentration in milligrams per liter
0.0
0.1
0.2
0.3
0.4
0
5
10
15
20
Stream Flow in cubic meters per second

TP

TP

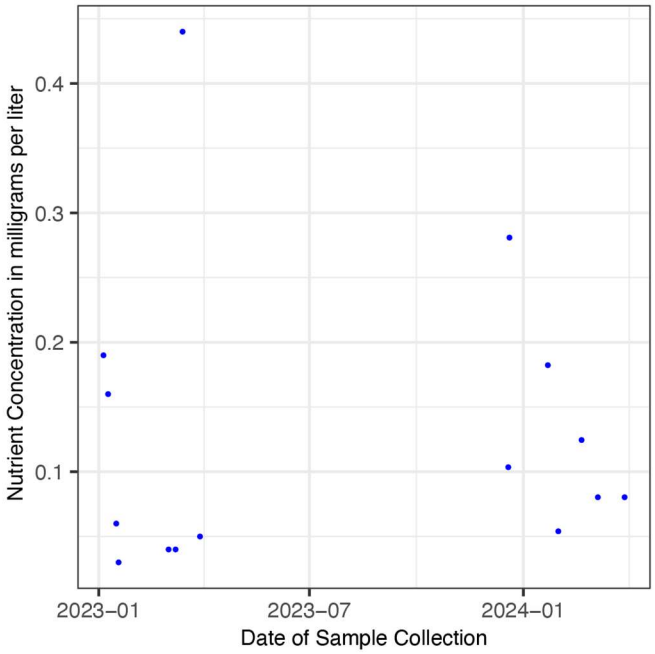
Nutrient Concentration in milligrams per liter
0.1
0.2
0.3
0.4
2023–01
2023–07
2024–01
Date of Sample Collection

Molesworth Creek (MCH)

DP

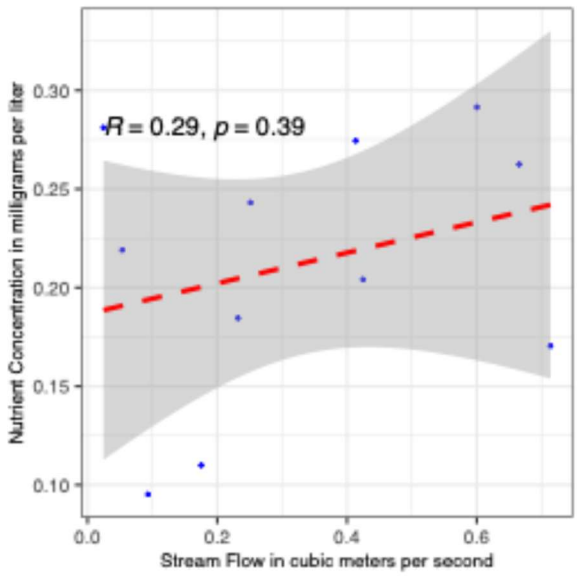

DP

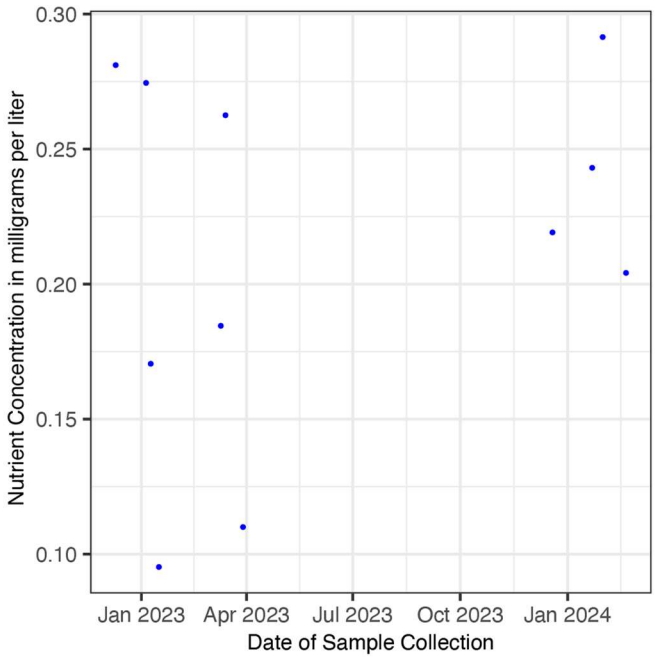

NH4

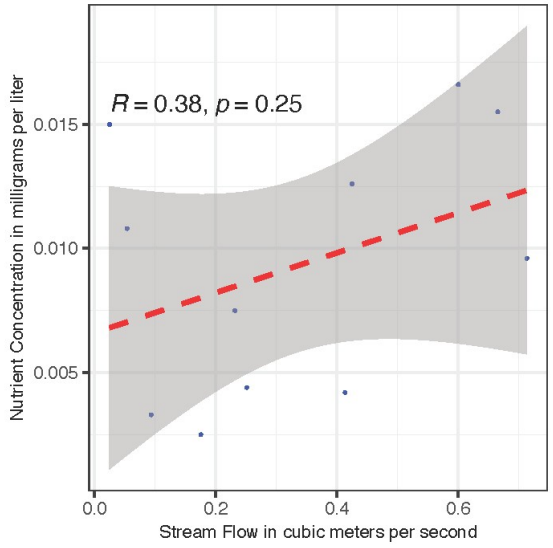

NH4

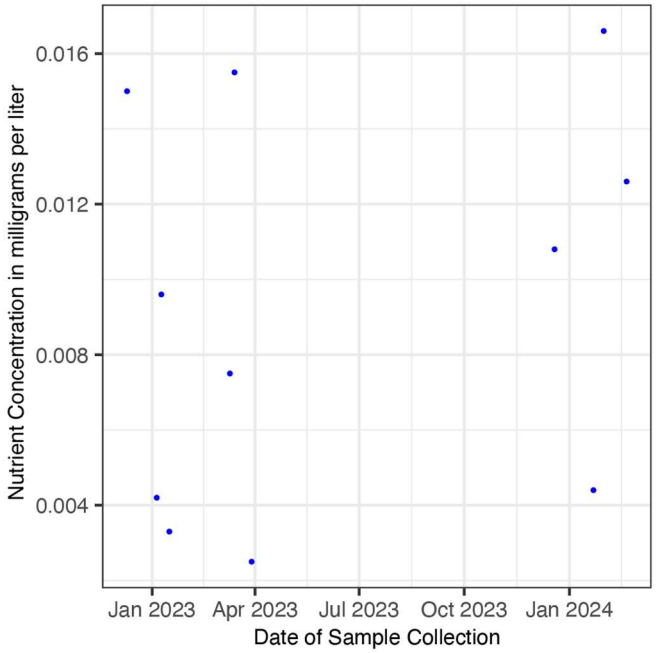

NO3

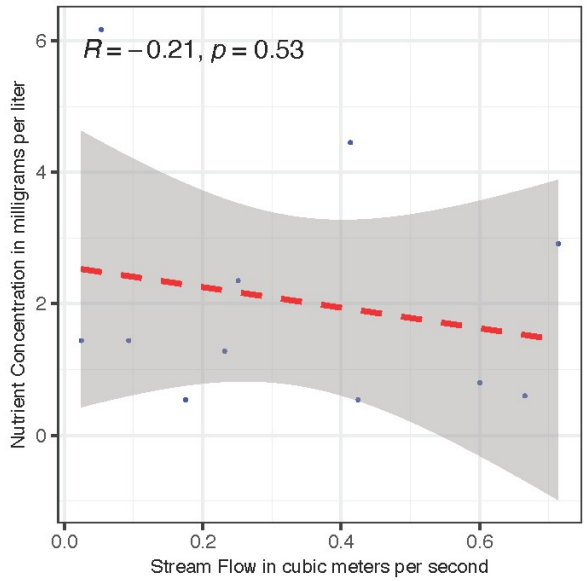

NO3

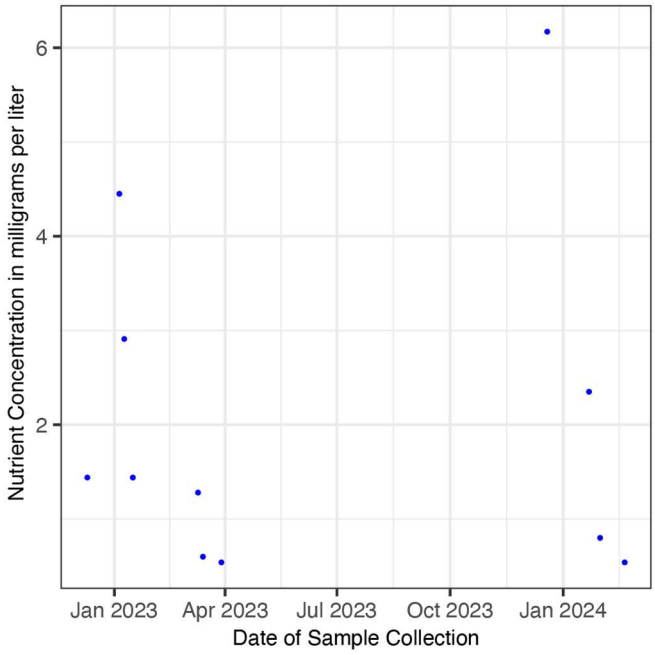

SRP

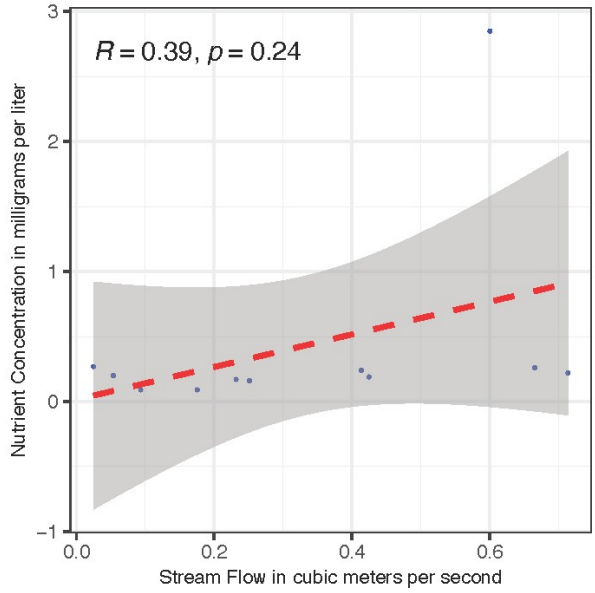

SRP

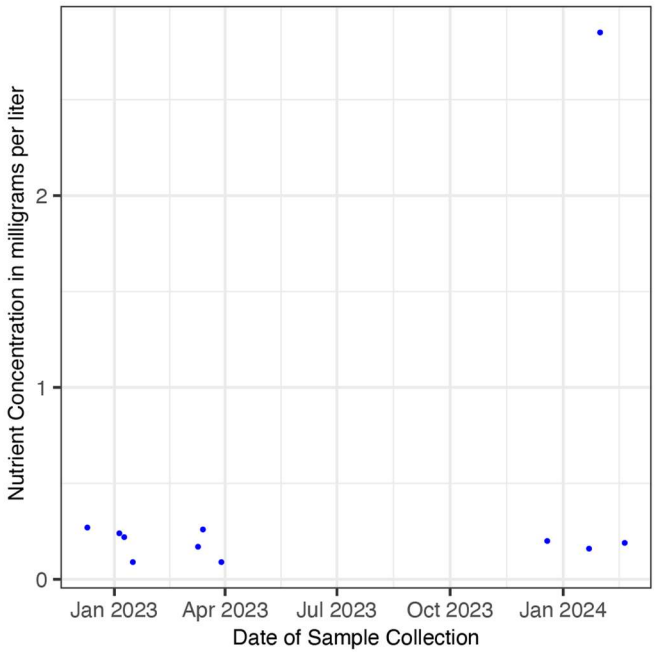

TKN

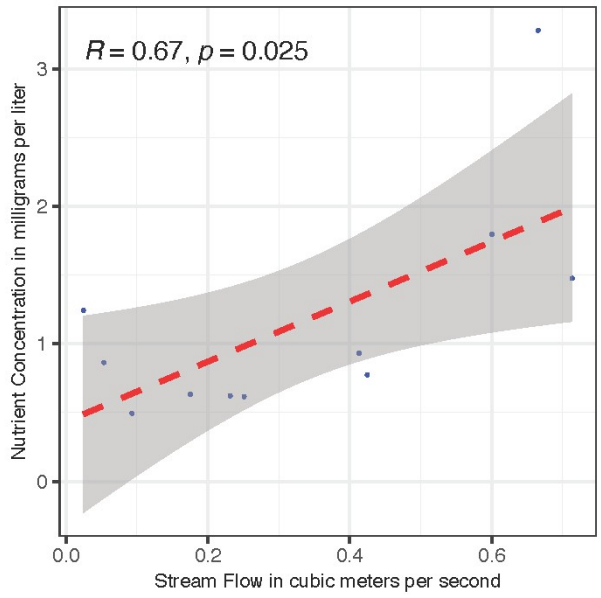
R = 0.67, p = 0.025
Nutrient Concentration in milligrams per liter
Stream Flow in cubic meters per second
0
1
2
3
0.0
0.2
0.4
0.6

TKN

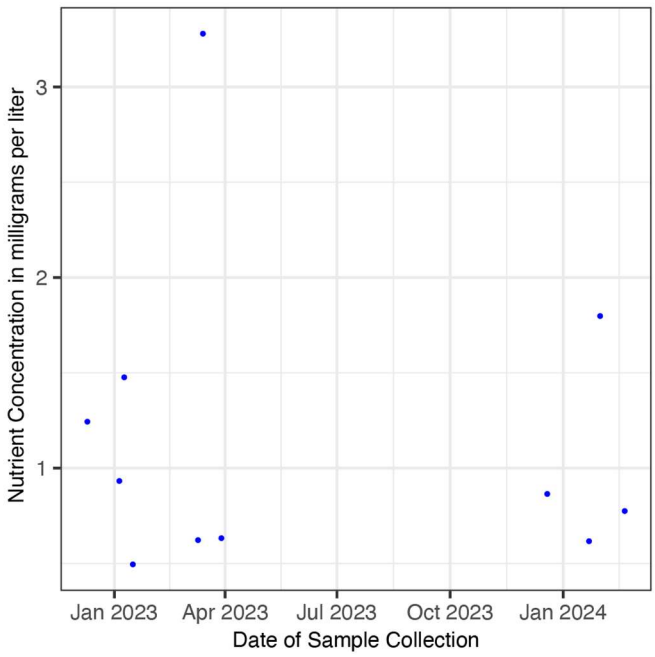
Nutrient Concentration in milligrams per liter
Date of Sample Collection
1
2
3
Jan 2023
Apr 2023
Jul 2023
Oct 2023
Jan 2024

TN

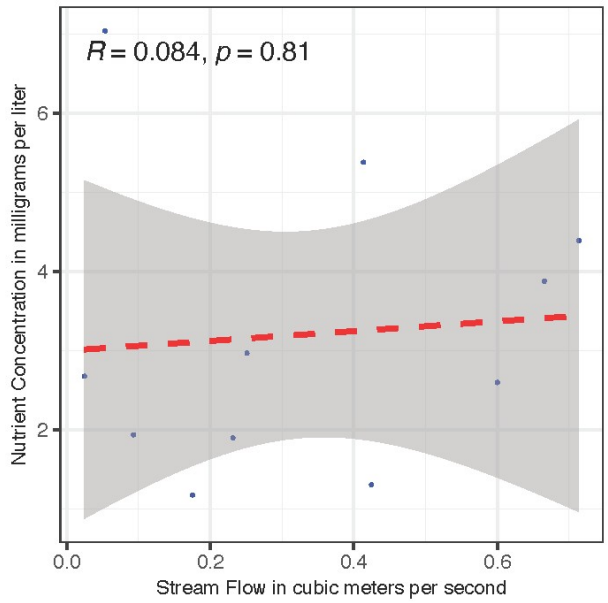
R = 0.084, p = 0.81
Nutrient Concentration in milligrams per liter
Stream Flow in cubic meters per second
2
4
6
0.0
0.2
0.4
0.6

TN

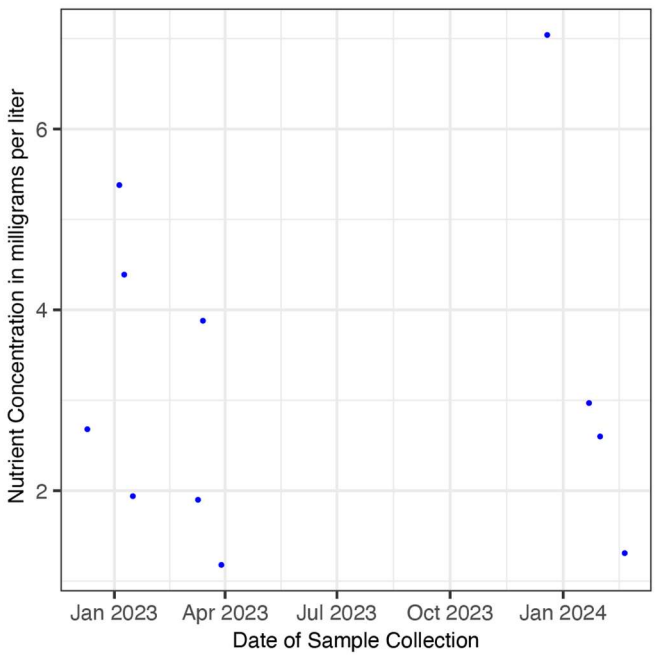
Nutrient Concentration in milligrams per liter
Date of Sample Collection
2
4
6
Jan 2023
Apr 2023
Jul 2023
Oct 2023
Jan 2024

TP

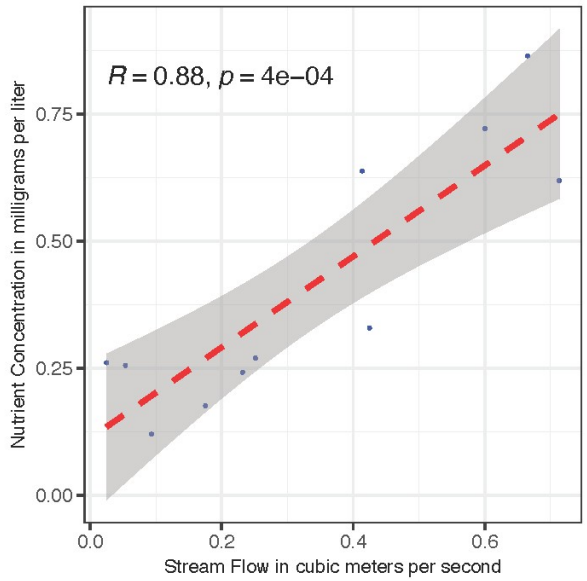

TP

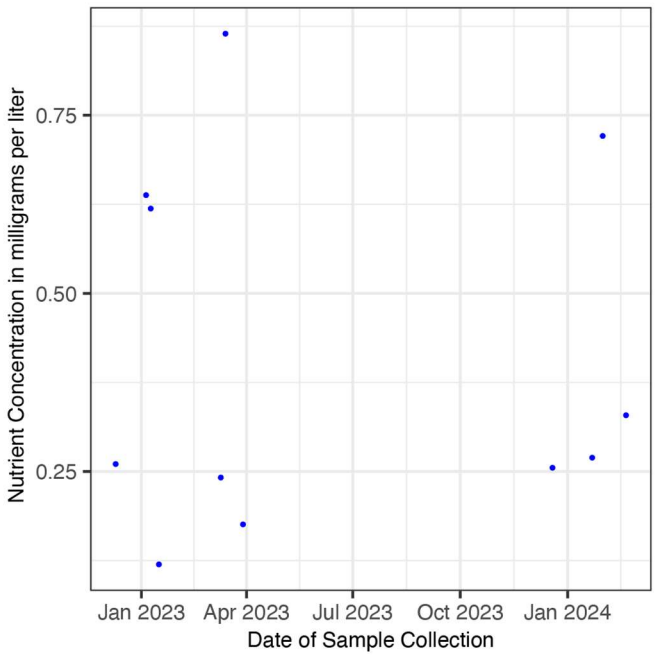

References Cited

Sushch, D., Alpers, C.N., Watanabe, P.T., Bennett, P.A., Brewster, G.D., Hansen, A., Le, A.K., Marvin-DiPasquale, M.C., Agee, J.L., Kieu, L., Kakouros, E., DePalma-Dow, A., Beaton, J., Liston, A.M., Sesma, S.M., Martinez, K.C., Cortes, A., and Schladow, S.G., 2025, Geochemical data for selected streams in the Clear Lake basin, Lake County, California: U.S. Geological Survey data release, https://doi.org/10.5066/P9AKO3CG

15.6 Upper Watershed Modeling (USGS)

15.6.2 SPARROW

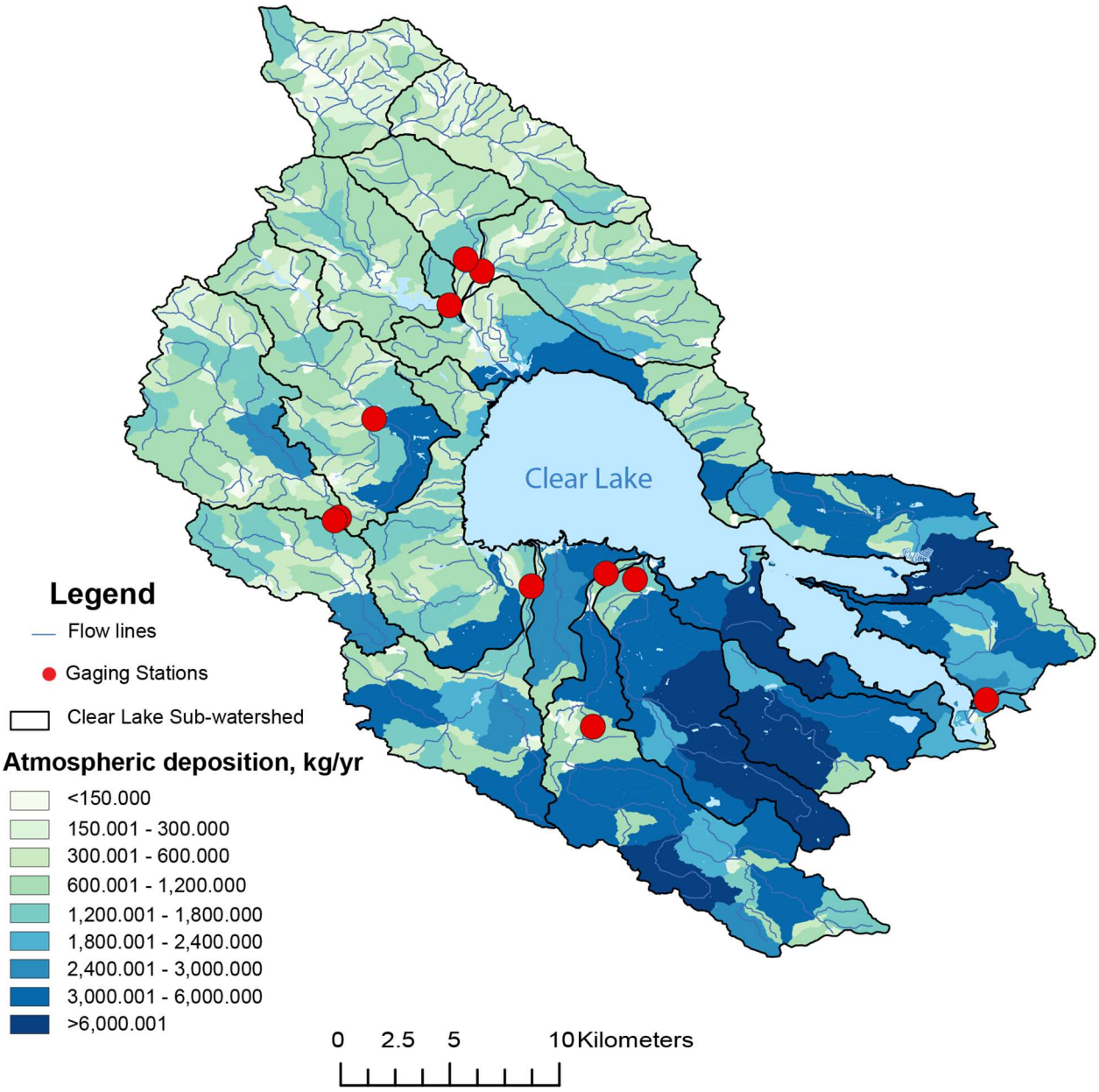

Figure 15.6.2.1. Map of Clear Lake Atmospheric deposition used to develop the Total Nitrogen (TN) SPARROW model for base year 2020. [kg/yr, kilogram per year]

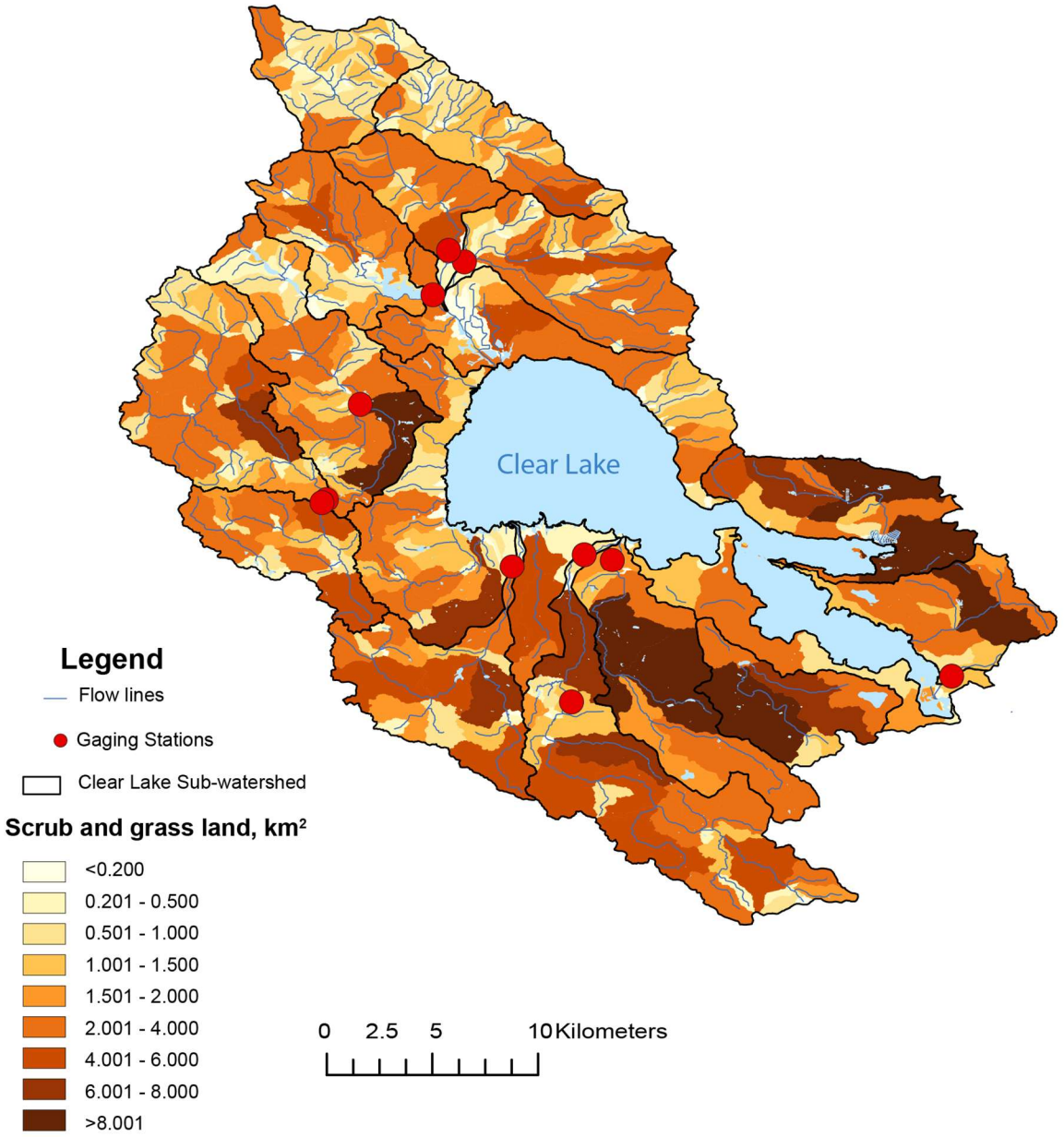

Figure 15.6.2.2. Map of spatial distribution of Scrub and grass land areas in Clear Lake used as a source variable in the Clear Lake SPARROW models, with 2020 base year. [km², square kilometer]

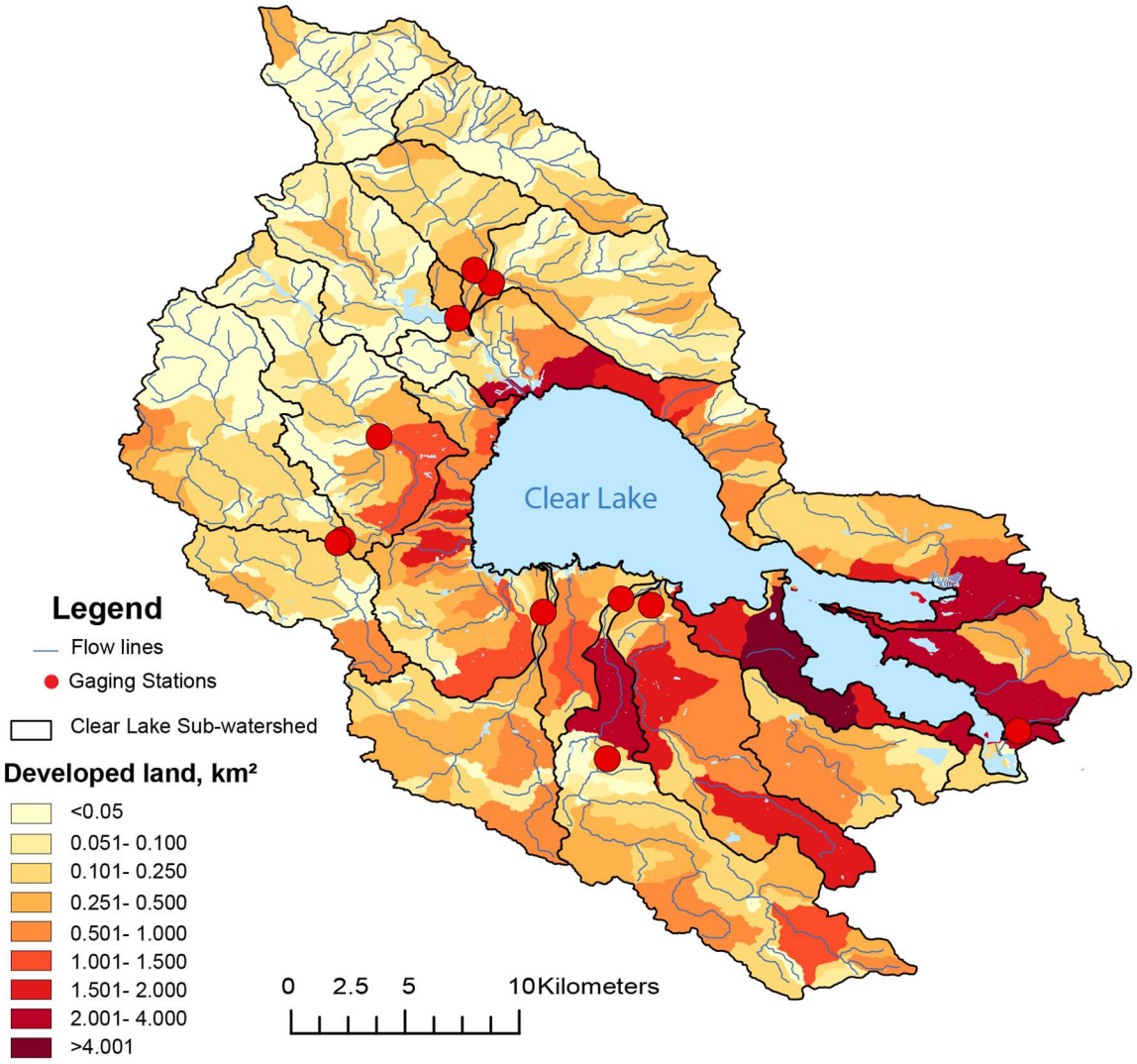

Figure 15.6.2.3. Map of spatial distribution of Developed land areas in Clear Lake used as a source variable in the Clear Lake SPARROW models, with 2020 base year. [km2, square kilometer]

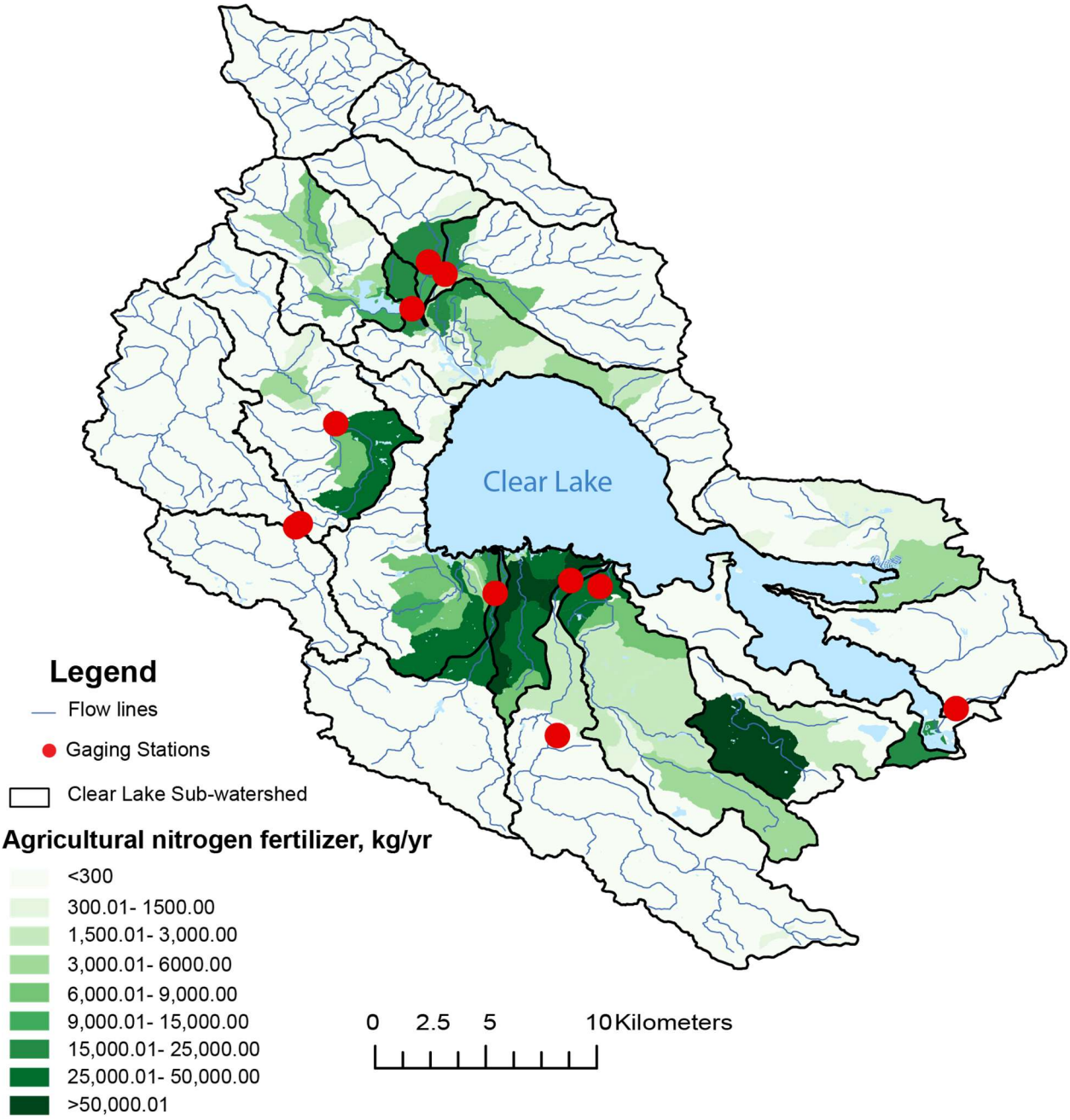

Figure 15.6.2.4. Map of spatial distribution of Nitrogen fertilizer applied in Clear Lake used as a source variable in the Clear Lake SPARROW models, with 2020 base year. [kg/yr, kilogram per year]

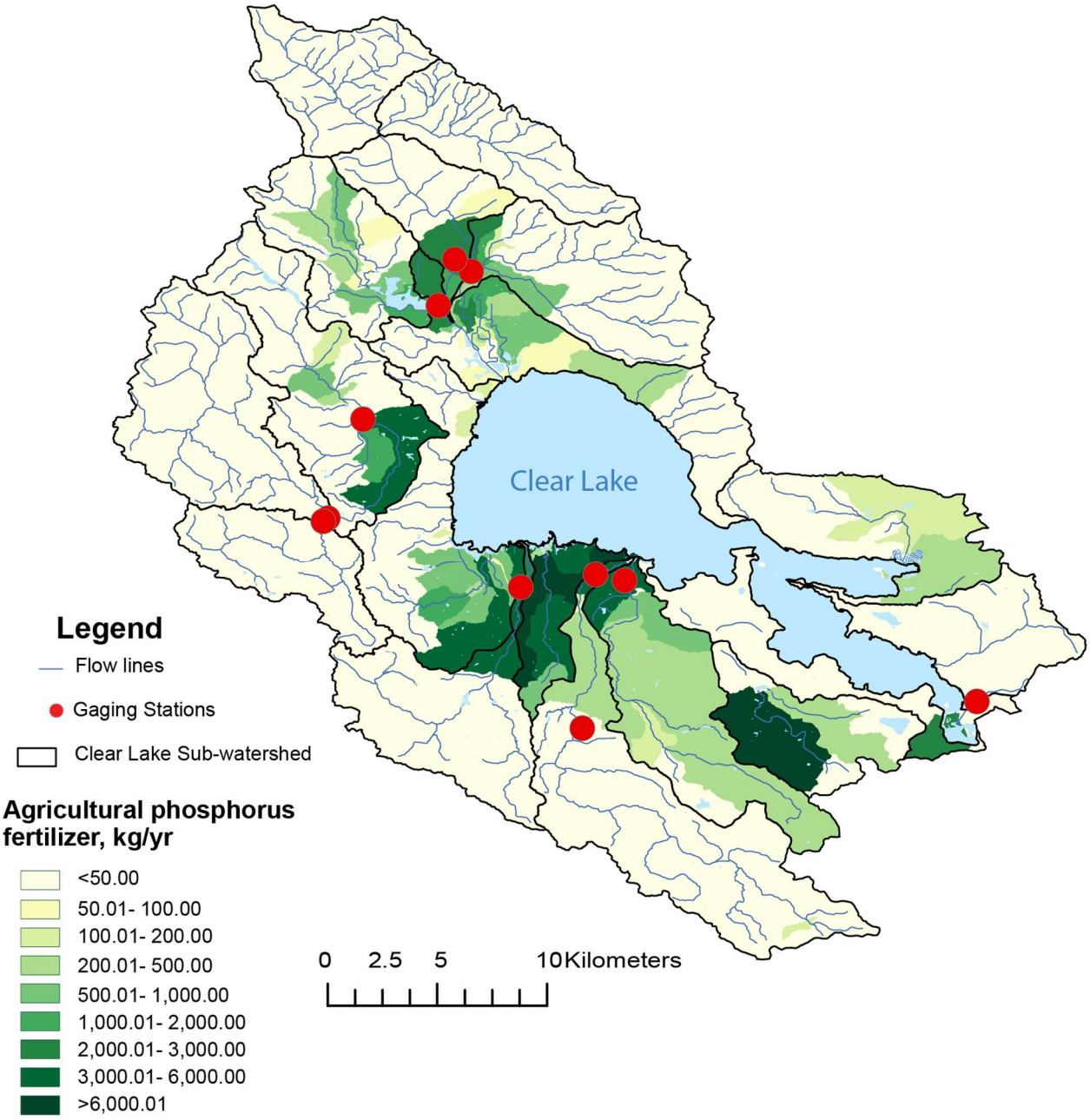

Figure 15.6.2.5. Map of spatial distribution of Phosphorus fertilizer applied in Clear Lake used as a source variable in the Clear Lake SPARROW models, with 2020 base year. [kg/yr, kilogram per year]

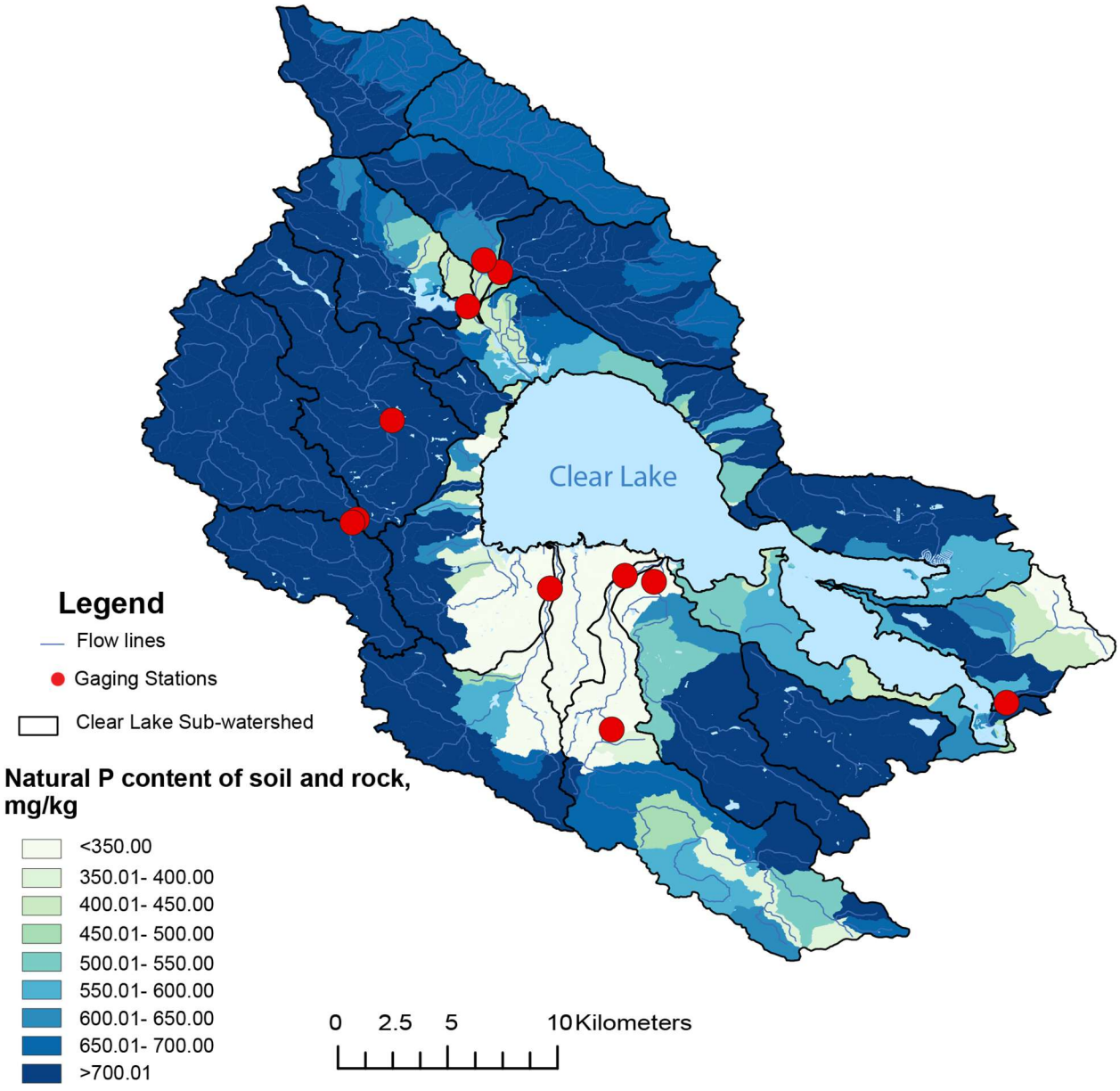

Figure 15.6.2.6. Map of spatial distribution of natural phosphorus content in soil and rocks in Clear Lake used as a source variable in the Clear Lake SPARROW models, with 2020 base year. [mg/kg, milligram per kilogram]

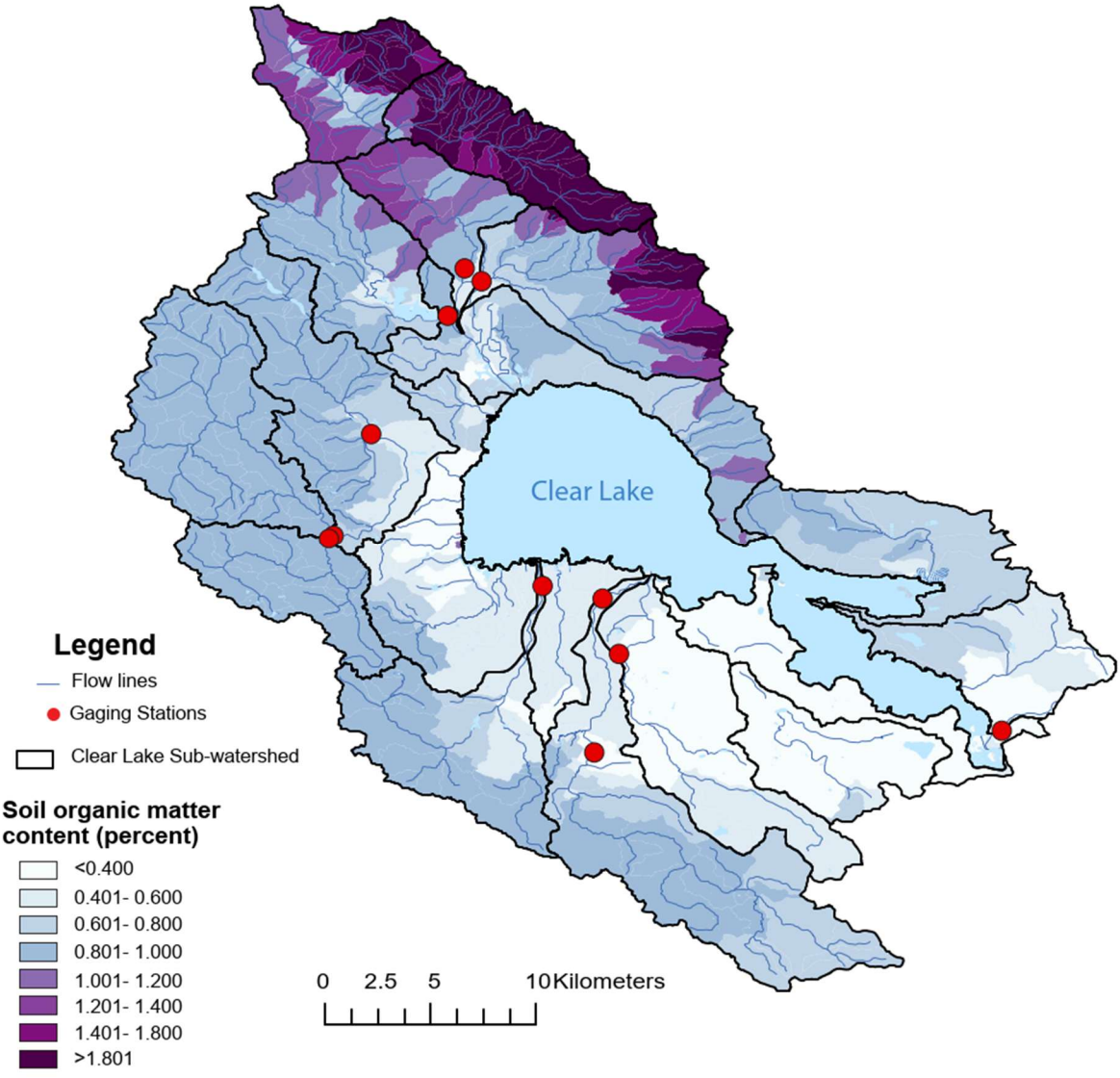

Figure 15.6.2.7. Map of spatial distribution of soil organic matter content Clear Lake used as a delivery variable in the Clear Lake SPARROW models, with 2020 base year.[percent]

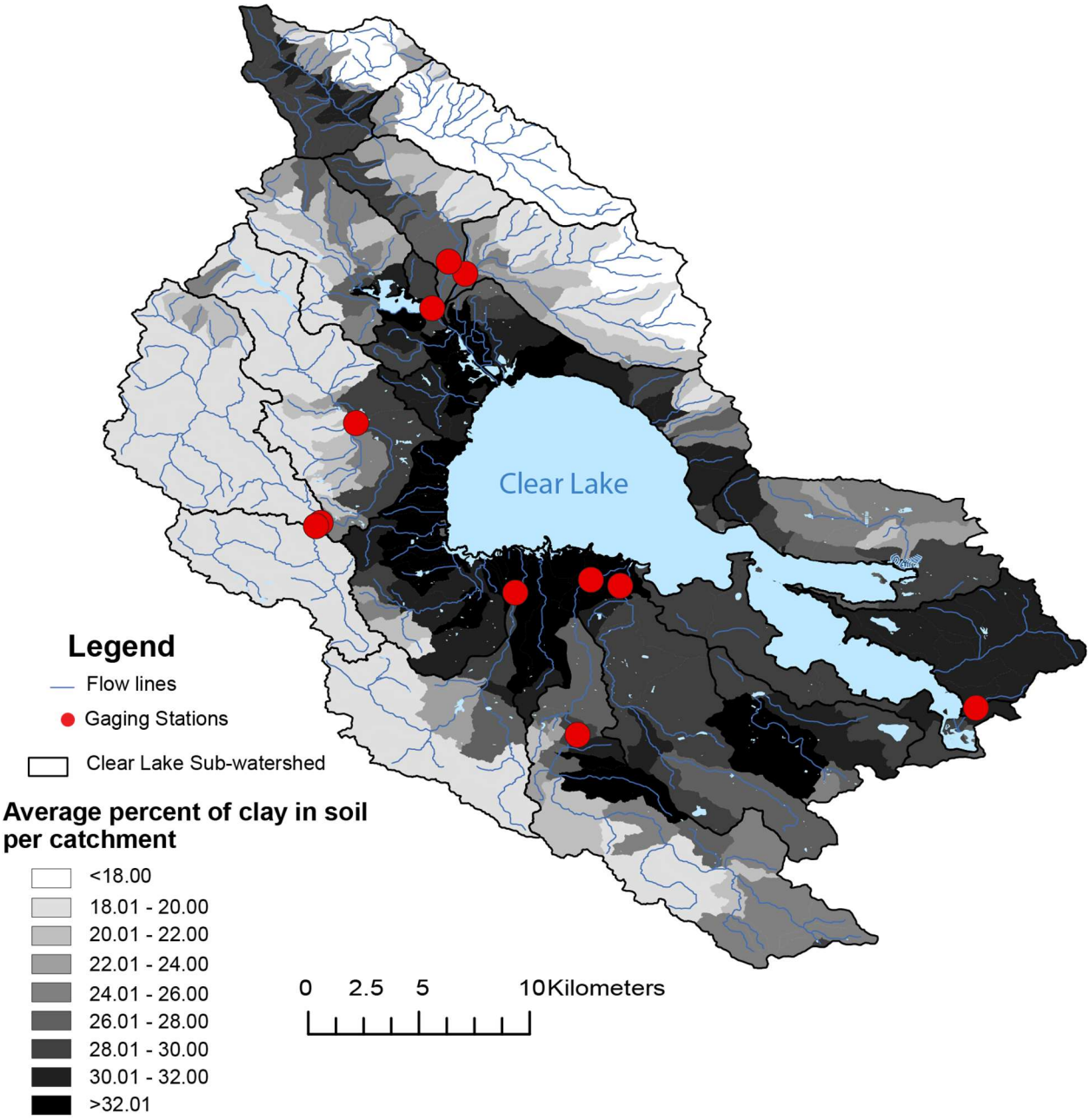

Figure 15.6.2.8. Map of spatial distribution of soil clay content Clear Lake used as a delivery variable in the Clear Lake SPARROW models, with 2020 base year.[percent]

15.6.4 Sediment Fingerprinting

Additional tables and figures for the section on Sediment Fingerprinting (6.4) are provided here.

Table 15.6.4.1. Proportions of geologic map units in tributaries to Clear Lake. Source: Saucedo et al. (2000)

Geologic Unit	Adobe Cr	Burns Valley	Clover Cr	Cole Cr	Kelsey Cr	Manning Cr	Middle Cr	Molesworth Cr	Rodman Slough	Schindler Cr	Scotts Creek (all)	Scotts Creek (upper)
Water	0.37%	0.02%	0.00%	0.40%	0.00%	0.00%	0.00%	0.00%	0.00%	0.00%	0.00%	0.00%
KJf	62.91%	3.41%	89.68%	0.00%	37.26%	31.50%	39.86%	0.00%	68.67%	53.64%	83.13%	99.93%
KJfm	0.00%	0.00%	0.02%	0.00%	0.63%	0.00%	13.17%	0.00%	4.24%	0.00%	0.00%	0.00%
KJfs	0.00%	0.00%	2.24%	0.00%	0.00%	0.00%	24.54%	0.00%	6.57%	0.00%	0.00%	0.00%
Mzv	9.87%	36.35%	0.00%	0.00%	2.46%	25.70%	0.00%	0.00%	2.68%	0.00%	4.32%	0.07%
Kl	0.00%	0.00%	0.00%	0.00%	0.00%	0.00%	6.36%	5.49%	2.90%	0.00%	1.22%	0.00%
um	5.51%	0.00%	0.00%	0.00%	12.22%	0.23%	0.00%	0.00%	0.18%	0.00%	0.34%	0.00%
Ku	0.00%	0.00%	0.00%	0.01%	2.23%	0.00%	14.75%	0.00%	6.30%	0.00%	4.56%	0.00%
Q	21.26%	0.00%	8.06%	15.23%	16.86%	42.57%	1.33%	0.00%	8.47%	30.68%	6.43%	0.00%
Qv	0.00%	9.31%	0.00%	84.35%	28.34%	0.00%	0.00%	16.56%	0.00%	0.00%	0.00%	0.00%
QPc	0.00%	49.46%	0.00%	0.00%	0.00%	0.00%	0.00%	77.92%	0.00%	0.00%	0.00%	0.00%
Qrv	0.00%	1.45%	0.00%	0.00%	0.00%	0.00%	0.00%	0.00%	0.00%	15.68%	0.00%	0.00%

Table 15.6.4.2. Proportions of geologic map units in tributaries to Clear Lake, grouped as in Trial 1, with drainage areas. Source: Saucedo et al. (2000).

	Group 1	Group 2	Group 3	Group 4
gic Unit	Scotts Cr & Adobe Cr & Manning Cr	Cole Cr & Kelsey Cr	Burns Valley / Molesworth Cr & Schindler Cr	Clover Cr & Middle Cr
Water	0.07%	0.16%	0.01%	0.00%
KJf	75.17%	22.66%	27.87%	57.46%
KJfm	0.00%	0.38%	0.00%	8.52%
KJfs	0.00%	0.00%	0.00%	16.66%
Mzv	7.10%	1.49%	16.05%	0.00%
Kl	0.89%	0.00%	0.37%	4.11%
um	1.30%	7.43%	0.00%	0.00%
Ku	3.34%	1.36%	0.00%	9.54%
Q	12.13%	16.22%	15.08%	3.71%
Qv	0.00%	50.29%	5.22%	0.00%
QPc	0.00%	0.00%	27.05%	0.00%
Qrv	0.00%	0.00%	8.35%	0.00%
Drainage Area				
square miles	141.42	72.32	24.78	76.79
hectares	36,627	18,730	6,418	19,889
% of modeled area	44.9%	22.9%	7.9%	24.4%

Geologic Unit	Description
Water	Water
KJf	Franciscan Complex Cretaceous and Jurassic sandstone with smaller amounts of shale chert limestone and conglomerate includes Franciscan mélange except where separated
KJfm	Mélange of fragmented and sheared Franciscan Complex rocks
KJfs	Blueschist and semi-schist of Franciscan Complex
Mzv	Undivided Mesozoic volcanic and metavolcanic rocks. Andesite and rhyolite flow rocks greenstone, volcanic breccia and other pyroclastic rocks in part strongly metamorphosed. Includes volcanic rocks of Franciscan Complex basaltic pillow lava, diabase, greenstone
Kl	Lower Cretaceous sandstone, shale, and conglomerate
um	Ultramafic rocks. Mostly serpentine. Minor peridotite, gabbro, and diabase, chiefly Mesozoic
Ku	Upper Cretaceous sandstone, shale, and conglomerate
Q	Alluvium lake playa and terrace deposits unconsolidated and semi-consolidated. Mostly nonmarine but includes marine deposits near the coast.
Qv	Quaternary volcanic flow rocks minor pyroclastic deposits
QPc	Pliocene and or Pleistocene sandstone shale and gravel deposits mostly loosely consolidated
Qrv	Recent volcanic flow rocks minor pyroclastic deposits

*Table 15.6.4.3. Trial 1 optimal geochemical parameters using in-mixing analysis based on Discriminant Function Analysis results. P_i is the proportion of source sample types classified correctly with parameter (i). W_i is parameter discriminatory weighting factor for parameter (i). [K, potassium; Rb, rubidium; Cr, chromium; Cs, cesium; Mg, magnesium; Li, lithium; LOI-2*TOC, loss on ignition minus two times total organic carbon; Ba, barium; Sr, strontium, U, uranium, Sc, scandium; Y, yttrium]*

Tracer	P_i	W_i
K	0.772	3.244
Rb	0.642	2.697
Cr	0.592	2.487
Cs	0.565	2.374
Mg	0.550	2.311
Li	0.542	2.277
LOI-2*TOC	0.516	2.168
Ba	0.496	2.084
Sr	0.495	2.080
U	0.495	2.080
Sc	0.426	1.790
Y	0.238	1

Table 15.6.4.4. Trial 1 error analysis for individual target samples estimated using 1000 Monte Carlo simulations.

SampleName	Mean error (%)	standard deviation
SFS-0907	2.47	0.11
SFS-0908	5.29	0.16
SFS-0909	5.43	0.14
SFS-0910	5.65	0.1
SFS-0912	4.77	0.08
SFS-0913	4.56	0.08
SFS-0902	10.53	0.23
SFS-0903	4.75	0.09
SFS-0904	5.29	0.1
SFS-0905	3.1	0.1
SFS-0906	4.88	0.07
SFS-0914	3.19	0.02
SFS-0915	3.61	0.05
SFS-0916	3.69	0.06
SFS-0917	3.51	0.04
SFS-0918	3	0.04
SFS-0919	2.54	0.03
SFS-0920	2.94	0.04
SFS-0921	3	0.04
SFS-0922	3.33	0.04
SFS-0923	3.22	0.04
SFS-0924	3.09	0.04
SFS-0925	2.98	0.04
SFS-0926	2.02	0.03
SFS-0927	1.62	0.04
Average	3.94	

Table 15.6.4.5. Trial 1 confusion matrix. Columns indicate actual distribution of samples. Rows indicate modeled distribution.

		Source Group 1	Source Group 2	Source Group 3	Source Group 4	
		ScottsC+AdobeC+ ManningC	ColeC+KelseyC	BVM+SchindlerC	CloverC+MiddleC	Total
Source Group 1	ScottsC+AdobeC+ManningC	72	0	2	1	
Source Group 2	ColeC+KelseyC	0	12	0	0	
Source Group 3	BVM+SchindlerC	0	0	15	0	
Source Group 4	CloverC+MiddleC	1	0	0	12	
	Total	73	12	17	13	115
	Percent correct	98.6%	100.0%	88.2%	92.3%	96.5%

Table 15.6.4.6. Trial 1 source verification test (SVT) results computed by running each source sample through the unmixing model as a target sample.

		Source Verification Test			
		Group 1	Group 2	Group 3	Group 4
		Adobe, Manning, & Scotts Cr	Cole & KelseyC	Burns Valley, Molesworth, & SchindlerC	Clover & MiddleC
Adobe, Manning, & Scotts Cr (N=73)	Mean	83	1	5	11
	SD	25	3	11	20
	Min	10	0	0	0
	Max	100	17	48	76
Cole & KelseyC (N=12)	Mean	4	59	25	12
	SD	7	36	26	28
	Min	0	0	2	0
	Max	22	94	100	73
Burns Valley, Molesworth, & SchindlerC (N=17)	Mean	24	0	75	2
	SD	31	0	31	4
	Min	0	0	0	0
	Max	100	0	100	16
Clover & MiddleC (N=13)	Mean	9	0	5	85
	SD	18	0	7	24
	Min	0	0	0	26
	Max	54	0	20	100

*SVT results show the mean, standard deviation, minimum and maximum values predicted by running each source sample as a target sample. N denotes the number of sources samples in each group. A high predicted contribution from the correct source indicates effective model prediction and discrimination between source types (e.g., Upper Scotts C predicted as Upper Scotts C). The best discriminated source groups are Group 1 with 83±25% (mean ± 1 SD) and Group 4 with 85±24% (mean ± 1 SD) of the source samples correctly classified.

*Table 15.6.4.7. Trial 2 optimal geochemical parameters using in-mixing analysis based on Discriminant Function Analysis results. P_i is the ;proportion of source sample types classified correctly with parameter (i). W_i is parameter discriminatory weighting factor for parameter (i). [Hf, hafnium; Zn, zinc; Mg, magnesium; Li, lithium; Cs, cesium; Nb, niobium; LOI-2*TOC, loss on ignition minus two times total organic carbon; $\delta^{15}N$, delta-15-nitrogen, the ratio of ^{15}N to ^{14}N relative to air; Mn, manganese; Ga, gallium; Cr, chromium; Sr, strontium]*

Tracer	P_i	W_i
Hf	0.669	2.111
Zn	0.553	1.745
Mg	0.533	1.684
Li	0.520	1.643
Cs	0.492	1.552
Nb	0.478	1.509
LOI-2*TOC	0.457	1.442
$\delta^{15}N$	0.427	1.347
Mn	0.410	1.293
Ga	0.400	1.263
Cr	0.386	1.220
Sr	0.317	1

Table 15.6.4.8. Trial 2 error analysis for individual target samples estimated using 1000 Monte Carlo simulations.

Sample name	Mean error (%)	Standard deviation
SFS-0350	1.12	0.003
SFS-0351	0.34	0.01
SFS-0352	0.59	0.00
Average	0.68	

Table 15.6.4.9. Trial 2 confusion matrix. Columns indicate actual distribution of samples. Rows indicate modeled distribution.

		Source Group 1	Source Group 2	Source Group 3	
		CloverC+MiddleC	Lower+MiddleScottsC	UpperScottsC	Total
Source Group 1	CloverC+MiddleC	23	2	1	
Source Group 2	Lower+MiddleScottsC	1	51	4	
Source Group 3	UpperScottsC	2	7	94	
	Total	26	60	99	185
	Percent correct	88.5%	85.0%	94.9%	90.8%

Table 15.6.4.10. Trial 2 source verification test (SVT) results computed by running each source sample through the unmixing model as a target sample.

		Source Verification Test		
		Group 1	Group 2	Group 3
		CloverC+MiddleC	LowerSC+MiddleSC	UpperScottsC
CloverC+MiddleC (N=26)	Mean	68	8	24
	SD	40	17	39
	Min	0	0	0
	Max	100	73	100
LowerSC+MiddleSC (N=60)	Mean	5	72	23
	SD	12	28	27
	Min	0	0	0
	Max	49	100	100
UpperScottsC (N=99)	Mean	18	12	69
	SD	31	20	38
	Min	0	0	0
	Max	100	82	100

*SVT results show the mean, standard deviation, minimum and maximum values predicted by running each source sample as a target sample. N denotes the number of sources samples in each group. A high predicted contribution from the correct source indicates effective model prediction and discrimination between source types (e.g., Upper Scotts C predicted as Upper Scotts C). The best discriminated source group was LowerScMiddleSC with 72%±28% (mean ± 1 SD) of the source samples correctly classified.

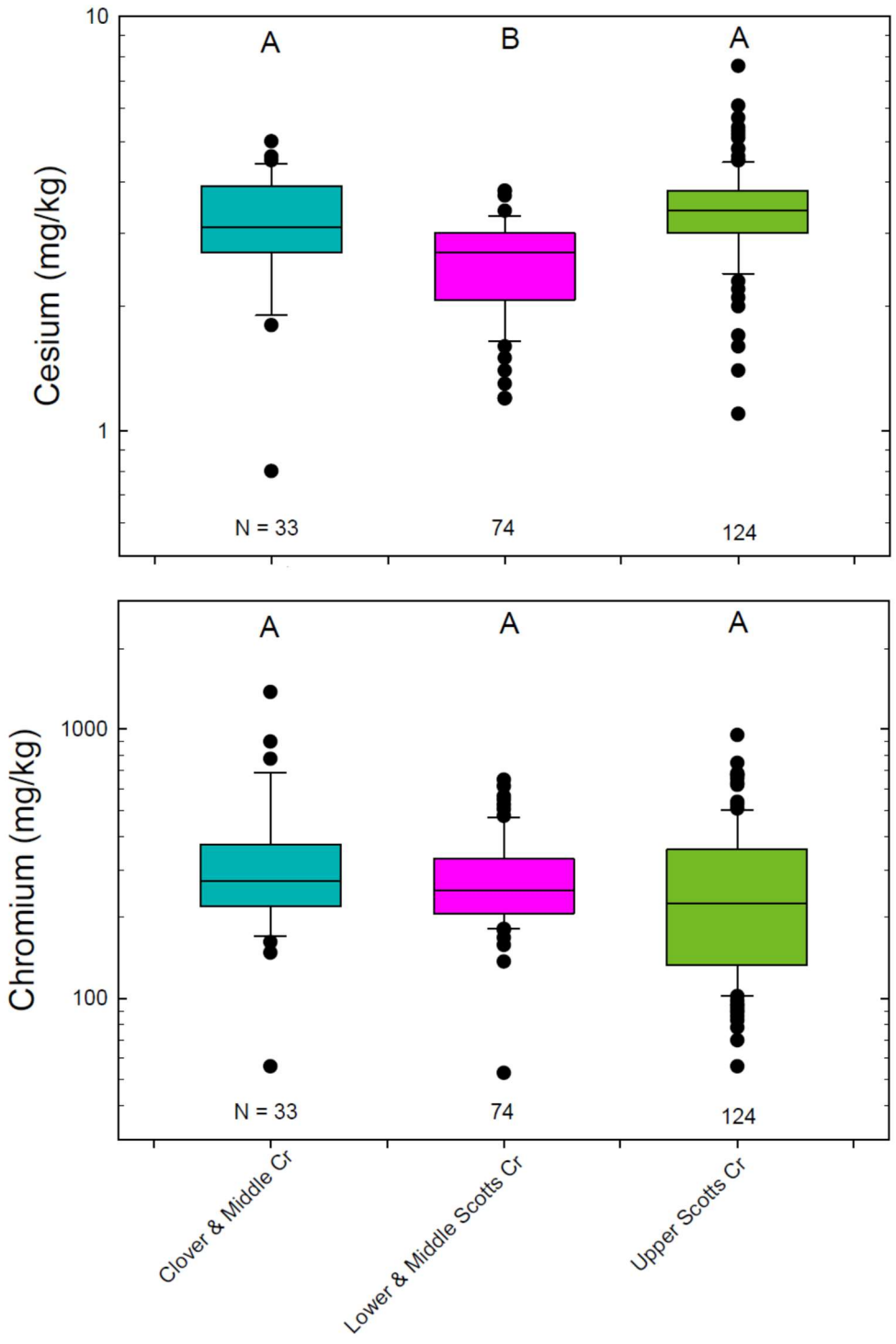

Figure 15.6.4.1. Box plots for cesium and chromium (logarithmic scale). Letters at top indicate statistical differences among the three source groups in Trial 2, using analysis of variance (ANOVA) on ranks. Numbers at bottom indicate the number of samples (N) from each source group. Boxes indicate interquartile range; horizontal lines indicate median; whiskers indicate 10th and 90th percentiles; circles indicate results below 10th percentile or above 90th percentile. Colors match Figures 6.4.18 and 6.4.19. Data summarized from Watanabe et al. (2025).

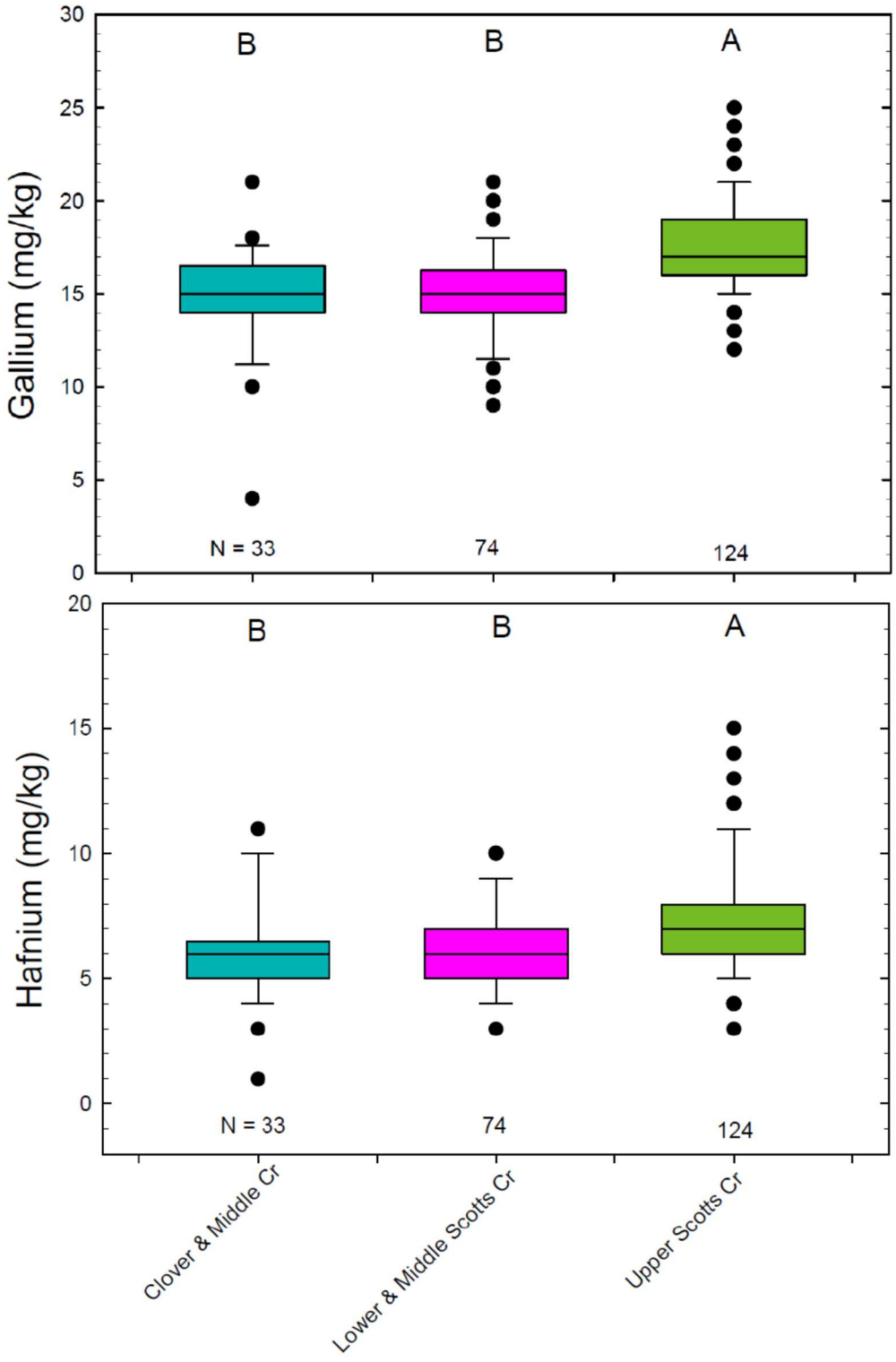

Figure 15.6.4.2. Box plots for gallium and hafnium (linear scale) and holmium (linear scale). Letters at top indicate statistical differences among the three source groups in Trial 2, using analysis of variance (ANOVA) on ranks. Numbers at bottom indicate the number of samples (N) from each source group. Boxes indicate interquartile range; horizontal lines indicate median; whiskers indicate 10th and 90th percentiles; circles indicate results below 10th percentile or above 90th percentile. Colors match Figures 6.4.18 and 6.4.19. Data summarized from Watanabe et al. (2025).

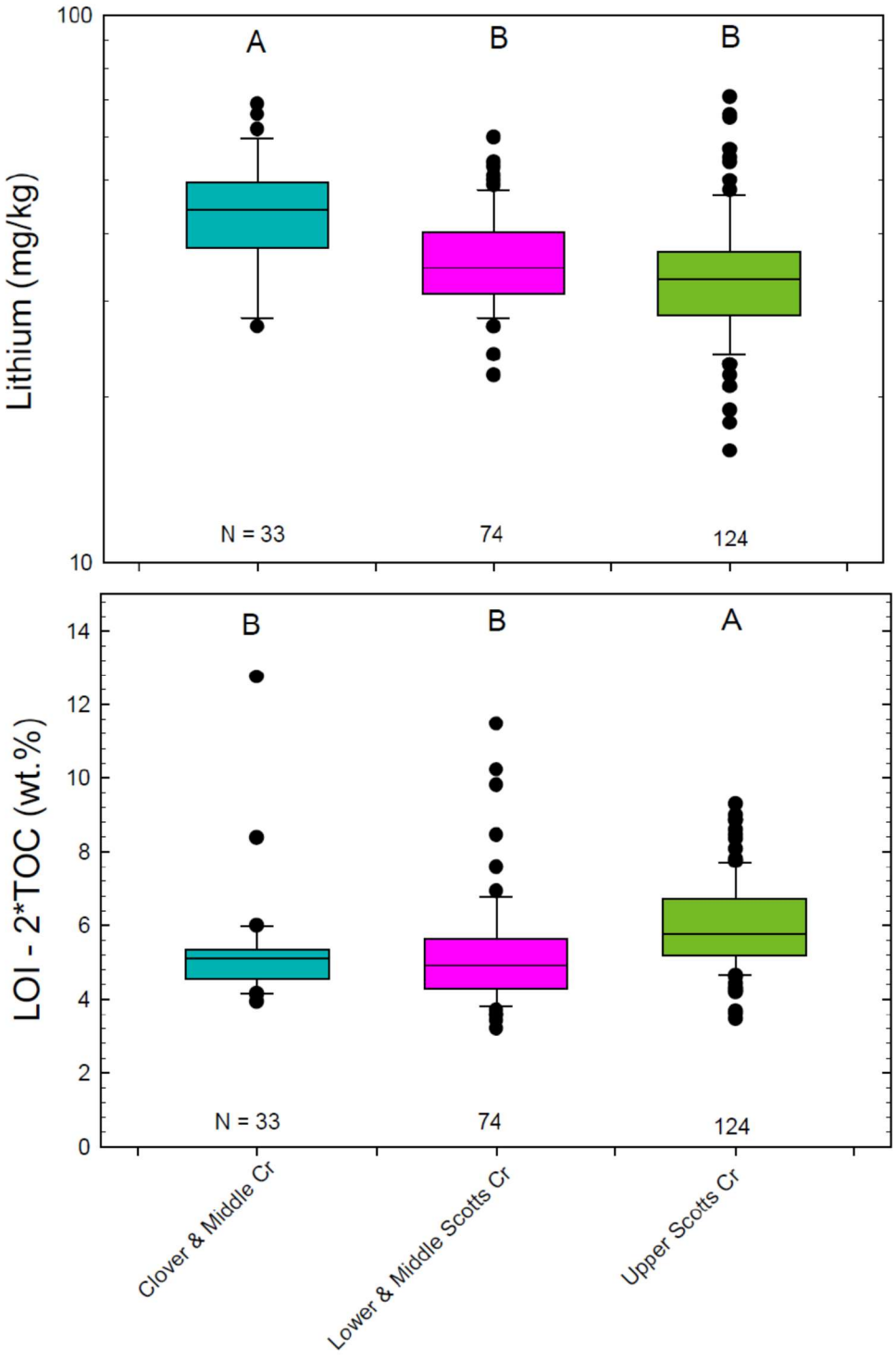

*Figure 15.6.4.3. Box plots for lithium (logarithmic scale) and loss on ignition minus two times total organic carbon (LOI-2*TOC, linear scale). Letters at top indicate statistical differences among the three source groups in Trial 2, using analysis of variance (ANOVA) on ranks. Numbers at bottom indicate the number of samples (N) from each source group. Boxes indicate interquartile range; horizontal lines indicate median; whiskers indicate 10th and 90th percentiles; circles indicate results below 10th percentile or above 90th percentile. Colors match Figures 6.4.18 and 6.4.19. Data summarized from Watanabe et al. (2025).*

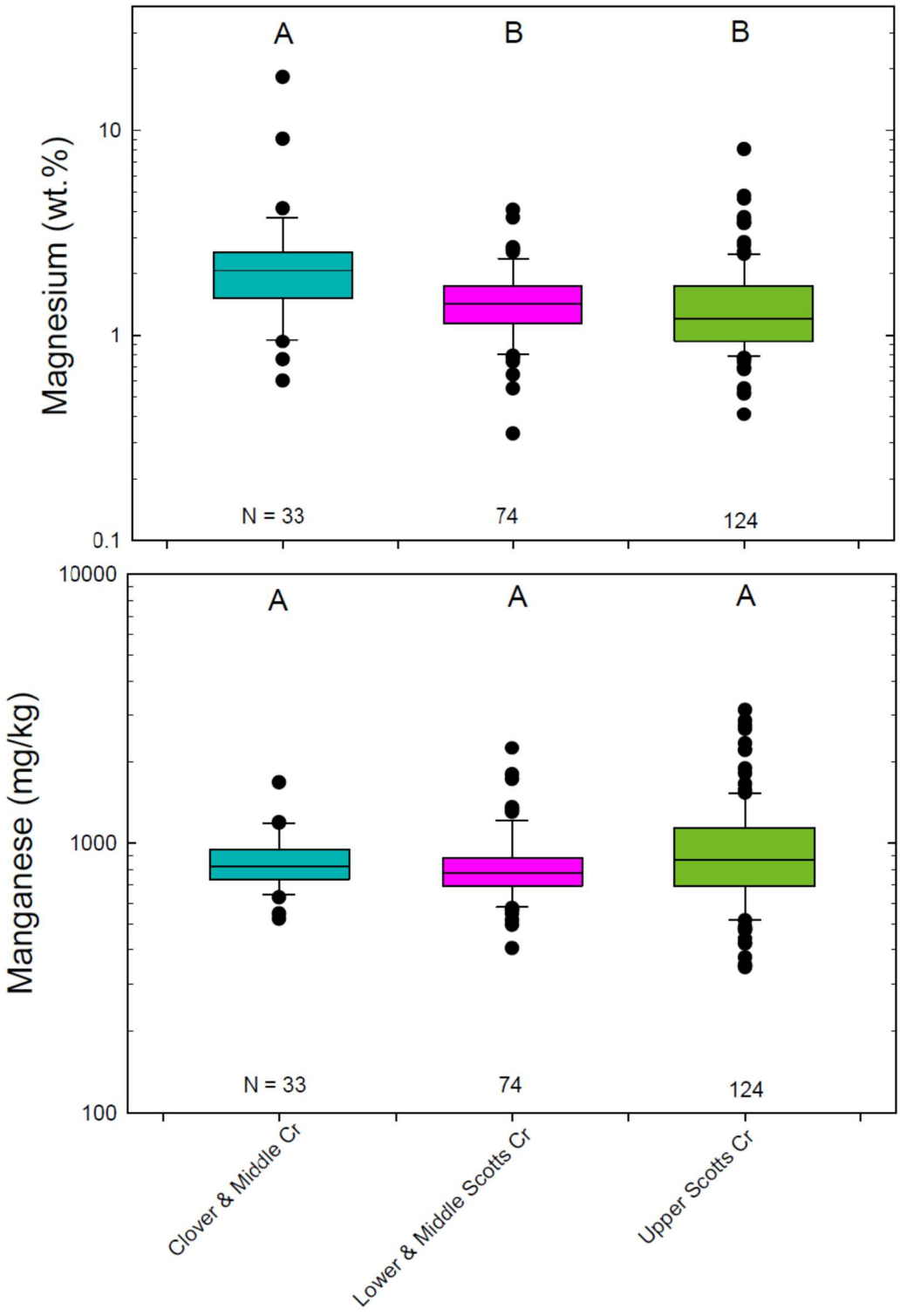

Figure 15.6.4.4. Box plots for magnesium and manganese (logarithmic scale). Letters at top indicate statistical differences among the six source groups in Trial 1, using analysis of variance (ANOVA) on ranks. Numbers at bottom indicate the number of samples (N) from each source group. Boxes indicate interquartile range; horizontal lines indicate median; whiskers indicate 10th and 90th percentiles; circles indicate results below 10th percentile or above 90th percentile. Colors match Figures 6.4.18 and 6.4.19. Data summarized from Watanabe et al. (2025).

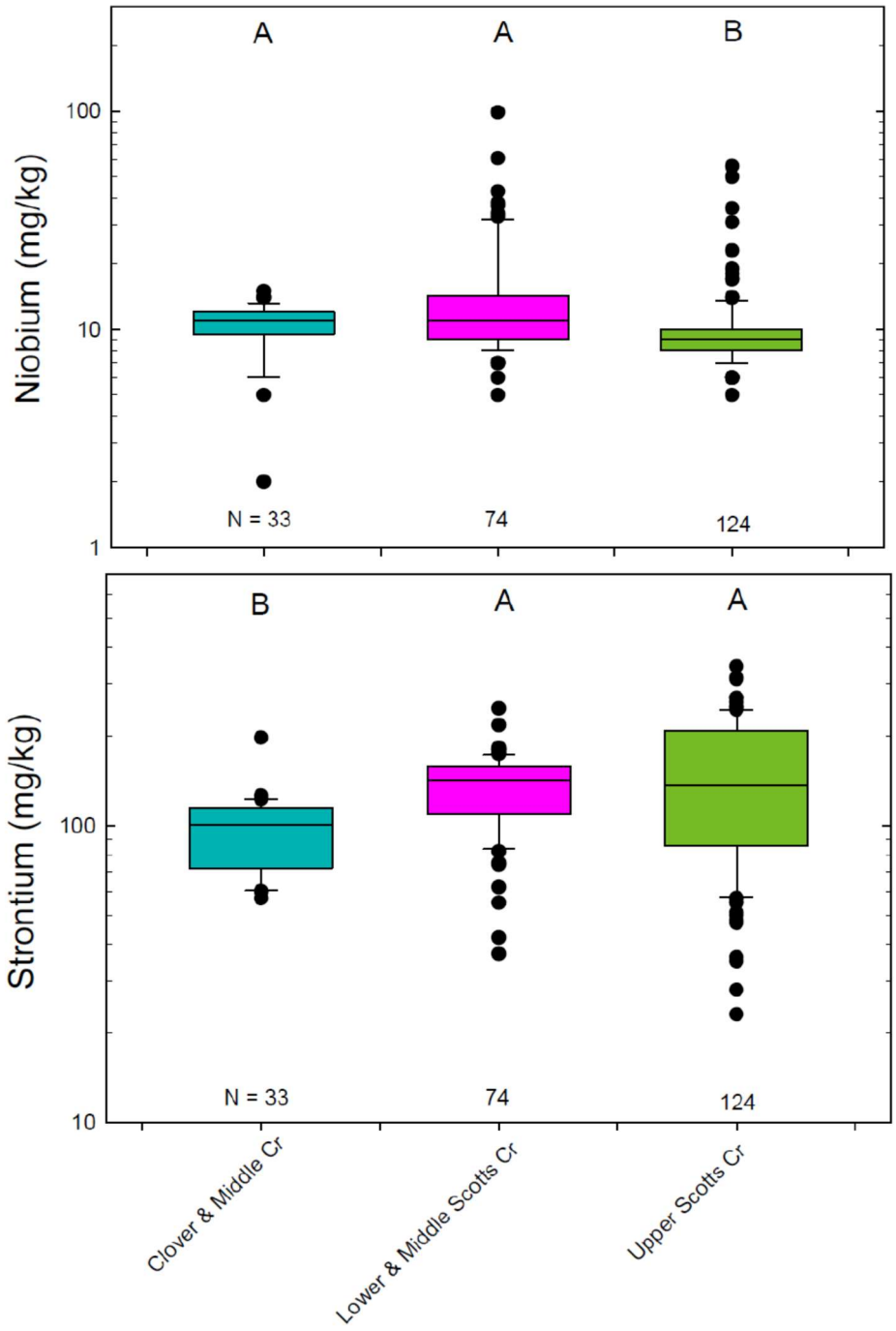

Figure 15.6.4.5. Box plots for niobium and strontium (logarithmic scale). Letters at top indicate statistical differences among the three source groups in Trial 2, using analysis of variance (ANOVA) on ranks. Numbers at bottom indicate the number of samples (N) from each source group. Boxes indicate interquartile range; horizontal lines indicate median; whiskers indicate 10th and 90th percentiles; circles indicate results below 10th percentile or above 90th percentile. Colors match Figures 6.4.18 and 6.4.19. Data summarized from Watanabe et al. (2025).

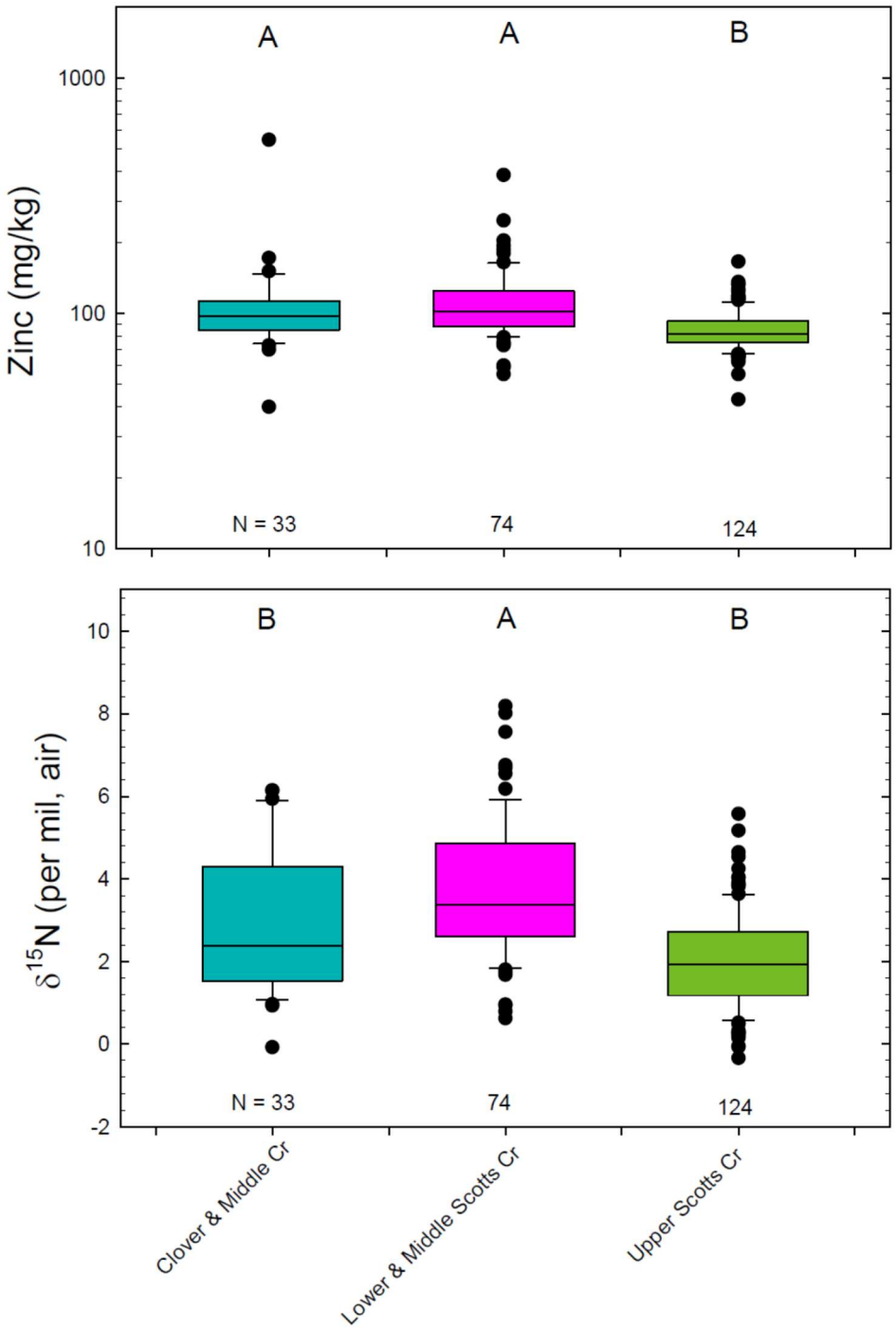

Figure 15.6.4.6. Box plots for zinc (logarithmic scale) and delta-15-N (linear scale). Letters at top indicate statistical differences among the three source groups in Trial 2, using analysis of variance (ANOVA) on ranks. Numbers at bottom indicate the number of samples (N) from each source group. Boxes indicate interquartile range; horizontal lines indicate median; whiskers indicate 10th and 90th percentiles; circles indicate results below 10th percentile or above 90th percentile. Colors match Figures 6.4.18 and 6.4.19. Data summarized from Watanabe et al. (2025).

15.7 In-Lake Monitoring (UCD-TERC)

15.7.1 Flow-TP regression curves

External loading estimates were calculated based on stream-specific flow vs TP regression curves estimated from stream nutrient samples collected across a range of flow conditions. All stream samples collected from Kelsey, Middle, and Scotts Creek between 2014 – 2021 are shown in Figure 15.7.1.1. Samples collected during the WY2018-19 first flush (November 2018) through January 2019, had significantly higher TP concentrations in Middle and Scotts Creek. Higher nutrient concentrations reflect the impacts of the Mendocino Complex which burned much of the Middle and Scotts Creek watersheds during summer 2019. Subsequent sampling events in February and March 2019 and January 2020 are lower (Figure 15.7.1.2), indicating a return to pre-2018 stream conditions. We chose to exclude stream samples from 2019-2021 and use only pre-2018 samples to estimate external loads due to the following reasons:

1. Due to the limited number of samples collected in Kelsey and Scotts Creek (*n* = 4) from 2018 – 2021, the flow vs TP regressions developed from these samples were not significant (Table 15.7.1.1).
2. Increased stream TP due to wildfires appeared to be temporary and likely did not impact external loads in 2020 – 2022.
3. Data from the 2021-2022 WY was not available at the time this analysis was conducted.

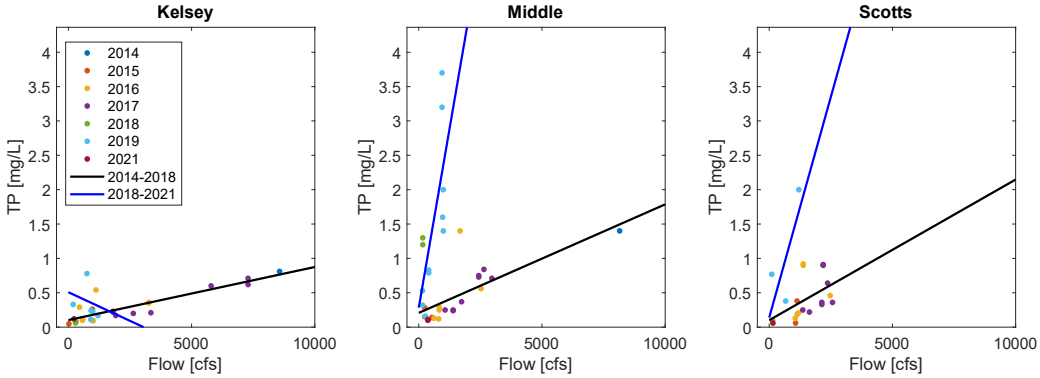

Figure 15.7.1.1. Stream TP measurements during storm sampling events (2014 – 2021). Samples are colored by sampling year. Black and blue lines show linear regressions for discharge vs TP curves based on 2014 – 2018 and 2019 – 2021 sampling data.

Table 15.7.1.1. Comparison of the number of observations used to develop linear regressions and r2, and p-values of regressions.

		Kelsey	Middle	Scotts
2014-2018	n	19	18	16
	R^2	0.75	0.63	0.10
	P value	<0.01	<0.01	0.1
2018 - 2021	n	4	12	4
	R^2	-0.40	0.50	0.45
	P value	0.75	<0.01	0.2

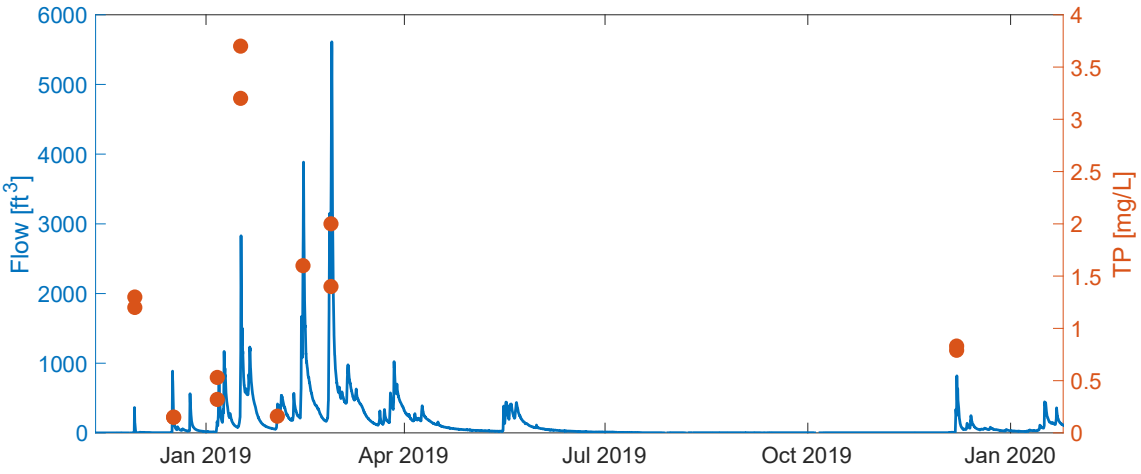

Figure 15.7.1.2. Timeseries of discharge and TP concentrations measured in Middle Creek (Nov 2018 – Feb 2020)

15.7.2 Spatial variability of meteorological conditions

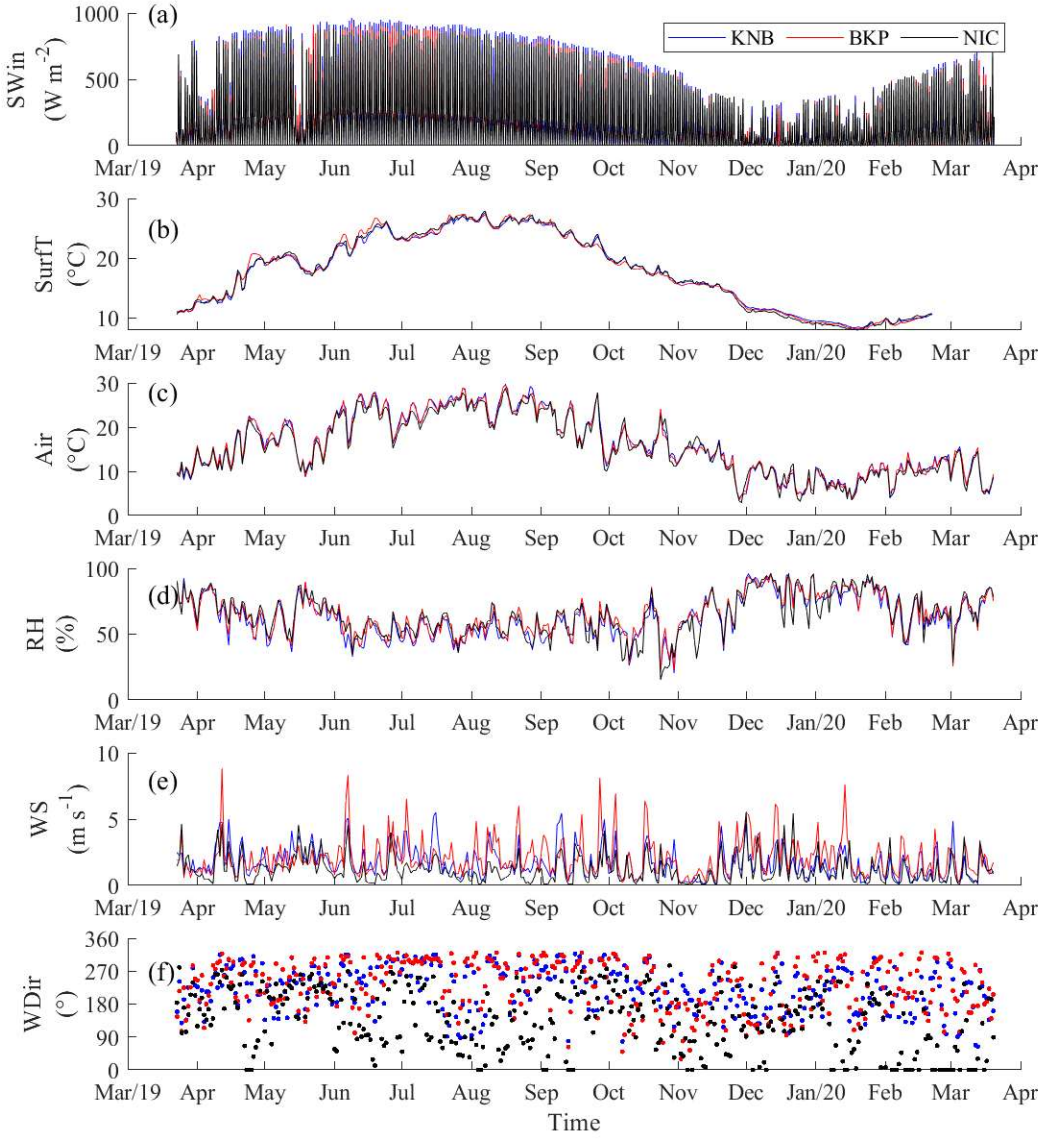

Figure 15.7.2.1. Daily time series of meteorological conditions and lake surface temperatures measured at the station upwind of the predominant wind direction for each basin: KNB for the Lower Arm (blue), BKP for the Oaks Arm (red), and NIC for the Upper Arm (black). Variables include (a) shortwave incoming radiation (SWin) – hourly values, (b) lake surface temperature (SurfT), (c) air temperature (Air), (d) relative humidity (RH), (e) wind speed (WS), and (f) wind direction (WDir).

15.7.3 Lake temperatures and dissolved oxygen at additional sites (UA-01, UA-08, NR-02)

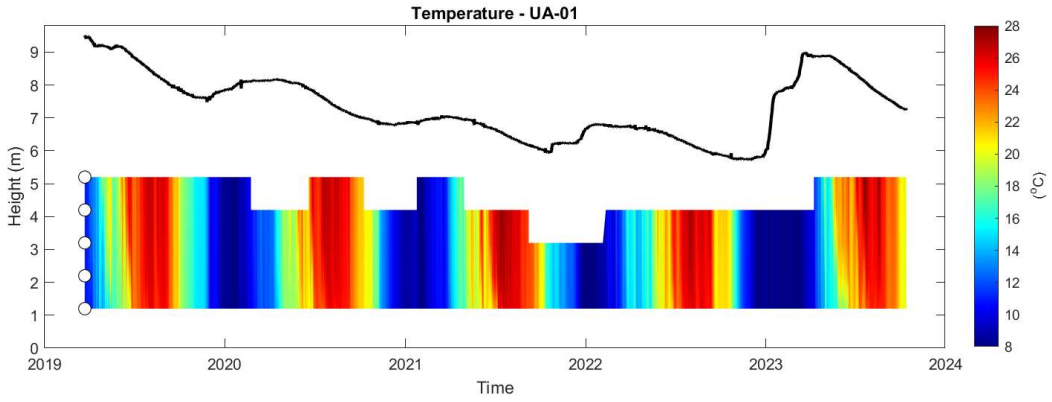

Figure 15.7.3.1. Time series in depth (as a function of distance from the bottom) of hourly lake temperature at multiple depths between 2019 and 2023 at UA-01. The white circles mark the location were we had instruments measuring temperature continuously. The top black line indicates the changes in lake level.

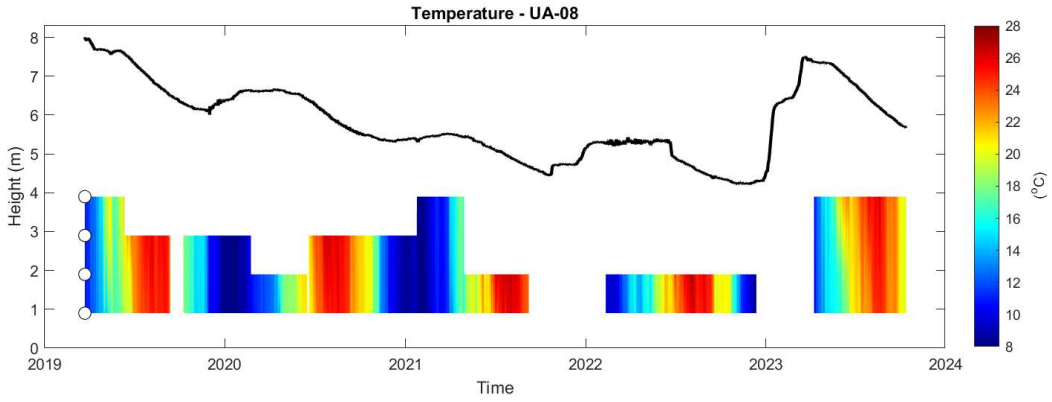

Figure 15.7.3.2. Time series in depth (as a function of distance from the bottom) of hourly lake temperature at multiple depths between 2019 and 2023 at UA-08. The white circles mark the location were we had instruments measuring temperature continuously. The top black line indicates the changes in lake level.

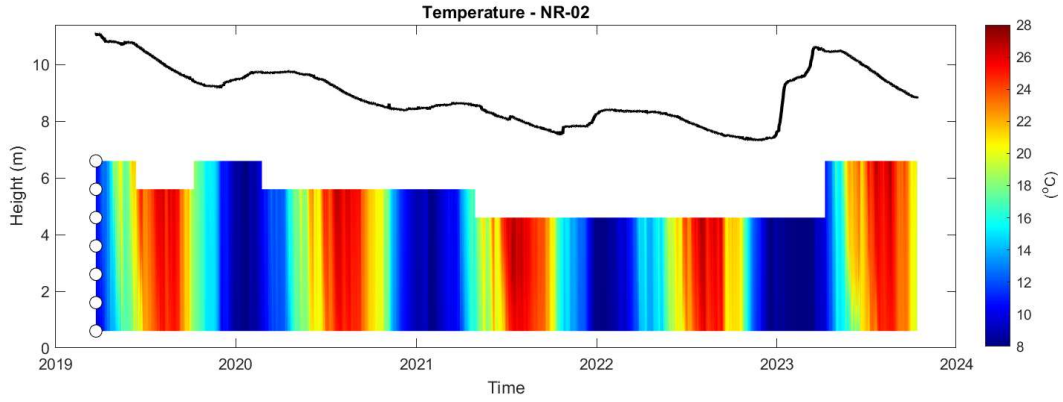

Figure 15.7.3.3. Time series in depth (as a function of distance from the bottom) of hourly lake temperature at multiple depths between 2019 and 2023 at NR-02. The white circles mark the location were we had instruments measuring temperature continuously. The top black line indicates the changes in lake level.

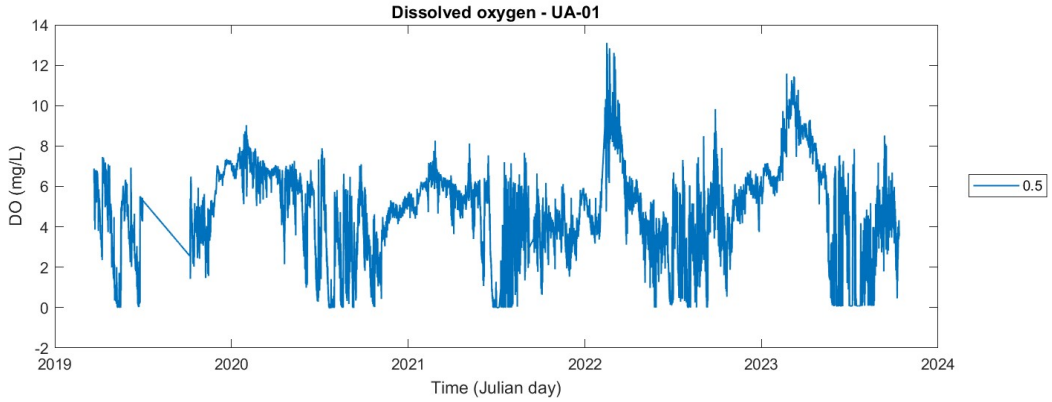

Figure 15.7.3.4. Time series of hourly dissolved oxygen (DO) near the bottom between 2019 and 2023 at UA-01. The white circles mark the location where we had instruments measuring temperature continuously. The top black line indicates the changes in lake level.

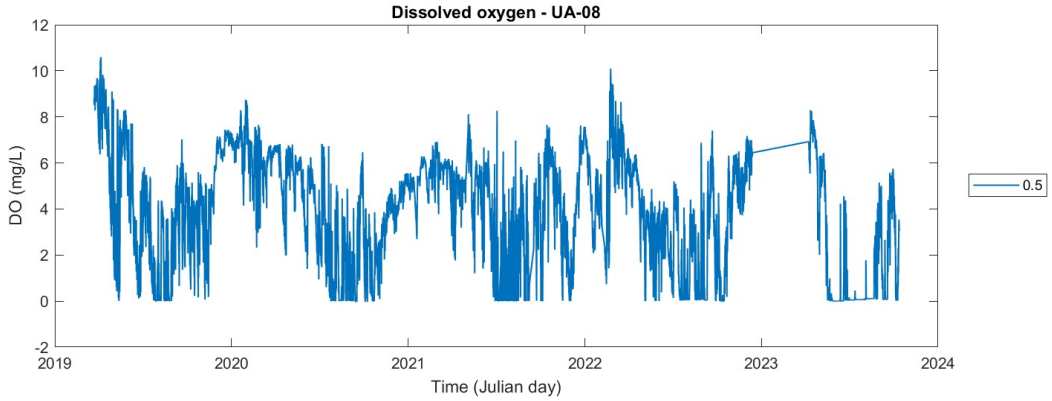

Figure 15.7.3.5. Time series of hourly dissolved oxygen (DO) near the bottom between 2019 and 2023 at UA-08. The white circles mark the location where we had instruments measuring temperature continuously. The top black line indicates the changes in lake level.

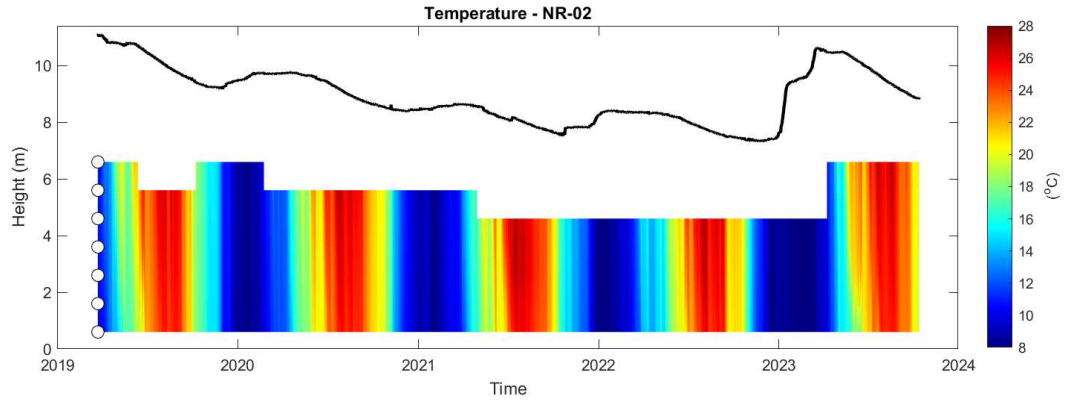

Figure 15.7.3.6. Time series in depth (as a function of distance from the bottom) of hourly dissolved oxygen (DO) at multiple depths between 2019 and 2023 at NR-02. The white circles mark the location where we had instruments measuring temperature continuously. The top black line indicates the changes in lake level.

15.7.4 Lake water quality properties measured at the deep sites and four depths during five years.

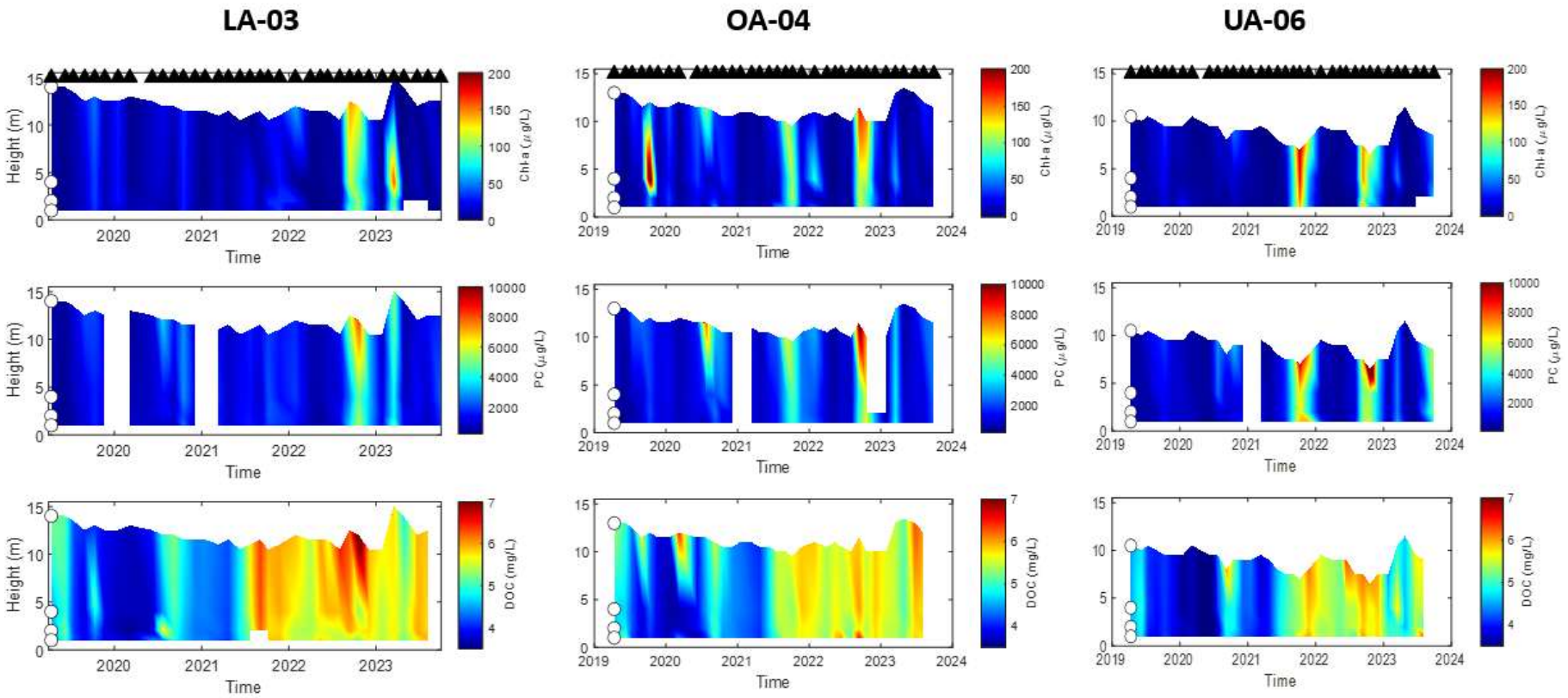

Figure 15.7.4.1. Time series in depth (as a function of distance from the bottom) of water quality constituents related to ***carbon*** *measured at four depths between 2019 and 2023 during our sampling events conducted every 6-8 weeks. Each row shows a different constituent: chlorophyll-a (chl-a), particulate carbon (PC), and dissolved organic carbon (DOC). Each column shows data from a different lake site: (left) LA-03, (middle) OA-04; (center) UA-06. The white circles mark the location where we collect discrete water samples. The top triangles indicate the dates when we collected water samples for laboratory analyses.*

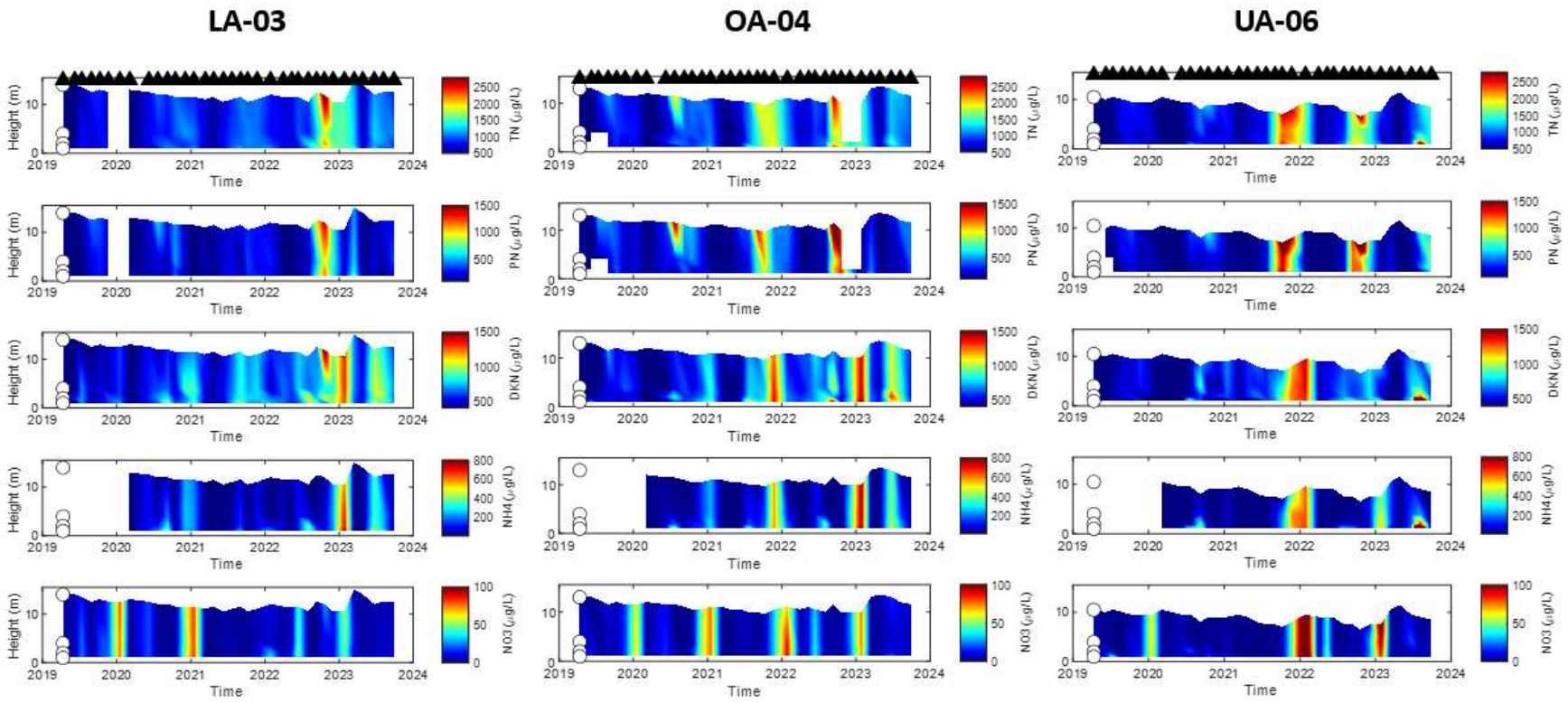

*Figure 15.7.4.2. Time series in depth (as a function of distance from the bottom) of water quality constituents related to **nitrogen** measured at four depths between 2019 and 2023 during our sampling events conducted every 6-8 weeks. Each row shows a different constituent: total nitrogen (TN), particulate nitrogen (PN), dissolved Kjeldhal nitrogen (DKN), ammonium (NH4), and nitrate (NO3). Each column shows data from a different lake site: (left) LA-03, (middle) OA-04; (center) UA-06. The white circles mark the location where we collect discrete water samples. The top triangles indicate the dates when we collected water samples for laboratory analyses.*

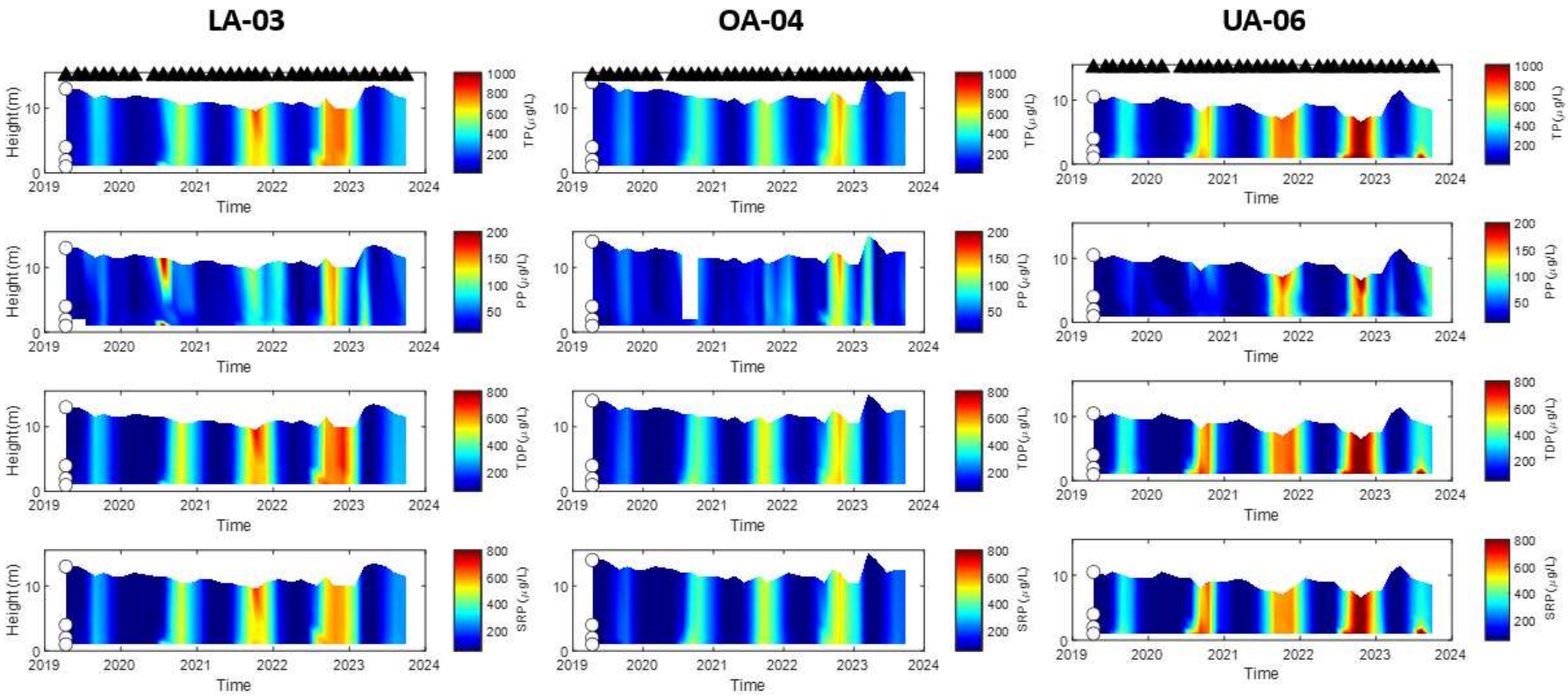

Figure 15.7.4.3. Time series in depth (as a function of distance from the bottom) of water quality constituents related to ***phosphorus*** *measured at four depths between 2019 and 2023 during our sampling events conducted every 6-8 weeks. Each row shows a different constituent: total phosphorus (TP), particulate phosphorus (PP), total dissolved phosphorus (TDP), and Orthophosphate Phosphorus PO_4, Soluble reactive phosphorus (SRP). Each column shows data from a different lake site: (left) LA-03, (middle) OA-04; (center) UA-06. The white circles mark the location where we collect discrete water samples. The top triangles indicate the dates when we collected water samples for laboratory analyses.*

15.8 In-Lake Modeling (UCD-TERC)

15.8.1 Water quality lake model: Calibration and validation initial and surface boundary conditions

- **Calibration: Initial and Surface Boundary Conditions (June-July 2020)**

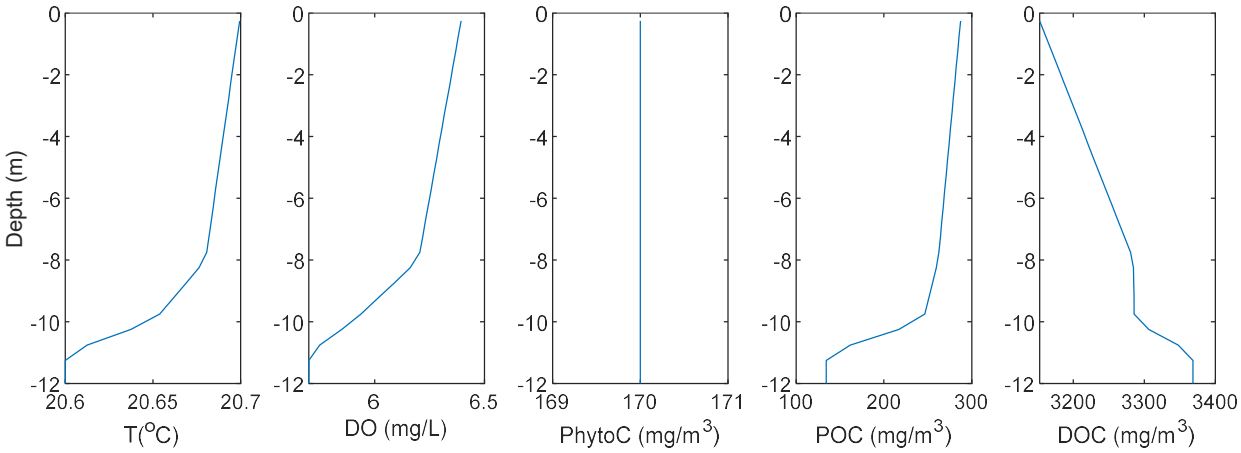

Figure 15.8.1.1. Lake profiles of initial conditions of the calibration run in June 2020: Temperature, dissolved oxygen, phytoplankton carbon, and carbon forms

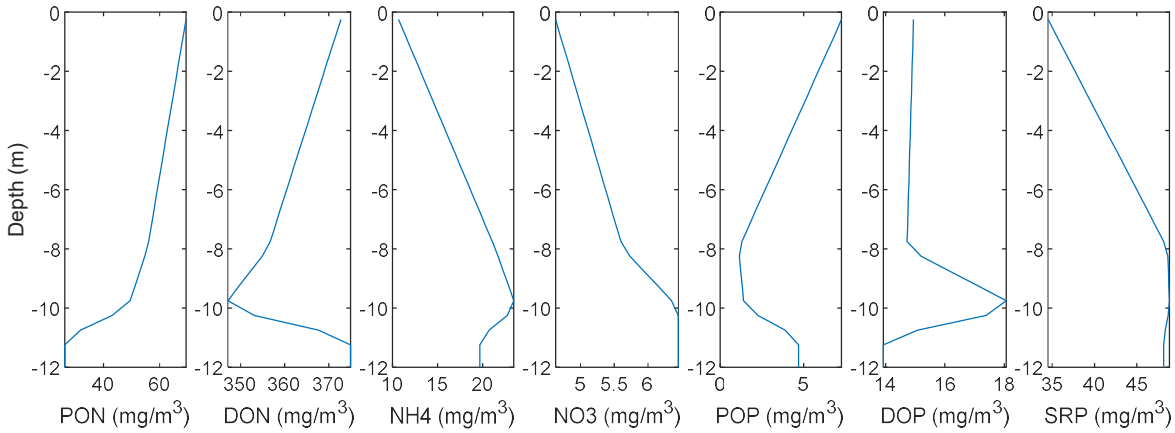

Figure 15.8.1.2. Lake profiles of initial conditions of the calibration run in June 2020: Nitrogen and phosphorus forms

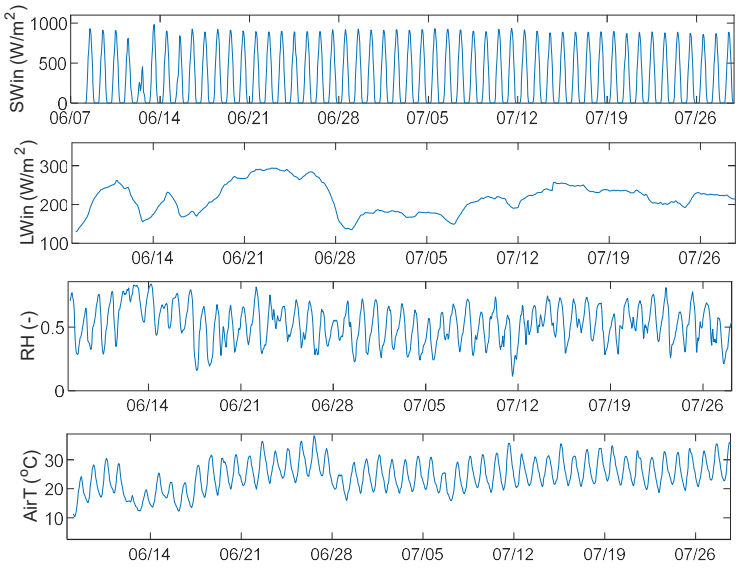

Figure 15.8.1.3. Time series of heat-related meteorological variables (incoming short-wave radiation SWin, incoming long-wave radiation LWin, relative humidity RH, and air temperature, AirT) at Clear Lake was used for the model calibration during the summer of 2020. Values are averaged across the lake.

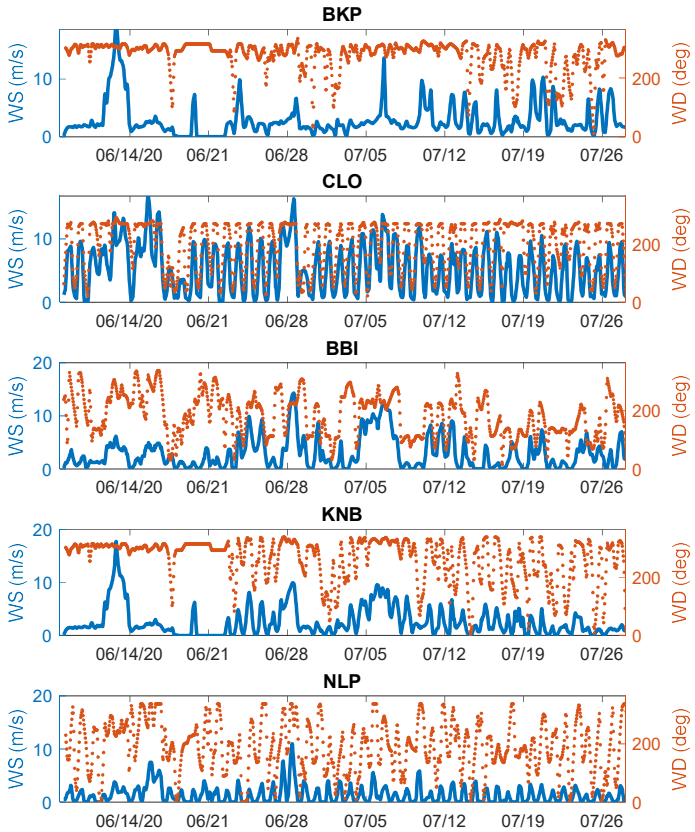

Figure 15.8.1.4. Time series of wind conditions (magnitude WS and direction WD) at Clear Lake used for the model calibration during summer 2020 at five stations across the lake: Buckingham Point (BKP), Konocti Bay (KNB), Beakbane Island (BBI), Clearlake Oaks (CLO), Nice (NIC)

- **Validation: Initial and Surface Boundary Conditions (July 2022)**

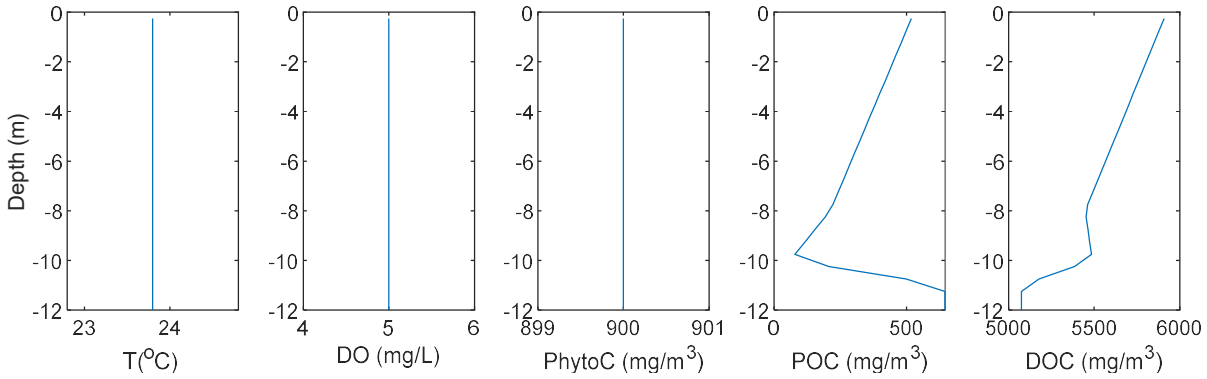

Figure 15.8.1.5. Lake profiles of initial conditions of the validation run in July 2022: Temperature, dissolved oxygen, phytoplankton carbon, and carbon forms

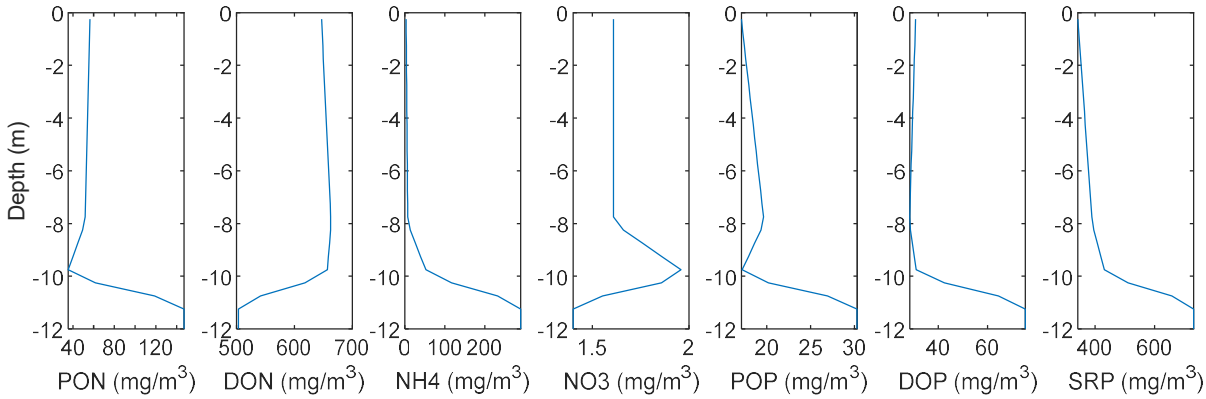

Figure 15.8.1.6. Lake profiles of initial conditions of the validation run in July 2022: Nitrogen and phosphorus forms

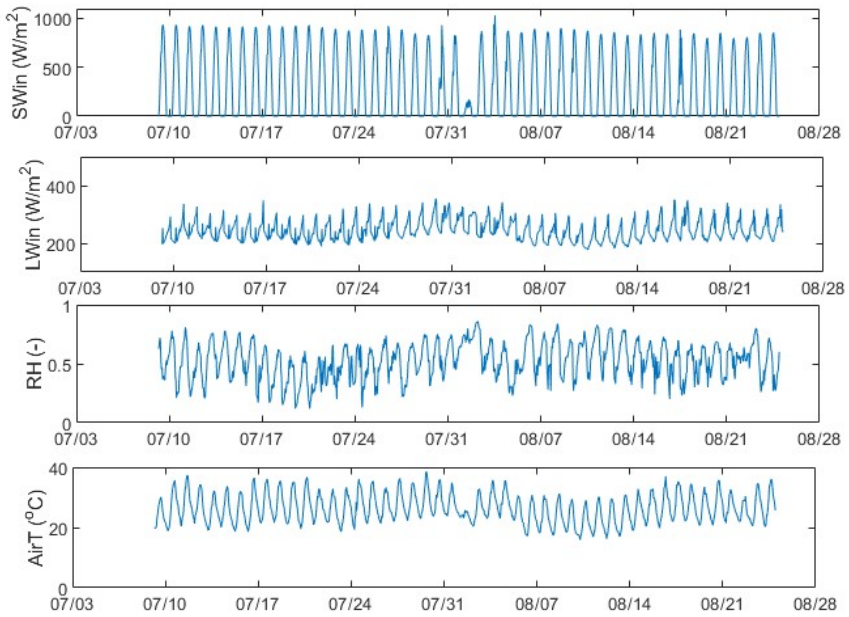

Figure 15.8.1.7. Time series of heat-related meteorological variables (incoming short-wave radiation SWin, incoming long-wave radiation LWin, relative humidity RH, and air temperature, AirT) at Clear Lake was used for the model validation during the summer of 202. Values are averaged across the lake.

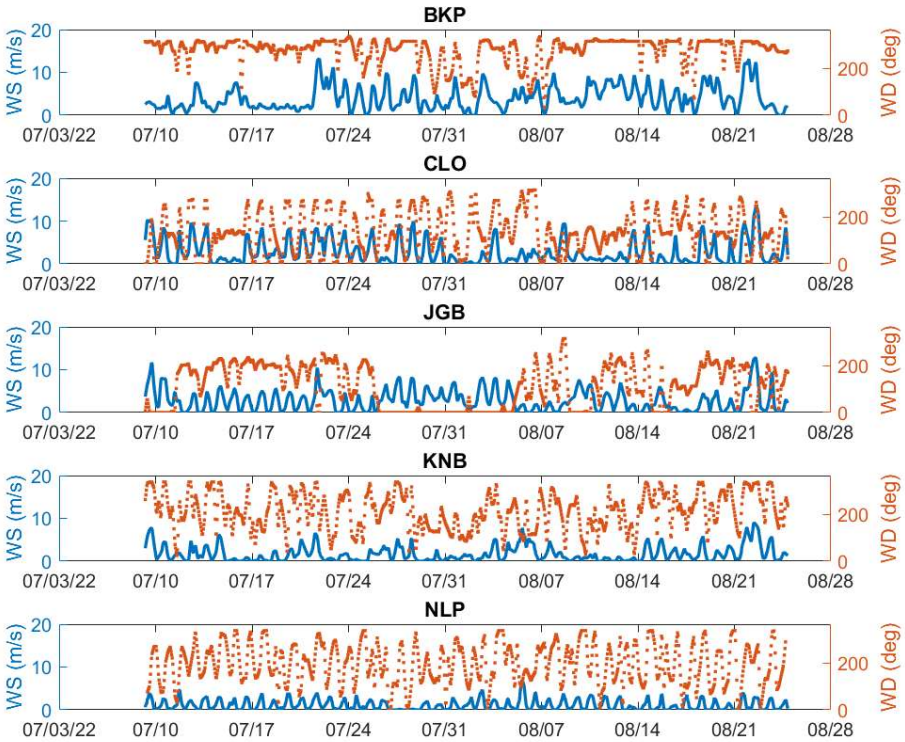

Figure 15.8.1.8. Time series of wind conditions (magnitude WS and direction WD) at Clear Lake used for the model validation during summer 202 at five stations across the lake: Buckingham Point (BKP), Konocti Bay (KNB), Beakbane Island (BBI), Clearlake Oaks (CLO), Nice (NIC)

15.8.2 Background of Hypolimnetic Oxygenation

The foundation for the use of oxygen as a restoration strategy of eutrophic lakes and reservoirs traces back to Mortimer (1942). The first application of artificially raising hypolimnetic oxygen to counter anoxia occurred in an Austrian aeration system. In the early years of HO, results were often variable, in part due to the availability of pure oxygen, design and performance issues, and oxygen storage logistics. As research on HO systems continued, technology improved, and pure oxygen became more readily available, HO has proven to be an effective technique with more predictive results. To date, more than 30 HO systems have been deployed in lakes and reservoirs worldwide (Gerling et al. 2014, Singleton and Little 2006).

Modern HO systems rely on oxygen either produced or stored adjacent to the lake. An on-site oxygen generator can be used to produce oxygen. These have a higher initial capital cost but lower operating costs in the long run. Liquid oxygen (LOX) can be delivered by a gas supplier. Such an arrangement has little or no maintenance expense but can result in a higher oxygen cost. Pure oxygen is preferred over the addition of air, as air is comprised of only 20% oxygen. It was envisaged for the Pilot Project that LOX be delivered, as the limited duration of the pilot project (less than 4 months) did not appear to warrant the extra capital costs. As part of the pilot project, a more detailed cost-benefit analysis of the oxygen supply could be conducted.

There are various systems used to transfer the oxygen from the storage or generation site into the lake and hypolimnion. HO transfer systems are generally categorized into three types: (1) direct injection via bubble plume diffusers (see for example Singleton et al. 2007) – in these systems a small bubble size ensures the oxygen quickly dissolves into the hypolimnion within a short distance from the injection depth; (2) in situ contact chambers such as the Speece Cone (see for example McGinnis and Little 1998) where oxygen dissolution occurs within a specially designed dissolution chamber housed at the bottom of the lake before releasing to the hypolimnion; and (3) side-stream saturation, for which water is withdrawn from the hypolimnion, oxygenated, and then returned (see for example Beutel and Horne 1999). Such systems have all operated for many years at a time, with a Speece cone system in Camanche Reservoir having been used for over twenty years. CA Waterboard currently has a hypolimnetic oxygenation study ongoing on Lake Hodges in San Diego. None of these systems have been found to cause the sustained disturbance of the sediments. A pilot study conducted by Dr. Horne in the 70s in the Oaks Arm used the aeration technique, and the goal was to mix the full water column instead of directly adding oxygen at the sediment-water interface.

In 1999, the first review on HO was compiled, focusing on the first two decades of HO (Beutel and Horne 1999). A 2006 review summarized the state of system design (Singleton and Little 2006). A comprehensive review of HO in 2016 summarized HO applications to reduce cyanobacterial blooms (Bormans et al. 2016). A more recent review of HO was conducted in 2019, which concluded that HO was largely successful in improving water quality in the studies reviewed, although the conclusions must be tempered with the fact that other in-lake and watershed nutrient restoration efforts have often been implemented in conjunction with HO (Preece et al. 2019). The impacts of hypolimnetic

oxygenation in three reservoirs in northern California specifically on mercury methylation are described in McCord et al. (2016).

References

Beutel, M. W., Horne, A. J., 1999, A review of the effects of hypolimnetic oxygenation on lake and reservoir water quality: Lake Reserv Manage, v. 15(4), p. 285–297. https://doi.org/*10.1080/07438149909354124*

Bormans, M., Marsalek, B., Jancula, D., 2016, Controlling internal phosphorus loading in lakes by physical methods to reduce cyanobacterial blooms: a review: Aquat Ecol, v. 50(3), p. 407–422. https://doi.org/10.1007/s10452-015-9564-x

Cortés, A., Forrest, A. L., Sadro, S., Stang, A. J., Swann, M., Framsted, N. T., Thirkill, R., Sharp, S. L., Schladow, S. G., 2021, Prediction of hypoxia in eutrophic polymictic lakes: Wat Resour. Res., v. 6, p. e2020WR028693. https://doi.org/10.1029/2020WR028693

Gerling, A. B., Browne, R. G., Gantzer, P. A., Mobley, M. H., Little, J. C., Carey, C. C., 2014, First report of the successful operation of a side stream supersaturation hypolimnetic oxygenation system in a eutrophic, shallow reservoir: Wat Res, v. 67, p. 129–143. https://doi.org/10.1016/j.watres.2014.09.002

McCord, S. A., Beutel, M. W., Dent, S. R., Schladow, S. G., 2016, Evaluation of mercury cycling and hypolimnetic oxygenation in mercury-impacted seasonally stratified reservoirs in the Guadalupe River watershed, California: Water Resour Res, v. 52(10), p. 7726–7743. https://doi.org/10.1002/2016WR019061

McGinnis, D. F., Little, J. C., 1998, Bubble dynamics and oxygen transfer in a Speece cone: Water Science and Technology, v. 37, p. 285-292. url: https://iwaponline.com/wst/article/37/2/285/7538/Bubble-dynamics-and-oxygen-transfer-in-a-speece

Mortimer, C. H., 1942, The exchange of dissolved substances between mud and water in lakes. Part III. The relation of seasonal variables in redox conditions in the mud to the distribution of dissolved substances in Esthwaite Water and Windermere, North Basin. Part IV. General discussion: J. Ecology, v. 30, p. 147–201. https://doi.org/10.2307/2256691

Preece, E. P., Moore, B. C., Skinner, M. M., Child, A., Dent, S., 2019, A review of the biological and chemical effects of hypolimnetic oxygenation: Lake and Reservoir Management, v. 35(3), p. 229-246. https://doi.org/10.1080/10402381.2019.1580325

Singleton, V. L., Gantzer, P., Little, J. C., 2007, Linear bubble plume model for hypolimnetic oxygenation: full-scale validation and sensitivity analysis: Water Resour Res, v. 43, p. W02405. https://doi.org/10.1029/2005WR004836

Singleton, V. L., Little, J. C., 2006, Designing hypolimnetic aeration and oxygenation systems: a review: Environ Sci Technol, v. 40(24), p. 7512–7520.